1-1-2005

Influence of compaction energy on soil engineering properties

Isaac Robert Drew
Iowa State University

Influence of compaction energy on soil engineering properties

by

Isaac Robert Drew

A thesis submitted to the graduate faculty

in partial fulfillment of the requirements for the degree of

MASTER OF SCIENCE

Major: Civil Engineering (Geotechnical Engineering)

Program of Study Committee:
David White, Major Professor
Edward Jaselskies
Max Morris

Iowa State University

Ames, Iowa

2005

Graduate College

Iowa State University

This is to certify that the master's thesis of

Isaac Robert Drew

has met the thesis requirements of Iowa State University

Signatures have been redacted for privacy

TABLE OF CONTENTS

LIST OF FIGURES

LIST OF TABLES

ABSTRACT

Strength and deformation parameters of compacted soil are known to be related to soil type and moisture content. However, little attention has been directed towards understanding the influence of compaction energy on these properties. This paper describes laboratory and field studies conducted to evaluate the relationship between soil type, soil moisture content, and compaction energy on seven cohesive soil types.

In the lab, specimens were compacted with impact energy at levels of 355, 592 (standard Proctor), 987, 1643, and 2693 kJ/m^3 (modified Proctor) over a wide range of moisture contents to determine dry unit weight, unconfined compressive strength and the secant (50 percent strain) stiffness. In total, 175 Proctor tests and 95 unconfined compression tests were performed. At each energy level, a soil was tested at 4 to 5 moisture contents with respect to its standard Proctor moisture range. In addition, 54 consolidated undrained triaxial tests were performed at the five energies and four moisture contents for one soil to evaluate changes in effective stress shear strength parameters.

This paper summarizes the results of statistical analyses performed on all lab and field tests conducted. The models that best explain variability in dry unit weight, strength, and stiffness are presented. Models are presented individually for each soil type and also inclusive of all soils grouped together. Independent variables used in the modeling include compaction energy, moisture content, confining pressure, Atterberg limits, material passing the No. 200 sieve, and clay fraction. In addition, a new compaction model, derived from a linear rate

equation, is presented and checked for validity in estimating soil dry unit weight as a function of compaction energy.

Results indicate that compaction energy, combined with moisture content, is a key factor in determining soil strength and stiffness parameters. It is concluded that the strength and stability of a compacted soil cannot be assessed in terms of relative compaction alone. Instead, this research encourages the use of strength and stiffness in the design and construction phases of earthwork operations, being the true functional requirements for compaction specifications.

CHAPTER 1. INTRODUCTION

The determination of relative compaction for fill soils is needed to ensure adequate performance of an overlying structure or pavement layer. Methods to monitor compaction typically involve process control (lift thickness and number of passes) and spot tests performed by onsite inspection personnel. The conventional method uses measurements of soil dry unit weight. In the field, measurement of soil dry unit weight is typically done with a nuclear gauge or sandcone test and compared to the maximum dry unit weight determined from a laboratory compaction test.

In 1997, a nationwide survey of state DOT's reported 41 states used standard Proctor as their primary test method for compaction quality assessment (Walsh et al. 1997). Ten states claimed to use modified Proctor, with some states using both methods. Regarding relative compaction, 95% of standard Proctor was reported as the most common specification used in the field (30 states).

Problems with fixating compaction specifications solely on 95% standard Proctor have been noted in the literature (Charles et al. 1998; Lawton et al. 1989; Trenter and Charles 1996). A common failure noted, when using this specification, is collapse compression and swelling of soils. This problem occurs when a fill is compacted at or above 95% standard Proctor, but is still dry of optimum moisture content. Additional moisture added to the fill results in swelling or collapse, depending on the overburden pressure applied. Therefore, it is suggested a soil's moisture content prior to compaction should play an equally important role

in composing a compaction quality specification. For example, the moisture content minimizing swell or collapse could be specified as a certain percentage wet of optimum.

In addition to moisture, the stability of soil is dependent on the amount of compaction energy delivered. Principles first established by Proctor (1933a), stated that for a given soil, different compactive efforts give rise to different dry unit weight-moisture content relationships. Maximum dry unit weight and optimum moisture content are notably affected by compaction energy in the former increasing with increased compactive effort and the latter decreasing with increasing compactive effort. Further, increased compactive effort, on clays dry of optimum and at optimum moisture content, have been observed to increase unconfined shear strength and stiffness (Attom 1997; Pagen and Jagannath 1969). Wet of optimum, compaction energy has been noted not to contribute to an increase in stability.

Often, the practice of a lab compaction method can lead to conclusions that are not representative of dry unit weight attained in the field (Kouassi et al. 2000). A misleading conclusion in the lab occurs in two ways. First, it occurs when the lab technique does not have the capacity to deliver the same amount of energy as a roller. Second, it occurs when the technique does not accurately represent how a soil is compacted by a roller.

While some agencies might neglect the importance of moisture and compaction energy, others have taken action by revising standards in compaction specifications. Still, most incorporate dry unit weight instead of other soil properties like strength or stiffness. The

insistence of agencies using dry unit weight as a measure of proper compaction stirs criticism, but nevertheless should be expected for several reasons.

First, the degree of variability in the measurement of strength and stiffness is significantly higher than dry unit weight. Therefore, when reporting to an owner, an agency would find comfort with results that expect little variation. Another reason why dry unit weight is preferred is ease in test method and cost. For example, an area consultant stated the use of nuclear gauge in the field as "much easier to use than dynamic cone penetrometer (strength test) and cheaper." (Joels Malama, personal communication, Jan. 15, 2005). Next, it seems reasonable to interpret the measurement of dry unit weight to correlating strength and stiffness, i.e. the higher the dry unit weight the soil, the greater the stiffness and strength, depending on the moisture content. Finally, it should not be surprising that a transition to a field test procedure based on strength or stiffness would be stalled due to majority opinion of industry personnel, including state DOT's and geotechnical consultant firms. In some vocations, past ideologies dominate the performance of test procedures, prohibiting new and progressive thinking from modifying or completely changing them. Geotechnical engineering is not exempt from this situation.

Maximum dry unit weight and optimum moisture content have been empirically related to soil index properties and compaction energy (Ring et al. 1962; Boltz et al. 1998). The empirical models developed have been useful in estimating results for field work and aided in the understanding of relationships between maximum dry unit weight, optimum moisture content, Atterberg limits, fines content, and compaction energy. However, additional

research is needed to better understand how compaction energy influences shear strength and stiffness.

Models derived from this research were concluded to be a tool in understanding the relationships between dry unit weight, undrained shear strength, secant modulus, and peak deviator stress with moisture content, compaction energy, and soil index properties. Major findings were that sensitivity of optimal conditions to compaction energy was dependent on soil plasticity; compaction energy explained more of the variability in dry unit weight dry of optimum and at optimum; variability in undrained shear strength was explained most by compaction energy; confining pressure explained more of the variability in two of the three stability parameters analyzed for CU loess specimens; and the practice of using 95% standard Proctor as a means to determine strength and stability is invalid.

Goal

The goal to alleviate the problem was to develop empirical models of strength and stiffness of soil as a function of compaction energy.

Objectives

1. Evaluate soil parameters as a function of compaction energy, moisture content, and index properties.
2. Derive prediction models that relate soil parameters to compaction energy, moisture content, and index properties.

3. Compare and contrast prediction models derived to previous work from the literature.
4. Verify the usefulness of prediction models by estimating soil behavior with lab soils not used in the statistical analyses.
5. Evaluate the potential to integrate lab research in estimating work performed in the field.

Benefits

The author anticipates the results of this work will encourage the use of strength and stiffness as parameters for quality control in earthwork construction. Empirical relationships between these parameters and compaction energy could be integrated into the field as a process specification, i.e. number of roller passes. It could also be used as an alternative or complimentary property of measurement to dry unit weight.

Thesis Organization

A background of how soil properties are affected by compaction energy, moisture content, and index properties is given in the following chapter. In addition, a summary of empirical relationships related to soil compaction is presented. Chapters 2 - 3 of this report review the methods used in the laboratory and discuss the results. Chapters 4 – 5 present methodology in field work and discuss the results from the field. Summaries for lab and field results are presented in Chapter 6 and 7. The conclusions and recommendations are presented in Chapter 8.

BACKGROUND

While soil compaction is complex, general relationships between soil engineering properties and soil index properties, moisture content, and compaction energy are predictable. A substantial amount of information can be found in the literature concerning these relationships. The intent of this review is to discuss how soil engineering properties are affected by the amount and type of compaction, moisture content, and index properties. A summary of empirical relationships of soil compaction is presented.

Influence of Compaction Energy on Soil Engineering Properties

Much of the literature focuses on dry unit weight as a key parameter of research. Investigation of other properties affected by compaction energy included strength, stiffness, permeability, and swell pressure.

Dry Unit Weight

Proctor (1933a) first systematically demonstrated the influence that compaction energy and moisture content have on the dry unit weight of soil. He introduced the use of a 2.5 kg. hammer, compacting soil into 3 equal layers at 25 strokes per layer. The soil was compacted in a cylinder, 11.4 cm in diameter and 17.8 cm in height. A penetrating needle was additionally used to test penetration resistance after a soil was compacted. His efforts on 200 different soil types showed that increases in compaction energy increased maximum dry unit weight and decreased the optimum moisture content (1933b). Other research in the literature affirms this principle (Attom 1997; Bell 1977; McRae and Rutledge 1952; Pagen and Jagannath 1969). One theory suggests that the addition of moisture lubricates soil particles

and allows them to slide, causing a denser state (Attom 1997). As more compaction energy is applied, lower moisture content is required to obtain the maximum dry unit weight. The test procedure would later be adapted as a test standard and common practice in attaining quality in earthwork construction.

Strength and Stiffness

Dry unit weight alone cannot, however, be relied on in determining the proper compaction of a soil (Proctor 1948b). A compacted soil must be tested for stability to make conclusions on its suitability in the field (Proctor 1933b). Stability of a material can be determined by measuring strength and stiffness.

Attom (1997) applied ten impact energies, ranging from 355 to 2693 kJ/m^3, on an expansive clay (CH). Table 1 gives the details of how compaction energy was applied to each specimen including hammer mass, drop height, number of blow applies, number of layers compacted, volume of cylinder, and value of energy.

Table 1. Compaction energy applied to clay specimens (after Attom, 1997)

Sample ID	Hammer Mass (kg)	Height of Drop (cm)	Number of Blows	Number of Layers	Volume of Cylinder (cm^3)	Energy Applied (kJ/m^3)
E1	2.5	30.5	15	3	934.5	355.6
E2	2.5	30.5	20	3	934.5	474.2
E3	2.5	30.5	25	3	934.5	592.7
E4	2.5	30.5	30	3	934.5	711.3
E5	2.5	30.5	20	5	934.5	790.3
E6	2.5	30.5	25	5	934.5	987.8
E7	2.5	30.5	30	5	934.5	1185.4
E8	4.5	45.7	15	5	934.5	1637.8
E9	4.5	45.7	20	5	934.5	2155.1
E10	4.5	45.7	25	5	934.5	2693.8

At four moisture contents dry of optimum, an increase in compaction energy increased unconfined compressive strength. Average measurements ranged from 68 kPa at 355 kJ/m^3 to 231 kPa at higher energies (987 to 2693 kJ/m^3). Figure 1 displays these results.

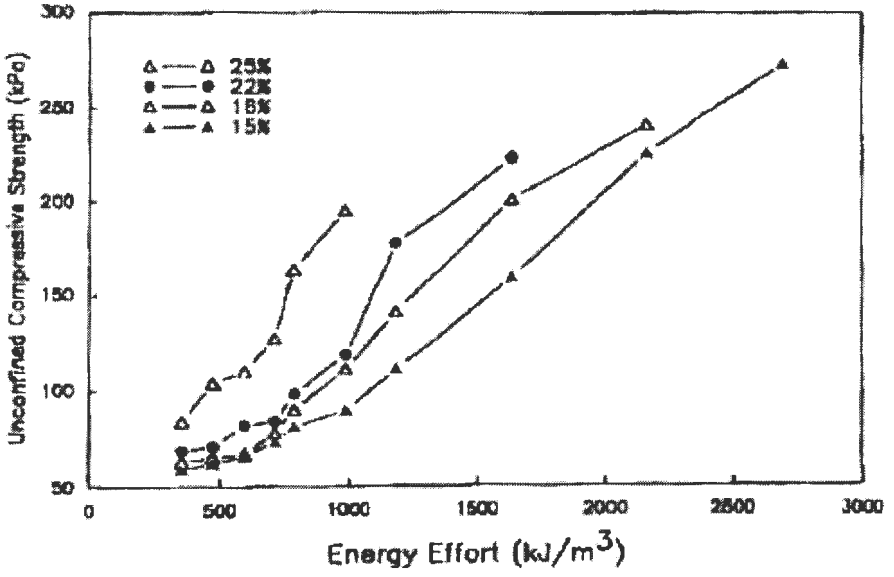

Figure 1. Compactive effort vs unconfined compressive strength for clays dry of optimum (after Attom 1997)

In the same manner, samples at optimum moisture (28.2%) increased in strength with a range of 106 to 288 kPa. The strength increase was explained as flocculated particles packing closer by increased energy, resulting in increased strength. Clay specimens compacted wet of optimum experienced a slight decrease in unconfined strength due to the dispersing of particles with increased energy effort.

Lambe's (1958) well referenced paper on compaction of clay notes the effect of compaction on strength parameters in clay. Comparing two specimens compacted at different energies and the same moisture dry of optimum, it was found that the lower energy specimen will have more random particle orientation than the higher energy specimen. In contrast, the higher energy specimen will have closer particle spacing than the lower energy specimen. It is the reduction in particle spacing that contributes to greater strength. Comparing the same situation with two specimens compacted wet of optimum, the higher energy specimen will still have closer particle spacing, but will be remolded more to a dispersed particle orientation than the lower energy specimen. This more parallel orientation in the higher energy specimen can actually cause lowering of shear strength. However, this is not always the case, i.e. the closer particle spacing can still offset the less random orientation and give the specimen a higher shear strength than the lower energy specimen. Lambe also compares two specimens compacted at the same energy level, with same dry unit weights, but moisture contents on opposite sides of optimum. When sheared after being compacted, the dry specimen yields higher shear strength since it has a more random structure, lower pore water tension, and lower electrical repulsion between particles. If the two specimens are saturated after compaction and then sheared the clay compacted dry of optimum will contain particle

electrical repulsion and pore water tension behavior similar to the clay compacted wet of optimum. However, while the strength of a sample compacted dry of optimum is reduced due to saturation, the orientation of the particles are still more random than particles wet of optimum and therefore still has higher shear strength.

Pagen and Jagannath (1969) used a gyratory device to compact kaolin clays (MH). The clays were compacted with a gyratory at vertical loads of 3336, 4893, 6672, and 9786 N at five moisture contents. Fifteen gyrations were performed in constructing each sample at a fixed angle of gyration of two degrees. Material was compacted in a mold with dimensions of 10.2 cm in internal diameter and 12.7 cm in height. Following each compaction procedure, three specimens (d = 3.3 cm, h = 7.2 cm) were extruded with stainless steel tubes from the larger

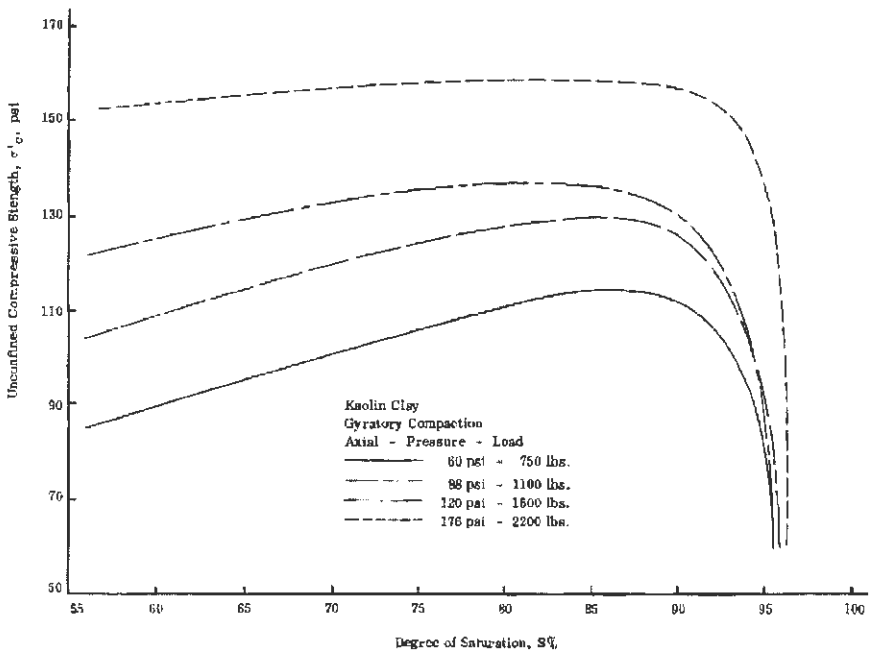

Figure 2. Unconfined compressive strength vs degree of saturation (Pagen and Jagannath 1969)

sample. It was observed that increased compaction energy increased the unconfined compressive strength and initial tangent modulus within a saturation range of 55%-95% (see Figure 2 and Figure 3). At each compaction level, a steady increase in strength and decrease in stiffness was noted, from 55% to 90% saturation. At 55% saturation, specimens ranged in shear strength from 585 to 1050 kPa. Compressive strengths ranged from 790 to 1090 kPa at 90% saturation. Tangent modulus ranged from 47,750 to 66,240 kPa at 55% and 41,950 to 51,335 kPa at 90%. Over 90% saturation both strength and modulus both dropped drastically.

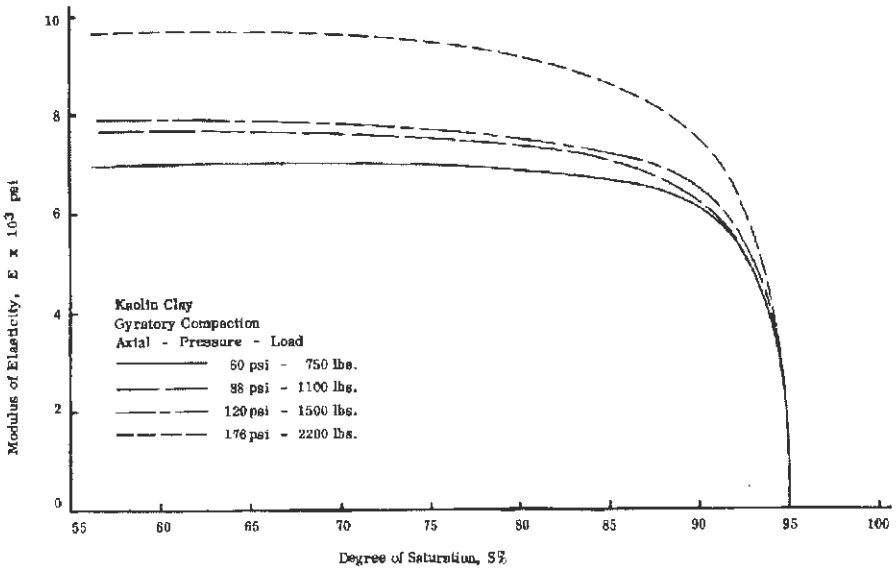

Figure 3. Modulus of elasticity vs degree of saturation for gyratory compaction (Pagen and Jagannath 1969)

Swelling

Increasing energy levels has been demonstrated to increase swell pressure in an expansive clay (CH) at dry and optimum moisture content (Attom 1997). Samples were prepared at impact compaction energies of 355, 592, 987, 1637, and 2693 kJ/m^3 (see Table 1), seated in a

consolidation cell with an initial load of 6.9 kPa, and saturated. The procedure was termed a zero swell test where swell pressure was defined as the amount of pressure that discontinued soil expansion. Figure 4 shows that dry of optimum, average swell pressure ranged from 1.3 kg/cm^2 (355 kJ/m^3) to 3.4 kg/cm^2 (987 to 2693 kJ/m^3). Swell pressure at optimum moisture increased from 1.6 kg/cm^2 (355 kJ/m^3) to 4.5 kg/cm^2 (2693 kJ/m^3). Increased swell pressure with increasing compaction energy was attributed to lower air voids in the soil with increasing energies. Wet of optimum, the compactive effort had little effect on swell pressure because of high initial moisture contents.

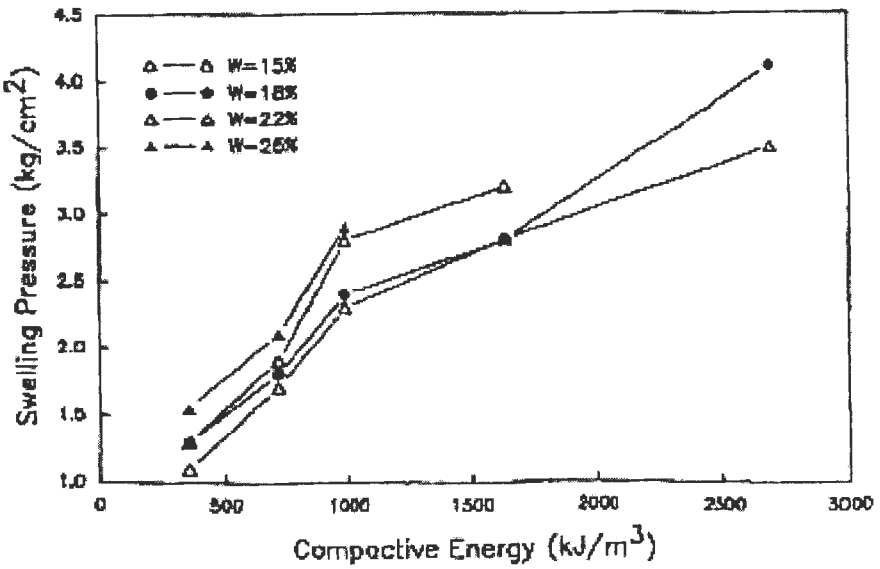

Figure 4. Compactive energy versus swelling pressure for clays dry of optimum (Attom 1997)

Permeability

Expansive clay (CH) specimens were also studied for changes in permeability at compacted impact energies of 355, 987, 1637, and 2693 kJ/m^3 (Attom 1997). Table 1 details how energy was applied. At optimum moisture content, permeability decreased from 5.9 x 10^{-9}

cm/sec to at 355kJ/m^3 to 1.8 x 10^{-11} cm/sec at 2693 kJ/m^3. Dry of optimum, permeability ranged from 9 x 10^{-9} to 5.37 x 10^{-7} cm/sec at 355 kJ/m^3 (see Figure 5). At higher compactive efforts (987 to 2693 kJ/m^3) permeability decreased, ranging from 1 x 10^{-11} to 2.8 x 10^{-9} cm/sec. As compaction energy increases, the voids decreases, reducing permeability. Plotted against moisture content, permeability, at every energy level, decreased from dry to optimum moisture contents and then increased beyond optimum. These conclusions are affirmed by work previously performed by Lambe (1958) on clays.

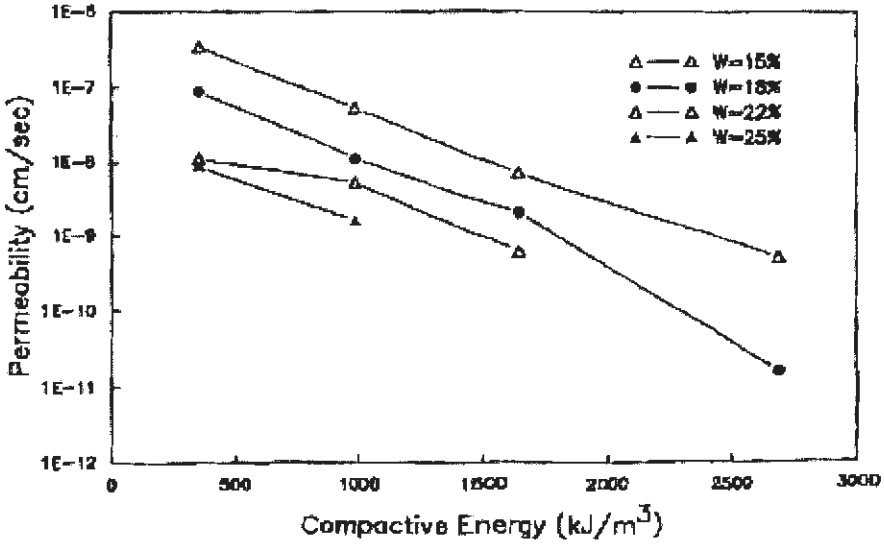

Figure 5. Compactive versus permeability for clays dry of optimum (Attom 1997)

Influence of Compaction Method on Soil Engineering Properties

The manner in which a soil is compacted can influence its final properties. Applying only one method of compaction can lead to a conclusion that underestimates or overestimates a soil's engineering properties. In the literature, the laboratory compaction methods for cohesive soils include impact, static, and kneading methods. (Vibratory compaction is also

used, but mainly for cohesionless soils). The purpose of evaluating various lab techniques is to compare and contrast resulting soil parameters and conclude how the various compaction methods affect soil engineering properties.

The most commonly used method is impact compaction, where a freefalling weight compacts a loose layer of material, densifying the layer by pressing out air voids. This is usually performed with a drop hammer as in the Proctor test. The determination of compaction energy is calculated by dividing the product of the height of the drop hammer, hammer weight, number of drop, and number of layer by the volume of the specimen.

Kneading compaction can be achieved in several ways. One method involves pressing a spring or hydraulically loaded steel rod into a soil, densifying the soil by moving up and around the tip of the rod. Another method involves using a gyratory machine that simultaneously compacts the soil with a static ram load and gyrates the mold holding the soil. The gyration is what simulates the kneading action. Energy determination for kneading compaction is not as straightforward as it is for impact compaction, but can be determined by calculating the area under a force versus displacement curve.

Static, or pressure, compaction is usually accomplished by pressing a loose layer of soil between two metal plates. Here, the soil is simply being displaced to a denser layer at a known axial force. Like kneading compaction, input energy for static compaction can be determined by calculating the area under a force versus displacement curve.

Vibratory compaction is performed with a vibratory table or by tamping the sides of a compaction mold. Cohesionless soils are used in this compaction application. Particles are initially placed into a compaction mold loosely and are vibrated into a denser state due to particle rearrangement during motion of the table. The determination of input energy in vibratory compaction is not as clear as the other compaction methods.

Method Comparison in Laboratory Tests

For sandy silty clays (CL-ML), Bell (1977) compacted specimens with kneading, static, and impact methods at various moisture contents. Static compaction was performed by pressing both ends of a Proctor steel cylinder (d = 11.4 cm, h = 17.8 cm) filled with clay. Kneading compaction was performed by pressing a triangular tamping foot into a Proctor mold filled with soil. The kneaded soil was compacted in three layers with 24 tamps per layer at a foot pressure of 3861 kPa. Energy for static and kneading was determined by calculating the area under a force versus displacement curve. The Proctor procedure was used in applying impact compaction. Energy was calculated using the product of number of layers and hammer blows, hammer weight, and drop height divided by the mold volume. It was observed that the static method was three to ten times more efficient in reaching 100% standard Proctor (18.8 kN/m^3 at 13.8% optimum) than kneading and impact methods at a given moisture content. The greater efficiency was determined by observing that at dry of optimum (10.6%) static compaction required 187 kJ/m^3 of energy to achieve maximum dry unit weight while kneading and impact required 435 and 626 kJ/m^3, respectively. Wet of optimum (15.7%), static compaction needed only 52 kJ/m^3 of energy with kneading and impact requiring 609

and 370 kJ/m^3 of energy. Figure 6 shows the efficiency of each compactive method obtaining maximum dry unit weight in the spectrum of moisture contents.

Undrained shear of each compacted sample was measured in direct shear tests. Direct shear specimens were obtained from the center third of the aforementioned compacted samples, trimming them to 6.4 cm in diameter and 2.5 cm in height. After trimming, a specimen was placed in the direct shear device and seated with a normal load of 47.9 kPa. Specimens were

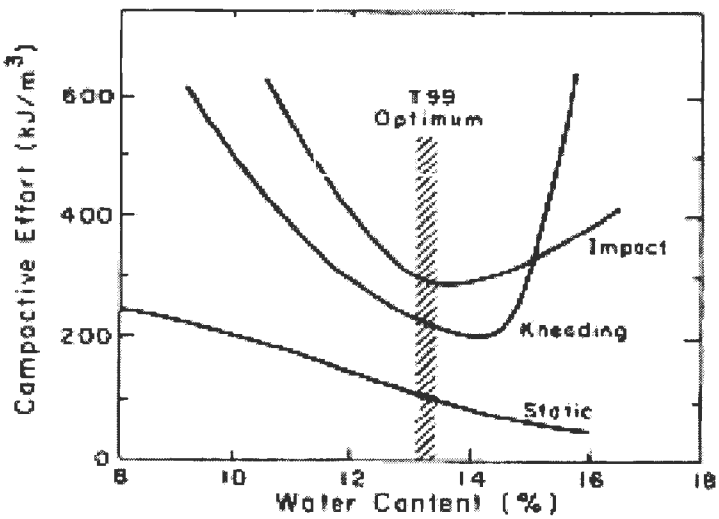

Figure 6. Compactive effort required to obtain maximum standard Proctor dry unit weight for three compaction methods (Bell 1977)

sheared at 0.01 mm/s. Kneading and impact specimens had nearly the same undrained shear strength (ranging from 128 to 240 kPa) at all moisture contents. Kneading was considered more efficient in attaining shear strength than impact at optimum and dry of optimum moisture content, i.e. it required less energy to produce the same strength of impact compaction. Wet of optimum, however, kneading compaction required a higher energy

output, making impact more efficient for strength. Although not yielding higher overall strength values than impact and kneading, it was concluded the static method was most efficient in regard to relative peak strength per unit of compactive effort as seen in Figure 7.

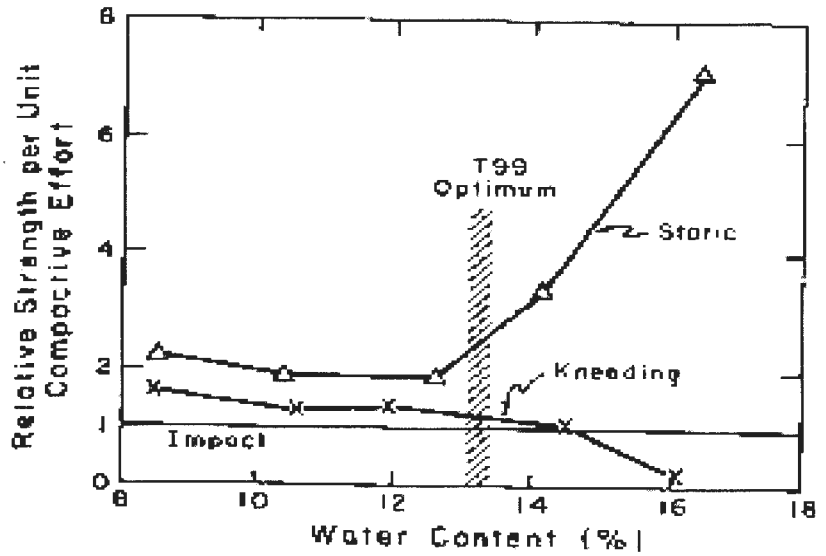

Figure 7. Relative peak strength per unit compactive effort with different compaction methods (Bell 1977)

Attom et al. (2001) studied the influence of different compaction methods on the unconfined compressive strength and swelling of three Jordan soils (CH, MH, and CL). Compaction methods used were impact, kneading, and static. The impact method used was modified Proctor (5 layers at 25 blows per layer). Static compaction was performed by compressing both ends of a standard unconfined compression mold fill with material. Kneading compaction specimens were prepared in a standard Proctor split mold and compacted with a Harvard Miniature Compactor. Impact specimens to be tested in unconfined compressive strength and swelling were extracted from the Proctor mold by pushing a standard unconfined compression mold into the material. All specimens were compacted at a dry unit

weight of 13 kN/m^3 at four moisture contents from 10% to 30%. Quantified compaction energy was not used in this research. Results indicated that at all moisture contents for CH soils, impact compaction resulted in compressive strengths 1.2 and 2.3 times higher than static and kneading respectively. Impact compaction also resulted in compressive strengths 1.2 and 2.3 times higher than static and kneading for MH soils at all moisture contents. The same trend was observed for the low plasticity clay (1.1 to 1.5 times higher strength). Impact compaction yielded swelling pressures1.2 and 1.6 times higher than static and kneading methods for CH soils and MH soils. Impact compaction on CL soils resulted in swelling pressures 1.3 to 2.0 times higher than static and kneading. At in-situ moisture and dry unit weight, undisturbed samples exhibited the highest shear strength and swelling at 1.35 and 1.5 times higher than the closest method (impact). As moisture content increased shear strength and swell pressure decreased for all three methods.

Pagan and Jagannath (1969) demonstrated on kaolin clays (MH) that compaction with a gyratory device produced higher unconfined compressive strength and tangent modulus than an impact method and alternative kneading procedure. Methodologies for the impact and alternative kneading procedures were not given in the report. The gyratory device procedure is mentioned earilier in this paper. These comparisons were made at the same dry unit weight values of kaolin clay (MH). Gyratory averaged 1.8 times higher modulus than impact and 1.4 times higher modulus than the alternative kneading method. Shear strength, for gyratory, was 1.3 and 2.1 times higher than kneading and impact respectively.

Table 2 is a summary of the research involving the comparison of different compaction methods. Comparing the results of strength, different conclusions are drawn between all three authors. This could be due to differences in soil type, application of energy, and type of strength test method. Soil types are not drastically different, all cohesive materials. The way in which methods were performed were different, specifically comparing the kneading proceudures. Attom et al. (2001) and Pagen and Jagannath (1969)used unconfined compressive strength while Bell (1977) used undrained strength from direct shear.

Table 2. Summary of conclusions from research using different compaction methods

Author	Soil	Compaction Methods Used	Dry Unit Weight (high to low)	Strength (high to low)	Swelling Pressure (high to low)	Modulus (high to low)
Bell (1977)	CL-ML	Kneading Static Impact	Static Kneading Impact	Static Kneading Impact	n/a	n/a
Attom et al. (2001)	CH,MH,CL	Kneading Static Impact	not compared	Impact Static Kneading	Impact Static Kneading	n/a
Pagen and Jagannath (1969)	MH	Gyratory Impact Kneading	not compared	Gyratory Kneading Impact	n/a	Gyratory Kneading Impact

Comparison of Laboratory Method and Field Results

Often, the practice of a lab compaction method can lead to conclusions that overestimate or underestimate a soil's performance in the field. This occurs when the lab technique does not accurately represent how a soil is compacted by a roller. Thus, a primary focus in the literature involved the discernment of lab techniques which best simulated how a material is compacted in the field.

Ping et al. (2002) compared field results of sandy soils (SW) to results from gyratory, impact, and vibratory tests. A padfoot and smooth drum vibratory roller were used on two test strips in the field. Gyratory compaction was performed by a Servopac Gyratory Compactor. Standard and modified Proctor tests were performed for impact compaction. The vibratory tests was performed in accordance with ASTM D 4253. It was noted that the gyratory test replicated the dry unit weight measured in the field, followed by modified proctor and vibratory. For both strips, dry unit weight for rollers was achieved 0.5-1.0 kN/m^3 greater than 100% modified Proctor (16.3 and 17.4 kN/m^3). Impact compaction was concluded as an inefficient lab test in determining in-situ conditions for sandy soils.

Kneading compaction was performed on silty clays (CL-ML) by McRae and Rutledge (1952) and compared to impact, static, and field results by a sheepsfoot roller. The kneading apparatus was operated by use of an air compressor and could perform both kneading and impact compaction. A 6 inch CBR mold was used in the apparatus. The mold was rotated after each penetration by a small air cylinder. The device's impact compaction setup included a 20-lb. weight dropping 9 inches, producing a similar energy blow to the modified Proctor test. Kneading samples were compacted in five layers with 40 strokes on each layer, using foot pressures of 700, 1400, and 2100 kPa. Impact compaction was performed on the same device using 660, 1240, and 1900 kJ/m^3 of compaction energy. The latter of the three energies created a maximum dry unit weight similar to the 300 psi kneading compaction. It was not noted how static compaction was achieved. However, figures indicated specimens were compacted by the static method at pressure of 500 and 1000 psi. Optimum lines of

kneading compaction, derived from moisture-dry unit weight curves, were observed to be closer to field optimum lines an zero-air voids curve, proceeded by impact and static tests.

In the development of a new kneading compaction device, Kousassi et al. (2000) conducted analyses on low plasticity clays (CL). The device used a California Bearing Ratio (CBR) mold to compact the material. Compaction was performed hy a steel disk (15 cm in diameter) that has three tamping feet attached to it. Each tamping foot was 5 cm in diameter and 2.5 cm in height. The feet were rotated at 45 degrees between successive loadings. After a trial and error proceedure, the device was standardized at five layers of compaction with 1.25 MPa of foot pressure. At this combination of soil layers and foot pressure, the dry unit weight compared best to in situ soil properties. Thus, compaction energy comparison was not sought after to standardize the proceedure of the kneading tool. The kneading samples were extruded from the CBR and compared with impact, static, and field specimens. Impact specimens were compacted using standard Proctor procedure. A uniaxial compactor was used to construct static specimens. All field samples were constructed with tamping rollers. Compared to standard Proctor, kneading had values of dry unit weight that were closer to samples from field. Kneading points wet of optimum were closer to the zero air curve as well. In general, the kneading method acquired higher dry unit weight measurements. The kneading method was also a better estimate of field samples when tested for limit state parameters (c, ϕ) and initial tangent modulus. Specimens constructed with the two methods, as well as static, were subjected to CU and UU compression at confining pressures of 50, 100, 200, and 400 kPa. The average CU tangent modulus of one clay was 70 MPa for static, 41 MPa for kneading, and 28 MPa for the tamping roller. Differences in CU

limit state parameters were minimal. Other clays tested in UU had average values of tangent modulus that were 1.5 to 3 times higher in static (15 to 33 MPa) than field specimens. The static method also yielded UU cohesion values twice that of field samples. For the two lab methods, an increase in moisture content decreased tangent modulus and limit state parameters.

Variation in Load Application

Bell (1977) investigated the significance of applying impact compaction differently on sandy silty clays (CL-ML) while maintaining a constant energy value (592 kJ/m^3). A total of nine application combinations were used to compact the material at optimum moisture (~ 13.8%). Table 3 displays all combinations used. The values of dry unit weight were compared to each other and to other Proctor tests conducted at compactive efforts from 284 to 2693 kJ/m^3. Differing application of energy resulted in similar dry unit weights, varying by 0.5 kN/m^3.

Table 3. Impact compaction variables and results (Bell, 1977)

Blows Per Layer	Height of Drop (mm)	Rammer Force (N)	Moisture Content (%)	Dry Unit Weight (kN/m^3)	Peak Strength (kN/m^2)
55	610	5.6	13.7	18.2	173
55	305	11.1	13.6	18.3	212
55	152	22.2	13.6	18.3	218
25	610	12.2	13.6	18.6	239
25	305	24.5	13.4	18.7	205
25	152	49.0	13.5	18.6	205
12	610	25.5	13.9	18.5	217
12	305	51.0	13.4	18.7	165
12	152	102.0	13.2	18.8	174

However, when plotted on a semi logarithmic graph with the other compactive efforts the range becomes significant (see Figure 8). Bell explains:

> The least efficient combination gives a dry unit weight that could have been obtained with only about 402 kJ/m^3 by the basic method, and the most efficient combination corresponds to a unit weight that would have required about 790 kJ/m^3 by the basic method...on this basis, the most efficient combination (133% efficiency) is approximately twice as efficient as the least efficient procedure (68% efficiency).

Further, the least and most efficient compaction methods yielded the same result of undrained shear strength (173 kPa) measured from a direct shear device. Highest undrained shear strength (239 kPa) was obtained at an intermediate energy effort of 1185 kJ/m^3. It was postulated that the high-energy rammer allowed for remolding of the soil, reducing its overall strength.

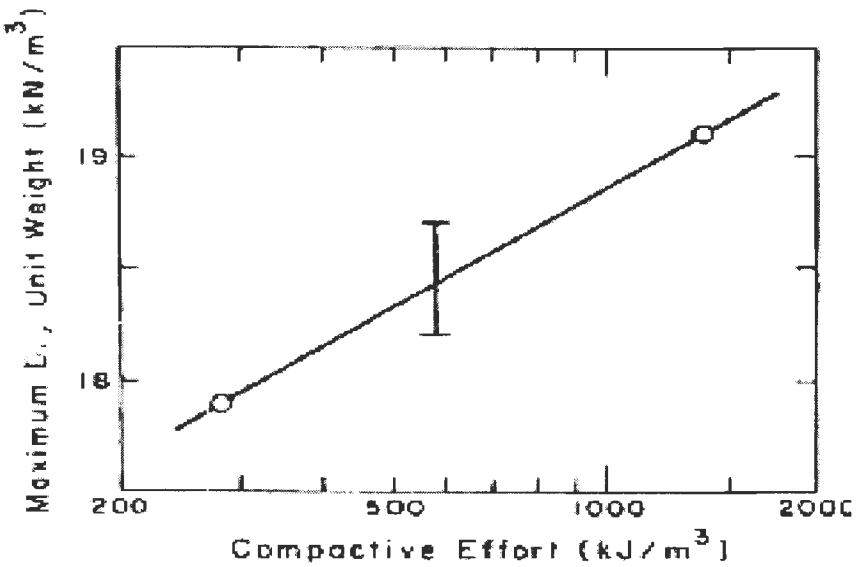

Figure 8. Maximum dry unit weight versus compactive effort for impact compaction with range of dry unit weights at 592 kJ/m^3 energy level (Bell 1977)

Ping et al. (2002) compacted sandy soils (SW) at various combinations of gyration angle (1.00 and 1.25 degrees), vertical pressure (100, 200. 300, 400, and 500 kPa), and number of gyrations (30, 60, and 90) on a Servopac Gyratory Compactor. It was shown that as the number of gyrations increases, the dry unit weight increases. Gyration angle also affected the dry unit weight. However, as the number of cycles increased the significance of the angle diminished. Vertical pressure was not a factor of influence on dry unit weight after reaching a load higher than 200 kPa. Pressure above or below 200 kPa did not increase the dry unit weight. Further, this stress level was equivalent to the average peak vertical stress under a roller measured in the field by load cells.

Empirical Relationships of Soil Compaction

Building off of Proctor's work, research has been performed to investigate the interrelation of soil gradation, plastic properties, optimum moisture content, and maximum dry unit weight (Woods and Litehiser 1938; Turnbull 1948; Jumikis 1958; Ramiah et al. 1970). The studies were on soils within limited regions, with one involving over 1300 soil types (Woods and Litehiser 1938). The general understanding of soil relationships has enabled derivation of empirical models with soil index properties, moisture content, and compaction energy.

Index Properties

Rowan and Graham (1948) presented equations to estimate optimum moisture content and maximum dry unit weight. The compaction parameters of 10 soils were estimated using specific gravity, shrinkage limit, shrinkage ratio and percent passing the No. 4 and No. 40

sieves. Davidson and Gardiner (1949) modified these equations after an analysis on 210 soils from 11 states with the following:

$$\gamma_d \text{ (pcf)} = 6250\ K_1/(SL(B/A) - 1) + 100/R) \qquad [1\text{-}1]$$

$$m_{opt} = SL\ (B/A) + K_2 \qquad [1\text{-}2]$$

where, SL is the shrinkage limit, R is the shrinkage ratio, A and B are the percentages of particles passing the No. 4 and No. 40 sieves, $K_1 = (312 - 2\ (PI))/300$, $K_2 = (PI/3) - 4$, and PI is the plasticity index.

Due to the larger range of soil types, a wider deviation, compared to Rowan and Graham (1948), was observed between parameter estimations and actual results, particularly with highly plastic soils. Plasticity index is included because of the observation.

An attempt to correlate optimum moisture content and maximum dry unit weight with plastic properties was made on 972 soils from 31 states by Yemington (1958). Figure 9 is the chart resulting from that work. The chart presents correlations of the two compaction parameters with plastic and liquid limit. It was used to estimate the amount of water needed for the first moisture-dry unit weight point in the lab. In addition, it was used as a check of optimum moisture contents observed in the field by technicians.

The chart in Figure 9 was evaluated with an additional set of 510 soil types sampled throughout the United States (Yemington 1958). Approximately 81% of the predicted optimum moisture contents were within 2% of the optimum moisture contents from the lab.

Further, 63% of maximum dry unit weight estimates were within 4 lb/ft^3 of the actual lab results. Evaluation of the chart with Alaskan and tropical soils resulted in poor correlations.

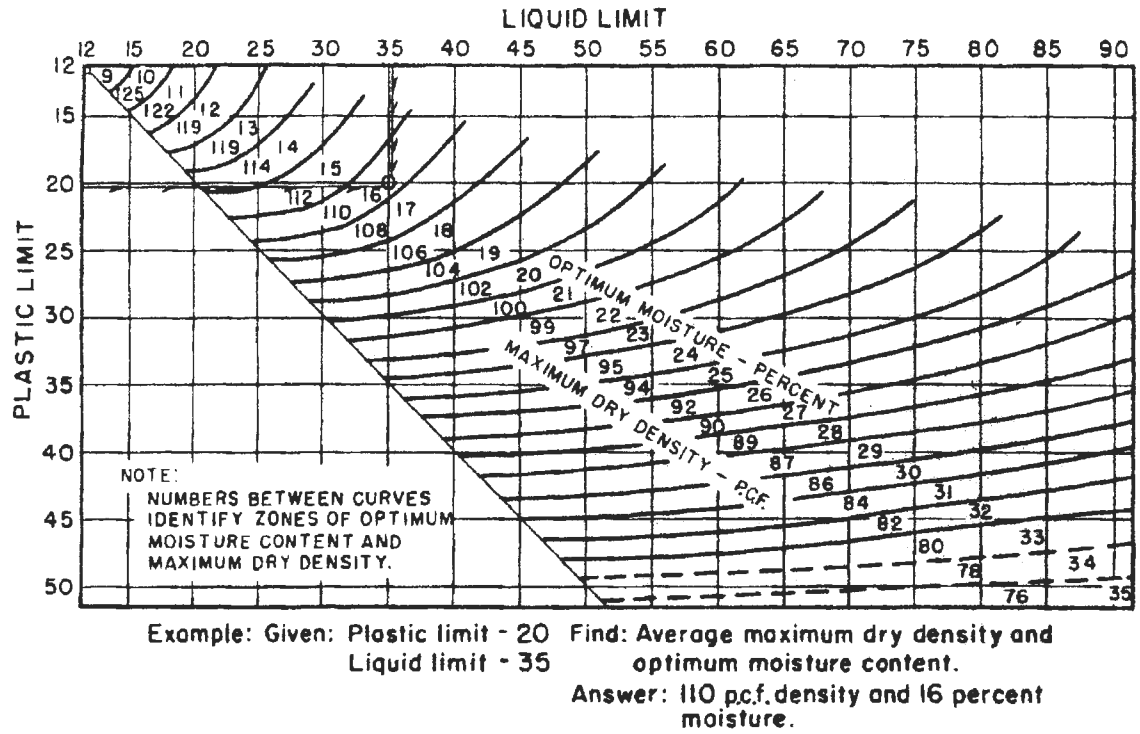

Figure 9. Relation of average maximum dry unit weight and optimum moisture content to plastic limit and liquid limit (after Yemington 1958)

Ring et al. (1961) performed additional research based on work by Yemington. A multiple linear regression analysis was conducted to estimate the optimum moisture content and maximum dry unit weight of 527 soils from 20 states. Independent variables included plastic and liquid limits, plasticity index, clay fraction, fineness average, and average particle size.

Several estimation models were developed from the analyses with the following highlighted in this report:

$$\text{Log } m_{opt} = 0.158 \log LL + 0.045 \log PL + 0.224 \log (PI + 15) + 0.033 \log (D'_{50}/100) + 0.229 \log (FA + 100) + 0.098 \log (CF + 40) - 3.401 \quad [1\text{-}3]$$

$$\text{Log } m_{opt} = 0.784 \log PL + 1.378 \log (FA + 100) - 6.586 \quad [1\text{-}4]$$

$$\gamma_{d\,max} \text{ (pcf)} = 147.525 - 0.020\, LL - 1.195\, PL - 0.198\, FA \quad [1\text{-}5]$$

$$\text{Log } \gamma_{d\,max} \text{ (pcf)} = 7.247 - 0.567 \log (PL + 20) - 0.110 \log FA \quad [1\text{-}6]$$

where, LL is liquid limit, PL is plastic limit, PI is plasticity index, D'_{50} is the average particle size, FA is the fineness average, and CF is the clay fraction. Fineness average is the average of the summation of percentage of particles finer than sieve No. 10, 40, 200, particle sizes 0.020, 0.005, and 0.001 mm.

The standard error of the estimate was calculated as 1.98% and 2.17% for equations 1-3 and 1-4. Standard error for equations 1-5 and 1-6 were 4.44 lb/ft^3 and 4.32 lb/ft^3 respectively. The standard errors from the models were 10.7% and 4.2% of the average parameter values. To demonstrate accuracy, 10 soils were selected to estimate the soil parameters with these new models and compared against all previous models mentioned in this report. The authors concluded the new models as slightly better predictors for both parameters.

Logarithm of Compaction Energy

Dry unit weight of soil has been empirically related to the logarithm of compaction energy (Boltz et al. 1998) in a linear equation:

$$\gamma_{d\,max} = \beta \log E + \delta \qquad [1\text{-}7]$$

where, β and δ are exponents that vary as a function of soil type and moisture content. Equation 1-7 was derived from a database of 22 clayey soil types and indicates that an increase in compaction energy will result in an incremental increase in relative compaction. Further investigation of β and δ led to correlations with liquid limit:

$$\beta = 2.27 \log LL - 0.94 \qquad [1\text{-}8]$$

and

$$\delta = 17.02 - 0.16\,LL \qquad [1\text{-}9]$$

If the liquid limit and single compaction curve ($\gamma_{d\,max,\,k}$, E_k) is known of a soil a maximum dry unit weight from compaction effort, E, can be estimated by combining equations 1-7 and 1-8:

$$\gamma_{d\,max,\,E} = \gamma_{d\,max,\,k} + (2.27\,LL - 0.94) \log (E/E_k) \qquad [1\text{-}10]$$

If only the liquid limit is known then maximum dry unit weight can be estimated by combining equations 1-7 and 1-9:

$$\gamma_{d\,max,\,E} = (2.27\,LL - 0.94)\log E - 0.16\,LL + 17.02 \qquad [1\text{-}11]$$

Soil Compaction Modeling

Fernandez and Corcoran (1999) created a soil compaction model to estimate all dry unit weight values of a soil. The research was in response to the majority of compaction earthwork specifications solely relying on dry unit weight from the standard Proctor test. Referring to the task of matching compaction requirements to specifications, the authors state:

> As engineers we face the first the challenge of defining the true functional requirements. Next, we face the challenge of setting specifications that will insure requirements are met. Third, we must select machines and processes that can meet the specifications and achieve the requirements efficiently. And finally, we must provide monitors and measures to qualify that specifications that specifications and requirements have been met and fulfilled.

The authors further state that simply by using relative compaction (i.e. from standard Proctor optimum values) as the requirements for specifications more often than not do not coincide with the optimal conditions needed for a soil to be compacted most efficiently. Therefore, the intention was to create a compaction model that assessed compaction efficiency using

understood relationships between soil dry unit weight, moisture content, and compaction energy. Equations used in the modeling included the following:

$$\rho = \rho_{min} + [(\rho_{max} - \rho_{min})\,(1 - 10^{-KE})] \qquad [1\text{-}12]$$

where, ρ is dry unit weight, ρ_{min} and ρ_{max} are the minimum and maximum dry unit weight corresponding to zero and infinite energy respectively, E is the compactive effort, K is the compactability term in m^3/kN-m.

Equation 1-12 represents the dry unit weight "growth curve", characterized by dry unit weight increasing with increasing compaction energy until reaching an asymptotic state. It is the K term, or compactability factor, that distinguishes the rate at which dry unit weight increases with increasing energy. K is described as the inverse of compaction energy required to attain 90% of range of dry unit weight between ρ_{max} and ρ_{min}. The higher the K-term the higher the compaction efficiency combination of moisture and energy, i.e. the rate of densification is higher and the required relative compaction is achieved sooner.

Two other equations derived for the purpose of modeling sensitivity were:

$$\rho = C/[(Steep*w^2 - 2\ Steep*w_{opt}*w + Steep*w_{opt}^2 + (C/\rho_{dmax})] \qquad [1\text{-}13]$$

$$w_{opt} = w_{optmin} + (w_{optmax} - w_{optmin})\ 10^{-KE} \qquad [1\text{-}14]$$

where, ρ_{dmax} is the maximum dry unit weight, C is a unit conversion constant = 801.3 Mg/m^3, Steep is a shape factor term reflecting the steepness of the compaction curve, w is the

moisture content, w_{opt} is the optimum moisture content, and w_{optmin} and w_{optmax} are the optimum moisture contents corresponding to infinite and zero energy, respectively.

Equation 1-13 models sensitivity of dry unit weight to moisture content. An increase in the steep value corresponds to the increase in sensitivity to moisture content in dry unit weight. Equation 1-14 applies the same concepts mentioned for Equation 1-12 for dry unit weight, except here it is for optimum moisture content.

For a complete model of compaction equations 1-12 to 1-14 were used with soil phase relationship equations:

$$\rho = (G_s \rho_w)/[1 + (G_s * w/S)] \qquad [1\text{-}15]$$

$$\rho_{dmax} = (G_s \rho_w)/[1 + (G_s * w_{opt}/S_{opt})] \qquad [1\text{-}16]$$

where, G_s is specific gravity of the soil, ρ_w is the unit weight of water, S is degree of saturation, and S_{opt} is the degree of saturations at optimum moisture content.

Compaction efficiency for a soil can be assessed by using Equations 1-12 – 1-16 and laboratory data. Input parameters entered include G_s, S_m, Steep, S_{opt}, K, w_{optmax}, and w_{optmin}. The article did not explain the exact procedure to attain input parameters other than noting that numerical iterations are used to complement lab data. The standard Proctor curves were produced for the iterations. K values from dry unit weight growth curves at different moisture contents can be compared for a single soil to assess efficiency. Also, a group of

soils can be used in the model to compare and contrast compaction efficiency and sensitivity to moisture content.

CHAPTER 2. LAB METHODOLOGY

The objective of the lab research was to determine relationships of soil properties as a function of compaction energy and moisture content. The lab research methodology involved the following tasks:

Task 1: Select four to five different soils from the region to perform laboratory tests.

Task 2: Devise a test plan for lab soils that involved measuring dry unit weight, undrained shear strength, secant modulus, cohesion, and friction angle.

Task 3: Collect data in the lab with conventional test equipment following standardized test procedures.

Task 4: Carry out statistical study to derive possible correlations between soil parameters and compaction energy/moisture content.

Laboratory Testing

Laboratory testing was performed in the soil labs of Iowa State University in Ames, Iowa. Grain size distributions, Atterberg Limits, and specific gravities were determined to properly classify the soils. Also, laboratory compaction, unconfined compression, and triaxial tests were conducted. All soils were air dried prior to testing. This research was performed to investigate relationships between dry unit weight, strength, stiffness, compaction energy and moisture content as well as other index properties.

The following laboratory tests were performed in general accordance with ASTM standards:

- Particle Size Analysis (ASTM D-422)
- Atterberg Limits Tests (ASTM D-4318)
- Soil Classification (ASTM D-2487)
- Specific Gravity (ASTM D-854)
- Proctor Compaction Tests (ASTM D-698 and ASTM D-1557)
- Unconfined Compression Tests (ASTM D-2166)
- Consolidated-Undrained Triaxial Tests (ASTM D-2850, D-4767)

It shall be noted that some of the soil specific gravities were determined using a helium pyncometer. The following sections detail test procedures used in the laboratory.

Proctor Compaction Tests

All lab soils were compacted at five energy levels (355, 592, 987, 1643 and 2693 kJ/m^3) for Proctor tests. The energy levels of 355 and 987 kJ/m^3 were attained by compacting the soil in three layers with a 2.5-kg. hammer at 15 and 42 blows per layer respectively. Both of these energy levels required a hammer height drop of 30 cm. The energy level of 1643 kJ/m^3 was attained by compacting the soil in five layers with a 4.5-kg. hammer at 15 blows per layer. This energy level required a hammer height drop of 46 cm. Method A (10.2 cm diameter mold) was used for all soils except the PPG till. Method C (15.2 diameter mold) was used for the PPG till.

Unconfined Compression Tests

The same five compaction energies were applied to specimens tested for undrained strength and stiffness (secant modulus) in an unconfined test apparatus. A 6.85-kg. hammer was used to compact soil in a cylindrical mold (7.1 cm diameter x 16.5). Energies, in ascending order, were attained by compacting the specimens at 7, 11, 18, 35, 50 total blows. The specimens were compacted on both sides. The hammer height drop for all energy levels was 46 cm. Specimens were compressed at a strain rate of 1.27 mm/min. Heights of the 94 specimens ranged from 13.8 to 15.4 cm. with a mean height of 14.3 cm. and a standard deviation of 0.4 cm. Unconfined compression tests were not performed on West Des Moines field soils.

Consolidated-Undrained Triaxial Tests

Consolidated-Undrained (CU) tests were performed on the Western Iowa loess. Two different machines were used: Wykeham Farrance (WF) and the ELE DS7 (ELE). Heights of the 54 specimens tested ranged from 13.7 to 15.4 cm. with a mean height of 14.4 cm. and a standard deviation of 0.3 cm. All specimens were back saturated, consolidated, and compressed without drainage. The procedures for sample preparation and back saturation differed between the two machines used. The testing procedures, including these differences, are discussed in the following sections.

Wykeham Farrance

Specimens were compacted in a standard cylindrical mold at compaction energies of 355, 592, 987, 1463, and 2693 kJ/m^3 with moisture contents ranging from 13% to 26%. At energy levels 355, 592, and 2693 kJ/m^3 specimens were compacted at approximately 13%, 19%,

21%, and 26% moisture content. At intermediate energies (987, and 1463 kJ/m^3) specimens were only compacted at moisture contents of 13% and 26%. In all, the entire envelope of the Proctor curves was covered using this test plan, i.e. within the compaction energy boundaries of modified Proctor and half of standard Proctor.

Three specimens were made for each compaction energy/moisture content combination and were consolidated at 35, 70, and 105 kPa respectively. Reconstituted specimens in this procedure were not cured in a humidity room prior to testing, but immediately placed in the test chamber.

After the test chamber was filled with water, specimens were back saturated with a confining pressure of 262 kPa and a pore pressure of 247 kPa. Highly saturated specimens, soft in structure, were back saturated at lower initial pressure increments, starting at 105 kPa confining pressure, to prevent consolidation. After approximately twenty minutes of this initial pressure, the pressure was incremented 35 kPa, saturated for another twenty minutes, and checked for saturation. Specimens that were not saturated to begin with were allowed to saturate for approximately two hours. A back pressure saturation check proceeded the two hours of saturation. The check was conducted by closing the saturation line valve, decreasing the confining pressure to zero and then increasing the confining pressure incrementally. Pore pressure values were noted and divided by confining pressure values (pp/σ_3) to calculate the B-value achieved in the specimen. For example, if the pore pressure value reading was 106 kPa at a confining pressure of 140 kPa the B-value was calculated as

106 kPa ÷ 140 kPa = 0.75. When a B-value of 0.95 had been achieved in the specimen (i.e. $pp/\sigma_3 = 0.95$) the specimen was allowed to consolidate.

During consolidation, volume change of the specimen was measured form the test chamber. Consolidation was complete when the volume change value stabilized. This process usually took about two to three hours. Specimens were then compressed at a strain rate of 1.27 mm/min. Pore pressure was measured during shearing of the specimen.

ELE DS7

Specimens were compacted in a standard cylindrical mold at compaction energies of 592 and 2693 kJ/m^3. Moisture contents of the specimens were around optimum. Three specimens were made for each compaction energy/moisture content combination and were consolidated at 35, 70, and 105 kPa. Constructed specimens in this procedure were cured for 24 hours in a humidity room prior to testing.

Upon filling the test chamber with water, a B-value was calculated by applying an initial confining pressure of 35 kPa and observing the change in pore pressure. Hence, a B-value was calculated in a similar way as the WF procedure ($\Delta pp/\Delta\sigma 3$). After establishing the value, a back pressure was applied to a specimen at a differential of 12.5 to 15 kPa of the confining pressure. The back pressure saturation was applied for 12 – 24 hours and another B-value was determined by increasing the confining pressure 35 kPa. This process continued until a B-value of 0.95 was observed. This was then was followed by consolidation.

In contrast to the WF apparatus, volume change during consolidation was measured through the specimen rather than through the chamber. Consolidation was allowed to continue until volume change in the specimen stabilized. Strain rate during compression was 1.27 mm/min.

Statistical Analysis

Statistical analysis was performed with the computer program SSPS. Laboratory and field values were analyzed with multiple regression analysis. Each regression model derived from an analysis was checked for its adjusted r^2 value, standard error of the estimate, F-statistic, and t-statistic.

Standard error was observed and compared with the standard deviation of the dependent variable. If the standard error was greater than the standard deviation, the regression model was no better a predictor than the mean of the dependent variable.

The F statistic was used to test the null hypothesis that the slopes of the multiple regression ($\beta_1, \beta_2, \beta_3 \ldots . \beta_p$) were zero. The F-statistic derived for any given regression analysis was compared to F-statistic values from an F distribution curve table and either accepted or rejected. If the null hypothesis was accepted or true (i.e. $\beta_p = 0$), this implied no independent variables would help explain the variation in the dependent variable. If the null hypothesis was rejected, at least one independent variable could help explain the variation in the dependent variable. The value of F in the distribution curve table was dependent on the degrees of freedom used in a given regression.

The t-statistic of the coefficients from a regression model was used to determine which independent variable was the strongest predictor. If the t-statistic of an independent variable fell between -2 and +2 ($\alpha = 0.05$), it could not be used as a predictor.

CHAPTER 3. LABORATORY RESULTS AND DISCUSSION

This chapter presents the index properties and parameters for all soils used in the laboratory phase of this project. Results from the statistical analysis on compaction, unconfined compression, and CU triaxial tests are also presented.

Soil Index Properties

Properties and classifications of the soils are presented in Table 4. Soil used in the lab are identified as glacial till (CL), weathered shale (CL), and loess (ML). The loess soil was collected from Western Iowa while the till and shale were collected from Central Iowa. The soils from field tests included lean clays (CL) from West Des Moines Iowa and glacial till (CL) from Peoria, Illinois. Liquid limits ranged from 19 to 49%. Plasticity indexes ranged from 6% to 19%. Gradation curves are provided in Appendix A. All applicable precision and bias information observed in ASTM standards for the properties in Table 4 are noted.

Proctor Compaction Tests

Figure 10 - Figure 16 present the results from Proctor compaction tests for all soils. The zero air voids curves (100% saturation) are indicated as solid lines with saturation lines from 50 to 90% as dashed lines. All soils responded in the similar ways as compaction energy was applied. Maximum dry unit weight increased and optimum moisture content decreased as compaction energy increased. Compaction curves were defined differently. For example, the loess' compaction curves were not as well defined as the tills. All Proctor compaction data is presented in tabular format in Appendix A.

Table 4. Properties of Midwest soils tested

Location	Glacial Till C. Iowa	Weathered Shale C. Iowa	Loess W. Iowa	Glacial Till W. Illinois (PPG)	Glacial Till W. Illinois (Edwards)	Clay C. Iowa (728)	Clay C. Iowa (GS)
Properties							
USCS	Sandy Lean Clay (CL)	Lean Clay (CL)	Silt (ML)	Sandy Lean Clay (CL)	Sandy Lean Clay (CL)	Lean Clay (CL)	Lean Clay (CL)
Liquid Limit[1]	24	35	29	19	29	42	49
Plastic Limit[2]	15	24	23	11	16	32	30
Plasticity Index	9	11	6	8	13	10	19
Specific Gravity	2.66	2.77	2.72	2.72	2.70	2.70	2.77
$W_{opt}(\%)_3$*	13.1	18.0	18.0	8.0	12.0	20.0	26.0
γ_{max} $(kN/m^3)_4$*	18.3	16.6	15.5	21.0	18.8	16.2	15.8
Gravel Fraction	1.4	0.0	0.0	14	4.2	0.4	0.0
Sand Fraction	46.3	9.1	2.9	42.5	26.9	1.2	2.8
Silt Fraction	37.7	51.7	90.6	34.6	43.8	69.1	63.8
Clay Fraction	14.6	39.2	6.5	8.9	25.1	29.3	33.4

1 - Standard deviation between 0.98 – 1.07 (2 soils tested by different operators in same lab)
2 - Standard deviation between 1.07 – 1.21 (2 soils tested by different operators in same lab)
3 - Standard deviation $\pm$ 0.86 (Multilaboratory precision)
4 - Standard deviation $\pm$ 0.26 (Multilaboratory precision)
* - Standard Proctor (592 kJ/m^3)

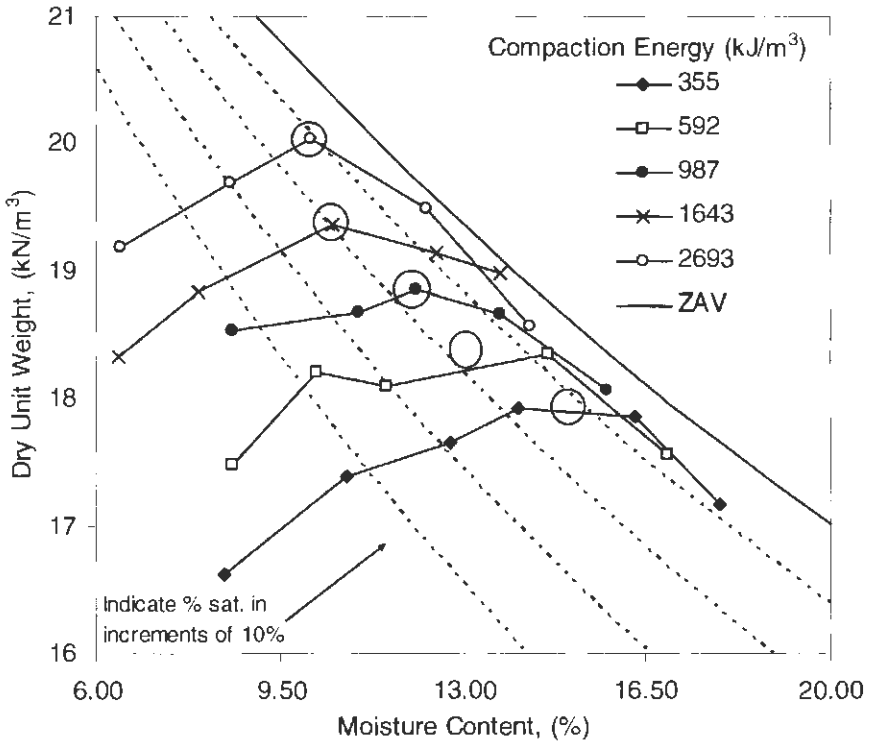

Figure 10. Laboratory compaction test results on Central Iowa till for various compaction energies

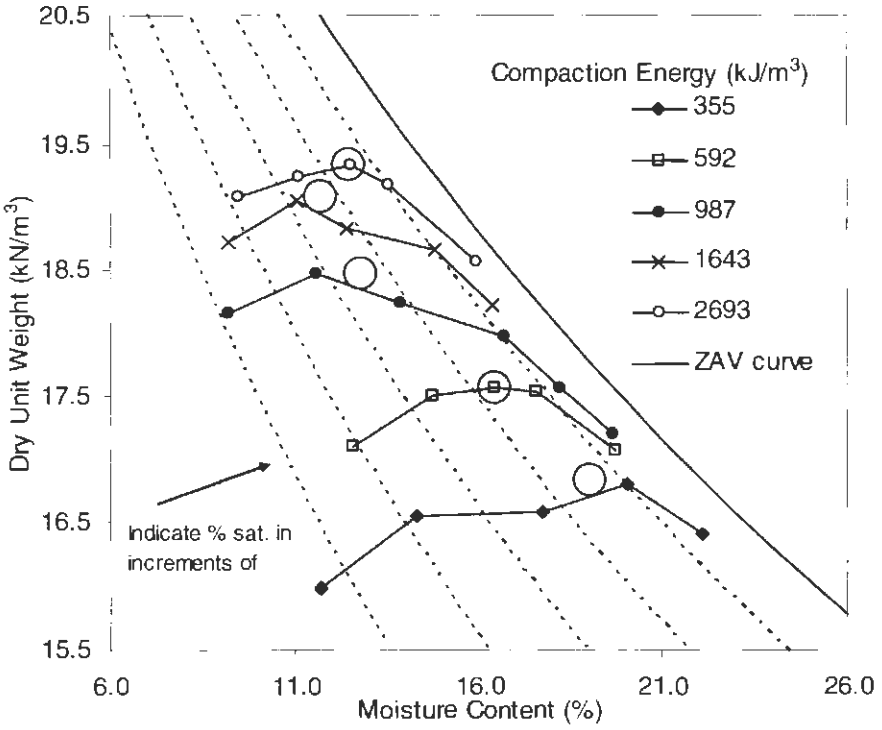

Figure 11. Laboratory compaction test results on weathered shale for various compaction energies

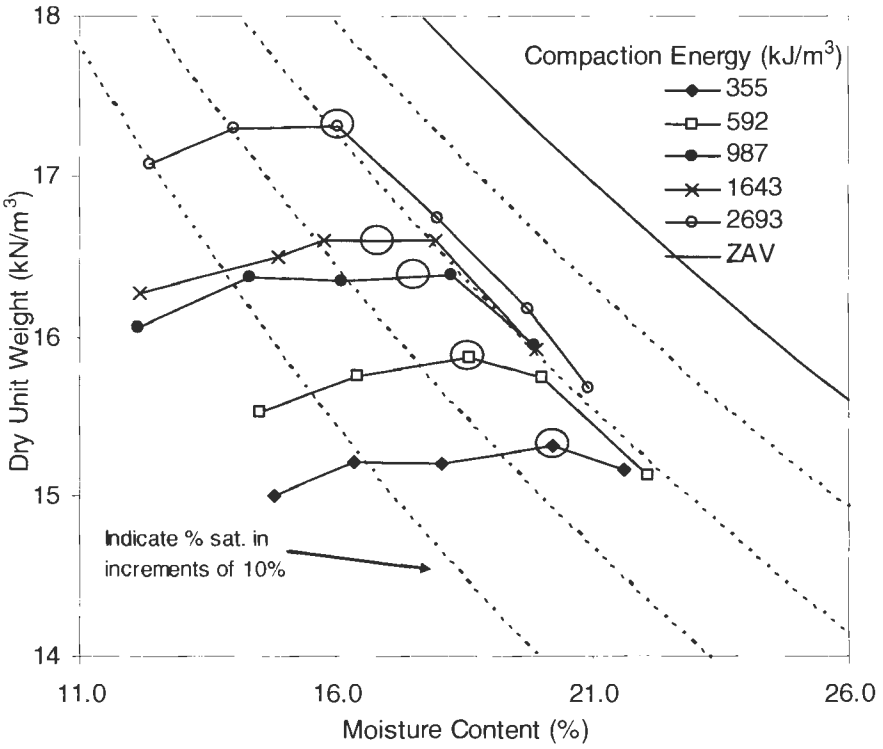

Figure 12. Laboratory compaction test results on Western Iowa loess for various compaction energies

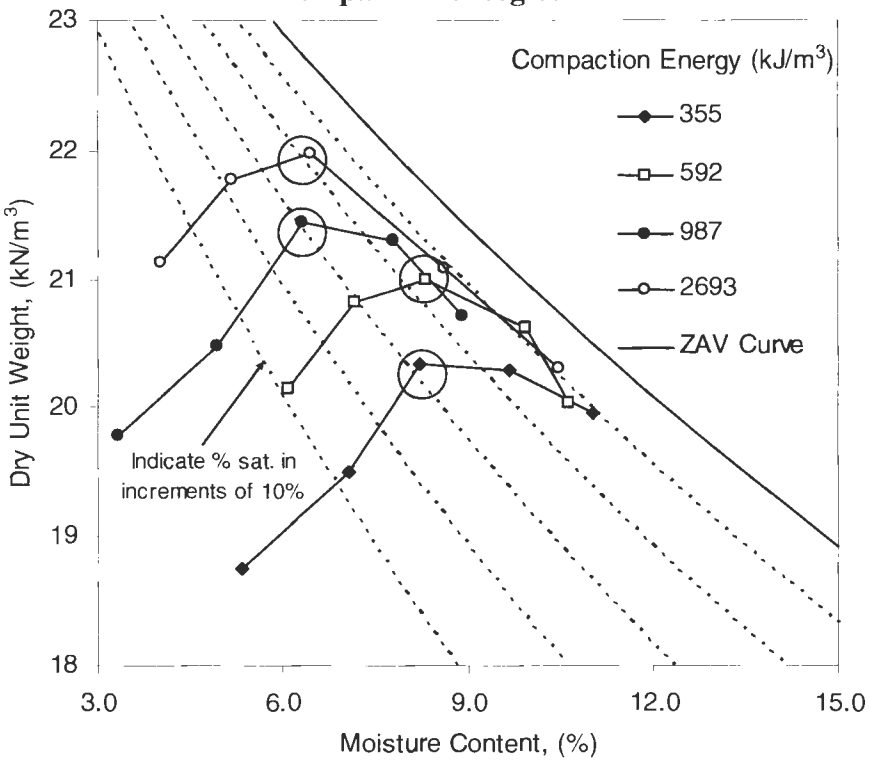

Figure 13. Laboratory compaction test results on PPG till for various compaction energies

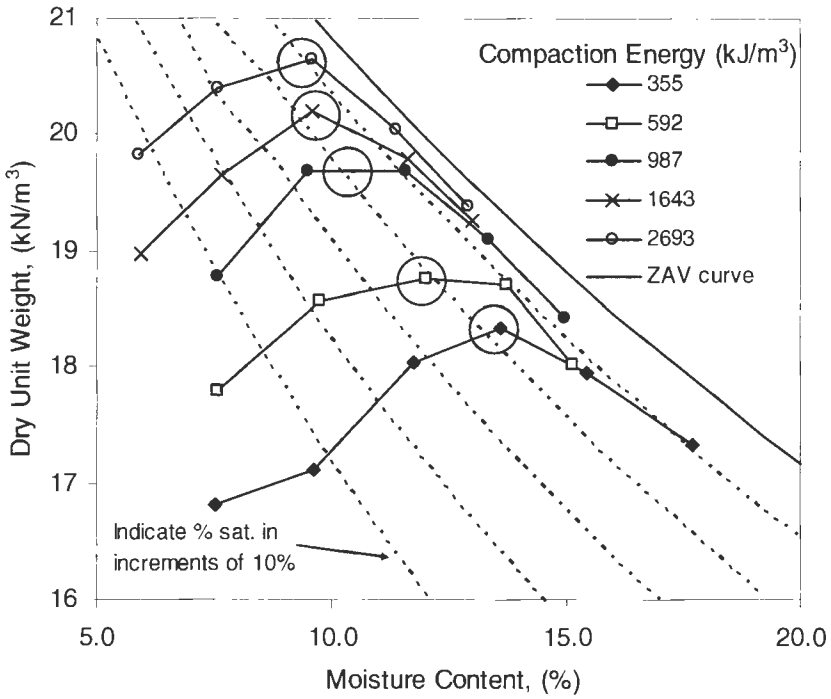

Figure 14. Laboratory compaction test results on Edwards till for various compaction energies

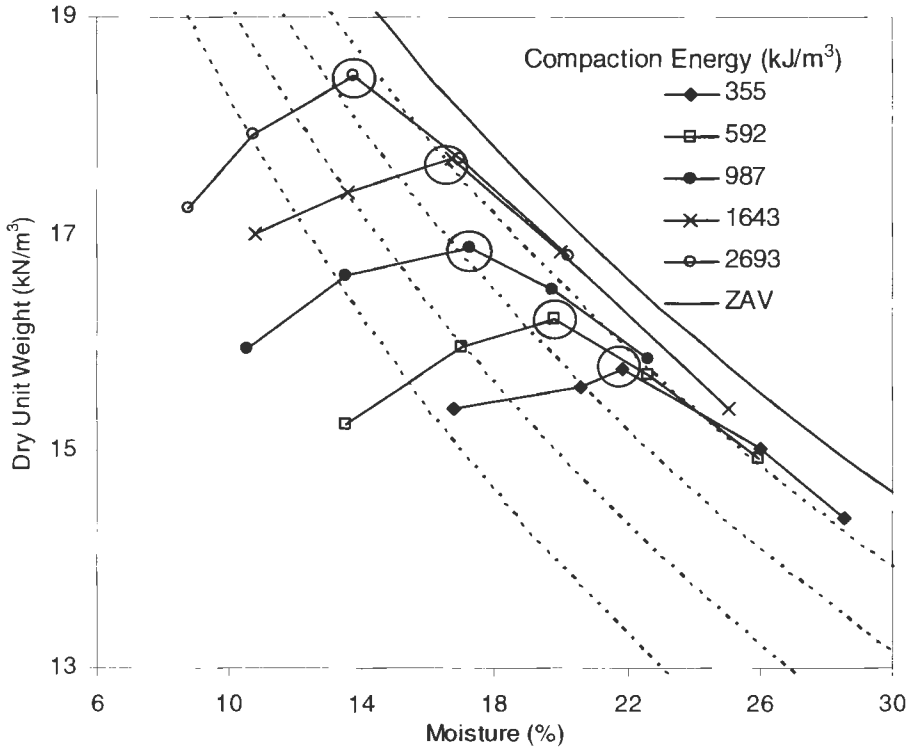

Figure 15. Laboratory compaction test results on West Des Moines clay 1 for standard Proctor energy

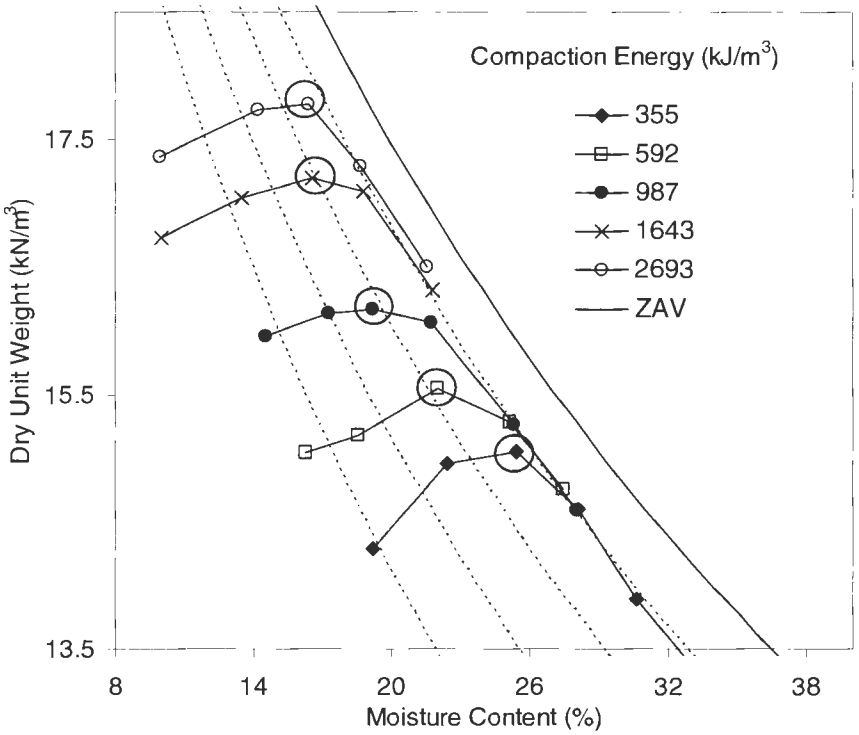

Figure 16. Laboratory compaction test results on West Des Moines clay 2 for standard Proctor energy

Relationships Between Compaction Energy and Optimal Conditions

Maximum dry unit weight and optimum moisture content for each soil plotted were against the logarithm of compaction energy. Points were selected by identifying the highest dry unit weight at each energy level. If the highest value of dry unit weight was observed by two measurements, the value was used and the optimum moisture content was interpolated between the two dry unit weights. All points used are indicated in Figure 10 to Figure 16 with a circle.

A linear correlation was observed between the parameters. Figure 17 through Figure 23 show the resulting linear correlations. Most maximum dry unit weights and optimum

moisture contents occurred between 75% and 90% saturation. Below this saturation range, dry unit weight increased with increasing moisture content. Above the range, dry unit weight decreased with increasing moisture content.

Most of the soils exhibit good correlations between the maximum dry unit weight, optimum moisture content and logarithm of energy (r^2 = 0.91-0.99). Lower correlations are observed between optimum moisture content and logarithm of energy in two soils (shale r^2 = 0.82, PPG till r^2 = 0.72).

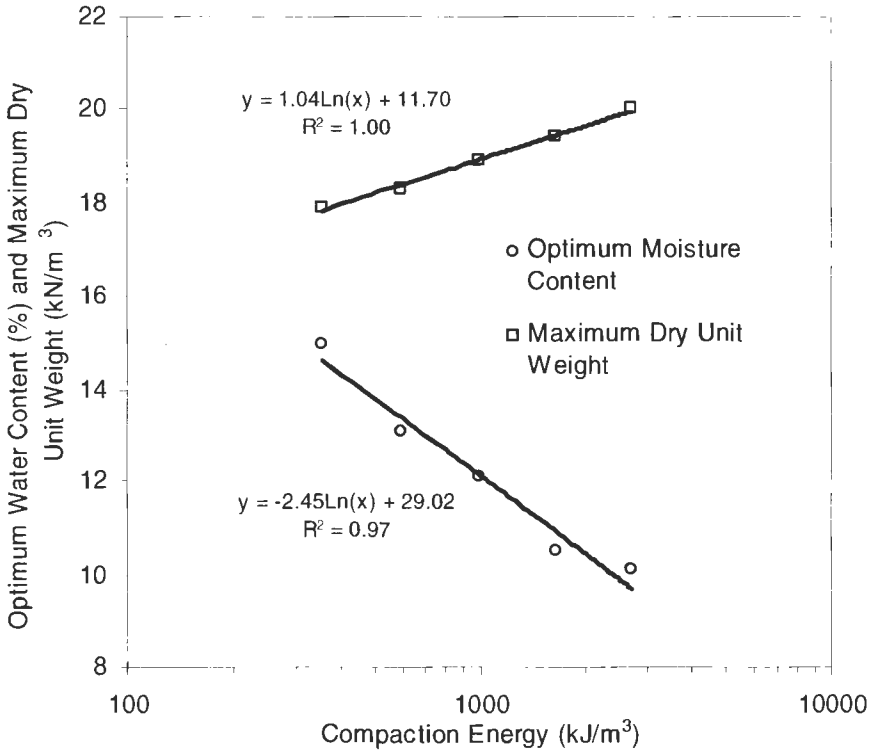

Figure 17. Semi-logarithmic relationship between compaction energy and optimum water content and maximum dry unit weight (Central Iowa till)

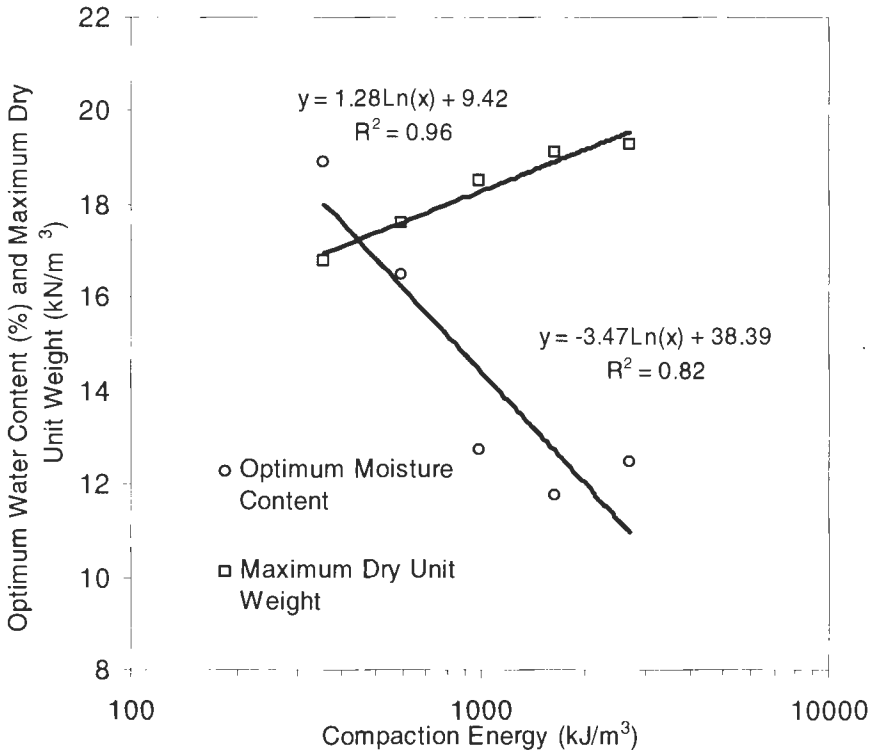

Figure 18. Semi-logarithmic relationship between compaction energy and optimum water content and maximum dry unit weight (weathered shale)

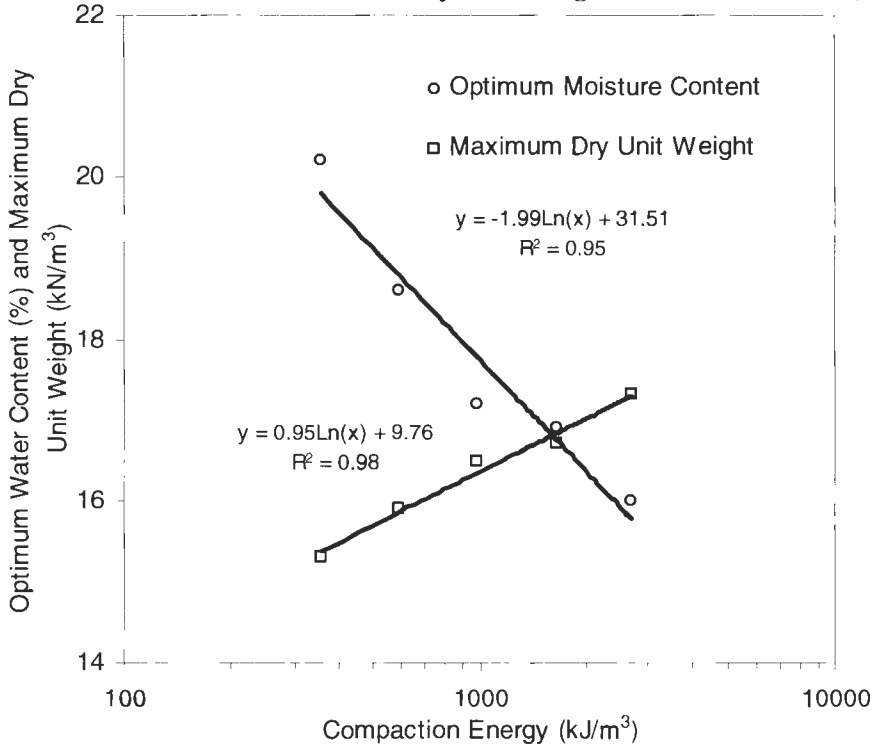

Figure 19. Semi-logarithmic relationship between compaction energy and optimum water content and maximum dry unit weight (Western Iowa loess)

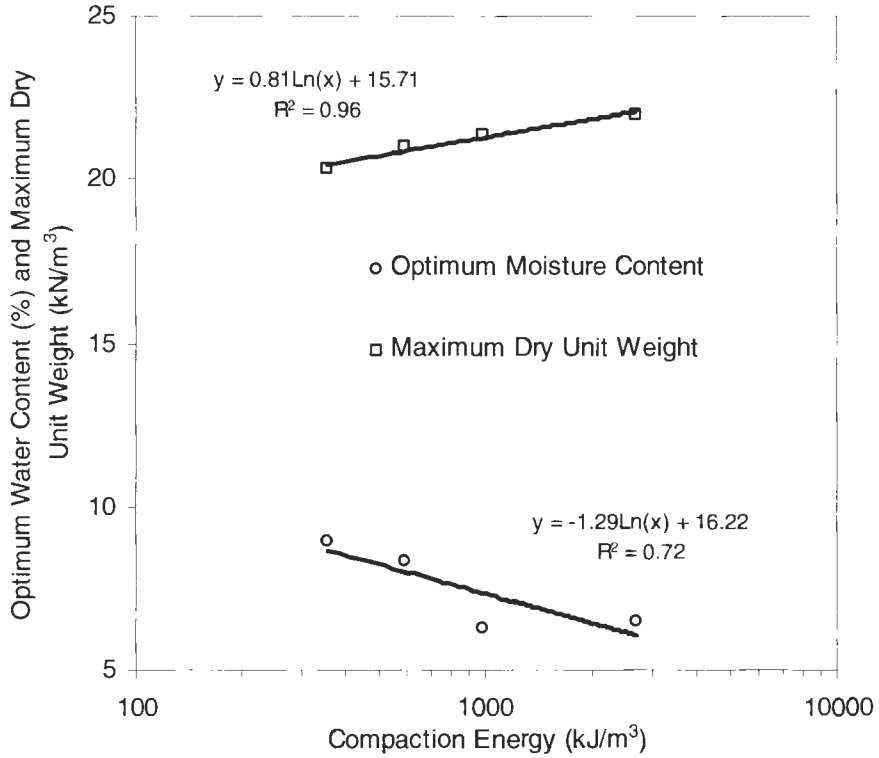

Figure 20. Semi-logarithmic relationship between compaction energy and optimum water content and maximum dry unit weight (PPG till)

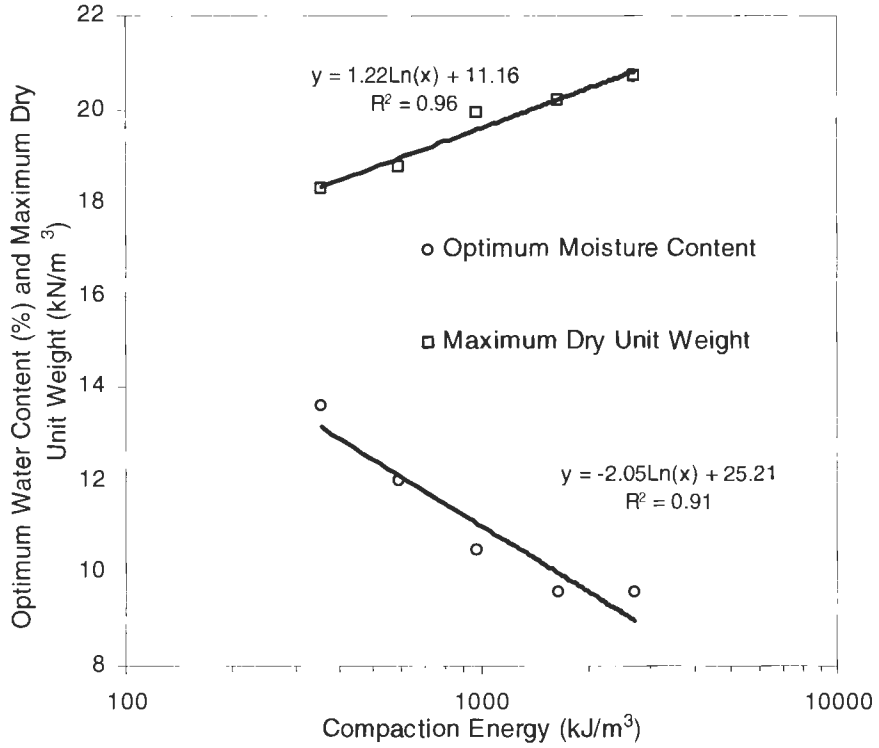

Figure 21. Semi-logarithmic relationship between compaction energy and optimum water content and maximum dry unit weight (Edwards till)

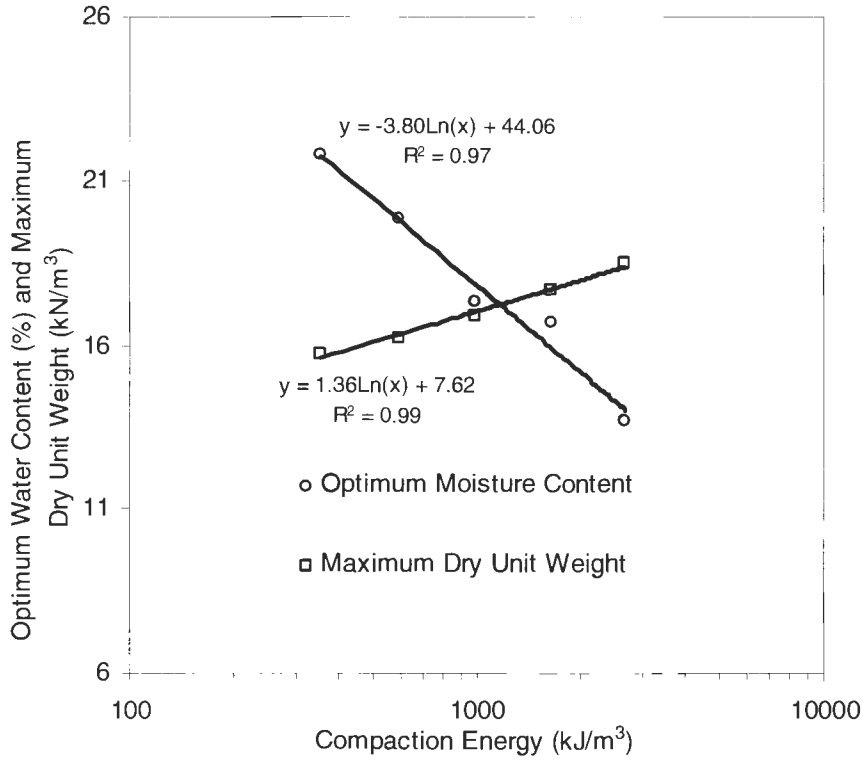

Figure 22. Semi-logarithmic relationship between compaction energy and optimum water content and maximum dry unit weight (WDSM clay 1)

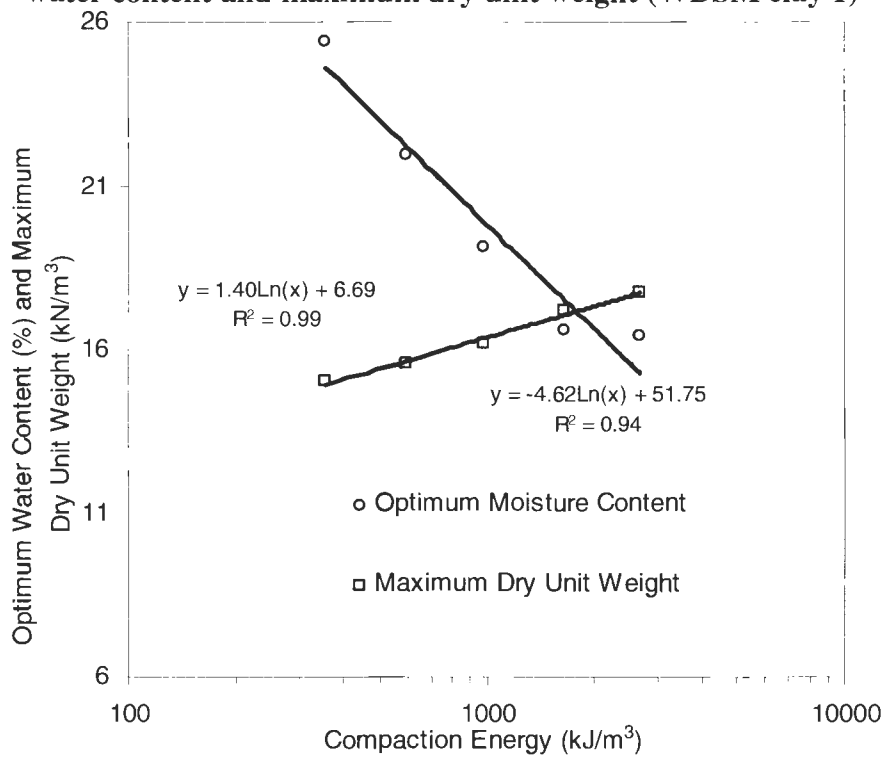

Figure 23. Semi-logarithmic relationship between compaction energy and optimum water content and maximum dry unit weight (WDSM clay 2)

For each soil, the slope of the lines (compaction sensitivity index) indicates the measure of sensitivity of maximum dry unit weight and optimum moisture content to compaction energy. As the slope coefficient increases, the sensitivity to compaction energy increases. These slopes were plotted against Atterberg limits and fines contents of the soils. Figure 24 and Figure 25 present the relationships of these index properties with the coefficient of compaction energy for maximum dry unit weight and optimum moisture content.

Sensitivity to compaction energy in maximum dry unit weight appeared to be most influenced by liquid limit and clay fraction while sensitivity in optimum moisture content was affected by liquid limit and plastic limit. As these parameters increased the sensitivity to compaction energy increased for maximum dry unit weight and optimum moisture content. Plastic limit, plasticity index, and fines passing the No. 200 also showed moderate correlation with the compaction sensitivity index for dry unit weight sensitivity ($r^2 = 0.51 - 0.65$). Plasticity index and both fines content parameters exhibited moderate correlation as well for optimum moisture content ($r^2 = 0.46 - 0.57$).

These results indicate that the sensitivity in the maximum Proctor conditions to compaction energy is linked to the liquid and plastic limits as well as clay fraction. An increase in clay content in increases the compressibility in a soil, thus increasing the sensitivity to applied energy. The liquid and plastic limits are then related to the amount of clay fraction, or fines content in general, i.e. increasing fines will increase Atterberg limits.

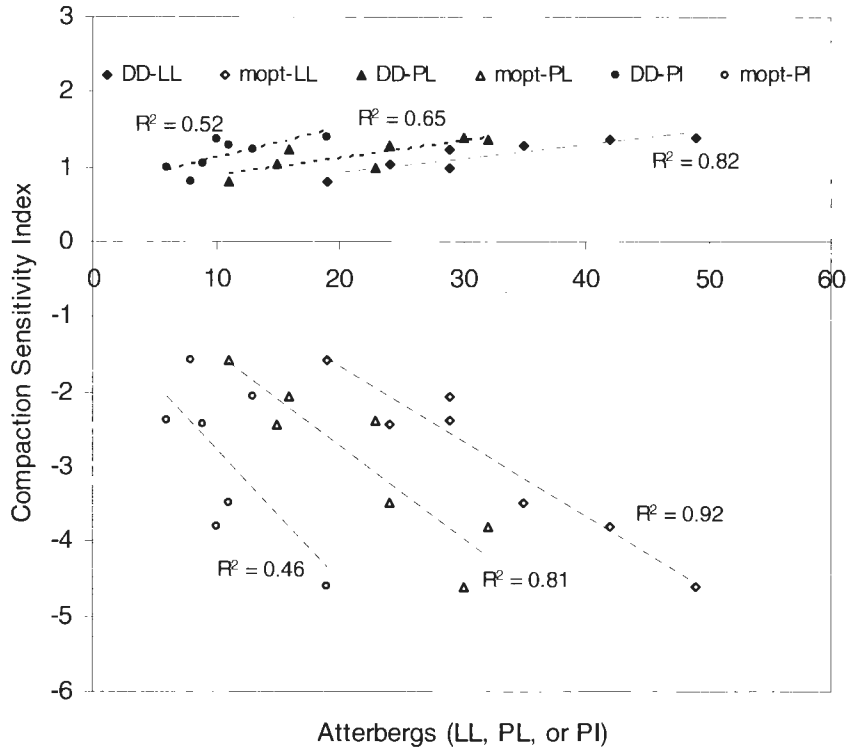

Figure 24. Relationships of Atterberg Limits and compaction sensitivity index

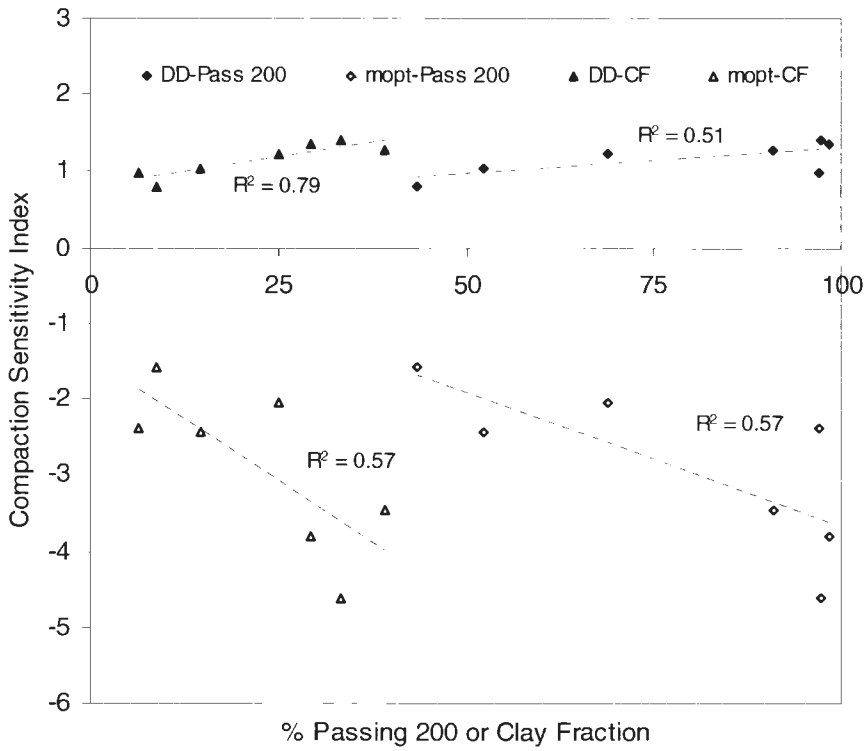

Figure 25. Relationships of fines contents and compaction sensitivity index

Relationships Between Compaction Energy and All Compaction Test Values

All dry unit weight measurements from compaction testing were also plotted versus the logarithm of compaction energy (see Figure 26 - Figure 30). Similar to the previous figures, these plots were created to observe the sensitivity to energy for all dry unit weights rather than merely the maximum conditions. From these observations, the objective was to develop a new model to estimate dry unit weight of a soil.

Each moisture content listed on the figures represents an average value for a given set of dry unit weights plotted against compaction energy. The maximum dry unit weight at standard Proctor energy is presented by a dashed line for reference. The achievement of 100% standard Proctor occurred at moisture contents $\leq$ 10.5%, 18.0%, 19.8%, 13.3%, and 21.8% for the Iowa till, shale, loess, and West Des Moines lean clays respectively. For the Illinois glacial tills attainment of 100% standard Proctor occurred at moisture contents $\leq$ 9.3% (PPG) and 13.1% (Edwards). To achieve 100% standard proctor dry of optimum involved a compaction energy $\geq$ 987 kJ/m^3.

Eventually, the dry unit weight reached an asymptotic state with increased compaction energy. The rate at which it reached this state depended on the soil's sensitivity to compaction energy. Fernandez and Corcoran (1999) explain the mechanical compaction process:

> During the early stage of the compaction process the soil transfers the compactive effort into densification at a high rate. As compaction progresses,

the rate of energy absorbed by the soil resulting volumetric strain is reduced producing diminishing returns in densification.

For all soils, a moisture content wet of optimum was observed that negated the achievement of 100% standard Proctor regardless of the amount of compaction energy applied. At this saturated condition, moisture content took full control of the end result in dry unit weight, resulting in an immediate asymptotic state across the energy spectrum.

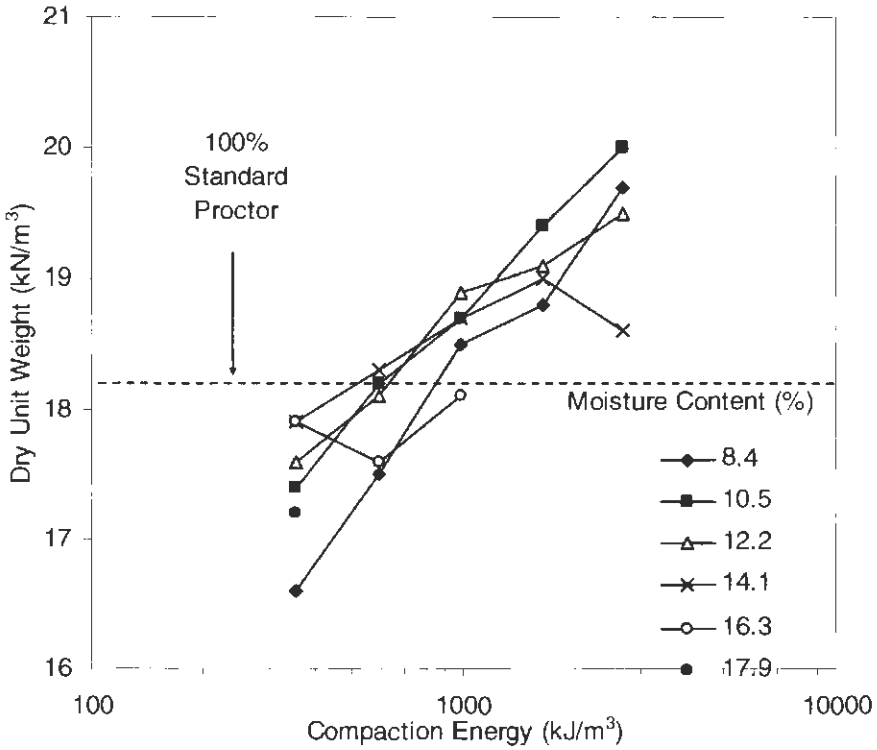

Figure 26. Influence of compaction energy on unit weight with average moisture contents (Central Iowa till)

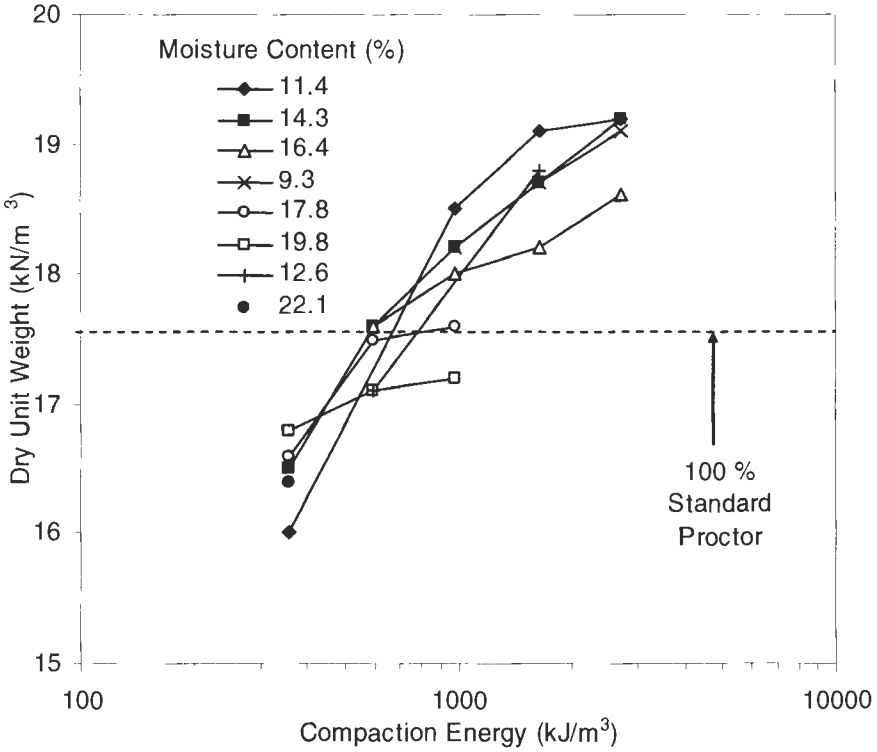

Figure 27. Influence of compaction energy on unit weight with average moisture contents (weathered shale)

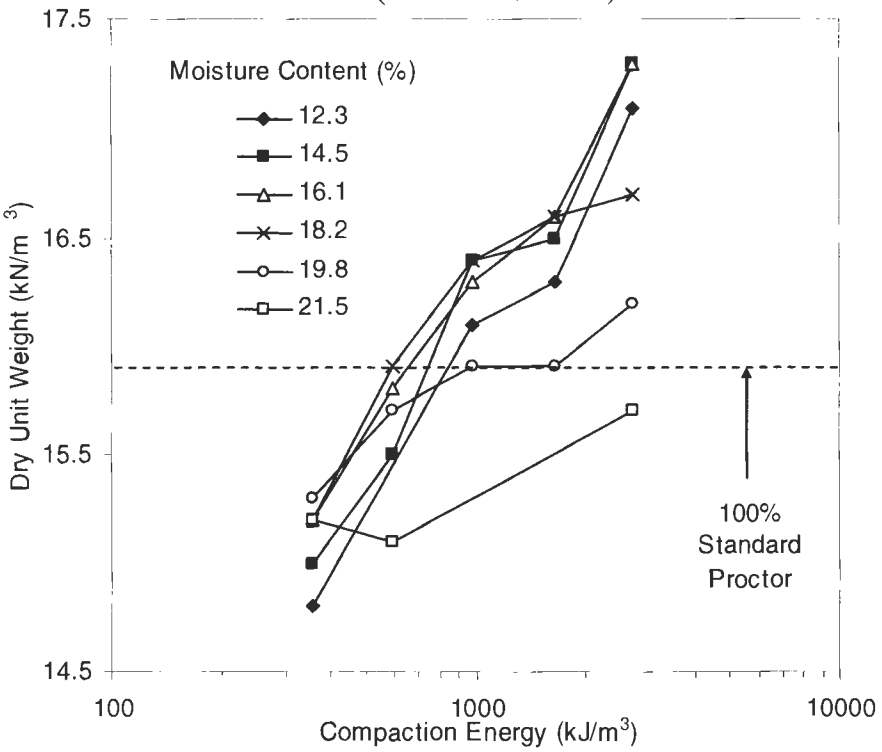

Figure 28. Influence of compaction energy on unit weight with average moisture contents (West Iowa loess)

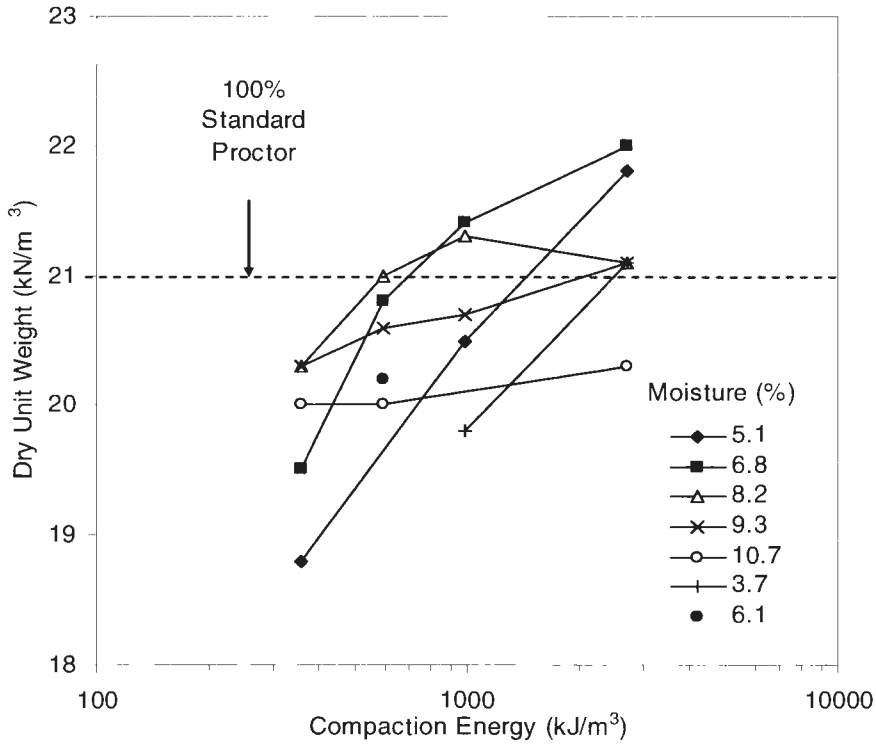

Figure 29. Influence of compaction energy on unit weight with average moisture contents (PPG till)

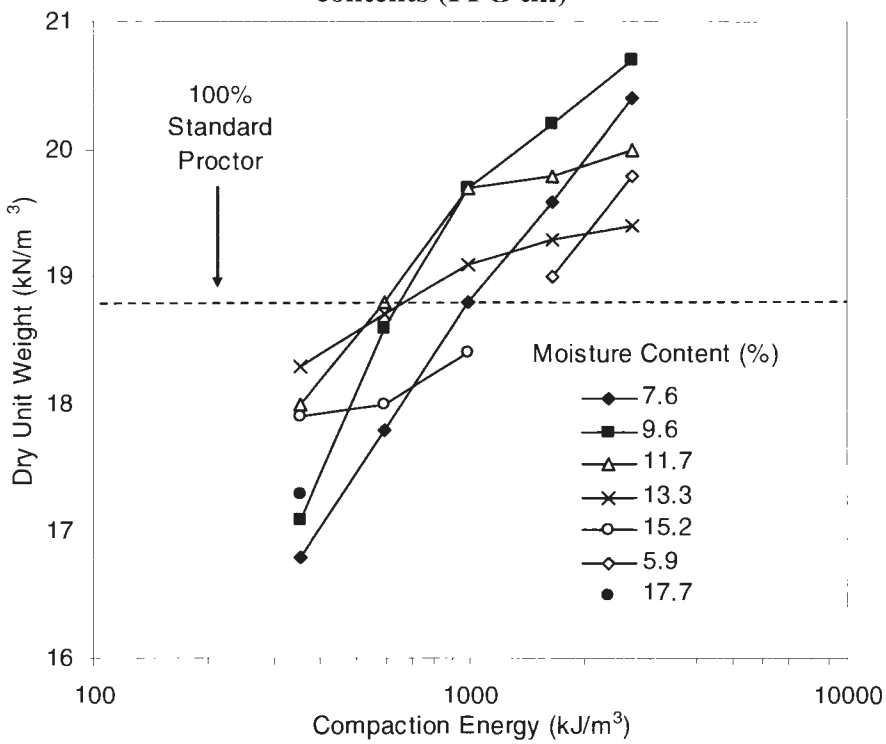

Figure 30. Influence of compaction energy on unit weight with average moisture contents (Edwards till)

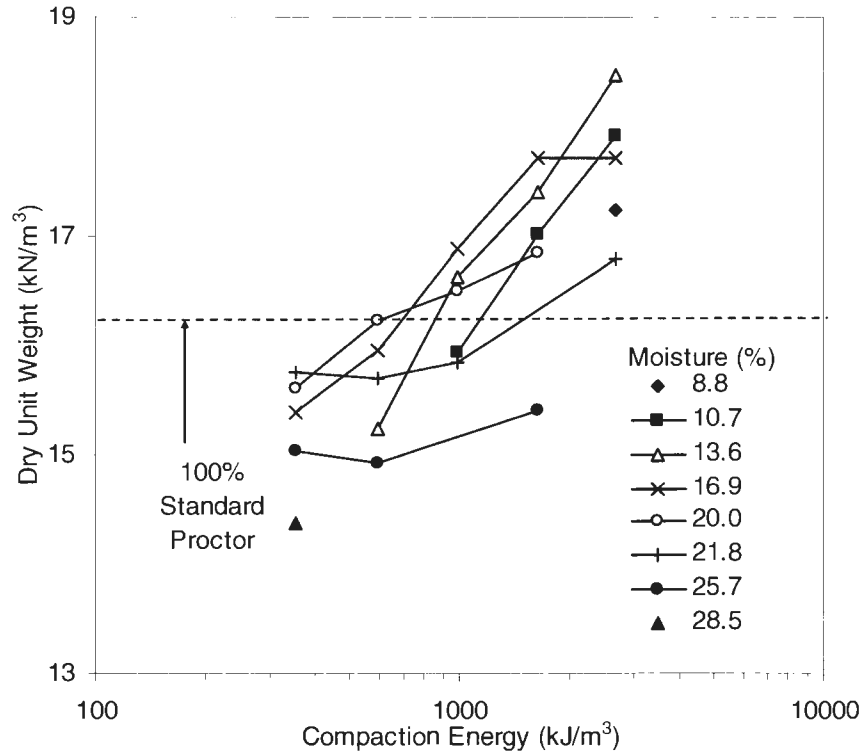

Figure 31. Influence of compaction energy on unit weight with average moisture contents (WDSM clay 1)

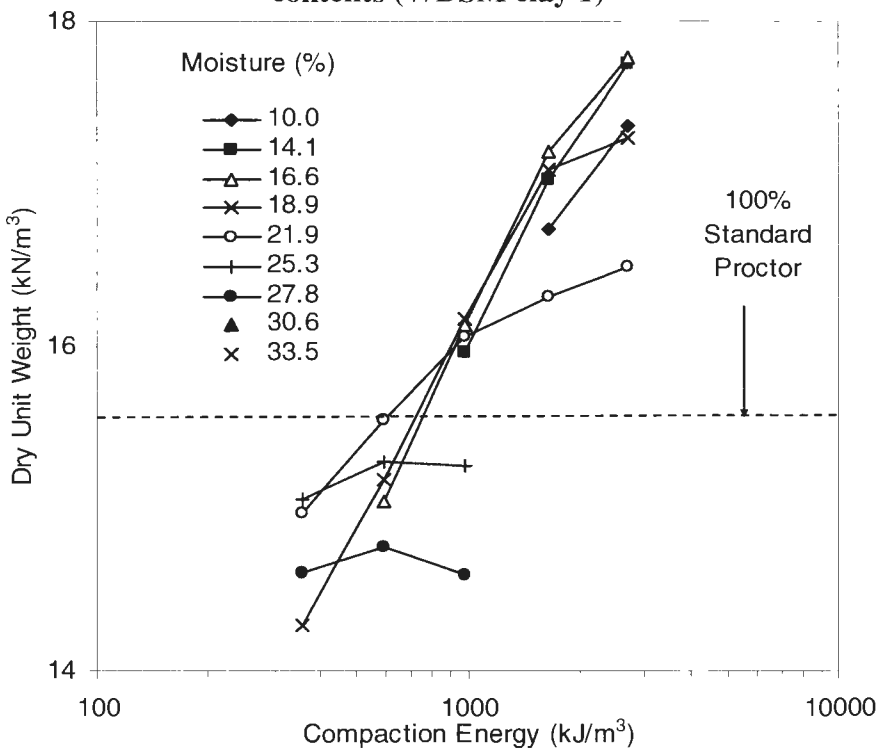

Figure 32. Influence of compaction energy on unit weight with average moisture contents (WDSM clay 2)

New Compaction Model

Inspired by the plots created and work by Handy (2002), a new model was developed that reproduced the asymptotic relationship observed between dry unit weight and compaction energy. The equation was derived from first-order, or linear rate equation principles. Linear rate equations are used to explain chemical and physical processes where a state of equilibrium is being established from an initial condition. A proportional relationship exists between the rate at which the equilibrium condition is approached and the departure from the original condition. Handy (2002) applied a geotechnical aspect to this principle in relating e – log P and compression index.

The linear rate equation derived allows one to estimate a dry unit weight value at a given moisture content by inputting a compaction energy value. The equation is as follows:

$$\gamma_{di} = \gamma_{do} + F \, Log_{10}(E_i/E_o) \qquad [3\text{-}1]$$

where, γ_{di} is the estimated dry unit weight, γ_{do} is a fixed known dry unit weight for a given moisture content and compaction energy, E_i is a compaction energy input variable, E_o is a compaction energy fixed value, and F is the compactability coefficient.

The compactability coefficient F at a given moisture content can be calculated as follows:

$$F = \frac{\gamma_{di} - \gamma_{do}}{Log_{10}(E_i/E_o)} \qquad [3\text{-}2]$$

where, γ_{di} and γ_{do} can be the known dry unit weights at energies 2693 and 355 kJ/m^3 and E_i and E_o can be compaction energy values of 2693 and 355 kJ/m^3.

It shall be noted that F changes with moisture content due to dry unit weight changing with moisture content. The term "known dry unit weight" is defined as the dry unit weight measured from a Proctor curve at the given energy. For this study, dry unit weights were attained at all Proctor curves in a set moisture range. Readings off the curves were taken at moisture content increments of 1%.

For this analysis, E_o was fixed at 355 kJ/m^3, i.e. 355 kJ/m^3 was utilized as the initial energy condition. Energy values ranging from 215 to 3325 kJ/m^3 were used for the compaction energy input variable, E, calculating the dry unit weight at increments of approximately 50 kJ/m^3. The initial dry unit weight (γ_{do}) used at each moisture content was the measured dry unit weight result at compaction energy 355 kJ/m^3.

Figure 34 is a plot of F-values as a function of moisture content for the Iowa till. In general, F decreases with increasing moisture content. All soil F-values exhibited this behavior as seen in Figure 35. Relations with Atterberg limits and fines contents parameters were investigated and are shown in Figure 36 to Figure 39. These figures show four values of F (1.0 to 4.0) plotted with individual index parameters (LL, PL, etc.) as a function of their corresponding moisture contents from Figure 35. It was observed that liquid limit, plastic limit, and fines passing No. 200 sieve correlated well with corresponding moisture contents for the four F-values chosen. Index parameters increased with increasing moisture contents.

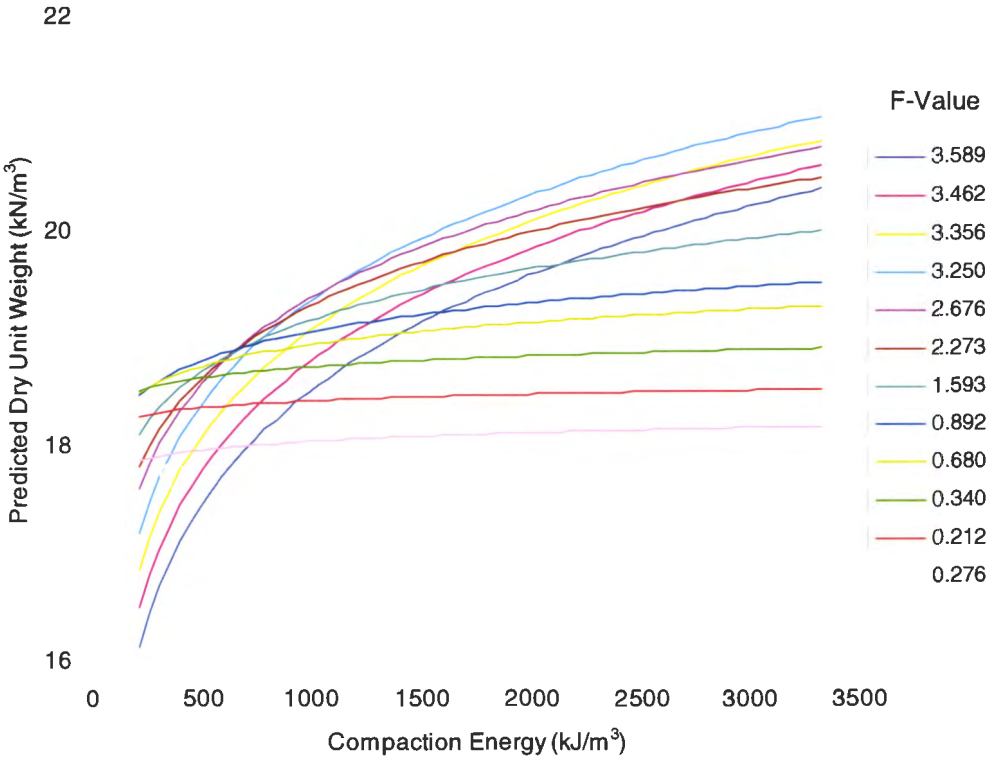

Figure 33. Prediction curves for dry unit weight using the linear rate model (Iowa till)

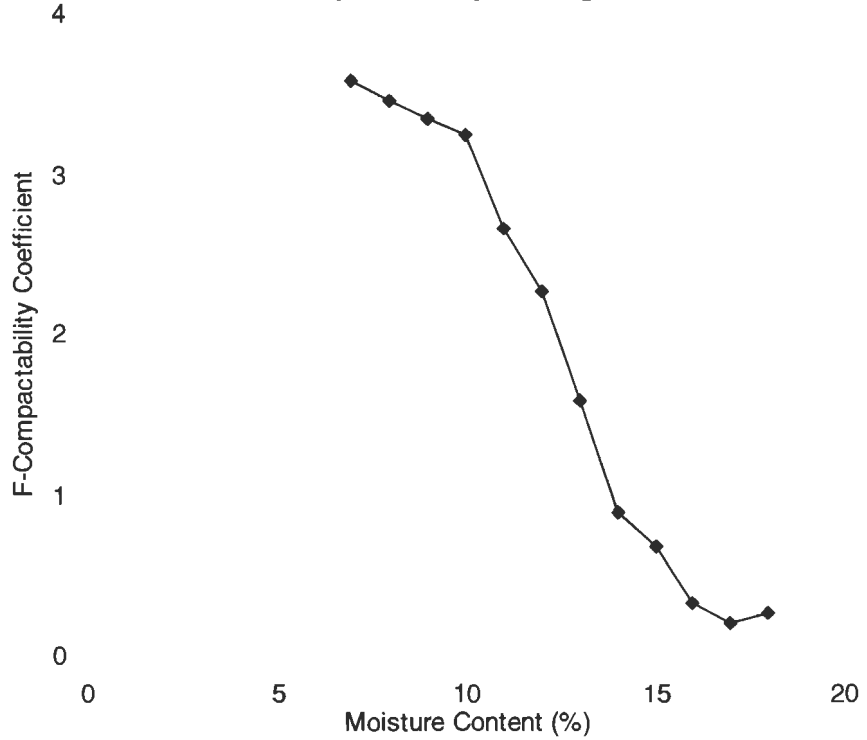

Figure 34. F-compactability coefficient as a function of moisture content for Central Iowa till

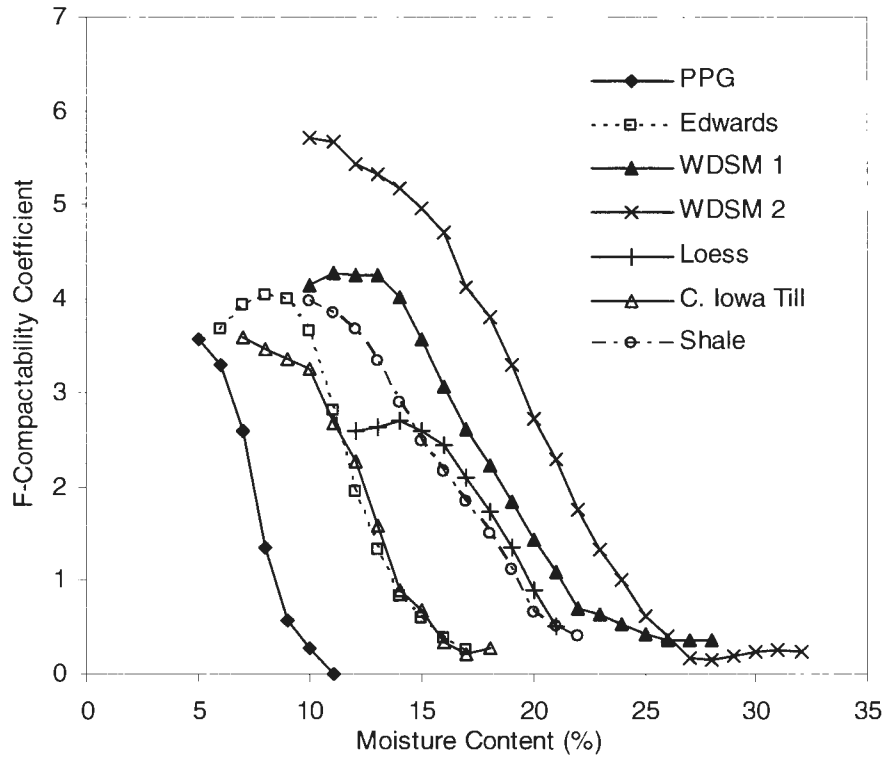

Figure 35. F-compactability coefficient as a function of moisture content for all soils

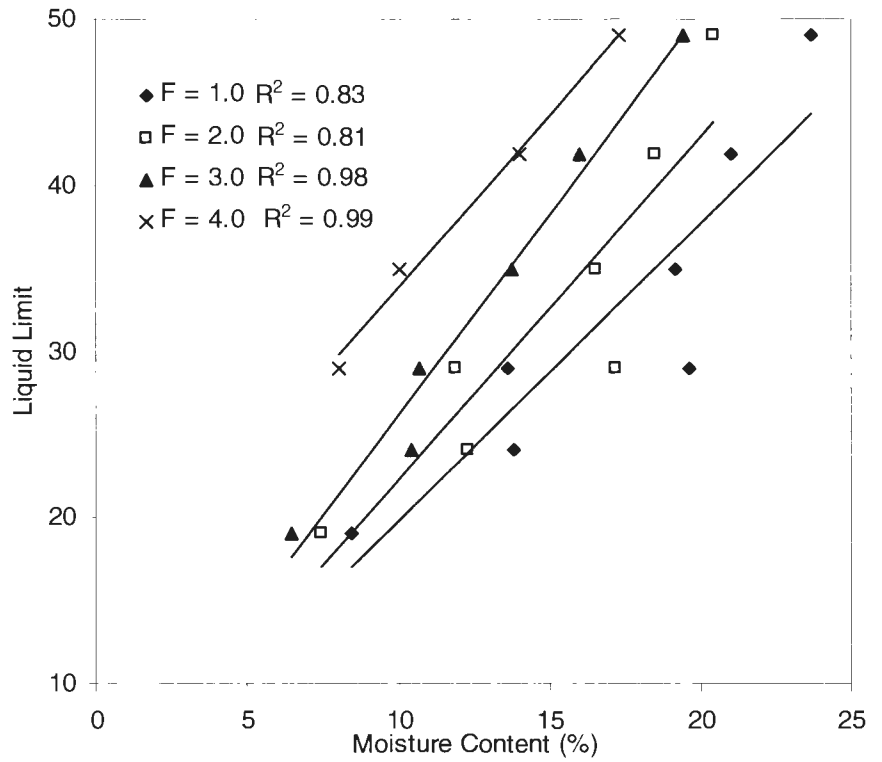

Figure 36. Relationships of liquid limit, moisture content and F-value

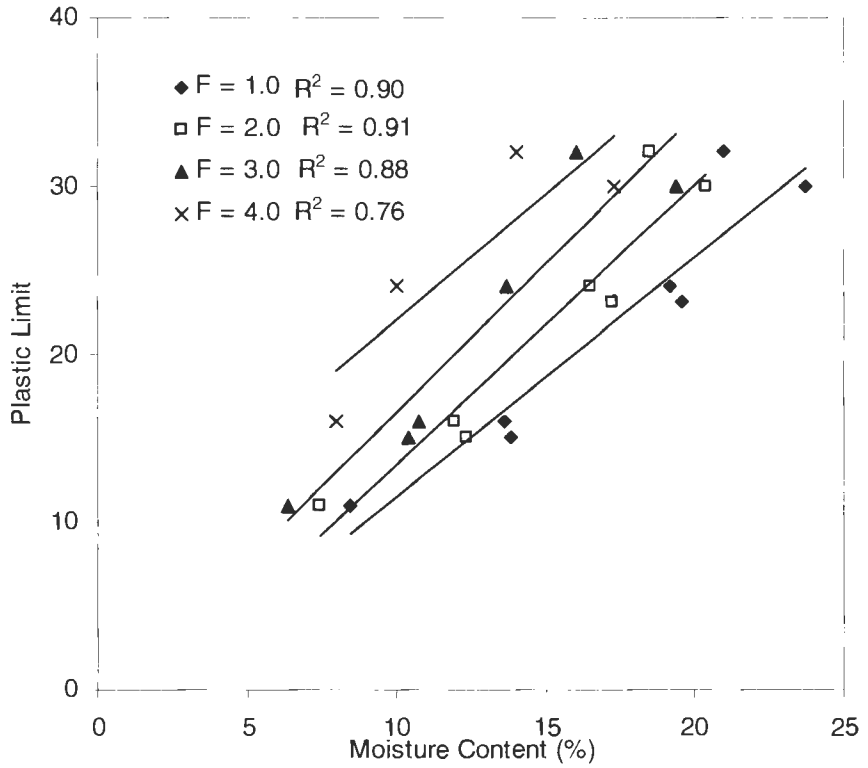

Figure 37. Relationships of plastic limit, moisture content and F-value

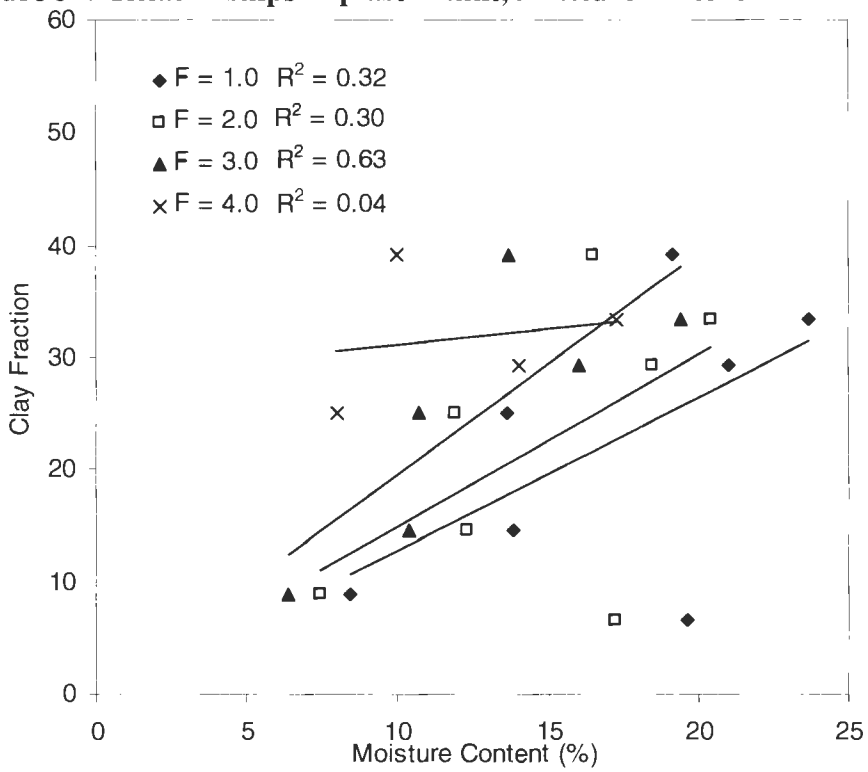

Figure 38. Relationships of clay fraction, moisture content, and F-value

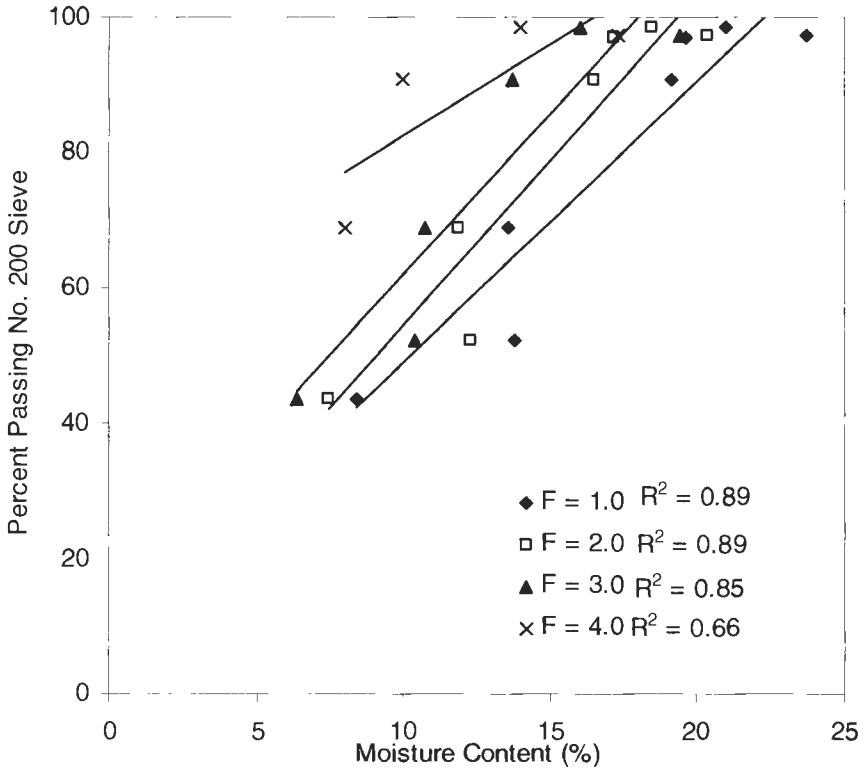

Figure 39. Relationships of percent passing No. 200 sieve, moisture content and F-value

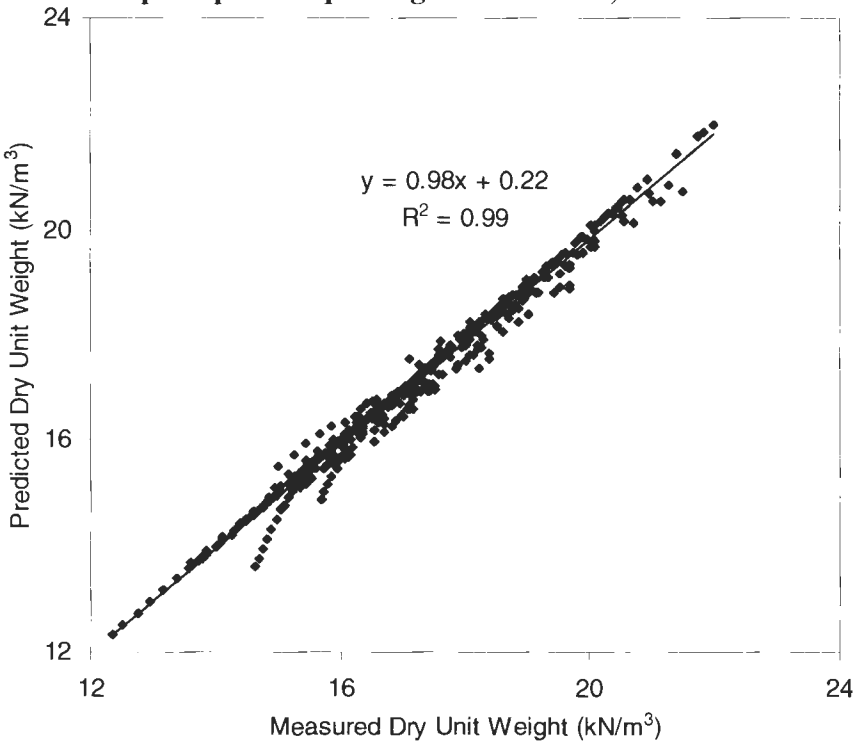

Figure 40. Measured vs. predicted unit weights from compaction model (all lab soils)

Also, trendlines moved right to left with increasing F-value. It was concluded the plots indicated that moisture content determined the compactability of a given soil. Further the plasticity characteristics of a soil determined the moisture contents at which compatability was determined. Equation 1-10 from Boltz et al. (1998), an equation similar to Eq. 3-1, shows that compactability of a soil is attributed to the LL. In this case, it appeared that moisture content attributed to the compactability of a soil rather than LL.

Most importantly, the validity of the compaction model was checked in comparing predicted dry unit weight and actual results from the laboratory. In all, 473 lab measurements were taken from 34 compaction curves of the 7 lab soils. Figure 40 displays the comparison between the measured and predicted. Excellent correlation (near unity at $r^2 = 0.99$) is observed between the parameters. The model appears to be an excellent predictor of dry unit weight for cohesive soils.

Moisture Content, Compaction Energy, and Relative Compaction

Figure 41 - Figure 45 shows how moisture content and compaction energy effect the relative compaction achieved. These figures, coined "bathtub curves", were created to gain another perspective on compaction efficiency. Compaction efficiency is determined by observing the relative compaction achieved for a given compaction energy and moisture content. The figures indicate the amount of compaction energy required to achieve different levels of relative compaction. The plots can be viewed in several ways. First, the achievement of relative compaction at individual moisture contents is observed. From the left side of the x-axis, more than one relative compaction is achieved at a given moisture content. For

example, at the moisture content of 10%, in Figure 41, all five levels of compaction are attained. However, by moving to higher moisture contents, a threshold is reached where an individual moisture content can only attain one level of compaction. These are the vertical straight-line portions of the curves favoring the right side of the x-axis.

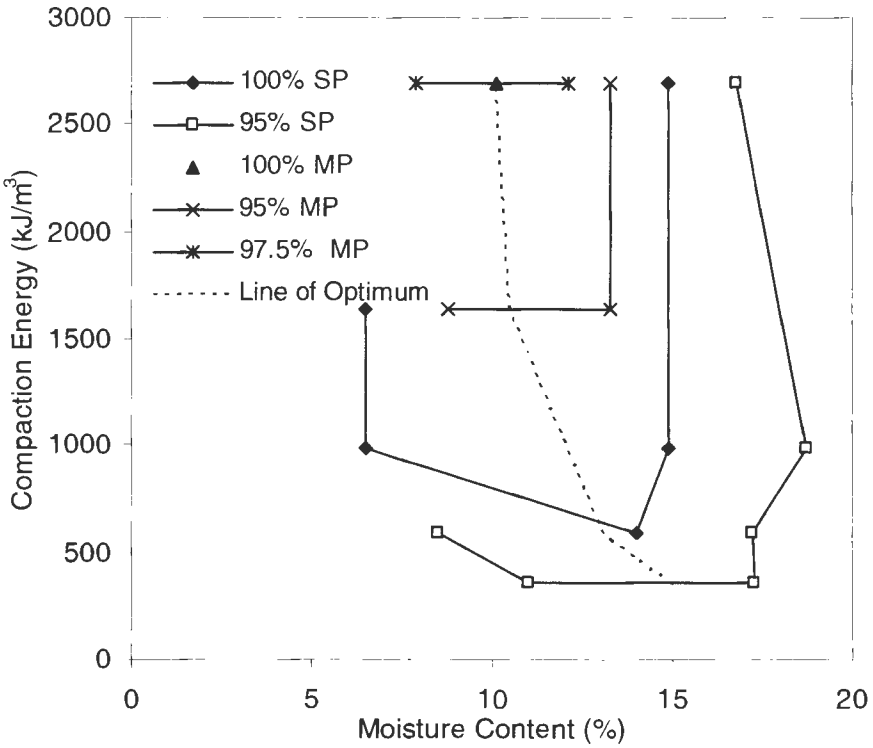

Figure 41. Energy as a function of moisture content for various degrees of compaction (Central Iowa till)

Another way to observe the plots are comparing sides of the line of optimum. The line of optimum, or boundary of optimum moisture content, is indicated on each figure as a dashed line. Optimum moisture contents occurred between 75% and 90% saturation. Same relative compaction was achieved at on both sides of optimum. However, moving from left to right on the x-axis, different levels of compaction are able to be obtained to a certain saturated state. Prior to this state, the energy applied is efficiently used. The line of optimum is an

approximation of this transition. Moving to the right, or wet of optimum, efficiency drops at moisture content at ≤ 3.5% from the line for all soils.

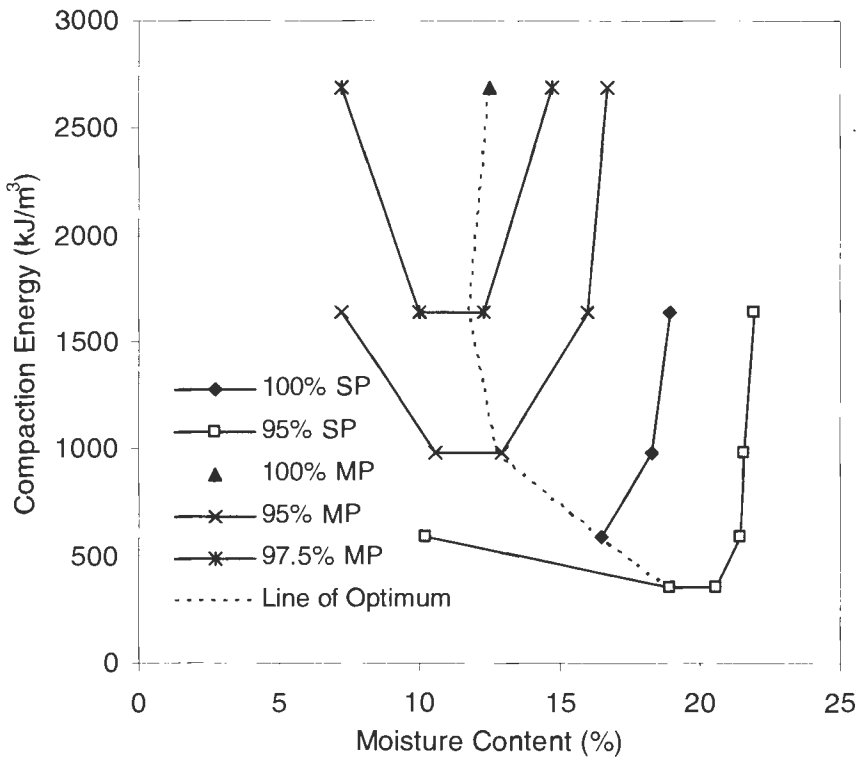

Figure 42. Energy as a function of moisture content for various degrees of compaction (weathered shale)

Compaction efficiency can also be assessed at a given compaction energy on the y-axis. A peak efficiency is attained for any given level of compaction energy, moving from left to right. Generally, but not always, this occurs at the low peak of a curve. For example, at 987 kJ/m^3 in Figure 44, 95% modified and 100% standard Proctor are attained at a moisture content of 5.75%. A relative compaction of 97.5% modified Proctor can be attained with the same energy at moisture contents between 6.5 and 7.5%. Therefore, by attaining a higher

relative compaction while using the same compactive effort, this combination of energy and moisture allows for greater efficiency.

Finally, compaction efficiency on the curves can be determined by comparing between different compaction energies. The lowest energy to achieve a given relative compaction is considered more efficient than higher energies achieving the same relative compaction. This can occur at different or same (wet of optimum) moisture contents. Thus, the highest efficiency for each relative compaction curve is observed at its lowest peak.

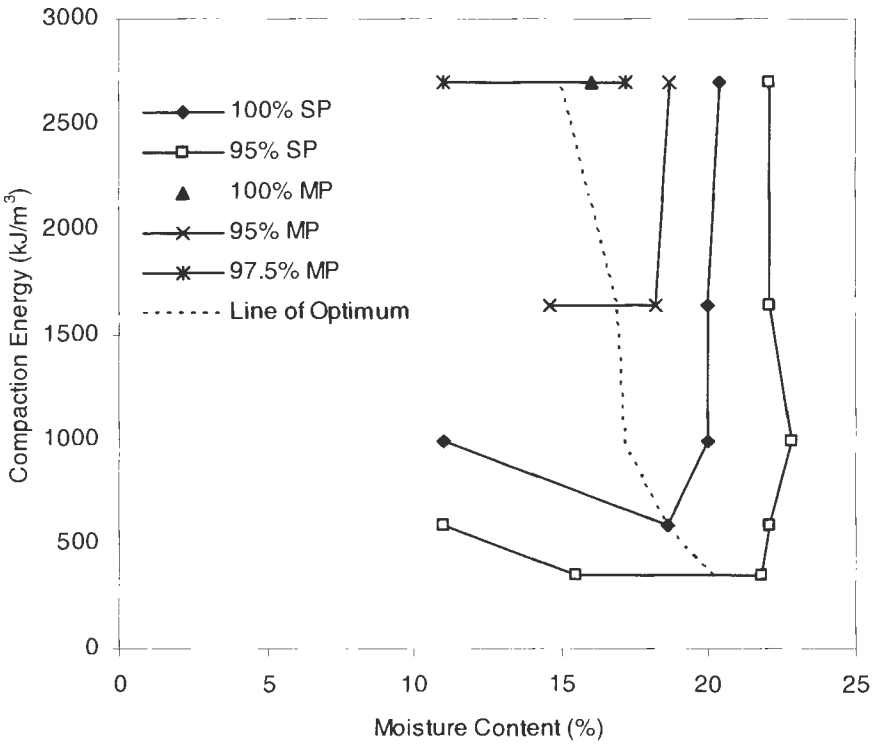

Figure 43. Energy as a function of moisture content for various degrees of compaction (Western Iowa loess)

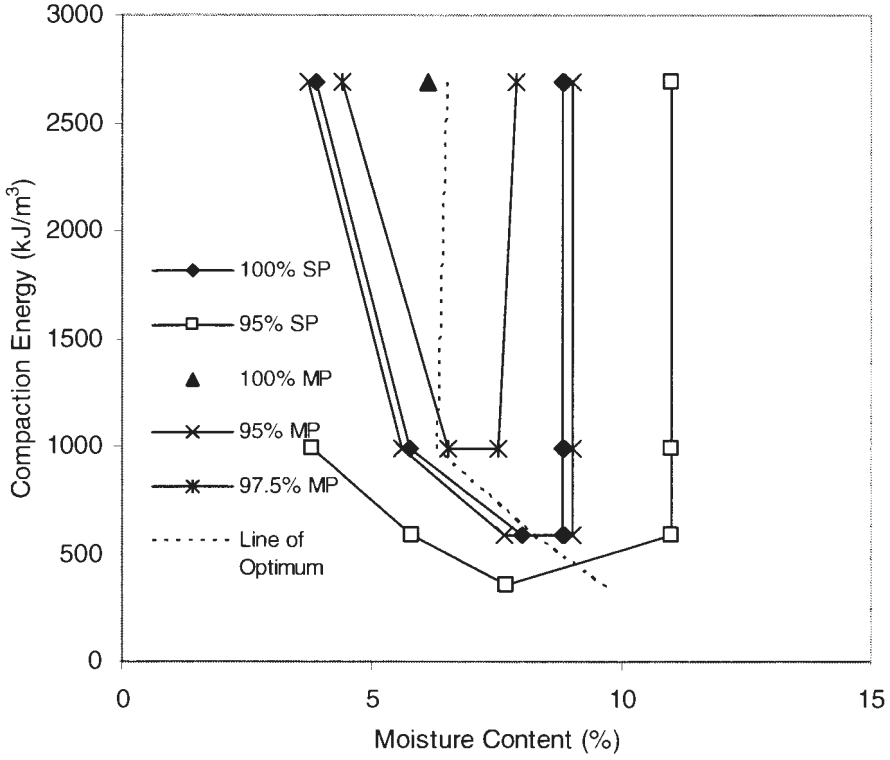

Figure 44. Energy as a function of moisture content for various degrees of compaction (PPG till)

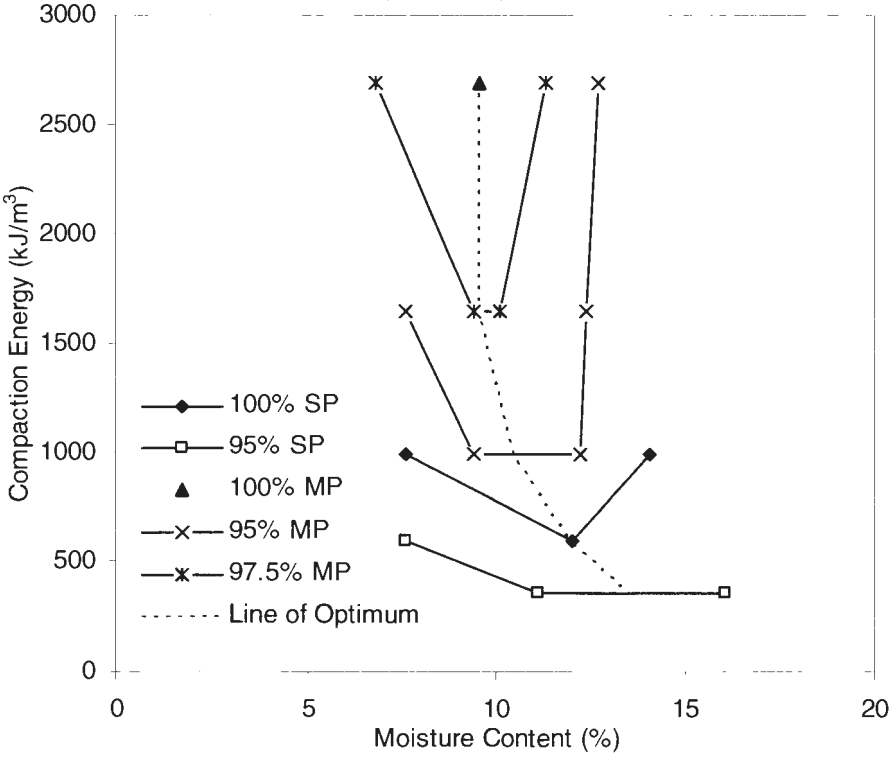

Figure 45. Energy as a function of moisture content for various degrees of compaction (Edwards till)

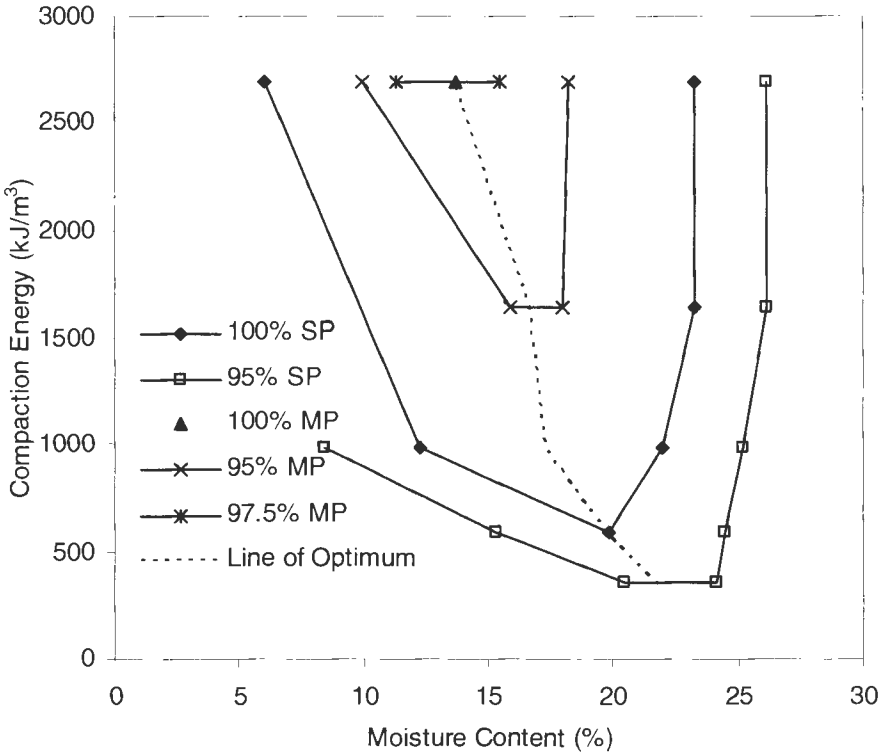

Figure 46. Energy as a function of moisture content for various degrees of compaction (WDSM clay 1)

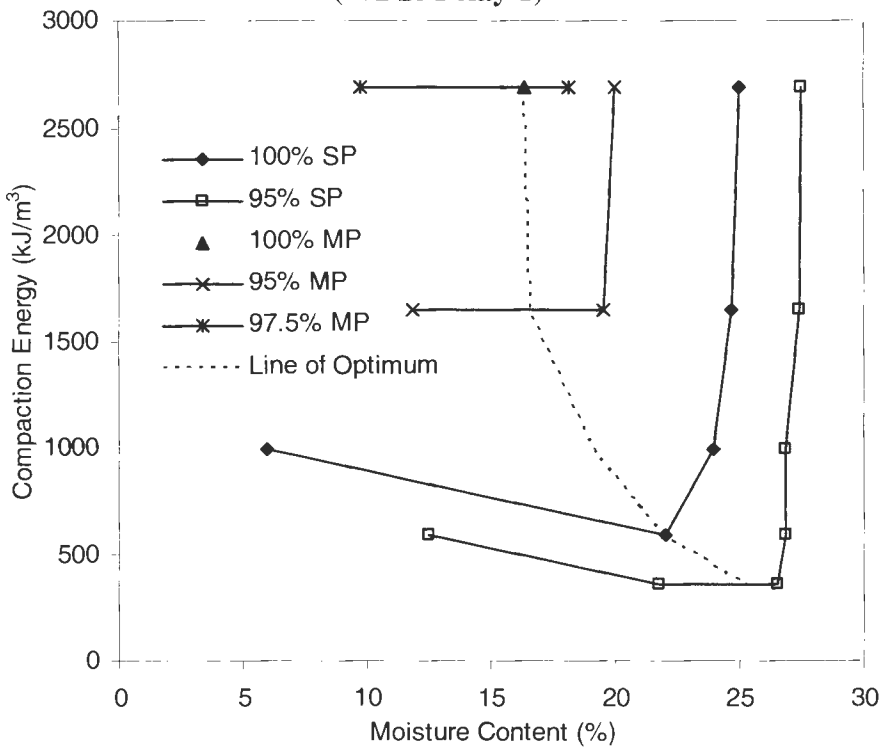

Figure 47. Energy as a function of moisture content for various degrees of compaction (WDSM clay 2)

Statistical Analyses of Compaction Test Data

Results of the Proctor tests from seven soils were investigated with a multiple regression analysis. Moisture content and logarithm of energy were defined as independent variables and dry unit weight as dependent. The following equations resulted from the analysis:

$$DD_{till} = 2.29(LogE) - 0.017(m\%) + 11.4 \quad [3\text{-}3]$$

$$DD_{shale} = 2.75(LogE) - 0.039(m\%) + 10.3 \quad [3\text{-}4]$$

$$DD_{loess} = 1.74(LogE) - 0.044(m\%) + 11.5 \quad [3\text{-}5]$$

$$DD_{PPG} = 1.645(LogE) - 0.04(m\%) + 15.5 \quad [3\text{-}6]$$

$$DD_{Edwards} = 2.87(LogE) - 0.02(m\%) + 10.1 \quad [3\text{-}7]$$

$$DD_{WDSM1} = 2.54(LogE) - 0.04(m\%) + 9.48 \quad [3\text{-}8]$$

$$DD_{WDSM2} = 2.66(LogE) - 0.023(m\%) + 9.31 \quad [3\text{-}9]$$

where, DD is the dry unit weight (kN/m^3), E is the compaction energy (kJ/m^3) and m% is the percent moisture content.

Statistical results are shown in Table 5. Adjusted r^2 values ranged from 0.39 to 0.89. Standard error of the estimate was recorded and compared with the standard deviation of the dry unit weight of each soil. All standard errors were less than their respective standard deviation. However, the Iowa till was close in comparing the two values. Therefore, regression models were slight to moderately accurate in estimation. Further, F-statistic values of the soils were greater than their percentage points on the F-distribution curve at $\alpha =$

0.05. Therefore, the null hypothesis was rejected and at least one independent variable helped explain the variation in dry unit weight.

Table 5. Statistical analysis on dry unit weight for laboratory soils

Equation	Soil	n	Adjusted r^2	Standard Error of Estimate	Standard Deviation	F-Statistic	t-statistics
3-3	Till	26	0.74	0.76	0.83	37.0	OK
3-4	Shale	26	0.89	0.32	0.99	106.9	NG(m%-1.9)
3-5	Loess	27	0.73	0.36	0.70	37.0	NG(m%-1.9)
3-6	PPG	20	0.39	0.61	0.79	7.17	NG(m%-0.6)
3-7	Edwards	26	0.76	0.51	1.03	40.3	NG(m%-0.6)
3-8	WDSM1	24	0.79	0.49	1.06	43.7	NG(m%-1.3)
3-9	WDSM2	27	0.88	0.42	1.83	98.0	OK

For all soils, the logarithm of energy proved to be a stronger predictor of dry unit weight rather than moisture content which is shown in Figure 26-Figure 30. In this linear analysis, the t-statistic of the moisture content could not be used as a predictor for the Illinois tills nor one of the West Des Moines clays.

The percent of variability explained by the independent variables are displayed in Table 6.Table 6 Percent variability was determined by squaring individual Pearson correlations (R values) between dependent and independent variables.

Table 6. Percent variability explained by variables regarding dry unit weight

Soil	Dry Unit Weight (kN/m^3)	
	Log E (% explained)	Moisture (% explained)
Till	76	8
Shale	89	33
Loess	72	8
PPG	44	1
Edwards	77	8
WDSM1	76	42
WDSM2	83	61

A major shortcoming of this approach is that there are two different dry unit weights for each moisture content (aside from optimum) as evidenced in earlier figures (Figure 10-Figure 16). Therefore, each Proctor curve was divided at the optimum moisture content and analyzed dry and wet of optimum separately. Equations for soil dry unit weight on the dry side of optimum are:

$$DD_{till\ dry} = 3.23(LogE) + 0.02(m\%) + 6.89 \quad [3\text{-}10]$$

$$DD_{shale\ dry} = 3.51(LogE) + 0.045(m\%) + 7.0 \quad [3\text{-}11]$$

$$DD_{loess\ dry} = 2.45(LogE) + 0.07(m\%) + 7.82 \quad [3\text{-}12]$$

$$DD_{PPG\ dry} = 3.12(LogE) + 0.042(m\%) + 8.90 \quad [3\text{-}13]$$

$$DD_{Edwards\ dry} = 4.02(LogE) + 0.027(m\%) + 4.61 \quad [3\text{-}14]$$

$$DD_{WDSM1\ dry} = 4.14(LogE) + 0.14(m\%) + 2.09 \quad [3\text{-}15]$$

$$DD_{WDSM2\ dry} = 4.18(LogE) + 0.08(m\%) + 2.35 \quad [3\text{-}16]$$

Equations for soil dry unit weight on the wet side of optimum include the following:

$$DD_{till\ wet} = 0.84(LogE) - 0.20(m\%) + 19.4 \quad [3\text{-}17]$$

$$DD_{shale\ wet} = 1.44(LogE) - 0.17(m\%) + 16.4 \quad [3\text{-}18]$$

$$DD_{loess\ wet} = 0.70(LogE) - 0.26(m\%) + 19.0 \quad [3\text{-}19]$$

$$DD_{PPG\ wet} = 0.58(LogE) - 0.32(m\%) + 21.9 \quad [3\text{-}20]$$

$$DD_{Edwards\ wet} = 1.20(LogE) - 0.27(m\%) + 19.0 \quad [3\text{-}21]$$

$$DD_{WDSM1\ wet} = 0.70(LogE) - 0.24(m\%) + 19.2 \quad [3\text{-}22]$$

$$DD_{WDSM2\ wet} = 1.04(LogE) - 0.20(m\%) + 17.2 \quad [3\text{-}23]$$

Statistical results for the revised equations are shown in Table 7 and Table 8. Adjusted r^2 values were improved by splitting the curves at optimum. Values ranged from 0.91 to 0.98 dry of optimum and 0.87 to 0.99 wet of optimum.

Table 7. Statistical analysis on dry unit weight for laboratory soils dry of optimum

Equation	Soil	n	Adjusted r^2	Standard Error of Estimate	Standard Deviation	F-Statistic	t-statistics
3-10	Till	18	0.97	0.15	0.86	259.7	OK
3-11	Shale	16	0.93	0.30	1.11	96.8	NG (m%-0.2)
3-12	Loess	19	0.96	0.14	0.76	245.1	OK
3-13	PPG	12	0.91	0.29	0.96	54.3	OK
3-14	Edwards	16	0.96	0.23	1.11	180.3	OK
3-15	WDSM1	15	0.97	0.16	0.99	191.8	OK
3-16	WDSM2	15	0.98	0.16	1.12	337.8	OK

Dry of optimum, the logarithm of energy was the stronger predictor of dry unit weight. The t-statistic of the moisture content could not be used as a predictor for the weathered shale.

Table 8. Statistical analysis on dry unit weight for laboratory soils wet of optimum

Equation	Soil	n	Adjusted r^2	Standard Error of Estimate	Standard Deviation	F-Statistic	t-statistics
3-17	Till	15	0.95	0.18	0.78	123.6	OK
3-18	Shale	18	0.99	0.11	0.89	573.0	OK
3-19	Loess	15	0.95	0.14	0.62	132.6	OK
3-20	PPG	12	0.87	0.22	0.62	38.7	OK
3-21	Edwards	15	0.98	0.14	0.94	289.8	OK
3-22	WDSM1	15	0.97	0.19	1.15	263.9	OK
3-23	WDSM2	17	0.98	0.19	1.27	339.0	OK

For all soils wet of optimum, moisture content was the strongest predictor for dry unit weight. Both independent variables could be used as predictors wet of optimum.

The percent of variability explained by the independent variables are displayed in Table 9. Percent variability was determined by squaring individual Pearson correlations (R values) between dependent and independent variables.

Table 9. Percent variability explained for dry unit weight dry and wet of optimum

Soil	Dry of Optimum		Wet of Optimum	
	Log E (% explained)	Moisture (% explained)	Log E (% explained)	Moisture (% explained)
Till	77	4	72	90
Shale	92	37	85	88
Loess	94	4	52	86
PPG	59	1	31	81
Edwards	79	2	76	88
WDSM1	83	19	53	96
WDSM2	96	44	77	96

Unconfined Compression Tests

Values of undrained shear strength and secant modulus are plotted as a function of the logarithm of compaction energy in Figure 48 - Figure 52 and Figure 53 - Figure 57. It shall

be noted that moisture contents given in these figures are average values of four or five test specimens. Undrained shear strength was calculated by dividing the unconfined compressive strength by two. Secant modulus was then determined by computing the slope of the line from the x-axis to the undrained shear strength. Each figure indicates the undrained shear strength of the specimen that exhibited the closest conditions at 100% standard Proctor.

Soils exhibited highest strength and stiffness values at dry of optimum and optimum conditions. As compaction energy increases, strength and secant modulus increases at moisture contents less than optimum. In general, an increase in shear strength was not observed well wet of optimum. Also, at these moisture contents, a general decrease in shear strength was noted at the highest compaction energy. This can be attributed to remolding of the highly saturated soils as more compaction energy is applied. The loess increased because it was only 2.5% wet of optimum (see Figure 50). Overall, secant modulus was highly variable, as anticipated. The variability in the results is due to variation in moisture contents between specimens. In particular the loess exhibited variability dry of optimum with an average moisture content of 12.2% for five specimens. The actual moisture conditions for the specimens compacted at 987, 1643, and 2693 kJ/m^3 were 10.8, 13.5, and 12.8% respectively.

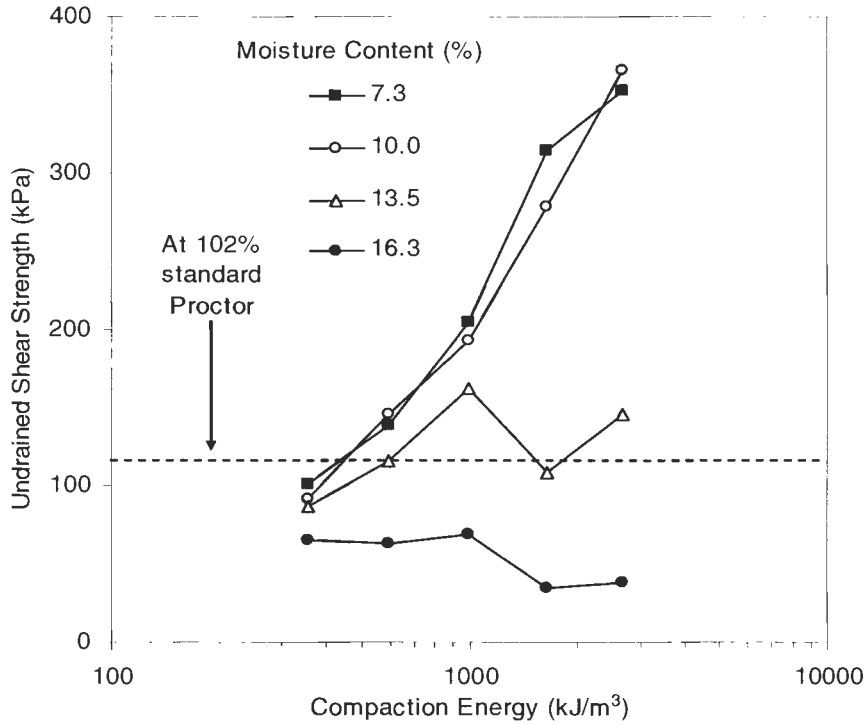

Figure 48. Semi-logarithmic relationship between undrained shear strength and compaction energy as a function of moisture content (Iowa till – m_{opt} = 13.1%)

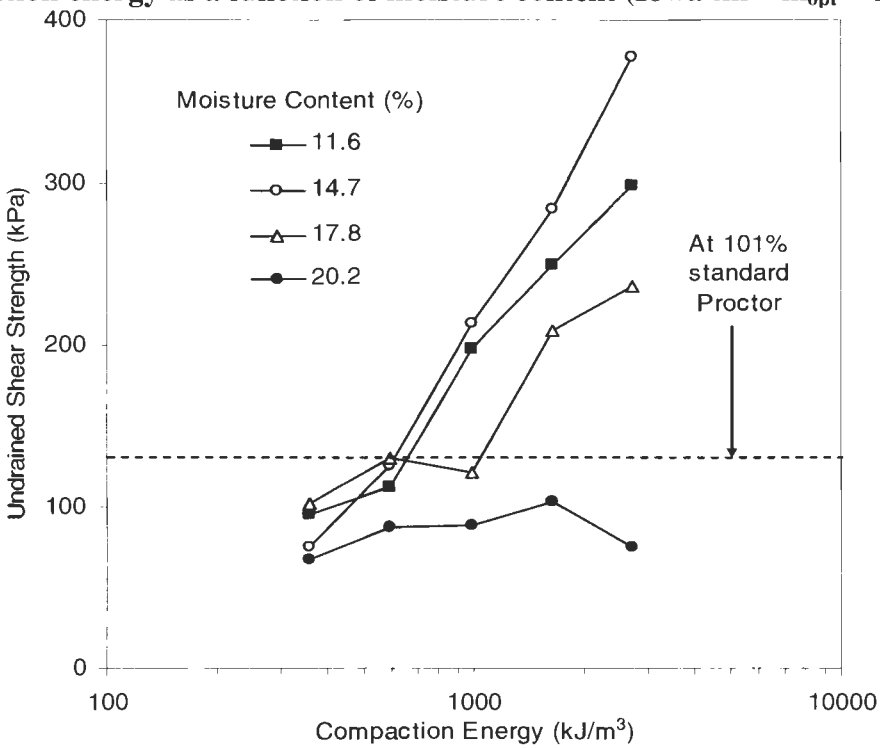

Figure 49. Semi-logarithmic relationship between undrained shear strength and compaction energy as a function of moisture content (weathered shale – m_{opt} = 18%)

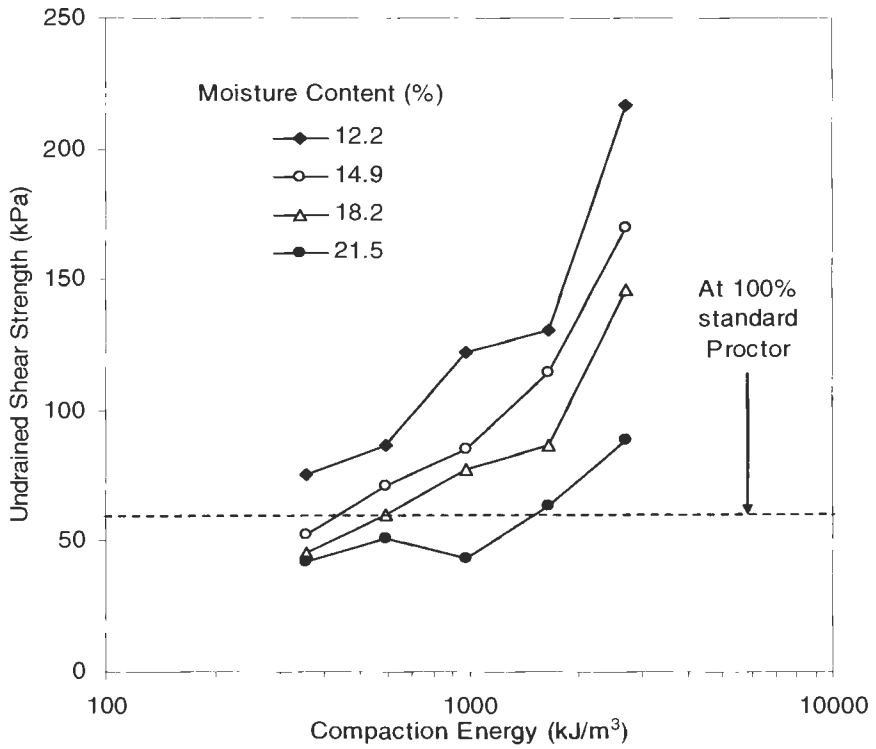

Figure 50. Semi-logarithmic relationship between undrained shear strength and compaction energy as a function of moisture content (Western Iowa loess – m_{opt} = 18%)

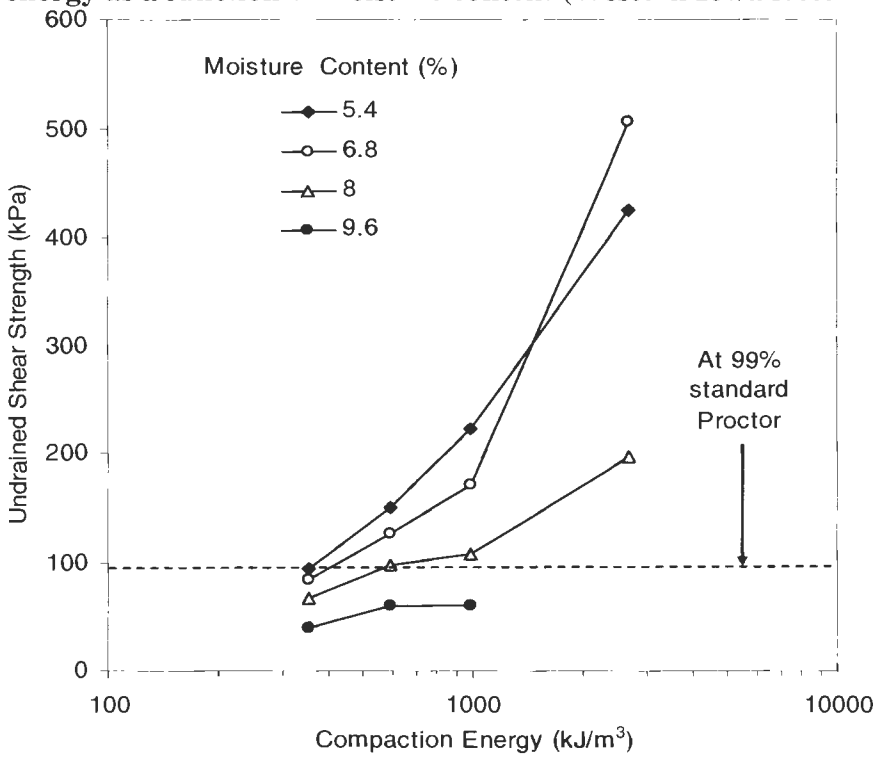

Figure 51. Semi-logarithmic relationship between undrained shear strength and compaction energy as a function of moisture content (PPG till – m_{opt} = 8%)

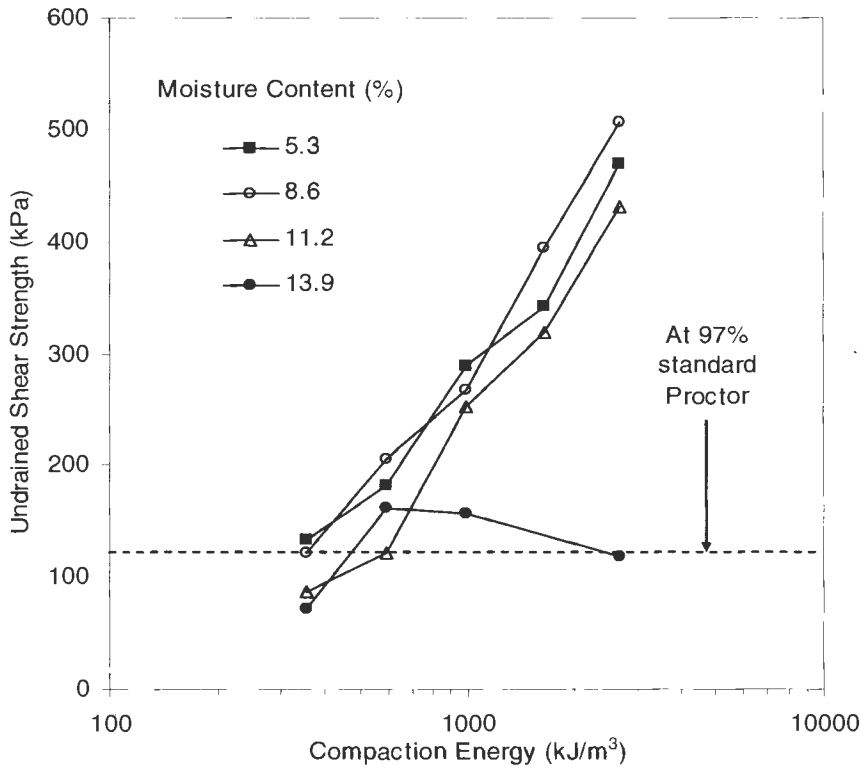

Figure 52. Semi-logarithmic relationship between undrained shear strength and compaction energy as a function of moisture content (Edwards till – m_{opt} = 12%)

Dry unit weights for the unconfined compression specimens are provided in Appendix B (Figures B1 – B5). Stress strain plots are compared between energy levels at similar moisture contents and between moisture contents at the same energy levels (Figures B6 – B49). All unconfined compression test data is presented in tabular format in Appendix B.

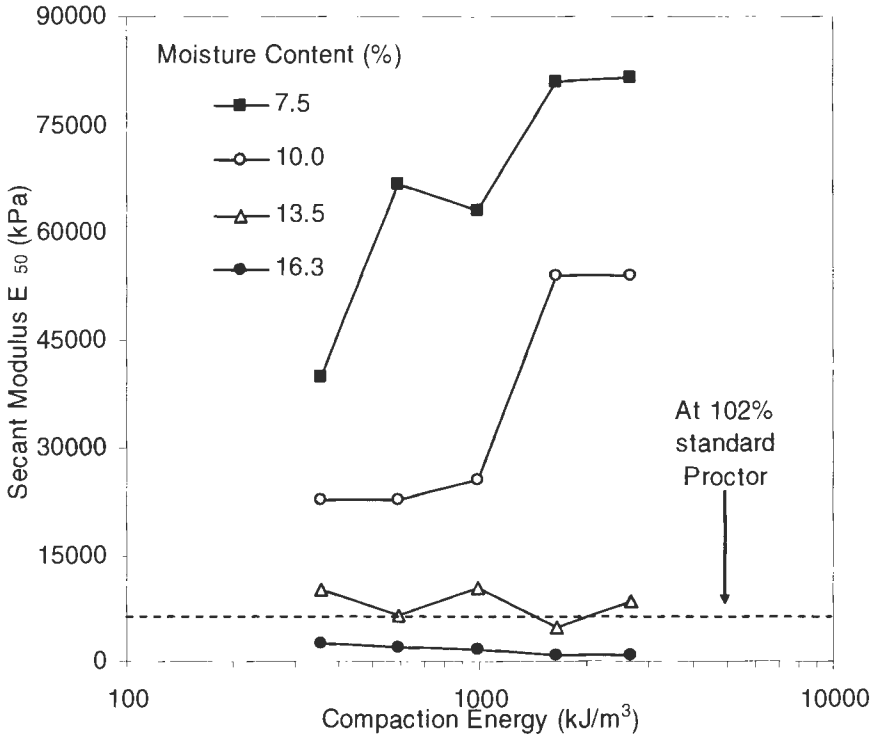

Figure 53. Semi-logarithmic relationship between secant modulus and compaction energy as a function of moisture content (Iowa till – m_{opt} = 13.1%)

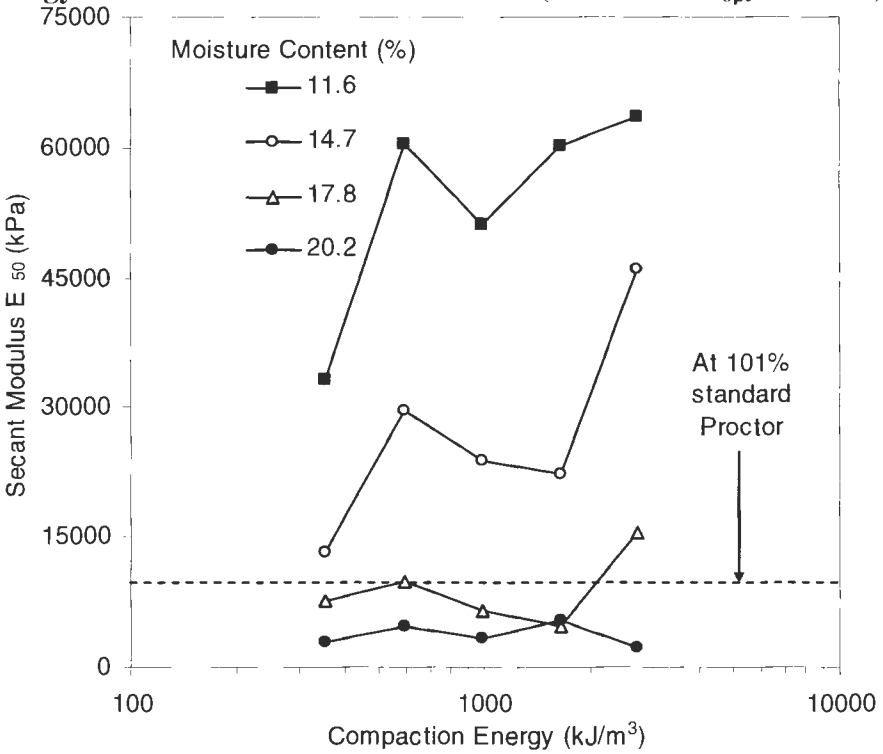

Figure 54. Semi-logarithmic relationship between secant modulus and compaction energy as a function of moisture content (weathered shale – m_{opt} = 18%)

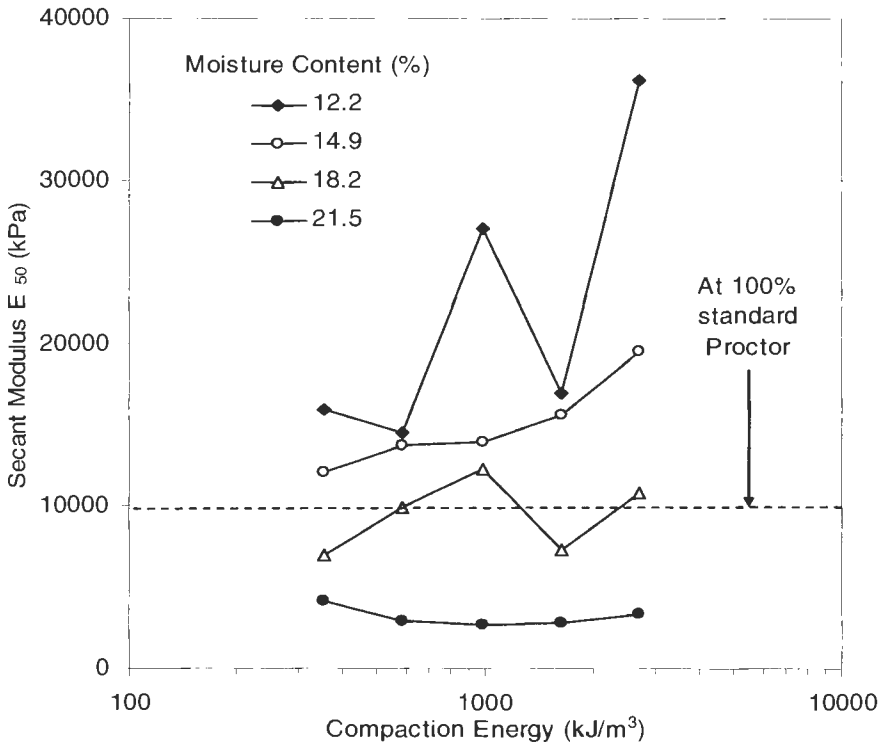

Figure 55. Semi-logarithmic relationship between secant modulus and compaction energy as a function of moisture content (Western Iowa loess – m_{opt} = 18%)

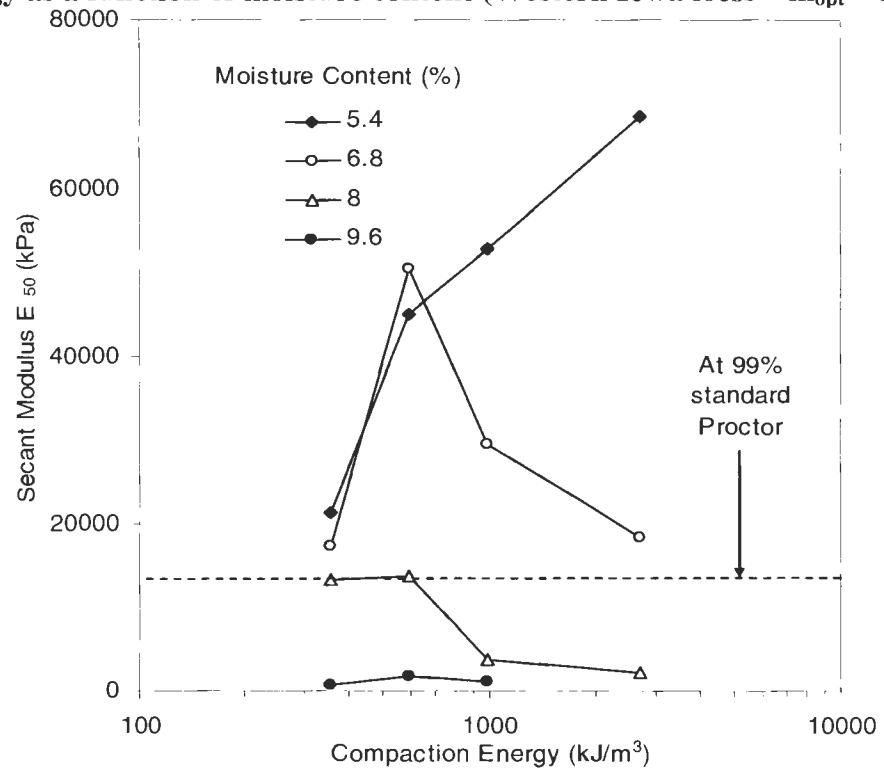

Figure 56. Semi-logarithmic relationship between secant modulus and compaction energy as a function of moisture content (PPG till – m_{opt} = 8%)

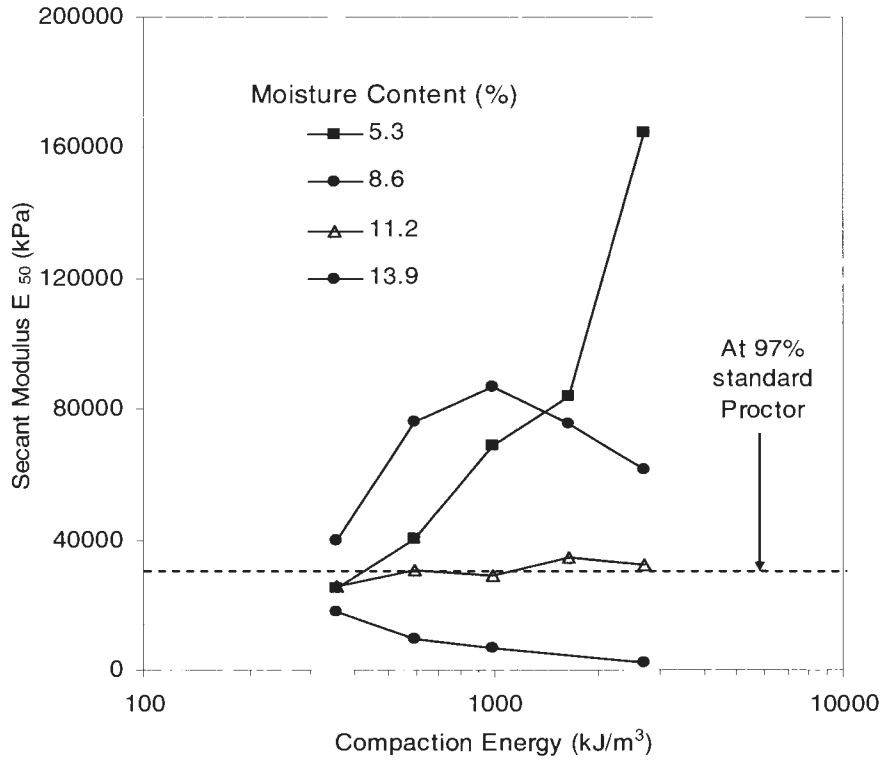

Figure 57. Semi-logarithmic relationship between secant modulus and compaction energy as a function of moisture content (Edwards till – m_{opt} = 12%)

Moisture Content, Compaction Energy, and Relative Strength/Stiffness

Similar to Figure 41 - Figure 47, moisture content is plotted against compaction energy at different percentages of the undrained shear strength and secant modulus at standard Proctor optimum (see Figure 58-Figure 67). While these curves are not as defined as those in Figure 41 - Figure 47, the same concepts can be applied in observations. Comparatively between moisture contents, the relative strength to standard Proctor is lowest generally at the wet moisture contents. Compaction efficiency, in terms of attaining strength, is low at wet conditions. Strengths below 100% standard Proctor strength are also at lower compaction energies that are not necessarily at high saturated conditions. However, as opposed to the wet specimens, an increase in energy applied to the drier specimens allowed for strengths

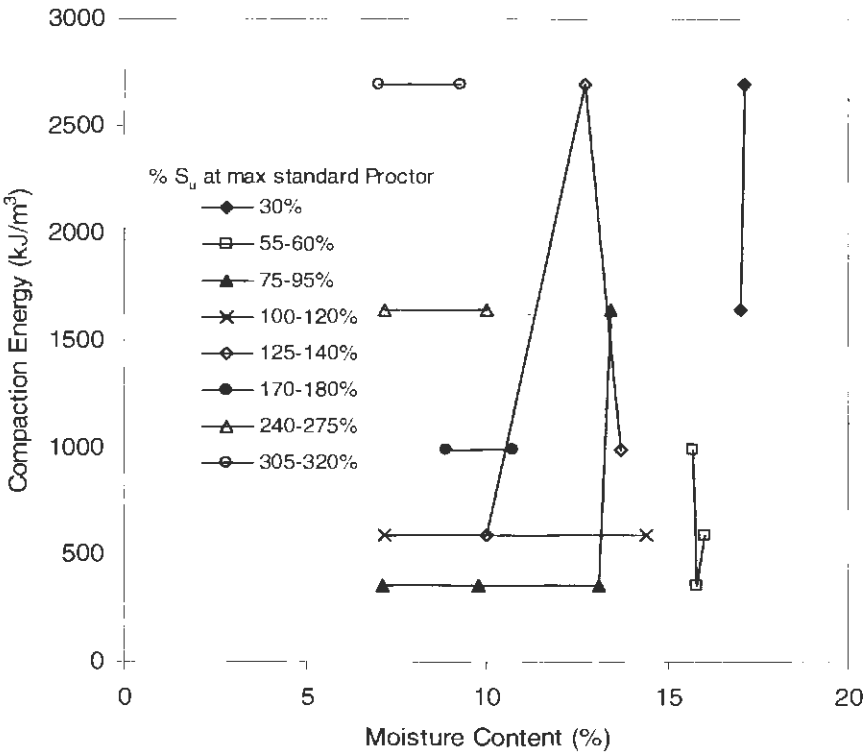

Figure 58. Energy as a function of moisture content for various degrees of undrained shear strength at standard Proctor (Central Iowa till)

exceeding 100% standard Proctor. Efficiency can again be assessed by comparing compaction energies within individual relative strength curves. However, caution should be used in making conclusions during these this observation, due to the percentage ranges used for the curves. In most cases for a given relative strength curve, the highest percentage of strength was attributed to the highest compaction energy applied. Regardless, a general observation in compaction efficiency can still be made within a given percentage of relative strength. Hence, the figures indicate energies achieving relative strengths that are close to strengths achieved at higher energies, which implies greater efficiency in compaction. Observations given for the strength curves are also true for the secant modulus curves. The secant modulus curves less defined than the strength curves, indicating higher variability.

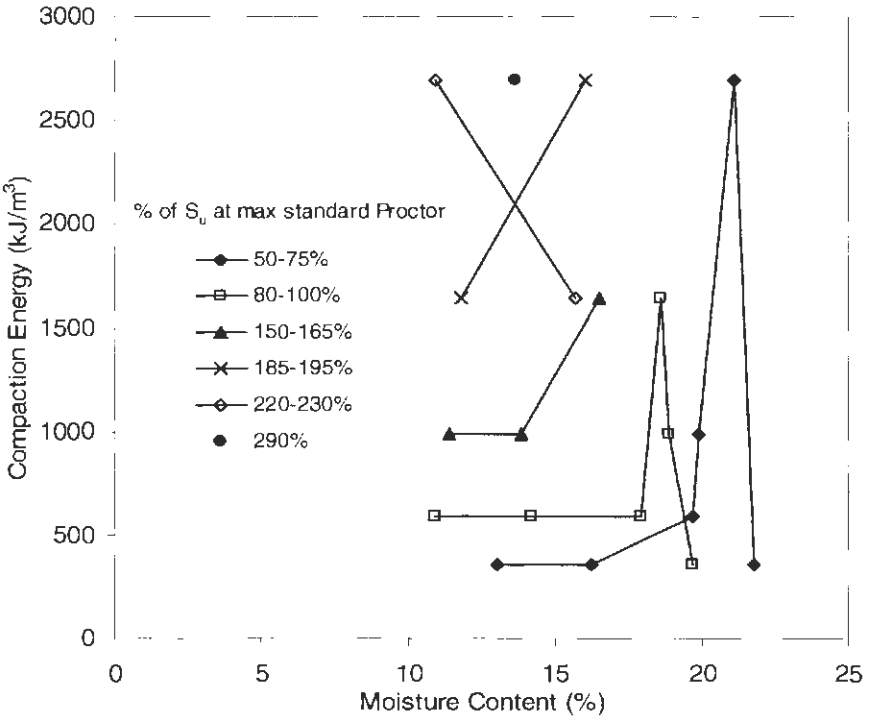

Figure 59. Energy as a function of moisture content for various degrees of undrained shear strength at standard Proctor (weathered shale)

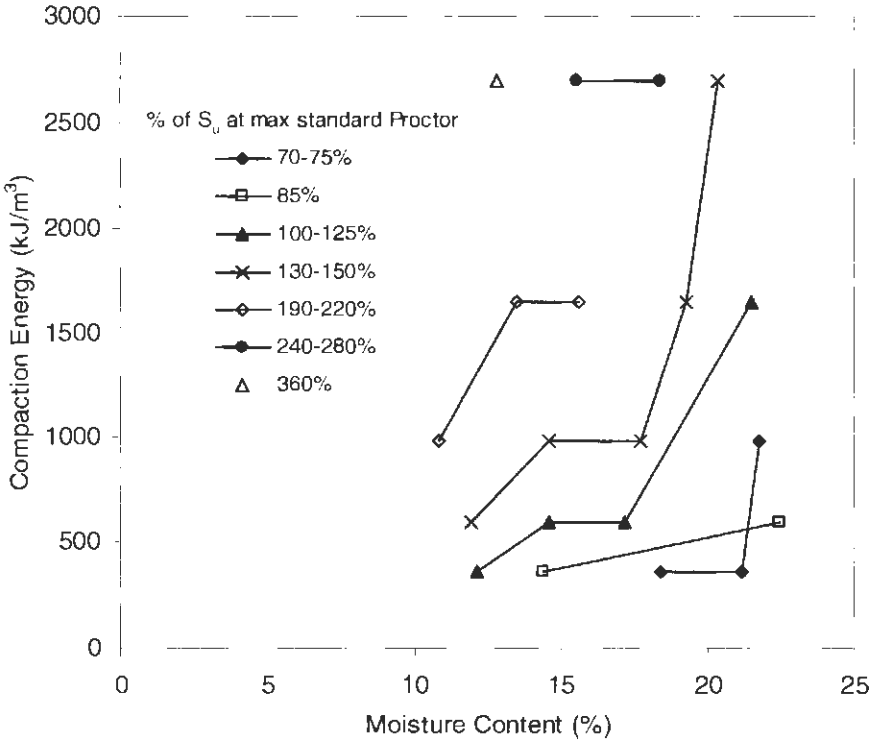

Figure 60. Energy as a function of moisture content for various degrees of undrained shear strength at standard Proctor (Western Iowa loess)

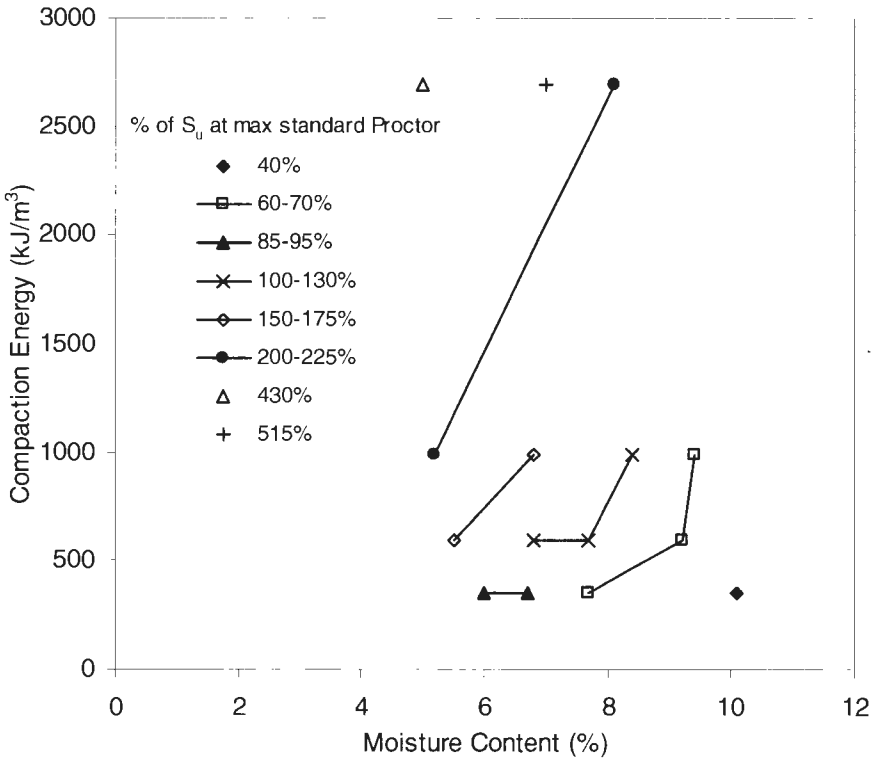

Figure 61. Energy as a function of moisture content for various degrees of undrained shear strength at standard Proctor (PPG till)

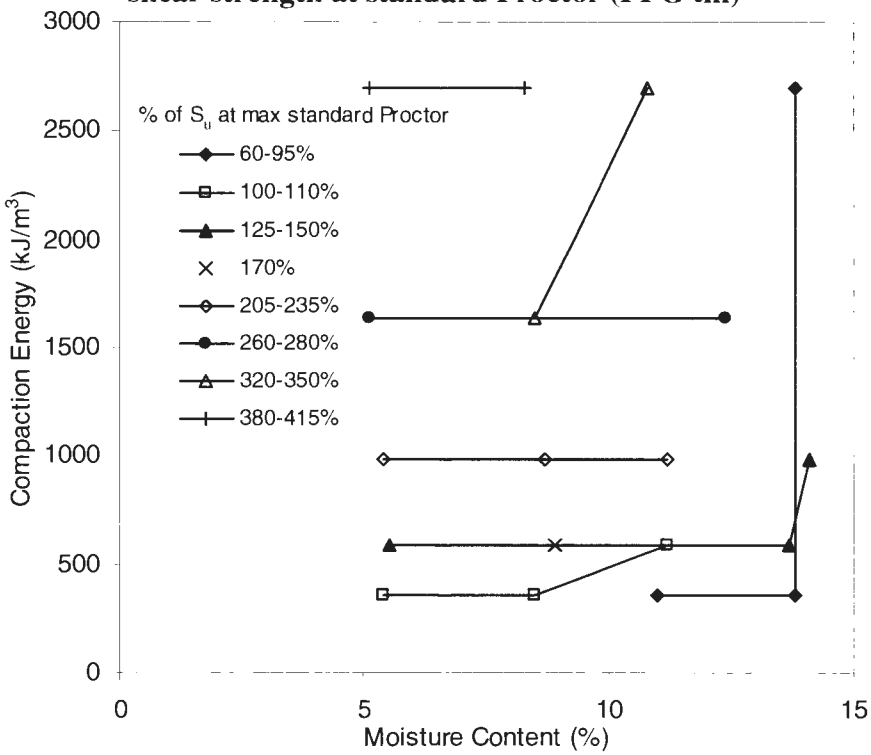

Figure 62. Energy as a function of moisture content for various degrees of undrained shear strength at standard Proctor (Edwards till)

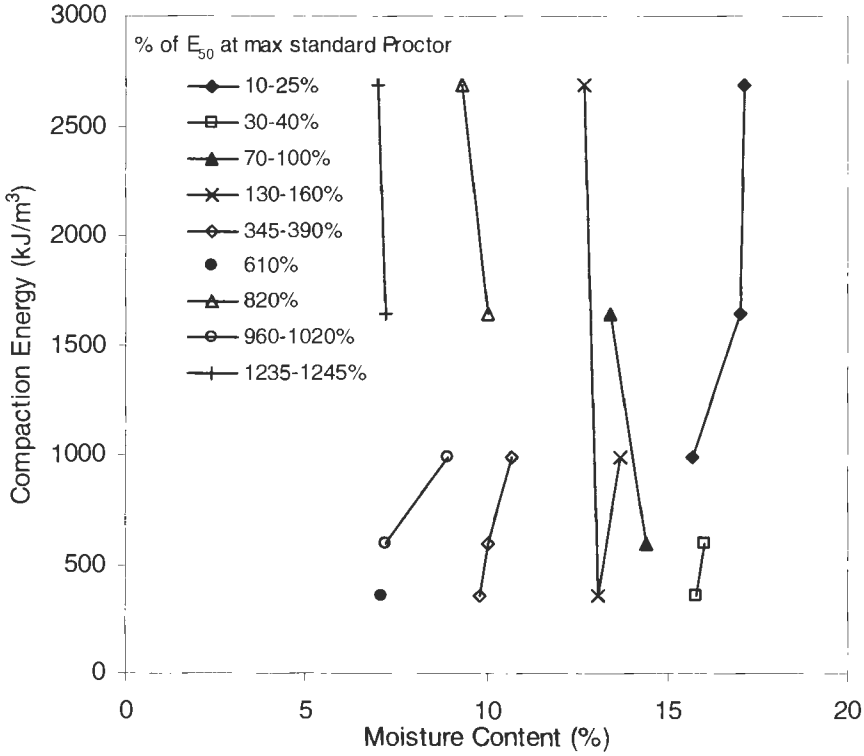

Figure 63. Energy as a function of moisture content for various degrees of secant modulus at standard Proctor (Central Iowa till)

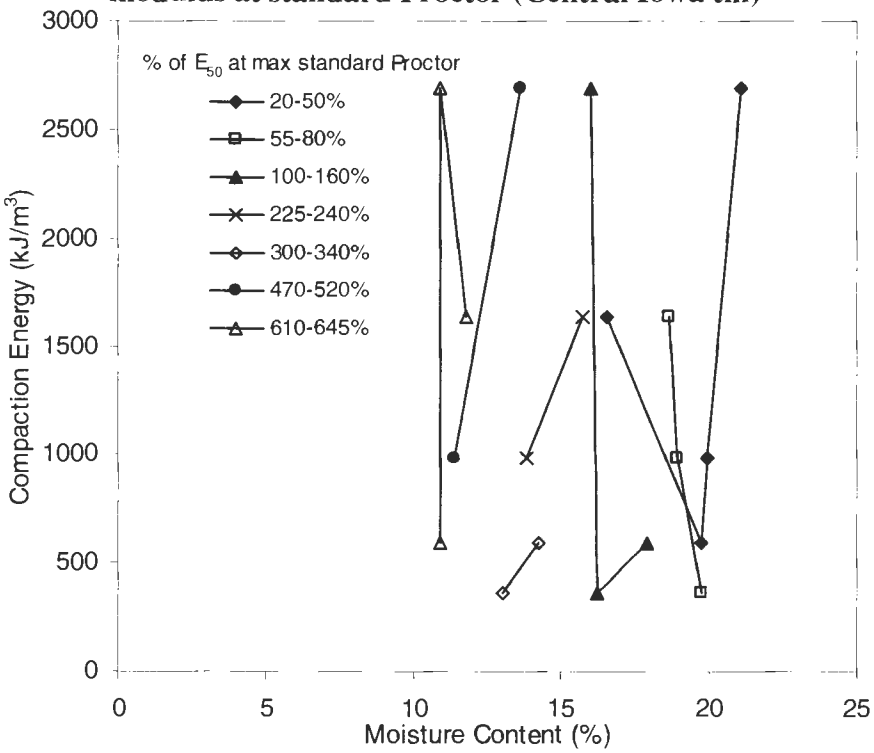

Figure 64. Energy as a function of moisture content for various degrees of secant modulus at standard Proctor (weathered shale)

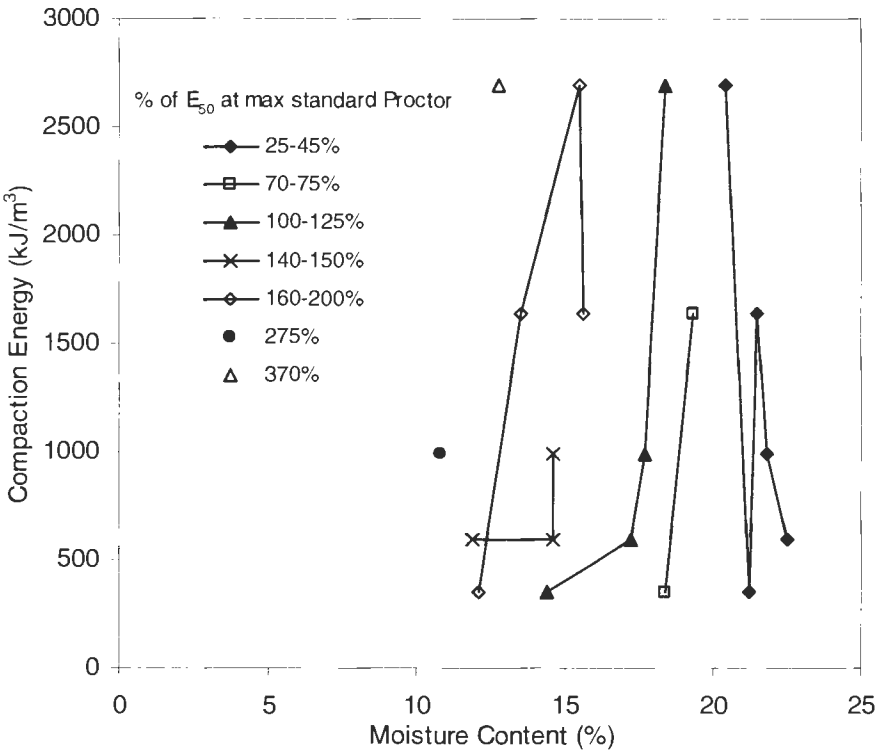

Figure 65. Energy as a function of moisture content for various degrees of secant modulus at standard Proctor (Western Iowa loess)

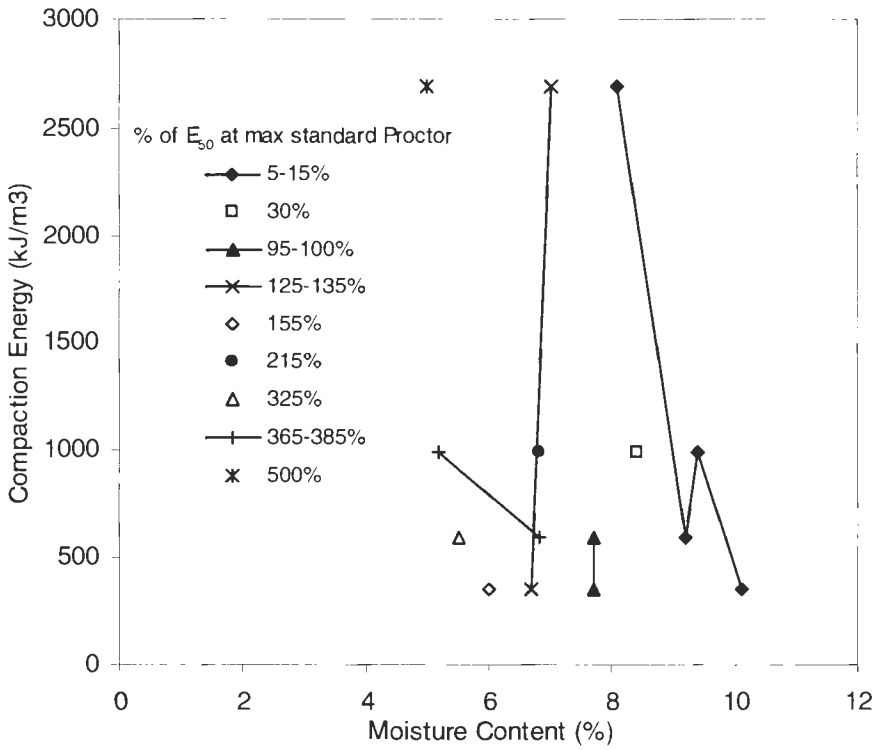

Figure 66. Energy as a function of moisture content for various degrees of secant modulus at standard Proctor (PPG till)

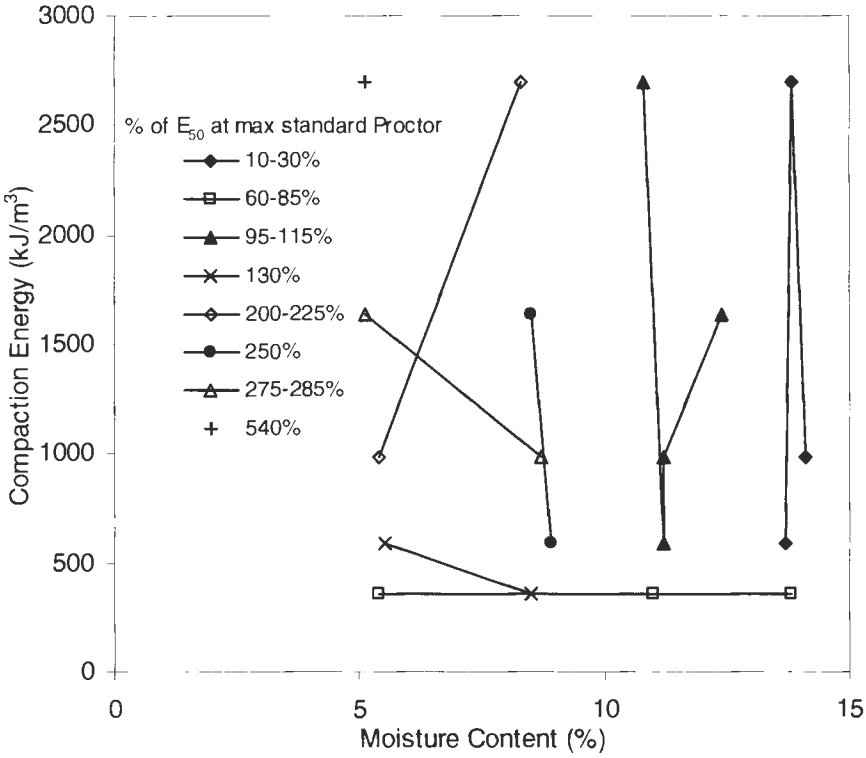

Figure 67. Energy as a function of moisture content for various degrees of secant modulus at standard Proctor (Edwards till)

Statistical Analyses of Unconfined Compression Tests

A multiple regression analysis was also performed for undrained shear strength (S_u) and secant modulus (E_{50}). Equations resulting from the multiple regression analysis are as follows:

$$Su_{till} = 168.0(LogE) - 20.7(m\%) - 104.7 \quad [3\text{-}24]$$

$$Su_{shale} = 173.0(LogE) - 12.1(m\%) - 161.4 \quad [3\text{-}25]$$

$$Su_{loess} = 115.1(LogE) - 6.9(m\%) - 138.0 \quad [3\text{-}26]$$

$$Su_{PPG} = 316.3(LogE) - 34.6(m\%) - 507.0 \quad [3\text{-}27]$$

$$Su_{Edwards} = 327.6(LogE) - 16.0(m\%) - 580.7 \quad [3\text{-}28]$$

$$E_{50(till)} = 21{,}736.1(LogE) - 7311.7(m\%) - 49{,}221.0 \quad [3\text{-}29]$$

$$E_{50(shale)} = 2497.7(LogE) - 5650.7(m\%) - 106{,}675.5 \quad [3\text{-}30]$$

$$E_{50(loess)} = 8739.3(LogE) - 1991.1(m\%) - 19{,}482.6 \quad [3\text{-}31]$$

$$E_{50(PPG)} = 3054.7(LogE) - 12{,}140.8(m\%) - 102{,}512.2 \quad [3\text{-}32]$$

$$E_{50(Edwards)} = 40{,}902.4(LogE) - 8124.9(m\%) - 3579.7 \quad [3\text{-}33]$$

Adjusted r^2 values for the undrained shear strength models ranged between 0.65 and 0.81 while, secant modulus r^2 values were between 0.54 and 0.84. Table 10 and Table 11 give a summary of the other statistical parameters.

Table 10. Statistical analysis on undrained shear strength for laboratory soils

Equation	Soil	n	Adjusted r^2	Standard Error of Estimate	Standard Deviation	F-Statistic	t-statistics
3-24	Till	20	0.72	54.1	101.5	25.0	OK
3-25	Shale	20	0.65	53.1	89.5	18.5	OK
3-26	Loess	20	0.81	20.1	46.2	41.6	OK
3-27	PPG	16	0.75	68.0	135.2	21.7	OK
3-28	Edwards	19	0.74	69.0	134.7	26.3	OK

All standard errors were less than their standard deviation. Therefore, regression models could be used in estimation. F-statistic values of the soils were checked at $\alpha = 0.05$ rejected the null hypothesis of $\beta = 0$. The t-statistics for undrained strength were outside the Student's t distribution curve and considered good predictors, with energy being the stronger predictor in four of the five soils. Moisture content was the stronger predictor for all secant modulus models. For shale and PPG till, compaction energy t-statistics did not meet passing criteria on the Student's t distribution curve.

Table 11. Statistical analysis on secant modulus for laboratory soils

Equation	Soil	n	Adjusted r^2	Standard Error of Estimate	Standard Deviation	F-Statistic	t-statistics
3-29	Till	20	0.83	11,775.4	28,556.4	47.3	OK
3-30	Shale	20	0.84	8799.8	21,681.3	49.2	NG (E-0.4)
3-31	Loess	20	0.76	4196.7	8511.6	30.6	OK
3-32	PPG	16	0.71	11,810.0	21,912.5	18.1	NG(E-0.4)
3-33	Edwards	19	0.54	26,388.2	38,727.9	11.4	OK

Table 12 gives the percent variability explained by variables energy applied and moisture content. Aside from the Iowa till, energy explained more of the variability in undrained strength than moisture. In contrast, moisture explained more of the variability in secant modulus, affirming comments made earlier of the t-statistics. Percent variability was determined by squaring individual Pearson correlations (R values) between dependent and independent variables.

Table 12. Percent variability explained by variables regarding strength and stiffness

	Undrained Shear Strength (Su)		Secant Modulus (E_{50})	
Soil	Log E (% explained)	Moisture (% explained)	Log E (% explained)	Moisture (% explained)
Till	24	49	4	79
Shale	47	34	4	85
Loess	53	23	6	68
PPG	63	27	3	75
Edwards	62	17	13	47

Sensitivity of Strength and Stiffness

The coefficients from equations 3-24 through 3-33 were investigated for relationships with Atterberg limits and fines content. As mentioned prior in this report, the coefficient is an indication of the sensitivity to the independent variables; in this case compaction energy and moisture content. As the slope coefficient increases, the sensitivity to compaction energy or

moisture content increases. Figure 68 to Figure 70 present the relationships of the index properties with the coefficients for undrained shear strength. Sensitivity in secant modulus is presented Figure 71 to Figure 73.

For undrained shear strength, sensitivity to moisture content correlates well with liquid and plastic limit with r^2 values of 0.71 and 0.82. Also there is moderate correlation between plastic limit and compaction energy coefficients ($r^2 = 0.53$). Plasticity index has fair correlation with the coefficient of compaction energy ($r^2 = 0.29$). For fines content parameters, percent passing the No. 200 sieve explains sensitivity to moisture content ($r^2 = 0.85$) and compaction energy ($r^2 = 0.39$).

For secant modulus, the best correlations were observed in regard to moisture content. Plastic limit and percent passing No. 200 sieve had good correlations with moisture content coefficients. Moderate correlation was seen between liquid limit and moisture content. Plasticity index gave the only noteworthy result relating to the coefficient of compaction energy ($r^2 = 0.38$).

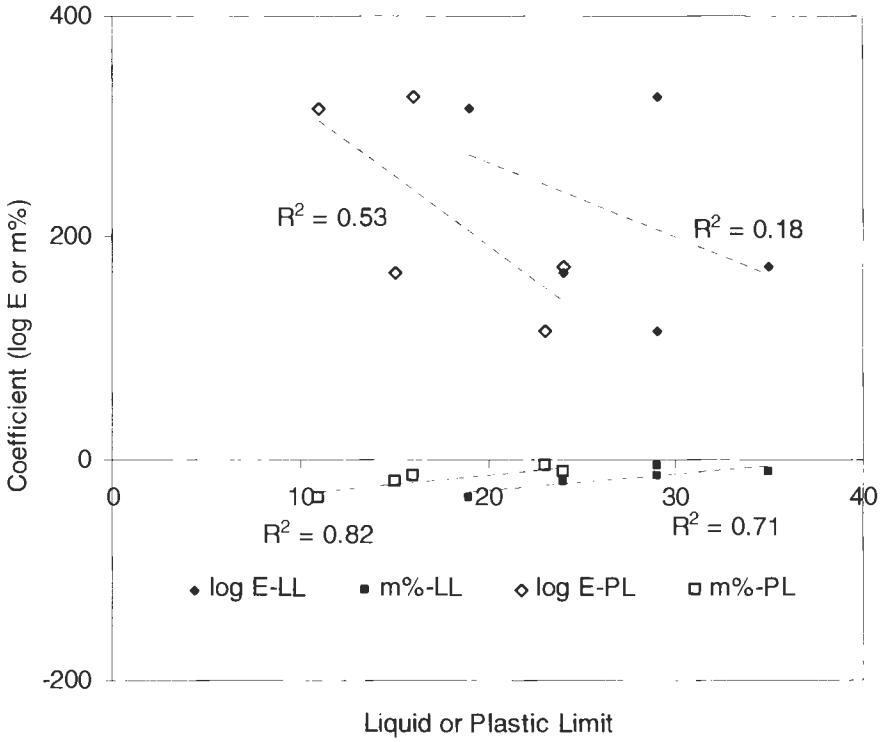

Figure 68. Relationships of Atterberg limits with compaction energy and moisture content coefficients for Midwest soils (undrained shear strength)

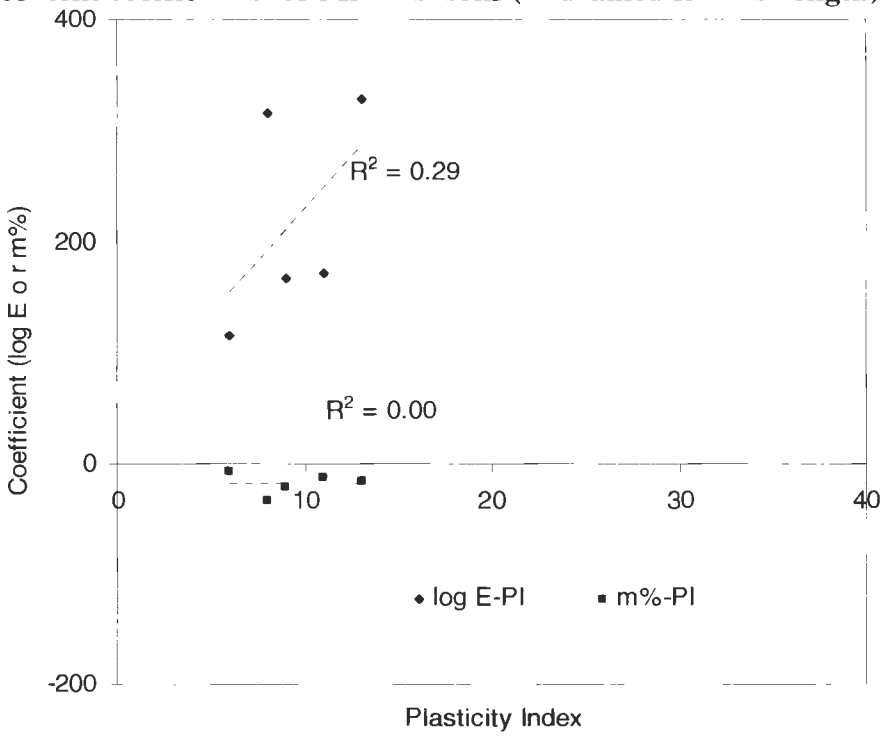

Figure 69. Relationships of plasticity index with compaction energy and moisture content coefficients for Midwest soils (undrained shear strength)

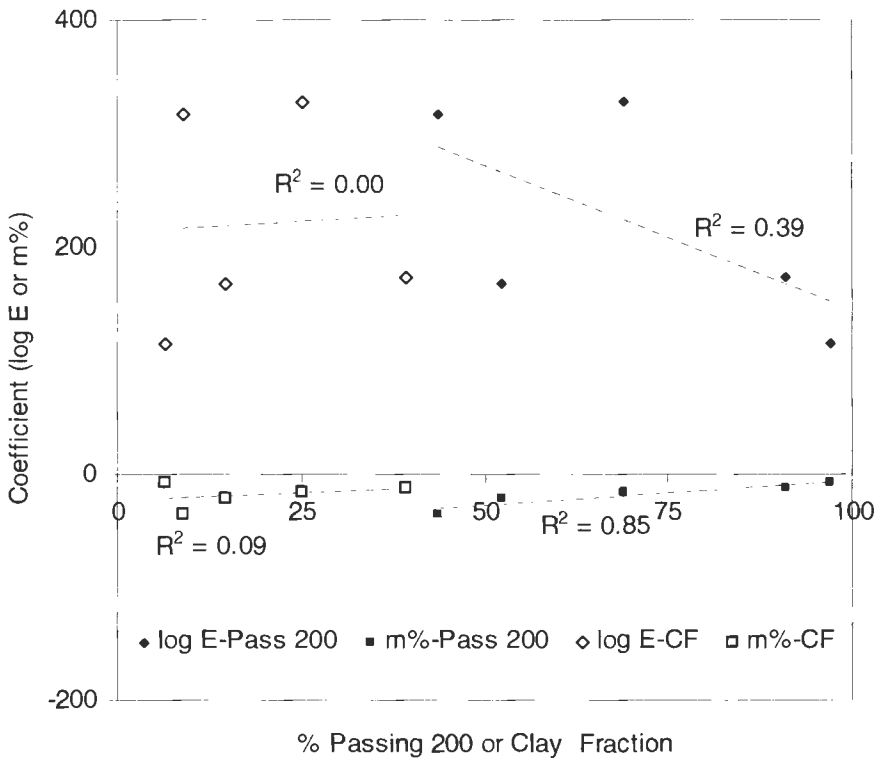

Figure 70. Relationships of fines content with compaction energy and moisture content coefficients for Midwest soils (undrained shear strength)

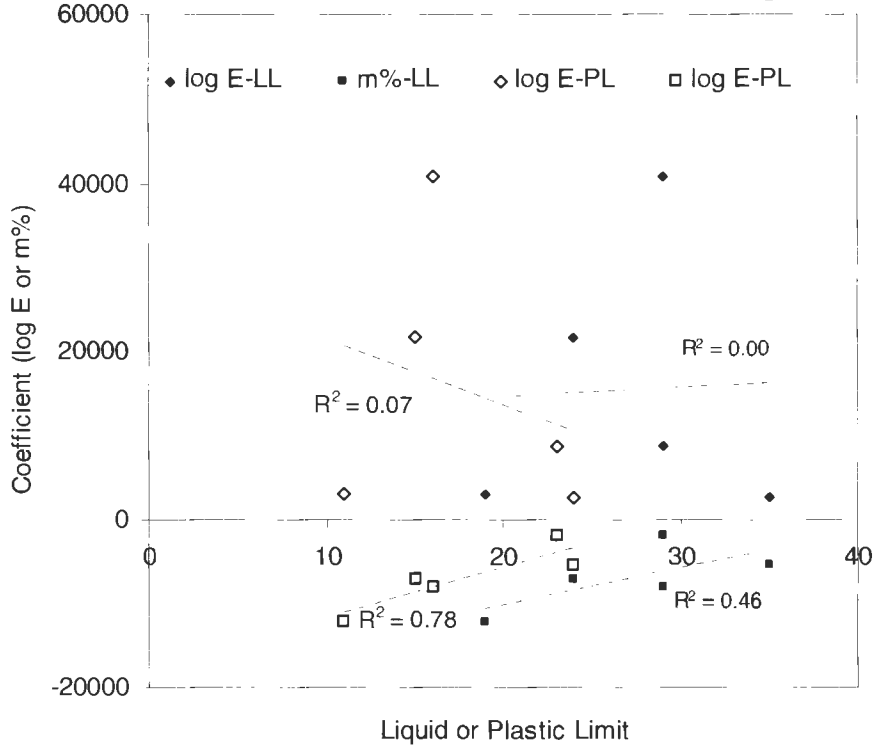

Figure 71. Relationships of Atterberg limits with compaction energy and moisture content coefficients for Midwest soils (secant modulus)

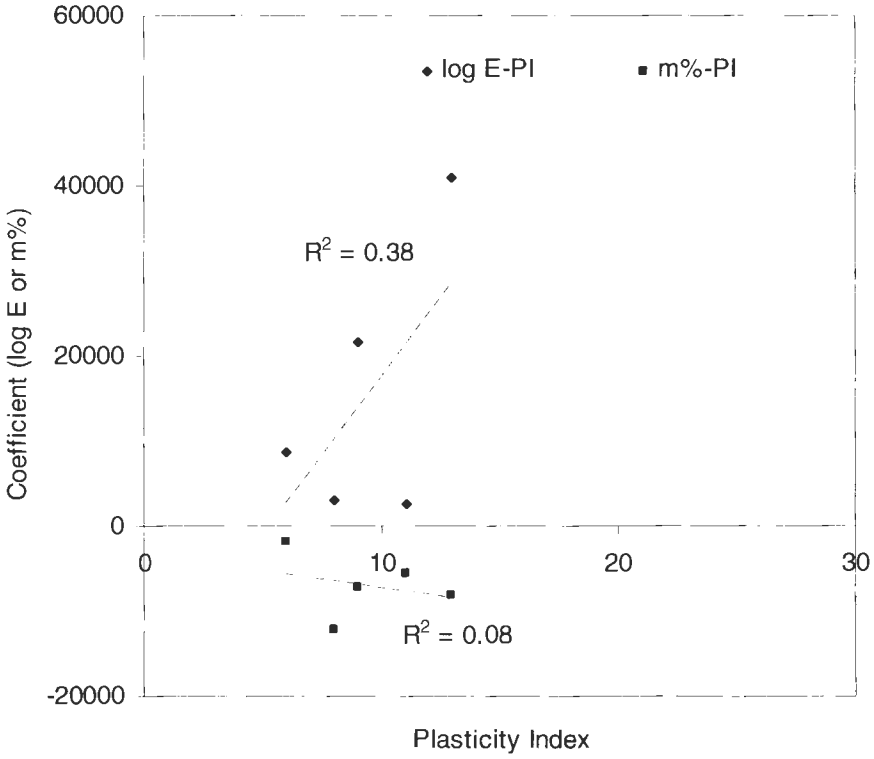

Figure 72. Relationships of plasticity index with compaction energy and moisture content coefficients for Midwest soils (secant modulus)

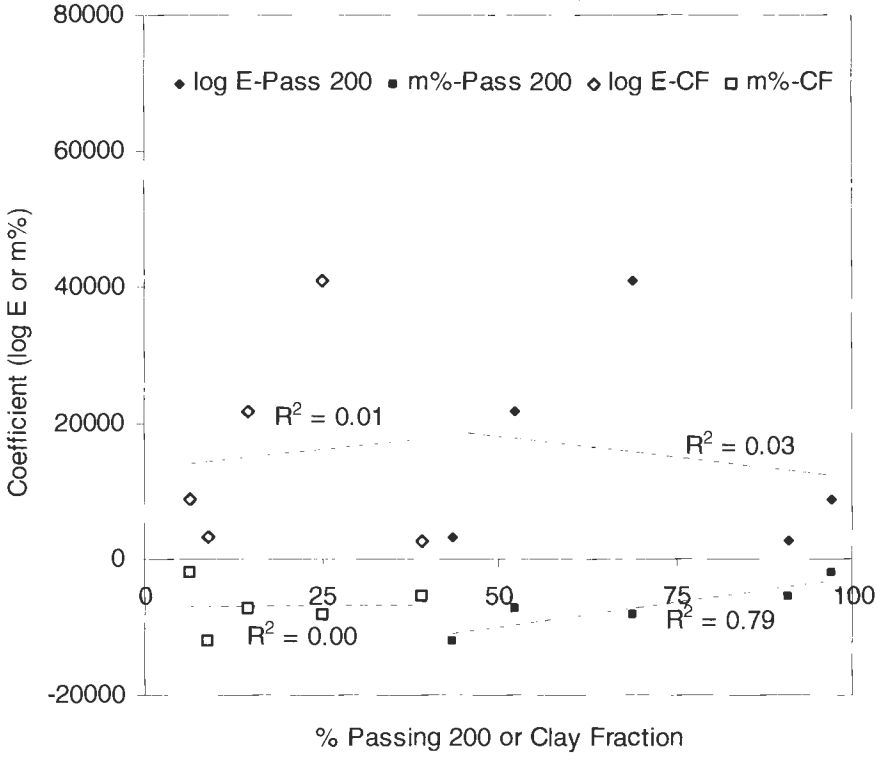

Figure 73. Relationships of fines content with compaction energy and moisture content coefficients for Midwest soils (secant modulus)

Statistical Analysis Using All Soil Data

All soil data was analyzed using the SPSS computer program. Empirical models for estimation were formulated from the analyses, similar to the previous models displayed. In addition to energy and moisture, index properties were inputted to determine potential improvement in estimating dependent variables. It shall be noted that index properties were taken at a fixed value from lab determination. Therefore, the assumption was made that these properties did not vary between lab specimens of the same soil. Also, the number of combinations used in deriving the equations in not exhaustive by any means. The following set of equations was determined for dry unit weight of Proctor compaction tests:

$$DD = 1.18(LogE) - 0.23(m\%) + 17.5 \quad [3\text{-}34]$$

$$DD = 2.47(LogE) - 10.0(LogLL) + 25.3 \quad [3\text{-}35]$$

$$DD = 1.58(LogE) - 0.20(m\%) - 5.5(LogLL) + 23.9 \quad [3\text{-}36]$$

$$DD = 1.98(LogE) - 0.10(m\%) - 0.05(Pass200) + 17.2 \quad [3\text{-}37]$$

$$DD = 2.53(LogE) - 1.52(LogLL) - 0.06(Pass200) + 17.2 \quad [3\text{-}38]$$

$$DD = 2.54(LogE) + 0.31(LogPI) - 0.07(Pass200) + 15.2 \quad [3\text{-}39]$$

$$DD = 2.53(LogE) - 0.07(Pass200) + 15.51 \quad [3\text{-}40]$$

$$DD = 2.48(LogE) - 17.2(LogLL) + 0.10(CF) + 33.5 \quad [3\text{-}41]$$

$$DD = 2.2(LogE) - 0.06(m\%) - 15.3(LogLL) + 0.06(CF) + 3.5(LogPI) + 30.0 \quad [3\text{-}42]$$

where, LL is liquid limit, PI is plasticity index, Pass 200 is percentage passing the No. 200 sieve, and CF is clay fraction.

Table 13 gives a summary of the statistical results from each dry unit weight model. Adjusted r^2 values as high as 0.90 (Eq. 3-42) were attained. However, some of the high values were attributed to collinearity between independent variables. The highest collinearity occurred between plasticity values and fines content. Variance inflation factor (VIF) was 3.6 for LL and Pass200 in equation 3-38. VIF was especially high for equation 3-42 which involved many independent variables. Other equations with slight collinearity were 3-36 and 3-37, where moisture interacted with plasticity and fine content values. The strongest predictor variable changed from equation to equation and is indicated in the table. Fines content passing the No. 200 seemed to dominate most equations, explaining 58% of the variability in dry unit weight (Eq. 3-37 through 3-40). The standard deviation for dry unit weight of all soils was 1.83 kN/m^3. Plots showing individual correlations for all lab dry unit weights are given in Appendix C.

Table 13. Statistical analysis on dry unit weight for 7 soil types

Equation	n	Adjusted r^2	Standard Error of Estimate	F-Statistic	t-statistics (<-2 or >+2)	Strongest Predictor
3-34	176	0.65	1.08	164.3	OK	m%
3-35	176	0.64	1.09	159.0	OK	Log LL
3-36	176	0.74	0.94	164.8	OK	m%
3-37	176	0.82	0.77	274.0	OK	Pass200
3-38	176	0.78	0.86	206.6	NG (LL-1.57)	Pass 200
3-39	176	0.78	0.87	203.6	NG (PI-0.49)	Pass 200
3-40	176	0.78	0.87	306.1	OK	Pass 200
3-41	176	0.84	0.73	313.1	OK	Log LL
3-42	176	0.90	0.59	307.3	OK	Log LL

Comparison with Other Authors

The maximum dry unit weight of a soil can be estimated using the relationship between logarithm of energy, liquid limit and maximum dry unit weight (Boltz et al., 1998). Table 14 displays the results of predicting modified maximum dry unit weight using Equation 1-10 from the literature. The equation yielded predicted values between -0.32 and 0.43 kN/m^3 from the observed lab results of modified maximum dry unit weight. The average error computed of 0.14 kN/m^3 and standard deviation of 0.27 kN/m^3 was reasonable when compared to work performed on soil by Boltz et al. (Table 15).

The average error was determined by averaging the differences calculated between the actual lab results and predicted values of modified dry unit weight. The standard deviation was the computed standard deviation of the differences between actual lab results and predicted values of modified dry unit weight.

Table 14. Estimating maximum dry unit weight based on logarithm energy-liquid limit relationship *

Soil	Liquid Limit	Standard Proctor (kN/m^3)	Predicted Modified (kN/m^3)	Actual Modified (kN/m^3)	Actual - Predicted (Error in kN/m^3)
C. Iowa Till	24	18.35	19.35	20.03	0.24
Shale	35	17.55	19.24	19.33	0.09
Loess	29	15.87	17.44	17.32	-0.12
PPG Till	19	21.01	22.30	21.98	-0.32
Edwards Till	29	18.76	20.33	20.64	0.31
WDM Clay1	42	16.23	18.04	18.47	0.43
WDM Clay2	49	15.55	17.46	17.78	0.32

* Equation used - $\gamma_{d\,max,\,E} = \gamma_{d\,max,\,k} + (2.27\,LL - 0.94) \log (E/E_k)$ (Boltz et al., 1998)

Table 15. Data results comparison with validation work performed in literature (validation results taken from Boltz et. al, 1998)

Validation	Average Error (kN/m^3)	Standard Deviation (kN/m^3)
Check A (22 soils-database)	-0.1	0.3
Check B (5 soils-lab tested)	-0.2	0.28
ISU Check (7 area soils)	0.14	0.27

Prediction equations for maximum dry unit weight summarized in the literature review were compared against equations derived from this study (Eq. 3-34, 3-39, 3-40, and linear rate compaction model). These model equations can be used for all dry unit weights and are not limited to estimating only maximum dry unit weight. Equations used from the literature include Equation 1-5 (Ring et al., 1961) and 1-10 (Boltz et al., 1998). Maximum dry unit weights for energies of 355, 987, 1643, and 2693 kJ/m^3 were estimated using equation 1-10. Equation 1-5 was limited to estimating maximum dry unit weights at 592 kJ/m^3. Equations from this study were used to estimate maximum dry unit weights at all energy levels and are separated out for clarity in the figures (see Figure 74 to Figure 76). Good correlations are observed for all prediction models (r^2 = 0.76-0.99). The regression equations were lower than the compaction model and Boltz et al. (1998) because they had been created from all soil dry unit weight data and were not limited to optimal conditions for derivation. The compaction model was high since only optimal conditions were estimated for the analysis.

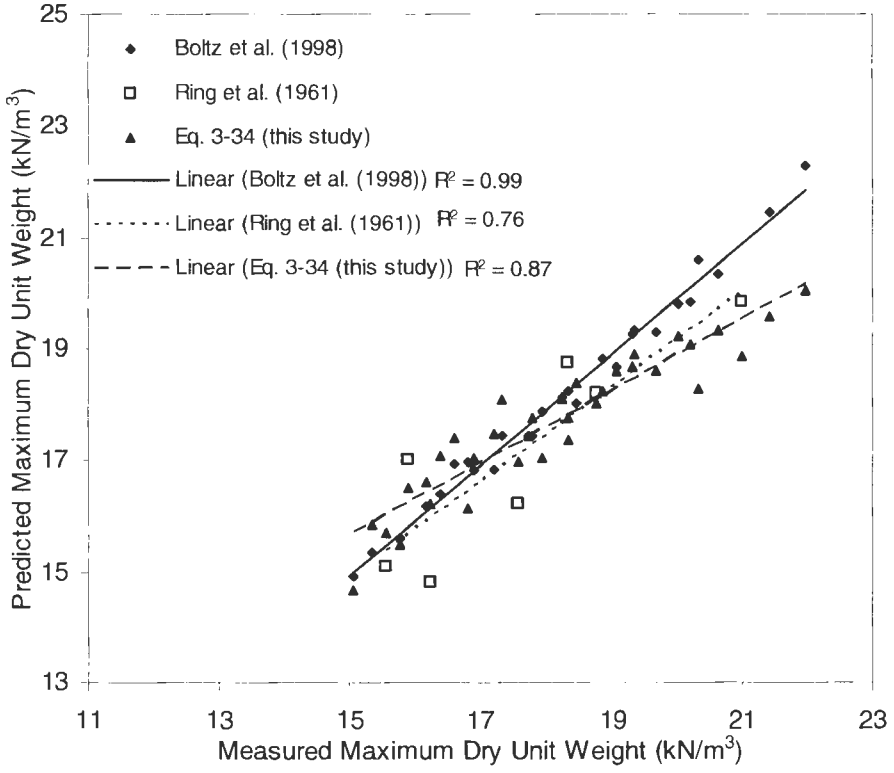

Figure 74. Predicted versus measured maximum dry unit weights for all soils (past authors and Eq. 3-34)

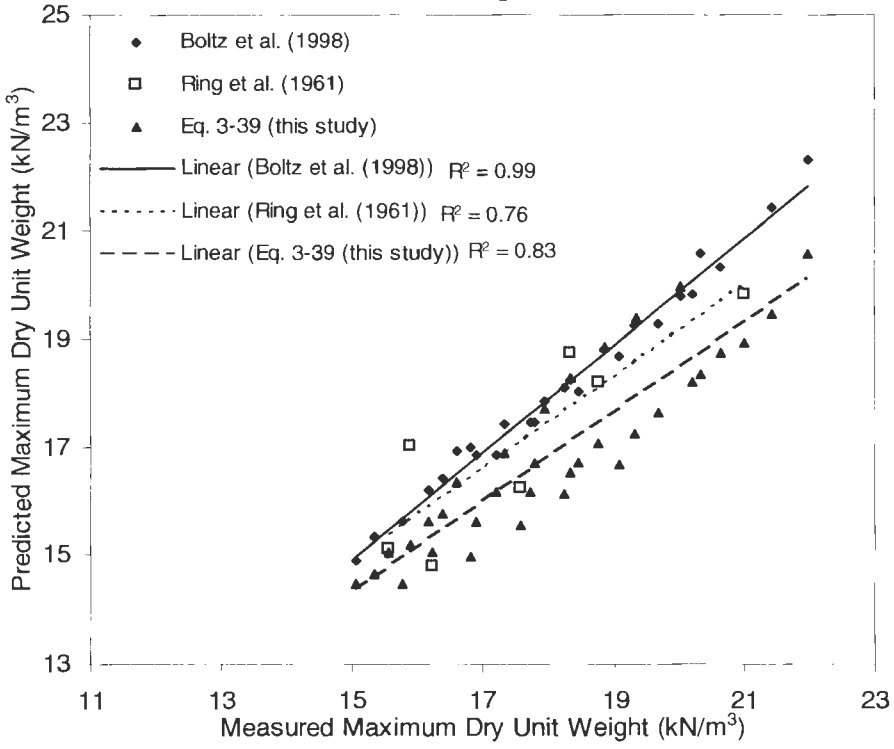

Figure 75. Predicted versus measured maximum dry unit weights for all soils (past authors and Eq. 3-39)

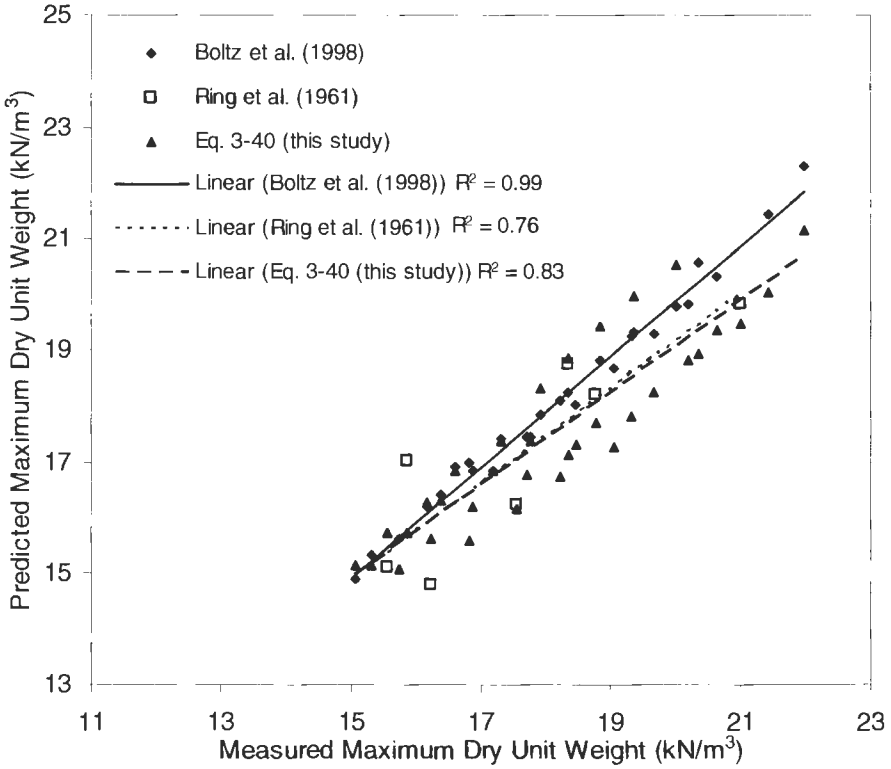

Figure 76. Predicted versus measured maximum dry unit weights for all soils (past authors and Eq. 3-40)

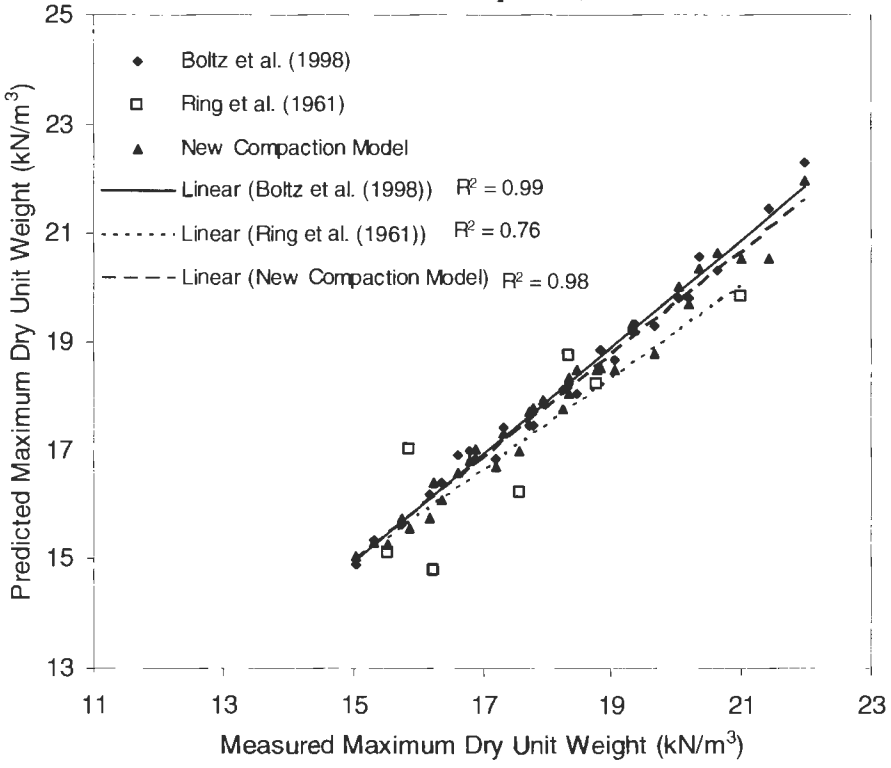

Figure 77. Predicted versus measured maximum dry unit weights for all soils (past authors and new compaction model)

Strength and Stiffness

Plotting data from strength and stiffness data as a function of saturation and normalized moisture content yielded moderate to good correlation (Figure 78 through Figure 80). These figures demonstrate the significance that moisture has on strength and stability. The best regressions attained were from an exponential relationship between moisture content and the various soil engineering properties. Secant modulus is observed as being greatly influenced by normalized moisture and percent saturation. The influence of these variables was investigated for strength and stiffness models. Other plots created to investigate undrained strength and stiffness correlations are displayed in Appendix C.

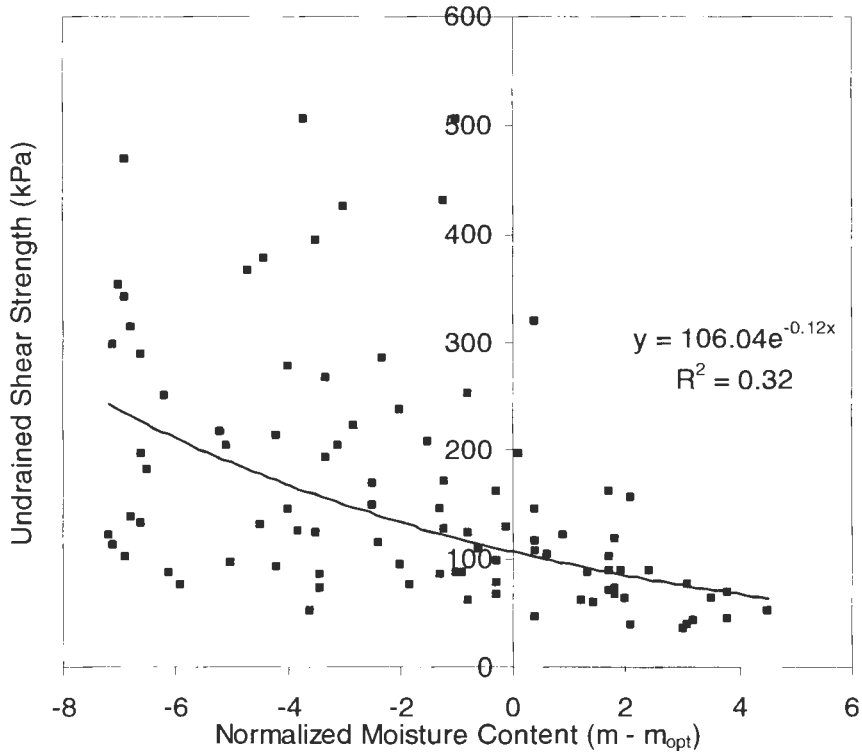

Figure 78. Undrained shear strength as a function of normalized moisture for all soils

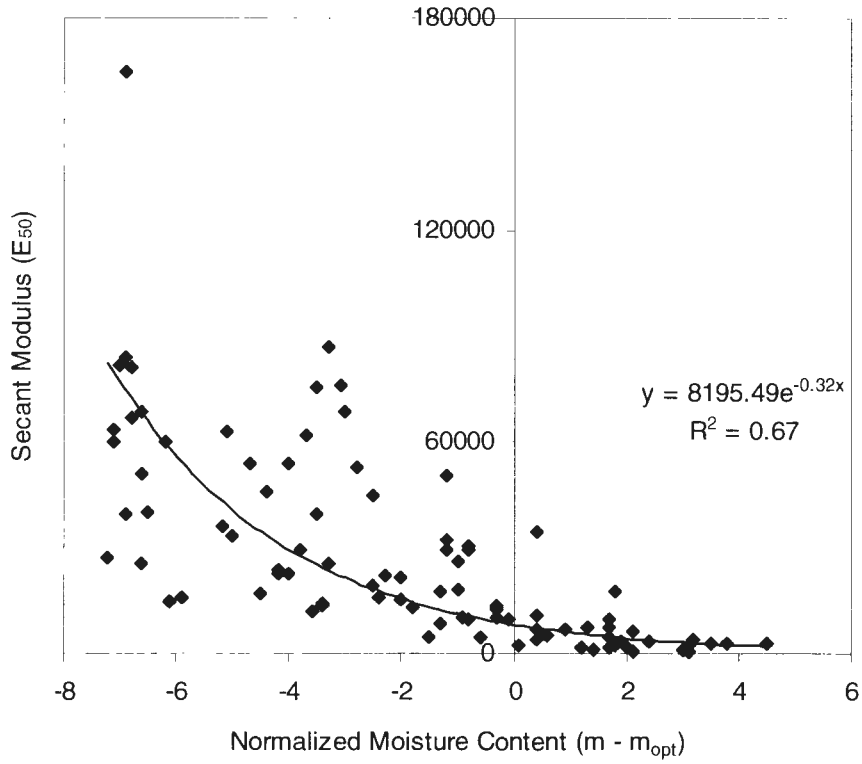

Figure 79. Secant modulus as a function of normalized moisture content for all soils

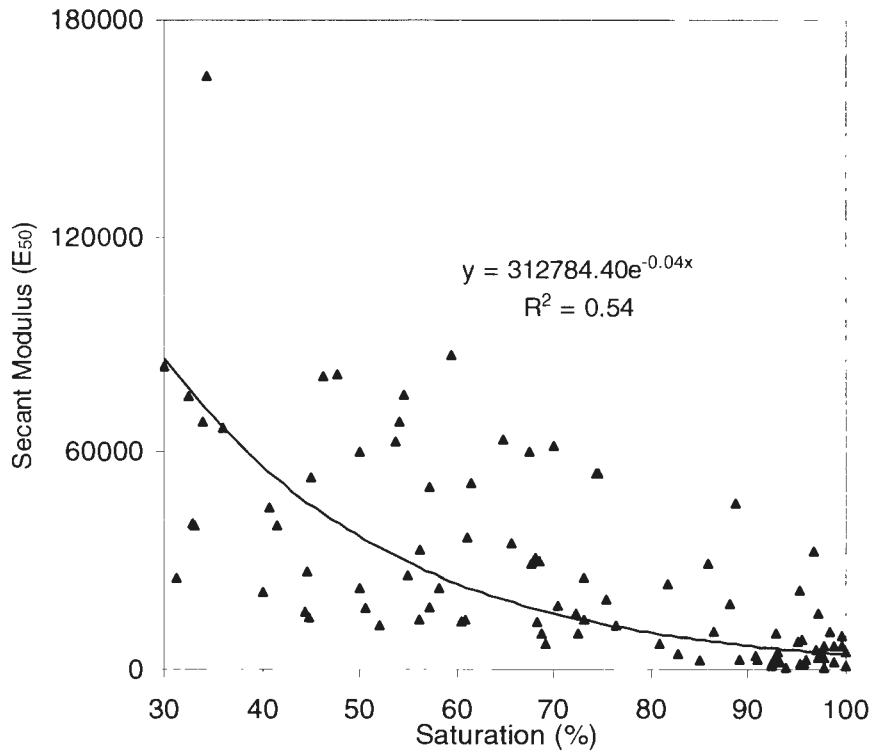

Figure 80. Secant modulus as a function of saturation for all soils

Undrained shear strength equations included the following:

$$Su = 225.0(LogE) - 12.1(m\%) - 356.1 \quad [3\text{-}43]$$

$$Su = 218.2(LogE) - 17.0(m\%) + 500.8(LogLL) - 991.9 \quad [3\text{-}44]$$

$$Su = 223.1(LogE) - 10.5(m\%) + 273.3(LogPI) - 633.4 \quad [3\text{-}45]$$

$$Su = 220.8(LogE) - 15.9(m\%) + 1.3(Pass200) - 390.4 \quad [3\text{-}46]$$

$$Su = 221.8(LogE) - 13.3(m\%) + 2.7(CF) - 384.0 \quad [3\text{-}47]$$

$$Su = 256.4(LogE) - 2.1(S\%) - 452.0 \quad [3\text{-}48]$$

$$Su = 210.1(LogE) - 15.7(nm\%) - 492.3 \quad [3\text{-}49]$$

The logarithm of energy yielded higher values than compaction energy alone. Therefore, Log E was used in the listed equations. Table 16 summarizes remaining statistical results from the strength equations. Adjusted r^2 values ranged from 0.49 to 0.70. Again, some of the higher values were to be approached with caution due to varying degree of collinearity between independent variables. Equations 3-43 and 3-46 were slightly collinear between moisture content, liquid limit, and fines content. The strongest predictor variable that dominated for strength was compaction energy.

Table 16. Statistical analysis on undrained shear strength for 5 soil types

Equation	n	Adjusted r^2	Standard Error of Estimate	F-Statistic	t – statistics (< -2 or >+2)	Strongest Predictor
3-43	95	0.60	72.0	70.2	OK	Log E
3-44	95	0.70	62.7	71.6	OK	m%,LogE
3-45	95	0.67	65.2	64.7	OK	LogE
3-46	95	0.63	69.4	52.9	OK	Log E
3-47	95	0.68	64.5	66.2	OK	Log E
3-48	95	0.49	81.5	44.8	OK	Log E
3-49	95	0.53	77.5	54.3	OK	Log E

The next set of equations resulted from statistical analyses on secant modulus:

$$E_{50} = 21{,}547.9(\text{LogE}) - 3723.3(\text{m\%}) - 9510.3 \quad [3\text{-}50]$$

$$E_{50} = 19{,}281.1(\text{LogE}) - 5326.5(\text{m\%}) + 167{,}439.4(\text{LogLL}) - 203{,}068 \quad [3\text{-}51]$$

$$E_{50} = 21{,}187.9(\text{LogE}) - 3406.3(\text{m\%}) + 51{,}144.2(\text{LogPI}) - 42{,}400.9 \quad [3\text{-}52]$$

$$E_{50} = 19{,}596.0(\text{LogE}) - 5469.1(\text{m\%}) + 607.8(\text{Pass200}) - 6462.0 \quad [3\text{-}53]$$

$$E_{50} = 20{,}798.8(\text{LogE}) - 3977.8(\text{m\%}) + 608.7(\text{CF}) - 3184.2 \quad [3\text{-}54]$$

$$E_{50} = 37{,}375.6(\text{LogE}) - 978.4(\text{S\%}) - 14{,}102.2 \quad [3\text{-}55]$$

$$E_{50} = 16{,}389.1(\text{LogE}) - 6033.5(\text{nm\%}) - 32{,}565.4 \quad [3\text{-}56]$$

Adjusted r^2 values for secant modulus models ranged from 0.44 to 0.62. Slight collinearity occurred in equation 3-51 and 3-53. The reason why less collinearity occurred in the strength and stiffness models was due to less independent variable inputs. The strongest predictor variable that dominated for secant modulus was moisture content. Saturation and normalized

moisture content slightly improved the prediction models in replacing moisture content. The two parameters explained 43% and 50%

Table 17. Statistical analysis on secant modulus for 5 soil types

Equation	n	Adjusted r^2	Standard Error of Estimate	F-Statistic	t – statistics (< -2 or >+2)	Strongest Predictor
3-50	95	0.44	20,959	37.3	OK	m%
3-51	95	0.62	17,274	51.3	OK	m%
3-52	95	0.48	20,235	29.2	OK	m%
3-53	95	0.56	18,798	38.6	OK	m%
3-54	95	0.50	19,712	32.4	OK	m%
3-55	95	0.58	18,131	65.1	OK	S%
3-56	95	0.52	19,344	51.7	OK	nm%

The potential for better correlations was investigated with exponential, power, or other functions that did not exhibit a linear relation. These modifications to the variables yielded the following equations:

$$Su = 0.08(E) - 138.9(\text{Log } m\%) + 405.8 \quad [3\text{-}57]$$

$$\text{Log } Su = 3.85 \times 10^{-4}(E) - 0.17(nm\%) - 0.015(nm\%)^2 + 4.3 \quad [3\text{-}58]$$

$$E_{50} = 7.11(E) - 44{,}465.6(\text{Log } m\%) + 127{,}319.6 \quad [3\text{-}59]$$

$$\text{Log } E_{50} = 3.8 \times 10^{-4}(E) - 0.045(S\%) + 12.5 \quad [3\text{-}60]$$

$$\text{Log } E_{50} = 3.3 \times 10^{-5}(E) - 0.4(nm\%) - 0.002(nm\%)^2 + 9.1 \quad [3\text{-}61]$$

The additional models, 3-58 and 3-61, yielded higher r^2 values than their counterpart linear related models (3-49 and 3-56). It is interesting to note that none of the new models yielding highest correlations involved neither exponential nor power functions, but rather logarithm

Table 18. Additional statistical analysis on undrained shear and secant modulus

Equation	n	Adjusted r^2	Standard Error of Estimate	F-Statistic	t – statistics (< -2 or >+2)	Strongest Predictor
3-57	95	0.58	73.4	65.8	OK	E
3-58	95	0.60	0.42	47.9	OK	E
3-59	95	0.46	20,610.0	40.1	OK	Log m%
3-60	95	0.59	0.81	69.3	OK	S%
3-61	95	0.69	0.70	70.7	NG (0.38-E)	nm%

and polynomial. Three of the equations (3-58, 3-59, and 3-61) involved the logarithm of the dependent variable, but only one improved the correlation.

Table 19 presents statistical results of the dependent variable focused on in the analysis. The discrepancy in variability noted at the beginning of the paper can be observed in this table, particularly in stiffness.

Table 19. General statistical data for all lab soils

Parameter	Mean	Standard Deviation	COV (%)
Dry Unit Weight	18.2	1.7	9.2
Undrained Strength	161.5	113.6	70.3
Secant Modulus	26,878.2	27,966.3	104.0

Validity in Using Relative Compaction

As anticipated, percent standard Proctor increased with increasing compaction energy in the lab (Figure 81 and Figure 82). Observing the slight correlations in Figure 83 there appears to be credibility in reasoning higher relative compaction leads to greater undrained shear strength. However, the correlation shown is only fair ($r^2 = 0.23$). Further, the figure indicates that at a given relative compaction, a difference in strength as high as twelve fold

can occur. This difference occurs at 99% standard Proctor. The validity of using relative compaction in properly assessing stability remains questionable as demonstrated in Figure 84.

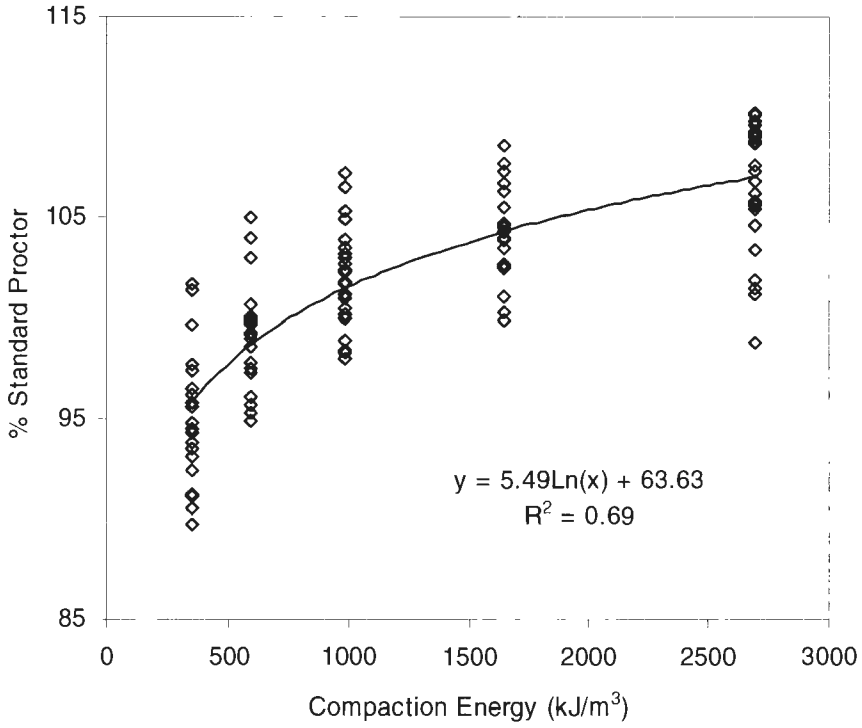

Figure 81. Percent standard Proctor vs compaction energy for Proctor compaction tests (all lab soils)

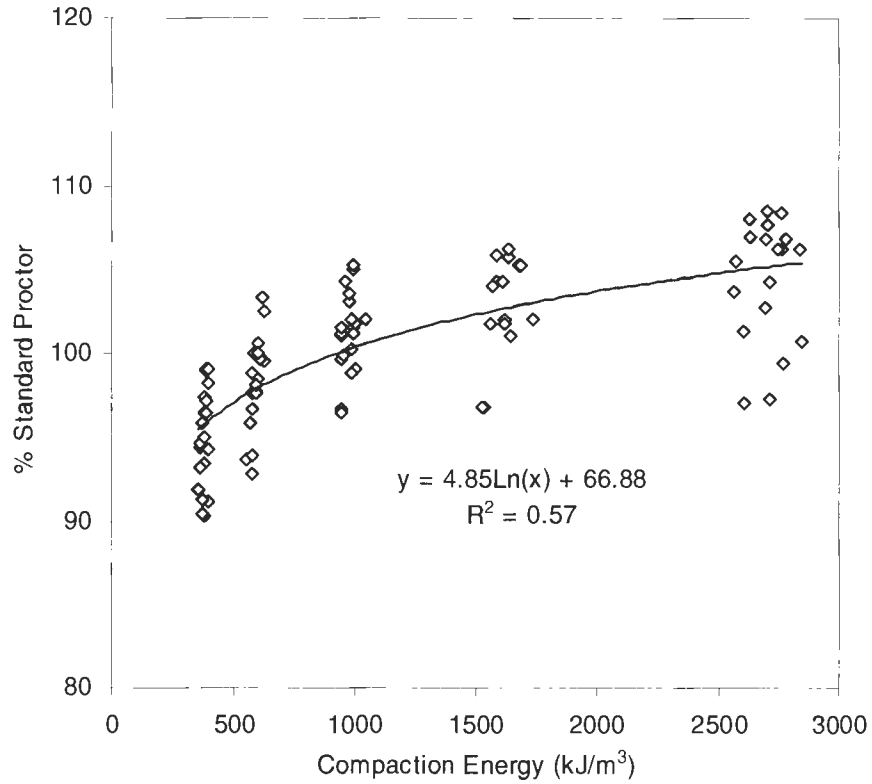

Figure 82. Percent standard Proctor vs compaction energy for unconfined compression tests (all lab soils)

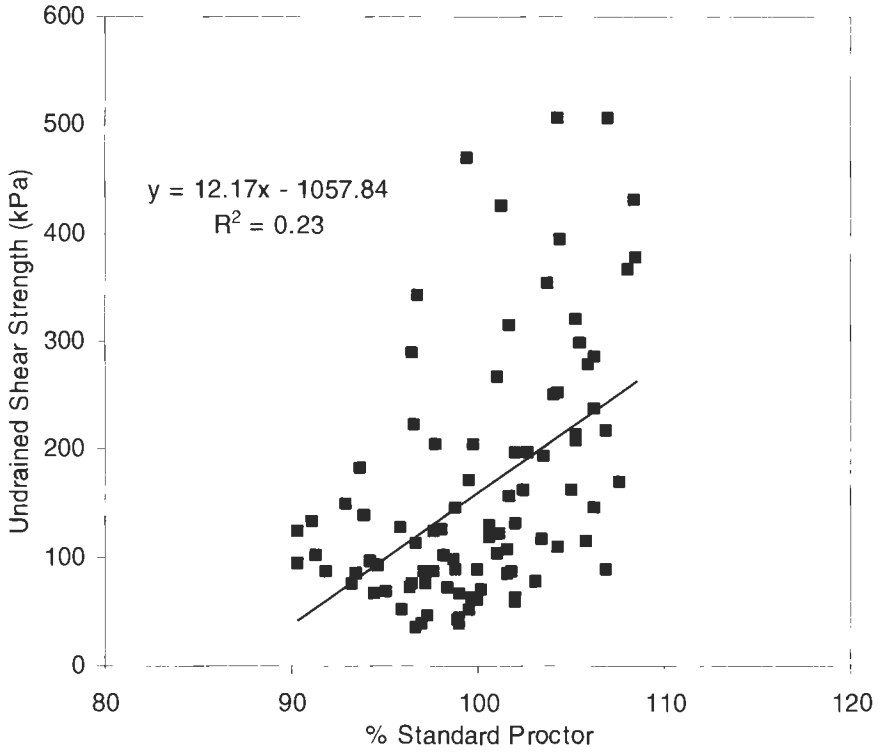

Figure 83. Undrained shear strength vs relative compaction (all lab soils)

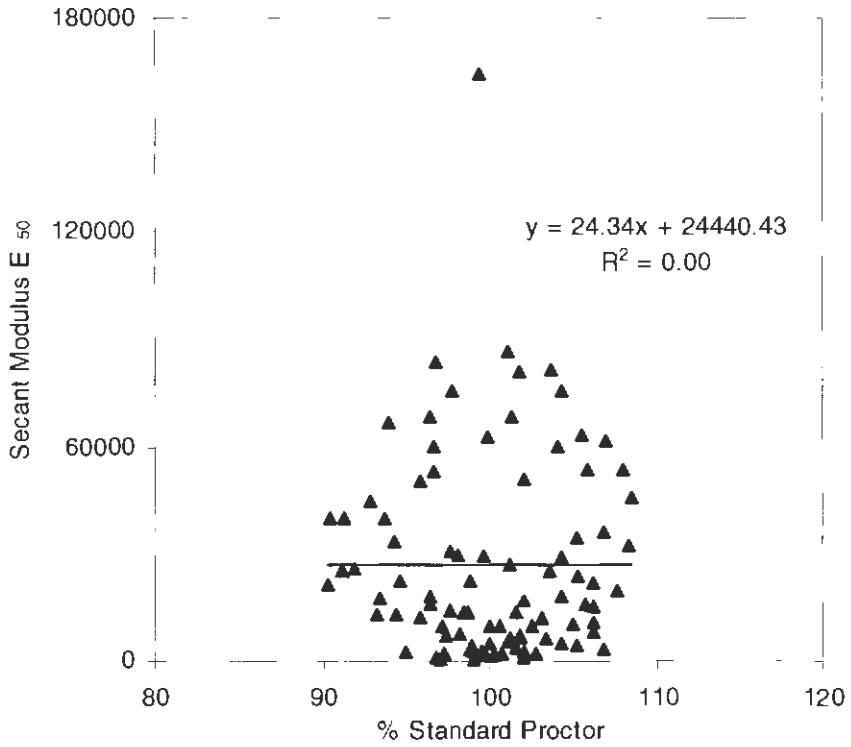

Figure 84. Secant modulus vs relative compaction (all lab soils)

CU Triaxial Tests

Results from 54 CU tests on the Wykeham Farrance triaxial machine are presented in Table 20. Table 21 gives the results of 6 CU tests on the ELE DS7 testing device. Specimens are identified by compaction energy applied, initial moisture content, and confining pressure used in consolidation and compression. For example, 355D-35 was a loess sample constructed at a compaction energy of 355 kJ/m^3, dry of standard optimum moisture content (~13%), and consolidated at 35 kPa. Terms BC and AC are before and after consolidation.

All data given are conditions observed at peak deviator stress strength failure. From each test, strength and stability parameters, σ_1/σ_3 and secant modulus, were determined as well as dry unit weight, moisture content and void ratio before and after consolidation. The pore

pressure coefficient and strain at failure were also recorded. Finally, the effective limit state parameters, cohesion (c') and friction angle (ϕ') , were determined using p' and q' at failure for tests at the confining pressures of 35, 70, and 105 kPa. The regression for p'- q' plots were recorded but are not shown in the tables. All p'-q' plots had r^2 between 0.994 and 1.000. Regression for p;-q' plots for 2693OPT and 592ELEOPT specimens were 0.970 and 0.888 respectively.

An envelope displaying the ranges of dry unit weight, moisture content, and compaction energy is given in Figure 85. Dashed lines represent the lower and upper threshold of compaction energies of 355 and 2693 kJ/m^3.

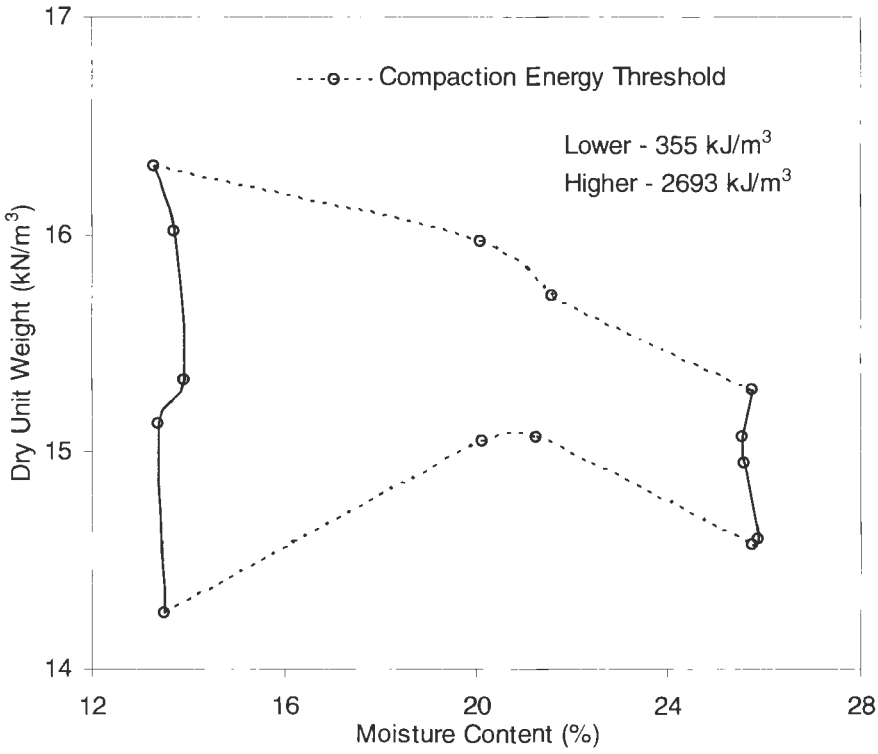

Figure 85. Envelope of moisture content and dry unit weight for WF specimens (Western Iowa loess)

Shortly after beginning the CU tests with the WF device, it was observed that low pore pressure coefficents were being measured during compression, as evidenced in Table 20. Therefore, the additional use of the ELE device was implemented in the testing plan to determine if a different back saturation procedure would result in higher coefficients of pore pressure in the loess. Upon the completion of six tests with the DS7, higher coefficients of pore pressure were established (see Table 21).

Late in the CU testing with the WF it was discovered that the procedure in recording of initial and final volume change was incorrect. Thus, volume changes for 33 of the test specimens were recorded higher than actual readings. Void ratio and dry unit weight after consolidation are omitted when applicable from to the observation made. The following specimens (given by ID) had a correct volume change recorded: 592OPT, 592OP+2, 2693OPT, 1463W, and 2693W.

All WF and ELE plots for stress-strain, p'- q', and pore pressure coefficient-strain are provided in Appendix D.

Table 20. Results from Wykeham Farrance triaxial tests on Western Iowa loess

Specimen	Dry Unit Weight (kN/m^3) BC	Dry Unit Weight (kN/m^3) AC	Moisture Content (%) BC	Moisture Content (%) AC	Void Ratio (e_{int}) BC	Void Ratio (e_o) AC	Strain at Failure (%)	Pore Pressure Coefficient A_f	σ_{1f} σ_{3f} (kPa)	Peak Deviator Stress ($\sigma_1-\sigma_3$) (kPa)	Secant Modulus E_{50} (kPa)	Cohesion (c') (kPa)	Friction Angle (ϕ')
355D-35	14.26	----	13.6	25.9	0.869	----	8.73	0.055	5.2	112	7,930	10.7	35.1
355D-70	14.24	----	13.6	24.6	0.871	----	11.8	0.044	4.5	201	11,600		
355D-105	14.26	----	13.3	23.7	0.868	----	10.1	0.036	4.1	286	15,914		
592D-35	15.43	----	13.4	23.5	0.727	----	8.0	-0.004	5.9	159	10,335	19.6	34.6
592D-70	15.01	----	13.2	22.2	0.774	----	9.4	-0.003	4.9	236	13,560		
592D-105	14.95	----	13.5	22.5	0.783	----	10.8	0.010	4.4	330	18,000		
987D-35	15.29	----	13.9	-----	0.743	----	9.9	-0.011	6.0	195	9,575	17.5	37.2
987D-70	15.19	----	13.9	25.9	0.753	----	7.3	-0.005	4.9	273	11,717		
987D-105	15.52	----	14.0	21.7	0.717	----	6.4	-0.004	4.8	393	20,070		
1643D-35	15.85	----	14.7	25.7	0.681	----	5.3	-0.009	7.8	238	10,800	36.1	36.7
1643D-70	16.28	----	13.3	20.5	0.637	----	4.7	0.008	6.5	363	19,412		
1643D-105	15.92	----	13.1	21.5	0.674	----	6.4	-0.005	5.2	443	23,337		
2693D-35	16.34	----	13.2	22.9	0.631	----	4.2	0.012	8.6	210	8,341	25.9	40.0
2693D-70	16.25	----	13.5	21.3	0.639	----	4.6	0.004	6.4	337	13,441		
2693D-105	16.36	----	13.2	20.7	0.629	----	4.2	0.006	5.7	463	20,610		
355OPT-35	15.28	----	19.2	23.6	0.744	----	7.7	-0.009	5.6	158	8,569	25.6	30.9
355OPT-70	15.10	----	19.2	23.3	0.765	----	11.4	-0.008	4.6	246	13,415		
355OPT-105	15.03	----	20.0	22.5	0.773	----	8.9	0.002	4.2	315	18,590		
592OPT-35	15.61	16.00	18.2	22.8	0.707	0.666	5.7	0.011	5.5	119	4,132	10.6	36.7
592OPT-70	15.73	16.27	18.2	23.6	0.694	0.638	7.1	0.023	4.8	211	6,588		
592OPT-105	15.68	16.32	18.2	21	0.700	0.633	8.1	0.009	4.4	316	13,175		
2693OPT-35	16.15	16.59	19.2	20.1	0.649	0.607	5.3	-0.014	8.3	242	8,169	0.0	50.9
2693OPT-70	15.92	16.42	20.1	20.7	0.674	0.623	6.2	-0.12	6.4	357	12,266		
2693OP-105	15.86	16.34	20.9	19.7	0.680	0.631	4.3	0.009	8.8	447	16,059		
355OP+2-35	15.0	16.4	21.2	25.6	0.778	0.625	5.6	0.000	4.8	122	6,013	3.0	37.9
355OP+2-70	15.0	16.0	21.3	24.0	0.775	0.664	7.3	0.010	4.2	200	11,800		
355OP+2-105	15.2	16.4	21.3	22.3	0.748	0.622	8.9	0.011	4.4	320	19,803		
592OP+2-35	15.09	15.51	21.8	24.3	0.766	0.718	10.3	-0.098	4.5	141	5,472	4.7	37.1
592OP+2-70	15.13	15.87	22.2	23.7	0.762	0.679	7.9	-0.022	4.4	218	6,192		
592OP+2-105	15.02	15.56	22.9	22.7	0.774	0.712	9.5	-0.014	4.2	333	16,030		

Table 20. Results from Wykeham Farrance triaxial tests on Western Iowa loess (cont.)

Specimen	Dry Unit Weight (kN/m^3) BC	Dry Unit Weight (kN/m^3) AC	Moisture Content (%) BC	Moisture Content (%) AC	Void Ratio (e_{int}) BC	Void Ratio (e_o) AC	Strain at Failure (%)	Pore Pressure Coefficient A_f	σ_{1f} / σ_{3f} (kPa)	Peak Deviator Stress ($\sigma_1-\sigma_3$) (kPa)	Secant Modulus E_{50} (kPa)	Cohesion (c') (kPa)	Friction Angle (ϕ')
2693O+2-35	15.72	----	21.8	21.9	0.695	----	7.3	-0.016	10.2	260	3,789	23.4	45.7
2693O+2-70	15.67	----	21.9	21.4	0.700	----	8.9	0.003	7.9	410	6,433		
2693O+2-105	15.75	----	21.1	20.6	0.691	----	8.2	0.006	7.3	576	10,588		
355W-35	14.6	----	25.2	24.6	0.827	----	8.2	0.059	6.9	141	3,322	22.5	33.4
355W-70	14.61	----	25.8	24.3	0.824	----	15.5	-0.058	4.6	296	5,484		
355W-105	14.5	----	26.2	23.2	0.843	----	12.5	0.007	4.2	315	9,363		
592W-35	14.6	----	26.1	25.2	0.828	----	10.7	0.042	6.9	146	2,834	20.7	34.4
592W-70	14.5	----	25.6	24.0	0.840	----	12.7	0.030	4.8	228	3,686		
592W-105	14.7	----	25.9	23.3	0.817	----	11.6	0.021	4.5	325	5,998		
987W-35	14.91	----	25.7	23.2	0.788	----	9.9	0.012	6.3	162	3,456	18.8	35.9
987W-70	15.03	----	25.8	23.2	0.778	----	12.3	0.026	5.0	242	3,946		
987W-105	14.89	----	25.3	22.8	0.789	----	10.8	0.020	4.4	334	6,554		
1643W-35	14.79	15.13	25.2	22.5	0.802	0.762	12.3	-0.052	5.5	159	3,636	12.4	36.9
1643W-70	15.17	15.70	25.5	22.9	0.756	0.697	6.6	0.015	4.7	228	8,535		
1643W-105	15.23	15.73	25.9	22.0	0.750	0.694	10.0	-0.010	4.5	360	9,380		
2693W-35	15.28	15.72	25.9	24.2	0.744	0.695	13.5	-0.036	5.6	152	3,958	13.5	36.0
2693W-70	15.22	15.67	26.3	22.8	0.750	0.701	12.2	-0.034	4.5	246	6,844		
2693W-105	15.35	15.83	25.0	22.4	0.736	0.683	13.4	-0.029	4.4	361	9,507		

Table 21. Results from DS7triaxial tests on Western Iowa loess

Specimen	Dry Unit Weight (kN/m^3) BC	Dry Unit Weight (kN/m^3) AC	Moisture Content (%) BC	Moisture Content (%) AC	Void Ratio (e_{int}) BC	Void Ratio (e_o) AC	Strain at Failure (%)	Pore Pressure Coefficent A_f	σ_{1f} / σ_{3f} (kPa)	Peak Deviator Stress ($\sigma_1-\sigma_3$) (kPa)	Secant Modulus E_{50} (kPa)	Cohesion (c') (kPa)	Friction Angle (ϕ')
592OPT-35	15.0	15.0	19.0	29.3	0.777	0.772	9.1	-0.258	3.6	250	7,966	3.2	32.2
592OPT-70	14.83	14.96	18.7	29.2	0.796	0.781	8.1	-0.191	3.0	302	10,895		
592OPT-105	15.44	15.60	19.1	25.1	0.730	0.708	13.1	-0.128	3.6	393	12,272		
2693OPT-35	16.62	16.69	18.6	21.2	0.603	0.597	8.8	-0.306	3.9	817	18,188	34.5	33.3
2693OPT-70	16.59	16.76	18.2	23.0	0.606	0.590	11.1	-0.294	3.8	986	22,717		
2693OPT-105	16.75	16.98	17.5	21.4	0.591	0.570	8.6	-0.29	3.7	1,117	33,024		

Relationships of Strength and Stiffness in CU Tests

In addition to compaction energy and initial moisture content, other independent parameters used to study influence on strength and stiffness were confining pressure surrounding the specimen and moisture content after saturation and consolidation. For the WF specimens, equations derived from the multiple regression analysis are the following:

$$\sigma_1/\sigma_3 = 1.05(E) - 0.024(m\%_{BC}) + 4.8 \quad [3\text{-}62]$$

$$\sigma_1/\sigma_3 = 0.001(E) + 0.1(m\%_{AC}) + 1.9 \quad [3\text{-}63]$$

$$\sigma_1/\sigma_3 = 1.03(E) - 0.02(\sigma_3) + 5.7 \quad [3\text{-}64]$$

$$\sigma_1/\sigma_3 = 0.001(E) - 0.26(m\%_{AC}) - 0.03(\sigma_3) + 12.4 \quad [3\text{-}65]$$

$$E_{50} = 0.12(E) - 683.9(m\%_{BC}) + 23{,}606.9 \quad [3\text{-}66]$$

$$E_{50} = -2.05(E) - 2292.8(m\%_{AC}) + 65{,}237.2 \quad [3\text{-}67]$$

$$E_{50} = -670.87(m\%_{BC}) + 120.7(\sigma_3) + 15{,}136.8 \quad [3\text{-}68]$$

$$\sigma_1 - \sigma_3 = 0.05(E) - 2.4(m\%_{BC}) + 257.6 \quad [3\text{-}69]$$

$$\sigma_1 - \sigma_3 = 0.03(E) - 46.0(m\%_{AC}) + 1318.8 \quad [3\text{-}70]$$

$$\sigma_1 - \sigma_3 = -28.8m\%_{AC}) + 2.2(\sigma_3) + 779.5 \quad [3\text{-}71]$$

$$\sigma_1 - \sigma_3 = 0.05(E) + 2.9(\sigma_3) + 1.0 \quad [3\text{-}72]$$

$$\sigma_1 - \sigma_3 = 0.04(E) - 9.7(m\%_{AC}) + 2.7(\sigma_3) + 253.6 \quad [3\text{-}73]$$

where, σ_1/σ_3 is the principal stress ratio, E_{50} is secant modulus, $\sigma_1 - \sigma_3$ is the peak deviator stress, E is compaction energy, $m\%_{BC}$ is moisture content before saturation and

consolidation, $m\%_{AC}$ is the moisture content after saturation and consolidation, and σ_3 is the confining pressure.

Table 22 summarizes statistical results for the set of equations. The logarithm of energy did not yield higher r^2 values and therefore was not used in the listed equations. Adjusted r^2 values ranged from 0.41 to 0.60 for σ_1/σ_3, 0.24 to 0.76 for E_{50}, and 0.16 to 0.84 for $\sigma_1 - \sigma_3$. The strongest predictor varied between the three parameters. Standard deviations for σ_1/σ_3, E_{50}, and $\sigma_1 - \sigma_3$ were 1.46, 5,509.6, and 103.6 respectively. Of the four equations for principle stress ratio, compaction energy was the strongest predictor for three of the equations. Moisture, both initial and final, predicted secant modulus the best. However, when three independent variables were used, confining pressure was the strongest predictor. Percent variability explained of the dependent variables is provided in Table 23.

Table 22. Statistical analysis on strength and stiffness for loess WF triaxial specimens

Equation	n	Adjusted r^2	Standard Error of Estimate	F-Statistic	t – statistics (< -2 or >+2)	Strongest Predictor
3-62	47	0.41	1.12	17.2	NG (m%-0.73)	E
3-63	47	0.41	1.11	17.2	NG (m%-0.77)	E
3-64	47	0.57	0.96	30.9	OK	E
3-65	47	0.60	0.93	23.0	NG (m%-1.90)	σ_3
3-66	47	0.35	4438.7	13.4	NG (E-0.17)	$m\%_{BC}$
3-67	47	0.24	4793.7	8.4	OK	$m\%_{AC}$
3-68	47	0.76	2674.9	75.6	OK	σ_3
3-69	47	0.16	94.9	5.4	NG (m%-0.86)	E
3-70	47	0.47	75.2	21.6	NG (E-0.22)	$m\%_{AC}$
3-71	47	0.77	50.0	76.7	OK	σ_3
3-72	47	0.84	41.8	119.3	OK	σ_3
3-73	47	0.84	41.0	83.4	NG (m%-1.63)	σ_3

Table 23. Percent variability explained by independent variables for WF triax results

Dependent Variable	Percent Variability Explained (%)			
	Compaction Energy	Initial Moisture	Final Moisture	Confining Pressure
σ_1/σ_3	43	1	10	17
E_{50} (kPa)	0	38	21	41
$\sigma_1 - \sigma_3$ (kPa)	18	2	50	63

Percent variability was determined by squaring individual Pearson correlations (R values) between dependent and independent variables. The highest percent variability explained occur in confining pressure relating to E_{50} and $\sigma_1 - \sigma_3$ (41% and 63%), final moisture with $\sigma_1 - \sigma_3$ (50%), and energy with stress ratio (43%). Individual relations are displayed in Figure 86 - Figure 97. Other WF triax regression plots can be found in Appendix E.

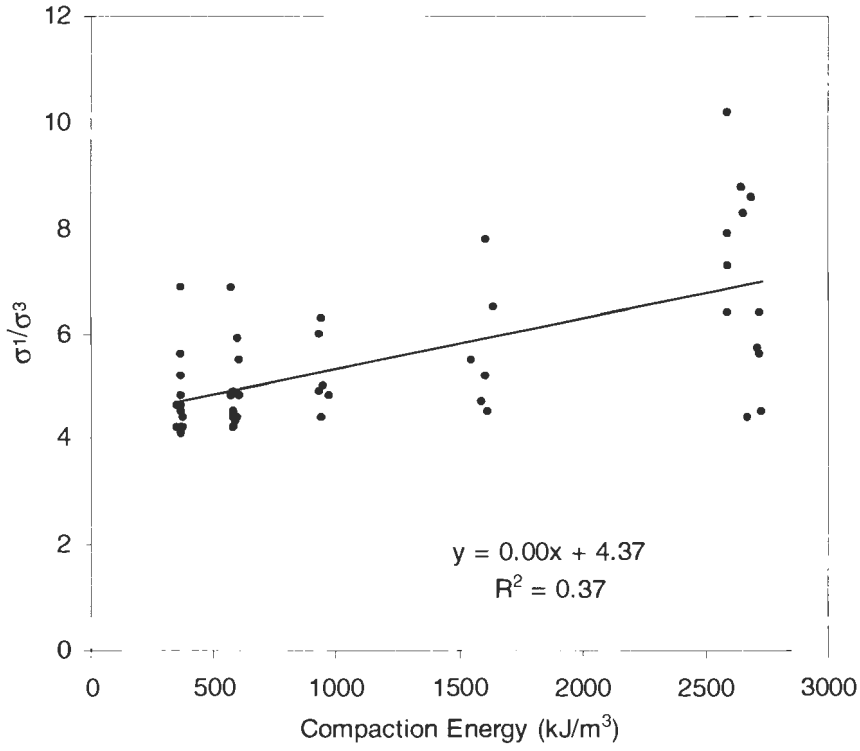

Figure 86. Regression of principle stress ratio and compaction energy for WF triax

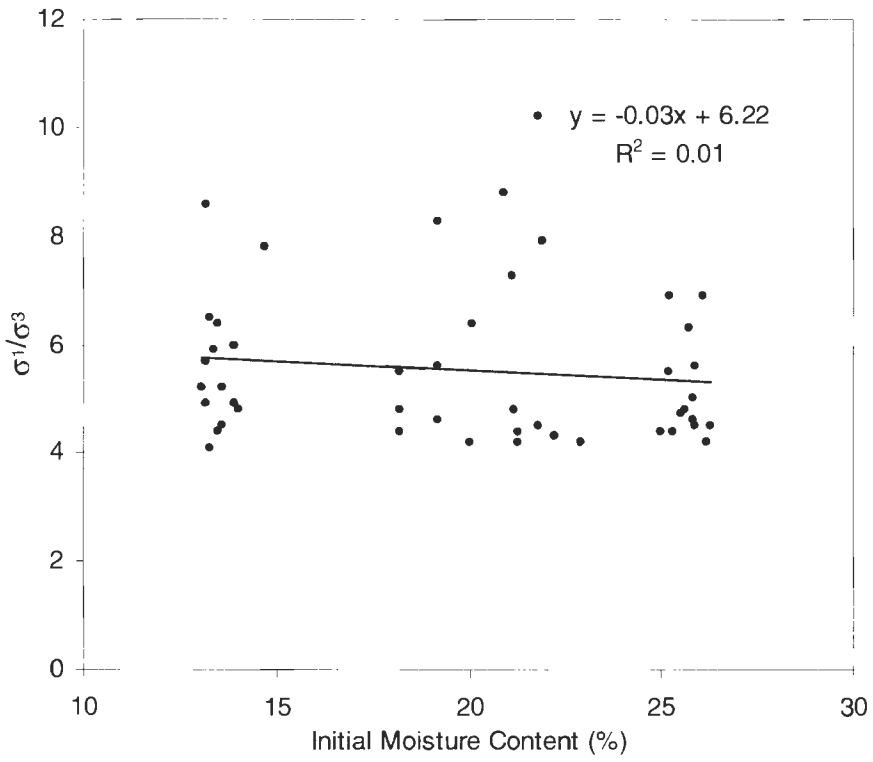

Figure 87. Regression of principle stress ratio and initial moisture content for WF triax

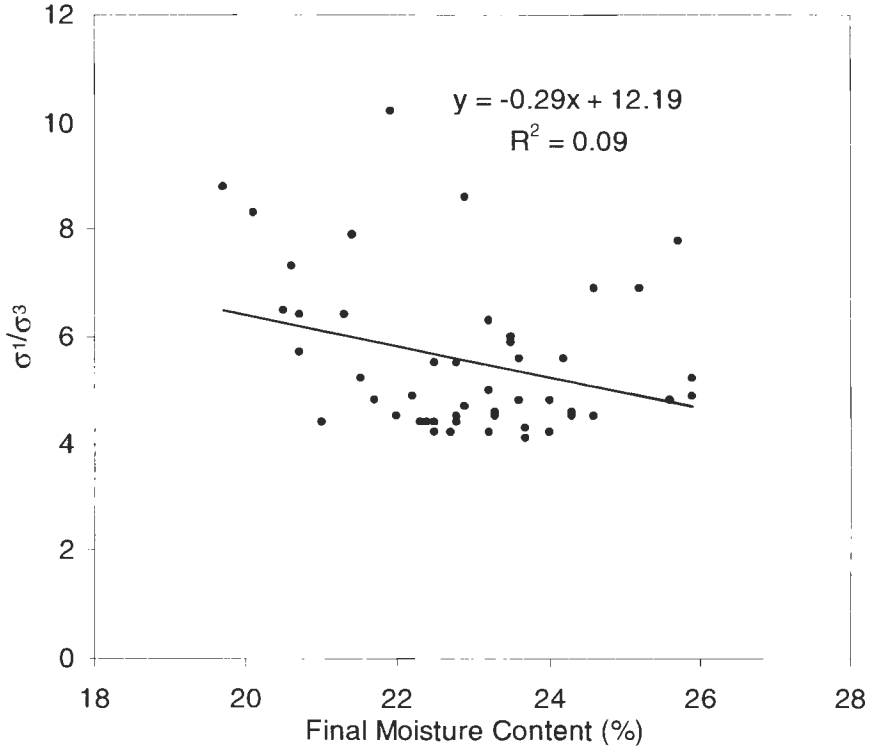

Figure 88. Regression of principle stress ratio and final moisture content for WF triax

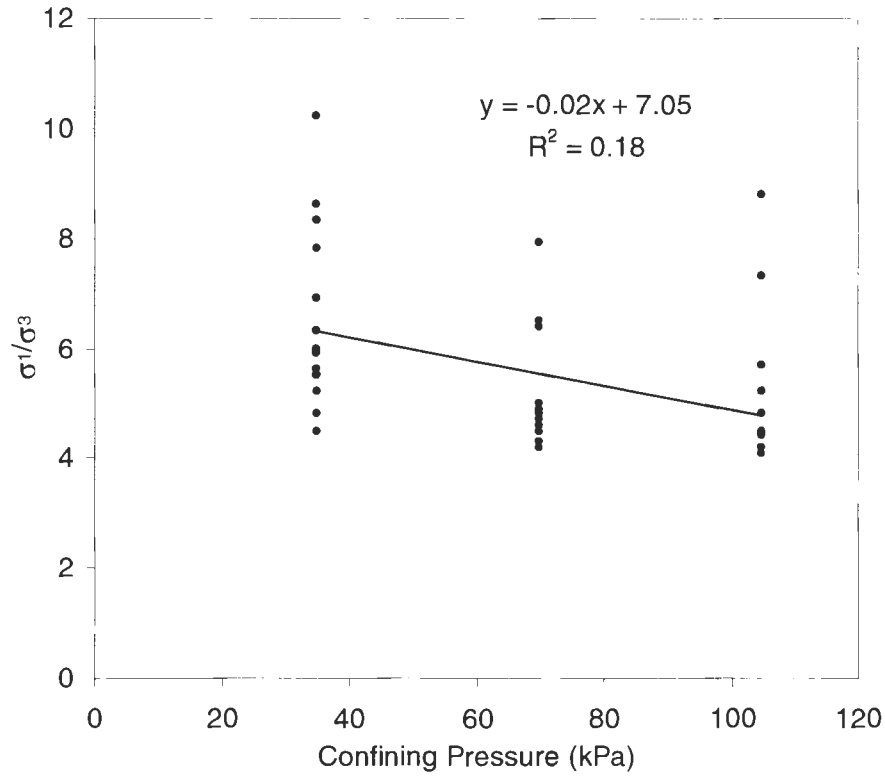

Figure 89. Regression of principle stress ratio and confining pressure for WF triax

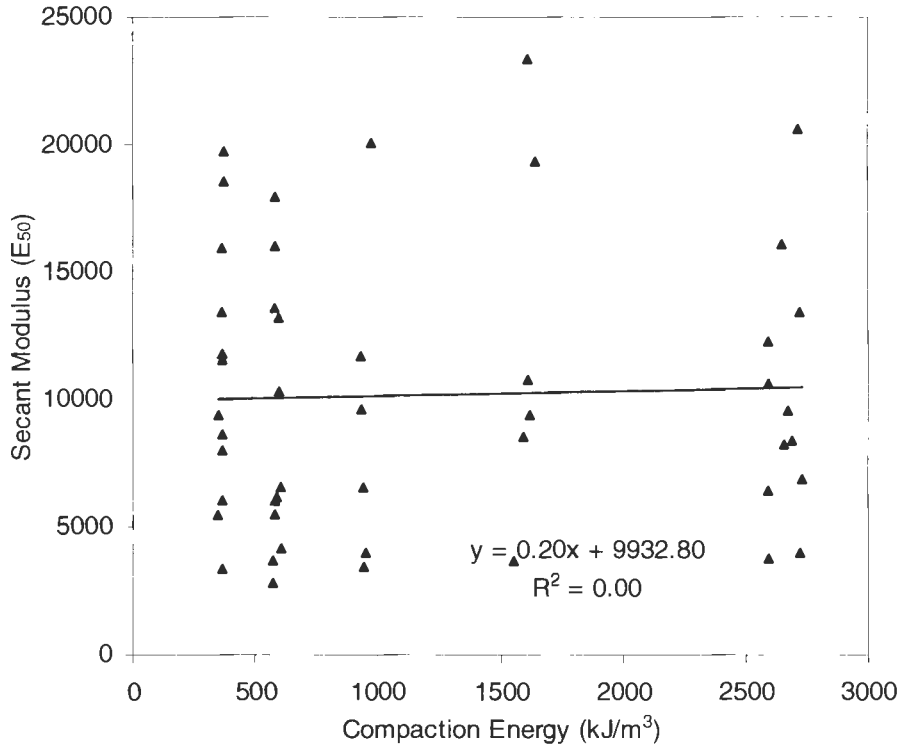

Figure 90. Regression of secant modulus and compaction energy for WF triax

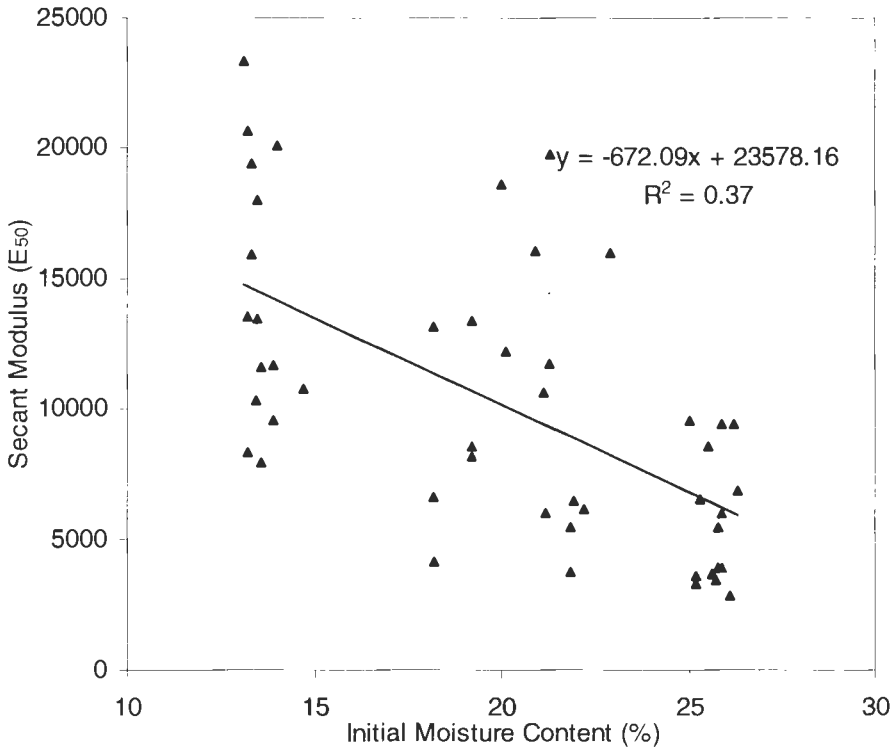

Figure 91. Regression of secant modulus and initial moisture content for WF triax

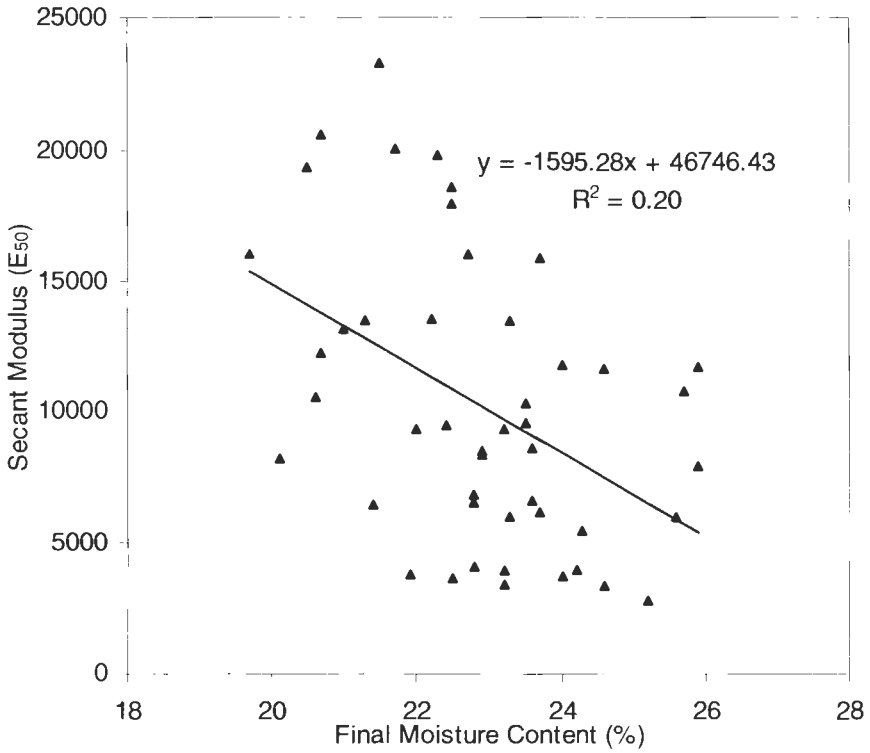

Figure 92. Regression of secant modulus and final moisture content for WF triax

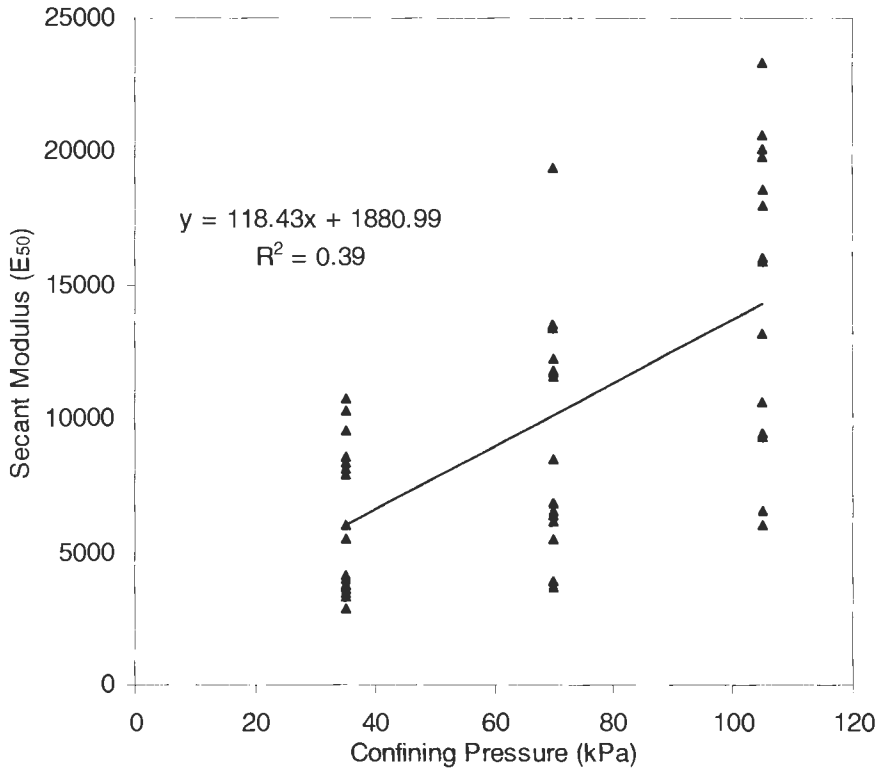

Figure 93. Regression of secant modulus and confining pressure for WF triax

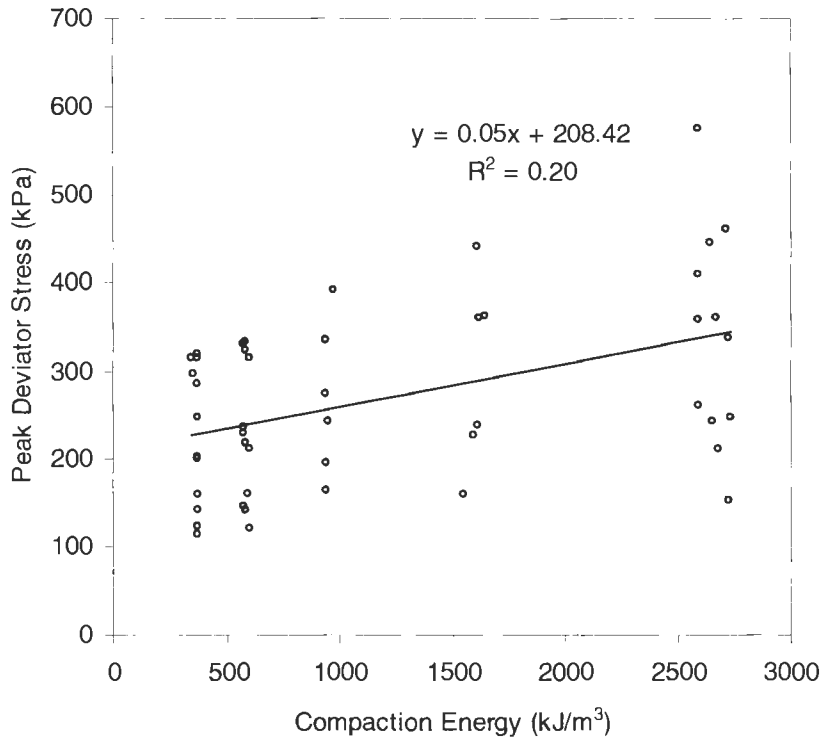

Figure 94. Regression of peak deviator stress and compaction energy for WF triax

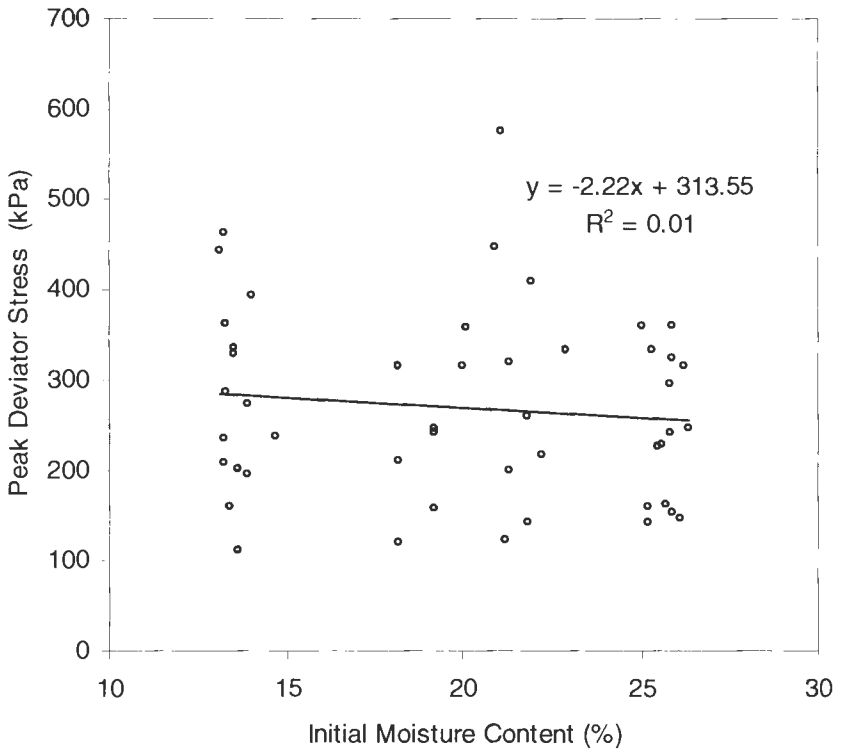

Figure 95. Regression of peak deviator stress and initial moisture content for WF triax

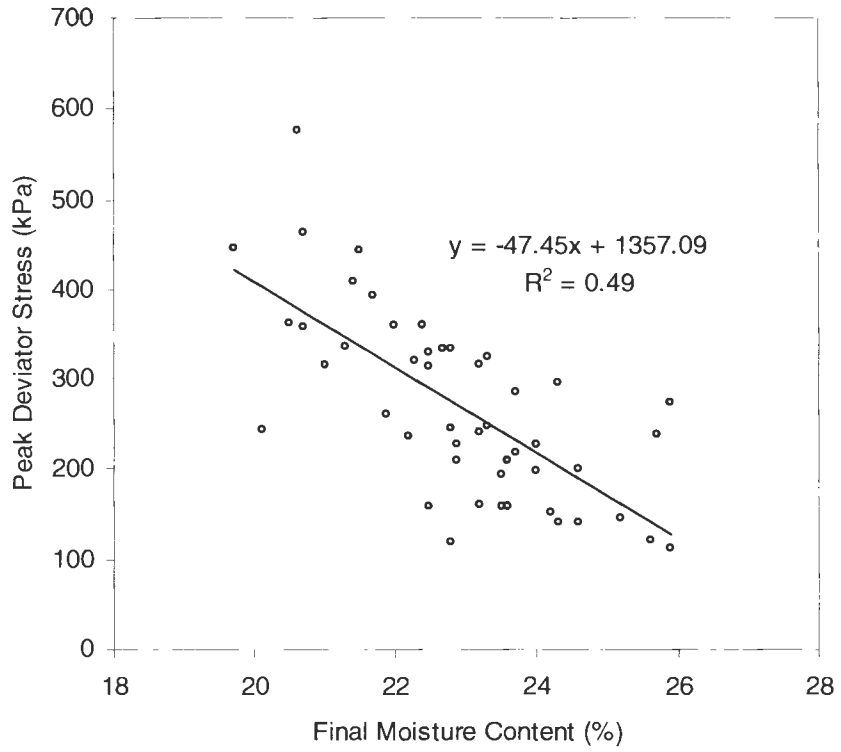

Figure 96. Regression of peak deviator stress and final moisture content for WF triax

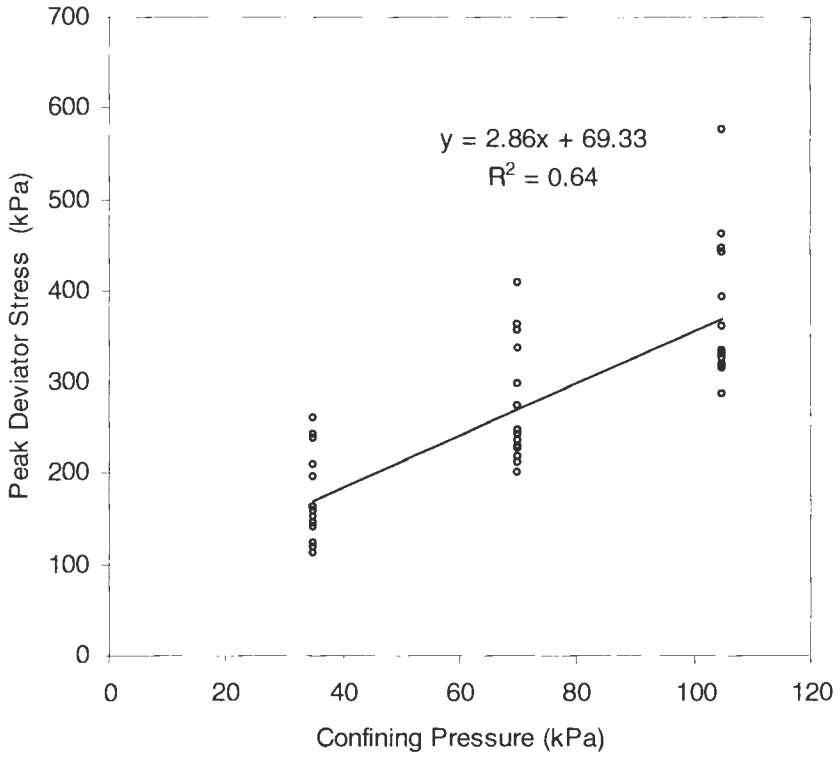

Figure 97. Regression of peak deviator stress and confining pressure for WF triax

While confining pressure is observed as having more influence on the parameters than compaction energy, the importance of energy is not overshadowed. In essence, the results in confining pressure can be directly linked to the importance in energy applied to soil, specifically in regard to earthwork construction. Consider that the condition of an initial loose layer of soil has little to no confining pressure. As energy is delivered, the soil densifies, causing internal prestresses to increase. Therefore, for a given moisture range, higher levels of compaction energy applied will lead to higher confining pressures within a soil structure. Moisture plays an important role, i.e. beyond a certain saturation level the soil will simply be remolded with increasing energy losing internal strength.

Limit State Parameter Relationships

The following set of equations, 3-74 through 3-77, were derived for relationships for cohesion (c') and the friction angle (ϕ') determined from p'-q' plots.

$$c' = 8.2 \times 10^{-4}(E) - 0.45\ (m\%_{BC})\ 24.6 \quad [3\text{-}74]$$

$$c' = 3.4 \times 10^{-3}(E) + 2.2(m\%_{AC}) - 37.7 \quad [3\text{-}75]$$

$$\phi' = 3.7(E) - 0.04(m\%_{BC}) + 33.8 \quad [3\text{-}76]$$

$$\phi' = 2.2 \times 10^{-3}(E) - 1.3\ (m\%_{AC}) + 64.3 \quad [3\text{-}77]$$

where, c' is the effective cohesion and ϕ' is the effective friction angle.

The statistical results from this multiple regression analyses are presented in Table 26. Plots for the individual regressions are given in Figure 98 to Figure 103.

Table 24. Statistical analysis on limit state parameters for loess WF triaxial specimens

Equation	n	Adjusted r^2	Standard Error of Estimate	F-Statistic	t – statistics (< -2 or >+2)	Strongest Predictor
3-74	16	0.0	9.9	0.44	NG (both)	n/a
3-75	16	0.0	10.0	0.30	NG (both)	n/a
3-76	16	0.44	3.6	6.9	NG (m%--0.2)	E
3-77	16	0.50	3.4	8.4	NG (both)	n/a

Moisture content and compaction energy values used in the regression analyses were average values between each respective set of three test specimens shown in Table 20. As indicated in Table 26 and Figure 98 -Figure 100, little correlation exists between cohesion of the Western Iowa loess and, independent variables, energy and moisture content. In contrast,

fair correlation (r^2 = 0.44 and 0.50) exists between effective friction angle of the loess and the three variables. In general, linear relations were exhibited in the correlations, which involved increasing friction angle with increasing compaction energy, and decreasing friction angle with increasing moisture content after consolidation.

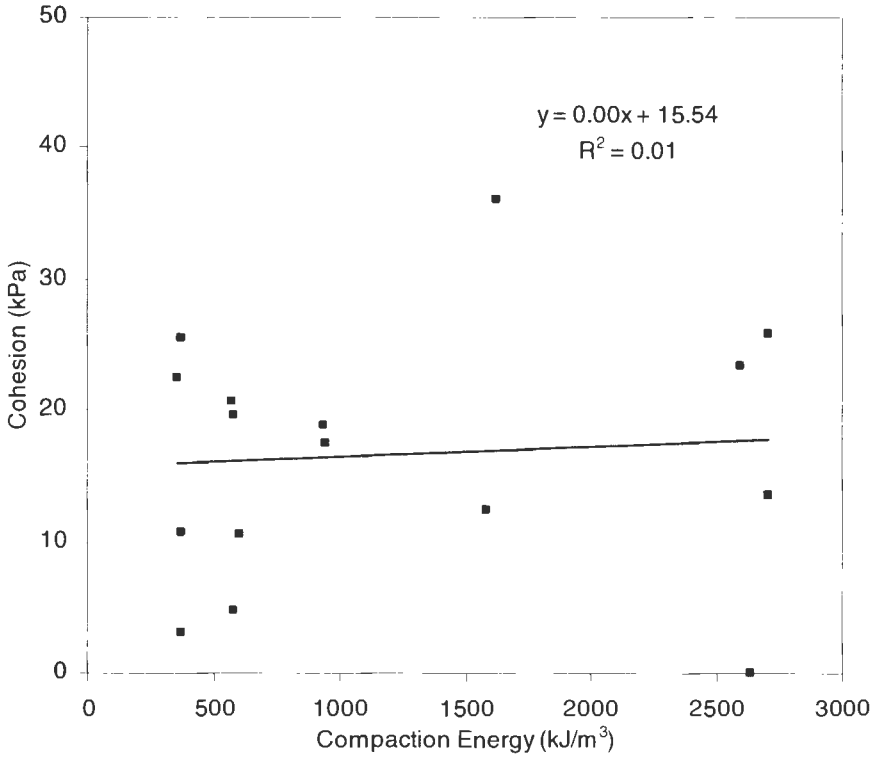

Figure 98. Regression of effective cohesion and compaction energy for WF triax

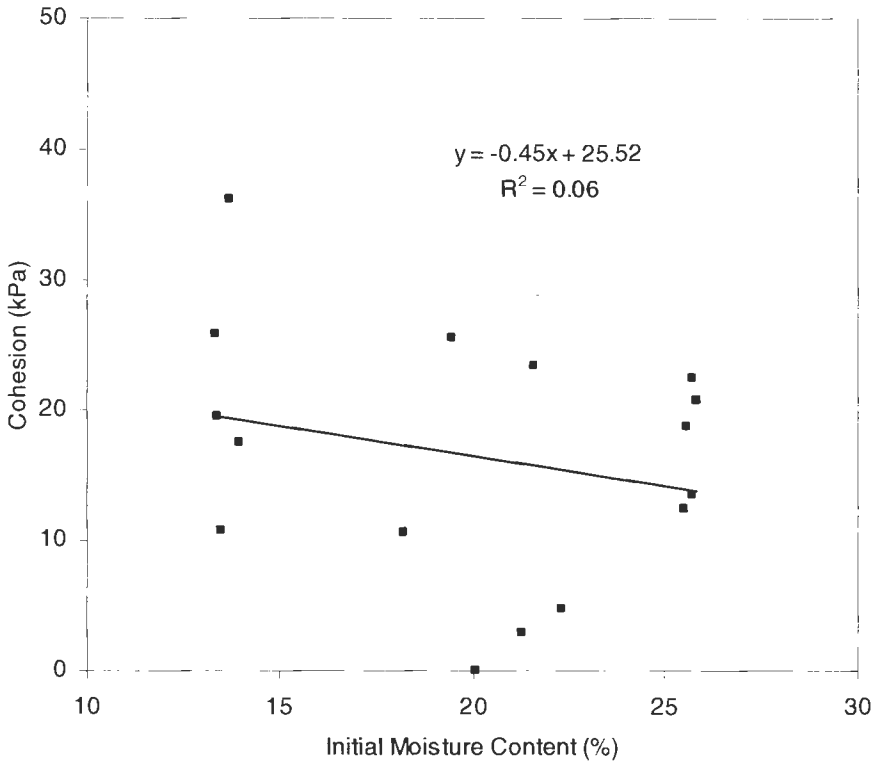

Figure 99. Regression of effective cohesion and initial moisture content for WF triax

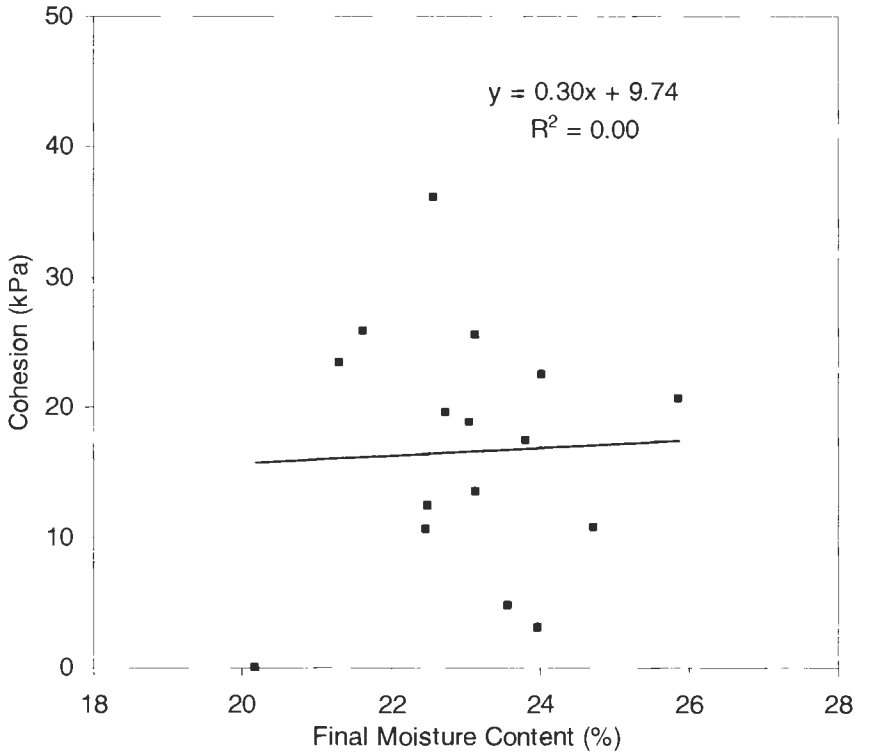

Figure 100. Regression of effective cohesion and final moisture content for WF triax

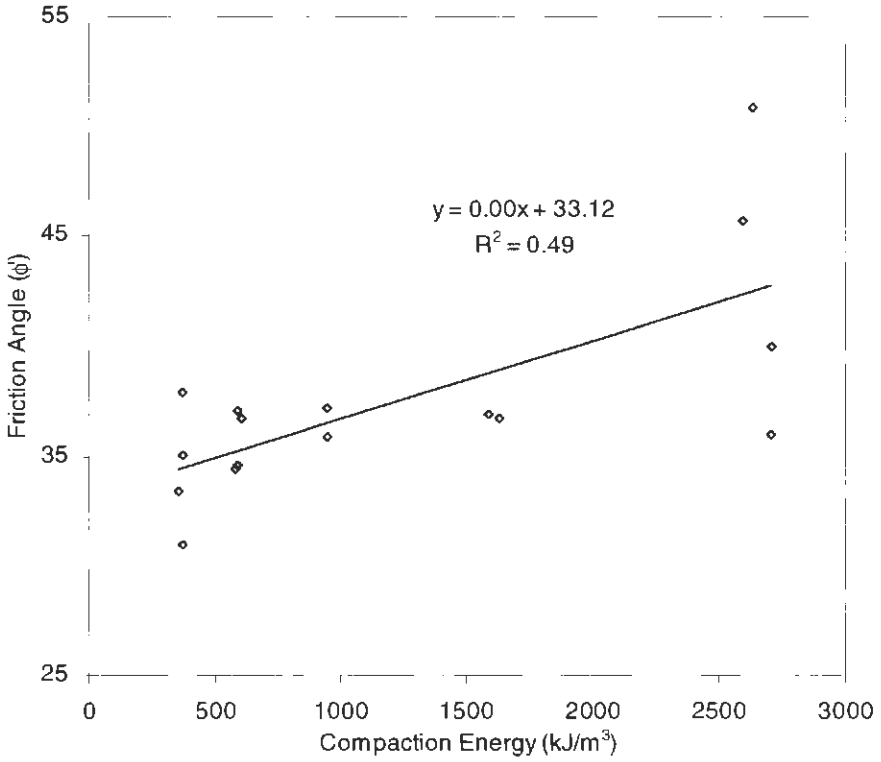

Figure 101. Regression of effective friction angle and compaction energy for WF triax

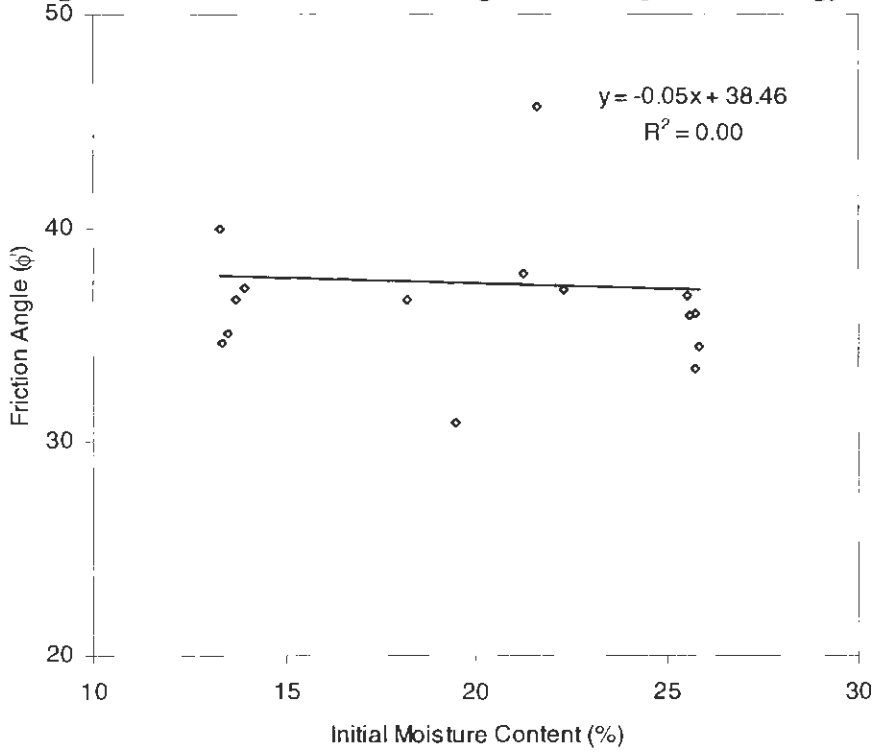

Figure 102. Regression of effective friction angle and initial moisture content for WF triax

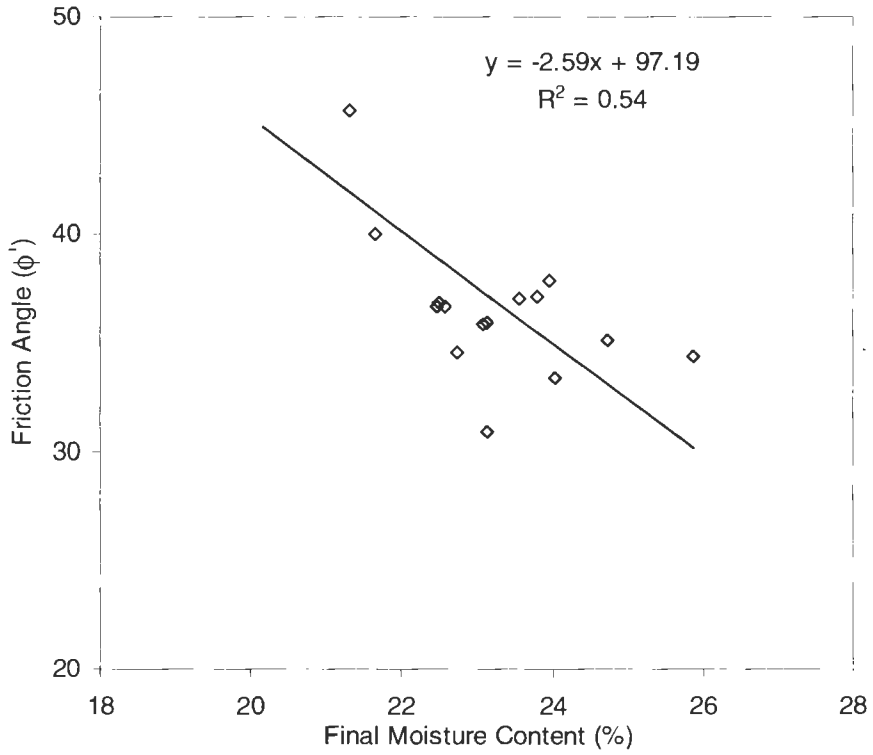

Figure 103. Regression of effective friction angle and final moisture content for WF triax

Comparison Between Wykeham Farrance and ELE Specimens

Comparisons of results were drawn between WF and ELE specimens at optimum moisture content (19%) for standard Proctor energy. Energies of the specimens were 592 and 2693 kJ/m^3. Figure 104 through Figure 108 are plots comparing independent variable results from compaction energy only. Other plots comparing the devices include moisture content and confining pressure and are given in Appendix E.

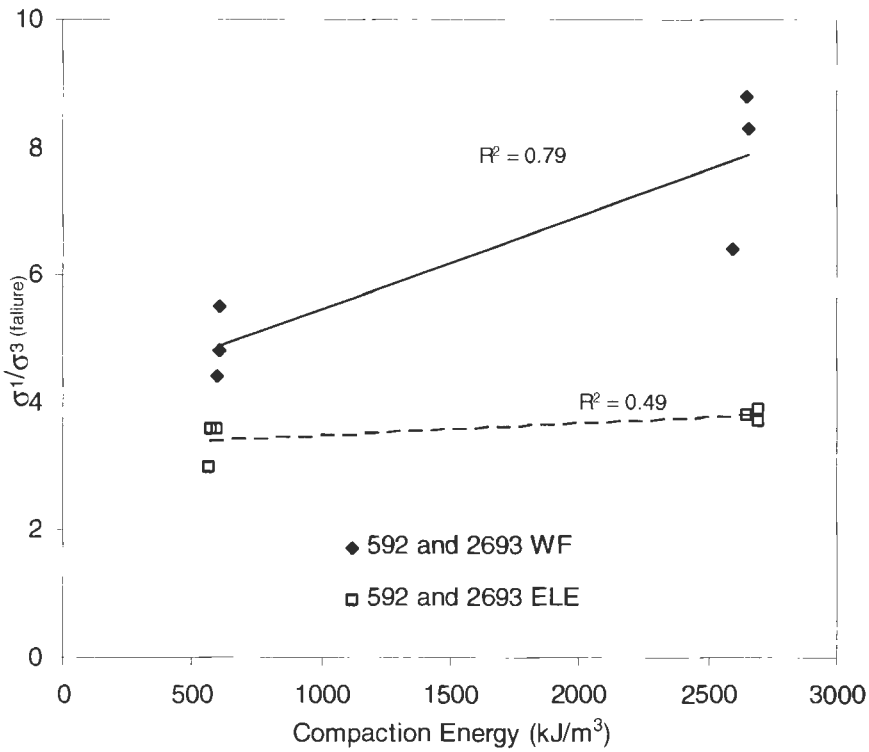

Figure 104. Comparison of principle stress ratio with compaction energy between WF and ELE

Principle stress ratios were higher for WF specimens. This is due to higher pore pressure registered during shearing of the ELE specimens. Higher pore pressure in the ELE specimens also explains the higher pore pressure coefficients observed during shearing (see Figure 107).

Table 25 gives an individual comparison of pore pressures readings at failure. The procedure with ELE established pore pressures on the order of 15 to 140 times higher than the WF.

Table 25. Comparison of pore pressures at failure for WF and ELE triaxial specimens

Specimen	Pore Pressure at Failure (kPa)		Difference in Magnitude
	WF	ELE	
592OPT-35	8.3	518.4	63
592OPT-70	13.1	463.3	35
592OPT-105	11.0	486.4	44
2693OPT-35	1.4	191.8	139
2693OPT-70	2.8	146.7	53
2693OPT-105	11.7	178.7	15

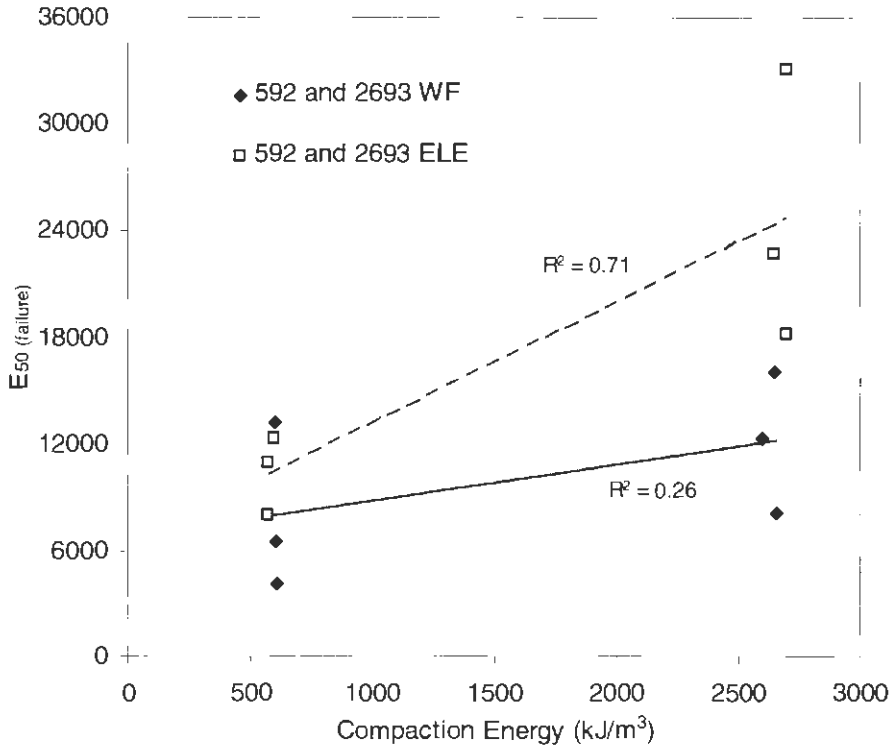

Figure 105. Comparison of secant modulus with compaction energy between WF and ELE

Regarding strength and stiffness, ELE specimens generally had higher values of undrained shear strength and secant modulus especially at higher compaction energies. Specimens from both devices increased in stress ratio, secant modulus, and shear strength with

increasing energy. In addition, specimens from both devices decreased in pore pressure coefficient A, or increased in dilation, with increasing compactive effort.

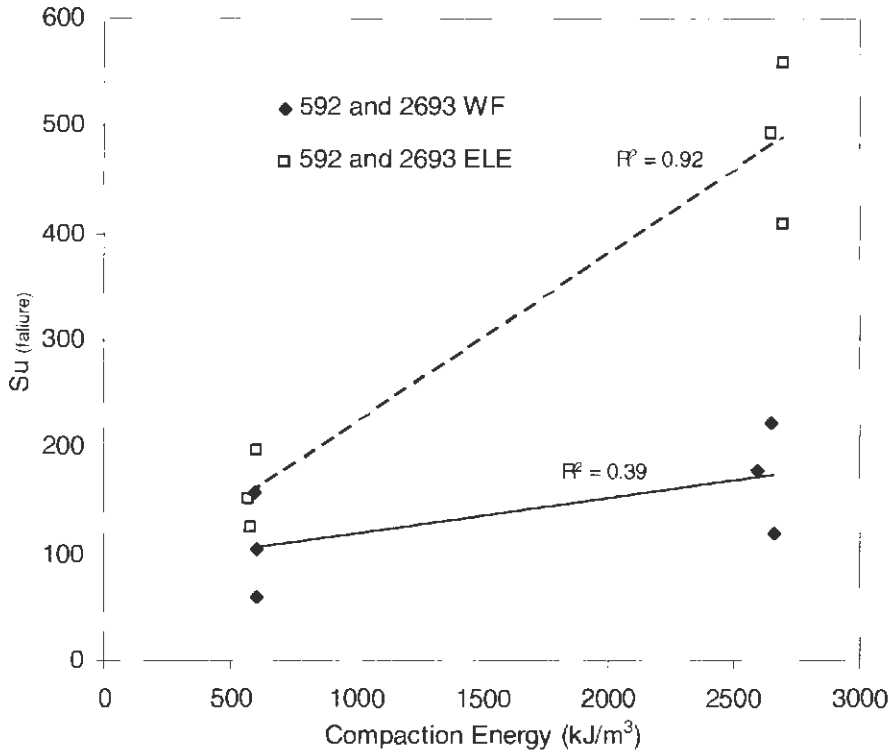

Figure 106. Comparison of undrained shear strength with compaction energy between WF and ELE

Effective limit state parameters of the two devices are similar for standard Proctor energy with cohesions of 4 and 10 kPa and friction angles of 32 and 37 degrees respectively. However, at modified Proctor energy ELE specimens yielded higher cohesion (c' = 35 kPa) than WF specimens. In contrast, the WF envelope resembled a cohesionless soil with c'= 0 and $\phi' = 51^{\circ}$.

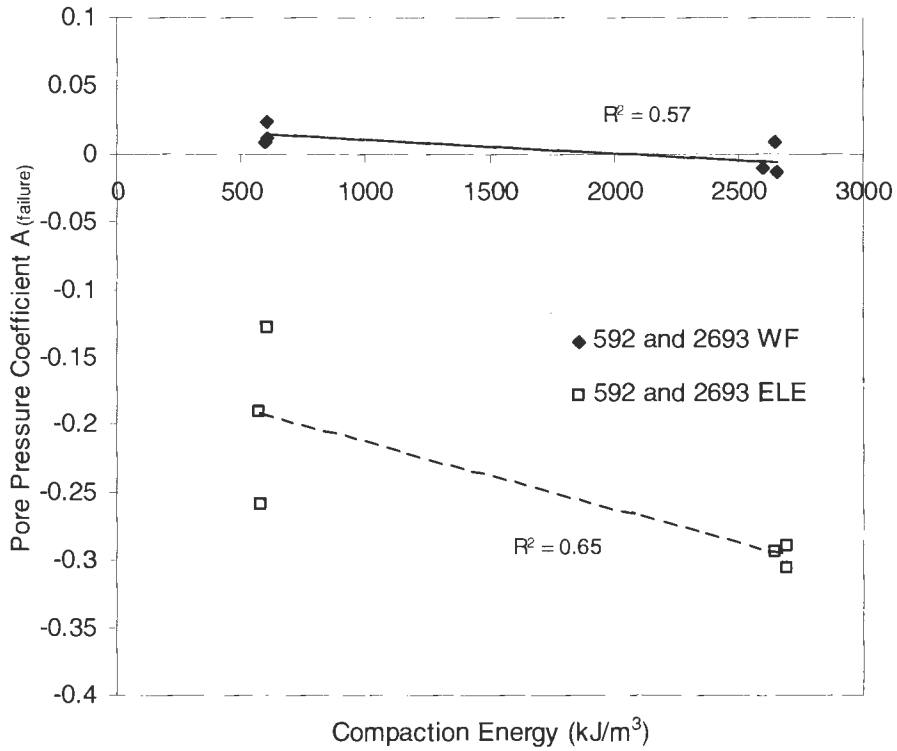

Figure 107. Comparison of pore pressure coefficient A with compaction energy between WF and ELE

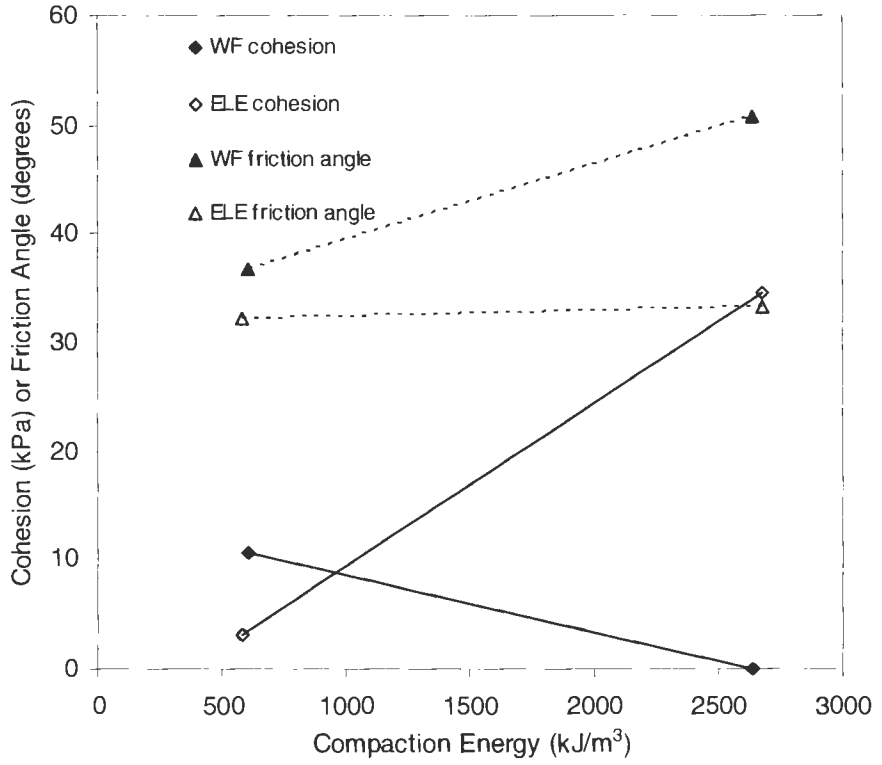

Figure 108. Comparison of effective limit state parameters with compaction energy between WF and ELE

Comparison with Unconfined Compression Tests

Loess samples tested in unconfined compression (shown earlier in this paper) were compared with triaxial samples. The unconfined compression samples represent the strength and stability of the loess in the compacted state immediately after construction. The specimens are undrained and unconsolidated. It shall be noted that strength and stiffness for these tests are conservative considering the specimens are not confined. The CU samples represent the strength and stability of the loess in the compacted state long after construction, where the loess has been allowed to saturate and consolidate from overburden loads and self weight of the soil.

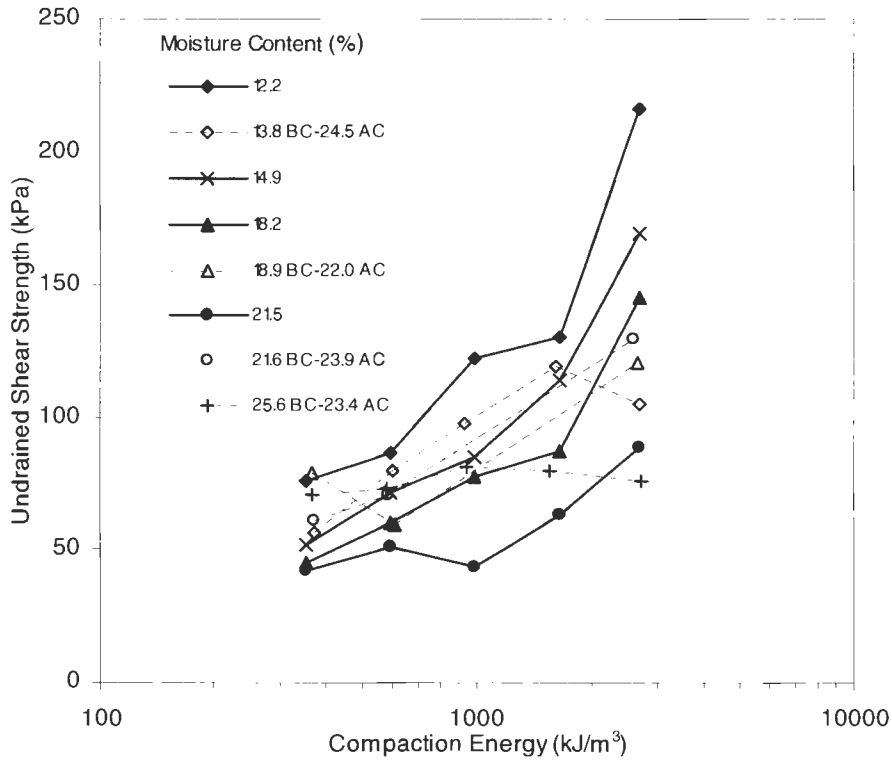

Figure 109. Undrained shear strength vs. compaction energy for UCS and CU specimens (σ_3 = 35 kPa)

Shear strength and stiffness comparison between UCS and CU specimens are provided in Figure 109 - Figure 114, where solid and open points on the plots represent UCS and CU respectively. Moisture contents given are average for each group of values across the energy spectrum.

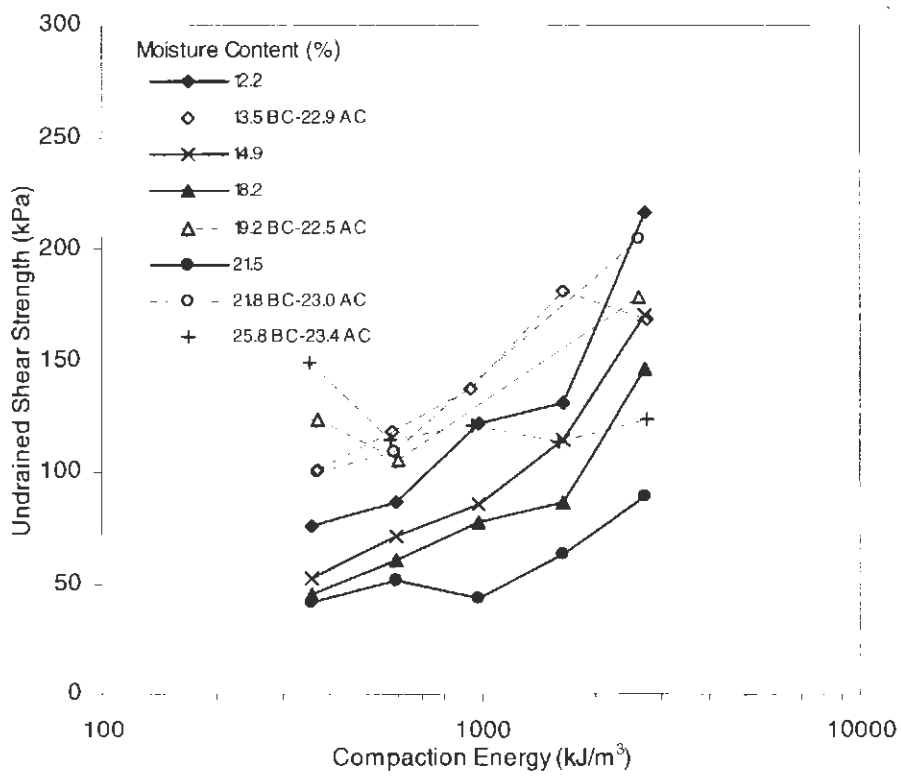

Figure 110. Undrained shear strength vs. compaction energy for UCS and CU specimens (σ_3 = 70 kPa)

An immediate observation of the graphs is that there is not as definite separation in triaxial specimen between moisture contents as there is with unconfined specimens, indicating a higher degree of variability. For CU specimens with σ_3 = 35 kPa, shear strengths were within the boundaries UCS shear strengths and tended to generally increased with increasing compactive effort. Dry of optimum, UCS specimens were higher than CU specimens,

particularly at 2693 kJ/m^3 of energy. At optimum moisture, strengths between the two were similar. Wet of optimum (+2 and +6%), CU test specimens generally exhibited higher shear strength than unconfined specimens. For stiffness dry of optimum, the magnitude of difference was more significant between CU and UCS specimens, where UCS was greater. Stiffness at optimum moisture was also slightly greater for UCS specimens. CU specimens at σ_3 = 35 kPa were more variable in stiffness as a function of energy than UCS specimens that tend to increase more with increasing compaction energy.

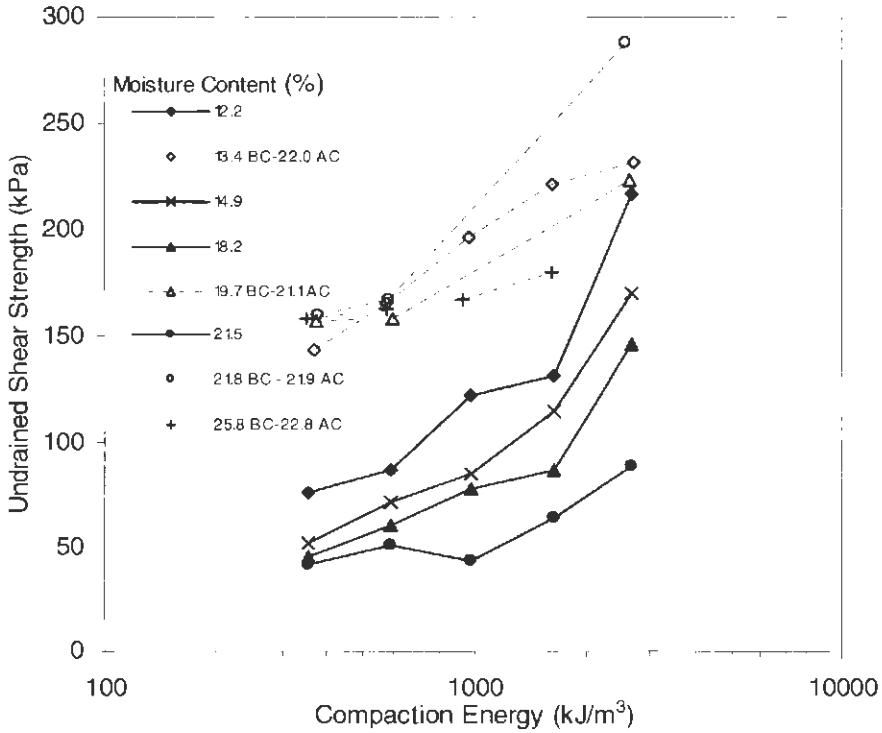

Figure 111. Undrained shear strength vs. compaction energy for UCS and CU specimens (σ_3 = 105 kPa)

At σ_3 = 70 and 105 kPa, CU specimens continue to increase in shear strength and stiffness, eventually surpassing UCS test shear strength values at 105 kPa confining pressure.

Essentially, the shear strengths established in the CU tests at these confining pressures are to be considered a truer representation of the loess' strength.

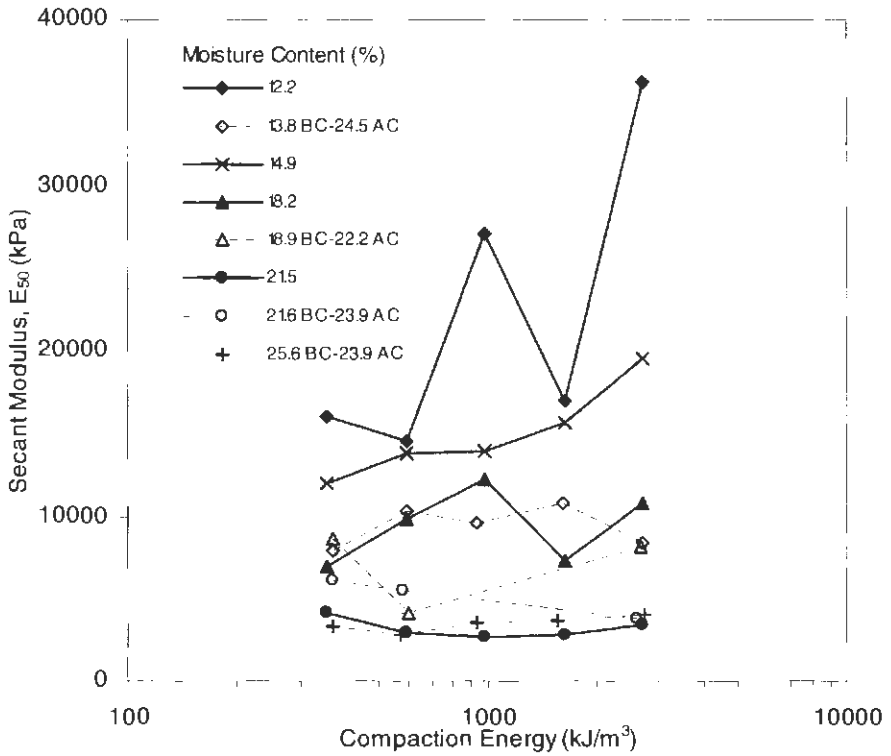

Figure 112. Secant modulus vs. compaction energy for UCS and CU specimens (σ_3 = 35 kPa)

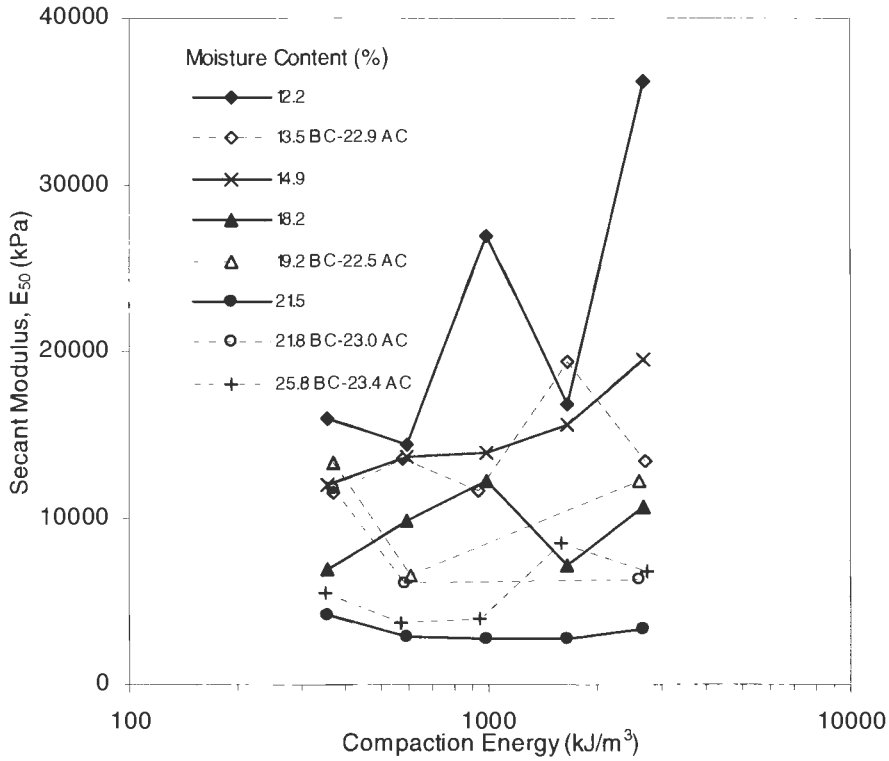

Figure 113. Secant modulus vs. compaction energy for UCS and CU specimens (σ_3 = 70 kPa)

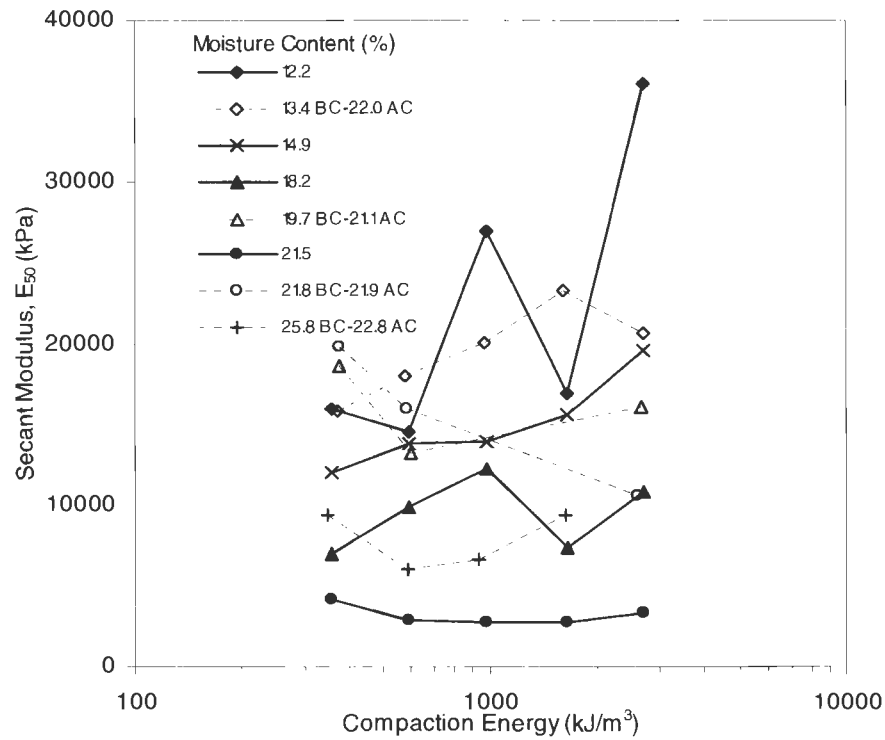

Figure 114. Secant modulus vs. compaction energy for UCS and CU specimens (σ_3 = 105 kPa)

CHAPTER 4. FIELD METHODOLOGY

The objective of the field research was to determine relationships of soil properties as a function of roller pass, moisture content, and compacted lift thickness. The field research methodology involved the following tasks:

Task 1: Devise a test plan for field strip construction of each field material based on laboratory results.

Task 2: Construct field strips, varying the conditions of roller pass, moisture content, and loose lift thickness.

Task 3: Collect data in the field with conventional test equipment.

Task 4: Carry out statistical analyses to derive possible correlations between soil parameters and compaction energy/moisture content.

Research Design for Field Soils

Three field tests were conducted in this phase of the research. Two of the field tests were performed under controlled conditions at two different sites in Peoria, Illinois. The third field test was located on an earthwork grading project in West Des Moines, Iowa. The general procedure to construct a field test strip involved the following: (1) aerate/till existing soil, (2) moisture condition soil with water truck (when necessary), (3) remix soil, (4) blade to level surface, and (5) compact soil with a Caterpillar CP – 533E roller. The test strips were constructed to vary in moisture content, roller passes, and loose lift thickness. Field and laboratory procedures are discussed in the following sections.

Field Measurements

To evaluate changes in soil properties as a result of compaction, 5 to 10 test points were randomly identified within each test strip and measured for dry unit weight (nuclear and drive core methods), water content (nuclear and oven methods), strength (dynamic cone penetrometer), and stiffness (Clegg impact soil test and Geogauge stiffness test).

Dry Unit Weight and Moisture Content

Bag samples and drive core specimens were collected at each test location to determine dry unit weight and moisture content in the lab using the oven method. Comparisons were made between the drive core dry and the nuclear dry unit weight measurements. The drive core samples were taken in the top 5 to 13 cm, whereas the nuclear tests averaged a measurement over the top 15 to 20 cm.

In-Situ Strength

Dynamic Cone Penetrometer (DCP) tests were performed to develop strength versus depth profiles and determine vertical and horizontal uniformity. Tests were conducted in accordance with ASTM D-6951. Each test performed penetrated down to or through the interface of upper and lower lifts. Compacted lift thicknesses were interpreted from the DCP plots by observing the change in the mean DCP index (DCPI) profile with depth. The mean DCP index was calculated as the weighted average of the index values in the upper lift, ignoring data from the underlying layer. Uniformity in a lift was determined by calculating the mean change in the DCPI. The unit of measurement for the DCP index was millimeters

per hammer blow. Equations for calculating the weighted average DCPI (Eq. 4-1) and mean change in DCPI (Eq. 4-2) are the following:

$$DCPI_{wt.\ avg.} = \frac{\Sigma\,(DCPI_i * z_i)}{H} \qquad [4\text{-}1]$$

$$DCPI_{mean\ change} = \frac{\Sigma\,[(DCPI_k - DCPI_i) * z_i]}{H} \qquad [4\text{-}2]$$

where, $DCPI_i = z_k - z_i/n$, z_i is the layer depth interval, $z_k - z_i$ is change in depth, n is the number of blows, H is the entire compacted lift, and $DCPI_k - DCPI_i$ is the change DCP index. The repeatability standard deviation for the DCP has been determined to be less than 2 mm/blow.

Clegg Impact Soil Test

The Clegg impact soil test device is primarily used to indicate soil stiffness but can also be used to gain an understanding of strength. All testing was performed in accordance with ASTM D-5874. The test involves dropping a hammer through a guide tube at a predetermined height. Fitted to the hammer is an accelerometer which measures the peak deceleration of the hammer's impact on the soil surface. A digital readout is displayed on a screen attached to hammer. The unit of measurement is termed the Clegg Impact Value (CIV), and has been correlated to California Bearing Ratio (CBR) and used to calculate elastic modulus. However, the use of CIV alone is a practical alternative to CBR and is used in this study. The coefficient of variation for impact values has been reported from one

source as 2% or greater for lab work and 4% or greater in earthwork involving uniform conditions. Earthwork with more variable conditions yields a COV of 20%.

Geogauge Stiffness Test

A GeoGauge was used to measure the structural layer stiffness (MN/m) and Young's Modulus (MPa) of the soil. The device works by applying a continuous vibrating force for 75 seconds and measuring the impedance at the surface of a compacted soil (Humboldt, 1999). The force vibrates at 25 steady state frequencies between 100 and 196 Hz. Resulting displacements are small ($< 1.27 \times 10^{-6}$ m) and are used to calculate the stiffness at each frequency. The average of the 25 stiffness measurements are averaged and displayed on the digital screen. By storing Poisson's ratio of the material, prior to testing, Young's modulus is derived and displayed. The coefficient of variation ranges between 1% to 10%.

Field Test 1 – Caterpillar Inc. Proving Grounds, Peoria, Illinois

Field Test 1 was located at an outdoor test facility in Peoria, Illinois. Testing was conducted in September of 2003. The test area was divided into three sections, each containing two 100-foot-long test strips. Each test strip contained 10 test points. The first section was compacted with roller one pass. Average moisture content for strips of section 1 was 8.6%. Test sections 2 and 3 were compacted with two and three roller passes. Test strips in section 2 had an average moisture content of 8.7% while strips in section 3 averaged 9.3%. The field material was observed as a glacial till (CL). Test strips were approximately 20 to 25 cm in loose lift thickness. Detailed identification for test strips are given in Table 27. Field tests performed included using nuclear gauge, DCP, Clegg impact, and Geogauge.

Field Test 2 – Edwards Test Facility, Peoria, Illinois

Field Test 2 was located in an indoor test facility in Peoria, Illinois. Testing was conducted March of 2004. This field test involved the construction of eight test strips, identified as A through H. The test strips varied in loose lift thickness, water content, and number of roller passes. The field material was a glacial till (CL). The test areas identified as test strips A through D were compacted first at six roller passes each. Loose lift thickness were 31 cm for test strip A and 41 cm for test strips B through D. Average moisture content for strips A to D were as follows: 9.5%, 13.6%, 15.4%, and 15.7%.

Test strip E was compacted with 10 roller passes at a loose lift thickness of 26 cm and an average moisture content of 8.9%. Test strips F and G were compacted at a thicker loose lift thickness of approximately 68 cm. Strip G had an average moisture content measurement of 12.8% while strip was 15.6%. Finally, test strip H was compacted with 10 roller passes at a loose lift thickness of 31 cm and a moisture content of 12.9%. Optimum moisture for the till was established in the laboratory as 12%. Table 31 provides the identification for all test strips with summarized data for each test.

Field measurements taken were dry unit weight (nuclear and drive cone methods), moisture content (nuclear and oven methods), strength (DCP), and stiffness (Clegg hammer). Measurements were taken after all roller passes were completed.

Field Test 3 – Wells Fargo Construction Site, West Des Moines, Iowa

Field Test 3 was located a construction site in West Des Moines, Iowa. Testing was conducted on July of 2004 at three different areas on the project site for this field test. Four test strips were constructed and identified as A, B, C, and CV. Test strip A and B were constructed from a preexisting lean clay (CL). Four passes were used to compact strip A, while six passes were used for B. Average moisture contents were 27.5% and 22.6% for A and B respectively. Loose lift thicknesses for strip A and B varied between 35 to 50 cm. Test strip C and CV were constructed from a borrow fill material (CL) at six passes each. The average moisture content for C and CV was 26.7%.Lift thickness for test strips C and CV was approximately 40 cm. Three to five test points were selected randomly from each test strip and measured between roller passes. The vibratory option on the roller was used when constructing passes 7 and 8 in test strip B. Also, strip CV was fully constructed with vibratory while C was compacted in the static mode. Test strip identifications are shown in Table 35 to Table 38.

CHAPTER 5. FIELD RESULTS AND DISCUSSION

The following chapter summarizes results measured in the field. Field tests are first presented individually and then collectively together in the last section. Comparison with lab and field dry unit weights is given at the beginning of each section followed by statistical analyses. After these sections is a segment concerning the stability and uniformity of the soil based on DCP, Clegg, and Geogauge results.

Caterpillar Inc. Proving Grounds, Peoria, Illinois

The dry unit weight values measured in the field were plotted in the Proctor curve figure established in the laboratory (see Figure 115). Here, the achievement of compaction relative to standard Proctor can be determined.

As anticipated, the test strips rolled with three passes attained the highest relative compaction. Only one point of the 60 points measured achieved 95% standard Proctor (see Table 26). The range and mode for each test section is noted. Table 26 is a summary for all test strips at one, two, and three roller passes respectively.

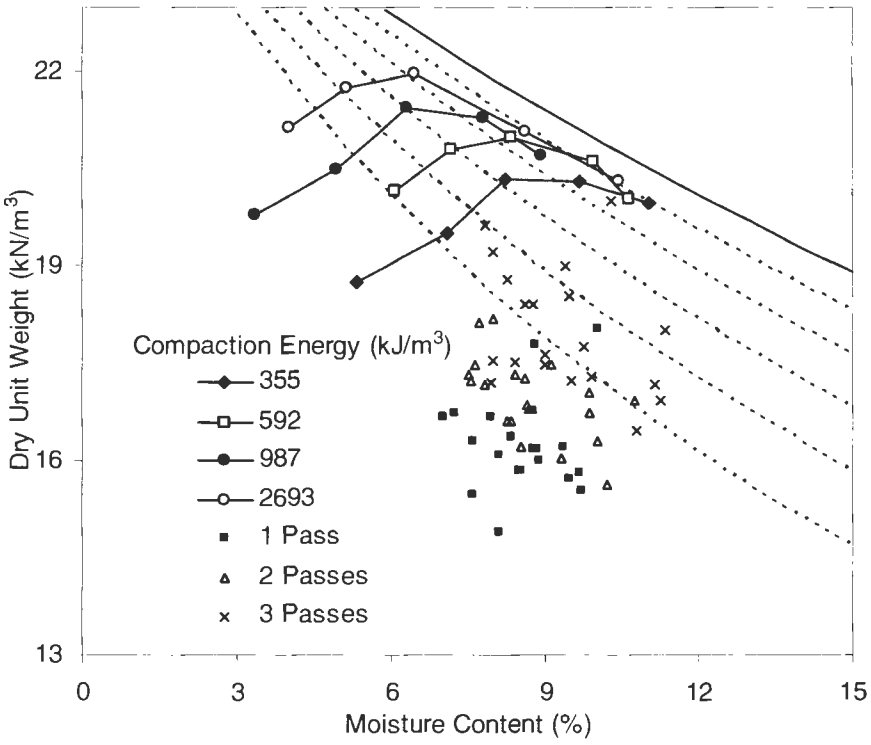

Figure 115. Dry unit weight in the field at different roller passes in relation to Proctor curves from the laboratory (PPG till)

Table 26. Statistics on relative compaction attained on field measurements (PPG till)

No. of Passes	No. of Measurements	Mean % Proctor	Standard Deviation (%)	No. of Points ≥ 95% Proctor	Range (%) (mode)
1	20	77	4	0	71–86 (4 at 77%)
2	20	81	3	0	75-85 (4 at 83%)
3	20	86	5	1	78-95 (4 at 82%)

A summary of average values from each test strip in given in Table 27. The number of test measurements is represented by the "n" column. The amount of roller passes influenced the dry unit weight of the till, increasing it with successive passes. Comparing test strips of 1 and 3 passes, DCP index showed a slight decrease and Geogauge measurements a slight increase. Stiffness measurement from Clegg appeared to not correlate with roller pass. It

shall be noted that only 42 measurements were taken for DCPI due to weather conditions later during in the period of testing. A detailed summary of all field test values is provided for in Table F1 - F6 Appendix F.

Table 27. Summary of in-situ measurements (PPG till, n = 10)

Test Strip	Number of Roller Passes	Average Values for Final Roller Pass						
		Dry Unit Weight (kN/m^3)	Percent Compact	Moisture Content (%)	Mean DCP Index (mm/blow)	Clegg Impact Value	Stiffness (MN/m)	Modulus (MPa)
1a	1	16.11	77	8.8	30	6.8	7.8	68.1
1b	1	16.41	78	8.3	30	6.5	7.8	67.7
2a	2	16.69	79	9.2	33	6.0	6.9	63.9
2b	2	17.27	82	8.3	28	6.4	6.4	56.1
3a	3	17.53	83	9.6	26	6.5	8.2	71.5
3b	3	18.50	88	9.1	12	7.0	9.2	80.1

Photos of the field tests performed at Peoria Proving Grounds are provided in Figure 116 through Figure 119.

Figure 116. Compaction being performed by CAT CP-533E roller

Figure 117. Measuring stiffness with Clegg impact hammer

Figure 118. GeoGauge used in measuring stiffness

Figure 119. Measuring strength with DCP

Statistical Analysis

Measurements from the field tests were evaluated using multi linear statistical analyses. Compaction energy and moisture content were the key independent variables used in the analysis. Normalized moisture content ($m - m_{opt}$) and the logarithm of compaction energy were also used in the analyses. Moisture content values were taken from nuclear gauge measurements. Compaction energy was represented by the number of roller passes. Relating roller passes to energy delivered to soils is affirmed by Proctor who stated the importance of knowing the number of roller passes needed to achieve a required dry unit weight (1933d). Dependent variables analyzed were dry unit weight (nuclear gauge), strength (DCP), and stiffness (Geogauge and Clegg Impact Hammer). The equations resulting from the analyses:

$$DD = 0.96(Pass) - 0.22(m\%) + 17.1 \quad [5\text{-}1]$$

$$DCPI = -5.4(Pass) - 0.012(m\%) + 37.4 \quad [5\text{-}2]$$

$$CIV = 0.13(Pass) - 0.23(m\%) + 8.3 \quad [5\text{-}3]$$

$$Stiff = 0.13(Pass) - 0.01(m\%) + 7.0 \quad [5\text{-}4]$$

$$Mod = 4.0(Pass) - 0.1(m\%) + 60.8 \quad [5\text{-}5]$$

where, Pass is the number of roller passes, m% is moisture content, DD is dry unit weight, DCPI is mean DCP index, CIV is Clegg impact value, Stiff is stiffness value from Geogauge, and Mod is modulus value from Geogauge.

Table 28 gives noteworthy statistical results from the analyses. Aside from equation 5-1, the models exhibited poor correlation, (r^2 between 0.02 – 0.10), with standard errors that are near the standard deviations of the dependent variables. Roller passes accounted for 46% of the variability of the dry unit weight while moisture content explained less than 1%. This is similar to laboratory results for PPG till. Percent variability was determined by squaring individual Pearson correlations (R values) between dependent and independent variables. Attempts to improve the correlation of the models proved unsuccessful when inputting logarithm of energy and normalized moisture content.

Table 28. Statistical analysis on PPG field test measurements

Equation	n	Adjusted r^2	Standard Error of Estimate	Standard Deviation	F-Statistic	t–statistics
5-1	60	0.49	0.76	1.06	29.1	OK
5-2	42	0.08	11.7	12.2	3.0	NG (both)
5-3	60	0.02	2.1	2.0	0.4	NG (both)
5-4	60	0.10	1.78	1.8	1.3	NG (both)
5-5	60	0.10	15.4	15.5	1.3	NG (both)

Individual regression graphs were created to determine non-linear relations between independent and dependent variables. No improvement was observed in regression for this particular case. This is most likely from little variation in moisture content, which relates exponentially to the field test measurements, particularly to the DCP. The number of roller passes also affected the regression, which behaves logarithmically with dry unit weight specifically. Only three roller passes were performed which likely inhibited the dry unit weight to reach an asymptotic state. This state probably would have occurred between six to eight roller passes. Also, measurements were not recorded after each roller pass; the exception of course being the test strip with only one pass. Therefore, since individual test strip data were not truly compared by pass the regression would be affected due to the inherent variability between test strips. Noteworthy figures of some dependent parameters as a function of pass and moisture content are given (Figure 120-Figure 125). A complete set of individual regression plots are given in Appendix G, including Geogauge plots and dependent parameters with normalized moisture content. Trendlines indicate moderate correlation in dry unit weight with roller pass and slight correlation in mean DCPI with roller pass. The remaining figures show poor correlation.

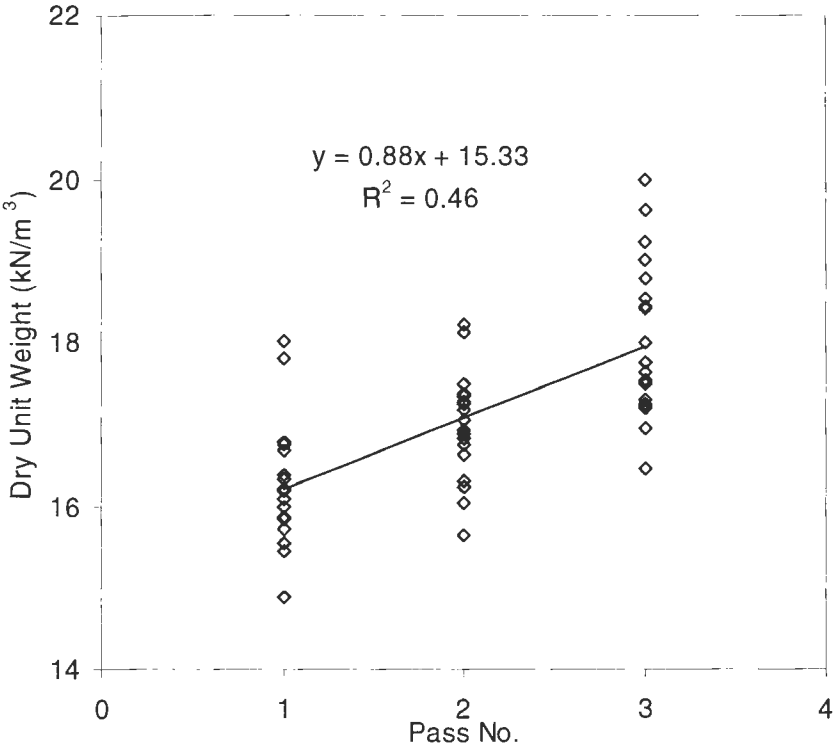

Figure 120. Regression of dry unit weight with roller pass (PPG)

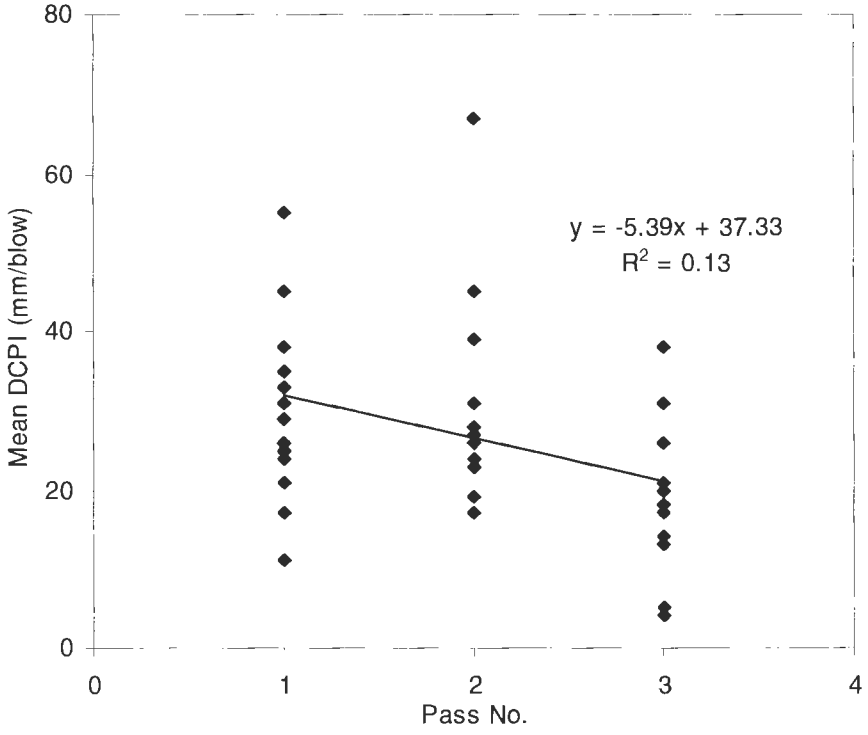

Figure 121. Regression of mean DCPI with roller pass (PPG)

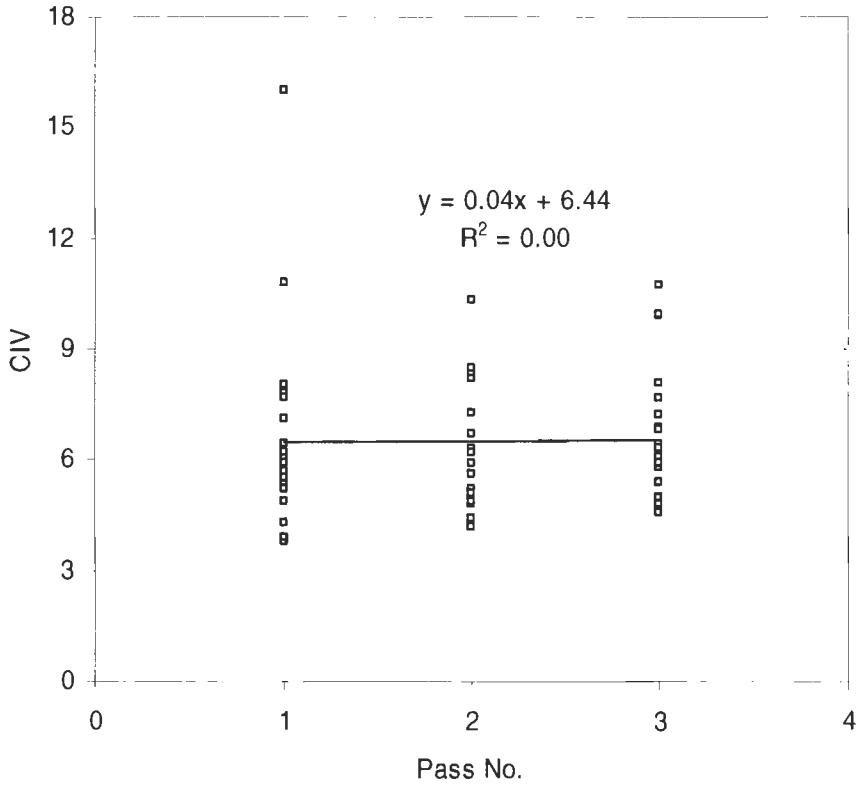

Figure 122. Regression of CIV with roller pass (PPG)

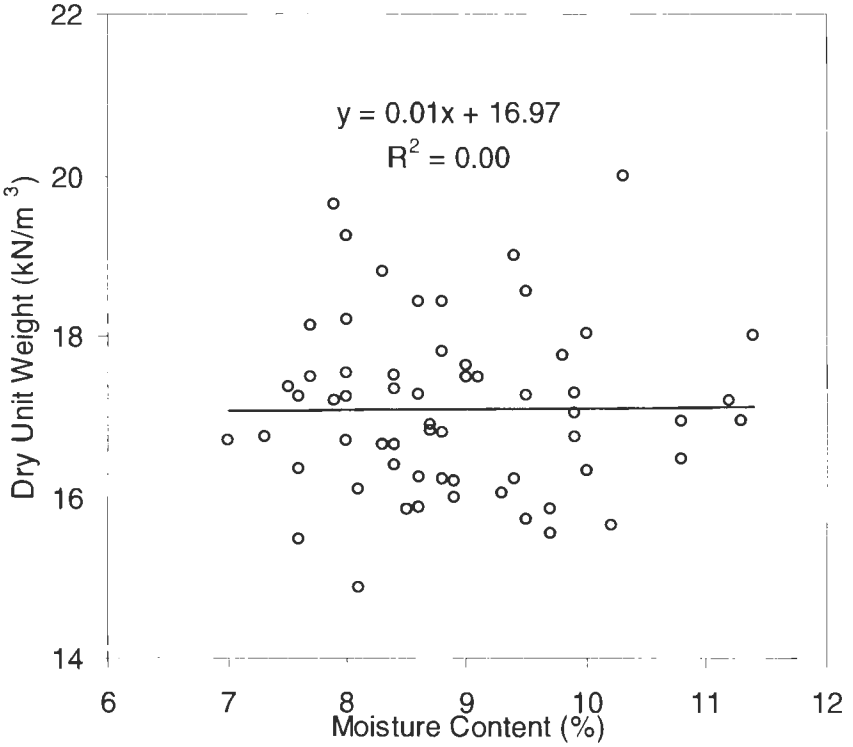

Figure 123. Regression of dry unit weight with moisture content (PPG)

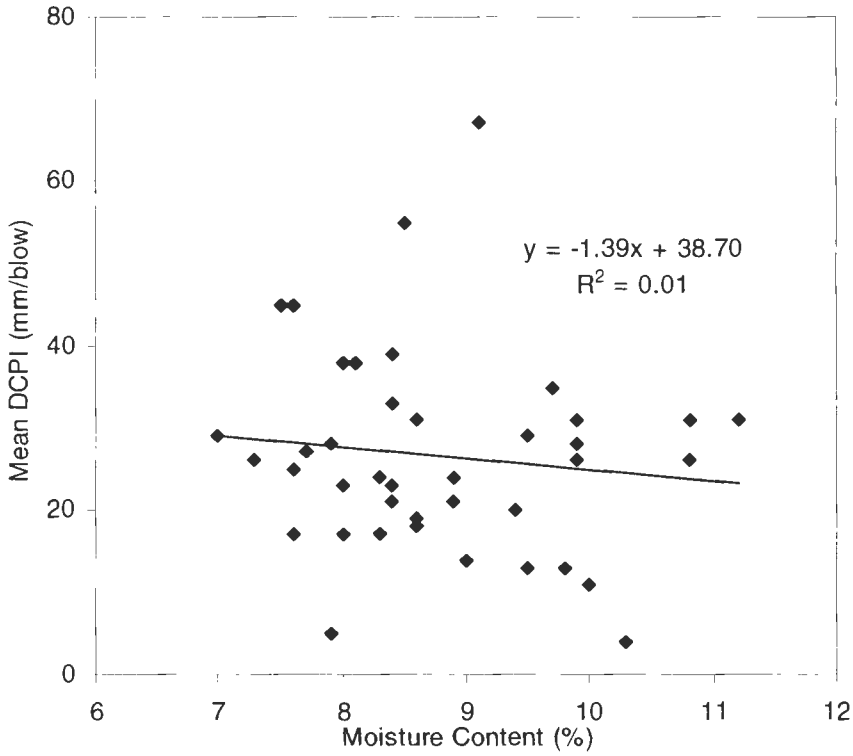

Figure 124. Regression of mean DCPI with moisture content (PPG)

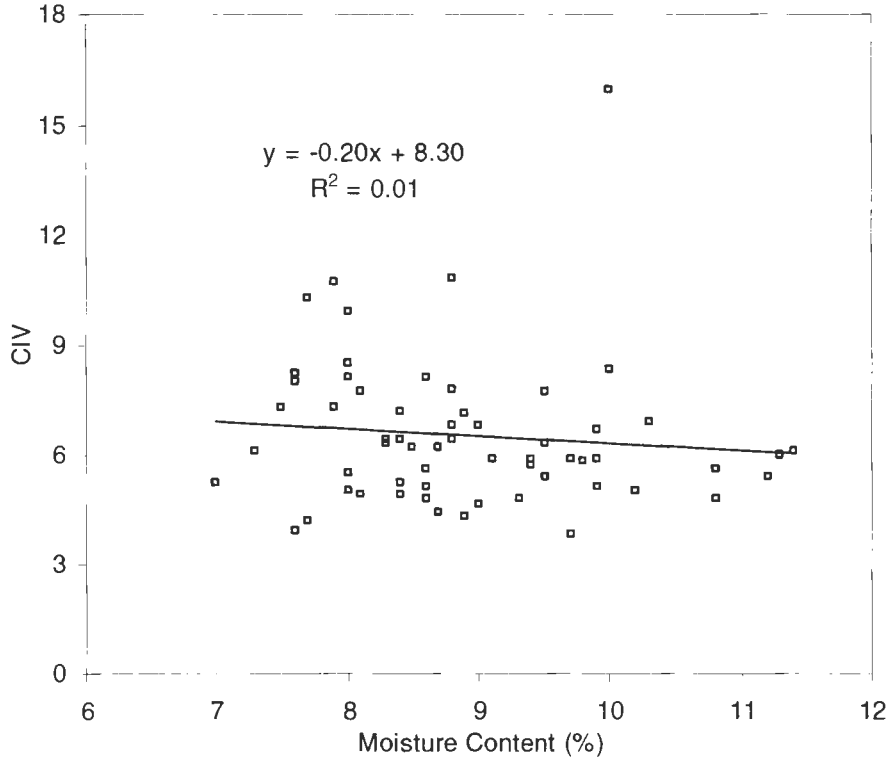

Figure 125. Regression of CIV with moisture content (PPG)

Stability and Uniformity

To interpret the stability and uniformity of the soil based on DCP results, a standard for a determination of quality is necessary. Compared to dry unit weight, little work has been performed to establish such a standard; particularly in Iowa. However, research on Iowa soils by White et al. (2002) resulted in the draft of proposed standards for the DCP, as well as a revised classification system of soils and moisture control. This work was used as a benchmark to classify soils and determine whether they met the appropriate DCP index threshold limits. The threshold limits used for this study are provided in Table 29.

Table 29. DCP threshold criteria used in study (after White et al., 2002)

Soil	Classification	Suitability Classification	Maximum Mean DCPI (mm/blow)	Maximum Mean Change in DCPI (mm/blow)	Moisture Control Range (% of m_{opt})
PPG	Low Plasticity Clay	Select	75	35	-1 to +3
Edwards	Low/Medium Plasticity Clay	Suitable	85	40	-1 to +3
WDSM Clay 1	Inorganic Silt of Medium Compressibility	Unsuitable	95	40	-2 to +4 ($m_{opt} \geq$ 20%)
WDSM Clay 2	Inorganic Silt of Medium Compressibility	Unsuitable	95	40	-2 to +4 ($m_{opt} \geq$ 20%)

Plots of mean DCPI, mean change in DCPI, moisture content, and compacted lift for each PPG test point are presented in Figure 126 - Figure 130. When applicable, plots were created using a four point moving average as suggested by White et al. (2002). The moisture control range and ideal zone of compacted lifts for earthwork construction (152 mm - 203 mm) are given in Figure 129 and Figure 130. It shall be noted that lifts could be higher by 50 to 100

mm and still be suitable. Therefore, it should not be regarded as a required standard in the industry. All four of the compaction criteria were met in the six test strips constructed with the Illinois till.

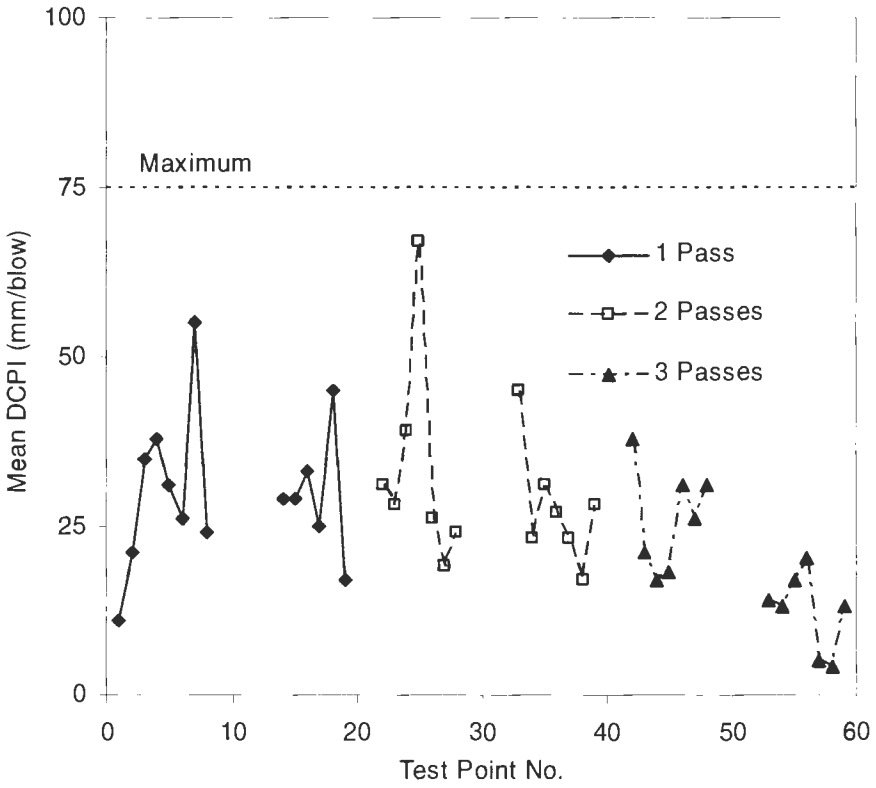

Figure 126. Mean DCPI for each test point (PPG)

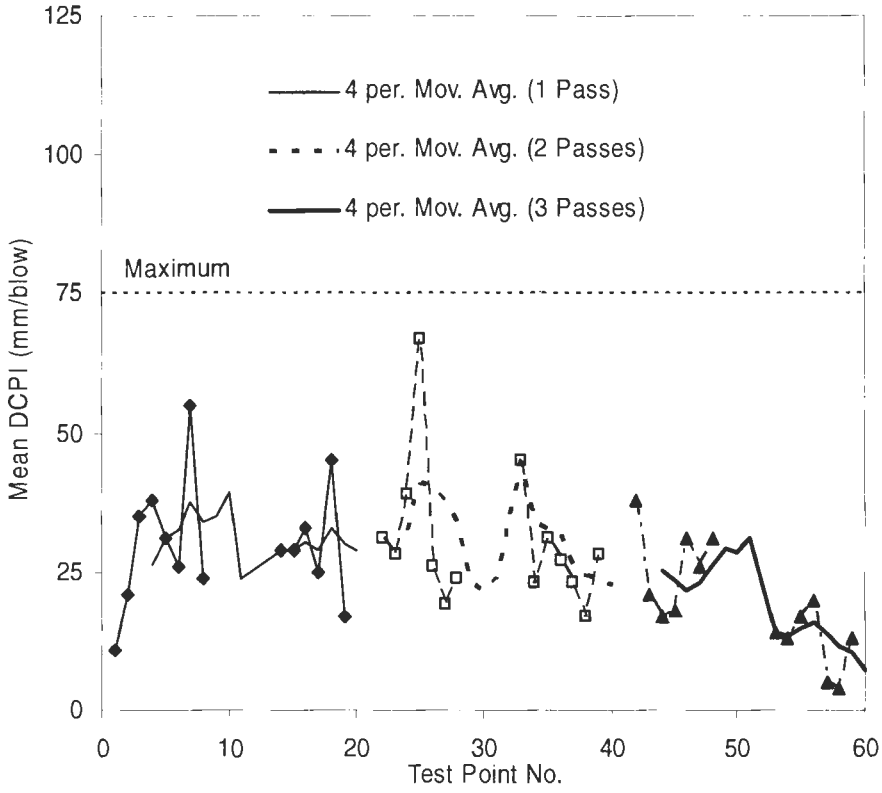

Figure 127. Mean DCPI with 4 point moving average (PPG)

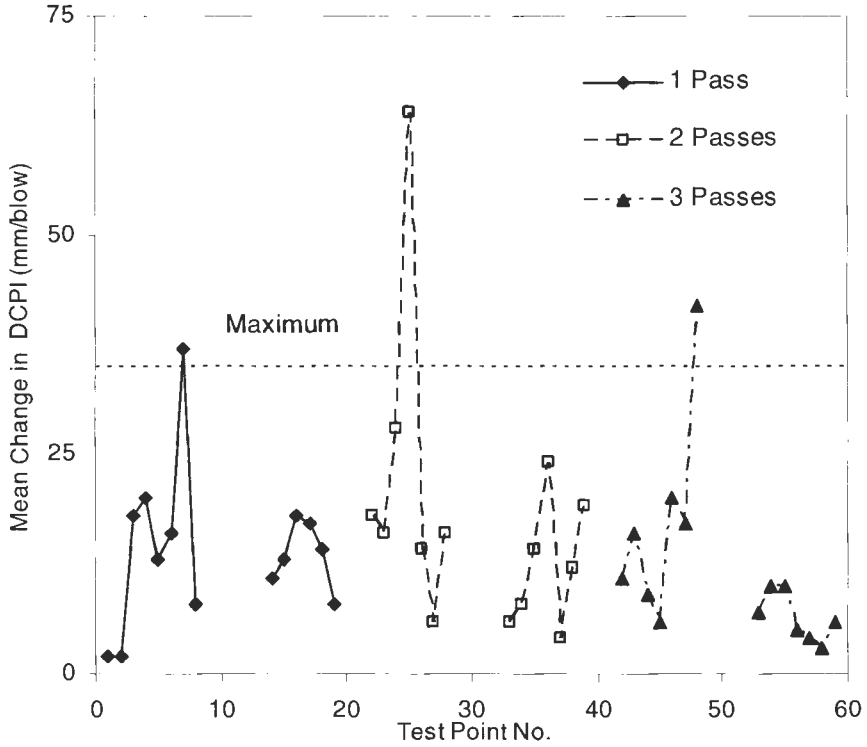

Figure 128. Mean change in DCPI for each test point (PPG)

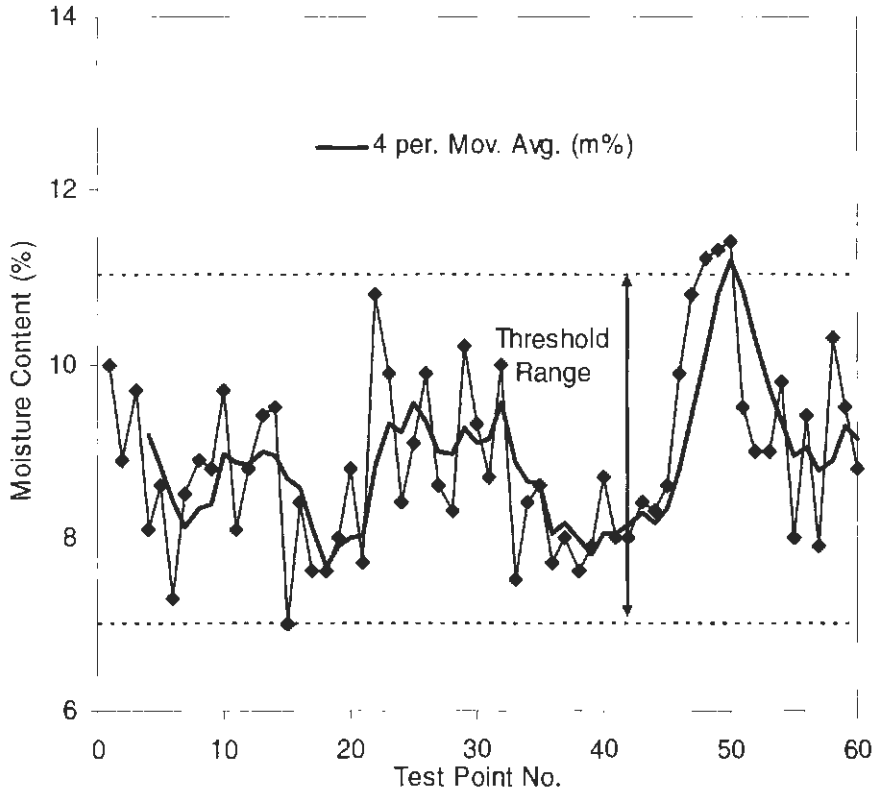

Figure 129. Moisture contents plotted with moisture range (PPG)

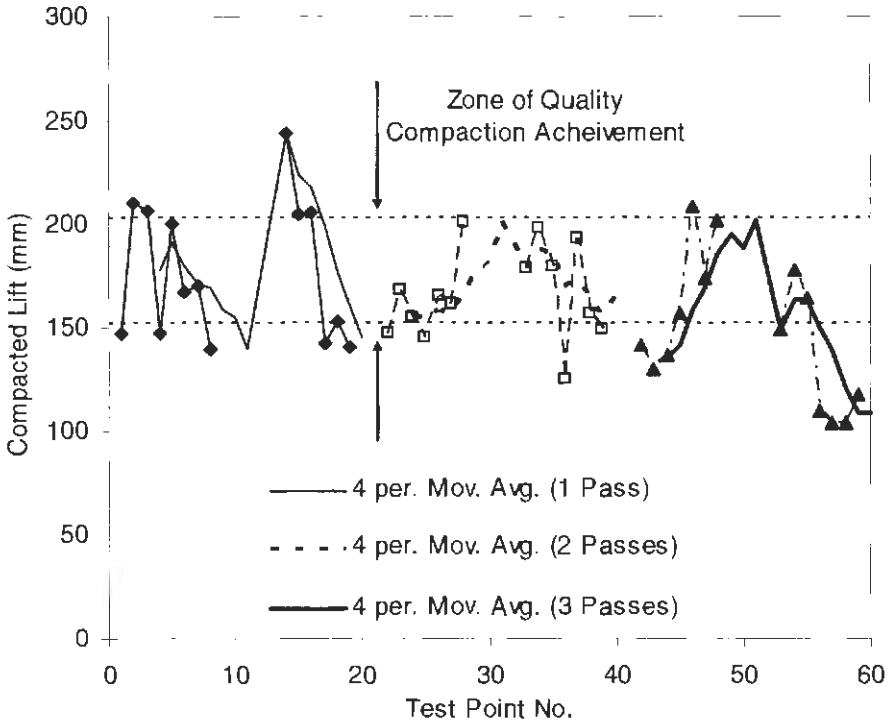

Figure 130. Compacted lifts plotted with ideal zone of compaction (PPG)

Stability measurements using Clegg and Geoguage are given in Figure 131 and Figure 132. In general, CIV, stiffness, and modulus do not vary much between roller passes. The high CIV value at one roller pass could be attributed to a dry spot or hitting a cobble at the surface of the test strip. Clegg values at two roller passes are lower than one roller pass at some points. This trend is also noted for Geogauge measurements. Collectively, CIV at three roller passes are slightly higher than the other test strips. Stiffness and modulus at three roller passes also exhibit this trend.

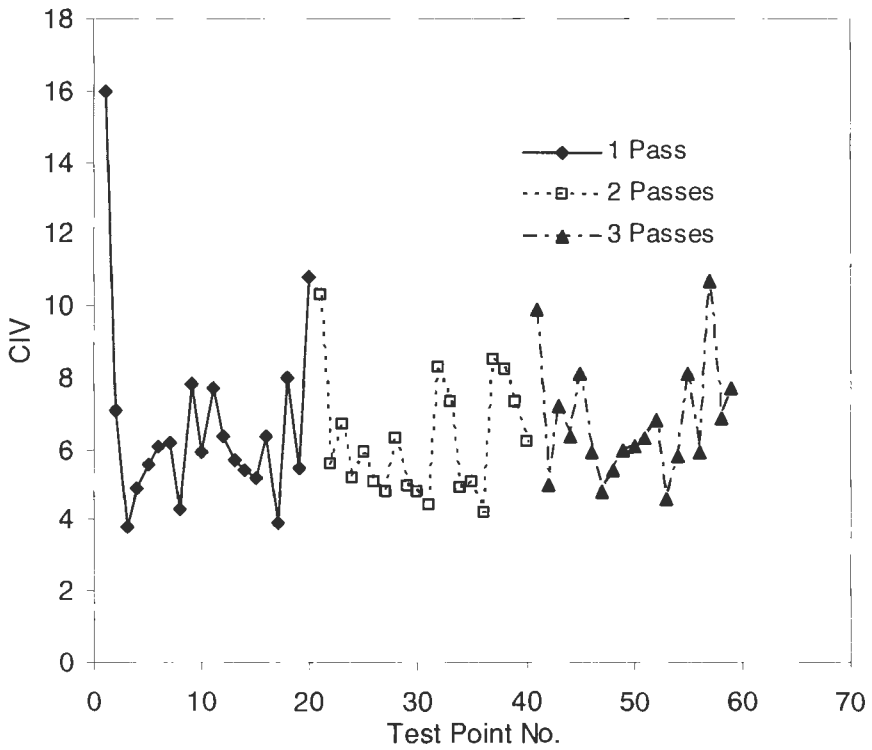

Figure 131. Clegg Impact Value for each test point (PPG)

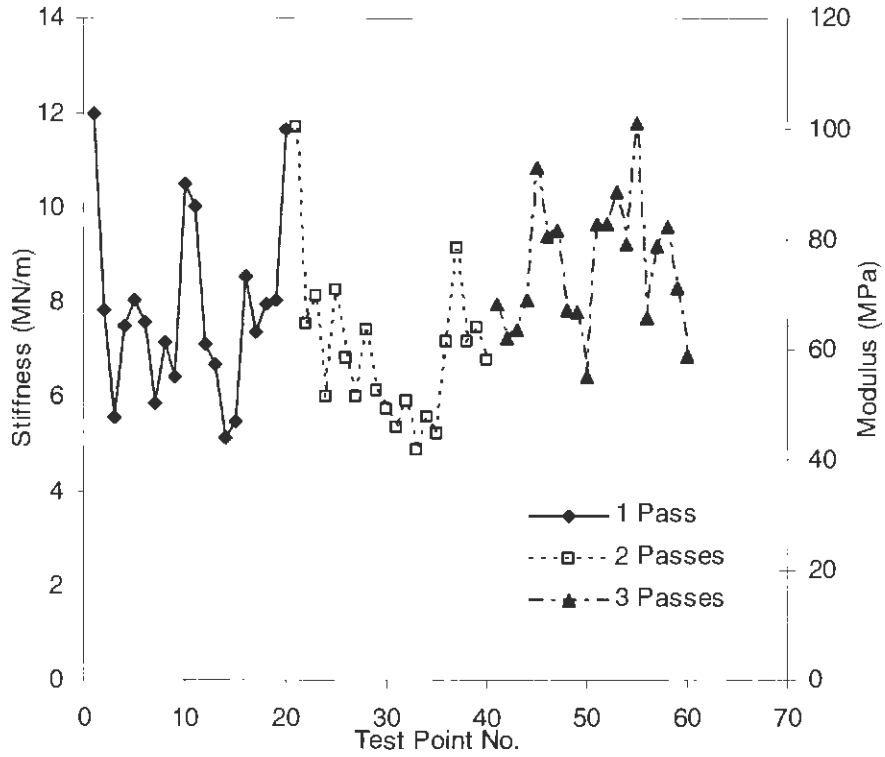

Figure 132. Stiffness and Modulus from Geogauge for each test point (PPG)

Edwards Test Facility, Peoria, Illinois

Figure 133 shows the laboratory standard Proctor curves and field test results attained for test strips compacted at six and ten roller passes. A majority of the points did not achieve 95% standard Proctor. Test strips with ten roller passes had a higher mean % Proctor and achieved six points at or above 95% standard Proctor (see Table 30). Table 30 is a summary for all test strips at six and ten roller passes respectively.

Table 31 gives a summary of average soil parameter measurements from each test strip. Initially, it was observed that moisture content contributed the greatest influence on DCPI and CIV. The affect of roller pass was not as obvious in this data set. A detailed summary of all field test values is provided for in Table F7 - F14 in Appendix F.

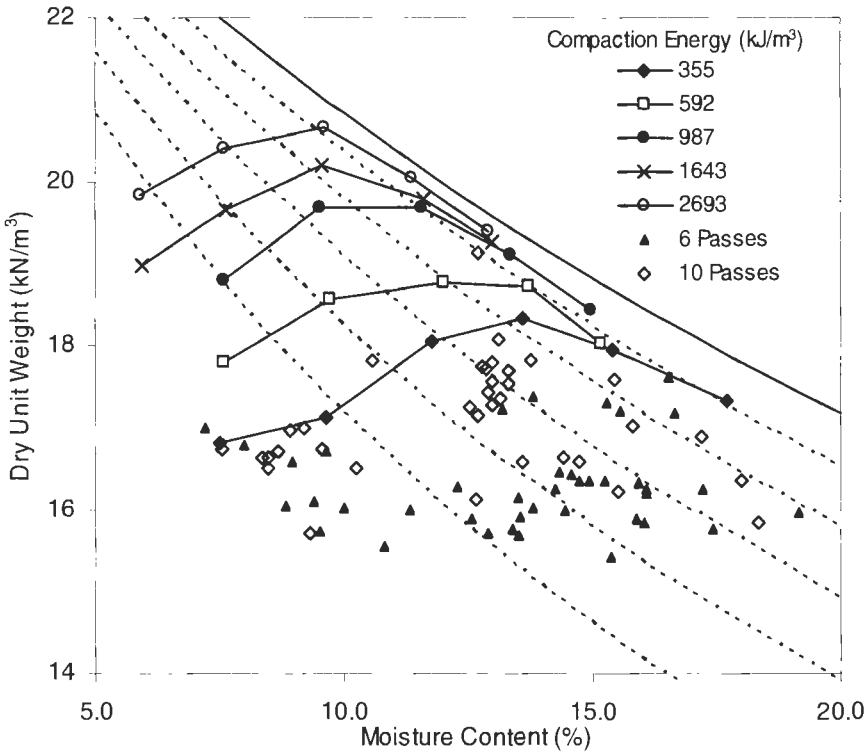

Figure 133. Dry unit weight in the field at different roller passes in relation to Proctor curves from the laboratory (Edwards till)

Table 30. Statistics on relative compaction attained on field measurements (Edwards till)

No. of Passes	No. of Measurements	Mean % Proctor	Standard Deviation (%)	No. of Points ≥ 95% Proctor	Range (%) (mode)
6	40	87	3	0	82–94 (9 at 85%)
10	35	91	4	6	84-102 (6 at 89%)

Table 31. Summary of in-situ measurements (Edwards Test Facility, n=10)

Test Strip	Loose Lift Thickness (cm)	Number of Roller Passes	Average Values for Final Roller Pass				
			Dry Unit Weight (kN/m^3)	Percent Compaction	Moisture Content (%)	Mean DCP Index (mm/blow)	Clegg Impact Value
A	30	6	16.22	86	9.5	24	13.0
B	40	6	16.00	85	13.6	49	9.0
C	40	6	16.58	88	15.4	81	5.7
D	40	6	16.39	87	15.7	80	5.1
E	25	10	16.61	89	8.9	16	20.3
F	68	10	16.80	90	15.6	64	7.6
G	66	10	17.20	92	12.8	45	11.6
H	30	10	17.72	94	12.8	22	13.0

Photos of the field tests performed at Edwards Test Facility are provided in Figure 134 and Figure 135.

Figure 134. Test strips A through D after compaction

Figure 135. Test strips F and G after tilling with RR350

Statistical Analysis

The linear multiple regression analysis on the Edwards test measurements yielded the following equations for the dependent variables DD, DCPI, and CIV:

$$DD = 0.19(Pass) - 0.01(m\%) + 15.0 \quad [5\text{-}6]$$

$$DCPI = -5.5(Pass) + 8.2(m\%) - 12.8 \quad [5\text{-}7]$$

$$CIV = 1.03(Pass) - 0.23(m\%) + 18.9 \quad [5\text{-}8]$$

In comparison to PPG field data, correlations improved slightly with Edwards data. This can be attributed to higher variation in moisture content. Slight correlation was seen for dry unit weight and DCP index equations (Table 32). The Clegg impact value equation had reasonable correlation with moisture content and roller pass. Particularly, moisture content was a stronger predictor in Clegg values, explaining 52% of the variability. Percent variability was determined by squaring individual Pearson correlations (R values) between

dependent and independent variables. Correlations were not improved by applying logarithm of roller passes or normalized moisture content. Normalized moisture content related with DCPI and CIV in the same manner as moisture content. Low correlation with roller pass can be attributed to the factors mentioned for the PPG field results, i.e. only using measurements from the last pass and not recording pass by pass.

Table 32. Statistical analysis on Edwards field test measurements

Equation	n	Adjusted r^2	Standard Error of Estimate	Standard Deviation	F-Statistic	t – statistics
5-6	75	0.26	0.63	0.73	14.0	NG
5-7	75	0.34	37.8	46.6	20.2	NG (P-2.5)
5-8	75	0.64	3.34	5.6	67.7	OK
5-9	75	0.78	0.31	1.67	135.8	OK
5-10	75	0.32	23.5	46.6	18.5	OK
5-11	75	0.78	0.31	1.67	135.8	OK
5-12	75	0.32	23.5	46.6	18.5	OK

Simple linear regressions for dry unit weight, DCPI, and CIV in the next set of graphs. Other graphs are presented in Appendix G. It was determined that DCPI related with moisture content values exponentially (see Figure 137 and Figure 142). Further analyses were performed to investigate the possibility of better correlation with exponential or other function that did not exhibit a linear relation. The mean DCPI linear equations were modified as follows:

$$\text{Log DCPI} = -0.09(\text{Pass}) + 0.18(\text{m\%}) + 1.95 \qquad [5\text{-}9]$$

$$\text{DCPI} = -5.4(\text{Pass}) - e^{0.0000004(\text{m\%})} + 87.1 \qquad [5\text{-}10]$$

$$\text{Log DCPI} = -0.09(\text{Pass}) + 0.18(\text{nm\%}) + 4.2 \qquad [5\text{-}11]$$

$$\text{DCPI} = -5.4(\text{Pass}) + e^{0.07(\text{nm\%})} + 87.0 \qquad [5\text{-}12]$$

Results of these equations show that taking the logarithm of the dependent variable increases the r^2 values, while the exponential regression exhibited lower correlations ($r^2 = 0.39$) than the linear model.

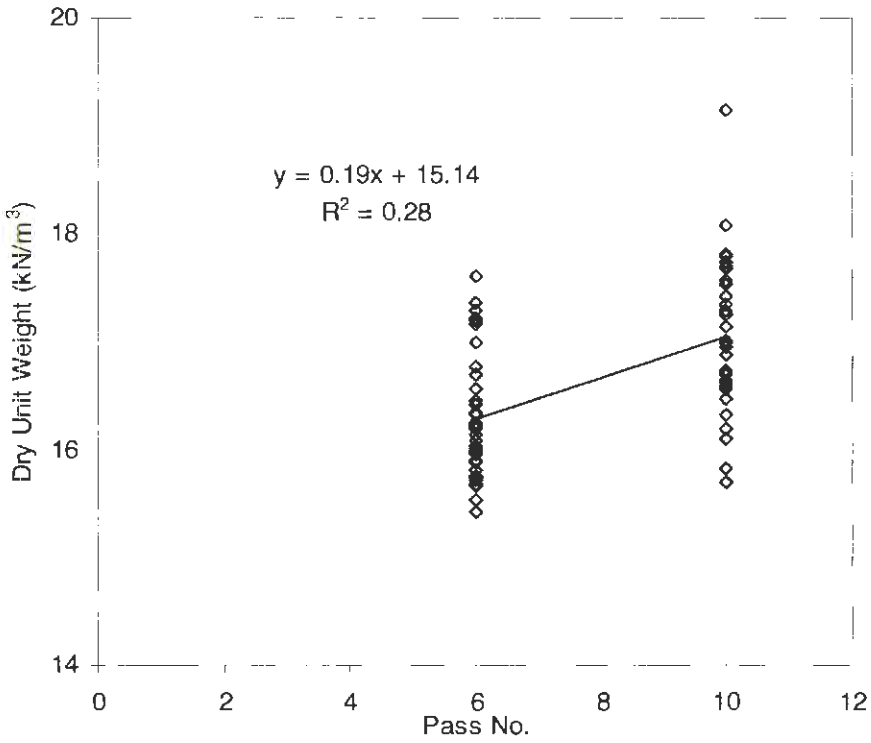

Figure 136. Regression of dry unit weight with roller pass (Edwards)

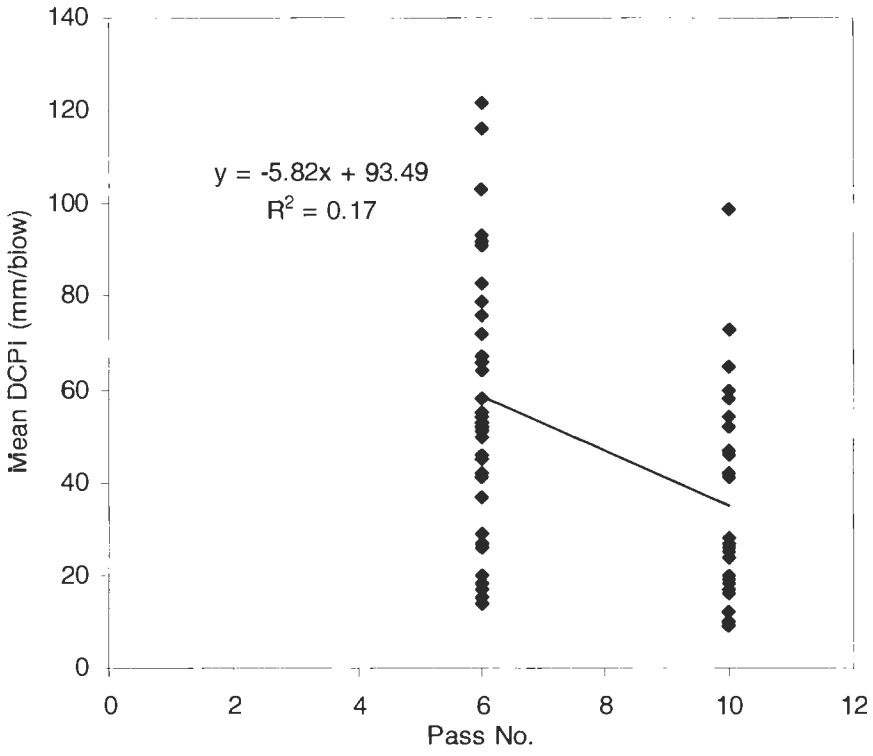

Figure 137. Regression of mean DCPI with roller pass (Edwards)

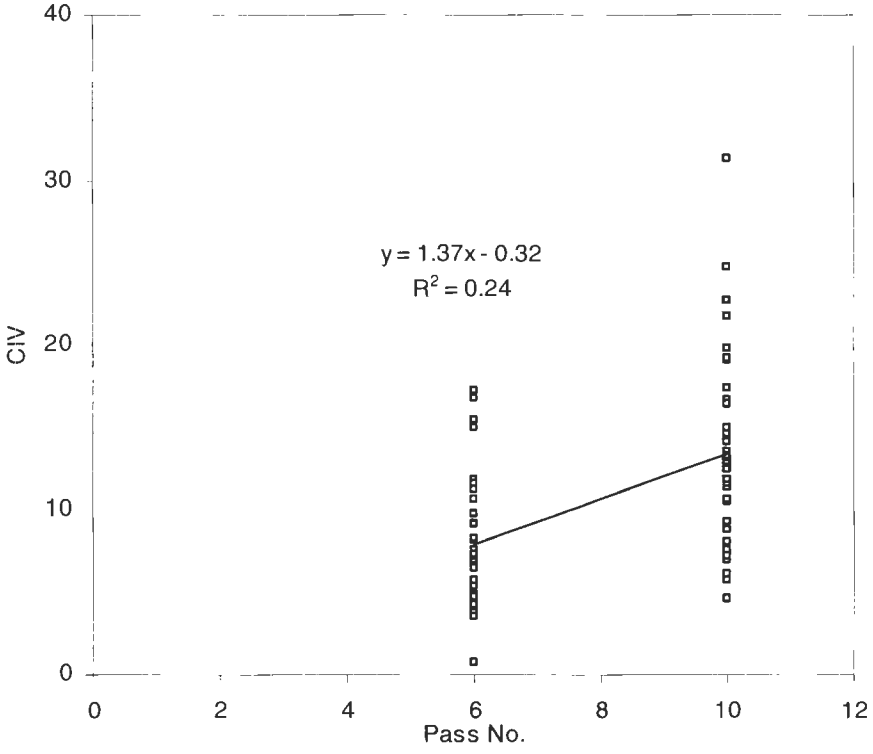

Figure 138. Regression of CIV with roller pass (Edwards)

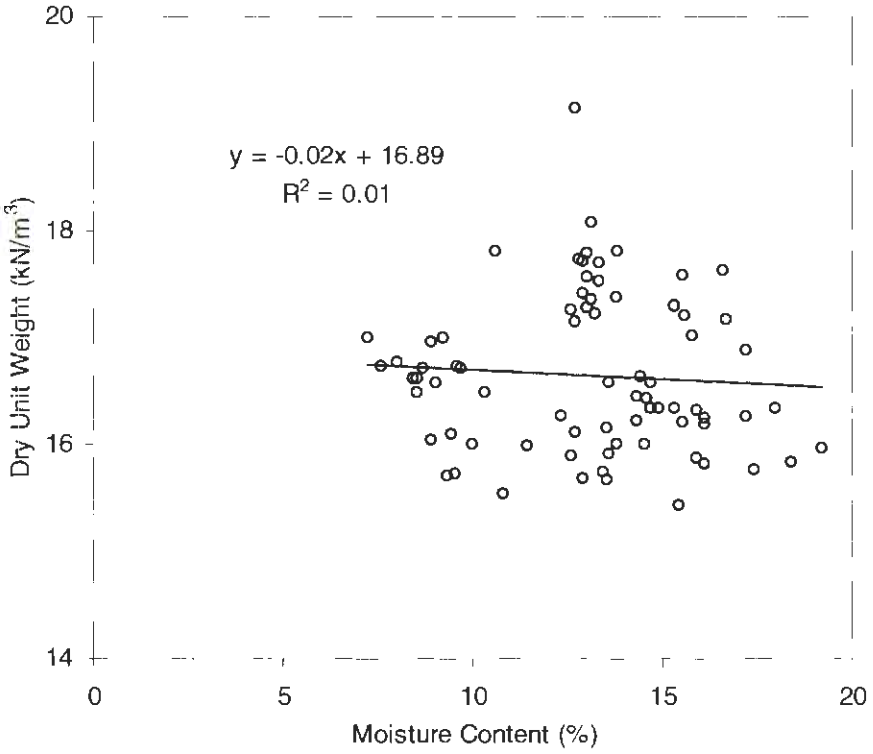

Figure 139. Regression of dry unit weight with moisture content (Edwards)

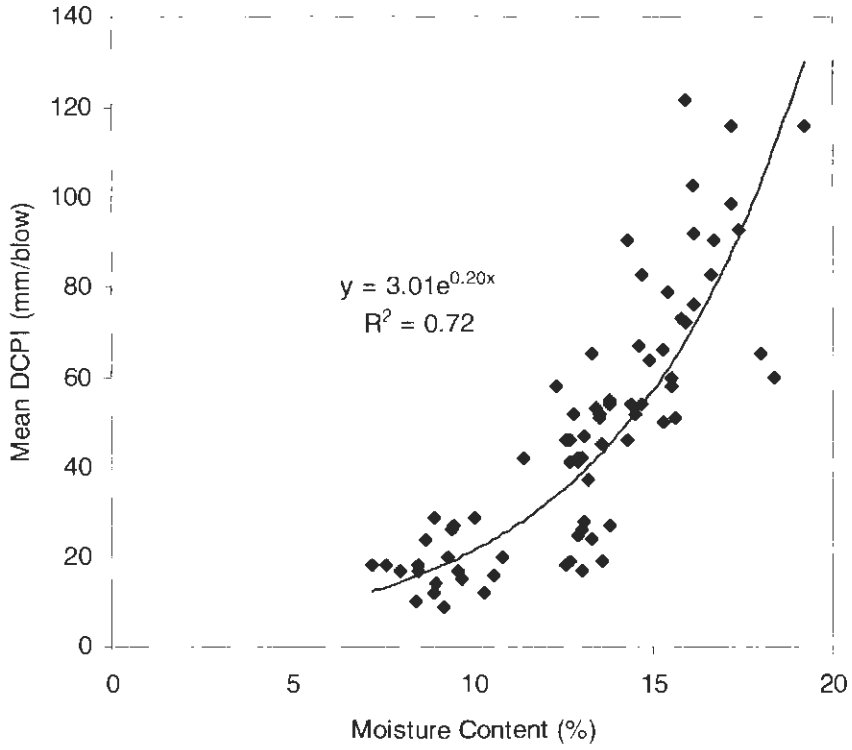

Figure 140. Regression of mean DCPI with moisture content (Edwards)

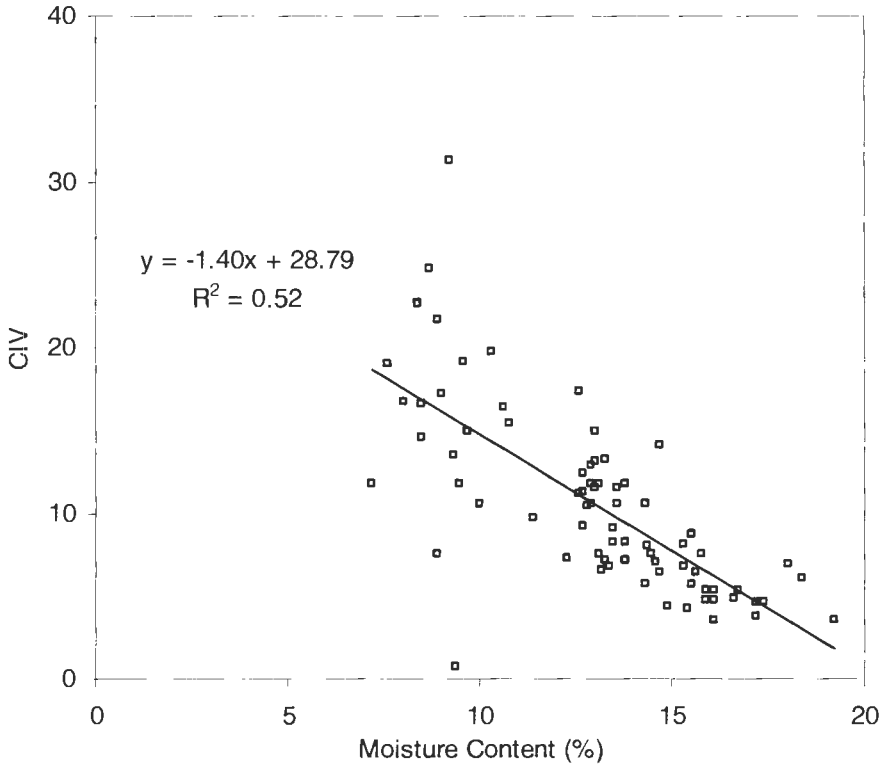

Figure 141. Regression of CIV with moisture content (Edwards)

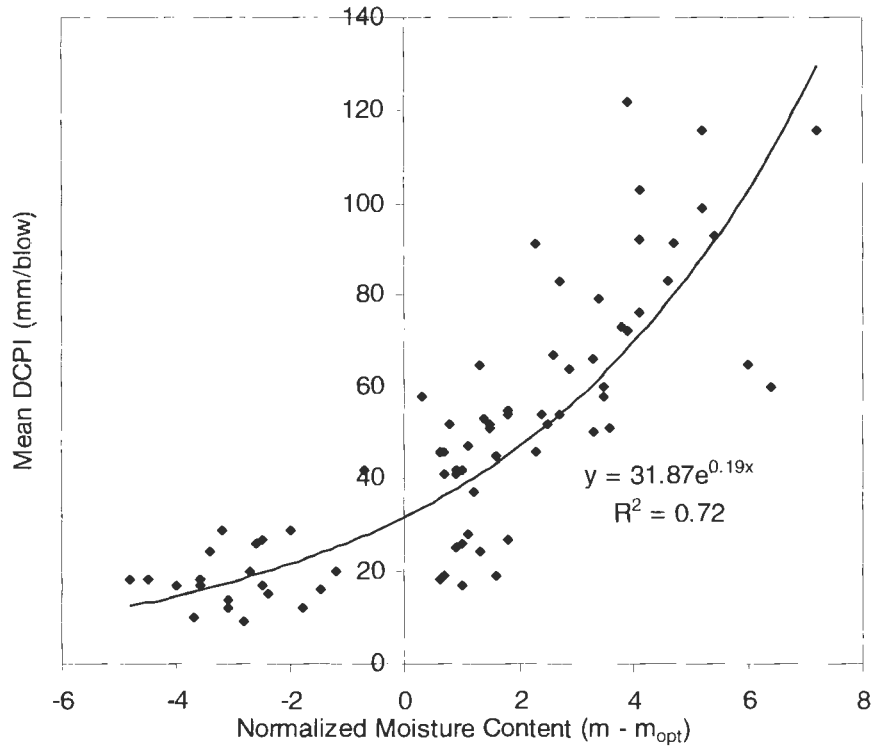

Figure 142. Regression of mean DCPI with normalized moisture content (Edwards)

Stability and Uniformity

Data for this field test was separated by number of roller passes. Figure 143 to Figure 147 present measurements from points on test strips with six roller passes, while Figure 148 to Figure 152 is data from ten roller passes. Test strips C and D indicated mean DCPI value above the maximum threshold. A problem with uniformity appeared only on strip D. While compacted lifts were higher than the range given, they were still suitable for real field conditions. Therefore, the stability and uniformity issues could be attributed to moisture content outside the threshold range which was the case seen in Figure 146. Also in this figure, strip A was observed to be dry of optimum. Strips E and H were compacted well, between 185 – 256 mm. Compacted lifts for strips F and G were high (440 – 634 mm), but still met DCPI standards. Strip F was slightly wet of the moisture control range and E was slightly dry.

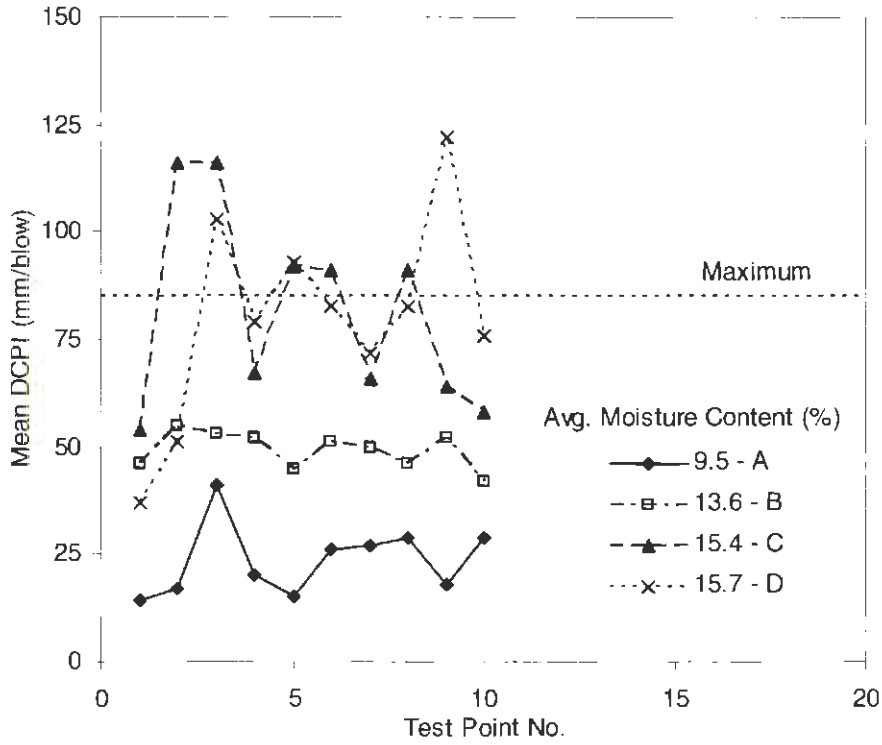

Figure 143. Mean DCPI for strips A-D (6 roller passes)

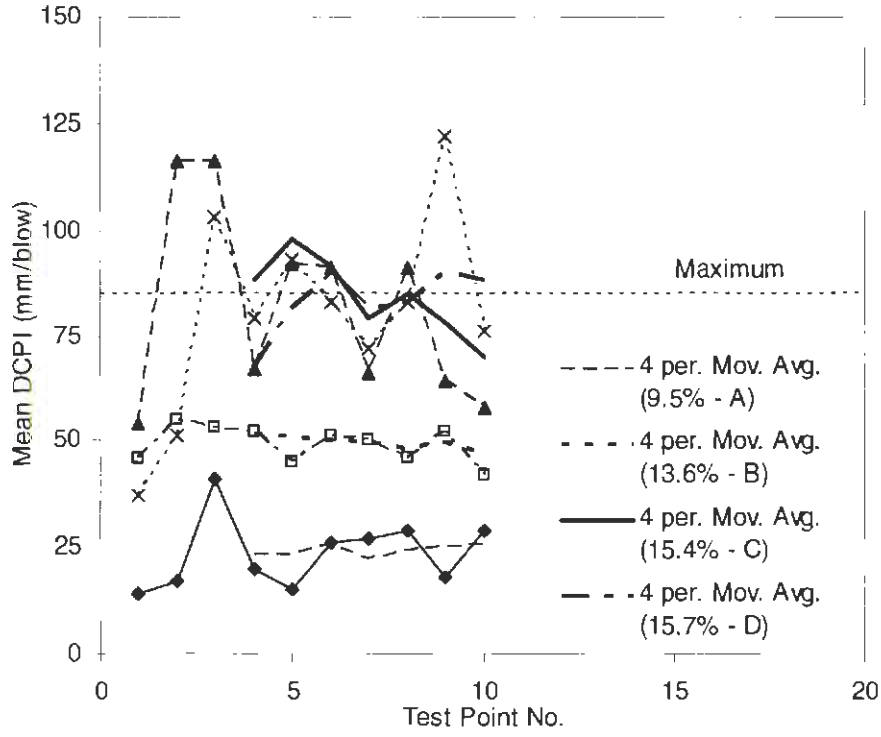

Figure 144. Mean DCPI for strips A-D with 4 point moving average (6 roller passes)

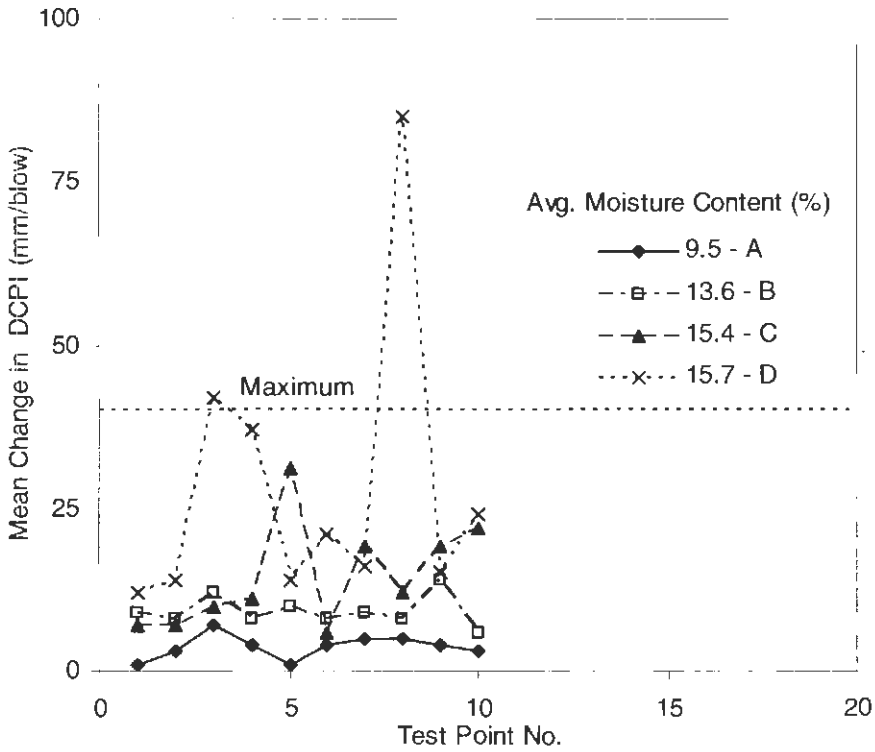

Figure 145. Mean change in DCPI for strips A-D (6 roller passes)

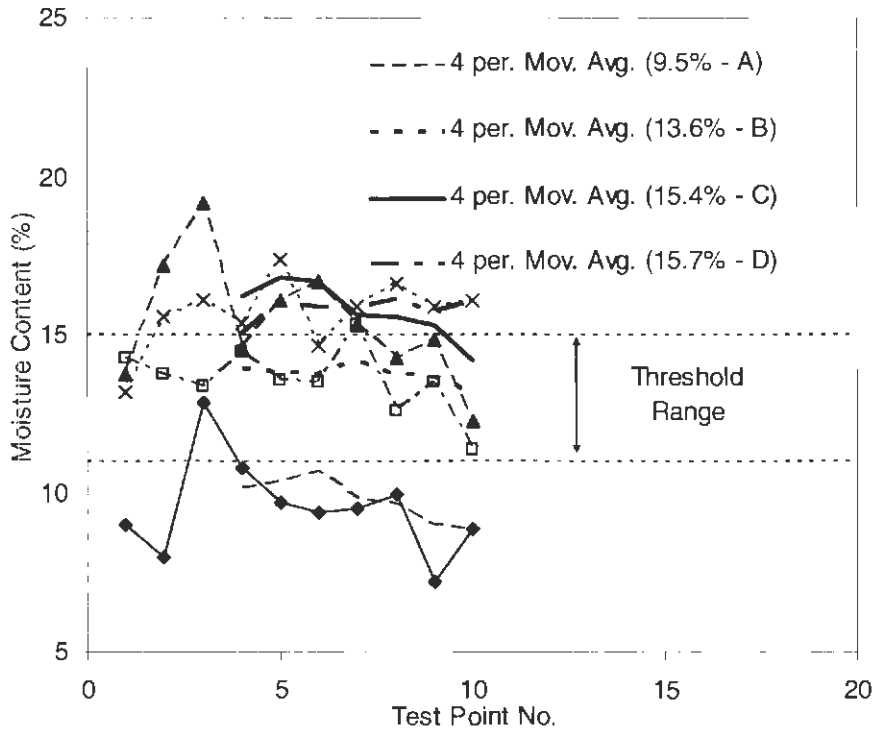

Figure 146. Moisture content for strips A-D with 4 point moving average

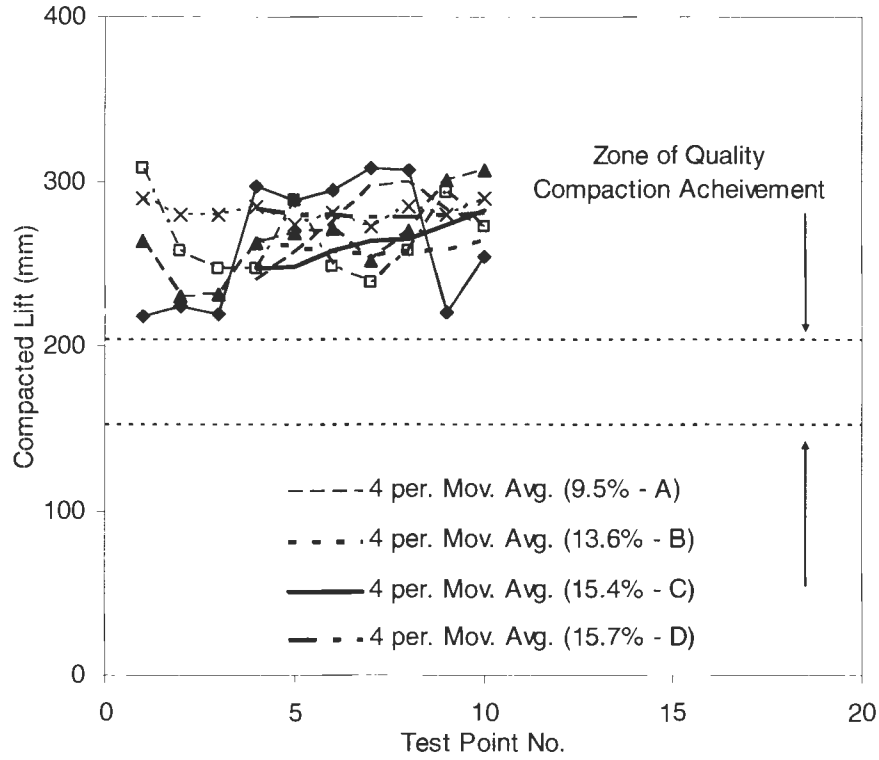

Figure 147. Compacted lifts for strips A-D plotted with ideal zone of compaction

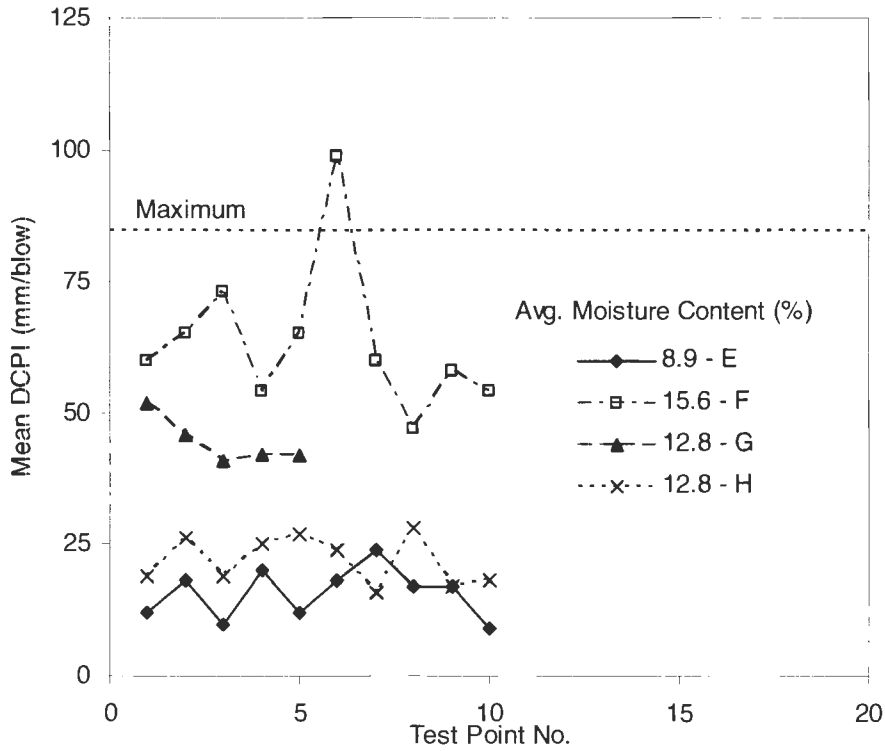

Figure 148. Mean DCPI for strips E-H (10 roller passes)

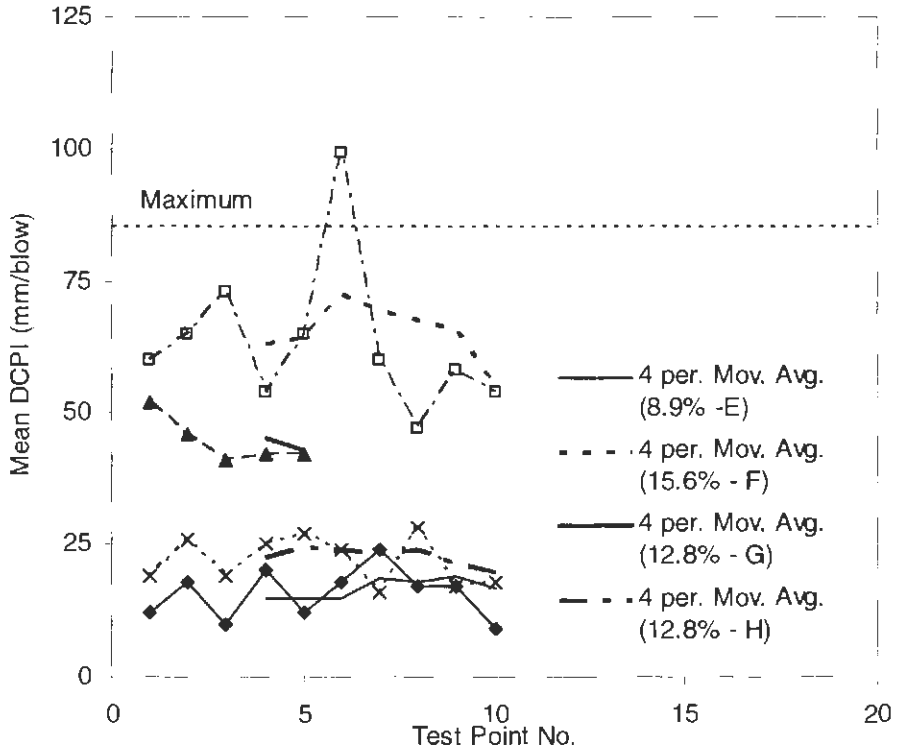

Figure 149. Mean DCPI for strips E-H with 4 point moving average (10 roller passes)

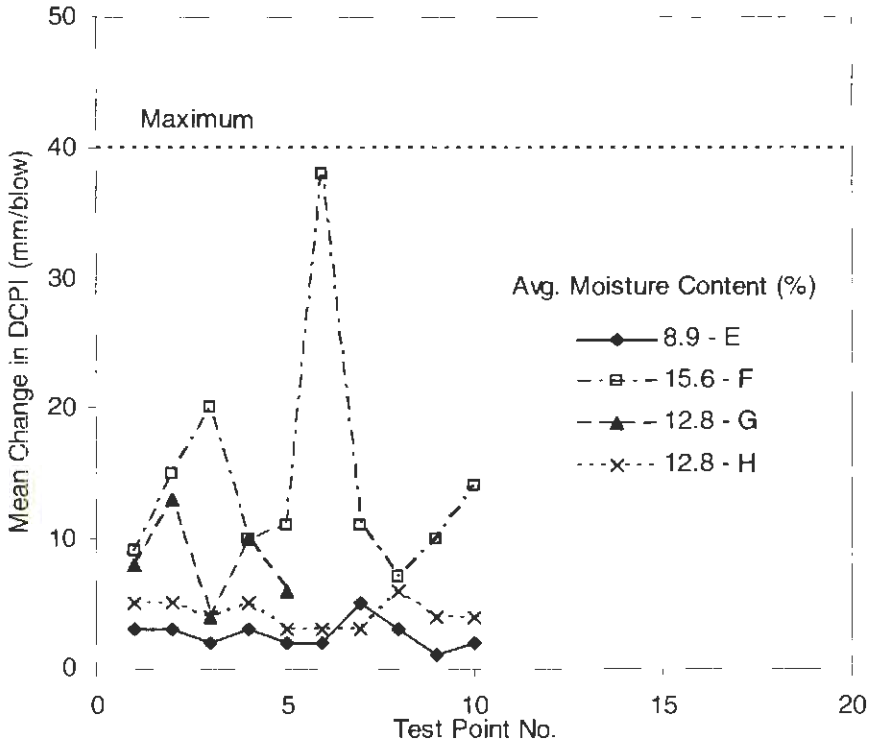

Figure 150. Mean change in DCPI for strips E-H (10 roller passes)

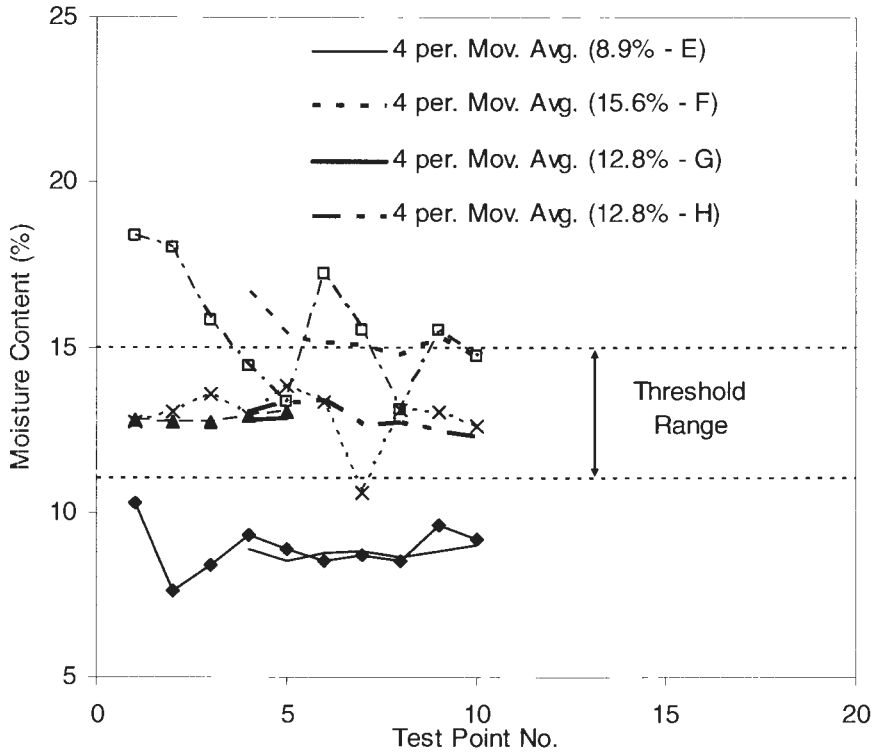

Figure 151. Moisture content for strips E-H with 4 point moving average

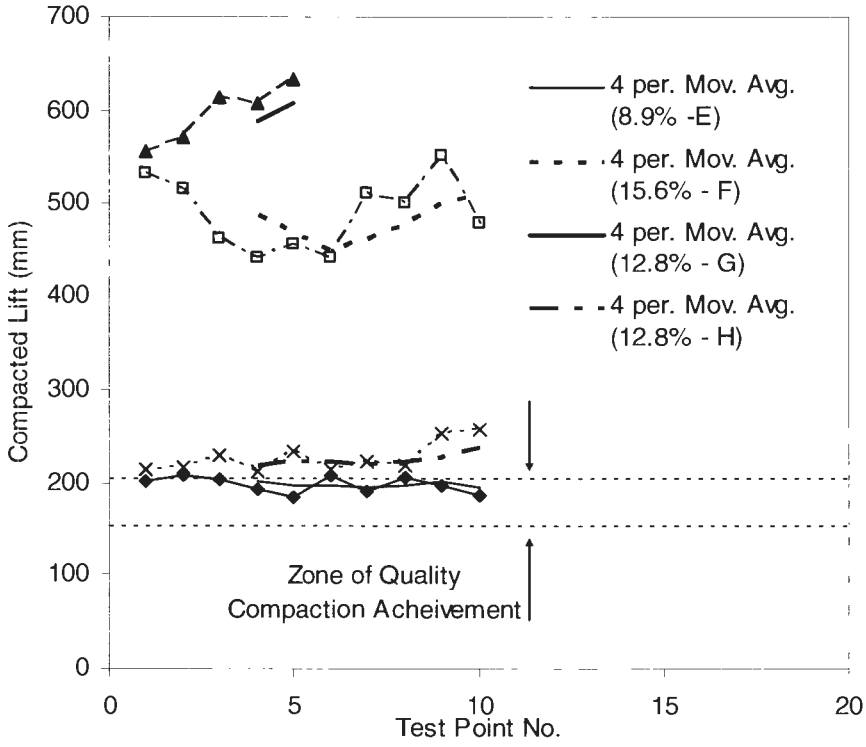

Figure 152. Compacted lifts for strips E-H plotted with ideal zone of compaction

Figure 153 and Figure 154 provide all CIV measurements for test strips A – H. For test strips rolled at six passes, strip A resulted in highest CIV values followed by strip B. Strip A had the lowest loose lift thickness (30.5 cm) and driest average moisture content of A – D. It is for certain that moisture content contributed to higher CIV for A, since B, which was drier than C and D, had higher CIV measurements and the same loose lift thickness. It is not for certain if the lower loose lift at A contributed to higher CIV measurements. Test strips C and D had similar values throughout their lengths. The question of whether loose lift thickness affected the CIV could be answered by looking at results from test strips E – H. Here, the same trend occurred where the highest CIV measurements were found in the driest conditions (strip E). This is followed by strips G and H which had the same average moisture content of 12.8% and then G at 15.8%. While G and H had similar CIV measurements at 12.8% moisture content they had different loose lift thicknesses. Therefore, loose lift thickness doesn't appear to be a determinate of CIV. These observations of moisture content's relation to CIV correspond to the statistical analyses of CIV.

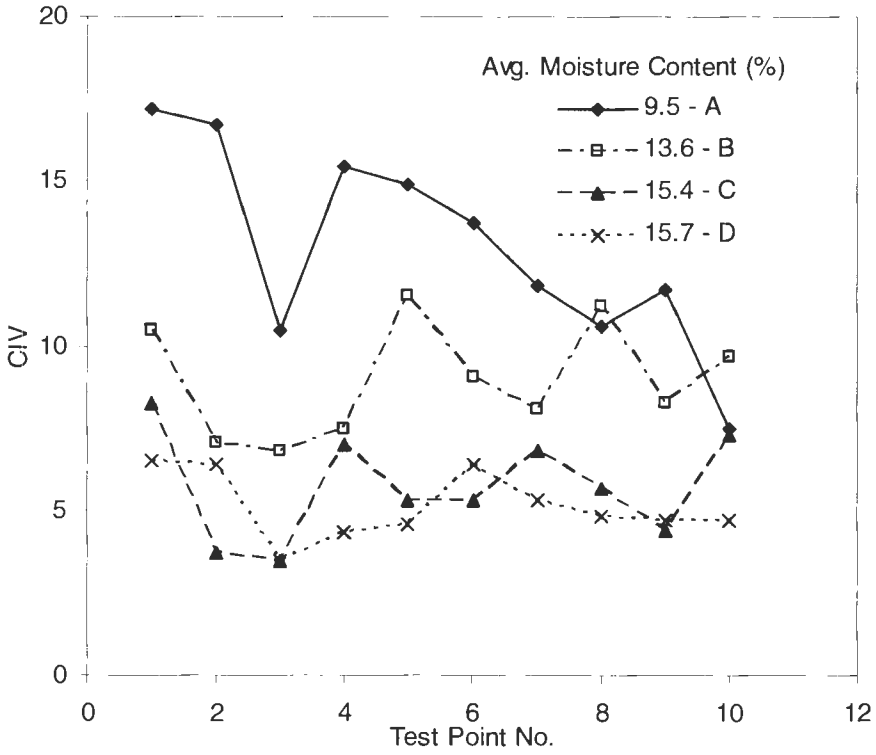

Figure 153. Clegg Impact Values for strips A – D (6 roller passes)

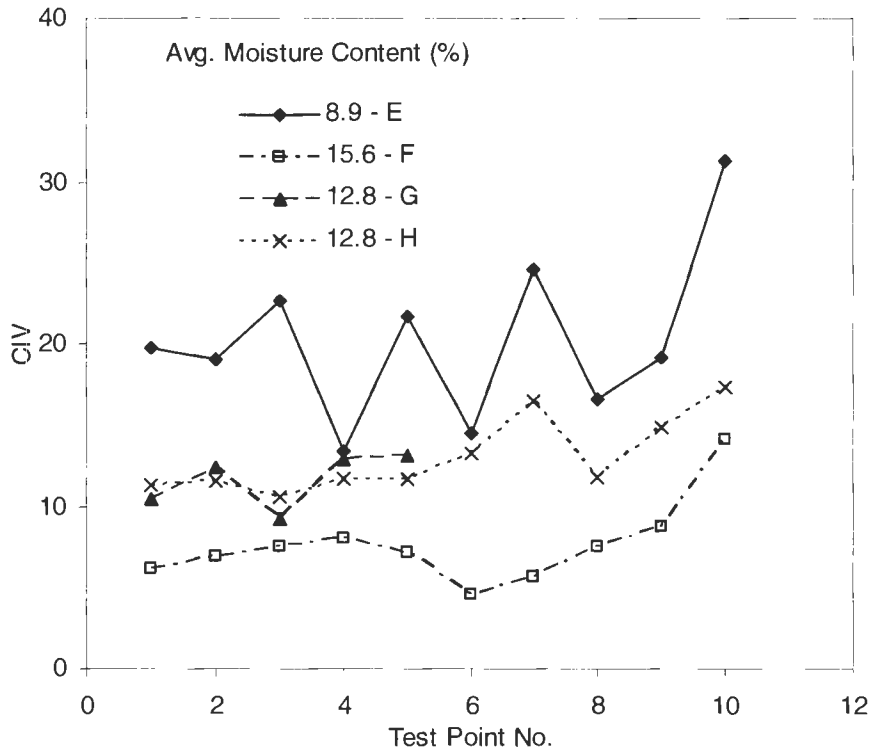

Figure 154. Clegg Impact Values for strips E – H (10 roller passes)

Wells Fargo Construction Site, West Des Moines, Iowa

Relative compaction achieved for existing and fill clay constructed are displayed in Figure 155 and Figure 156. The achievement 95% standard Proctor was not attained. Data in Table 33 and Table 34 indicate an increase in mean % Proctor by pass. Table 33 and Table 34 are summaries for all test strips at one to four and six roller passes respectively.

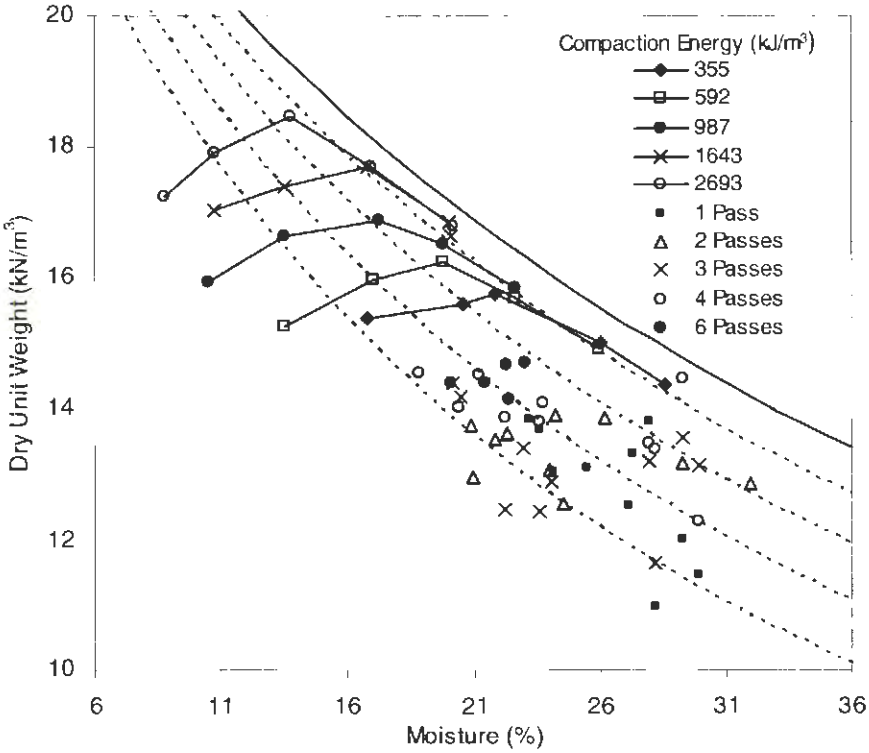

Figure 155. Dry unit weight in the field at different roller passes in relation to Proctor curves from the laboratory (existing clay)

Table 33. Statistics on relative compaction attained in field (existing clay)

No. of Passes	No. of Measurements	Mean % Proctor	Standard Deviation (%)	No. of Points ≥ 95% Proctor	Range (%) (mode)
1	10	79	6	0	77–86 (2 at 81,85%)
2	10	82	3	0	77-86 (2 at 81,85%)
3	10	81	5	0	72-89 (2 at 77,81%)
4	10	85	4	0	76-90 (2 at 87,90%)
6	5	89	1	0	87-91 (2 at 89%)

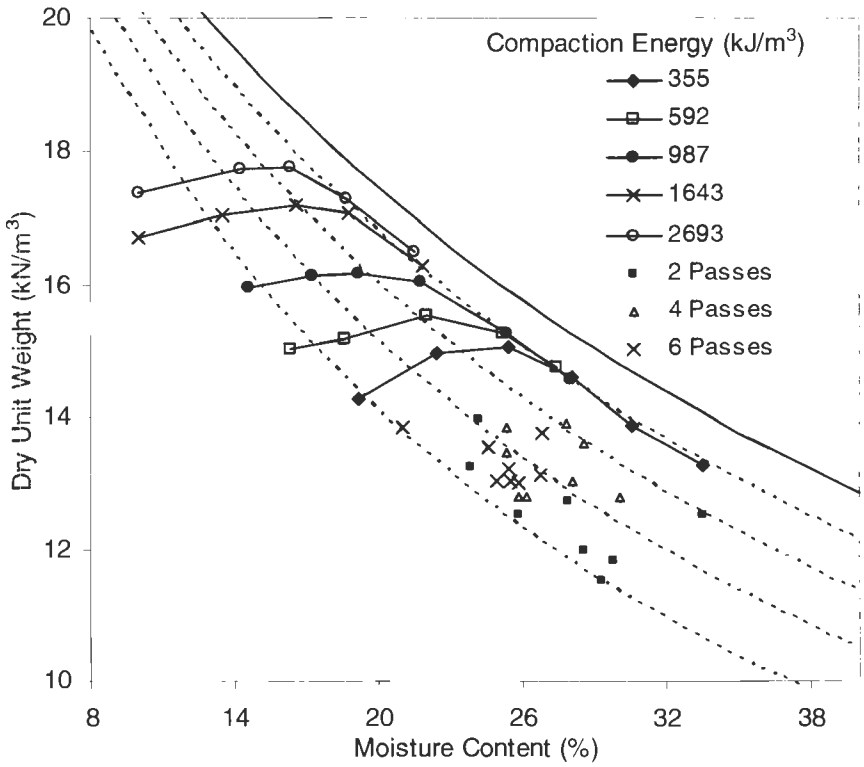

Figure 156. Dry unit weight in the field at different roller passes in relation to Proctor curves from the laboratory (fill clay)

Table 34. Statistics on relative compaction attained in field (fill clay)

No. of Passes	No. of Measurements	Mean % Proctor	Standard Deviation (%)	No. of Points ≥ 95% Proctor	Range (%) (mode)
2	8	79	5	0	73–88 (2 at 79%)
4	8	84	3	0	81-88 (3 at 81%)
6	8	84	2	0	82-88 (3 at 82%)

A summary of average values from successive roller passes is presented in Table 35 through Table 38. With increasing roller passes, values of dry unit weight and Clegg impact generally increased while DCPI decreased in test strip B, C, and CV. Average values in test strip A varied by pass. Table F15 - F29 in Appendix F provides further detail of measurements taken in the field.

Photos of the field tests performed in West Des Moines are provided in Figure 157-Figure 160.

Table 35. Summary of in-situ measurements (West Des Moines - test strip A)

Pass Number	Average Values from Successive Roller Passes					
	n	Dry Unit Weight (kN/m^3)	Percent Compaction	Moisture Content (%)	Mean DCP Index (mm/blow)	Clegg Impact Value
1	5	12.39	76	27.8	130	2.9
2	5	13.23	82	26.9	132	3.7
3	5	12.81	79	27.8	102	2.7
4	5	13.49	83	27.8	101	3.4

Table 36. Summary of in-situ measurements (West Des Moines - test strip B)

Pass Number	Average Values from Successive Roller Passes					
	n	Dry Unit Weight (kN/m^3)	Percent Compaction	Moisture Content (%)	Mean DCP Index (mm/blow)	Clegg Impact Value
1	5	13.18	81	25.4	159	2.8
2	5	13.45	83	22.4	155	3.1
3	5	13.48	83	22.0	123	3.6
4	5	14.23	88	21.3	124	3.8
6	5	14.47	89	21.9	139	3.8

Table 37. Summary of in-situ measurements (West Des Moines - test strip C)

Pass Number	Average Values from Successive Roller Passes					
	n	Dry Unit Weight (kN/m^3)	Percent Compaction	Moisture Content (%)	Mean DCP Index (mm/blow)	Clegg Impact Value
2	3	12.44	79	26.4	67	4.8
4	3	13.15	83	25.8	65	6.4
6	3	13.07	83	25.7	60	6.4

Table 38. Summary of in-situ measurements (West Des Moines - test strip CV)

Pass Number	Average Values from Successive Roller Passes					
	n	Dry Unit Weight (kN/m^3)	Percent Compaction	Moisture Content (%)	Mean DCP Index (mm/blow)	Clegg Impact Value
2	5	12.62	80	28.8	60	6.1
4	5	13.36	84	28.0	54	6.9
6	5	13.48	85	24.7	51	6.9

Figure 157. Compaction being performed by CAT CP-533E roller (Test strip A)

Figure 158. Test strip B after compaction

Figure 159. Test strips C and CV after compaction

Figure 160. Padfoot detail on strip C after compaction

Statistical Analysis

Equations 5-13 -5-15 resulted from the statistical analysis of the existing clay on the West Des Moines site. Fill clay brought into the site is represented by equations 5-16 to 5-18:

$$DD = 0.23(Pass) - 0.11(m\%) + 15.6 \quad [5\text{-}13]$$

$$DCPI = -5.0(Pass) - 0.3(m\%) + 155.0 \quad [5\text{-}14]$$

$$CIV = 0.09(Pass) - 0.10(m\%) + 5.5 \quad [5\text{-}15]$$

$$DD = 0.11(Pass) - 0.11(m\%) + 15.7 \quad [5\text{-}16]$$

$$DCPI = -3.0(Pass) - 1.4(m\%) + 107.8 \quad [5\text{-}17]$$

$$CIV = 0.44(Pass) - 0.18(m\%) + 0.23 \quad [5\text{-}18]$$

Standard error, F-statistics, and t-statistics are shown in Table 39. Similar to the PPG field test, poor correlations were observed in the DCPI and CIV equations. Inputting normalized moisture as an independent variable did not improve the correlations. An attempt to improve the correlation with logarithm of compaction energy was confirmed successful for fill clay models, yielding the following equations for dry unit weight and Clegg values:

$$DD = 1.11(\text{Log Pass}) - 0.11(m\%) + 15.4 \quad [5\text{-}19]$$

$$CIV = 3.9(\text{Log Pass}) - 0.19(m\%) + 0.98 \quad [5\text{-}20]$$

Some of the low correlation in this field test could again be attributed to the low range of moisture content between strips.

Table 39. Statistical analysis on West Des Moines field test measurements

Equation	n	Adjusted r^2	Standard Error of Estimate	Standard Deviation	F-Statistic	t – statistics
5-13	45	0.48	0.63	0.88	21.2	OK
5-14	41	0.02	45.3	44.8	0.6	NG (both)
5-15	45	0.19	0.82	0.9	6.0	NG (both)
5-16	24	0.34	0.53	0.66	6.9	NG (m%-2.3)
5-17	24	0.04	13.2	13.5	1.4	NG (both)
5-18	18	0.29	0.87	1.0	4.5	NG (m%-1.8)
5-19	24	0.37	0.52	0.66	7.7	NG(logP-1.9)
5-20	18	0.36	0.83	1.0	5.7	NG (m%-2.0)

Figure 161 to Figure 172 give a visualization of linear regression for both clays. The plots showing relationship of dry unit weight and CIV with logarithm of pass are Figure 167 and Figure 169.

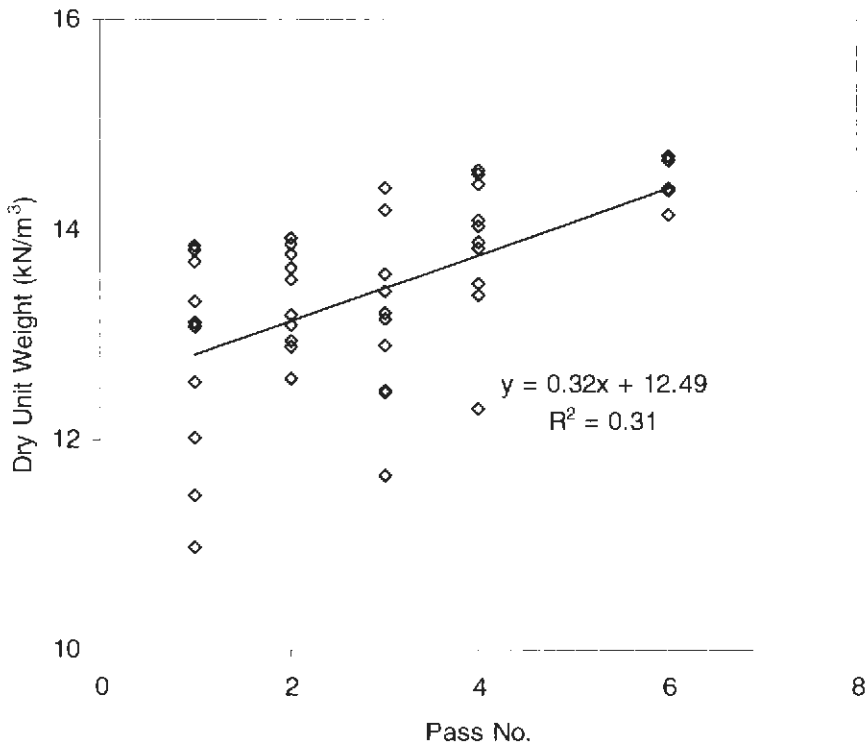

Figure 161. Regression of dry unit weight with roller pass (existing clay)

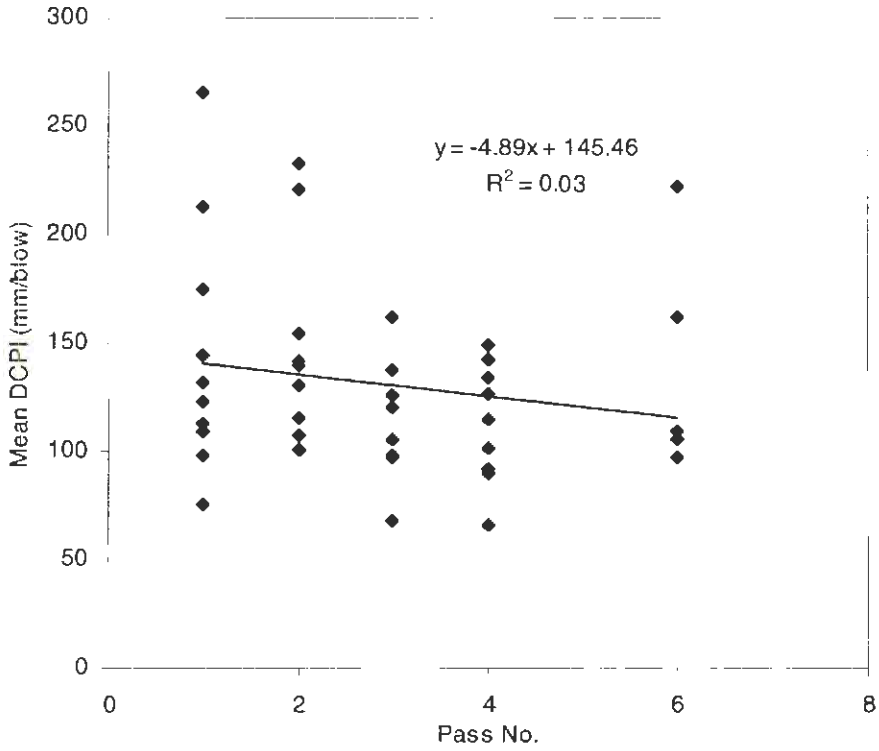

Figure 162. Regression of mean DCPI with roller pass (existing clay)

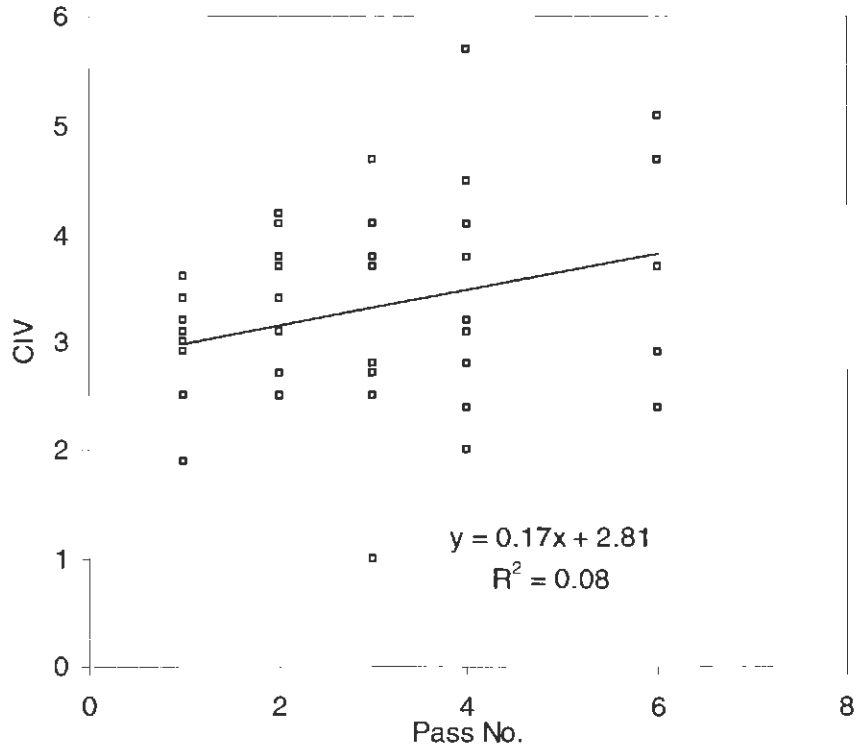

Figure 163. Regression of CIV with roller pass (existing clay)

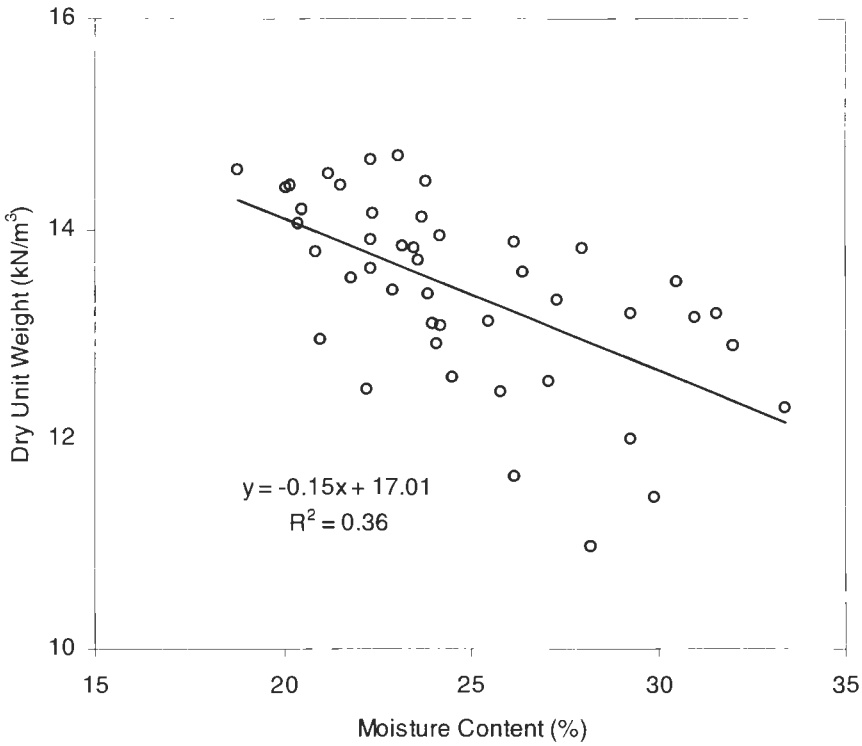

Figure 164. Regression of dry unit weight with moisture content (existing clay)

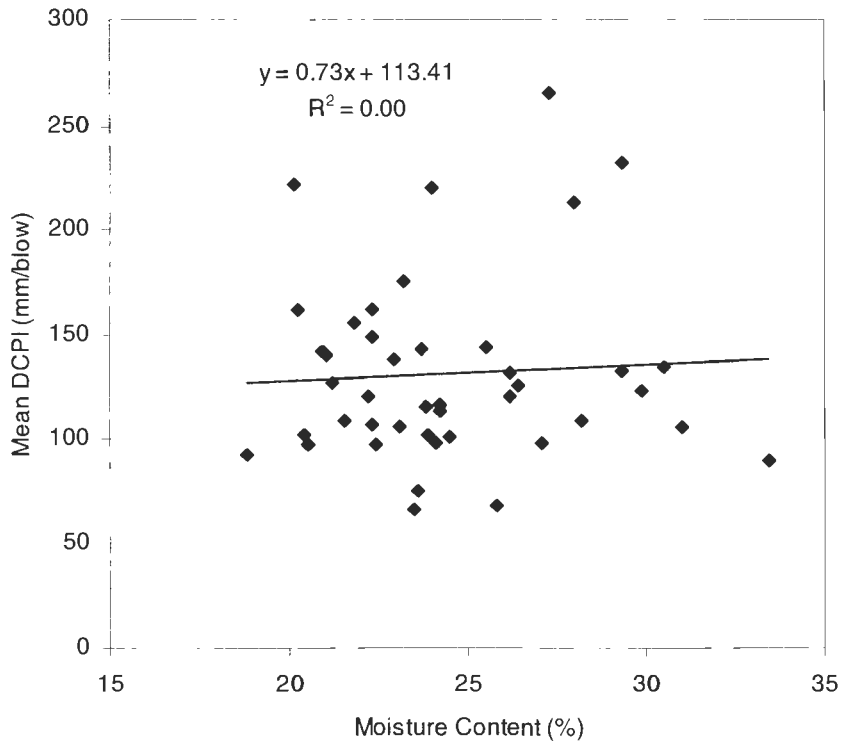

Figure 165. Regression of mean DCPI with moisture content (existing clay)

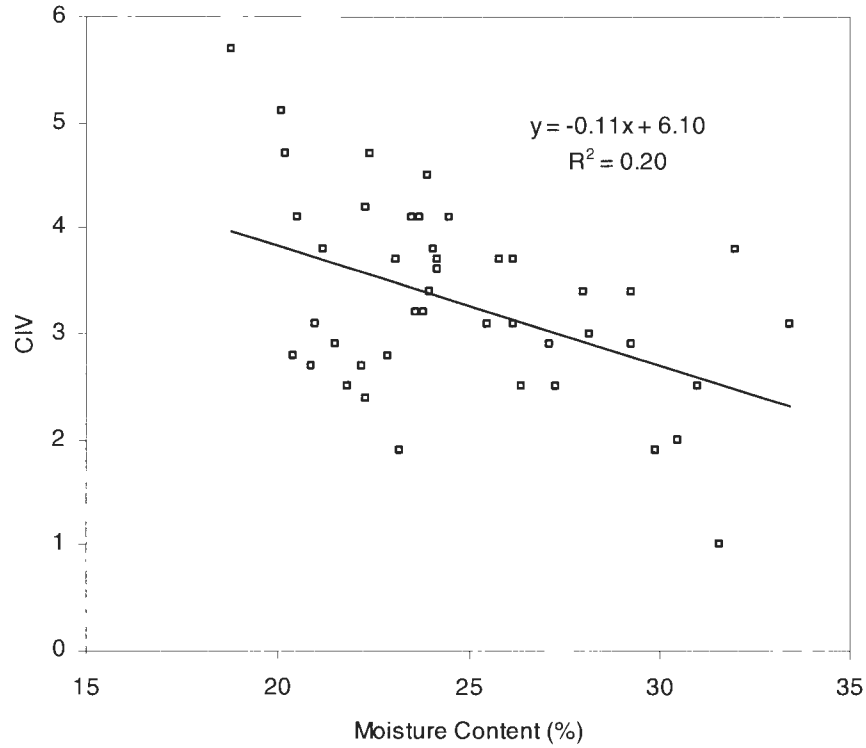

Figure 166. Regression of CIV with moisture content (existing clay)

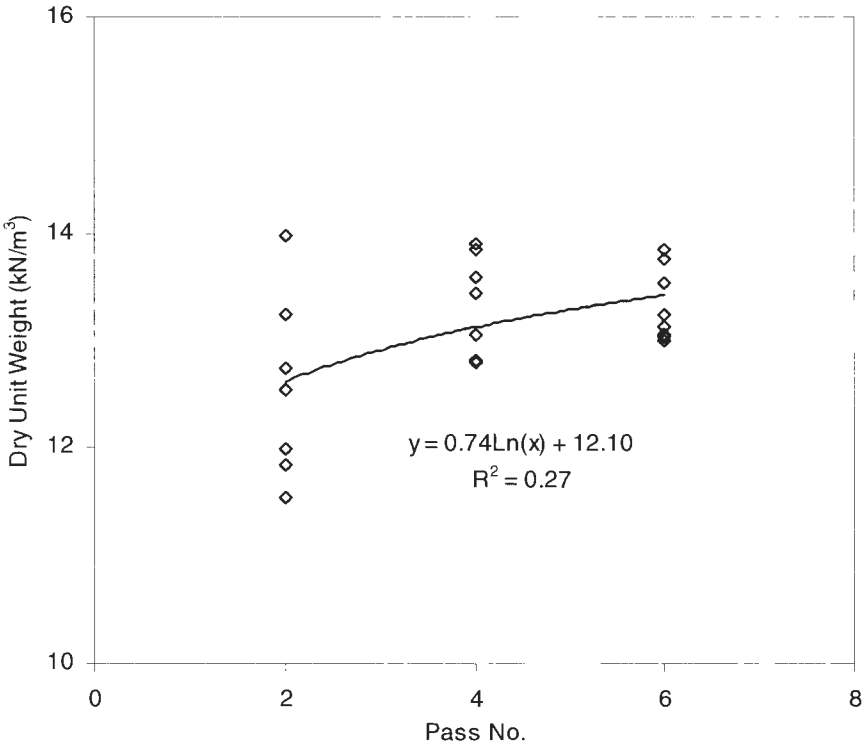

Figure 167. Regression of dry unit weight with roller pass (fill clay)

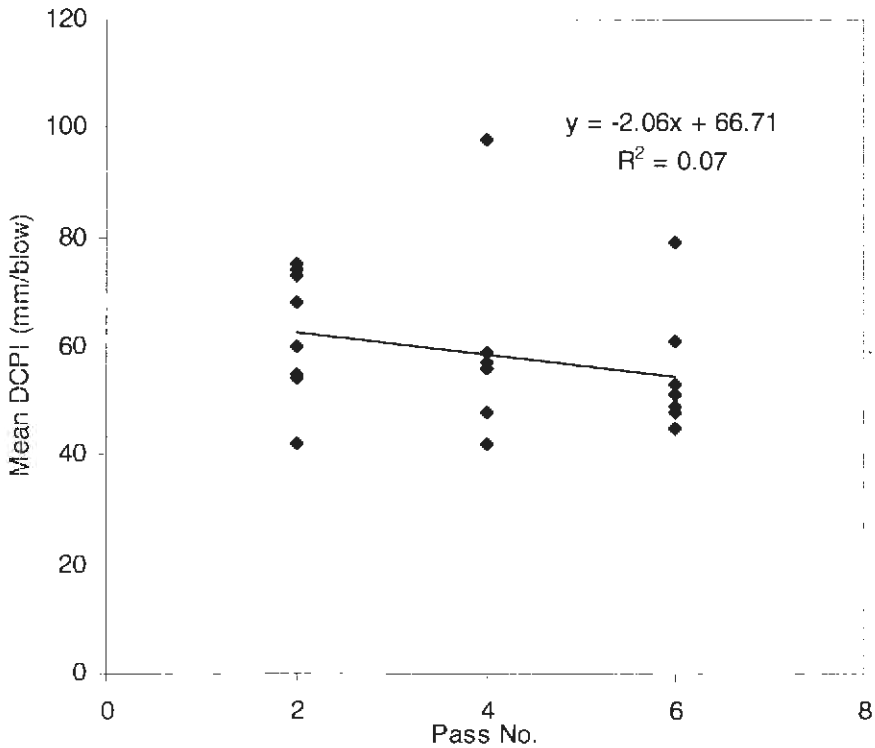

Figure 168. Regression of mean DCPI with roller pass (fill clay)

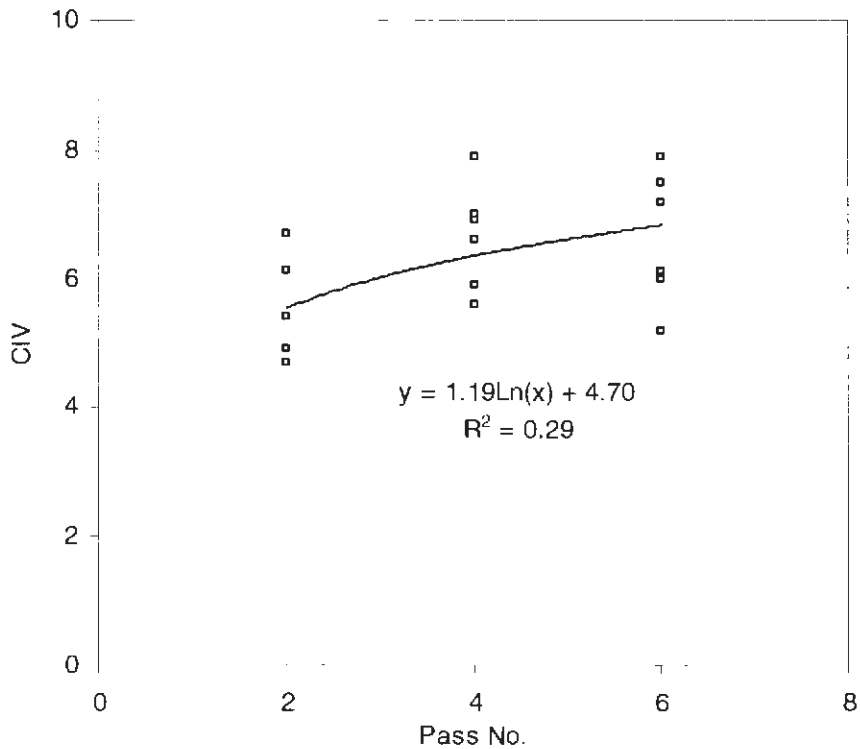

Figure 169. Regression of CIV with roller pass (fill clay)

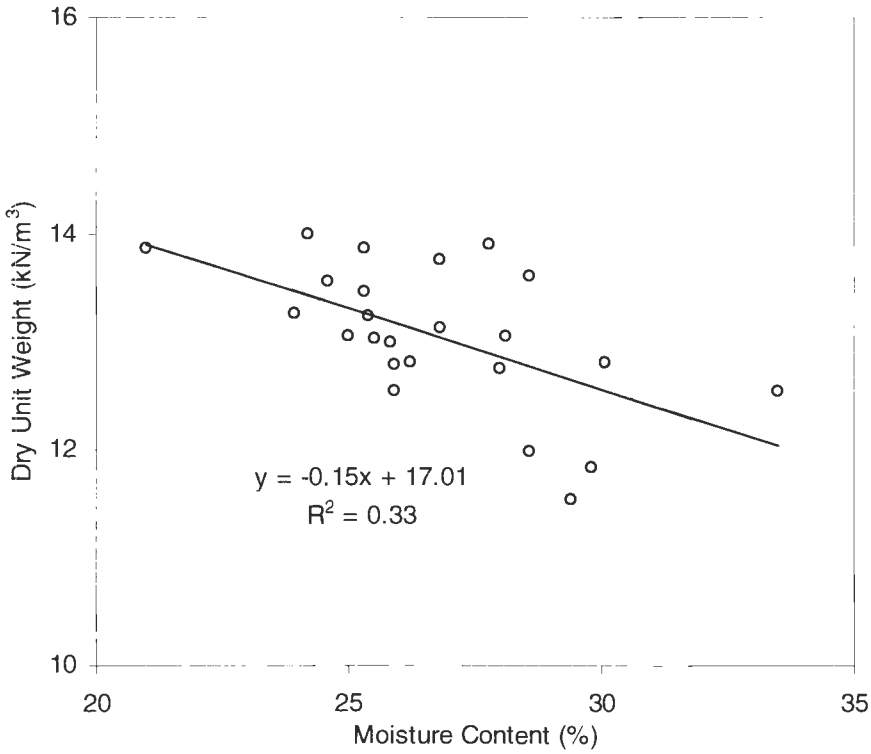

Figure 170. Regression of dry unit weight with moisture content (fill clay)

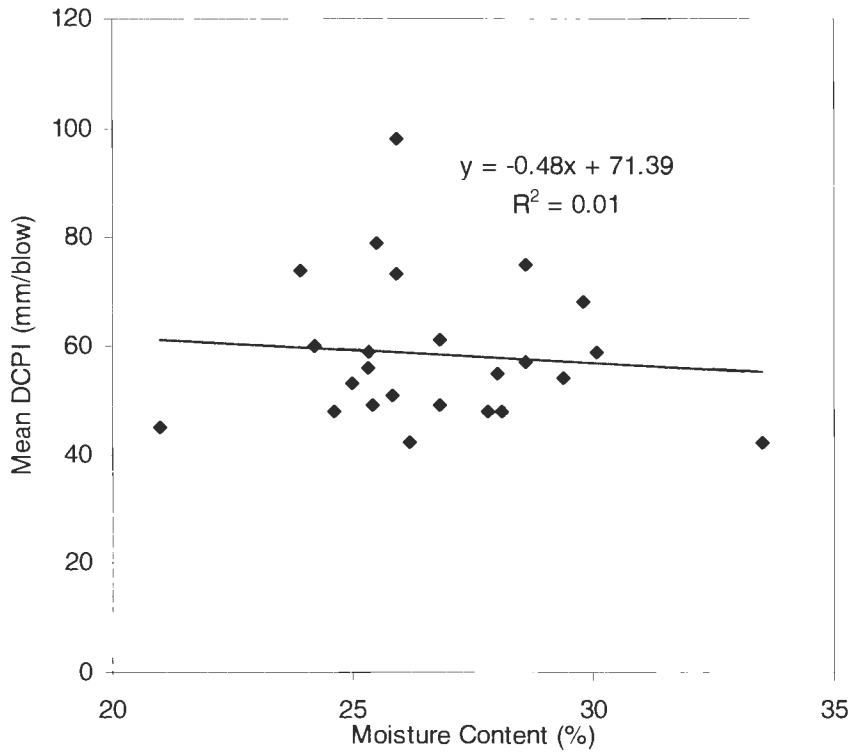

Figure 171. Regression of mean DCPI with moisture content (fill clay)

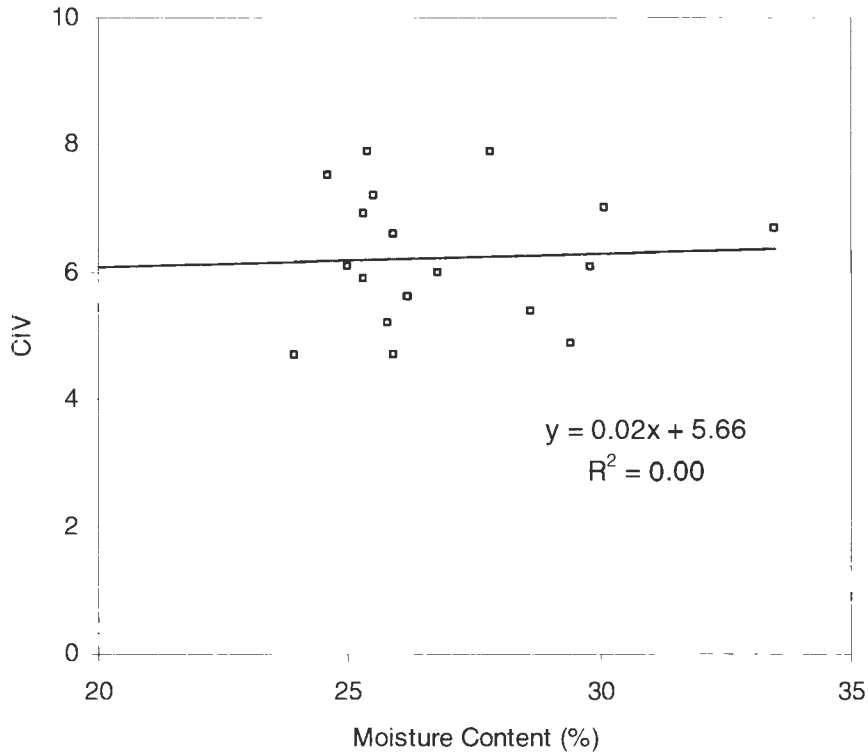

Figure 172. Regression of CIV with moisture content (fill clay)

Stability and Uniformity

Test strips constructed with the existing clay were examined individually for stability and uniformity. A point of interest, in the observations from this field test, was the data trends between passes. Data measured in test strip A are in Figure 173-Figure 176, with Figure 177 to Figure 180 giving pass by pass data from test strip B. Mean DCPI generally improved with increasing roller pass in strip A. Eventually, the measurements neared the maximum, but were still slightly above. Uniformity was quite variable between points and somewhat between passes. Pass 3 appeared to indicate the greatest improvement in uniformity. Moisture contents for these points were well wet of the moisture range and could explain for some of this variability. Lift thicknesses were observed as slightly decreasing as a function of increasing passes. Overall the compacted lift was within a reasonable thickness.

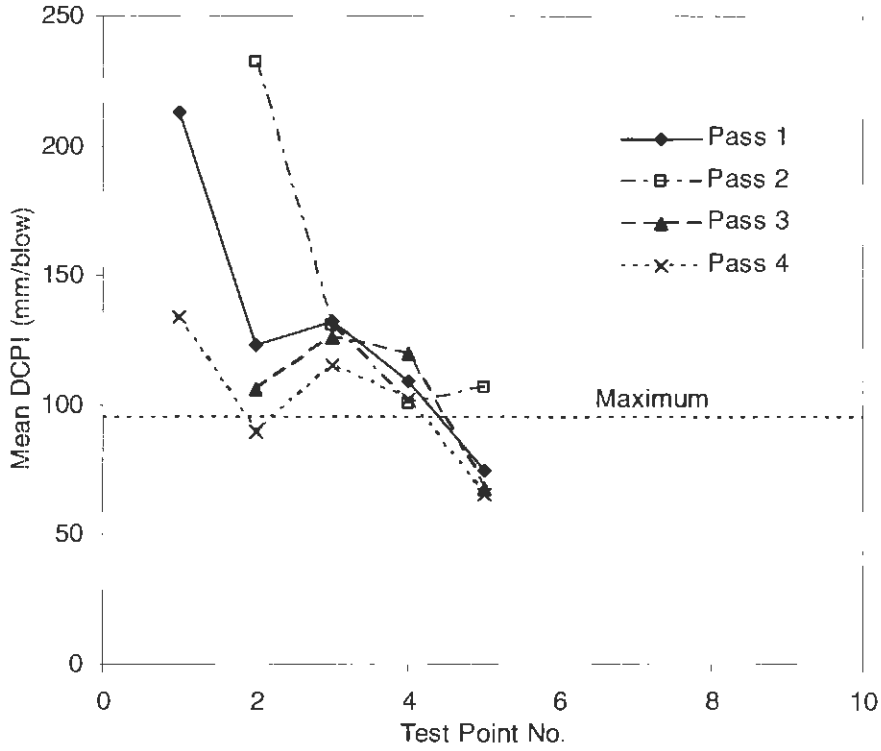

Figure 173. Mean DCPI by pass for test strip A

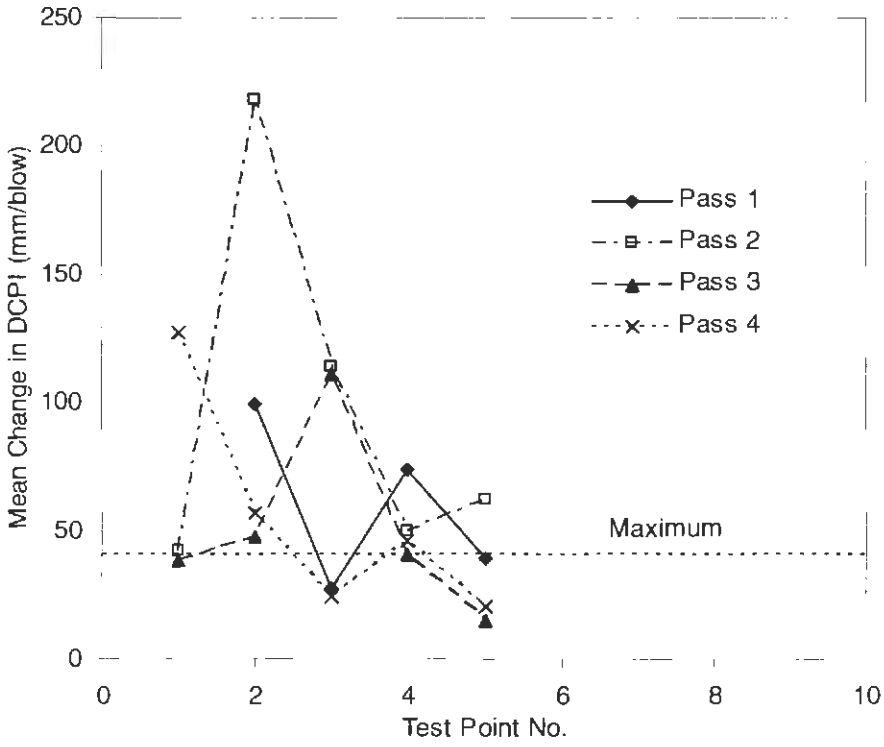

Figure 174. Mean change in DCPI by pass for test strip A

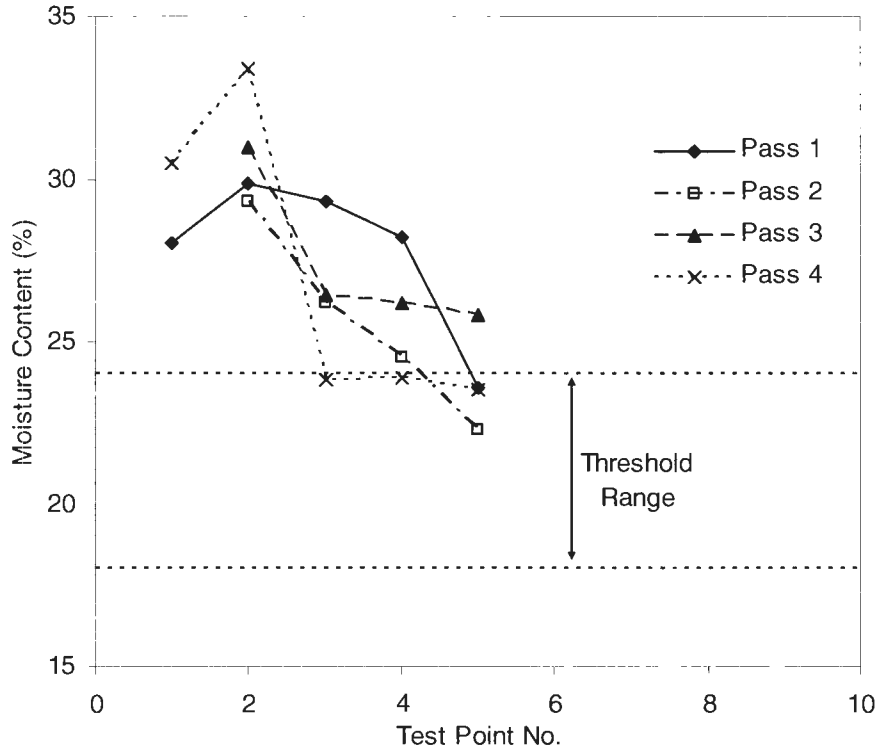

Figure 175. Moisture contents by pass for test strip A

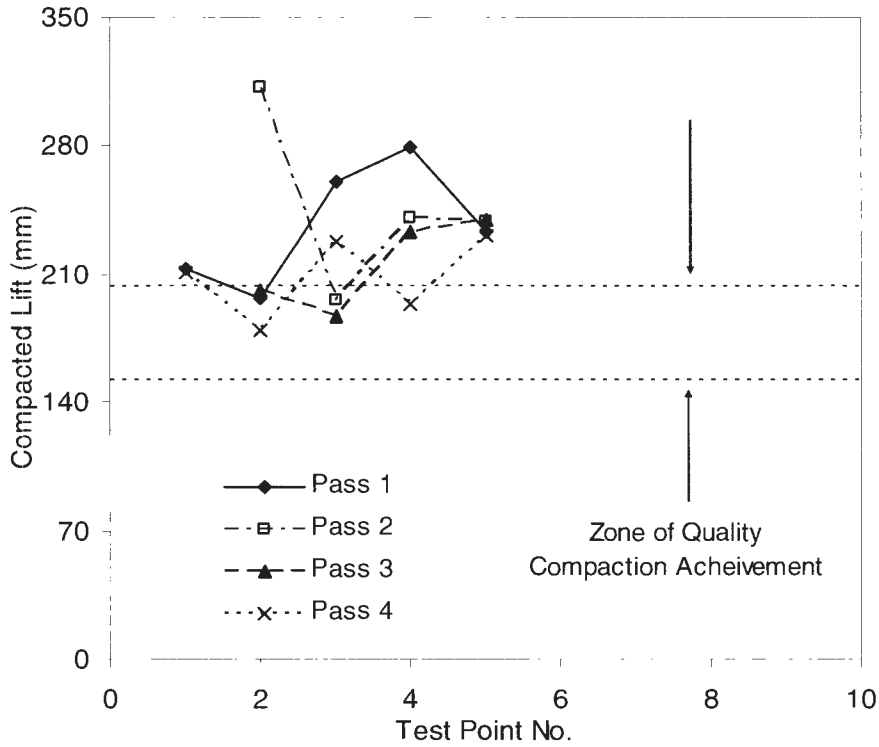

Figure 176. Compacted lifts for test strip A plotted with ideal zone of compaction

For test strip B the mean DCPI slightly improved with increasing roller passes, but most measurements were above the maximum limit of 95 mm/blow. Uniformity of this strip progressively was less by increasing passes as indicated by Figure 178. Aside from measurements after pass 1, the moisture contents were within the threshold for the unsuitable material. A great visualization of decreasing lift thickness by pass was observed in the final figure. Since the moisture range was satisfied, the problem in uniformity could be due to lift thickness.

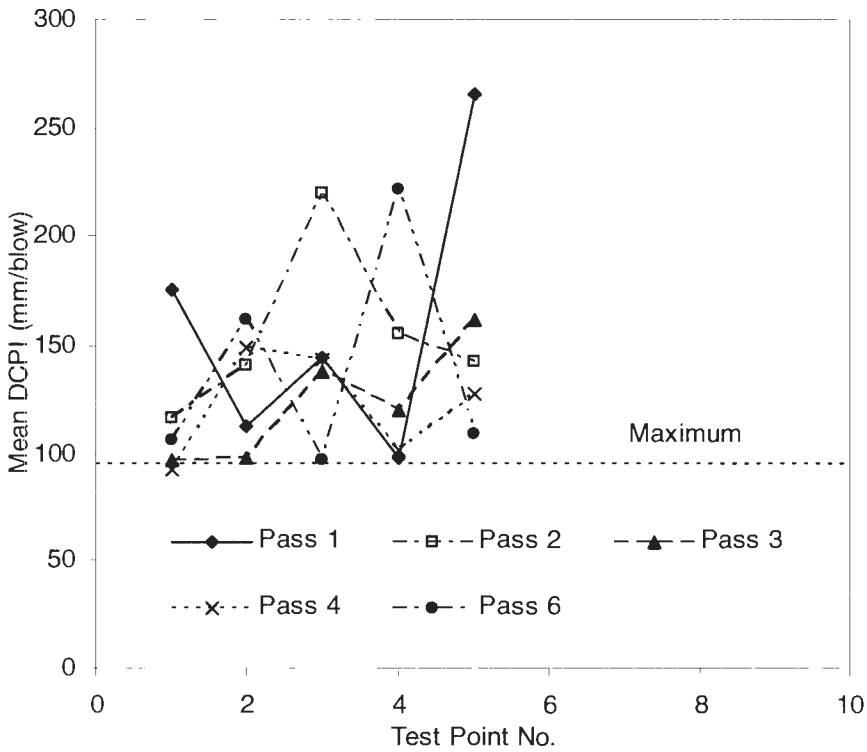

Figure 177. Mean DCPI by pass for test strip B

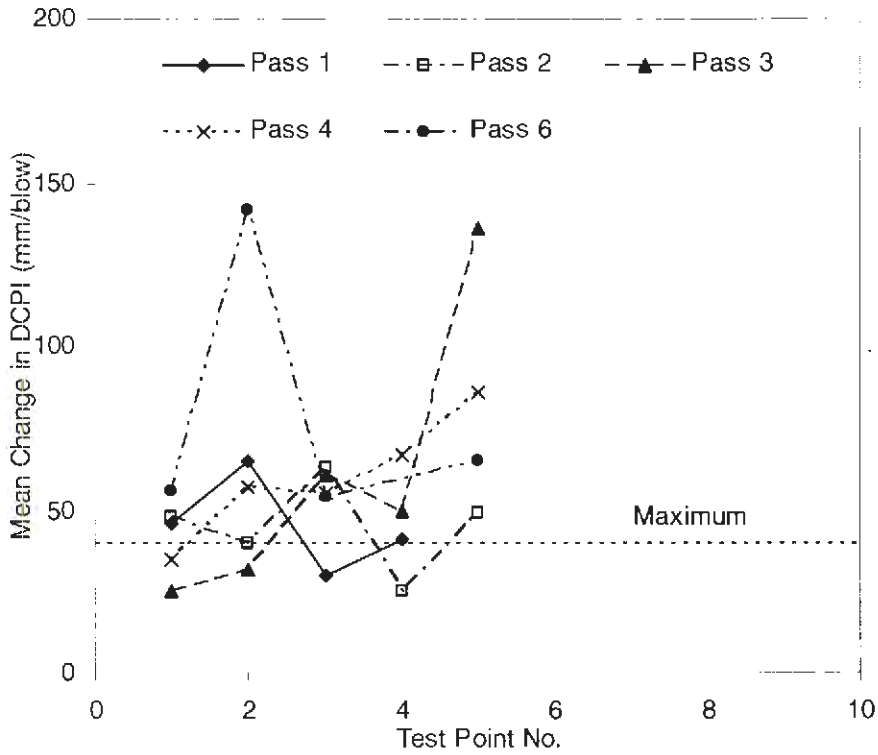

Figure 178. Mean change in DCPI by pass for test strip B

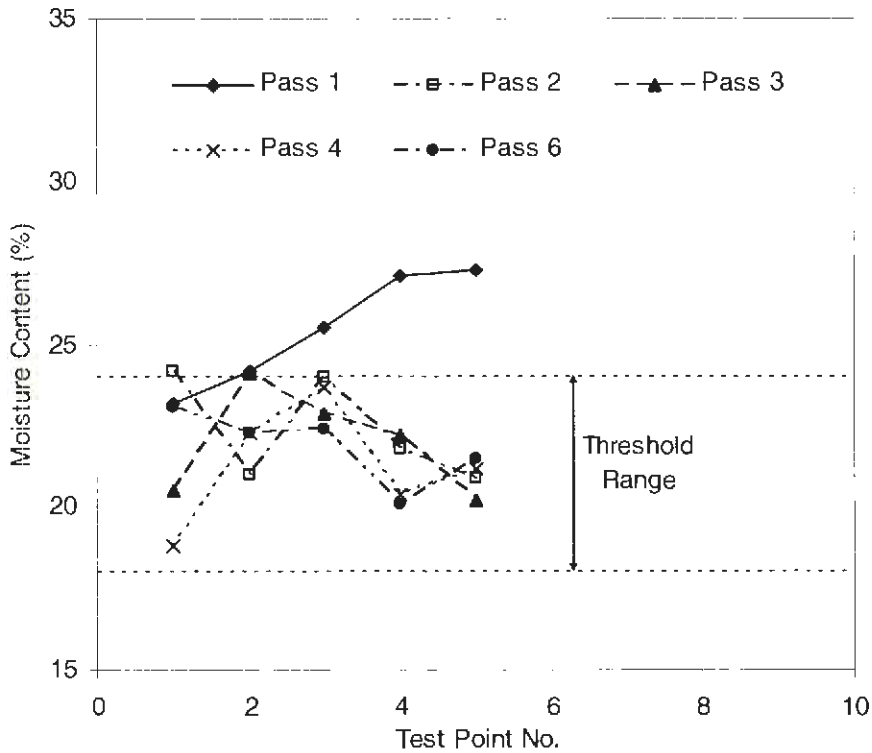

Figure 179. Moisture contents by pass for test strip B

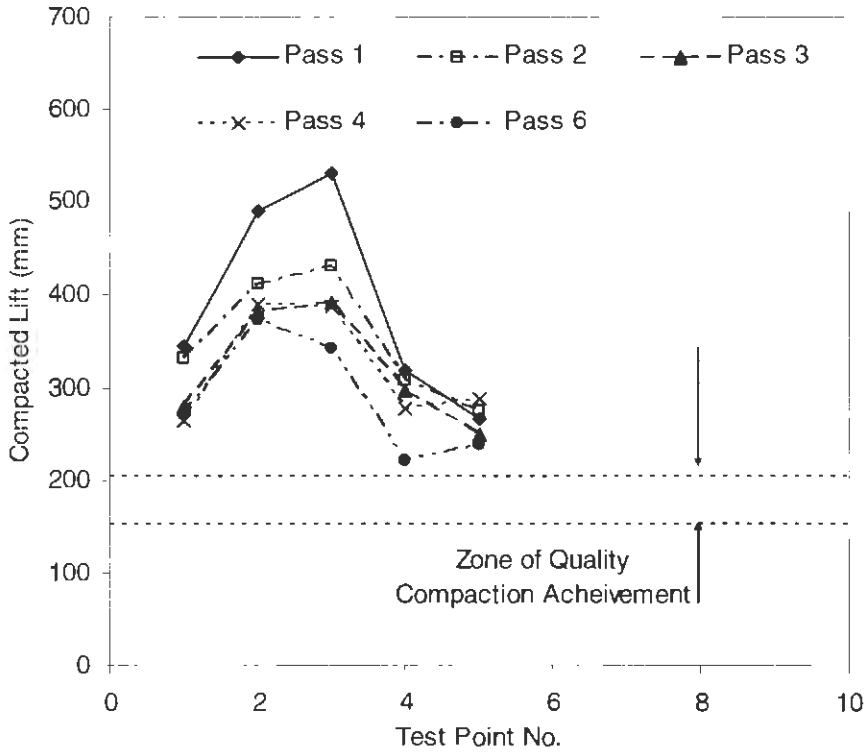

Figure 180. Compacted lifts for test strip B plotted with ideal zone of compaction

Fill clay data is depicted in the next set of graphs. Figure 181 to Figure 184 contain in-situ measurements from the test strip without vibratory (C). The second set of figure is measurements from the strip with vibratory (CV). Mean DCPI and change in DCPI for test strip C varied between passes. Values stayed below the suggested maximum limit for unsuitable soils, with the exception of one point. Moisture content measured in the lift remained within the specified limits and the compacted lift was reasonable for earthwork construction. The lift was observed to be high at the ends and low in the middle, reflected in Figure 184. Mean DCPI and change in mean DCPI generally decreased with roller pass for test strip CV. For the most part, the depth of compacted lift was acceptable, even though one side is on the borderline (335 – 350 mm). Beside a few points, moisture range criteria were satisfied.

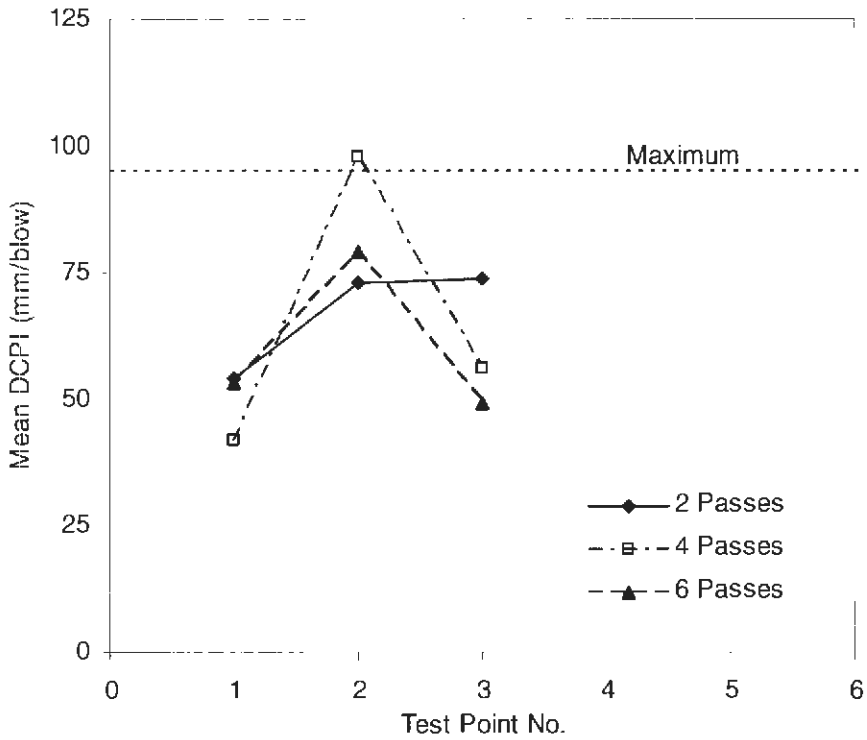

Figure 181. Mean DCPI by pass for test strip C

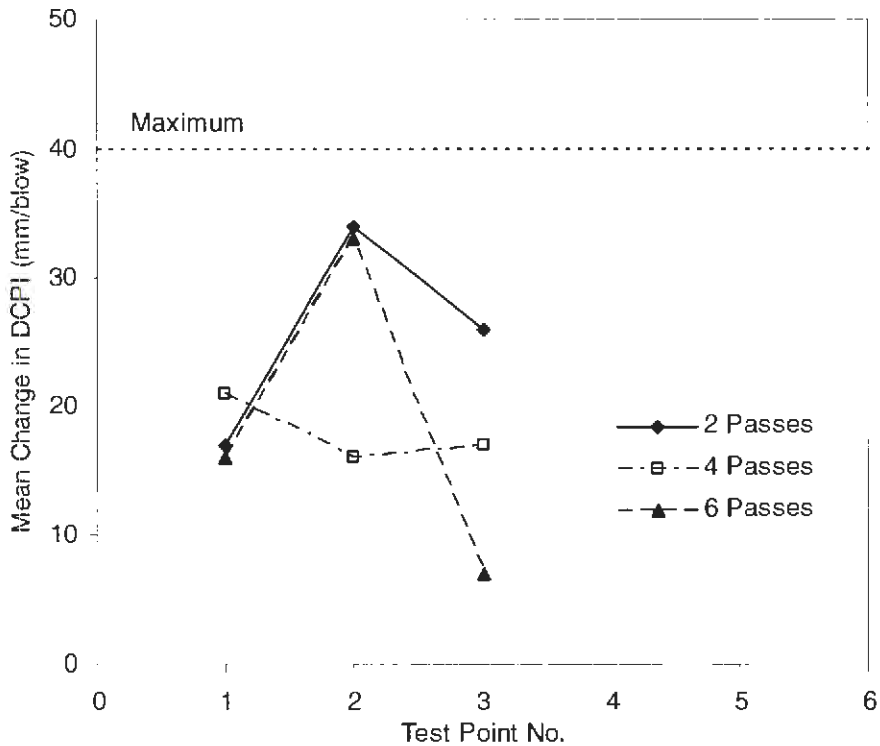

Figure 182. Mean change in DCPI by pass for test strip C

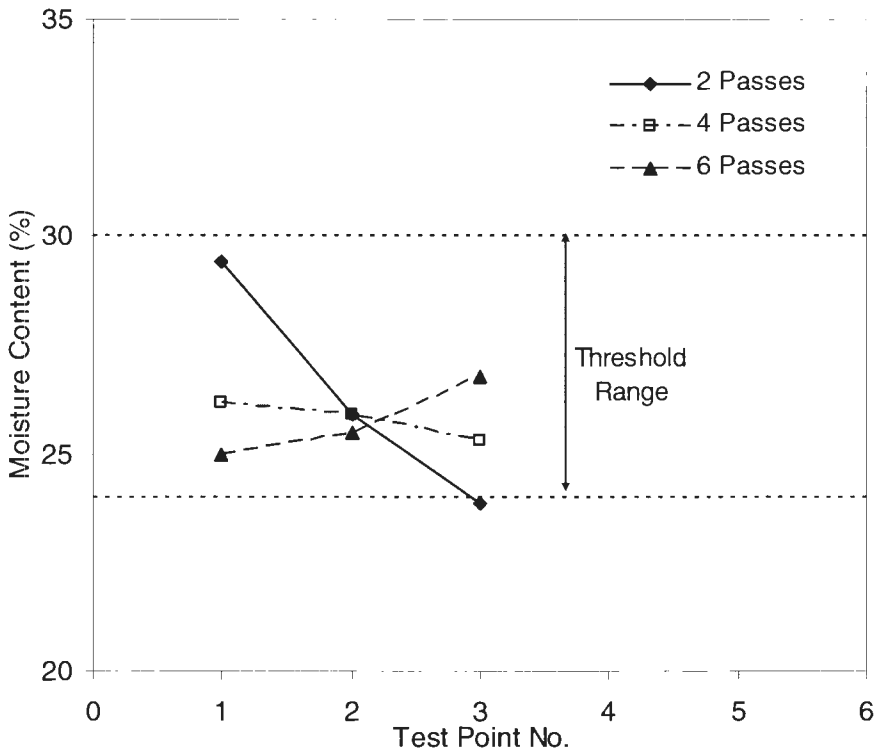

Figure 183. Moisture contents by pass for test strip C

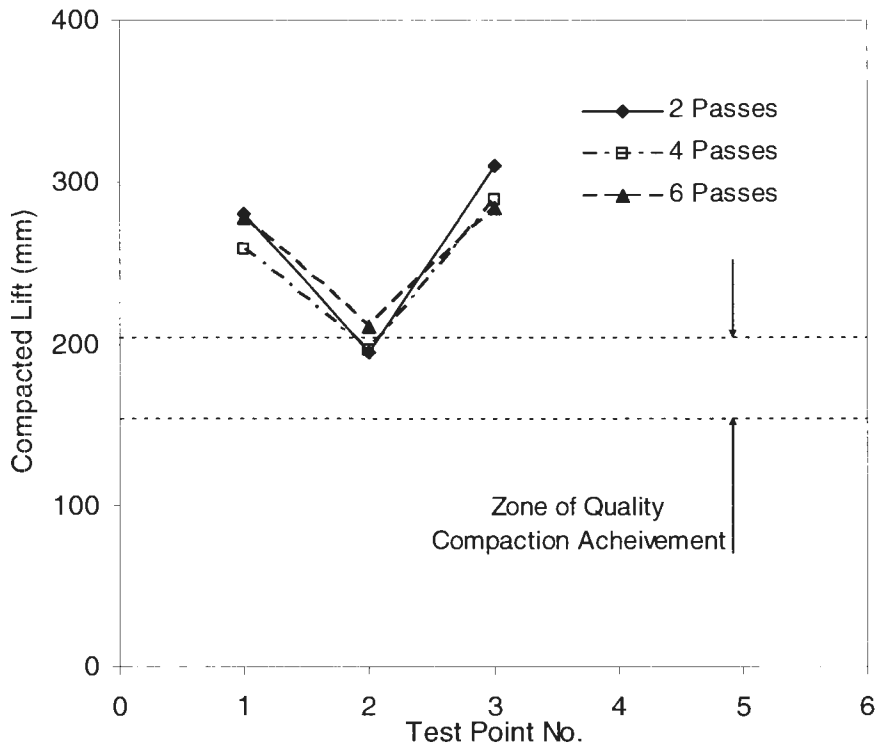

Figure 184. Compacted lifts for strip C plotted with ideal zone of compaction

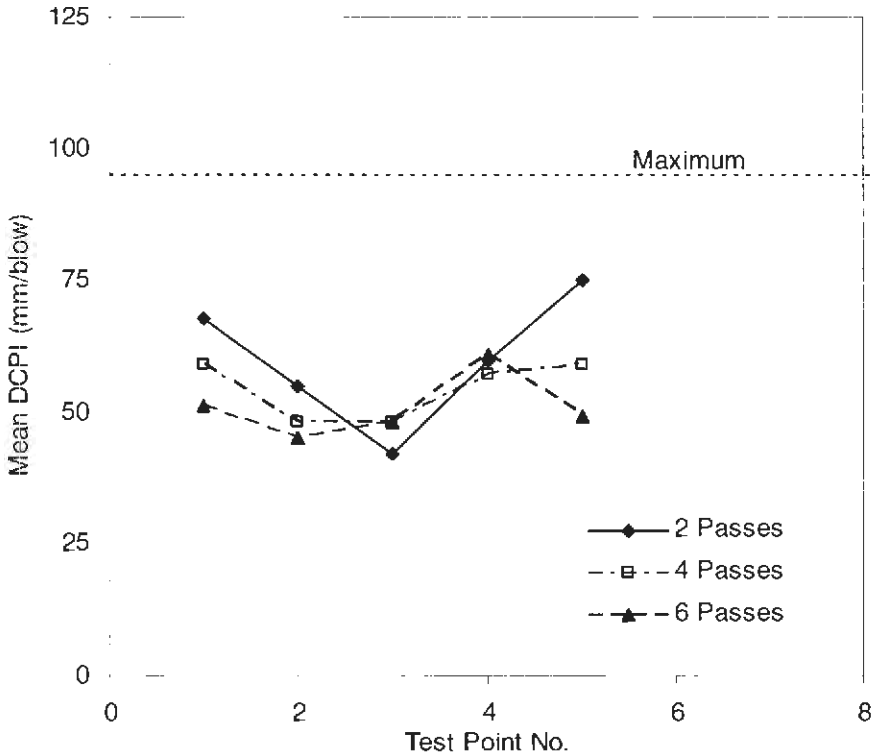

Figure 185. Mean DCPI by pass for test strip CV

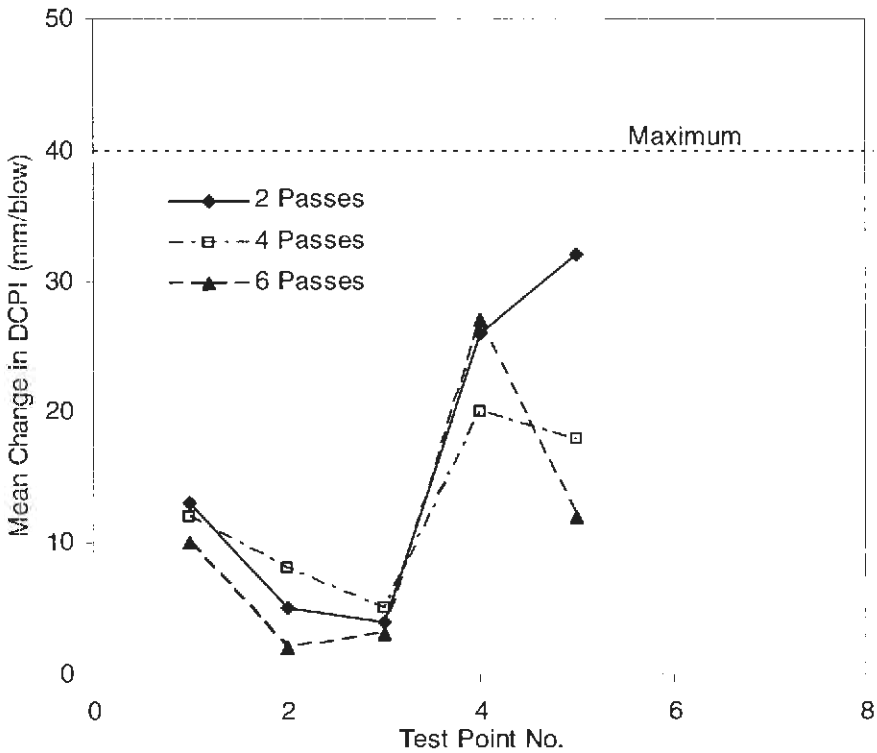

Figure 186. Mean change in DCPI by pass for test strip CV

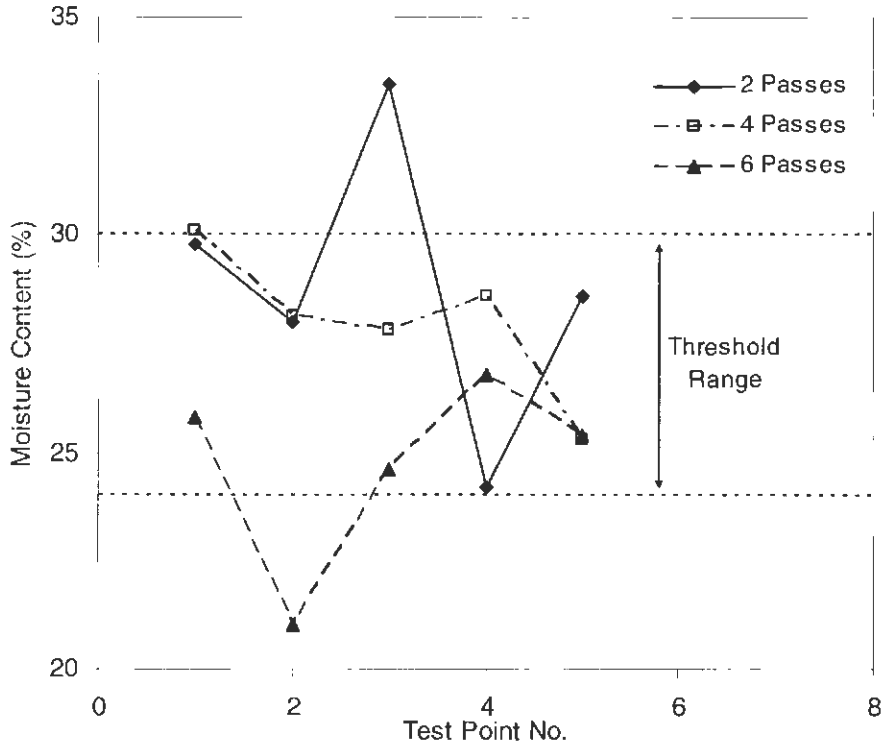

Figure 187. Moisture contents by pass for test strip CV

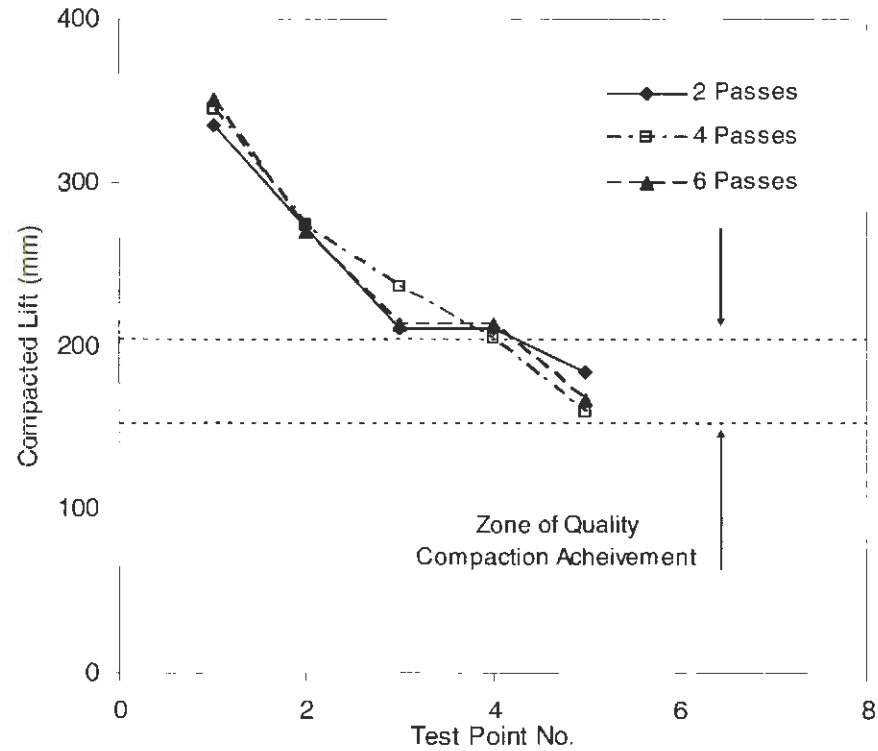

Figure 188. Compacted lifts for strip CV plotted with ideal zone of compaction

Comparing the two strips, it was noted that vibratory application appeared to construct a lift with lower values of mean DCPI and change in mean DCPI. Thus, strength and uniformity was improved.

CIV measurements by pass for given for WDSM clays in Figure 189 to Figure 192. Impact values increased from pass one to two, dropped after three passes, and increased after four passes. Points in test strip B had various combinations of increasing and decreasing CIV between roller passes. Test strips C and CV improved from two to four roller passes, and increased after six passes at some points.

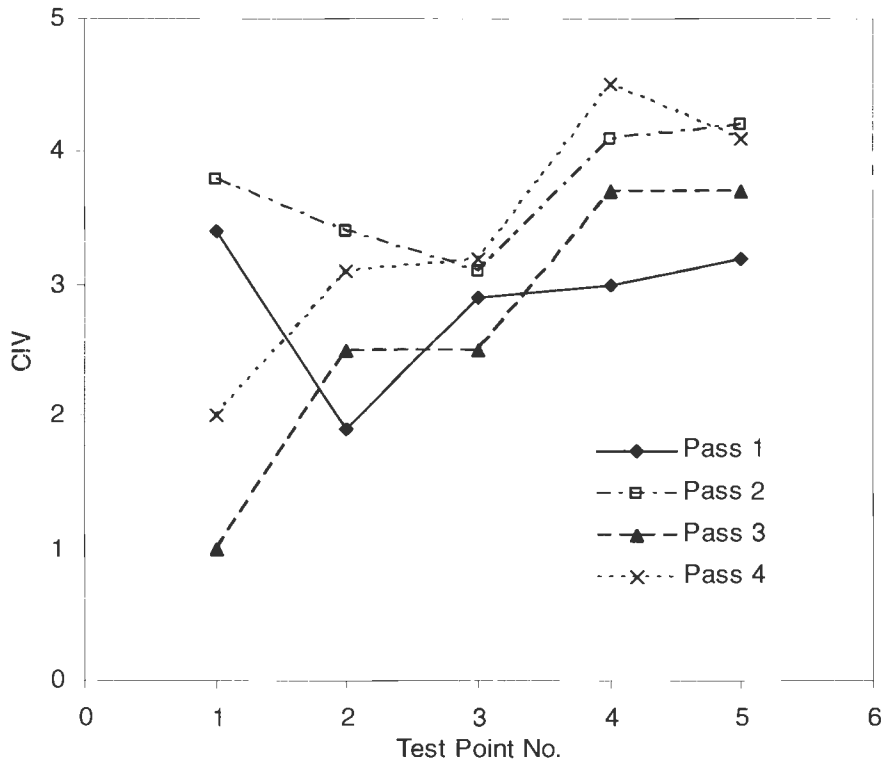

Figure 189. Clegg Impact Values by pass for test strip A

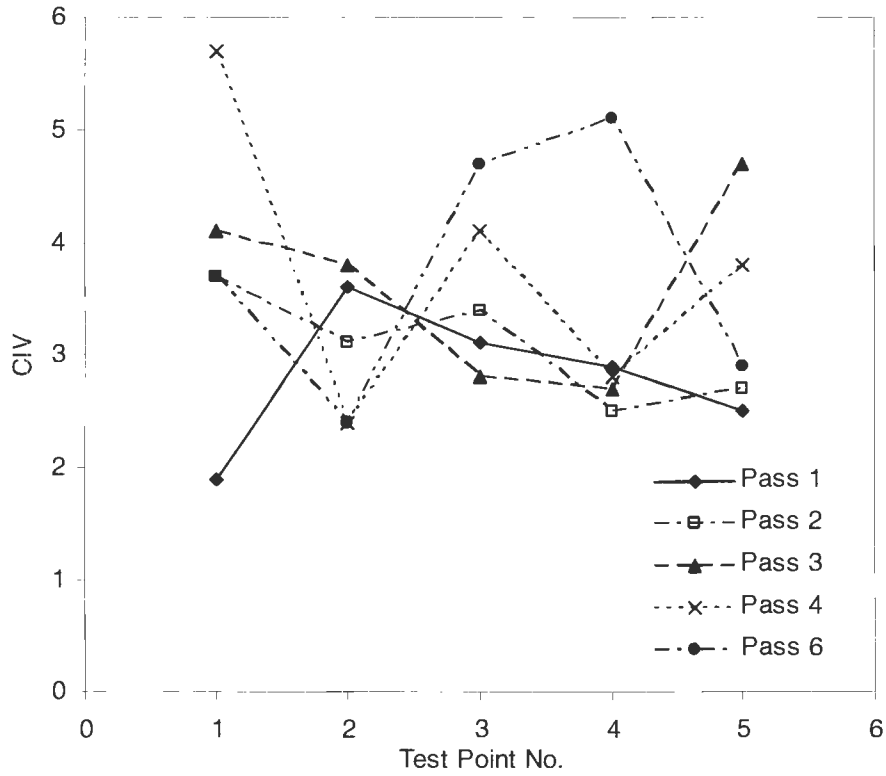

Figure 190. Clegg Impact Values by pass for test strip B

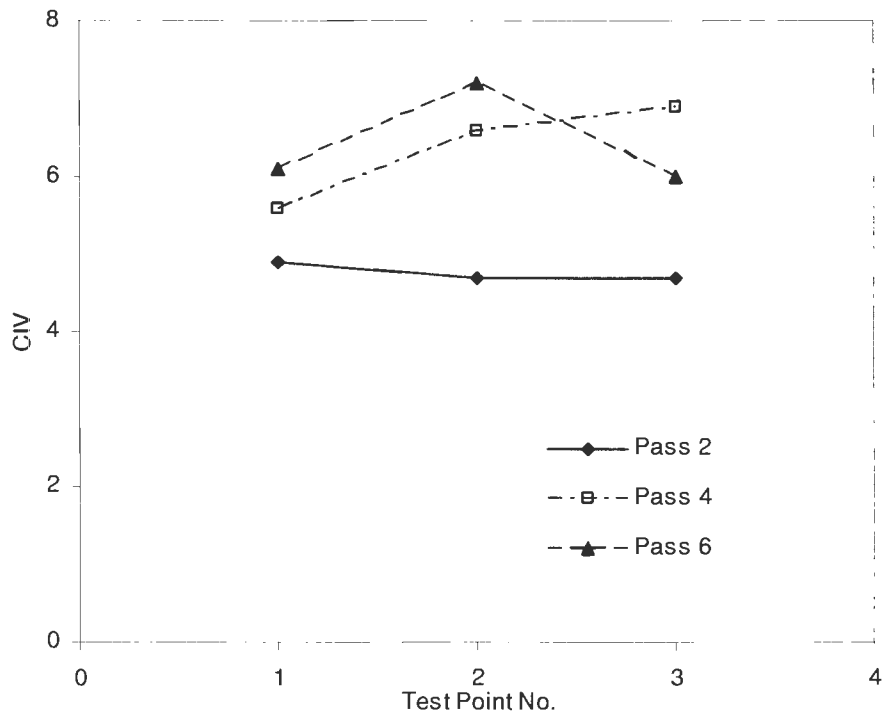

Figure 191. Clegg Impact Values by pass for test strip C

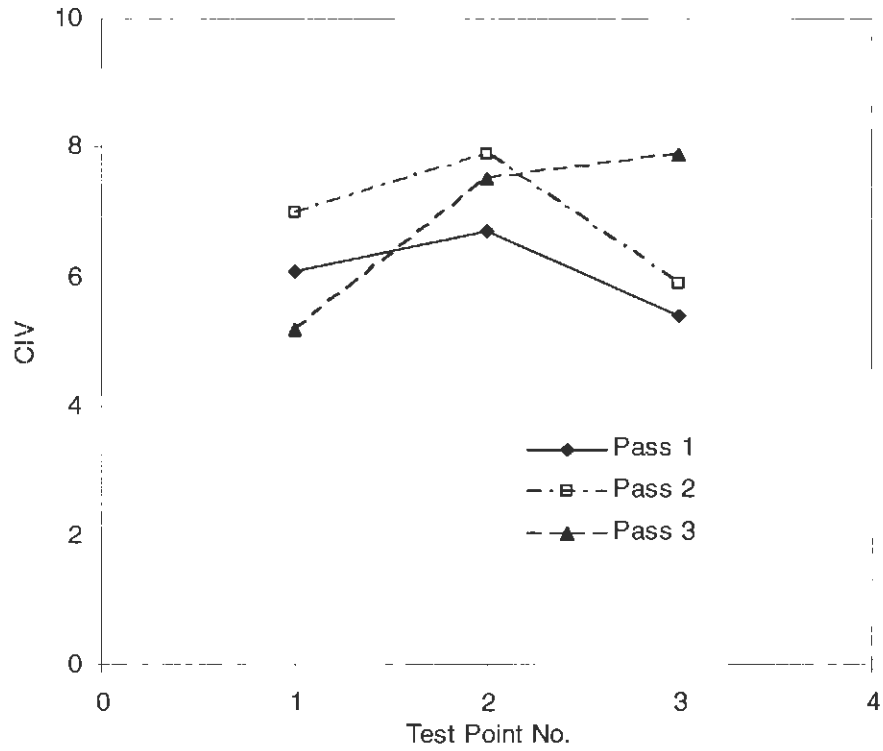

Figure 192. Clegg Impact Values by pass for test strip CV

Statistical Analysis of All Soils

Measurements from all sites were analyzed together in an attempt to further explain soil behavior. In addition to independent variables mentioned prior to this section, fines content (percent passing No. 200 sieve), clay fraction, liquid limit, and percent standard Proctor were inputted. Percent standard Proctor was also investigated as a dependent variable. While percent standard Proctor should be primarily understood as a dependent variable, it was inputted as an independent variable to check the validity of utilizing relative compaction as the standard for quality assessment in the field, e.g. 95% standard Proctor. It shall be noted fines content, clay fraction, and liquid limit were taken at a fixed value from lab determination. Therefore, the assumption was made that these parameters did not vary throughout the soil in a respective test strip.

Equations yielding the best correlations were as follows:

$$DD = 1.27(\text{Log Pass}) - 0.22(m\%) + 18.4 \quad [5\text{-}21]$$

$$DD = 0.25(\text{Pass}) - 0.075(\text{Fines}) + 19.9 \quad [5\text{-}22]$$

$$DD = 0.42(\text{Pass}) - 0.19(CF) + 18.0 \quad [5\text{-}23]$$

$$DD = 0.22(\text{Pass}) - 0.16(LL) + 19.5 \quad [5\text{-}24]$$

$$DCPI = -2.0(\text{Pass}) + 4.1(m\%) + 4.7 \quad [5\text{-}25]$$

$$DCPI = -4.2(\text{Pass}) + 1.5(\text{Fines}) - 27.7 \quad [5\text{-}26]$$

$$DCPI = -4.0(\text{Pass}) + 0.53(m\%) + 1.4(\text{Fines}) - 25.4 \quad [5\text{-}27]$$

$$CIV = 0.82(\text{Pass}) - 0.25(m\%) + 7.3 \quad [5\text{-}28]$$

$$CIV = 0.75(\text{Pass}) - 0.66(nm\%) + 5.0 \quad [5\text{-}29]$$

$$CIV = 0.95(\text{Pass}) - 0.065(\text{Fines}) + 7.5 \quad [5\text{-}30]$$

$$\%SP = 1.3(\text{Pass}) - 0.06(m\%) + 79.5 \quad [5\text{-}31]$$

$$\%SP = 1.3(\text{Pass}) - 0.20(nm\%) + 79.0 \quad [5\text{-}32]$$

Relevant statistical data are presented in Table 40. The models for dry unit weight resulted in excellent correlation ($r^2 = 0.80 - 0.84$). Moderate correlations were observed in mean DCPI ($r^2 = 0.46 - 0.50$), CIV ($r^2 = 0.45 - 0.56$) and percent compaction ($r^2 = 0.50$ and 0.51). T-statistics did not pass for moisture content in equation 5-27 and 5-32 or for normalized moisture in equation 5-32.

Table 40. Statistical analysis on all field test measurements

Equation	n	Adjusted r^2	Standard Error of Estimate	F-Statistic	t – statistics (<-2 or >+2)	Strongest Predictor
5-21	204	0.80	0.86	397.4	OK	m%
5-22	204	0.83	0.78	511.1	OK	Fines
5-23	204	0.83	0.80	478.0	OK	CF
5-24	204	0.84	0.77	524.4	OK	LL
5-25	182	0.46	35.5	74.9	OK	m%
5-26	182	0.50	34.1	90.8	OK	Fines
5-27	182	0.50	34.1	60.6	NG (m%-0.7)	Fines/Pass
5-28	198	0.51	3.2	102.3	OK	Pass
5-29	198	0.56	3.0	123.9	OK	Pass
5-30	198	0.45	3.4	81.0	OK	Pass
5-31	204	0.50	4.0	104.2	NG(m%--1.6)	Pass
5-32	204	0.51	4.0	106.2	NG(nm%--1.9)	Pass
5-33	182	0.68	0.44	100.1	NG($m\%^3$-1.1)	Pass
5-34	182	0.61	30.3	142.4	NG(Pass-0.9)	Fines
5-35	182	0.69	0.44	70.3	NG($m\%^2/m\%^3$)	Pass
5-36	204	0.36	3.7	56.6	NG(nm%--1.4)	Pass

Pass proved to be the strongest predictor for CIV and percent compaction while moisture content and index properties helped explain variability the best for dry unit weight and DCP data. For equation 5-27, roller pass and fines content were equal in prediction strength for mean DCPI. Since relations that were not linear and had better r^2 values were observed in DCPI and CIV measurements (see Figure 197 to Figure 200) further multiple regression analyses were performed to investigate the possibility of better correlation with exponential or other functions that did not exhibit a linear relation. The additional equations for DCPI and CIV of all soils were as follows:

$$\text{Log DCPI} = -0.07(\text{Pass}) + 0.5(\text{m\%}) - 0.02(\text{m\%})^2 + 1.2 \times 10^{-4}(\text{m\%})^3 + 0.2 \quad [5\text{-}33]$$

$$\text{DCPI} = 0.7(\text{Pass}) + e^{1.7\text{E-}41(\text{fines})} + 35.1 \quad [5\text{-}34]$$

$$\text{Log DCPI} = -0.1(\text{Pass}) + 0.4(m\%) - 0.1(m\%)^2 + 6.0 \times 10^{-5}(m\%)^3 \quad [5\text{-}35]$$
$$+ 0.07(\text{Fines}) - 4.5 \times 10^{-4}(\text{Fines})^2 - 13.5$$

$$\text{CIV} = 0.9(\text{Pass}) - e^{-6.1E\text{-}6(nm\%)} + 3.2 \quad [5\text{-}36]$$

Using polynomial (eq. 5-33 and 5-35) and exponential fits for DCPI increased r^2 values to 0.68, 0.69, and 0.61. However, the exponential fit for CIV with normalized moisture did not improve correlation, decreasing it to an r^2 value of 0.36.

All standard errors were less than their dependent variables standard deviation. Mean, standard deviation, and coefficient of variation are given in Table 41. As anticipated, dry unit weight and relative compaction has low variability, while the strength and stiffness measurements were highly variable. DCPI has a similar coefficient of variation as undrained strength from the unconfined compression tests.

Table 41. General statistical data for all field soils

Parameter	Mean	Standard Deviation	COV (%)
Dry Unit Weight	15.6	1.9	12.1
DCPI	63.2	48.1	76.1
CIV	7.2	4.6	63.1
% Standard Proctor	84.5	5.7	6.7

Individual linear and non-linear plots for all field soil data are exhibited in the next set of figures (Figure 193-Figure 202). Poor correlation with roller pass was observed for dry unit weight and mean DCPI, while CIV had moderate correlation. Figure 196 and Figure 197 showed good correlation for dry unit weight and mean DCPI with moisture content, with

CIV showing moderate correlation. The next two figures display the moderate correlation the two parameters had with normalized moisture content. The best trendline fits for DCPI and CIV was with power and exponential equations. Figure 201 and Figure 202 indicate the influence of fines content on dry unit weight and DCPI. Plots not displayed here, are presented in Appendix G.

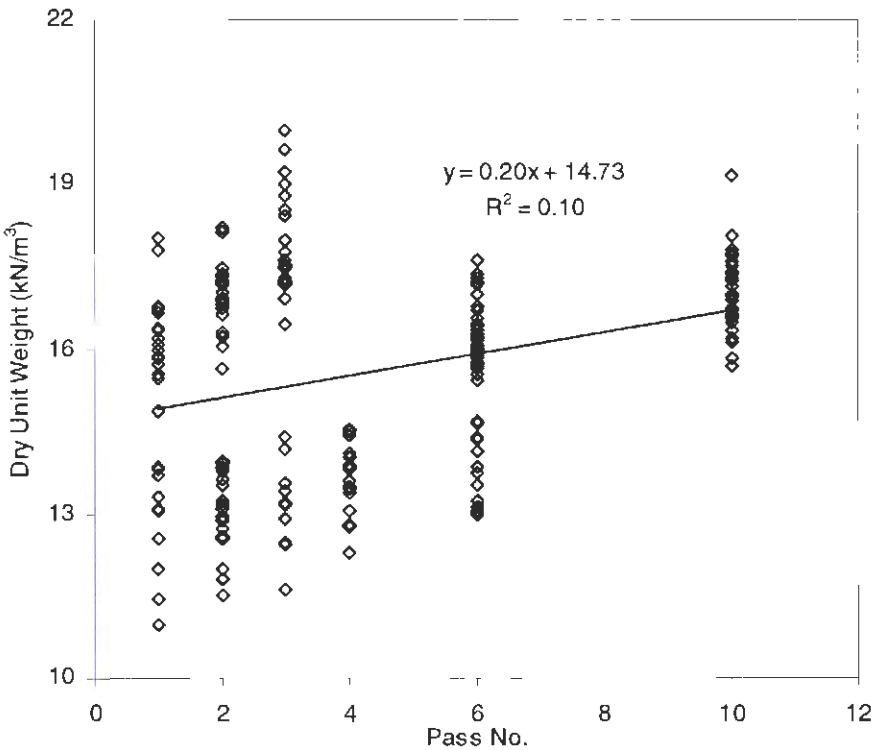

Figure 193. Regression of dry unit weight with roller pass (all field soils)

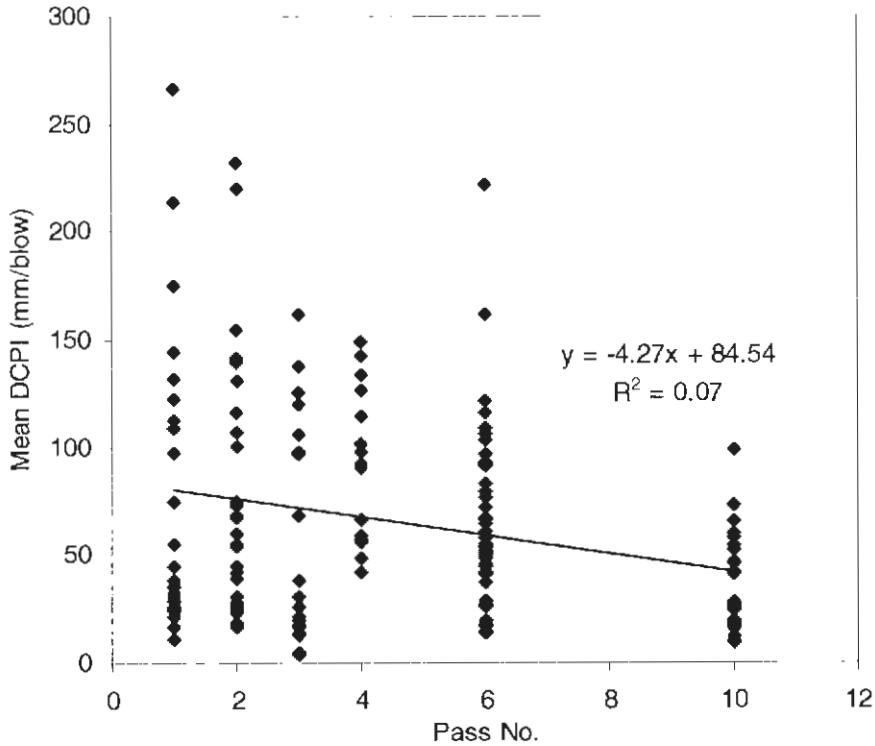

Figure 194. Regression of mean DCPI with roller pass (all field soils)

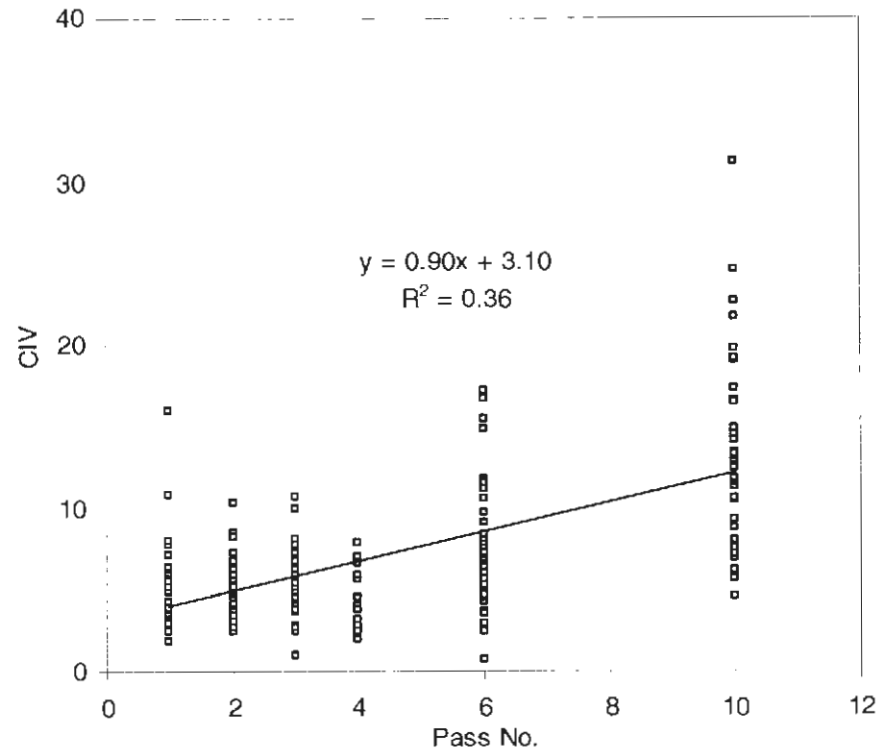

Figure 195. Regression of CIV with roller pass (all field soils)

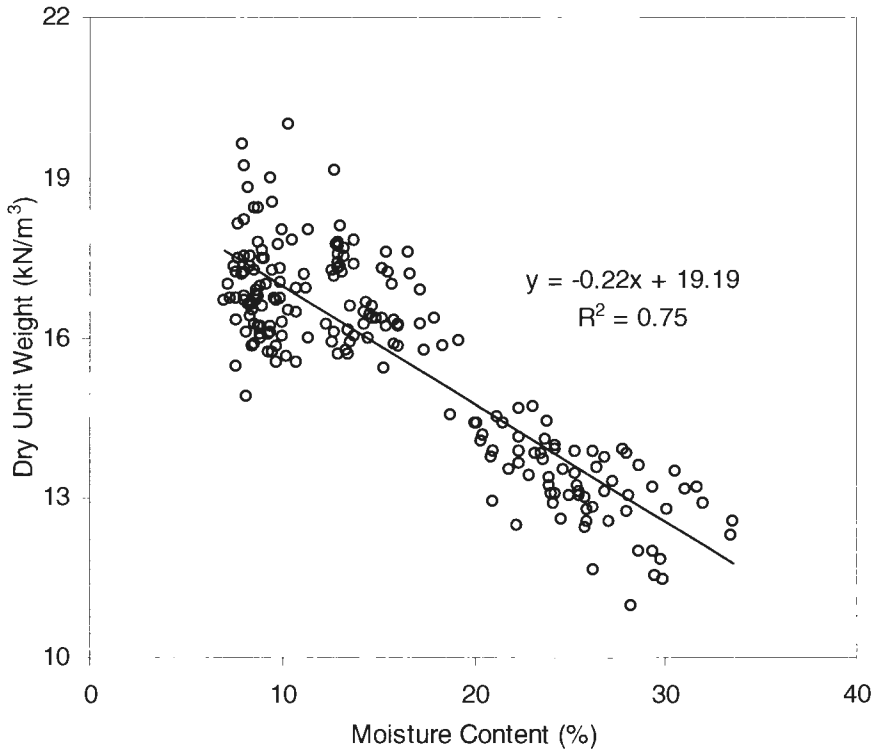

Figure 196. Regression of dry unit weight with moisture content (all field soils)

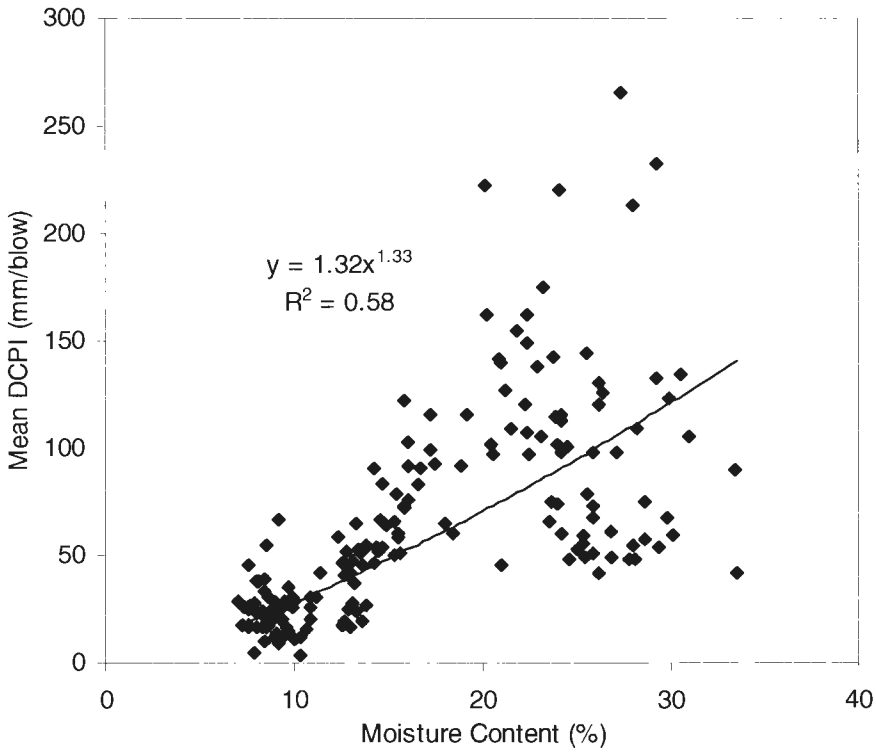

Figure 197. Regression of mean DCPI with moisture content (all field soils)

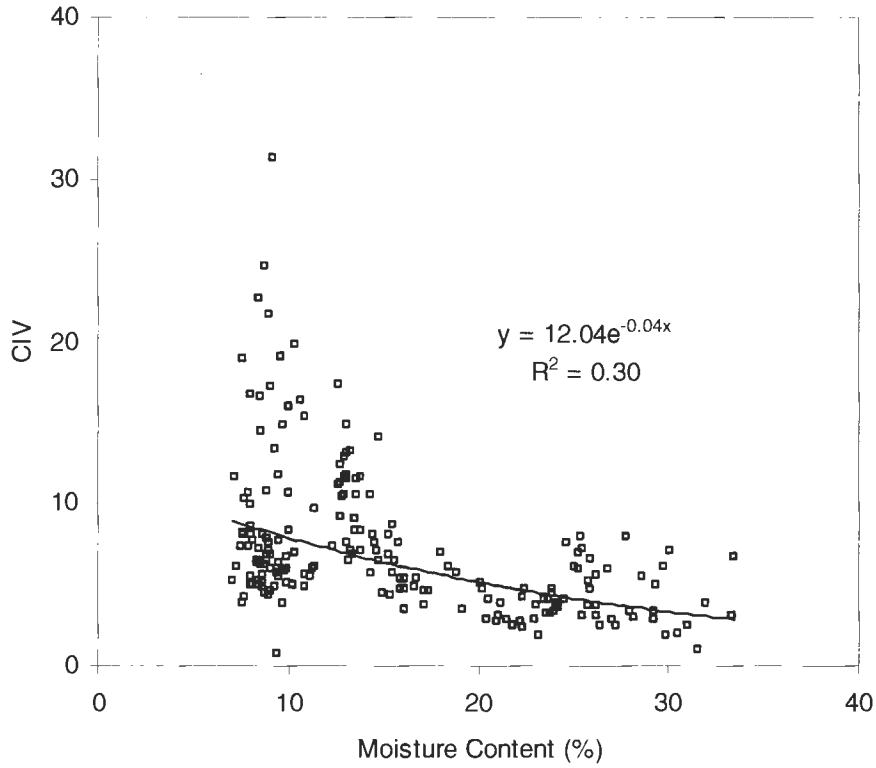

Figure 198. Regression of CIV with moisture content (all field soils)

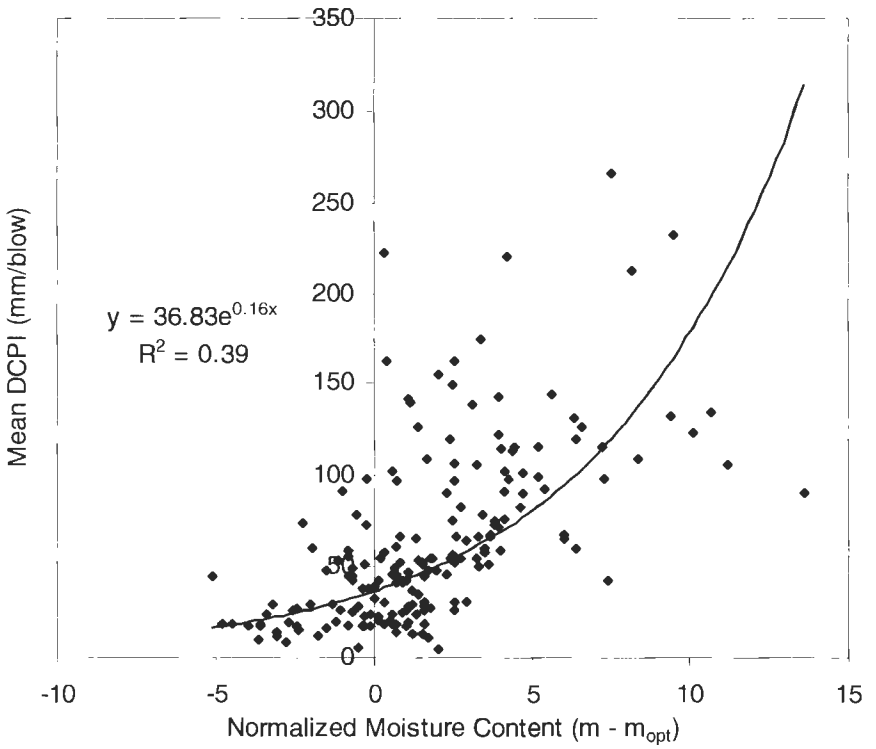

Figure 199. Regression of mean DCPI with normalized moisture content (all field soils)

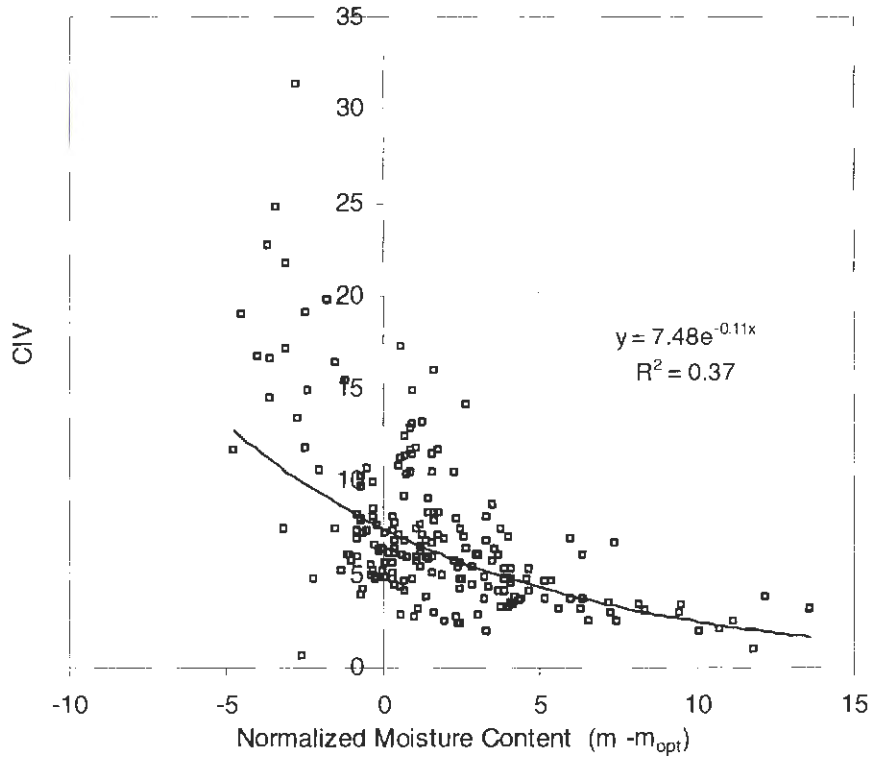

Figure 200. Regression of CIV with normalized moisture content (all field soils)

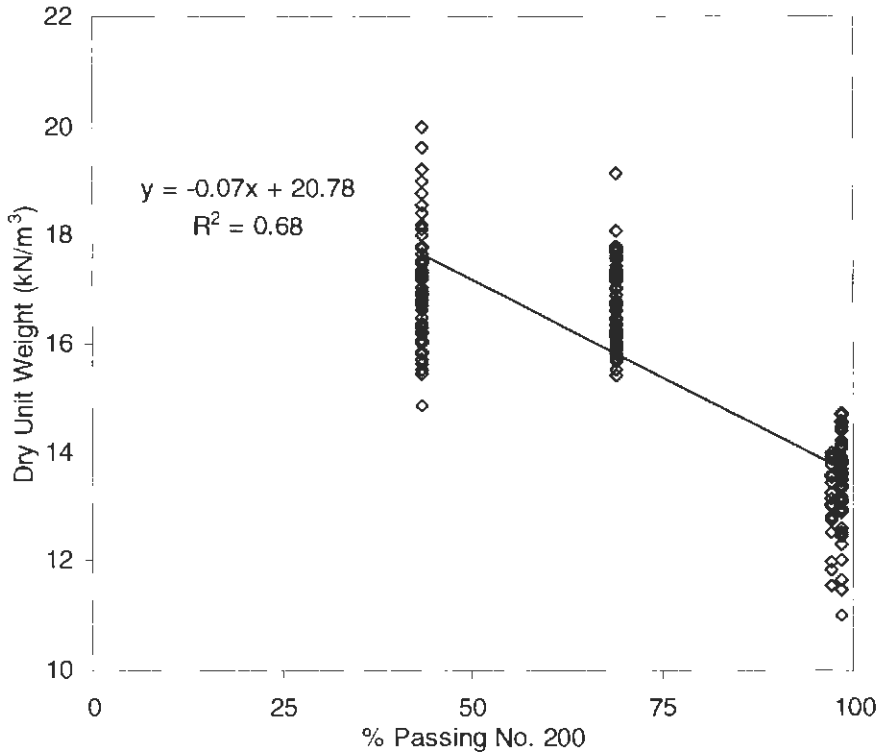

Figure 201. Regression of dry unit weight with fines content (all field soils)

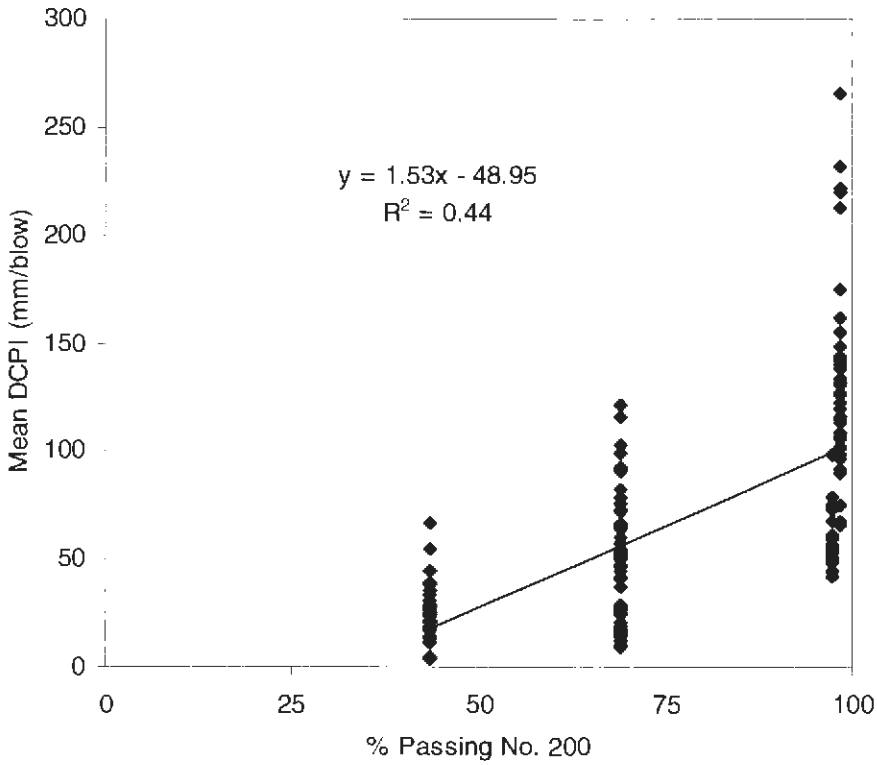

Figure 202. Regression of mean DCPI with fines content (all field soils)

Validity in Using Relative Compaction

As anticipated, percent standard Proctor increased with increasing roller passes in the field (Figure 203). Observing the slight correlation in Figure 204, there appears to be credibility in reasoning higher relative compaction leads to greater stability with Clegg values. However, the correlation is fair ($r^2 = 0.19$) and differences in CIV occur as high as 27.6 (eight fold difference). This occurs at 91% relative compaction. Also, the zone of influence on the Clegg is minimal (on the order of ≤ 150 mm in depth) and should not be taken as a complete representation of the compacted lift profile. The validity of using relative compaction in properly assessing strength remains questionable as demonstrated by the DCP in Figure 205. The DCP has a higher zone of influence (up to 1000 mm in depth) and therefore gives a greater understanding of the compacted lift profile.

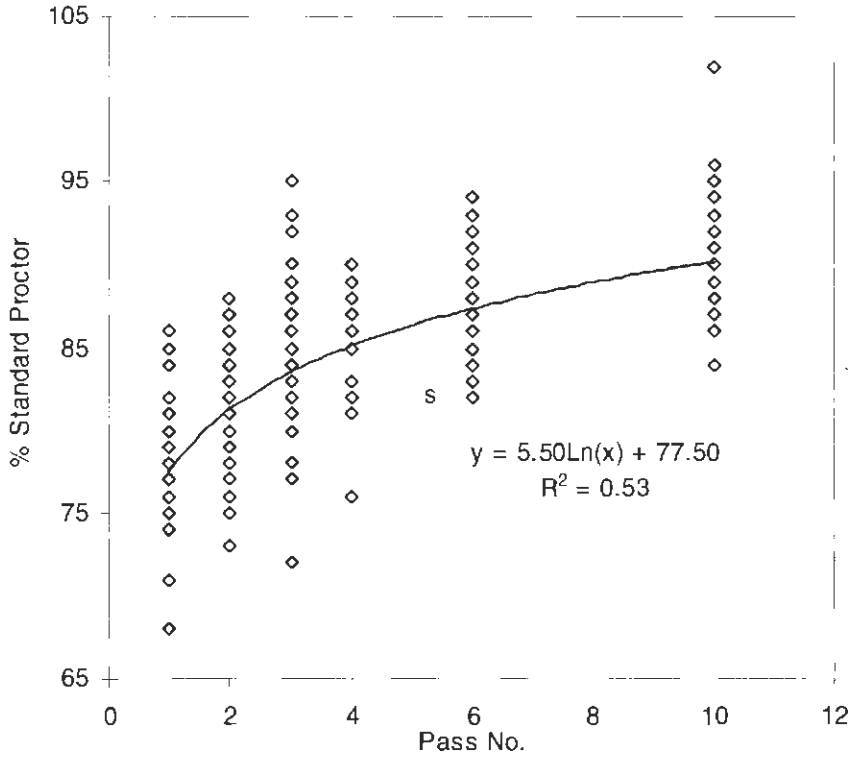

Figure 203. Percent standard Proctor as a function of roller passes (all field soils)

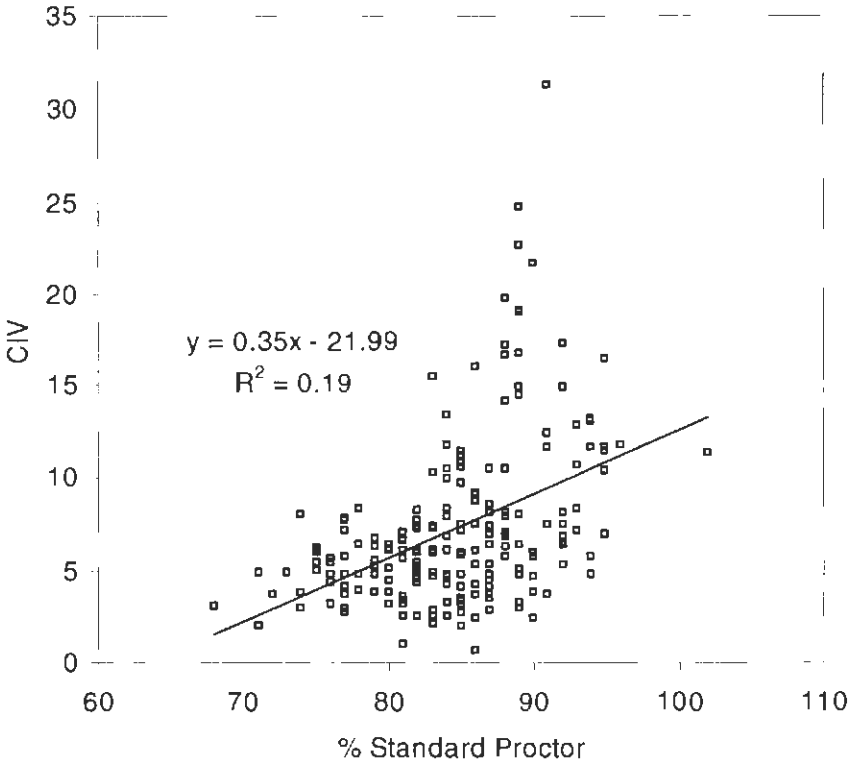

Figure 204. CIV as a function of relative compaction (all field soils)

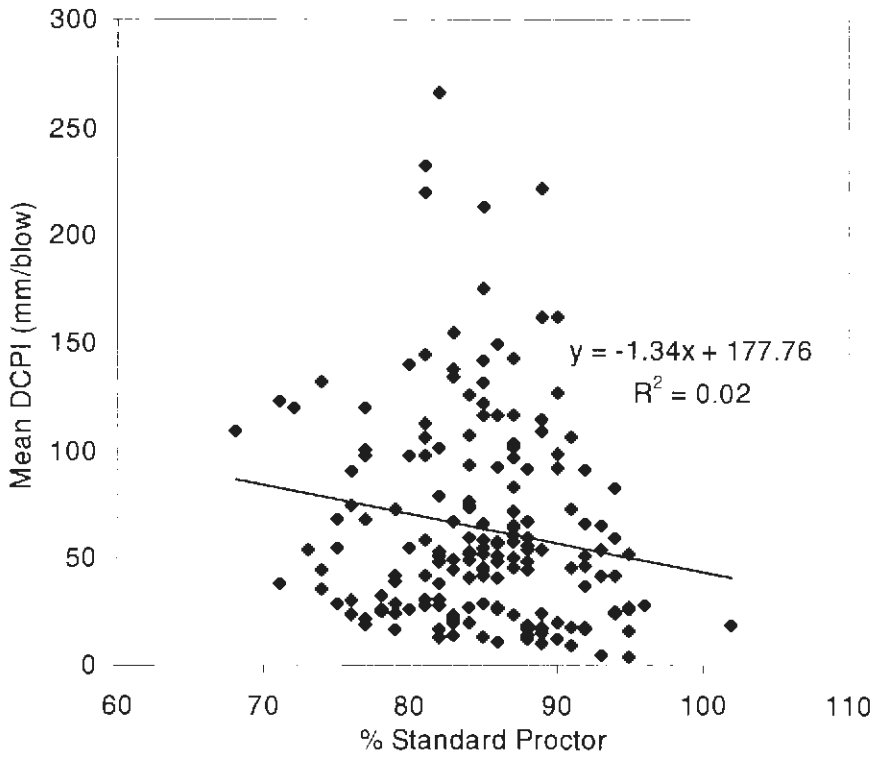

Figure 205. Mean DCPI as a function of relative compaction (all field soils)

Integrating Lab Research to Estimating Field Work

The final objective of this paper involved evaluating the potential of integrating the models developed for strength and stability to work performed in the field. To accomplish the objective, field results from the Peoria Proving Grounds and Edwards Test Facility were compared to laboratory results. Lab data used included strength and stiffness readings from unconfined compression tests. Mean DCPI and Young's modulus from the Geogauge were used from the field data. Thus, Young's modulus values were determined from UCS results, i.e. the secant modulus was not used in this analysis. Young's modulus comparisons were only observed for PPG till since the Geogauge was not used at the Edwards Test Facility. Clegg impact values could not be used the study. It shall be noted that the Clegg Impact Hammer can be used to determined target parameters like dry unit weight, strength, and

stiffness (ASTM D-5874). However, the Clegg test could not be used here because it was not used in the lab to establish semi-empirical relations from till specimens before sheared in the UCS test. Finally, unconfined compression tests were not conducted on West Des Moines clays, and therefore were not be used in the comparative analysis between lab and field.

The key obstacle to overcome in comparing lab and field results was determining mean DCPI values from undrained shear strength and vice versa. Research by Malama (2005) and White et al. (1999) were used to correlate lab UCS to DCPI with the following equations:

$$\text{Log DCPI} = -0.357(\text{Log UCS})^2 + 0.372(\text{Log UCS}) + 1.966 \qquad [5\text{-}37]$$

$$\text{Log UCS} = -0.727(\text{Log DCPI})^2 + 1.548(\text{Log DCPI}) + 1.832 \qquad [5\text{-}38]$$

where, UCS is the unconfined compressive strength (kPa) and DCPI is the mean DCP index (mm/blow). The models each have an r^2 value of 0.84 and are only valid for a DCPI greater than 10.

In essence, Equation 5-37 involves estimating DCPI based of a soil based on UCS values from the lab. Equation 5-38 entails the opposite case. This analysis benefited from using the former of the two models, since the outcome here was to implement a quality control procedure involving a predetermined strength and/or stiffness parameter from the lab.

An implementation involving UCS would be advantageous in the analysis for the following reasons:

1.) Unconfined compressive strength correlates more with energy than stiffness, which is more dependent on moisture parameters.

2.) The unconfined compression test, as opposed to triax or direct shear, is a simple and more economical procedure.

3.) The test is a conservative measurement of strength, which is always a crucial item in terms of design. Either UCS could be used, or undrained shear strength, i.e. ½ UCS = S_u.

Applications of a target parameter could vary depending on the structure and type of work, i.e. state or private. If state work is involved, the aforementioned work by White et al (2002) would suffice for target UCS values based on threshold criteria for DCP index. For private applications, target parameters could be established based on a firm's preferences and tolerances in their respective practice of design.

For both field tests, DCPI from the field and UCS converted to DCPI were plotted against either lab compaction energy or roller pass. Stiffness from UCS in the lab was also plotted with Geogauge stiffness measurement against compaction energy and roller pass. It was determined that roller passes could not be easily compared to a compaction energy produced

in the laboratory. It was concluded this could be due to inherent variability in soil, difference in lab and field compaction techniques, lack of true pass by pass data, and narrow ranges of moisture content.

Integrating Lab and Field Models

Ideally, the lab models from this research could be used in estimating the number of passes needed to achieve a target strength of stiffness parameter. It was observed in this study that while compaction energy does influence the stiffness in soil, moisture parameters play a much more important role in the determination of stiffness. Results shown in Table 11 and Table 17 give an indication of this. On the other hand, the compaction energy was more dominant a predictor in strength than moisture parameters (see Table 10 and Table 17). Therefore, it was advantageous to focus on the shear strength models derived to determine the ways to integrate the models.

A simple spreadsheet was set up to forecast lab compaction energies at different moisture contents based on a target unconfined compressive strength. The equations used in the spreadsheet included Equations 3-27 and 3-28 (individual regression models for PPG and Edwards till) and Equations 3-43 – 3-47, which were models of all lab soils tested in unconfined compression. Similar to the new compaction model, from Chapter 3, predictions were taken at moisture content increments of 1%, but this time for energy prediction. A target UCS value was inputted as a variable into the equation by first converting it to

undrained shear strength, since the models derived from this research were based on the shear strength.

The energies predicted in the modeling could be used in coordination with number of roller passes. In this case, however, a more robust DCPI data set is needed to derive better correlations with roller pass, i.e. pass by pass data is needed. One such unpublished data set has been completed on the Edwards till (as well as a topsoil, sand, and fill clay) and is recommended to be used for additional research in this modeling.

Another way attempted to integrate was to use the UCS/DCPI correlation equation (5-38) with DCPI equations for all field measurements (Eq. 5-25 – 5-27 and 5-33) derived from this study. By solving for Log DCPI, a prediction equation for UCS was derived. In the equation roller pass number was used as an input variable. The following in an example derivation between equations 5-25 and 5-38:

$$DCPI = -2.0(Pass) + 4.1(m\%) + 4.7 \qquad [5\text{-}25]$$

$$Log\ UCS = -0.727(Log\ DCPI)^2 + 1.548(Log\ DCPI) + 1.832 \qquad [5\text{-}38]$$

solving 5-25 for Log DCPI we have,

$$Log\ DCPI = -2.0Log(Pass) + 4.1Log(m\%) + Log(4.7) \qquad [5\text{-}25]$$

now placing Log DCPI from 5-25 into 5-38,

$$\text{Log UCS} = -0.727(-2.0\text{Log(Pass)} + 4.1\text{Log(m\%)} + \text{Log(4.7)})^2 + 1.548(-2.0\text{Log(Pass)} + 4.1\text{Log(m\%)} + \text{Log(4.7)}) + 1.832 \quad [5\text{-}39]$$

Equations like 5-39 were derived using the same derivation but with different field models. With this equation, the number of passes can be inputted as a variable to establish an estimate for UCS. A spreadsheet was set up using increments of 1% for moisture content; used when applicable. Model equations from all field results were used in the derivations since a robust data set of pass by pass data was not collected during individual field tests.

It was observed that much of predicted strength values were close to zero, indicating flaws in the specific equations used to derive the model or flaws in the overall theory. It is recommended that the unpublished pass by pass data from Edwards Test Facility be used to advance the efforts of this research and either validate or rescind the modeling used.

CHAPTER 6. SUMMARY ON LAB AND FIELD RESULTS

Cohesive soils from the Midwest were selected to perform laboratory and field tests. A test plan for the soils was devised that included the measurement of dry unit weight, strength, and stiffness at different combinations of moisture content and compaction energy. The lab and field data was collected using conventional lab equipment, following standardized test procedures. A statistical study was conducted to derive possible correlations between soil parameters and independent variables including compaction energy and moisture content. This chapter gives a summary of the results from the lab and field tests.

Lab Soils

For all lab soils, maximum dry unit weight increased and optimum moisture content decreased as compaction energy increased. Plotted against compaction energy, a semi-logarithmic relationship existed between the two optimal parameters and energy. Good correlation was observed for most soils ($r^2 = 0.91 - 0.99$).

It was concluded that the sensitivity of optimal conditions to compaction energy was closely related to the liquid limit, plastic limit, and clay fraction. An increase in the clay fraction, increased the compressibility of soil, thus increased the sensitivity to applied energy.

At each moisture content dry unit weight reached an asymptotic state with increased energy. The rate at which it reached this state depended on the soil's sensitivity to compaction energy. In highly saturated conditions the asymptotic state was reached immediately, regardless of an increase in compactive effort.

A new compaction model, derived from first-order linear rate principles, reproduced the asymptotic relationship between dry unit weight and energy. Estimates of dry unit weight from the model were compared to all measurements from the lab and yielded great correlation ($r^2 = 0.99$). The F-value, or compatibility coefficient, from the linear rate model was directly affected by moisture content.

By plotting compaction energy against moisture content at different levels of relative compaction, the compaction efficiency was determined in several ways. Efficiency was compared between individual moisture contents and compaction energies, on relative compaction curves, and at the line of optimum.

Individual dry unit weight compaction models, derived from multiple regression, yielded fair to good correlation. However, energy accounted for explaining most of the variability in the models. Models split at optimum moisture content and analyzed separately yielded higher correlations and allowed for moisture content to explain variability in dry unit weight, particularly wet of optimum. Moisture content, liquid limit, and fines content were the strongest predictor in compaction models for all soil data. In comparing compaction models from the literature review and those derived in this study.

Highest shear strength and stiffness occurred at dry of optimum and optimum moisture conditions. At moisture contents less than optimum the strength and stiffness of a soil increased with increasing compaction energy. An increase in these parameters was generally

not observed wet of optimum. Decreases in strength and stiffness with increased energy was attributed to remolding of soil.

Individual undrained shear strength and secant modulus models yielded fair to good correlation. Compaction energy accounted for explaining most of the variability in the shear strength while moisture content explained the variability in secant modulus. For all strength and stiffness data, models derived had moderate to good correlation. Independent variables explaining the variability in strength and stiffness were the same as individual models.

Results of undrained strength and secant modulus were noted as being sensitive to moisture content more than compaction energy applied. Index properties that yielded greatest correlation with moisture were liquid limit, plastic limit, and fines passing the No. 200 sieve. Good correlations with compaction coefficients and index properties were not observed.

The practice of using relative compaction as an absolute means in determining strength and stability of a soil was demonstrated to be invalid. While slight correlation ($r^2 = 0.23$) existed between relative compaction and undrained shear strength, a difference in strength as high as twelve-fold occurred at given percentages of standard Proctor. Further, stiffness showed poor correlation ($r^2 = 0.00$) with relative compaction.

Strength and stiffness models developed from loess WF specimens yielded moderate to good correlation with compaction energy, moisture content (before and after consolidation), and confining pressure. When used in the multiple regression analysis, confining pressure was

the strongest predictor for dependent parameters. Compaction energy explained variability the best for principal stress ratio, while initial moisture and confining pressure explained most of the variability in secant modulus. Confining pressure and final moisture explained most of the variability in peak deviator stress. It was concluded that the confining pressure applied can be considered a direct reflection of the amount of compaction energy used in earthwork construction. Higher levels of compaction energy applied to an initial loose layer of soil leads to higher confining pressure within a soil structure.

Poor correlation was observed between cohesion and independent variables. Moderate to fair correlation was observed for friction angle. Friction angle increased with increasing compaction energy and decreased with increasing moisture content after consolidation.

Field Results

For the field test at Peoria Proving Grounds, only one of 60 measurements of dry unit weight, was $\geq$ 95% standard Proctor. Despite low measures of relative compaction, DCP index values met threshold criteria (based on White et al., 2002), due to properly compacted lifts and a suitable moisture range. With increasing roller pass DCPI decreased and CIV/Geogauge values increased. Statistical analyses from the data set yielded poor to moderate correlation. This was attributed to a lack of a true data set of pass by pass field measurements and narrow range of moisture used.

At the Edward Test Facility, more measurements of 95% standard Proctor were achieved (at ten passes). DCPI at Edwards did not met threshold criteria on two of the strips that were

compacted wet of optimum. With increasing roller pass, DCPI decreased and increasing CIV with increased. The statistical analyses yielded moderate to good correlation because of the wider distribution in moisture content. The statistical modeling would have benefited from a data set of pass by pass test measurements.

The lean clays used in the West Des Moines field tests did not achieve 95% standard Proctor. Most DCPI measurements were over the allowable DCPI criteria for the existing clay. Increasing passes appeared to decrease DCPI. Fill clay test strips met DCPI criteria due to a narrower range of moisture content. Stiffness observed in Clegg values for both clays generally increased with increasing pass. The statistical modeling yielded poor to fair correlation mostly due to a limited range in moisture content. The impact of pass by pass test measurements was not completely seen in the modeling because of the narrow range in moisture.

Compaction models of all field measurements resulted in dry unit weight models yielding the best correlation, followed by CIV, DCPI, and percent compaction. For CIV measurements, roller pass proved to be the strongest predictor. Roller passes and fines content were equal in predicting DCPI for one model derived that included moisture content. Moisture content, fines, and liquid limit were strongest in predicting dry unit weight. Replacing linear models with polynomial and exponential fits increased r^2 values for DCPI models. Dry unit weight had a much lower coefficient of variation than DCPI and CIV.

CHAPTER 7. CONCLUSIONS AND RECOMMENDATIONS

The objectives for this thesis are restated as the following:

1. Evaluate soil parameters as a function of compaction energy, moisture content, and index properties.
2. Derive prediction models that relate soil parameters to compaction energy, moisture content, and index properties.
3. Compare and contrast prediction models derived to previous work from the literature.
4. Verify the usefulness of prediction models by estimating soil behavior with lab soils not used in the statistical analyses.
5. Evaluate the potential to integrate lab research in estimating work performed I in the field.

Soil parameters including dry unit weight, undrained shear strength, and secant modulus were evaluated as a function of compaction energy, moisture content and index properties. Results from the lab agree well with research from the literature.

In addition to evaluating soil parameter in ways documented from the past, new venues of research were explored inspired by work previously performed in linear rate theory applied to soil mechanics and soil compaction modeling involving the estimation of dry unit weight of soil based on moisture, energy, and index properties. The linear rate compaction model shows great promise in its ability to estimate dry unit weight. The multiple regression

compaction models derived go a step beyond estimating dry unit weight and estimate parameters of strength and stability. Despite more variability than dry unit weight, the strength and stiffness models give a general idea of what to expect with a given energy, moisture content, and index property.

The dry unit weight models from this paper were compared with work by past authors. Work by another author (Boltz et al., 1998) yielded a better estimation of dry unit weight than the actual equations derived from the lab results. This was due to the model equations being derived from all compaction data beside optimal conditions.

The integration of lab models to the field was investigated. Correlations between DCPI and UCS (Malama, 2005) were also used as a guide to compare lab and field results of UCS and DCPI respectively. The results indicate the correlation as a useful tool in anticipating DCPI measurement in the field. However, defining lab compaction energy as a quantity of roller pass was not clear when comparing actual and converted DCPI measurements. It was concluded this could be due to inherent variability in soil, difference in lab and field compaction techniques, lack of true pass by pass data, and narrow ranges of moisture content. Another approach to integrate lab data was to use the field models for DCPI in conjunction with the DCPI/UCS equation. A shear strength model spreadsheet resulted from this work. Slight potential was observed using the spreadsheet, but it was concluded that poor results could be due to a non-robust field data set, flaws in the specific equations used to derive the model, or flaws in the overall theory.

Due to time constraints, the fourth objective was not fulfilled in this research. It is therefore recommended that the models derived from this study be used on a different soil for validation of models. Also, it is recommended that a continuing database of soils be collected to further the effort of modeling Midwest soils in strength and stability. In particular, a soil database, based on triaxial specimens would be advantageous, since the nature of the test represents compacted soil long after construction. An ongoing effort and pursuit of research in this subject will someday turn the field of earthwork construction towards specifications on parameters that define true functional requirements. It is further recommended that further field tests be conducted that includes pass by pass in-situ data and a wider range of moisture content and index properties. This data could be used to further investigate the potential to integrate data from the laboratory to the field.

APPENDIX A. DISTRIBUTION CURVES AND PROCTOR DATA

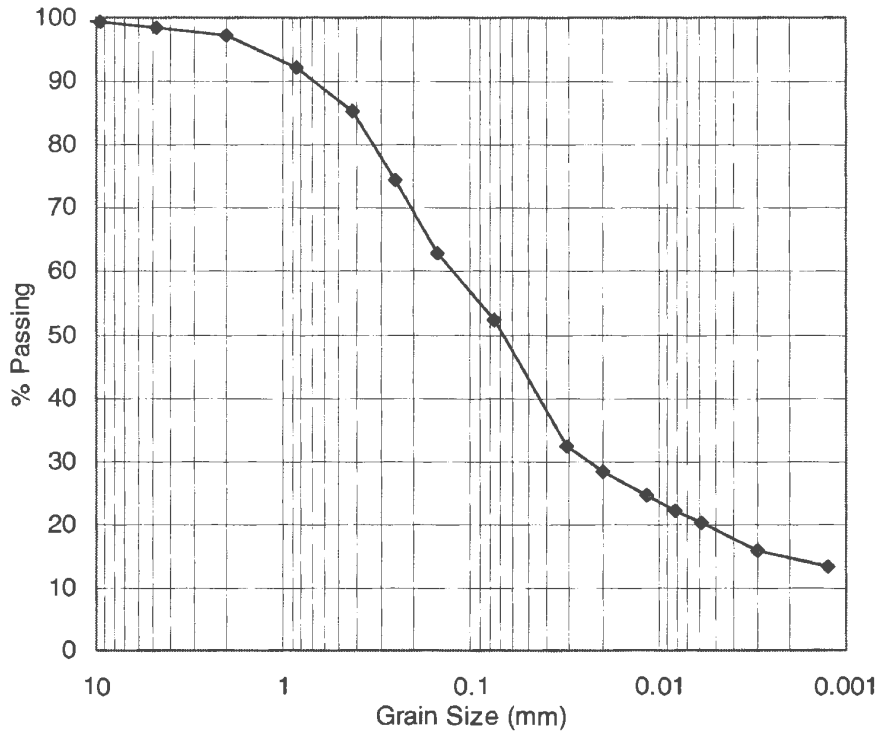

Figure A1. Grain size distribution of Central Iowa till

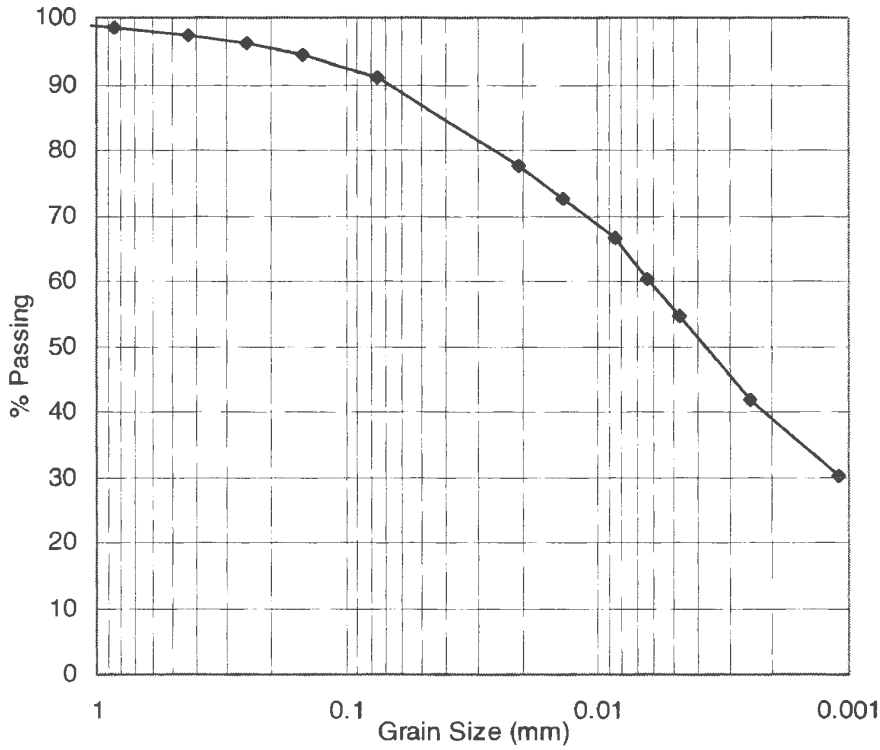

Figure A2. Grain size distribution of weathered shale

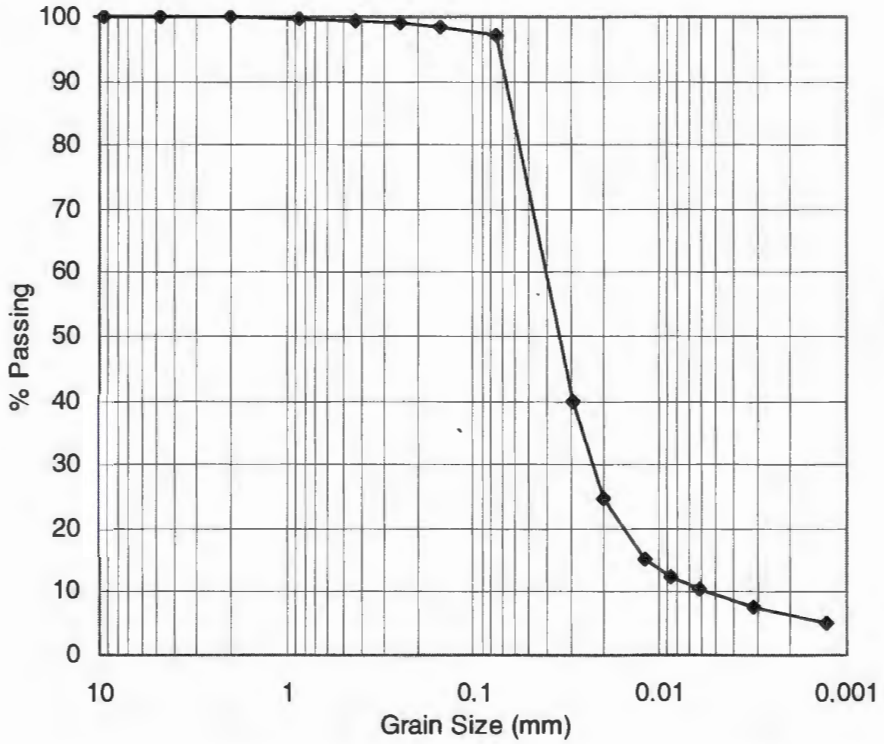

Figure A3. Grain size distribution of Western Iowa loess

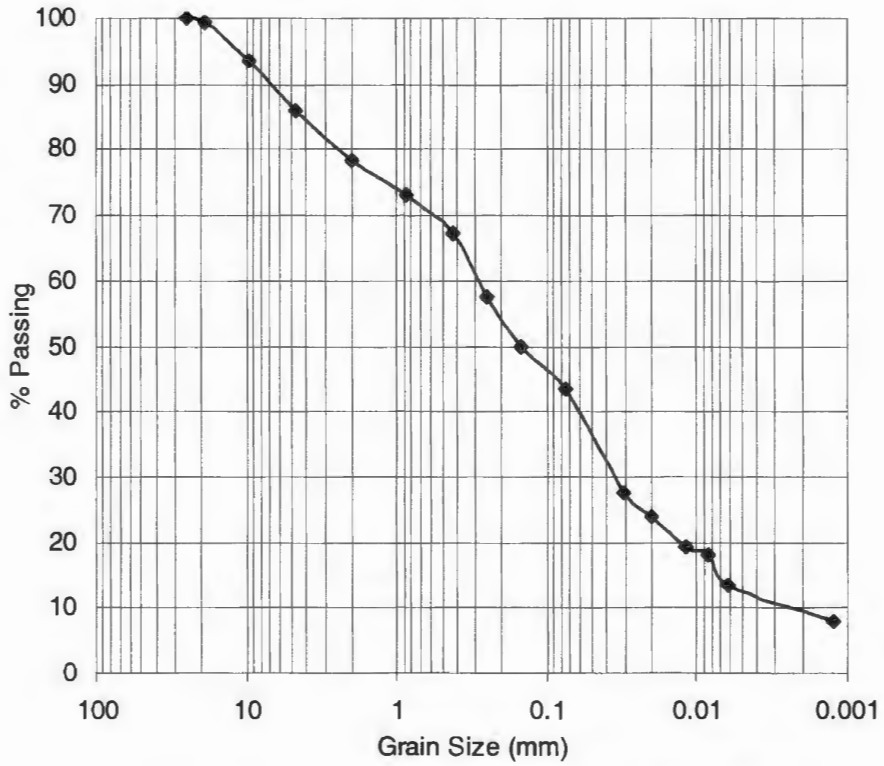

Figure A4. Grain size distribution of PPG till

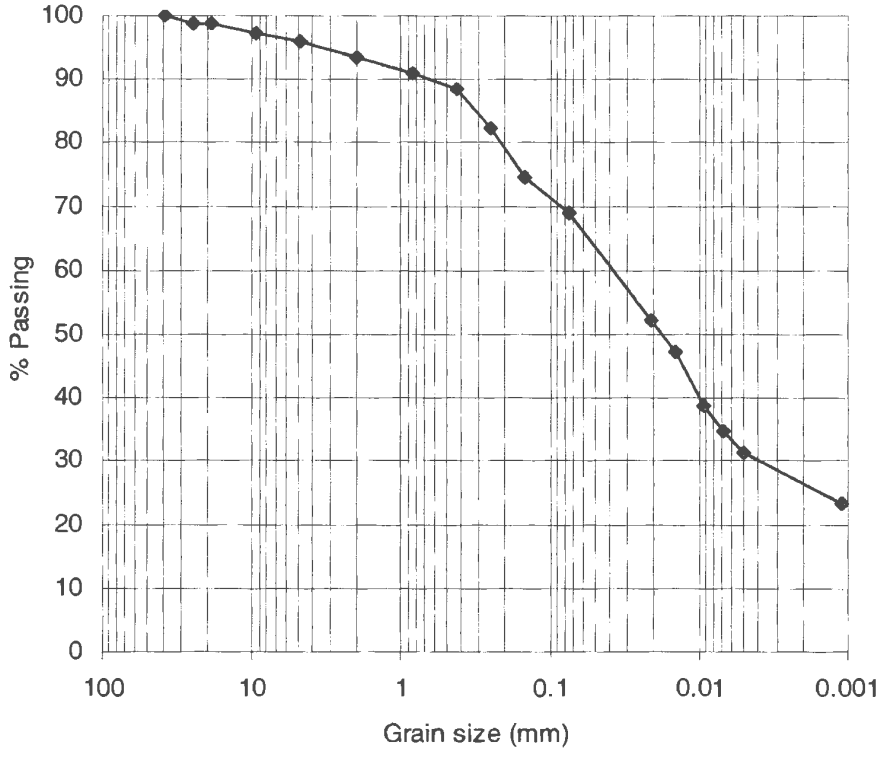

Figure A5. Grain size distribution of Edwards till

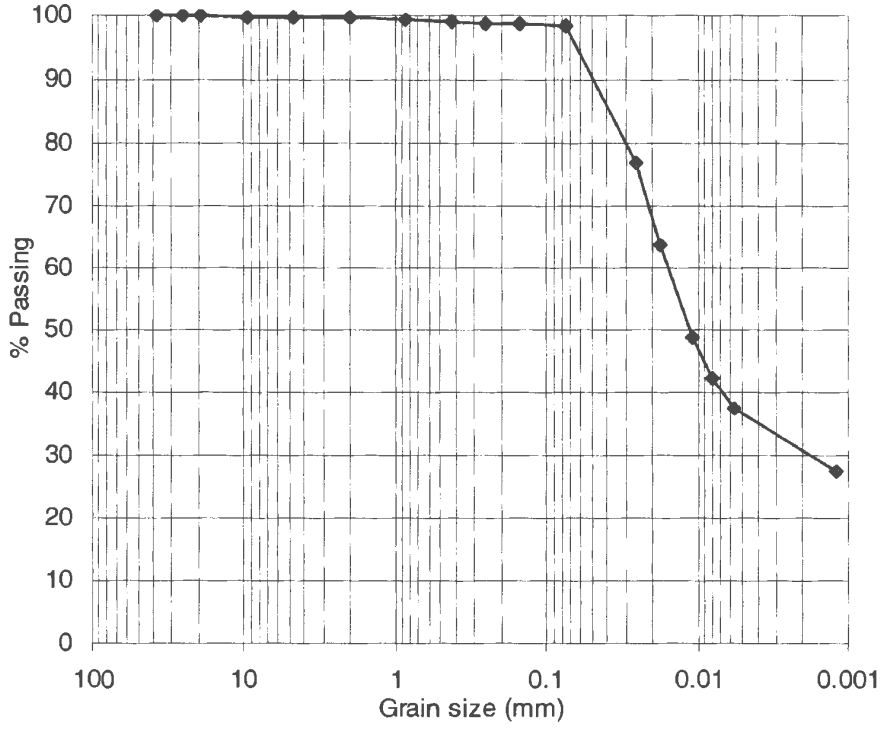

Figure A6. Grain size distribution of West Des Moines clay 1 (existing)

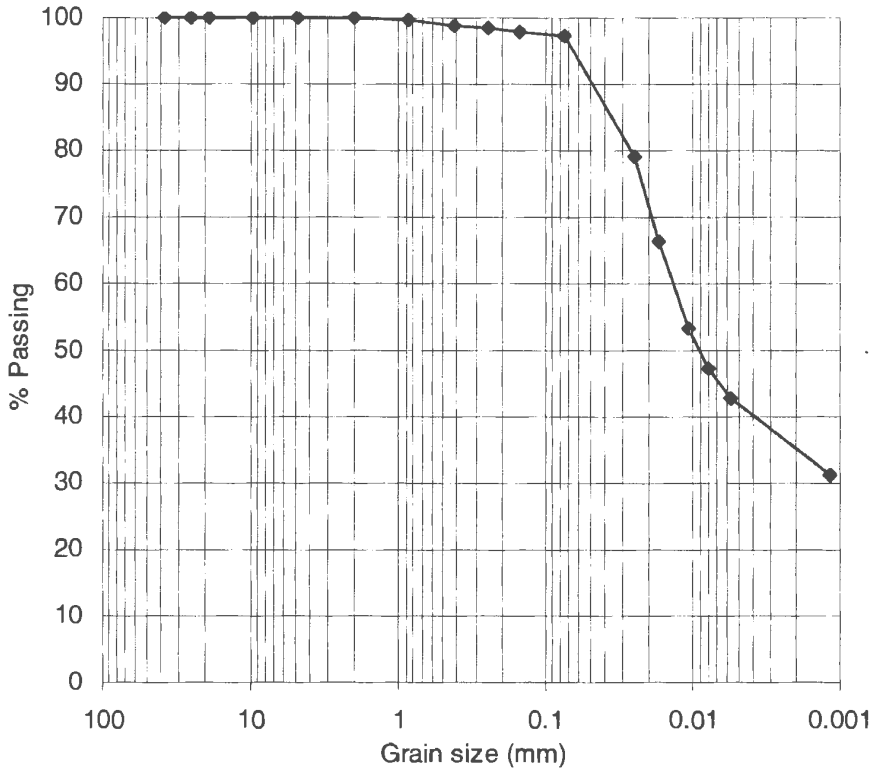

Figure A7. Grain size distribution of West Des Moines clay 2 (fill material)

Table A1. Proctor Compaction Test Results (Central Iowa Till)

Compaction Energy (kJ/m^3)	Moisture Content (%)	Dry Unit Weight (kN/m^3)
355	8.4	16.61
355	10.8	17.39
355	12.8	17.65
355	14.0	17.93
355	16.3	17.87
355	17.9	17.17
592	8.6	17.49
592	10.2	18.21
592	11.5	18.10
592	14.6	18.35
592	16.9	17.56
987	8.6	18.53
987	11.0	18.68
987	12.1	18.85
987	13.7	18.65
987	15.8	18.06
1643	6.4	18.33
1643	7.9	18.83
1643	10.5	19.36
1643	12.5	19.15
1643	13.7	18.98
2693	6.5	19.19
2693	8.6	19.70
2693	10.1	20.04
2693	12.3	19.48
2693	14.3	18.57

Table A2. Proctor Compaction Test Results (weathered shale)

Compaction Energy (kJ/m^3)	Moisture Content (%)	Dry Unit Weight (kN/m^3)
355	11.7	15.99
355	14.3	16.55
355	17.7	16.59
355	20.1	16.81
355	22.1	16.41
592	12.6	17.11
592	14.8	17.50
592	16.5	17.56
592	17.6	17.53
592	19.7	17.08
987	19.2	18.16
987	11.6	18.47
987	13.9	18.24
987	16.7	17.98
987	18.2	17.55
987	19.7	17.20
1643	9.2	18.73
1643	11.1	19.06
1643	12.4	18.84
1643	14.8	18.65
1643	16.4	18.23
2693	9.5	19.08
2693	11.1	19.24
2693	12.5	19.33
2693	13.6	19.18
2693	15.9	18.56

Table A3. Proctor Compaction Test Results (Western Iowa loess)

Compaction Energy (kJ/m^3)	Moisture Content (%)	Dry Unit Weight (kN/m^3)
355	12.3	14.77
355	14.8	15.00
355	16.4	15.21
355	18.1	15.20
355	20.2	15.32
355	21.6	15.16
592	14.5	15.53
592	16.4	15.76
592	18.6	15.87
592	20.0	15.75
592	22.1	15.13
987	12.1	16.06
987	14.3	16.37
987	16.1	16.35
987	18.3	16.38
987	19.9	15.95
1643	12.2	16.26
1643	14.8	16.50
1643	15.8	16.59
1643	18.0	16.60
1643	19.9	15.92
2693	12.4	17.07
2693	14.0	17.30
2693	16.0	17.32
2693	18.0	16.73
2693	19.8	16.17
2693	20.9	15.68

Table A4. Proctor Compaction Test Results (PPG Till)

Compaction Energy (kJ/m^3)	Moisture Content (%)	Dry Unit Weight (kN/m^3)
355	5.3	18.76
355	7.1	19.50
355	8.2	20.34
355	9.7	20.29
355	11.0	19.95
592	6.1	20.15
592	7.2	20.82
592	8.3	21.00
592	9.9	20.62
592	10.6	20.04
987	3.3	19.78
987	4.9	20.48
987	6.3	21.44
987	7.8	21.31
987	8.9	20.71
2693	4.0	21.14
2693	5.2	21.78
2693	6.5	21.98
2693	8.6	21.09
2693	10.5	20.30

Table A5. Proctor Compaction Test Results (Edwards Till)

Compaction Energy (kJ/m^3)	Moisture Content (%)	Dry Unit Weight (kN/m^3)
355	7.5	16.82
355	9.6	17.12
355	11.8	18.04
355	13.6	18.34
355	15.4	17.94
355	17.7	17.33
592	7.6	17.80
592	9.7	18.58
592	12.0	18.77
592	13.7	18.72
592	15.1	18.02
987	7.6	18.79
987	9.5	19.68
987	11.6	19.68
987	13.3	19.10
987	15.0	18.43
1643	5.9	18.97
1643	7.6	19.65
1643	9.6	20.20
1643	11.6	19.79
1643	13.0	19.26
2693	5.9	19.83
2693	7.6	20.41
2693	9.6	20.65
2693	11.4	20.04
2693	12.9	19.39

Table A6. Proctor Compaction Test Results (WDSM1 clay)

Compaction Energy (kJ/m^3)	Moisture Content (%)	Dry Unit Weight (kN/m^3)
355	16.8	15.39
355	20.6	15.60
355	21.8	15.75
355	26.0	15.03
355	28.5	14.37
592	13.5	15.25
592	17.0	15.96
592	19.8	16.23
592	22.6	15.70
592	26.0	14.93
987	10.5	15.94
987	13.5	16.62
987	17.3	16.89
987	19.8	16.50
987	22.6	15.84
1643	10.8	17.02
1643	13.5	17.41
1643	16.7	17.71
1643	20.0	16.85
1643	25.0	15.40
2693	8.8	17.25
2693	10.7	17.93
2693	13.7	18.47
2693	16.9	17.71
2693	20.2	16.80

Table A7. Proctor Compaction Test Results (WDSM2 clay)

Compaction Energy (kJ/m^3)	Moisture Content (%)	Dry Unit Weight (kN/m^3)
355	19.2	14.29
355	22.4	14.96
355	25.4	15.05
355	28.1	14.60
355	30.6	13.89
355	33.5	13.27
592	16.3	15.04
592	18.6	15.18
592	22.0	15.55
592	25.1	15.29
592	27.4	14.76
987	14.5	15.96
987	17.3	16.13
987	19.2	16.17
987	21.7	16.07
987	25.3	15.26
987	28.0	14.59
1643	10.0	16.70
1643	13.5	17.04
1643	16.6	17.20
1643	18.8	17.09
1643	21.8	16.31
2693	10.0	17.37
2693	14.2	17.74
2693	16.4	17.78
2693	18.7	17.29
2693	21.5	16.50

APPENDIX B. UNCONFINED COMPRESSION TEST DATA

Table B1. Unconfined Compression Test Results (Central Iowa Till)

Compaction Energy (kJ/m^3)	Moisture Content (%)	Undrained Shear Strength (kPa)	Secant Modulus (kPa)
355	7.1	101.7	39,8881.3
355	9.8	91.4	22,668.6
355	13.1	86.5	10,073.2
355	15.8	65.8	2568.3
592	7.2	138.6	66,787.4
592	10.0	145.5	22,678.2
592	14.4	115.1	6561.7
592	16.0	63.4	1931.9
987	8.9	204.4	63,037.3
987	10.7	193.1	25,512.6
987	13.7	162.0	10,407.6
987	15.7	69.3	1582.3
1643	7.2	314.1	81,130.5
1643	10.0	278.2	53,905.2
1643	13.4	107.9	4718.1
1643	17.0	34.1	853.6
2693	7.0	352.7	81,635.9
2693	9.3	365.8	53,868.7
2693	12.7	144.8	8487.4
2693	17.1	37.9	733.6

Table B2. Unconfined Compression Test Results (weathered shale)

Compaction Energy (kJ/m^3)	Moisture Content (%)	Undrained Shear Strength (kPa)	Secant Modulus (kPa)
355	13.0	95.1	33,268.4
355	16.2	74.8	13,263.8
355	19.7	102.0	7615.1
355	21.8	67.2	2838.8
592	10.9	112.4	60,421.7
592	14.2	125.5	29,665.4
592	17.9	129.6	9849.6
592	19.7	87.9	4772.4
987	11.4	197.2	51,085.5
987	13.8	213.0	23,751.1
987	18.9	121.0	6569.1
987	19.9	88.6	3301.0
1643	11.8	249.6	60,287.4
1643	15.7	284.4	22,219.4
1643	16.5	208.2	4658.2
1643	18.6	103.1	5294.1
2693	10.9	298.9	63,458.0
2693	13.6	377.1	45,993.0
2693	16.0	236.8	15,520.0
2693	21.1	75.5	2259.1

Table B3. Unconfined Compression Test Results (Western Iowa loess)

Compaction Energy (kJ/m^3)	Moisture Content (%)	Undrained Shear Strength (kPa)	Secant Modulus (kPa)
355	12.1	75.5	15,964.8
355	14.4	52.1	12,038.9
355	18.4	45.2	6963.0
355	21.2	41.7	4171.3
592	11.9	86.5	14,499.0
592	14.6	71.0	13,759.9
592	17.2	60.3	9840.9
592	22.5	51.0	2875.8
987	10.8	122.0	27,046.0
987	14.6	85.2	13,963.9
987	17.7	77.6	12,232.7
987	21.8	43.4	2715.2
1643	13.5	130.7	16,915.9
1643	15.6	114.5	15,642.1
1643	19.3	86.9	7269.1
1643	21.5	63.4	2796.5
2693	12.8	216.5	36,214.0
2693	15.5	170.0	19,543.9
2693	18.4	145.8	10,766.8
2693	20.4	88.9	3353.6

Table B4. Unconfined Compression Test Results (PPG Till)

Compaction Energy (kJ/m^3)	Moisture Content (%)	Undrained Shear Strength (kPa)	Secant Modulus (kPa)
355	6.0	93.4	21,324.8
355	6.7	84.1	17,383.0
355	7.7	66.2	13,237.9
355	10.1	39.0	773.9
592	5.5	150.0	44,988.9
592	6.8	126.2	50,469.6
592	7.7	98.3	13,843.9
592	9.2	60.3	1667.9
987	5.2	222.0	52,985.9
987	6.8	171.0	29,450.2
987	8.4	107.6	3788.6
987	9.4	59.6	1197.8
2693	5.0	425.1	68,669.0
2693	7.0	505.4	18,324.2
2693	8.1	196.5	2256.6

Table B5. Unconfined Compression Test Results (Edwards Till)

Compaction Energy (kJ/m^3)	Moisture Content (%)	Undrained Shear Strength (kPa)	Secant Modulus (kPa)
355	5.4	133.1	25,304.9
355	8.5	122.7	40,002.2
355	11.0	86.2	25,855.6
355	13.8	72.4	17,840.5
592	5.5	181.7	40,141.9
592	8.9	205.1	75,970.0
592	11.2	122.7	30,681.7
592	13.7	162.0	9638.7
987	5.4	288.5	68,701.3
987	8.7	266.8	86,971.0
987	11.2	251.7	29,262.6
987	14.1	156.9	6520.2
1643	5.1	343.0	83,768.2
1643	8.5	393.7	75,709.7
1643	12.4	319.9	34,681.8
2693	5.1	468.8	164,807.1
2693	8.3	506.4	61,895.9
2693	10.8	430.9	32,319.2
2693	13.8	118.2	2433.0

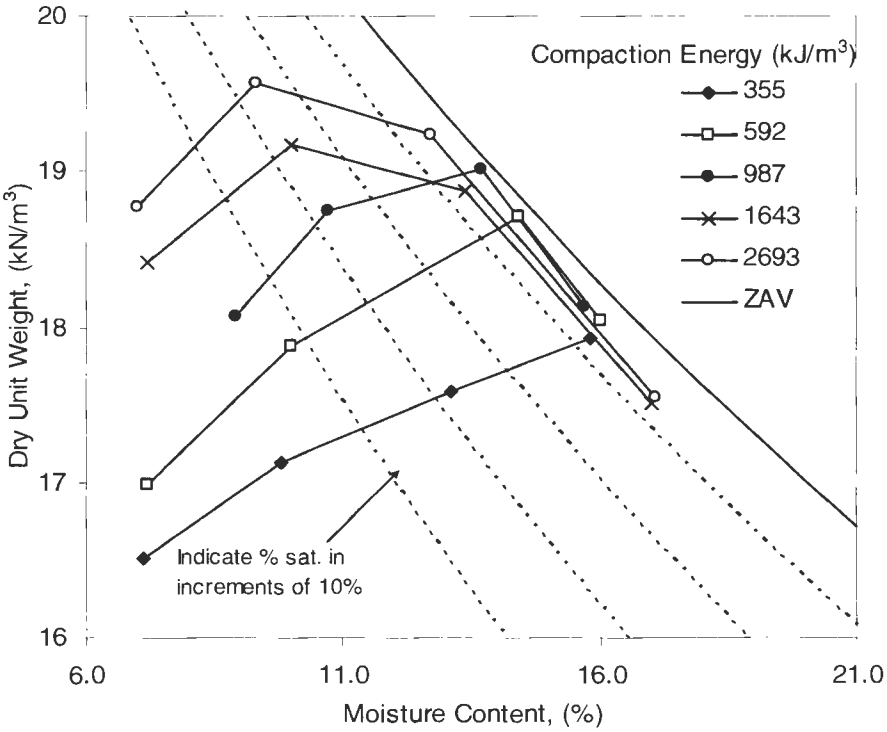

Figure B1. Dry unit weight results from unconfined compression tests for various compaction energies (Central Iowa till)

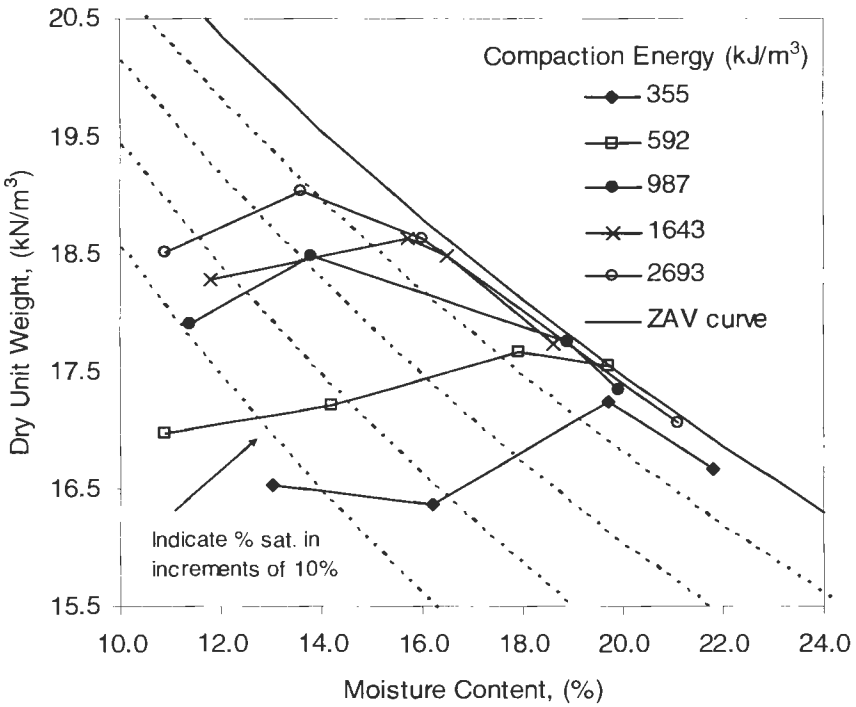

Figure B2. Dry unit weight results from unconfined compression tests for various compaction energies (weathered shale)

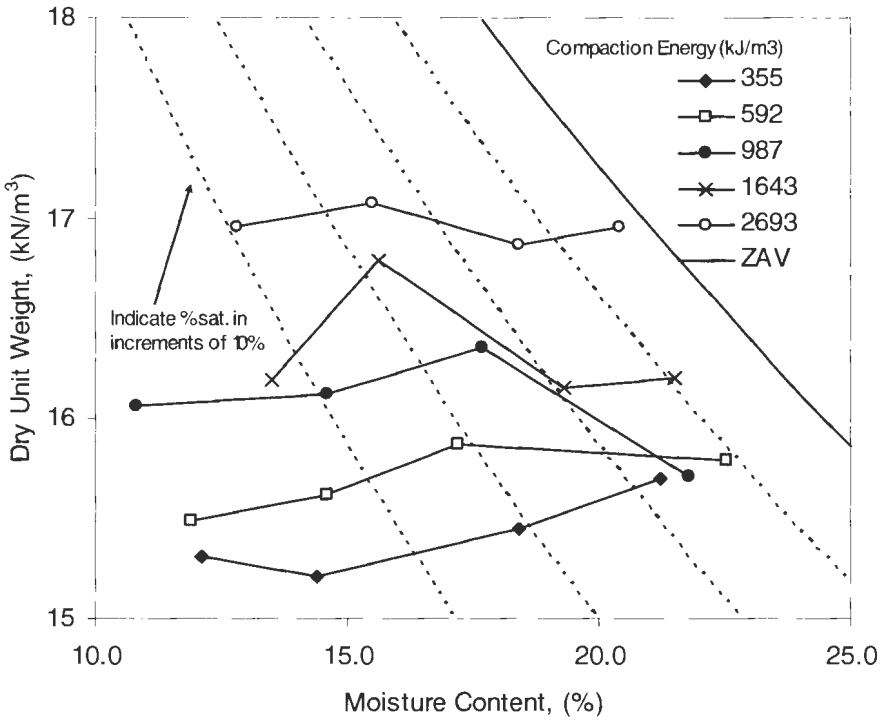

Figure B3. Dry unit weight results from unconfined compression tests for various compaction energies (Western Iowa loess)

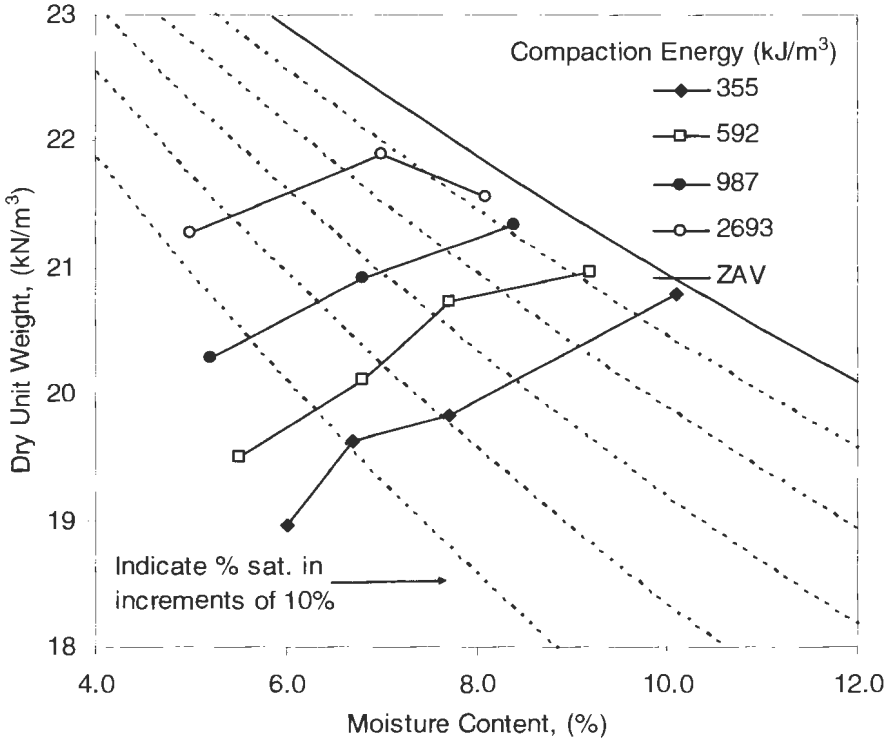

Figure B4. Dry unit weight results from unconfined compression tests for various compaction energies (PPG till)

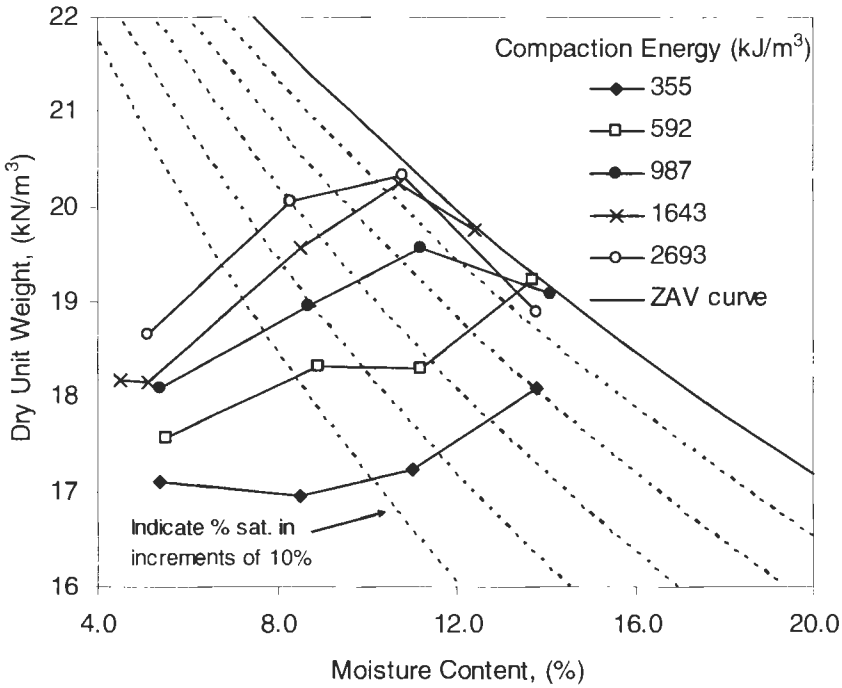

Figure B5. Dry unit weight results from unconfined compression tests for various compaction energies (Edwards till)

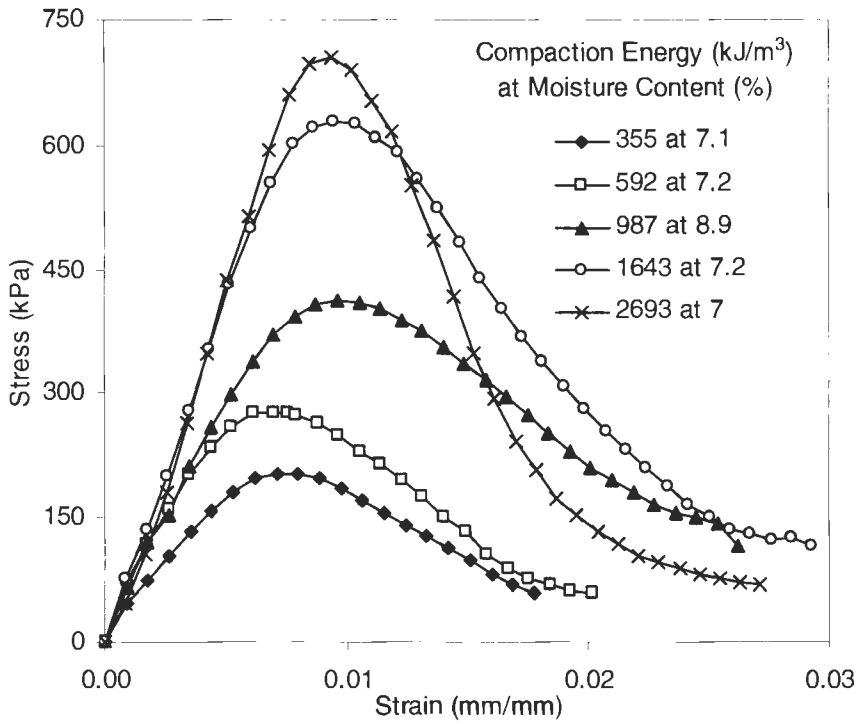

Figure B6. Unconfined compression results for various compaction energies at approximately 7.0% moisture content (Central Iowa till)

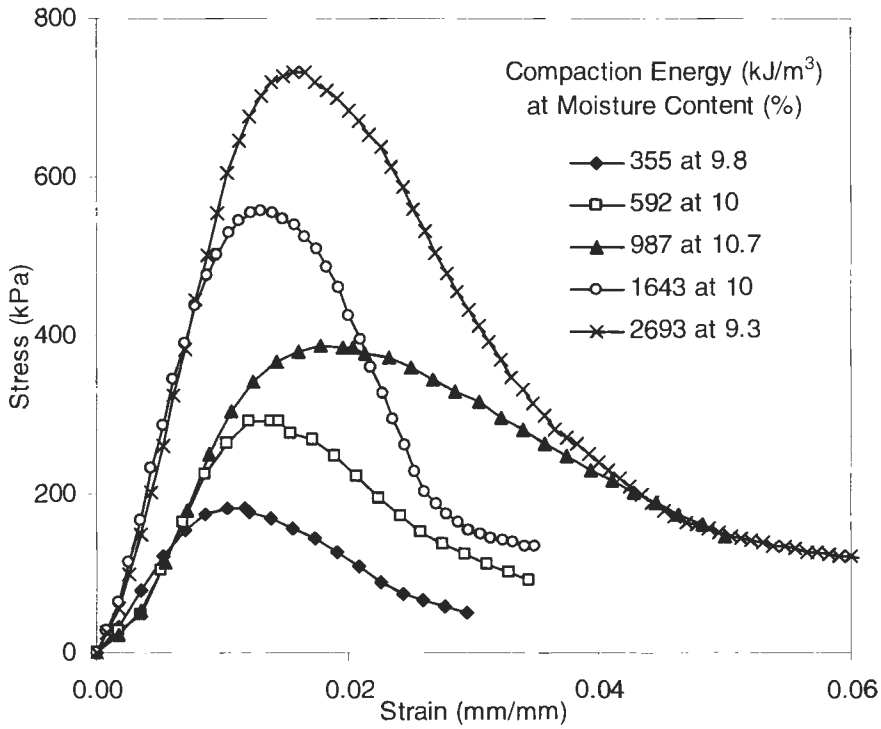

Figure B7. Unconfined compression results for various compaction energies at approximately 10.5% moisture content (Central Iowa till)

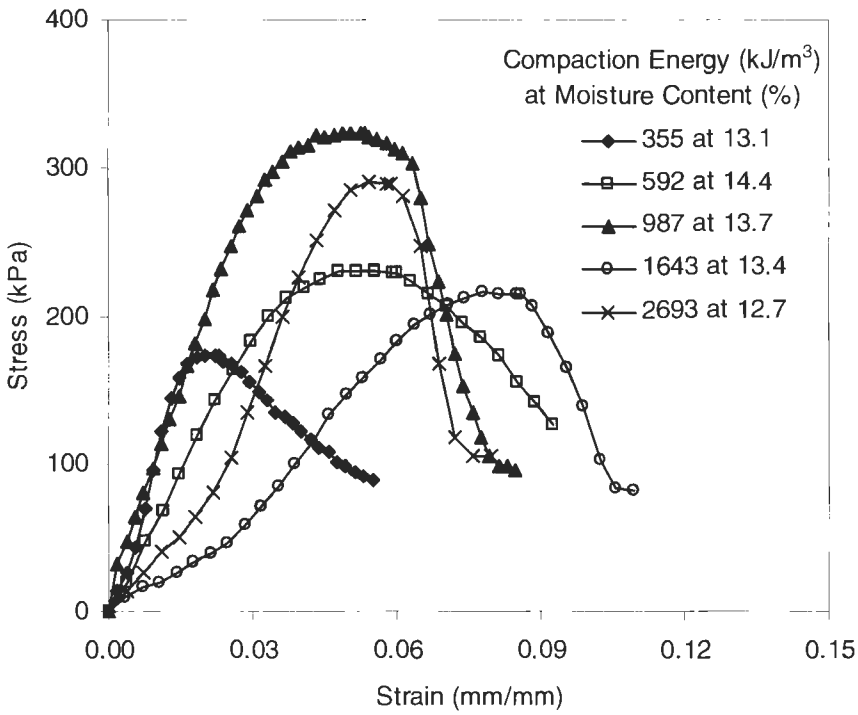

Figure B8. Unconfined compression results for various compaction energies at approximately 13.5% moisture content (Central Iowa till)

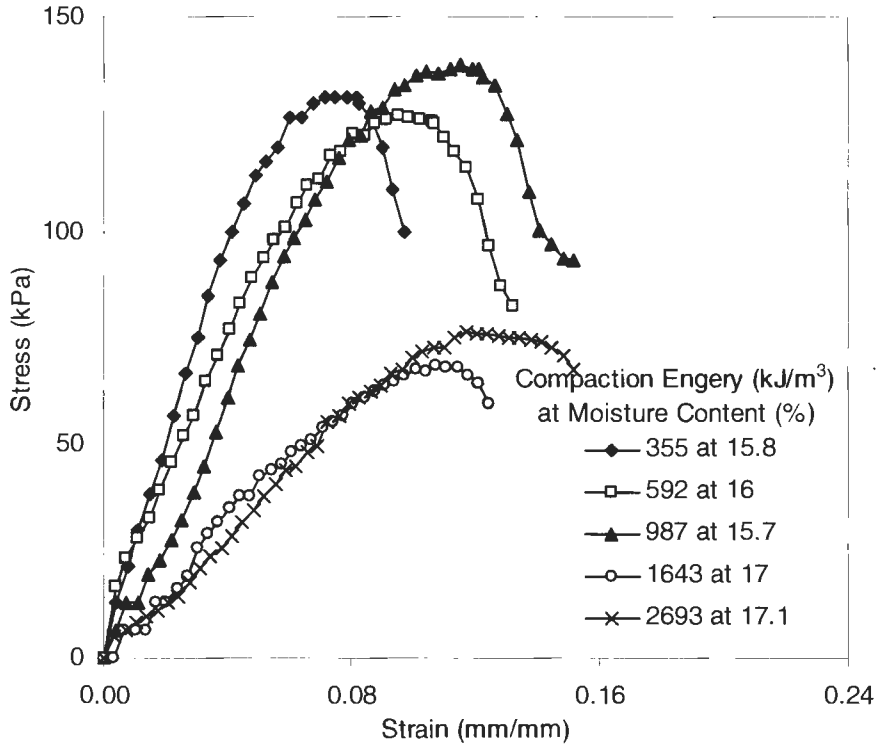

Figure B9. Unconfined compression results for various compaction energies at approximately 16.5% moisture content (Central Iowa till)

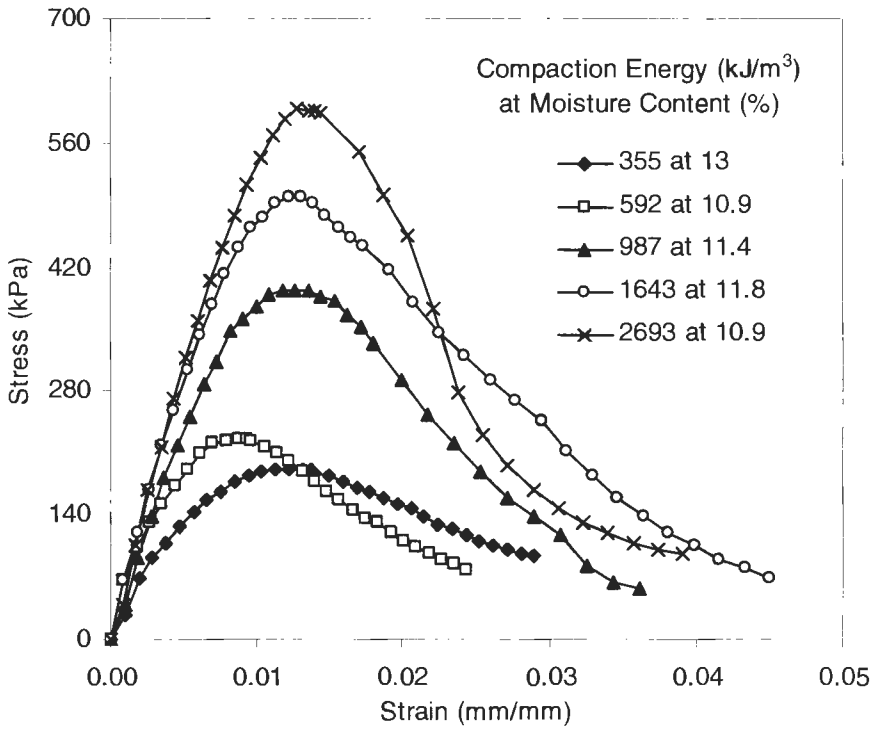

Figure B10. Unconfined compression results for various compaction energies at approximately 11.0% moisture content (weathered shale)

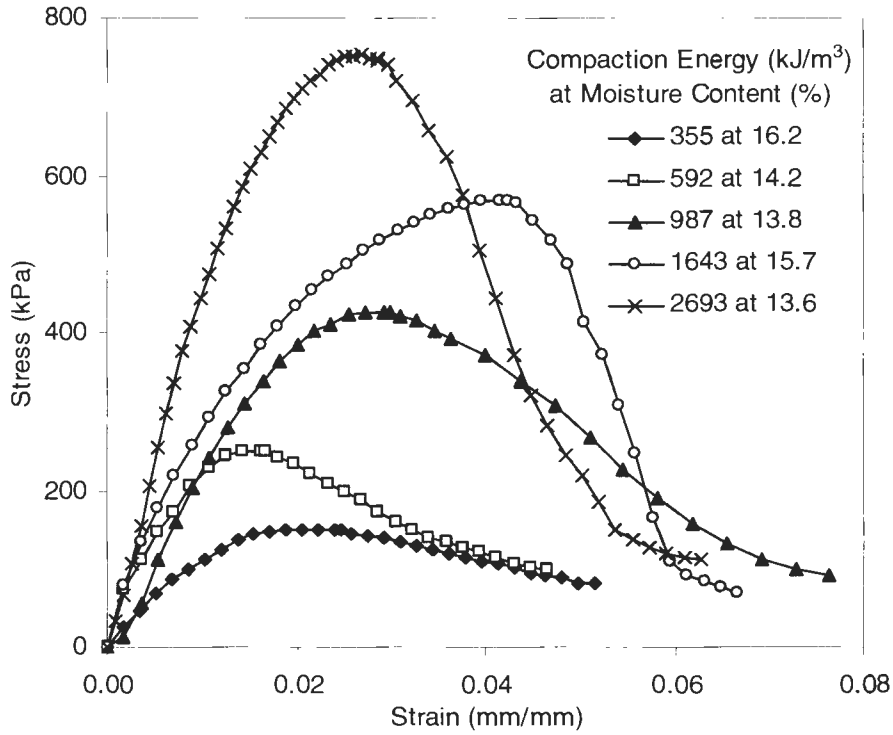

Figure B11. Unconfined compression results for various compaction energies at approximately 14.5% moisture content (weathered shale)

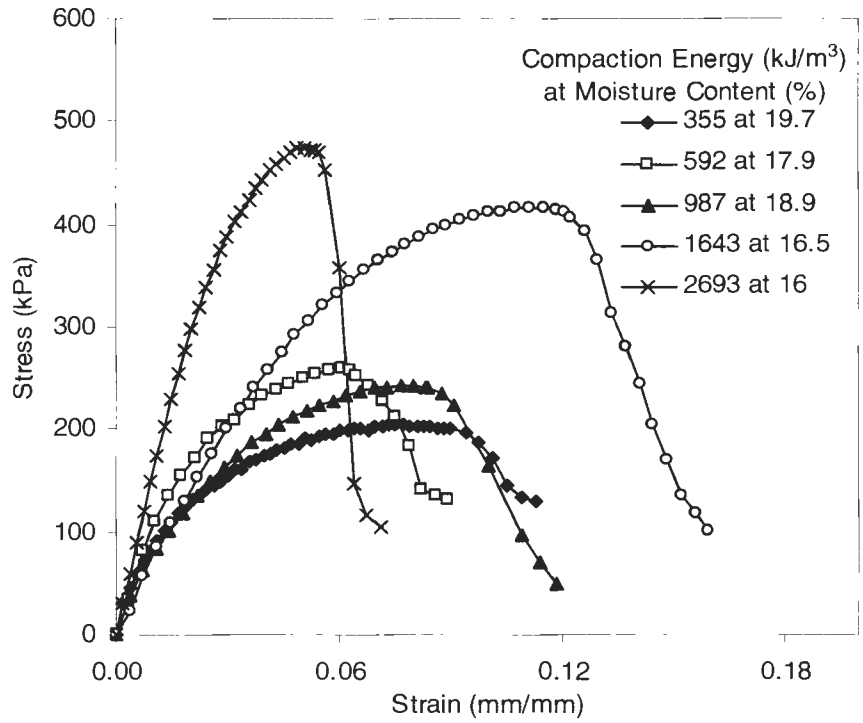

Figure B12. Unconfined compression results for various compaction energies at approximately 17.5% moisture content (weathered shale)

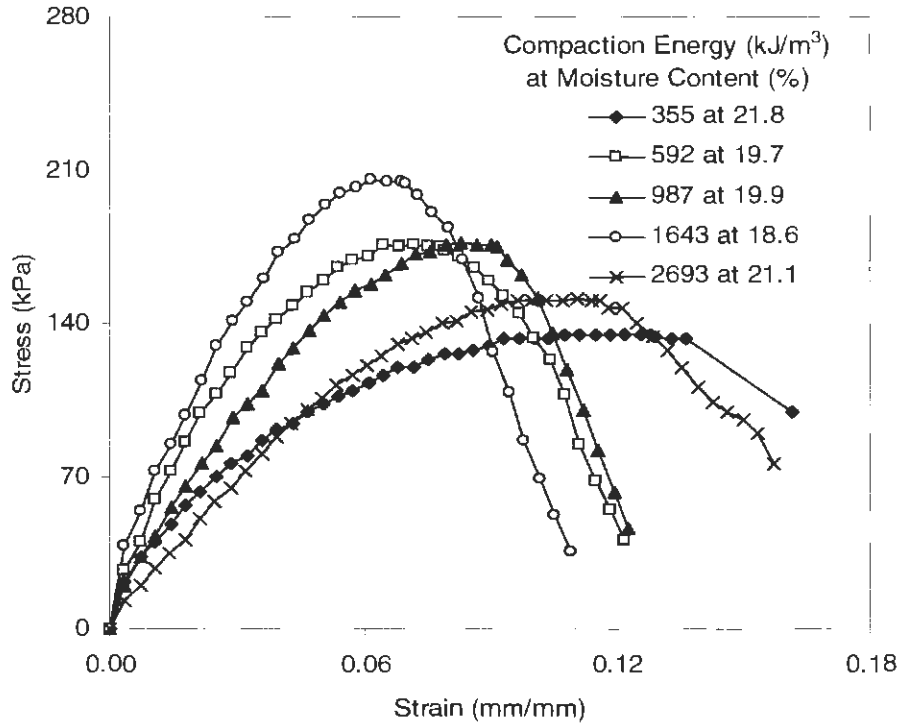

Figure B13. Unconfined compression results for various compaction energies at approximately 20.5% moisture content (weathered shale)

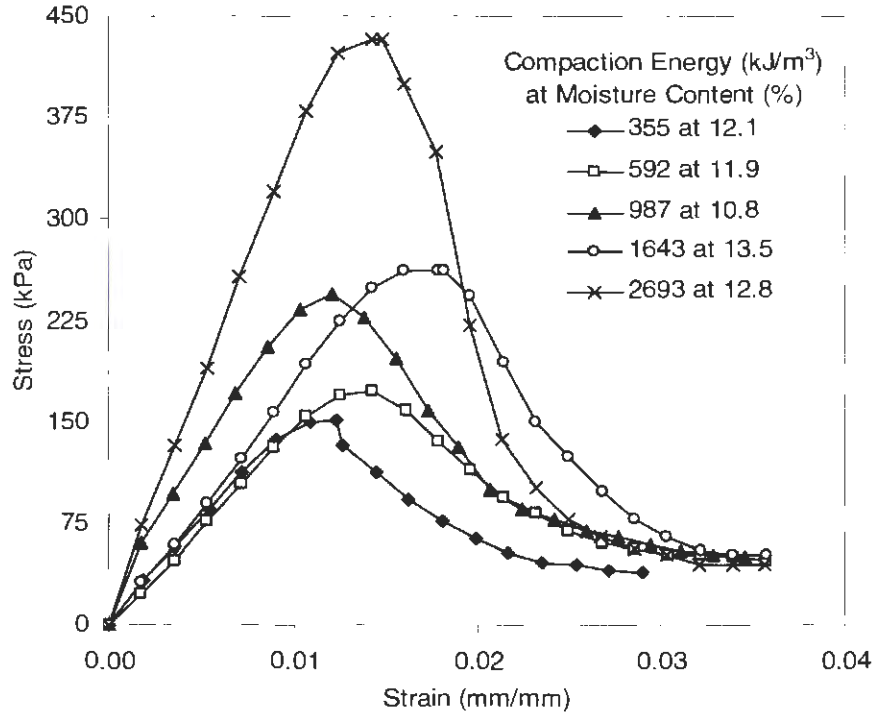

Figure B14. Unconfined compression results for various compaction energies at approximately 12.5% moisture content (Western Iowa loess)

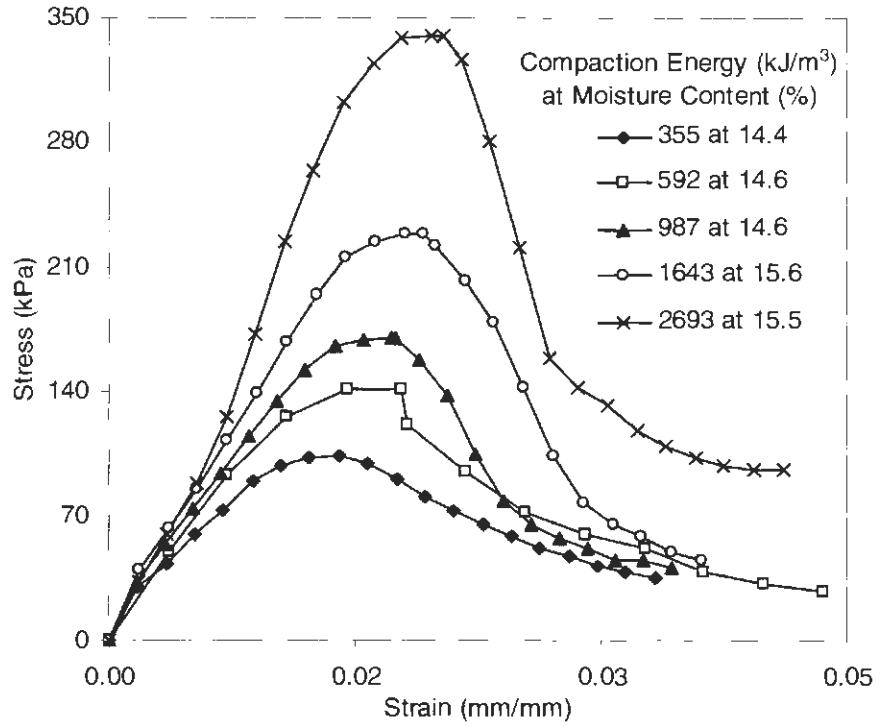

Figure B15. Unconfined compression results for various compaction energies at approximately 15.0% moisture content (Western Iowa loess)

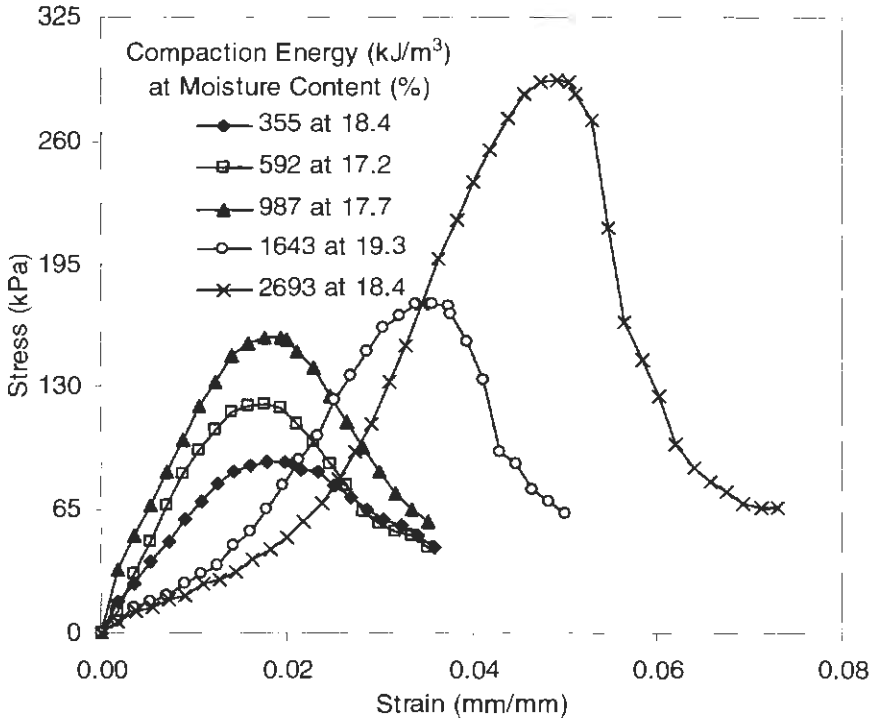

Figure B16. Unconfined compression results for various compaction energies at approximately 18.0% moisture content (Western Iowa loess)

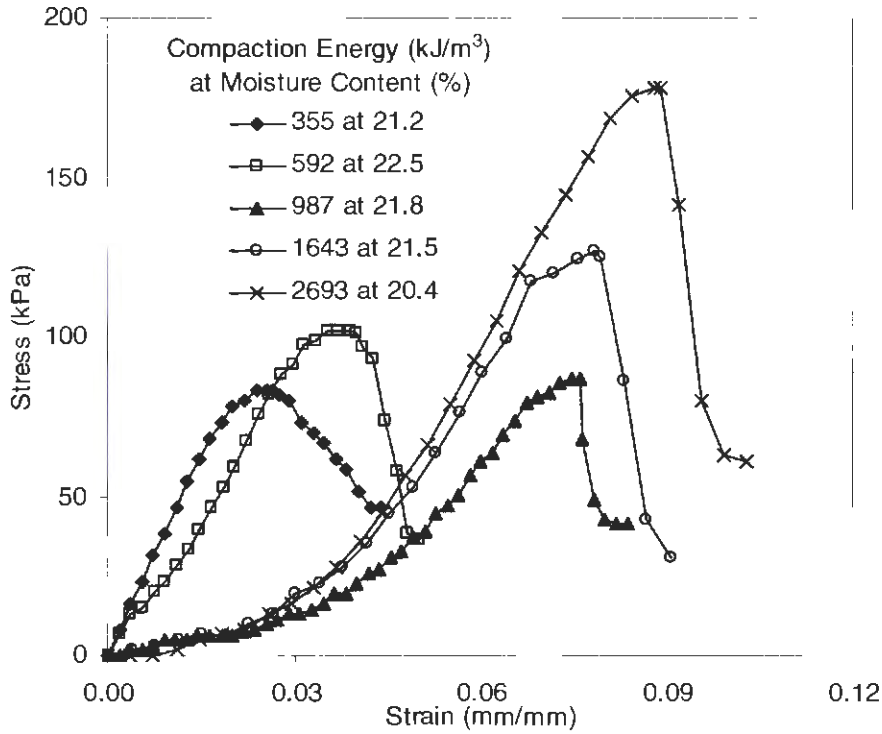

Figure B17. Unconfined compression results for various compaction energies at approximately 21.5% moisture content (Western Iowa loess)

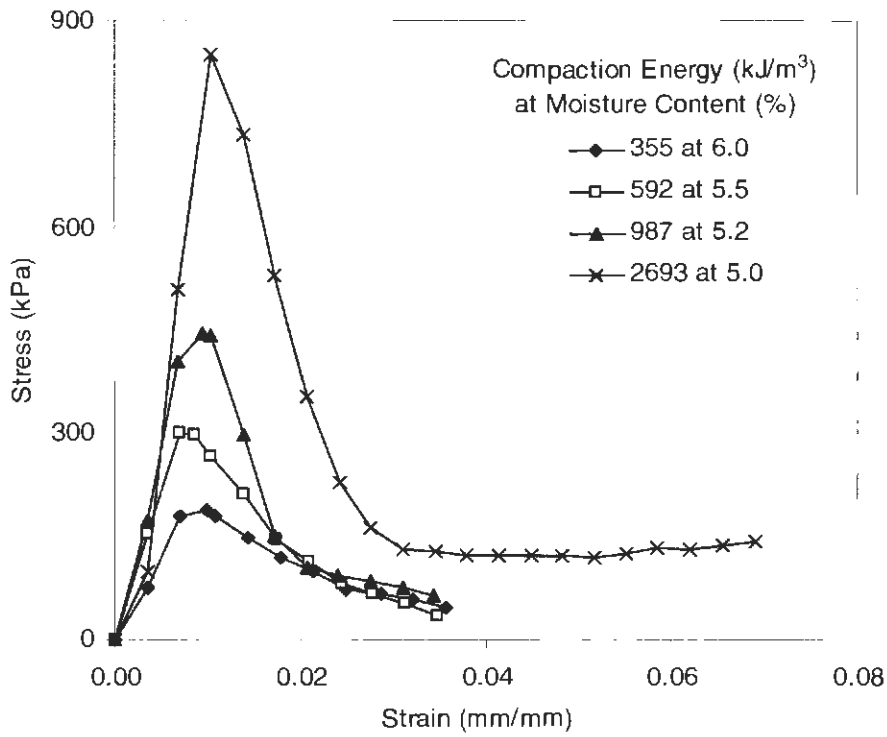

Figure B18. Unconfined compression results for various compaction energies at approximately 5.0% moisture content (PPG till)

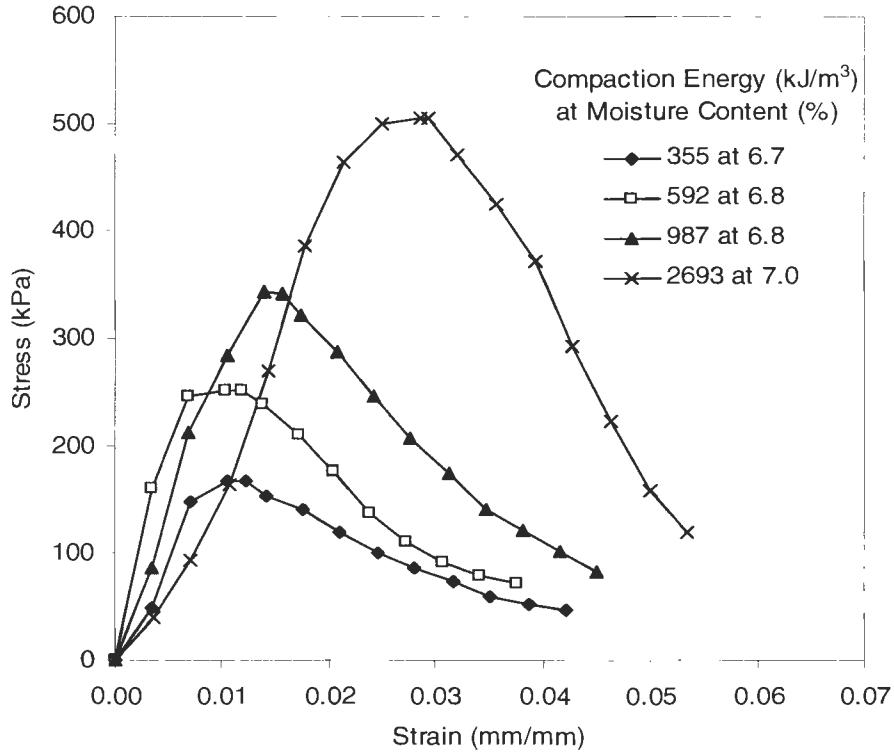

Figure B19. Unconfined compression results for various compaction energies at approximately 7.0% moisture content (PPG till)

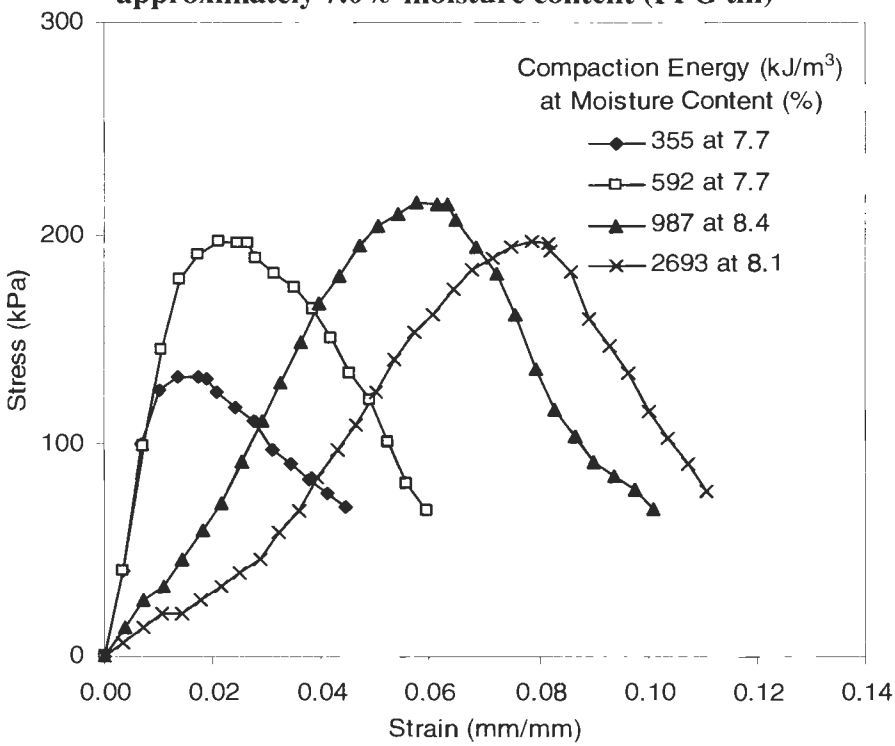

Figure B20. Unconfined compression results for various compaction energies at approximately 8.0% moisture content (PPG till)

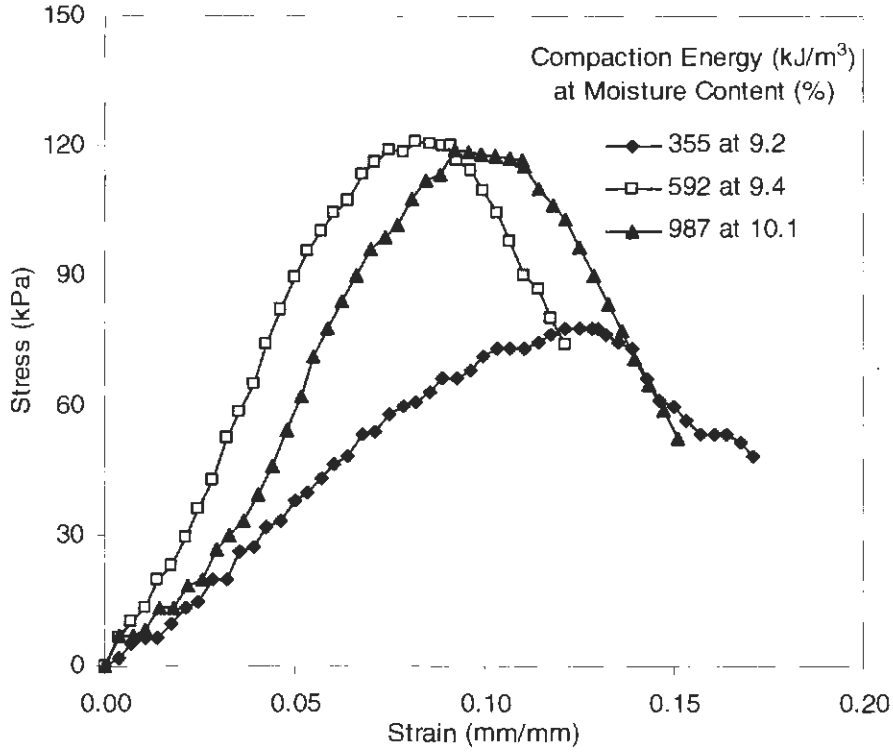

Figure B21. Unconfined compression results for various compaction energies at approximately 10.0% moisture content (PPG till)

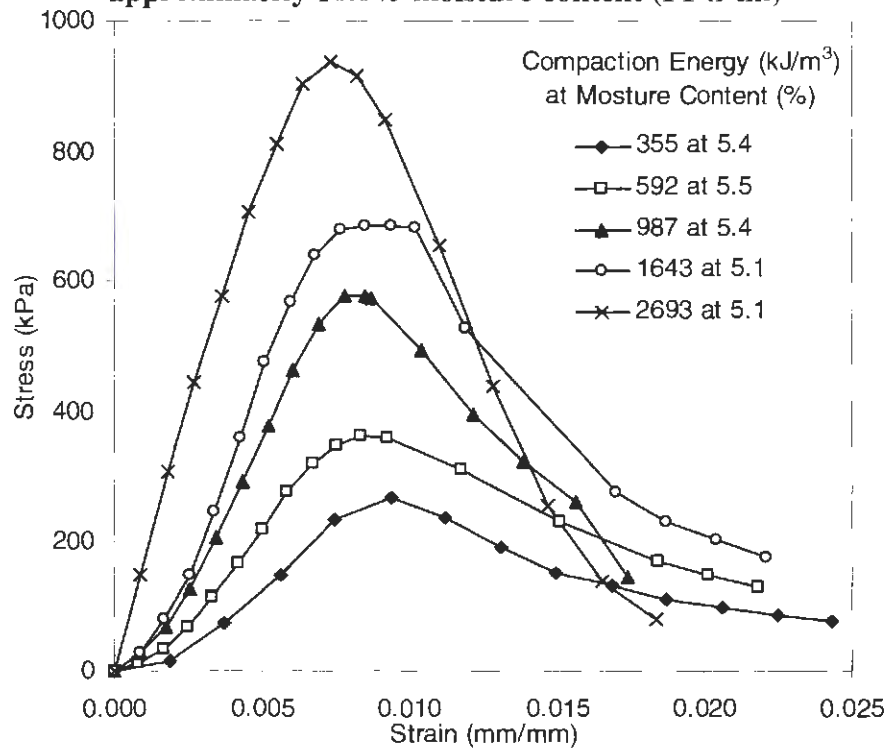

Figure B22. Unconfined compression results for various compaction energies at approximately 5.0% moisture content (Edwards till)

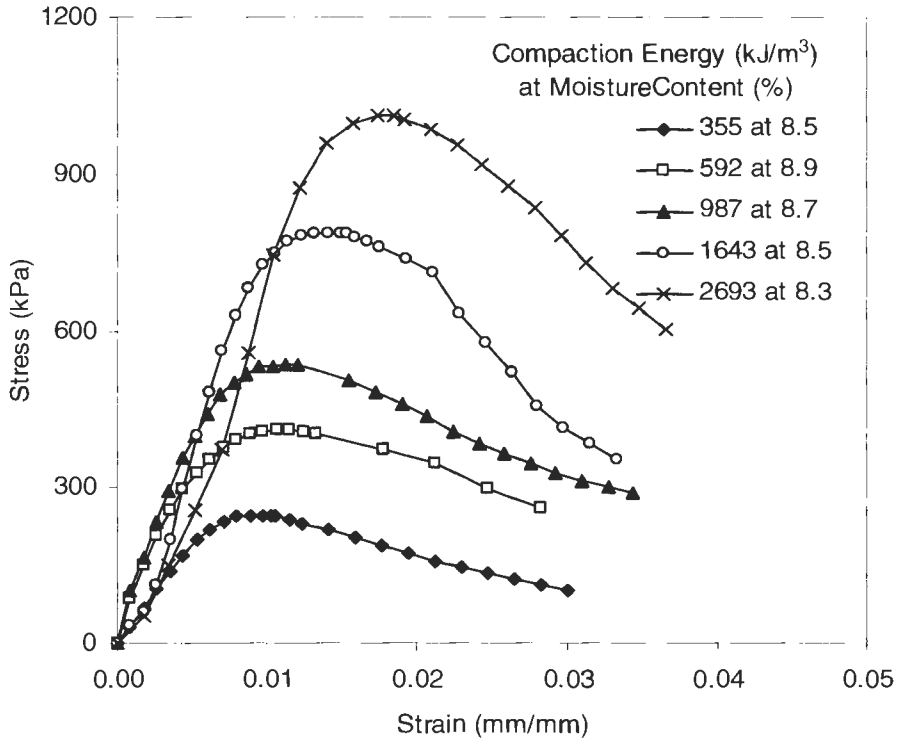

Figure B23. Unconfined compression results for various compaction energies at approximately 8.5% moisture content (Edwards till)

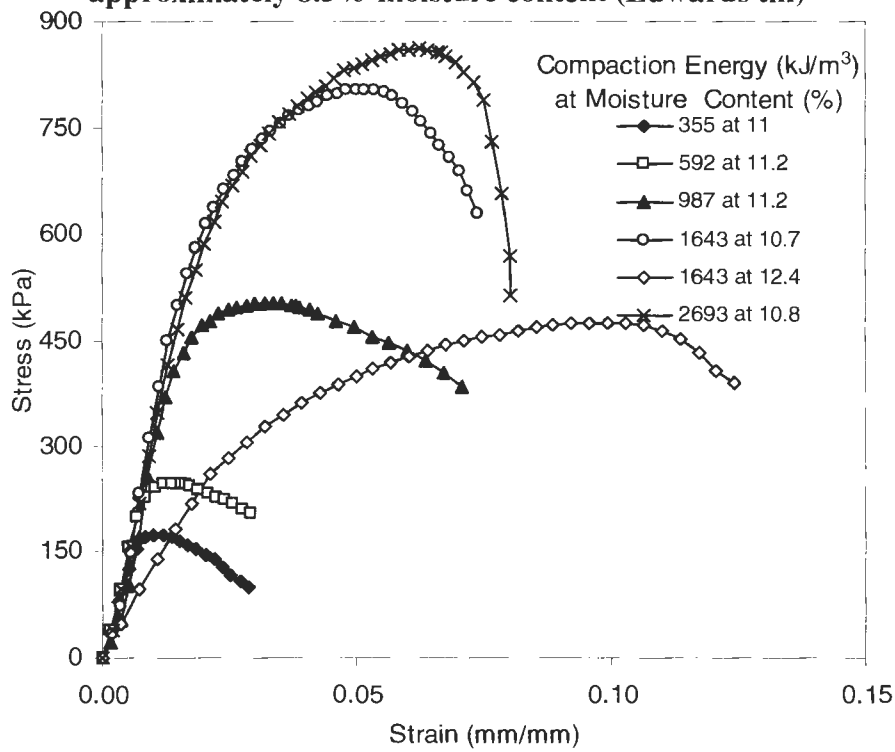

Figure B24. Unconfined compression results for various compaction energies at approximately 11.0% moisture content (Edwards till)

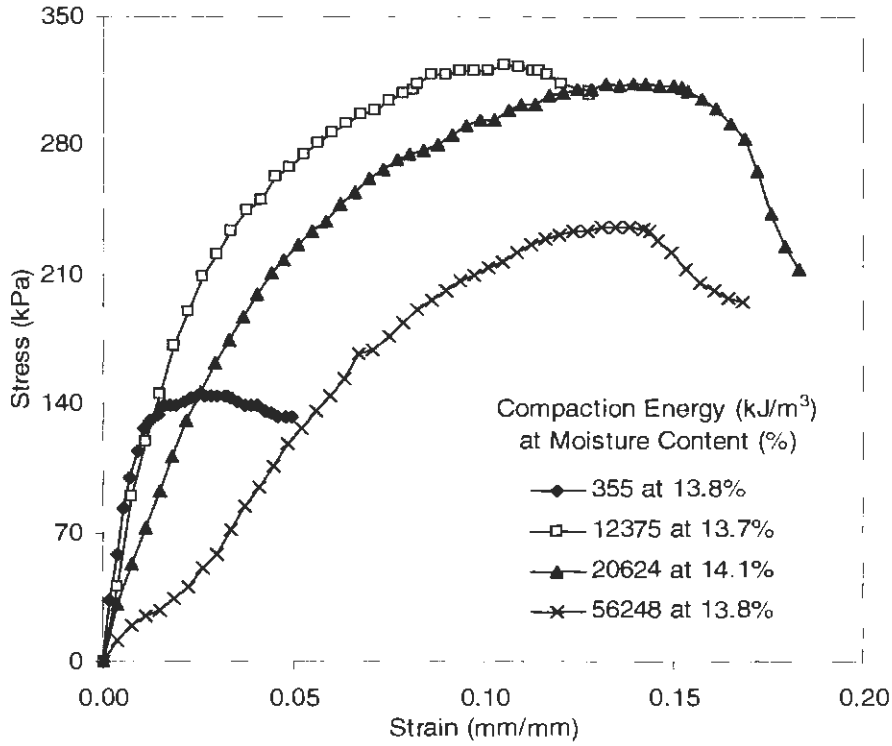

Figure B25. Unconfined compression results for various compaction energies at approximately 14.0% moisture content (Edwards till)

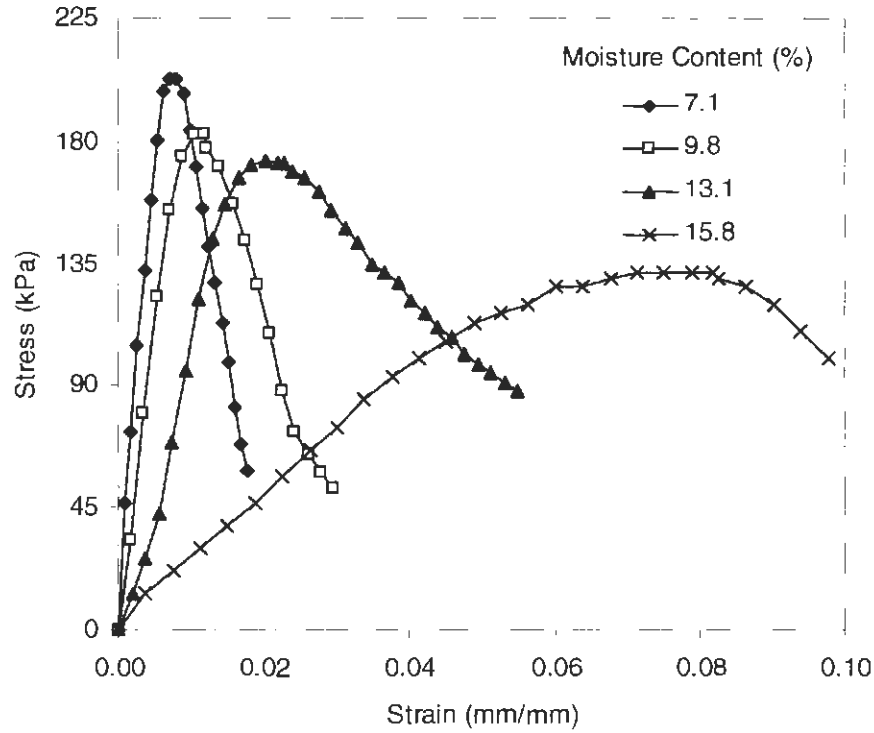

Figure B26. Unconfined compression results delivered with a compaction energy of 355 kJ/m^3 at various moisture contents (Central Iowa till)

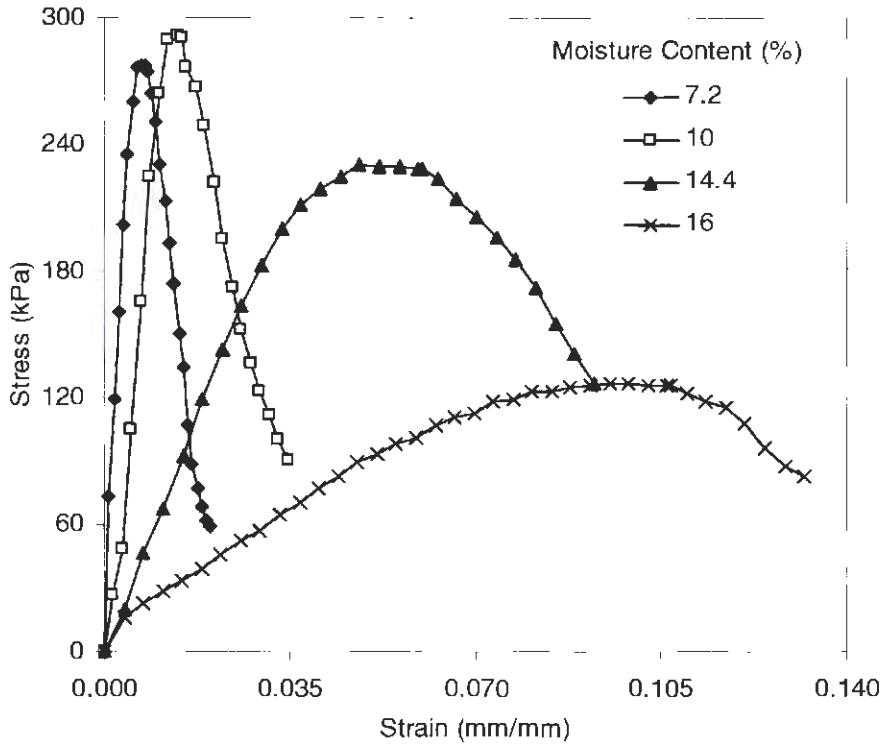

Figure B27. Unconfined compression results delivered with a compaction energy of 592 kJ/m^3 at various moisture contents (Central Iowa till)

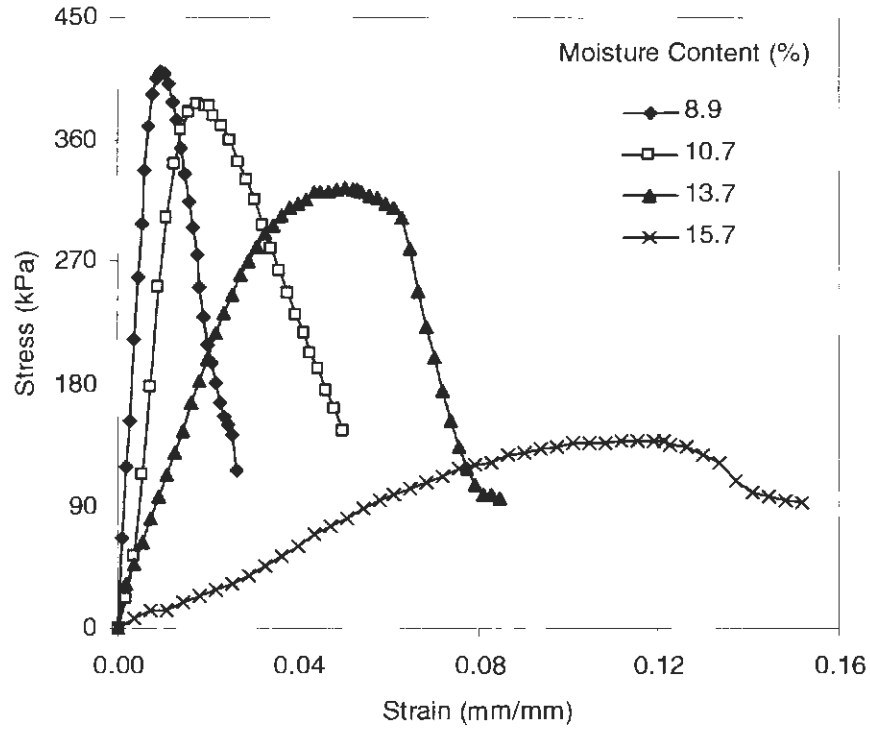

Figure B28. Unconfined compression results delivered with a compaction energy of 987 kJ/m^3 at various moisture contents (Central Iowa till)

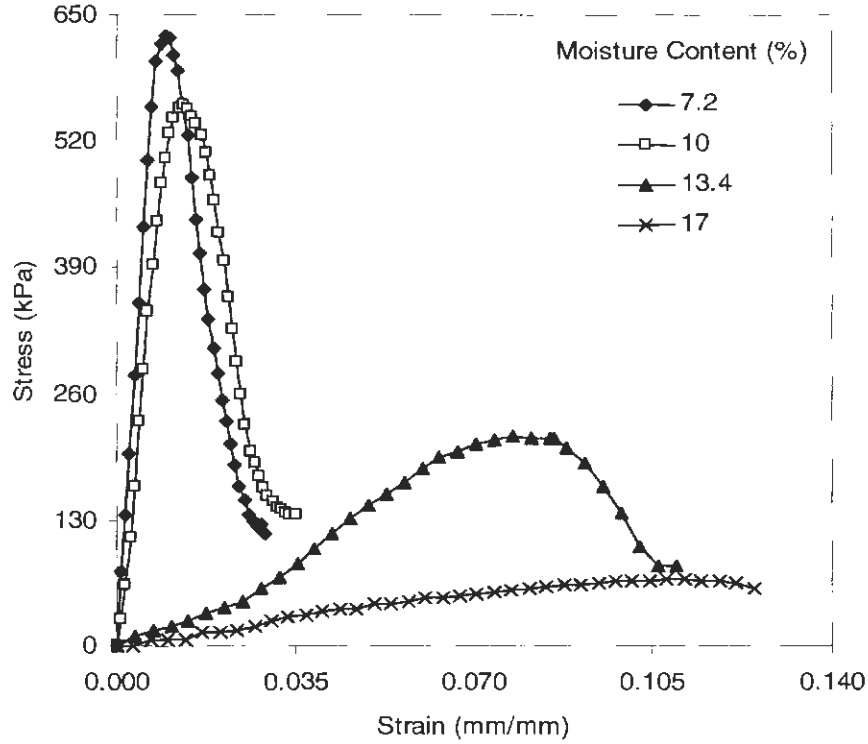

Figure B29. Unconfined compression results delivered with a compaction energy of 1643 kJ/m^3 at various moisture contents (Central Iowa till)

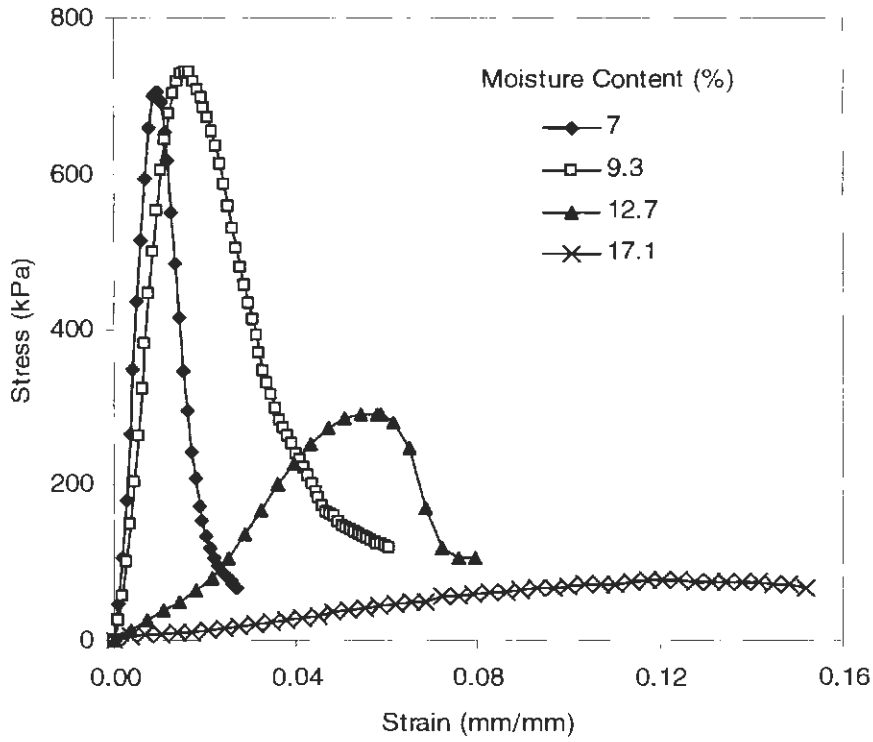

Figure B30. Unconfined compression results delivered with a compaction energy of 2693 kJ/m^3 at various moisture contents (Central Iowa till)

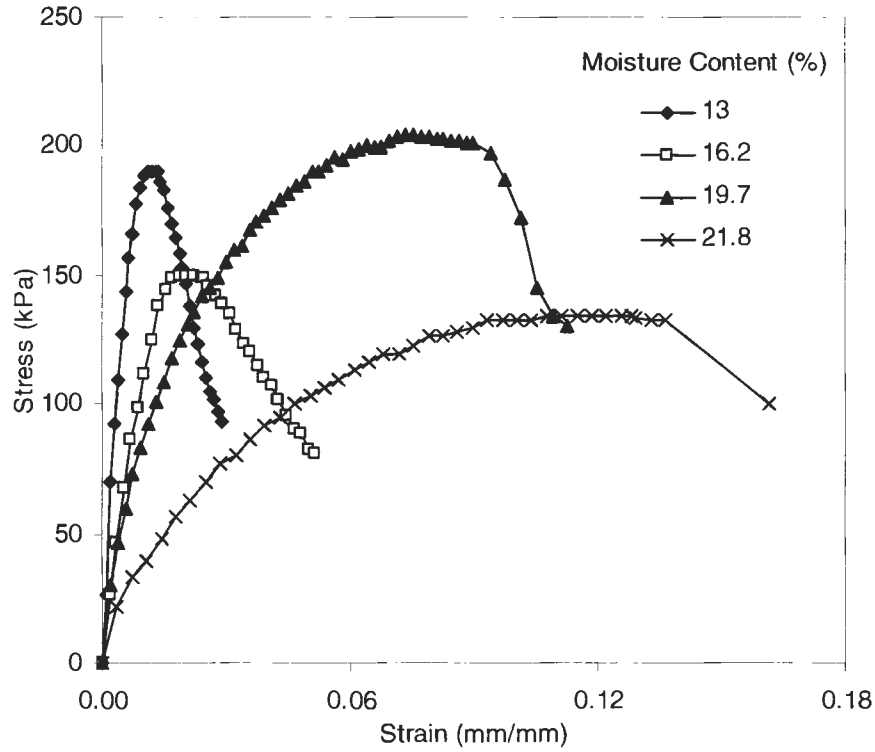

Figure B31. Unconfined compression results delivered with a compaction energy of 355 kJ/m^3 at various moisture contents (weathered shale)

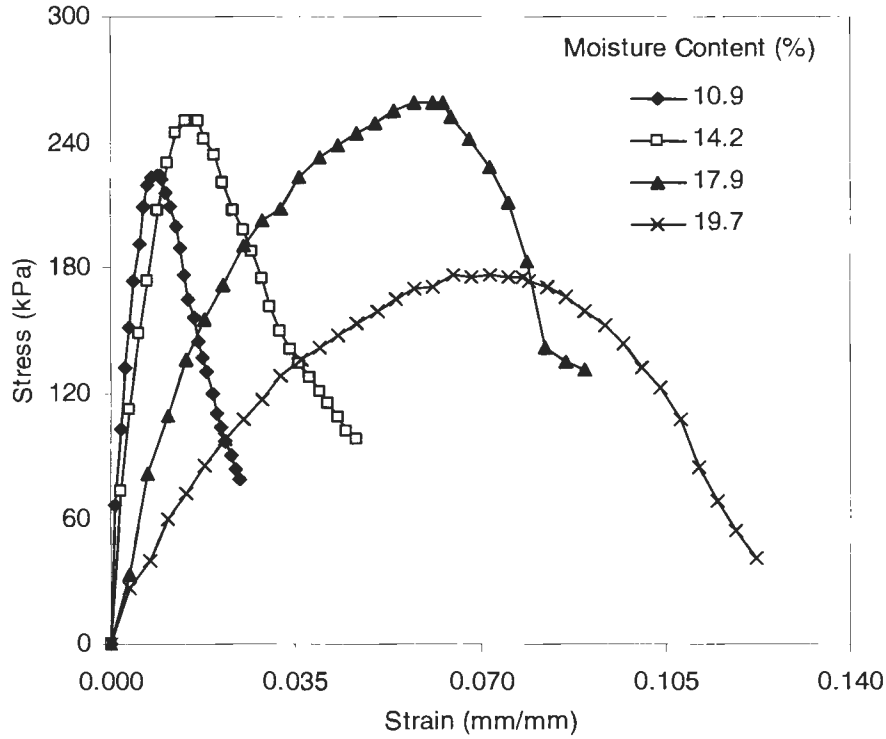

Figure B32. Unconfined compression results delivered with a compaction energy of 592 kJ/m^3 at various moisture contents (weathered shale)

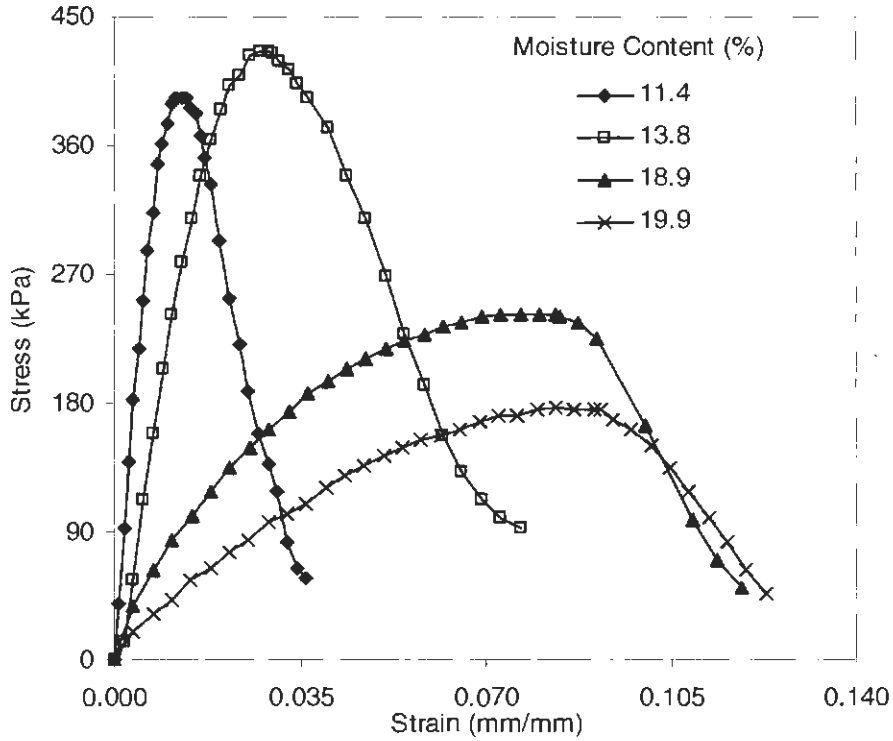

Figure B33. Unconfined compression results delivered with a compaction energy of 987 kJ/m^3 at various moisture contents (weathered shale)

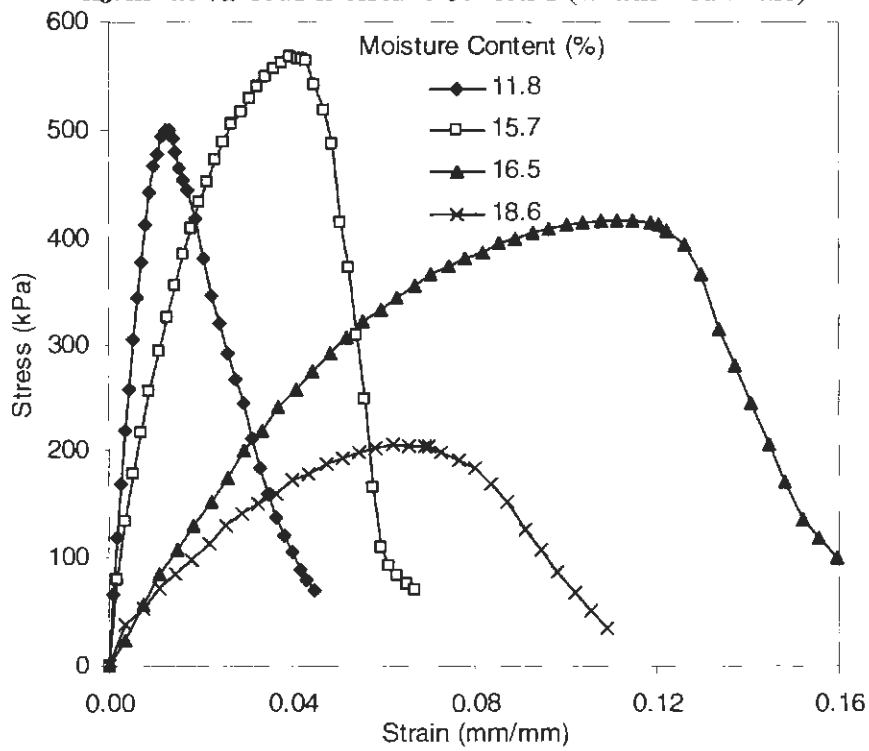

Figure B34. Unconfined compression results delivered with a compaction energy of 1643 kJ/m^3 at various moisture contents (weathered shale)

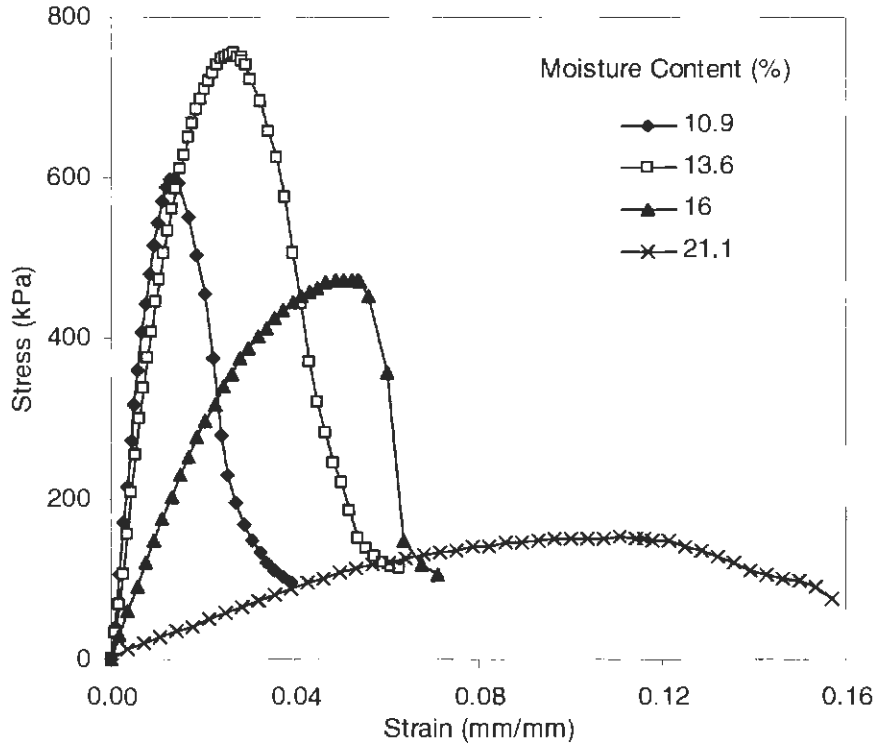

Figure B35. Unconfined compression results delivered with a compaction energy of 2693 kJ/m^3 at various moisture contents (weathered shale)

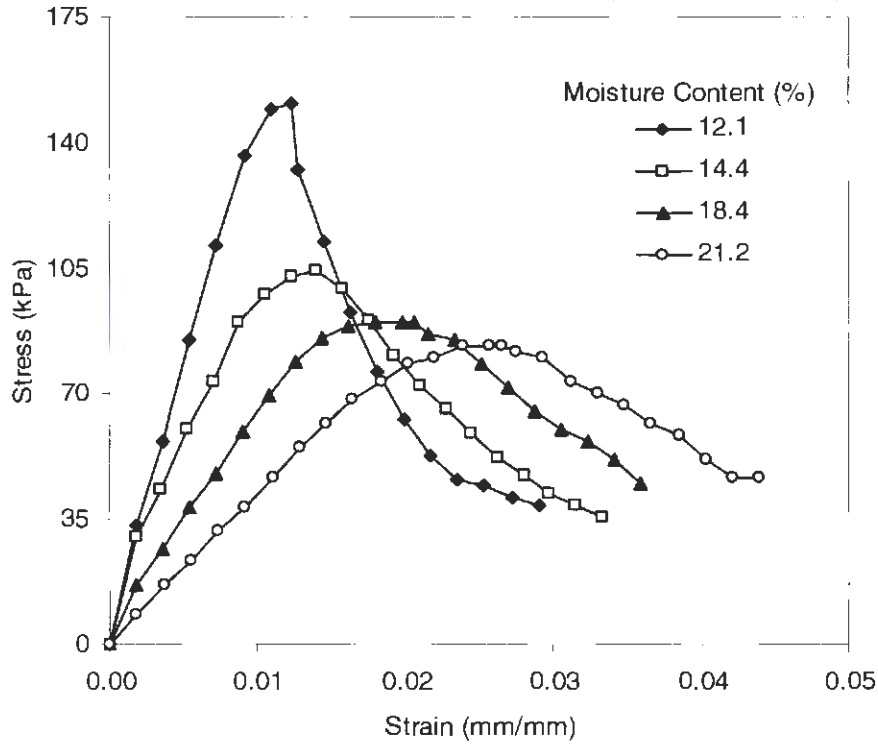

Figure B36. Unconfined compression results delivered with a compaction energy of 355 kJ/m^3 at various moisture contents (Western Iowa loess)

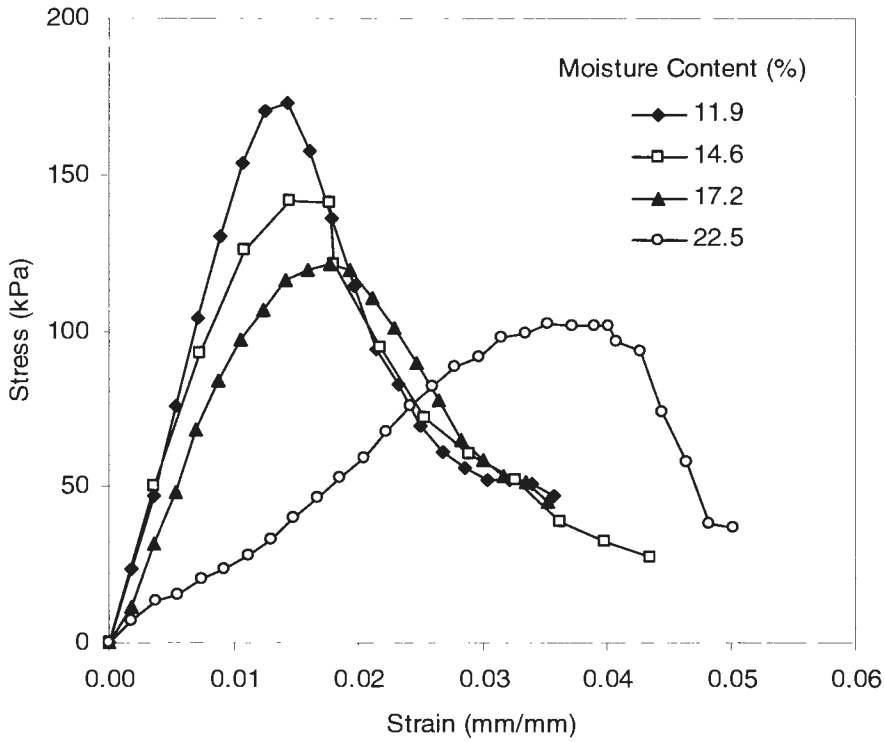

Figure B37. Unconfined compression results delivered with a compaction energy of 592 kJ/m^3 at various moisture contents (Western Iowa loess)

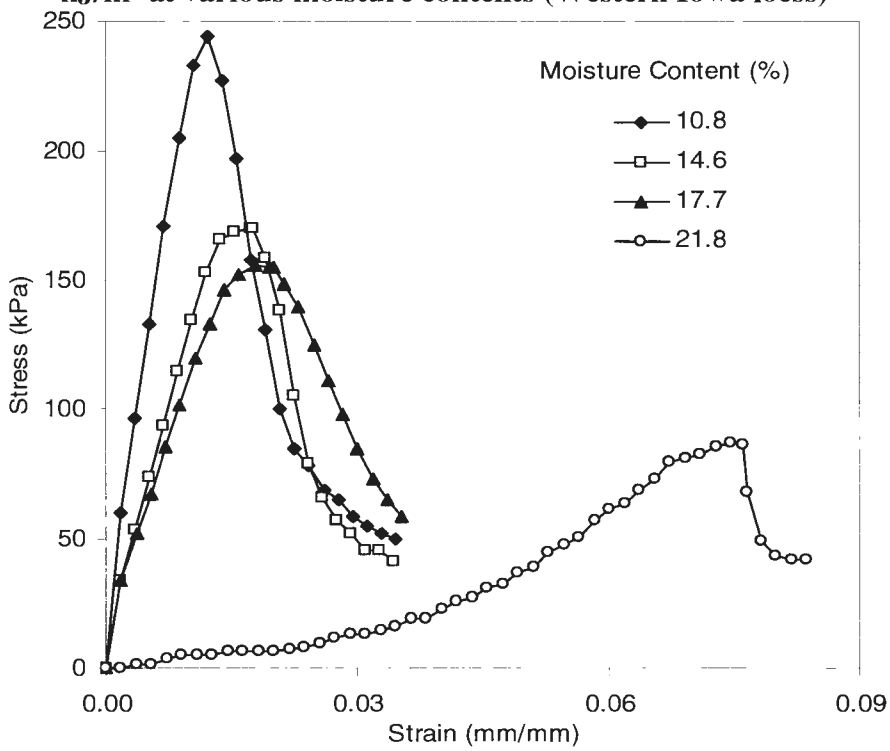

Figure B38. Unconfined compression results delivered with a compaction energy of 987 kJ/m^3 at various moisture contents (Western Iowa loess)

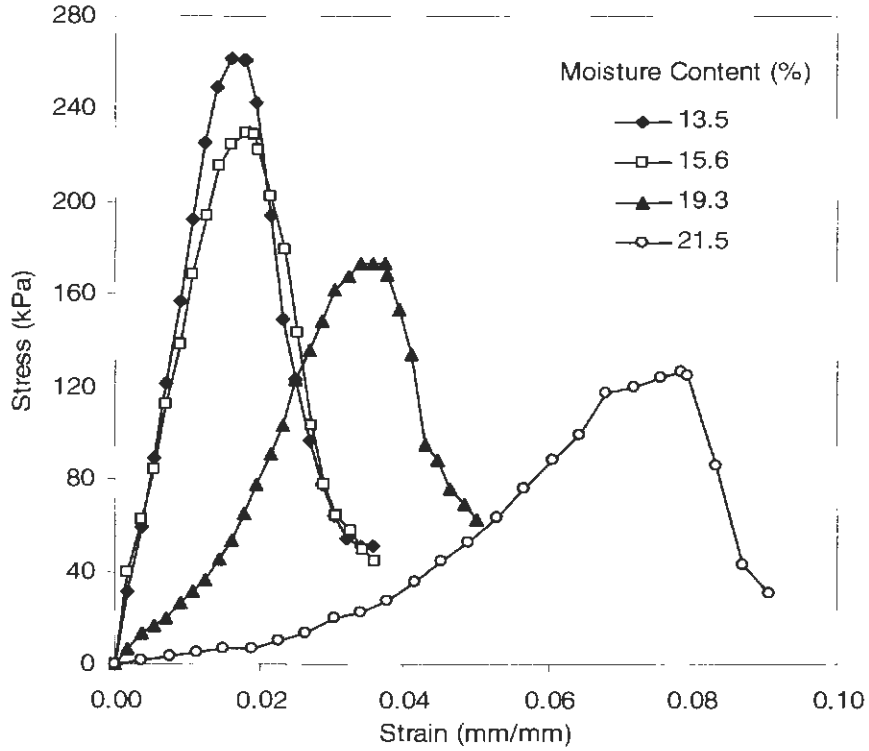

Figure B39. Unconfined compression results delivered with a compaction energy of 1643 kJ/m^3 at various moisture contents (Western Iowa loess)

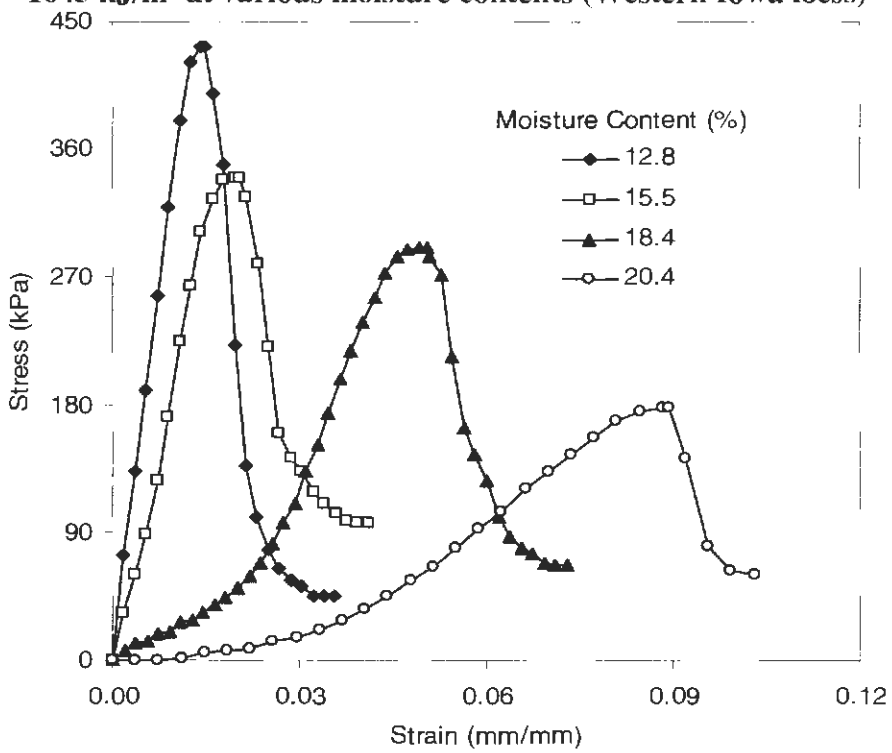

Figure B40. Unconfined compression results delivered with a compaction energy of 2693 kJ/m^3 at various moisture contents (Western Iowa loess)

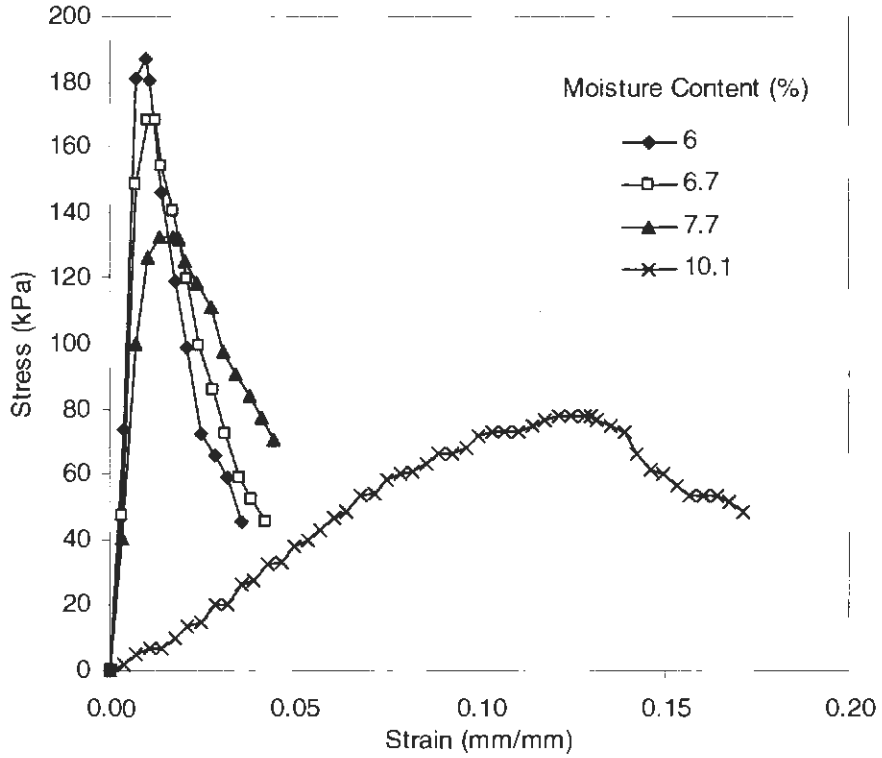

Figure B41. Unconfined compression results delivered with a compaction energy of 355 kJ/m^3 at various moisture contents (PPG till)

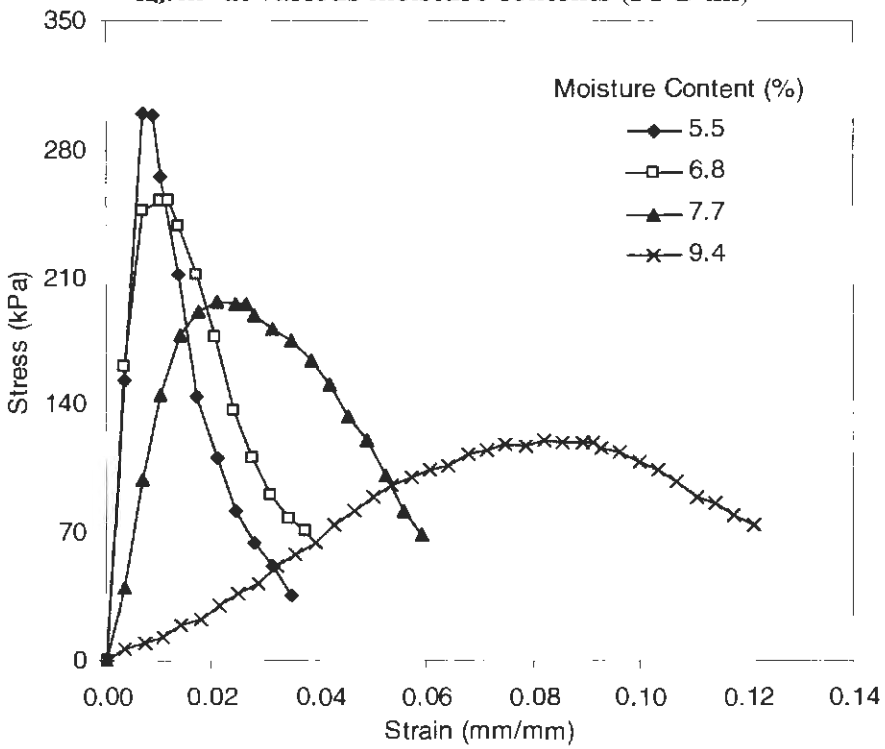

Figure B42. Unconfined compression results delivered with a compaction energy of 592 kJ/m^3 at various moisture contents (PPG till)

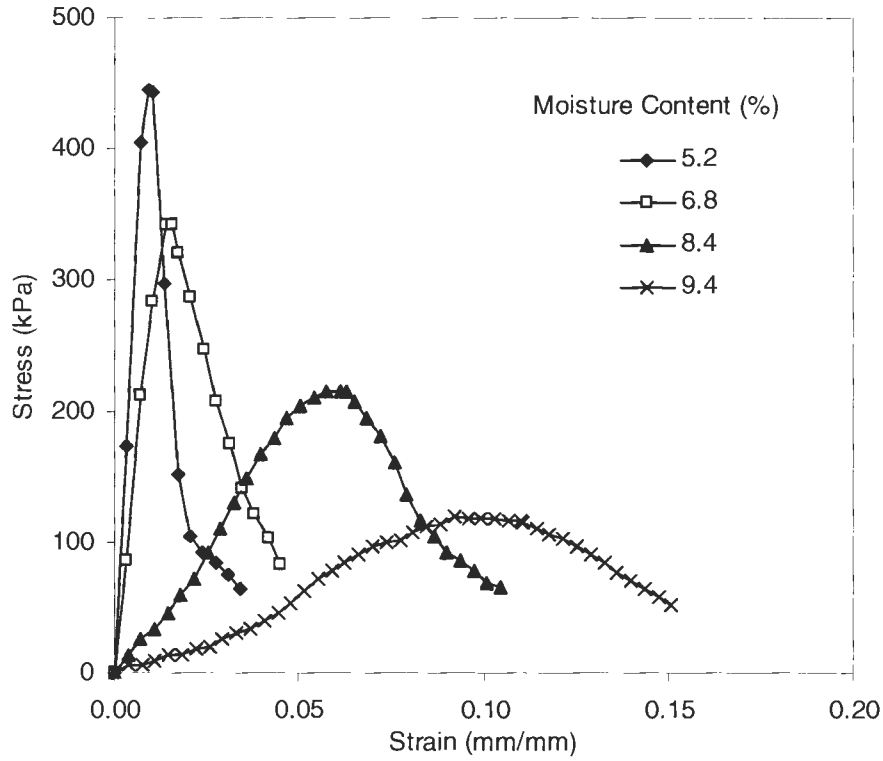

Figure B43. Unconfined compression results delivered with a compaction energy of 987 kJ/m^3 at various moisture contents (PPG till)

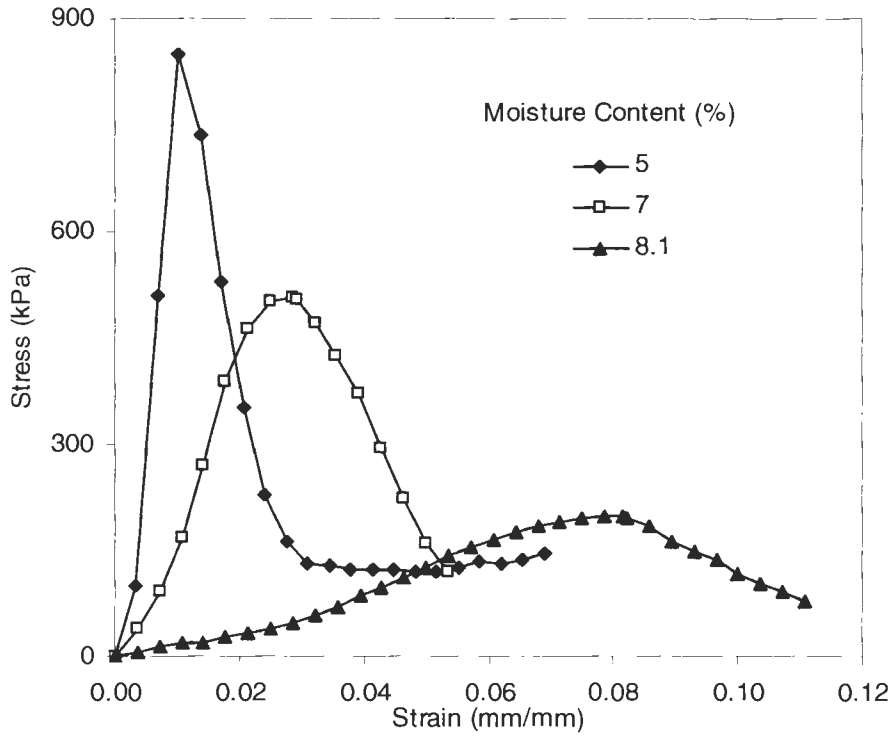

Figure B44. Unconfined compression results delivered with a compaction energy of 2693 kJ/m^3 at various moisture contents (PPG till)

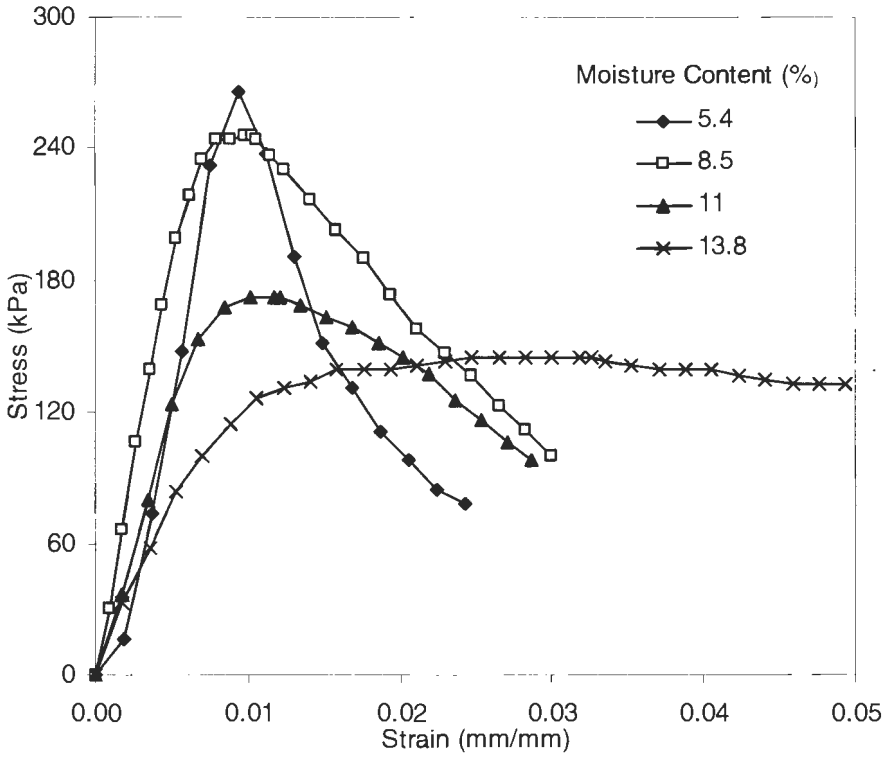

Figure B45. Unconfined compression results delivered with a compaction energy of 355 kJ/m^3 at various moisture contents (Edwards till)

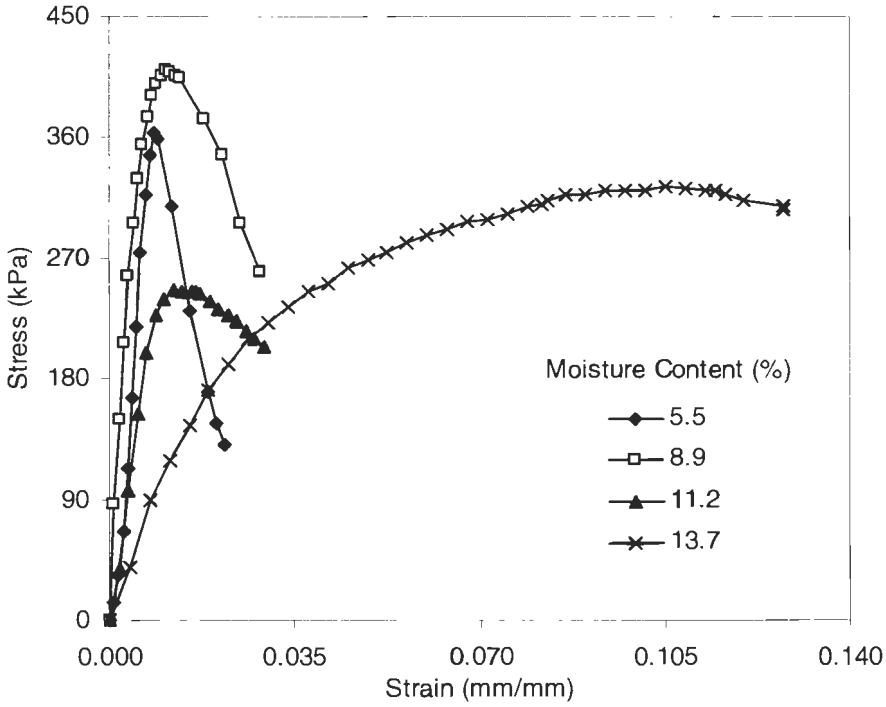

Figure B46. Unconfined compression results delivered with a compaction energy of 592 kJ/m^3 at various moisture contents (Edwards till)

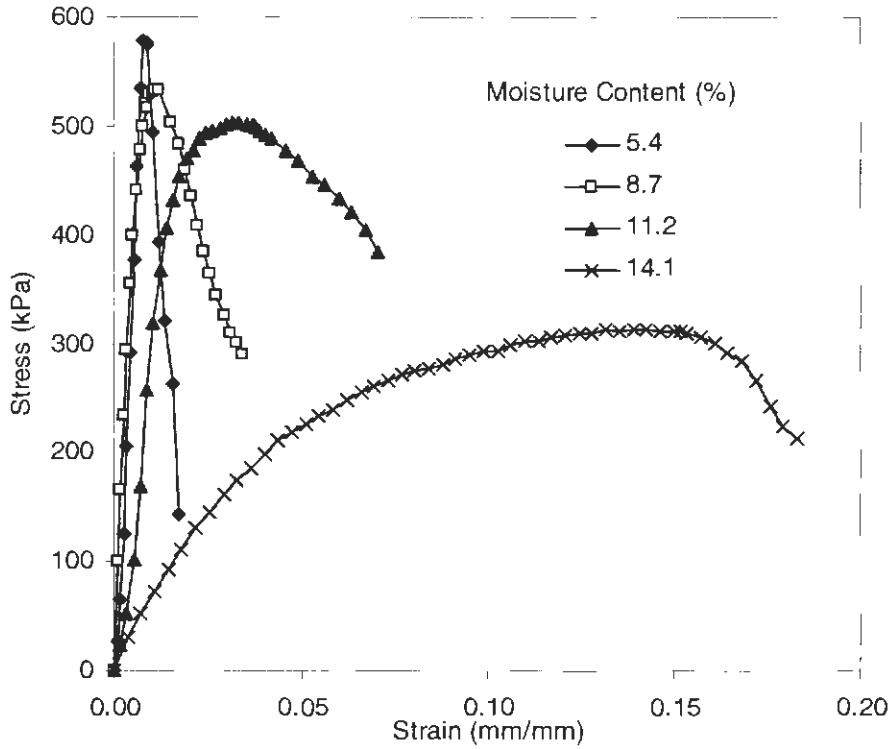

Figure B47. Unconfined compression results delivered with a compaction energy of 987 kJ/m^3 at various moisture contents (Edwards till)

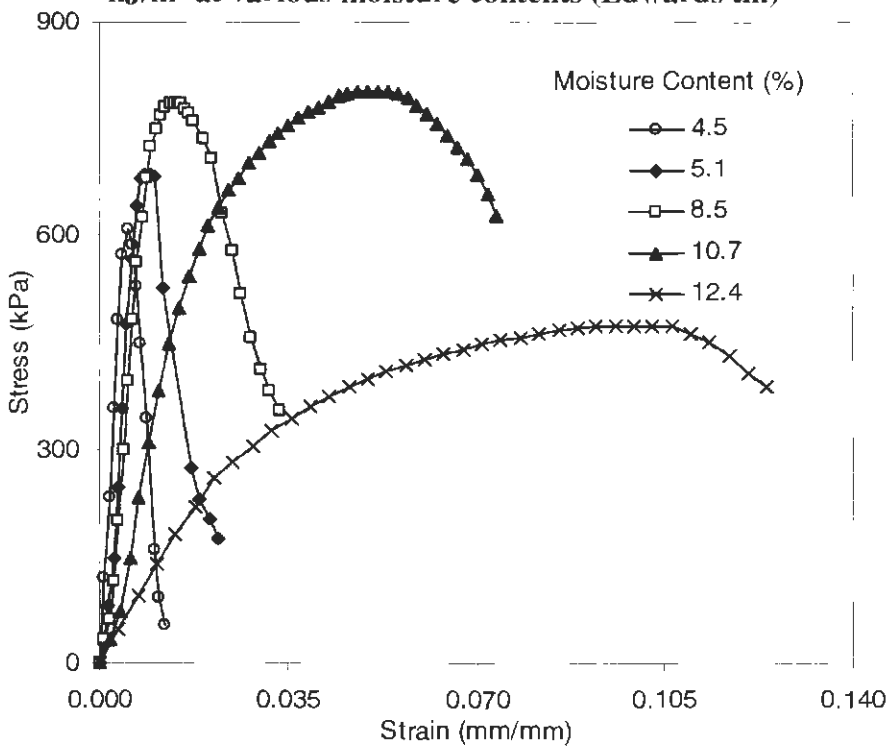

Figure B48. Unconfined compression results delivered with a compaction energy of 1643 kJ/m^3 at various moisture contents (Edwards till)

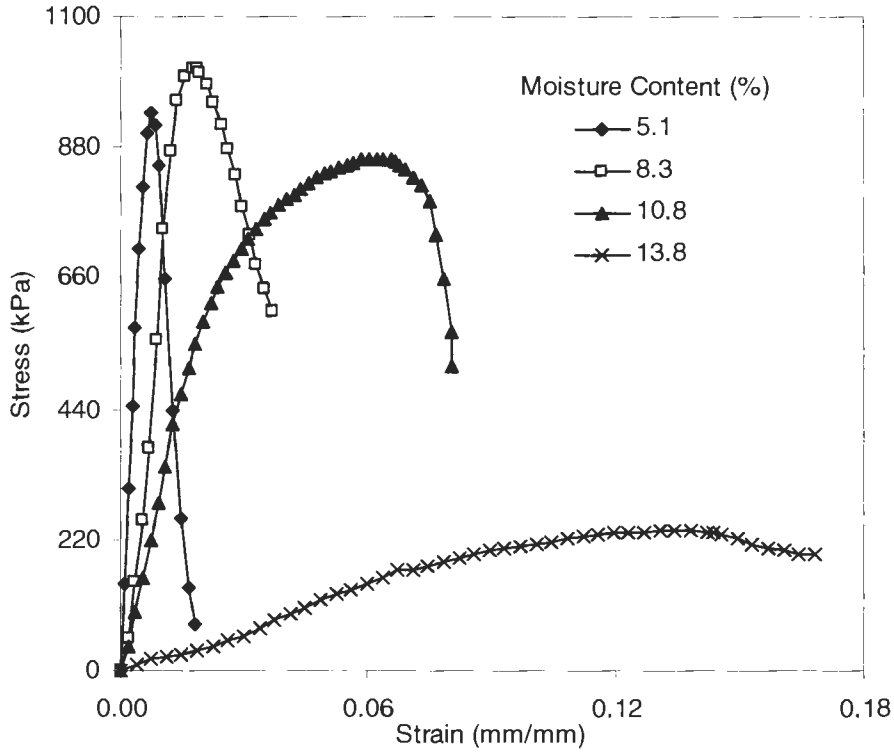

Figure B49. Unconfined compression results delivered with a compaction energy of 2693 kJ/m^3 at various moisture contents (Edwards till)

APPENDIX C. LABORATORY REGRESSION FIGURES

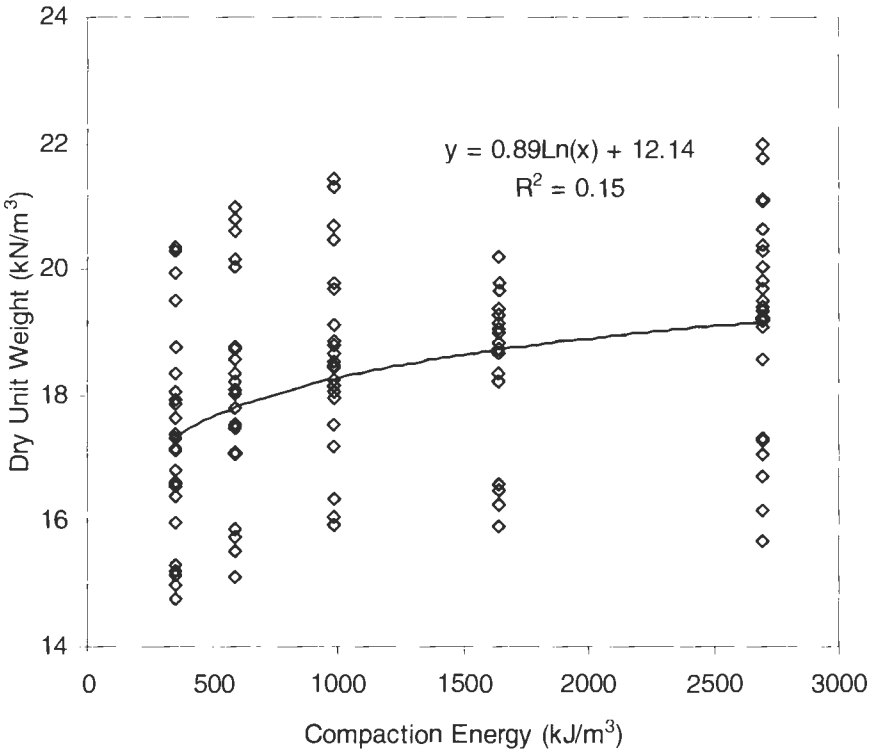

Figure C1. Regression for dry unit weight with compaction energy for all compaction tests

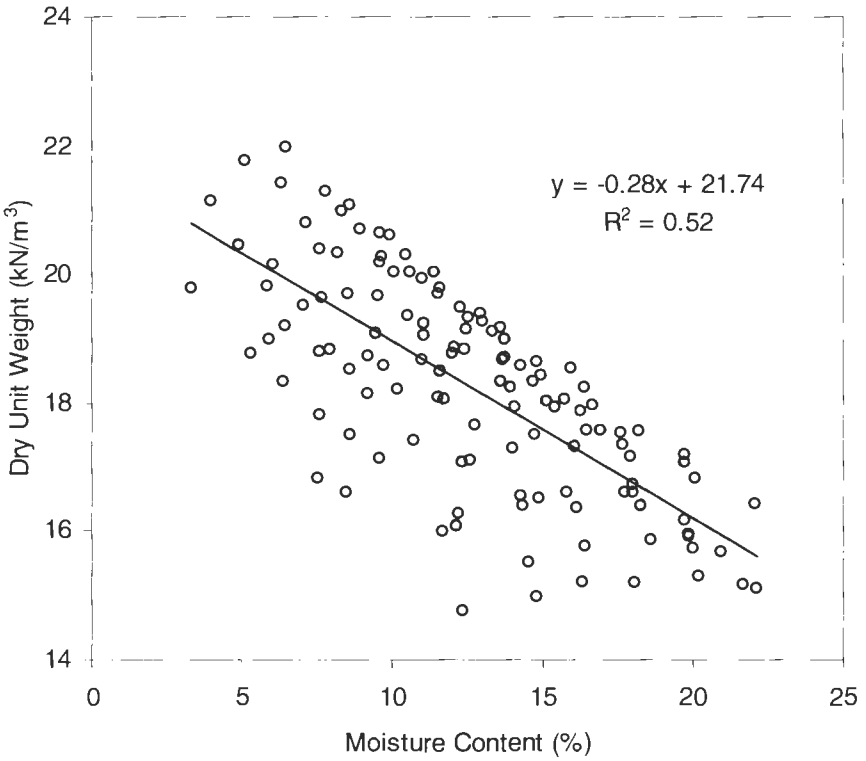

Figure C2. Regression for dry unit weight with moisture content for all compaction tests

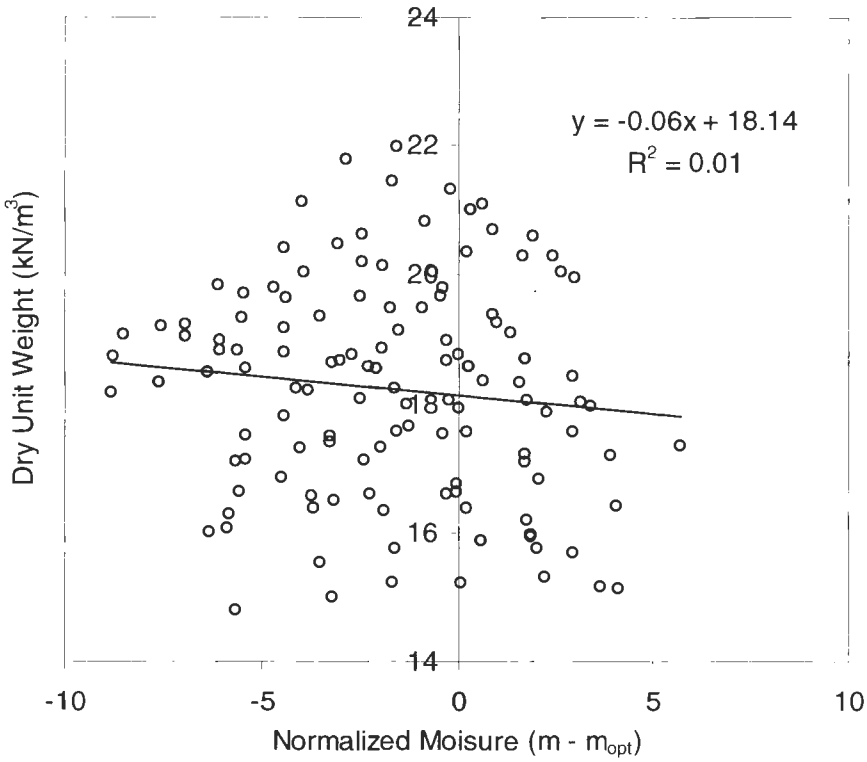

Figure C3. Regression for dry unit weight with normalized moisture content for all compaction tests

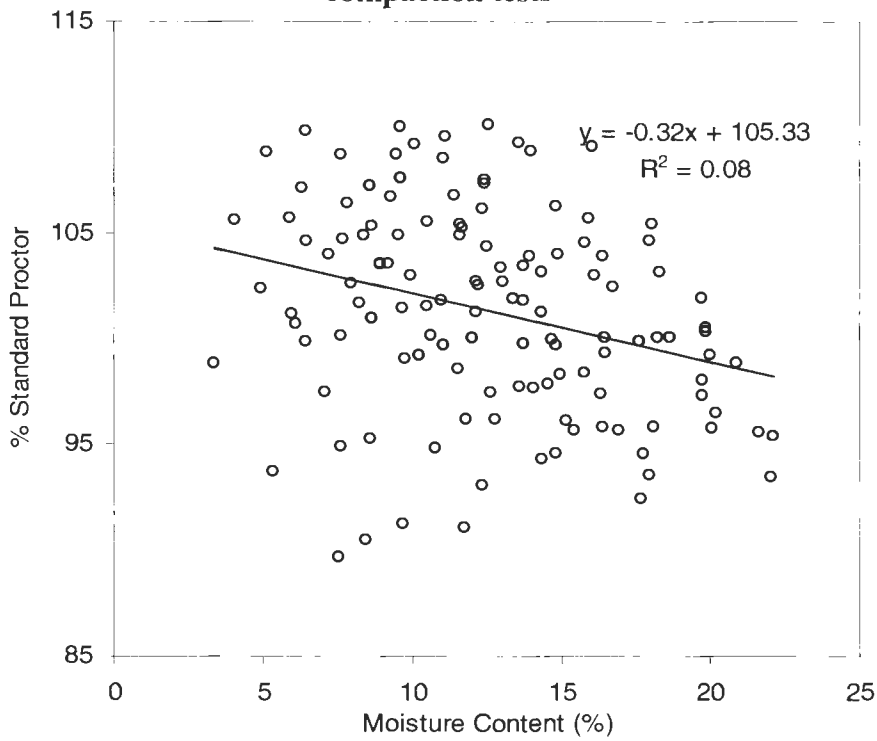

Figure C4. Regression for relative compaction with moisture content for all compaction tests

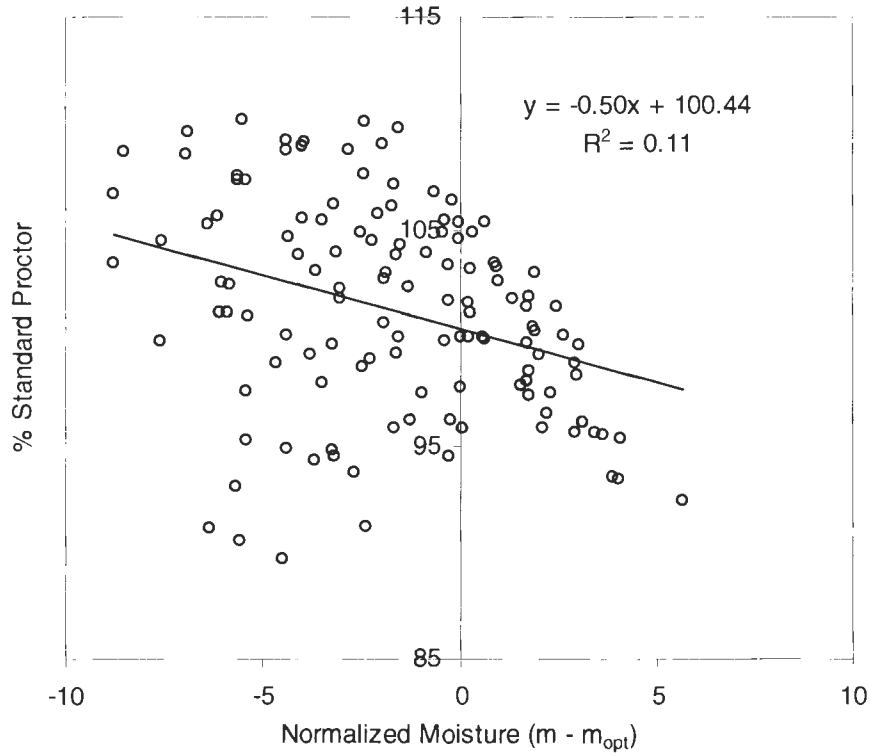

Figure C5. Regression for relative compaction with normalized moisture content for all compaction tests

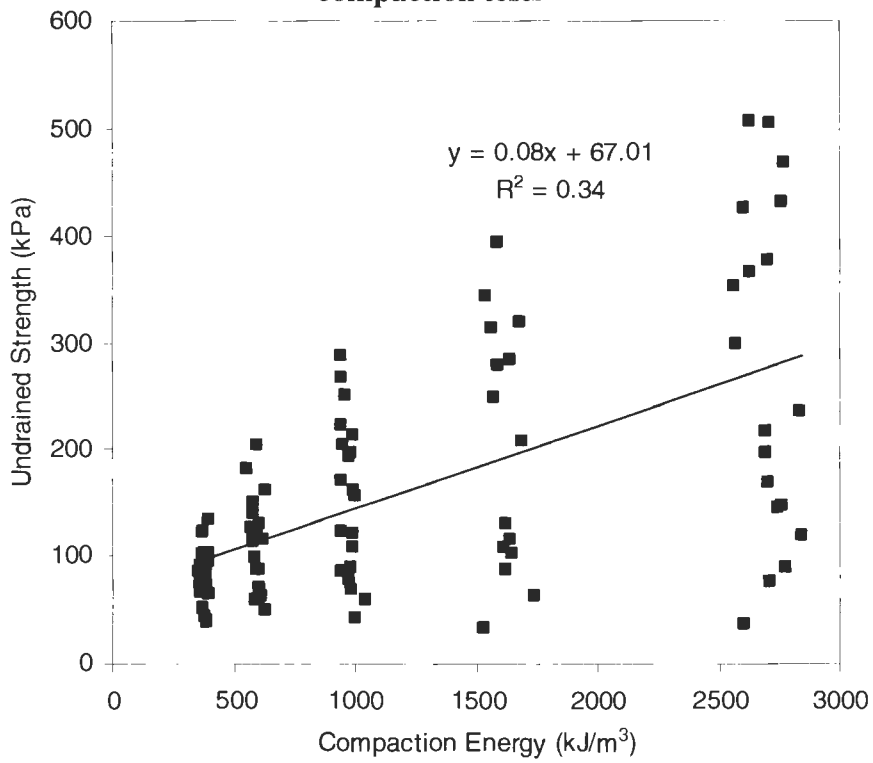

Figure C6. Regression for undrained shear strength with compaction energy for all unconfined tests

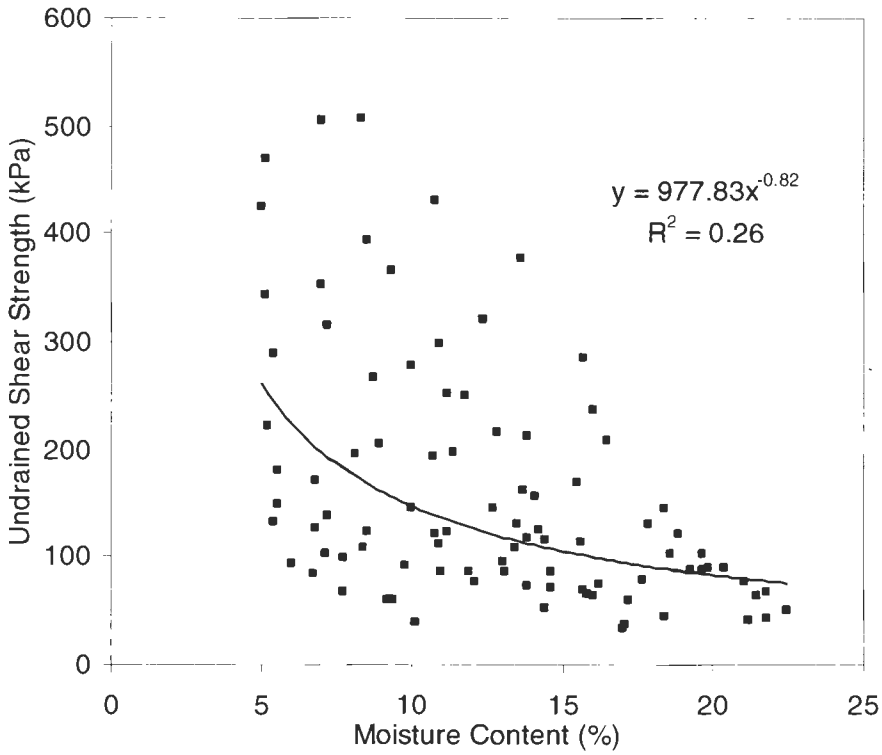

Figure C7. Regression for undrained shear strength with moisture content for all unconfined tests

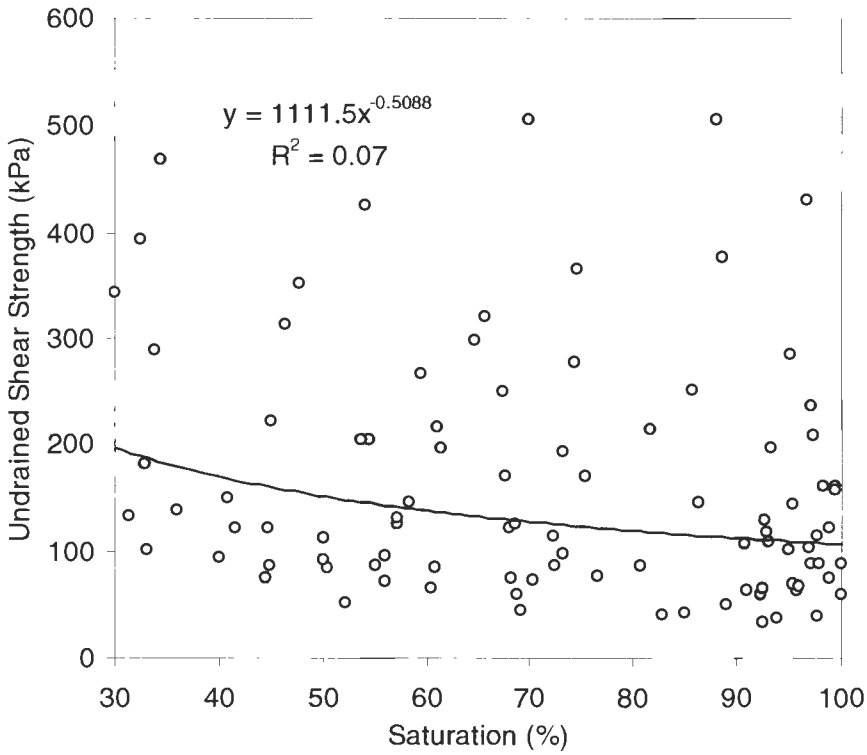

Figure C8. Regression for undrained shear strength with saturation for all unconfined tests

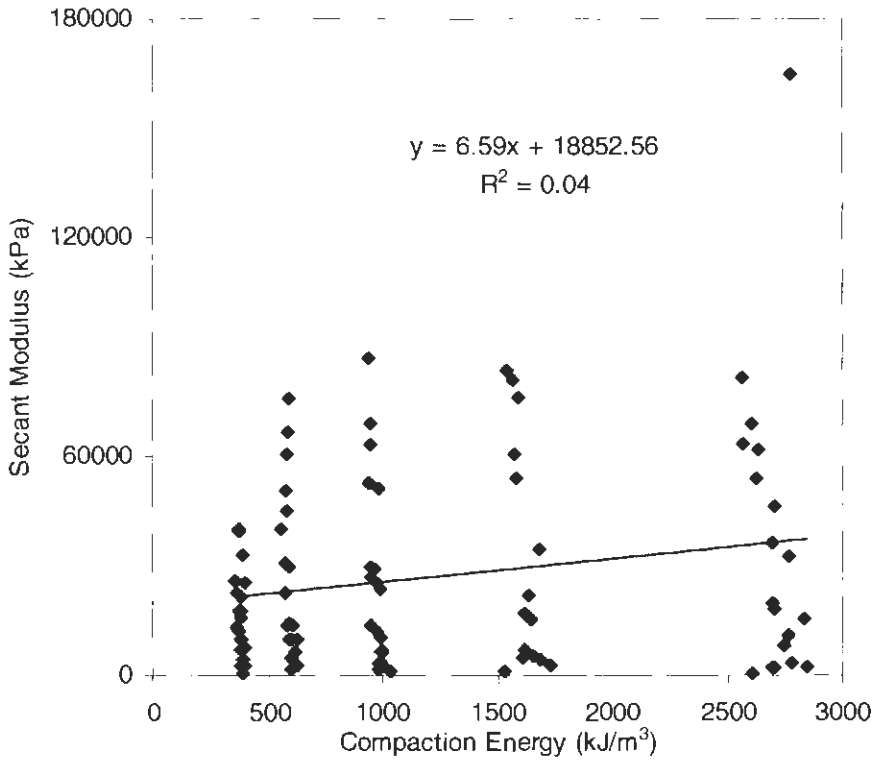

Figure C9. Regression for secant modulus with compaction energy for all unconfined tests

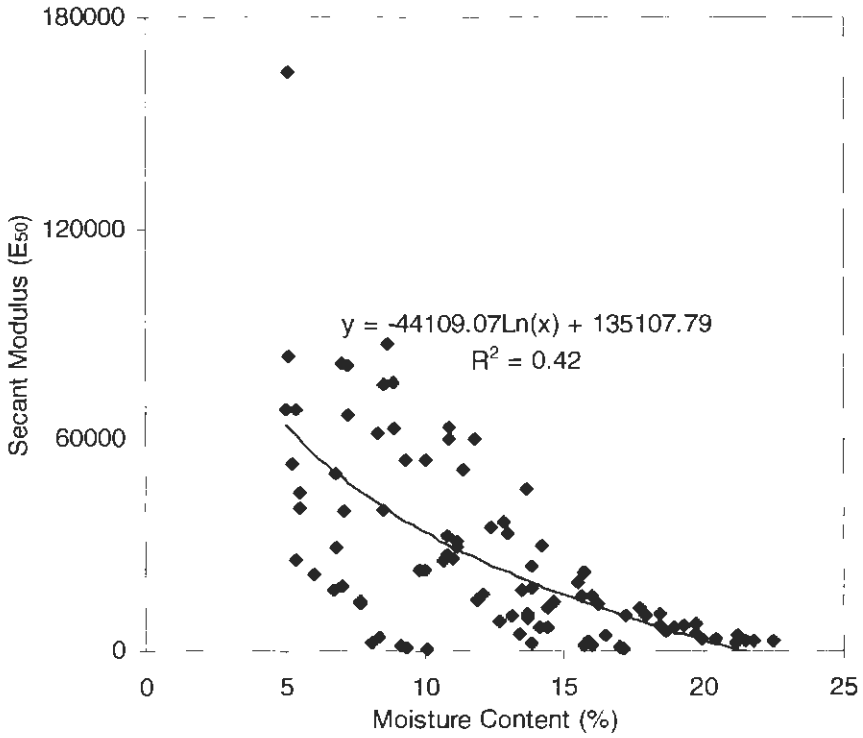

Figure C10. Regression for secant modulus with moisture content for all unconfined tests

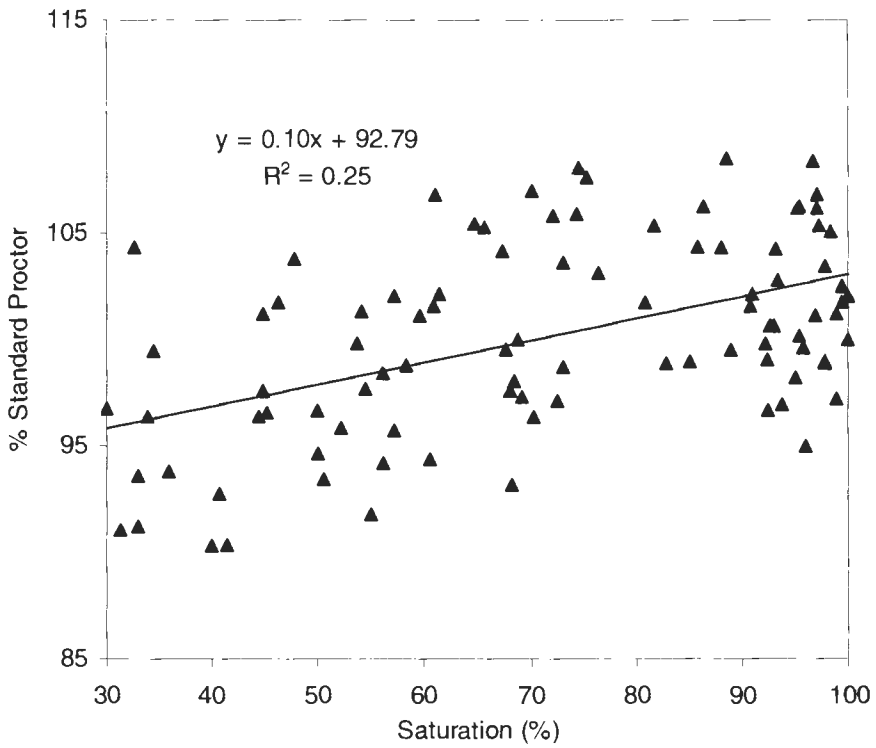

Figure C11. Regression for relative compaction with saturation for all unconfined test

APPENDIX D. TRIAXIAL TEST FIGURES

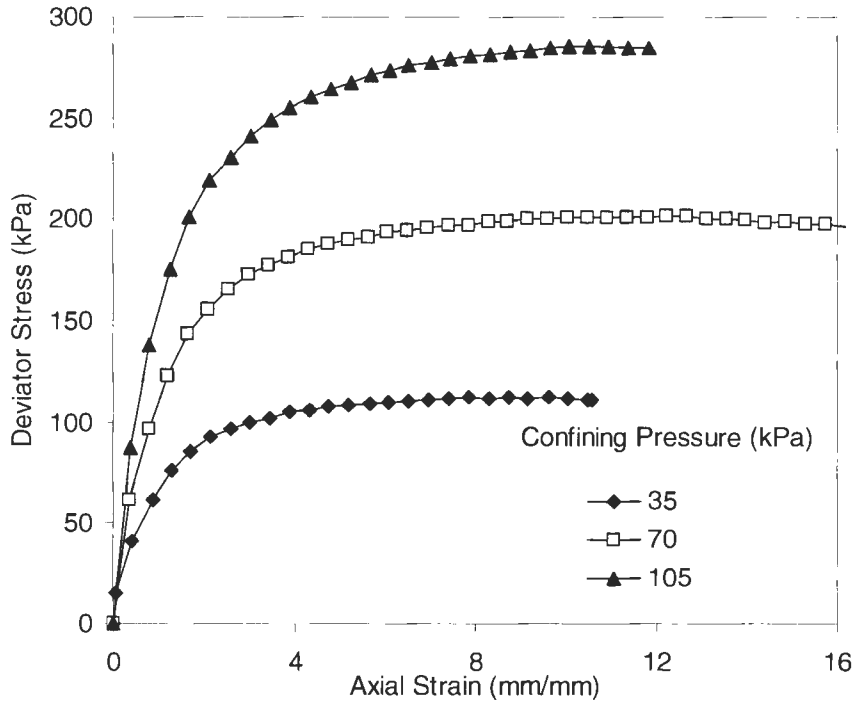

Figure D1. Stress-strain plots for WF triaxial specimens at compaction energy of 355 kJ/m^3 and average initial moisture content of 13.5%

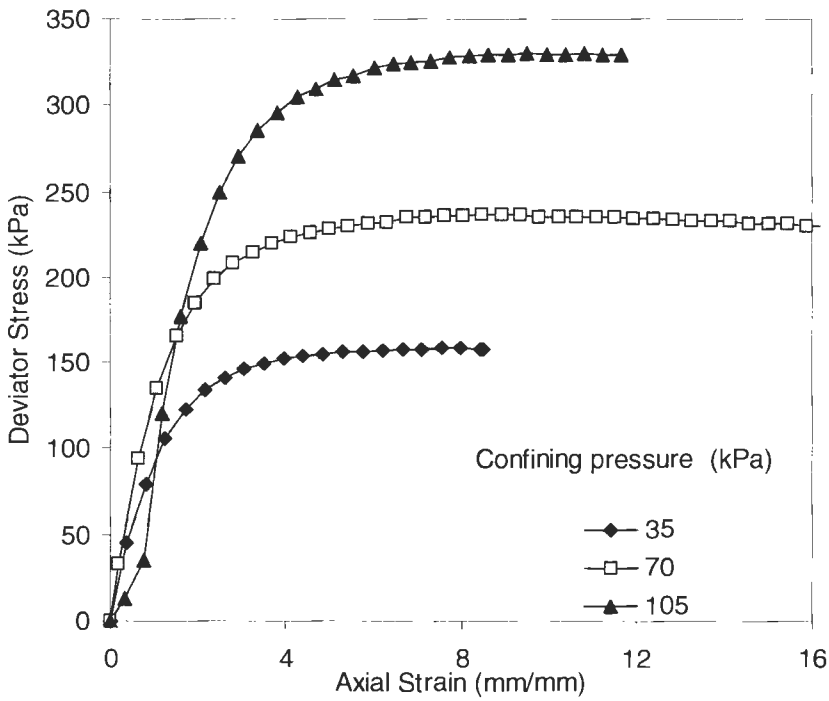

Figure D2. Stress-strain plots for WF triaxial specimens at compaction energy of 592 kJ/m^3 and average initial moisture content of 13.4%

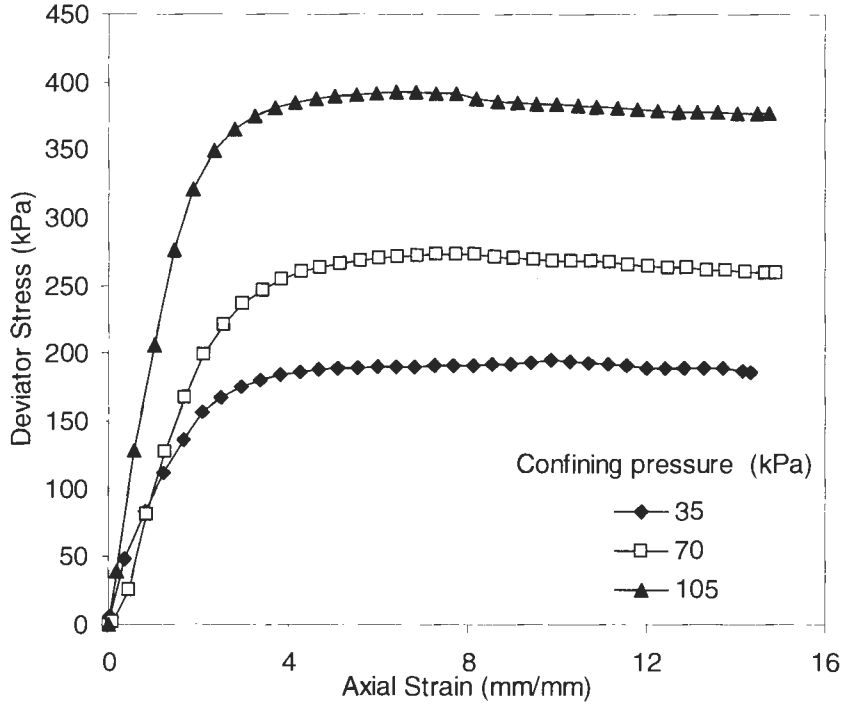

Figure D3. Stress-strain plots for WF triaxial specimens at compaction energy of 987 kJ/m^3 and average moisture initial content of 13.9%

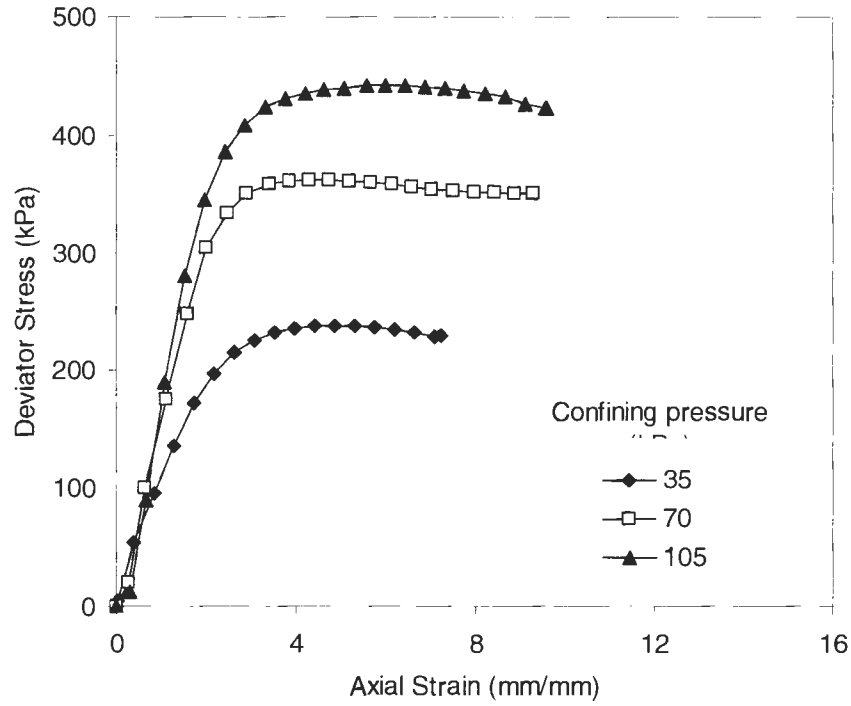

Figure D4. Stress-strain plots for WF triaxial specimens at compaction energy of 1643 kJ/m^3 and average initial moisture content of 13.7%

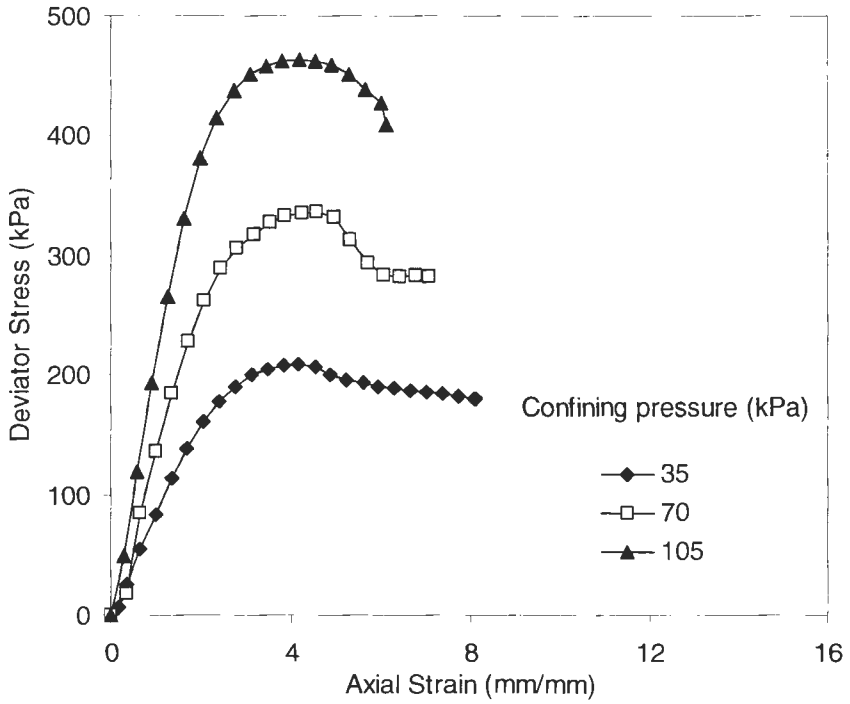

Figure D5. Stress-strain plots for WF triaxial specimens at compaction energy of 2693 kJ/m^3 and average initial moisture content of 13.3%

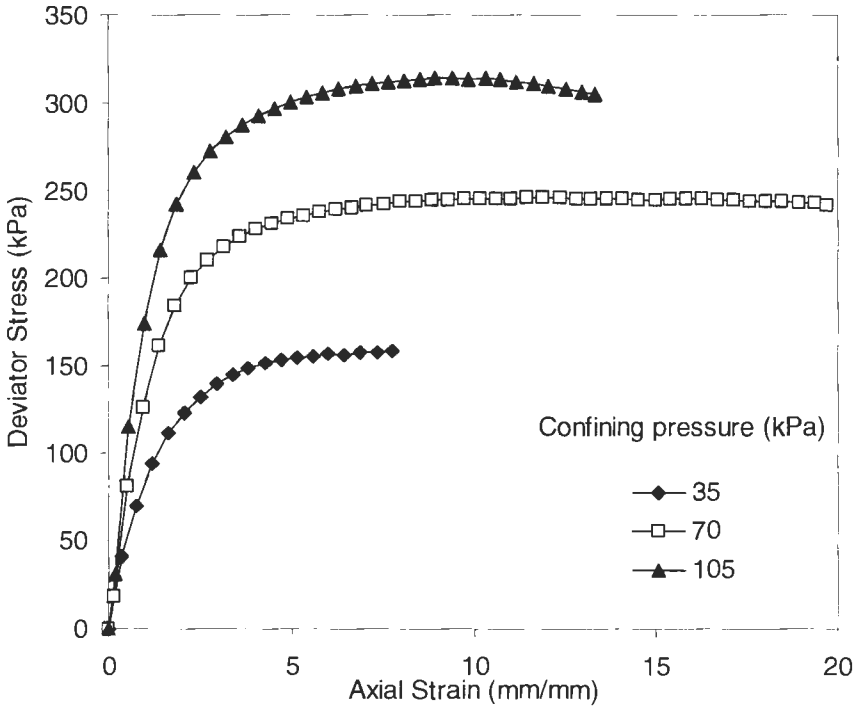

Figure D6. Stress-strain plots for WF triaxial specimens at compaction energy of 355 kJ/m^3 and average initial moisture content of 19.5%

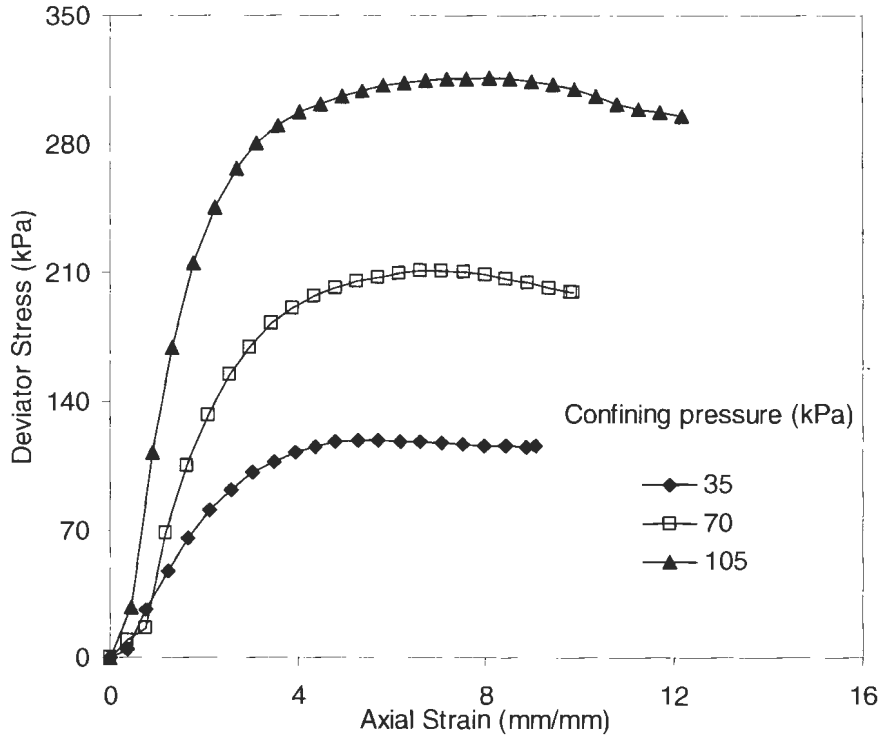

Figure D7. Stress-strain plots for WF triaxial specimens at compaction energy of 592 kJ/m^3 and average initial moisture content of 18.2%

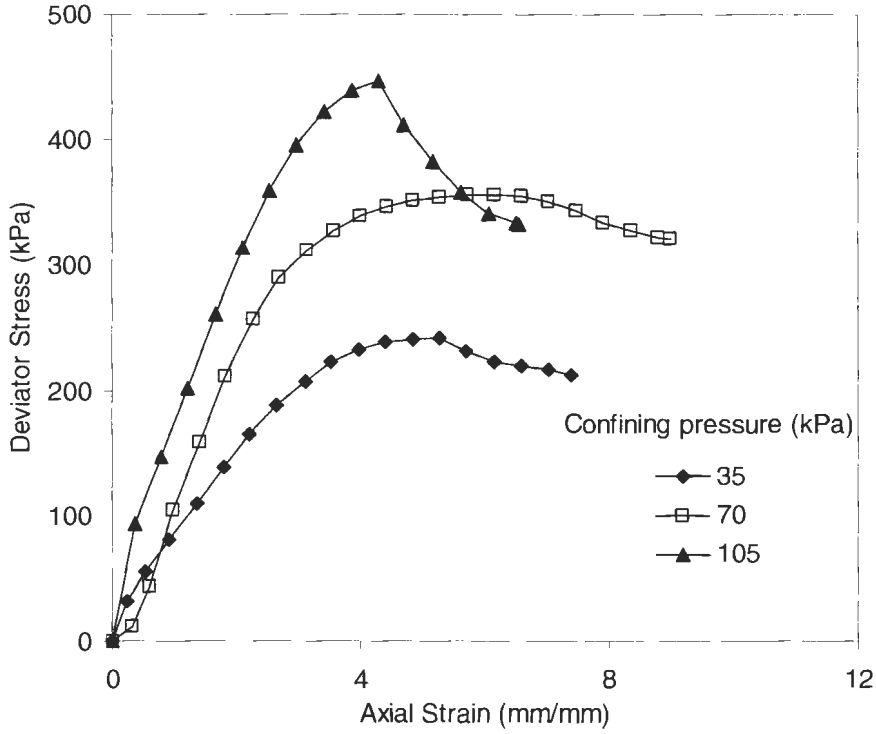

Figure D8. Stress-strain plots for WF triaxial specimens at compaction energy of 2693 kJ/m^3 and average initial moisture content of 20.1%

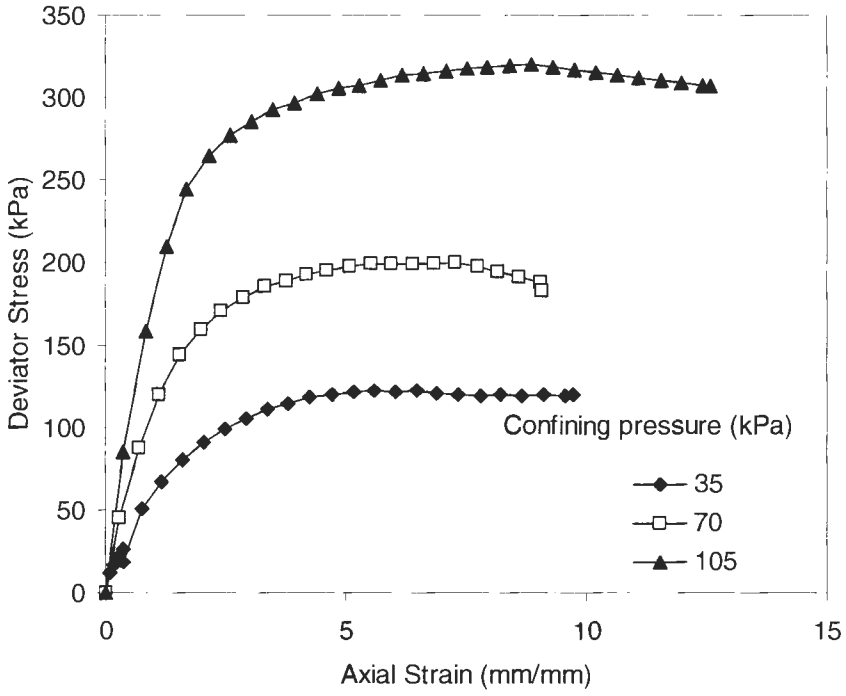

Figure D9. Stress-strain plots for WF triaxial specimens at compaction energy of 355 kJ/m^3 and average initial moisture content of 21.3%

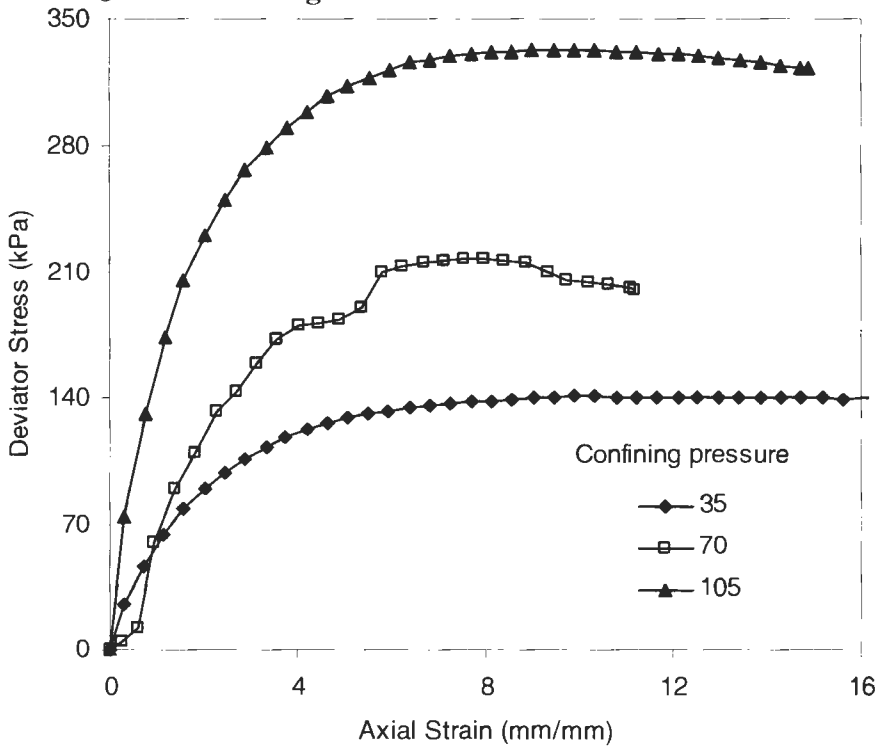

Figure D10. Stress-strain plots for WF triaxial specimens at compaction energy of 592 kJ/m^3 and average initial moisture content of 22.3%

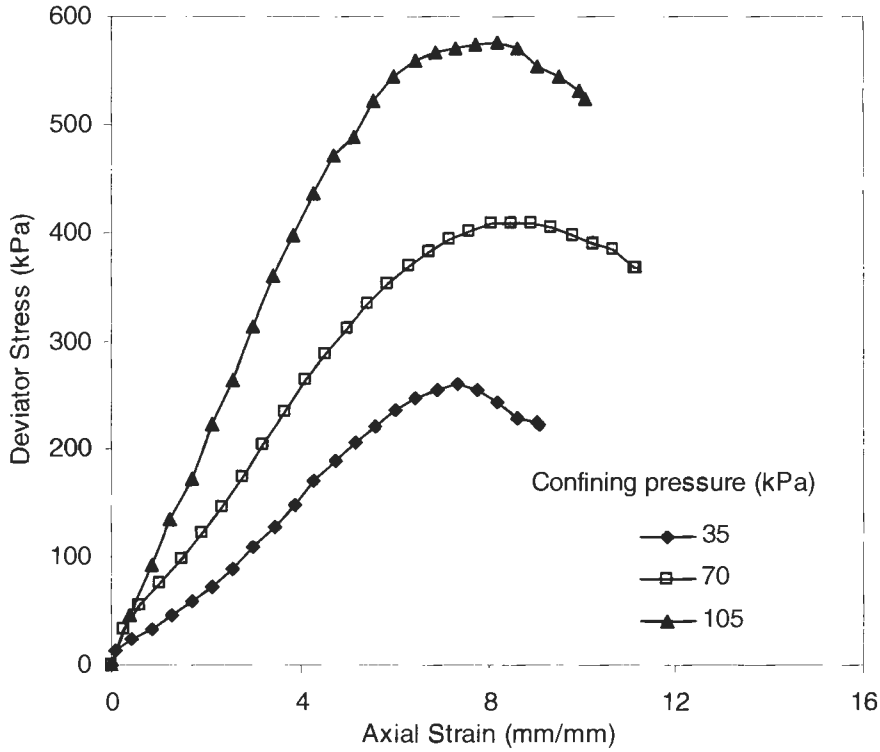

Figure D11. Stress-strain plots for WF triaxial specimens at compaction energy of 2693 kJ/m^3 and average initial moisture content of 21.7%

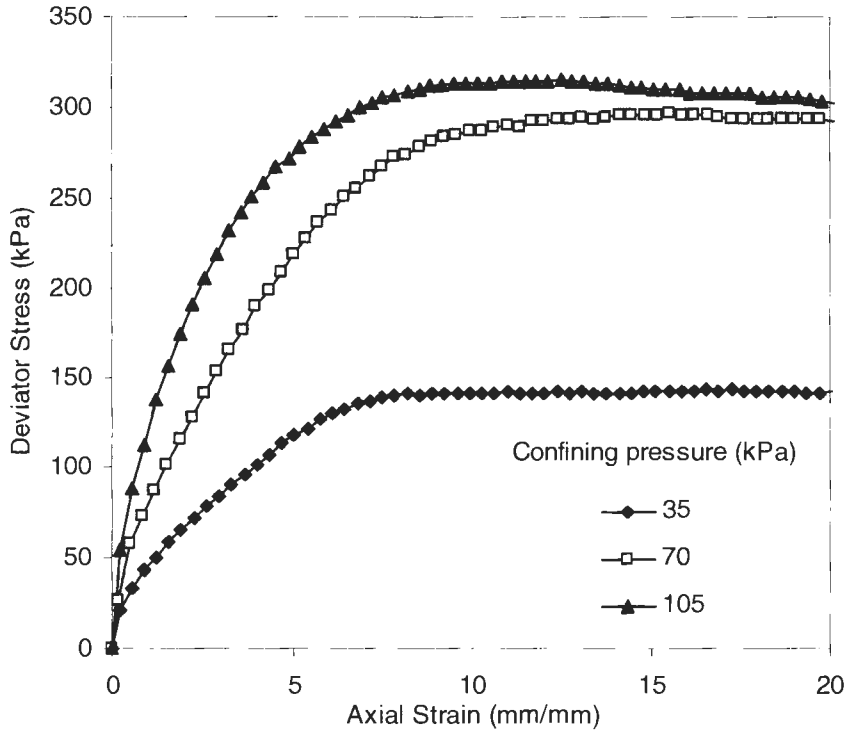

Figure D12. Stress-strain plots for WF triaxial specimens at compaction energy of 355 kJ/m^3 and average initial moisture content of 25.7%

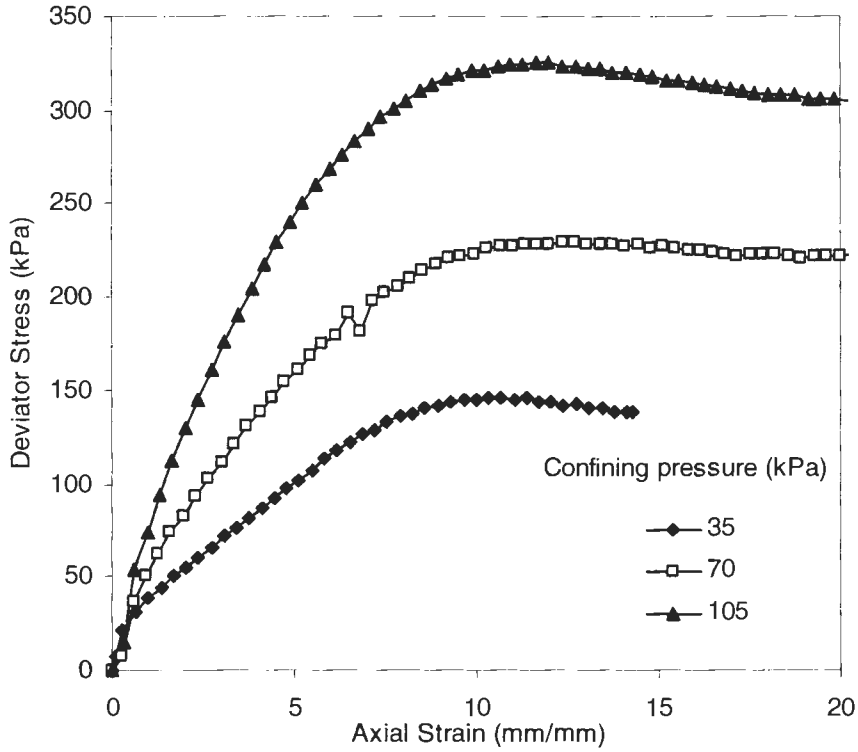

Figure D13. Stress-strain plots for WF triaxial specimens at compaction energy of 592 kJ/m^3 and average initial moisture content of 25.9%

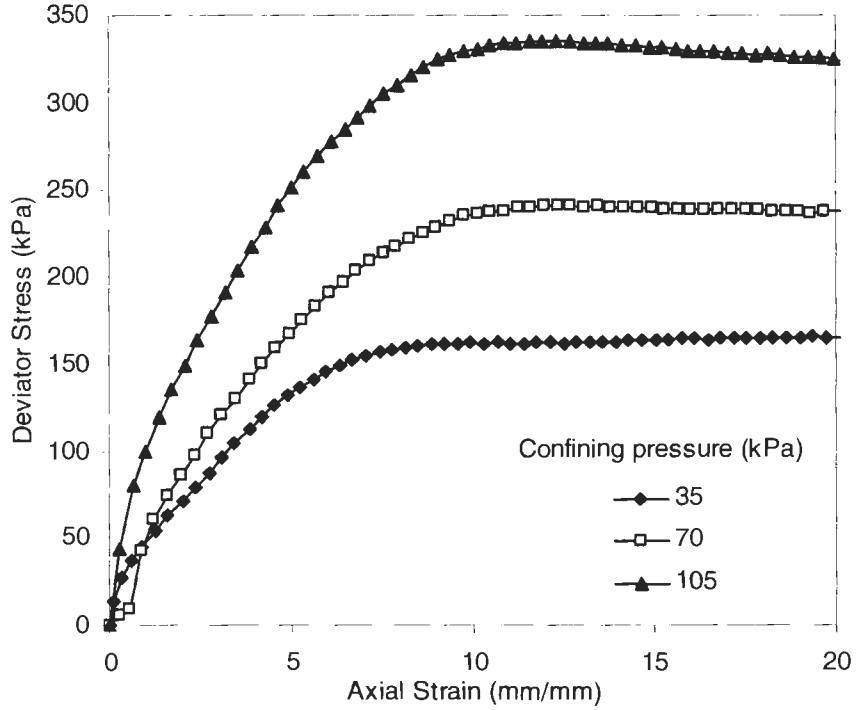

Figure D14. Stress-strain plots for WF triaxial specimens at compaction energy of 987 kJ/m^3 and average initial moisture content of 25.6%

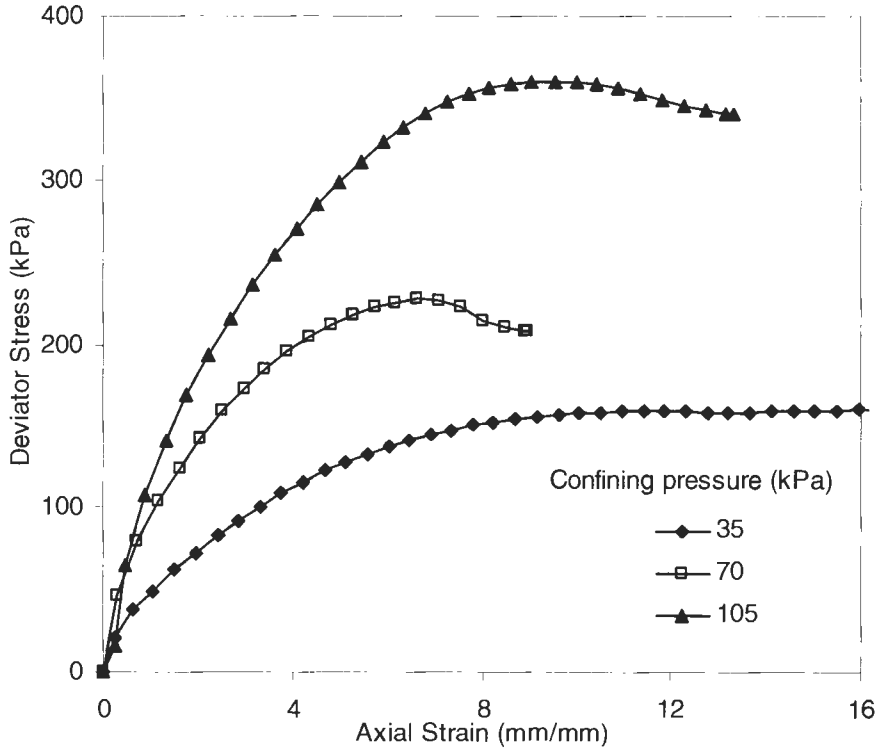

Figure D15. Stress-strain plots for WF triaxial specimens at compaction energy of 1643 kJ/m^3 and average initial moisture content of 25.5%

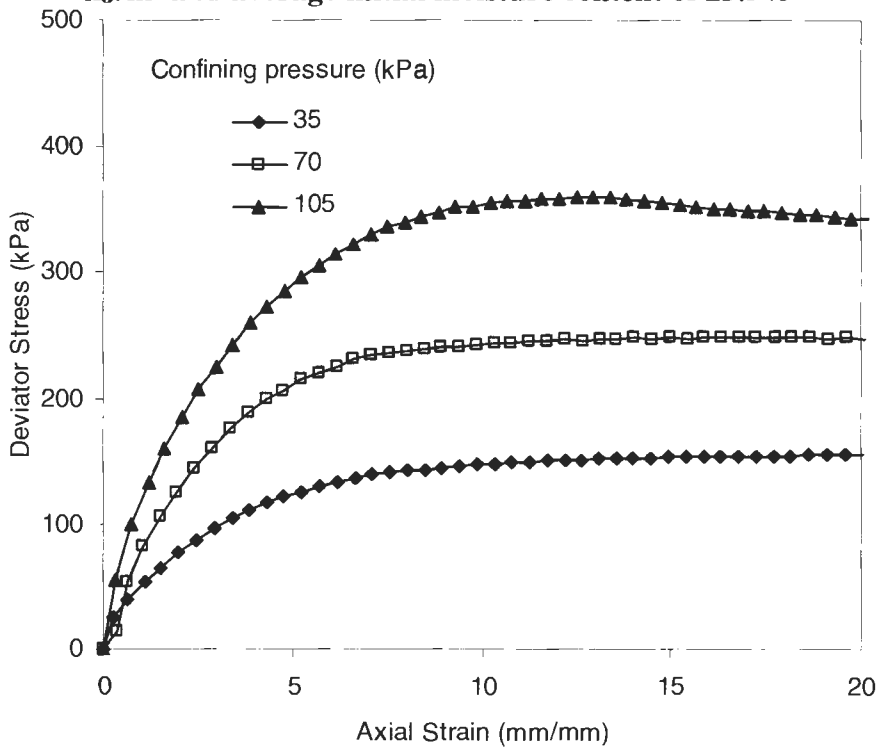

Figure D16. Stress-strain plots for WF triaxial specimens at compaction energy of 2693 kJ/m^3 and average initial moisture content of 25.7%

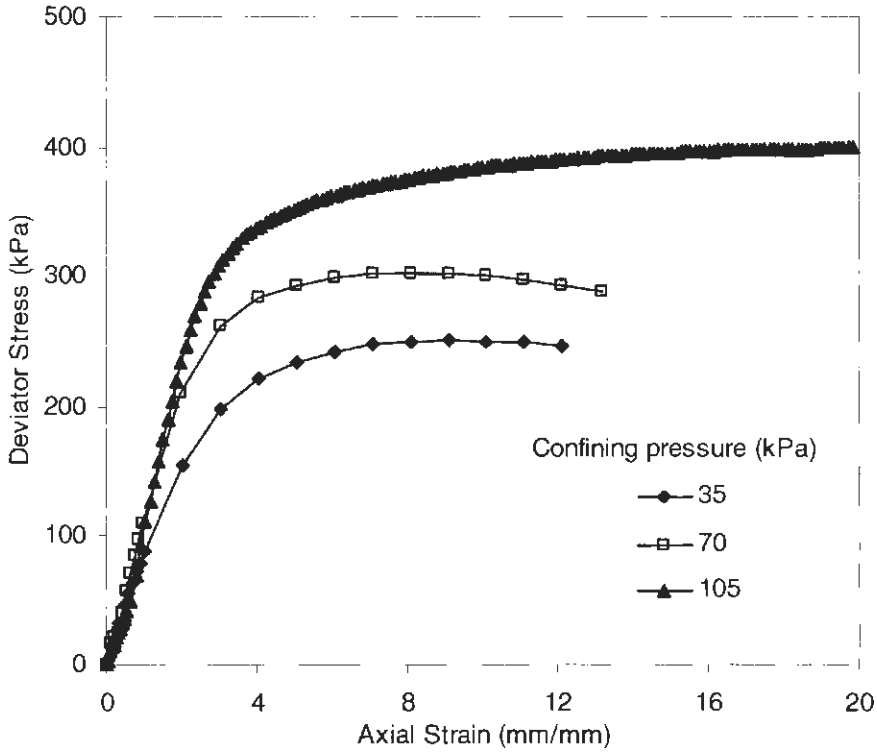

Figure D17. Stress-strain plots for ELE triaxial specimens at compaction energy of 592 kJ/m^3 and average initial moisture content of 18.9%

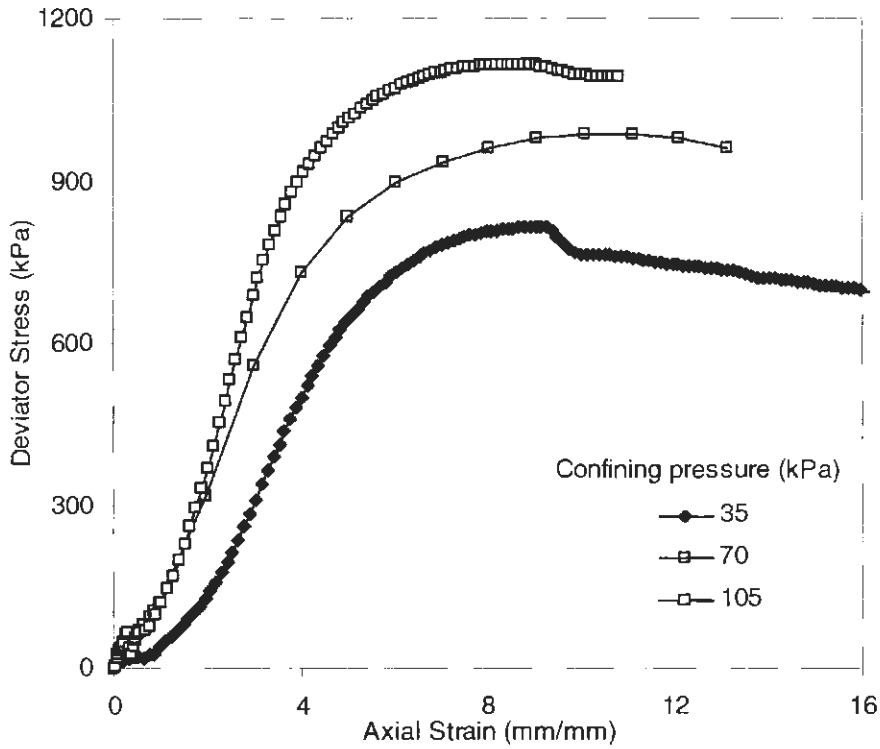

Figure D18. Stress-strain plots for ELE triaxial specimens at compaction energy of 2693 kJ/m^3 and average initial moisture content of 18.1%

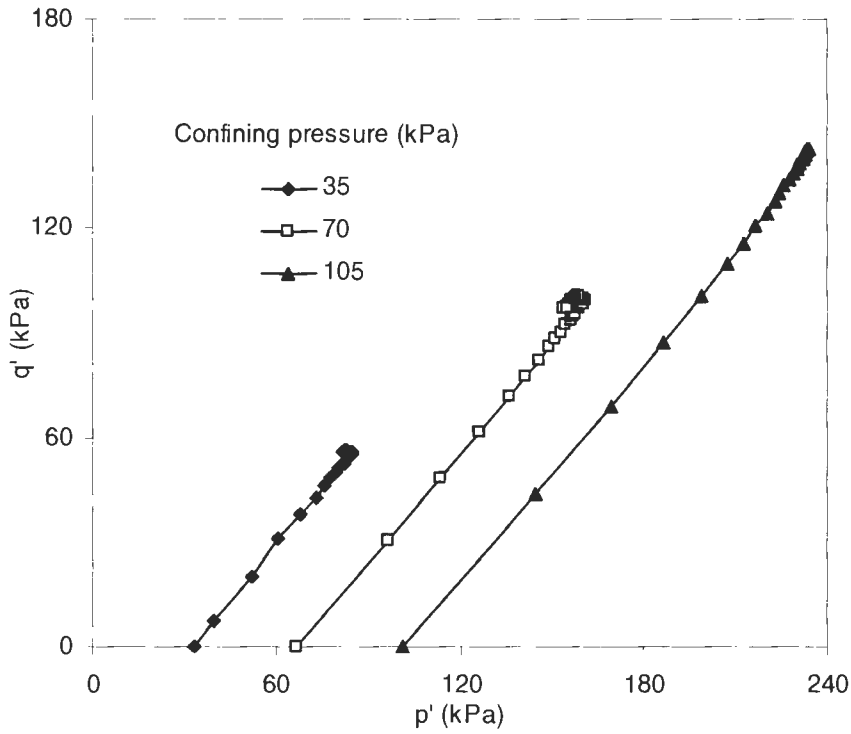

Figure D19. p' – q' plots for WF triaxial specimens at compaction energy of 355 kJ/m^3 and average initial moisture content of 13.5%

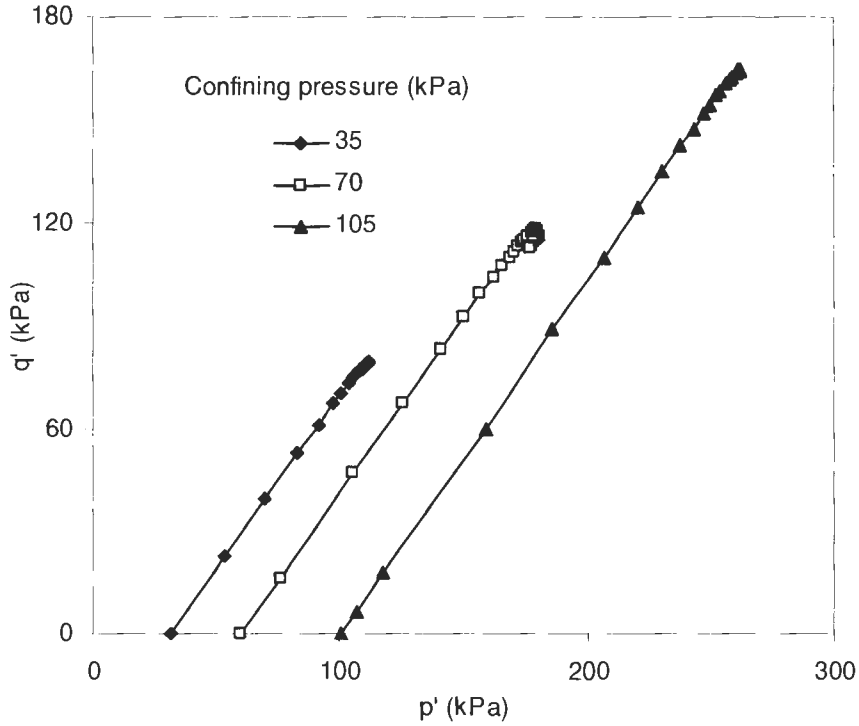

Figure D20. p' – q' plots for WF triaxial specimens at compaction energy of 592 kJ/m^3 and average initial moisture content of 13.4%

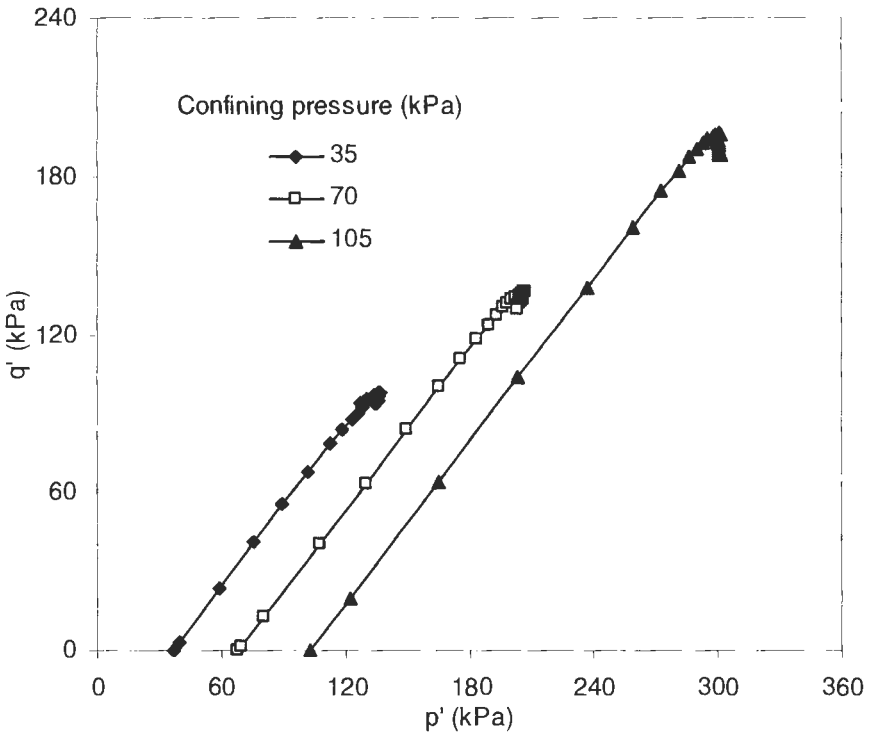

Figure D21. p' – q' plots for WF triaxial specimens at compaction energy of 987 kJ/m^3 and average initial moisture content of 13.9%

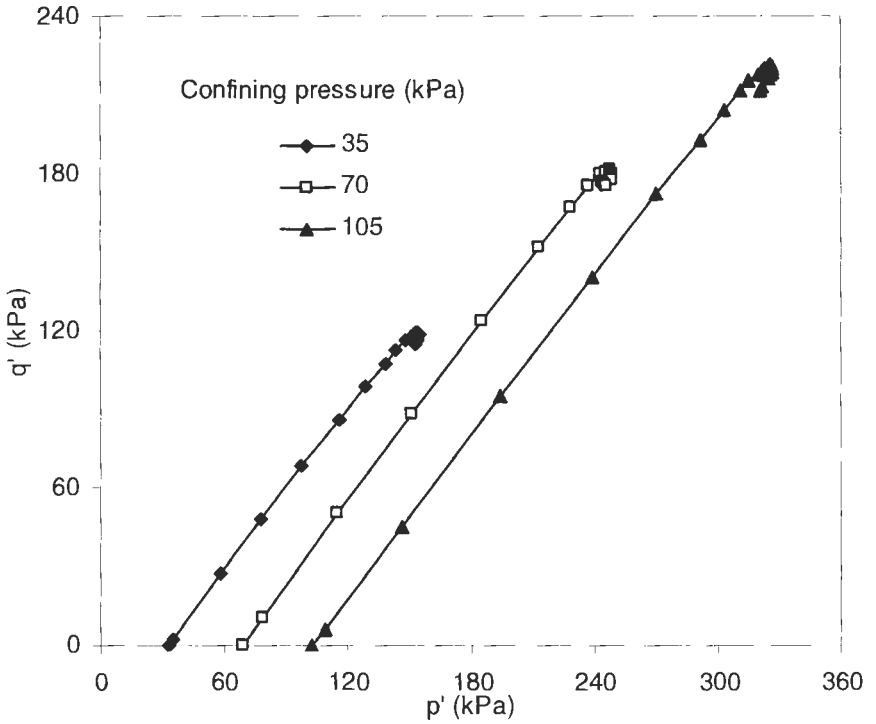

Figure D22. p' – q' plots for WF triaxial specimens at compaction energy of 1643 kJ/m^3 and average initial moisture content of 13.7%

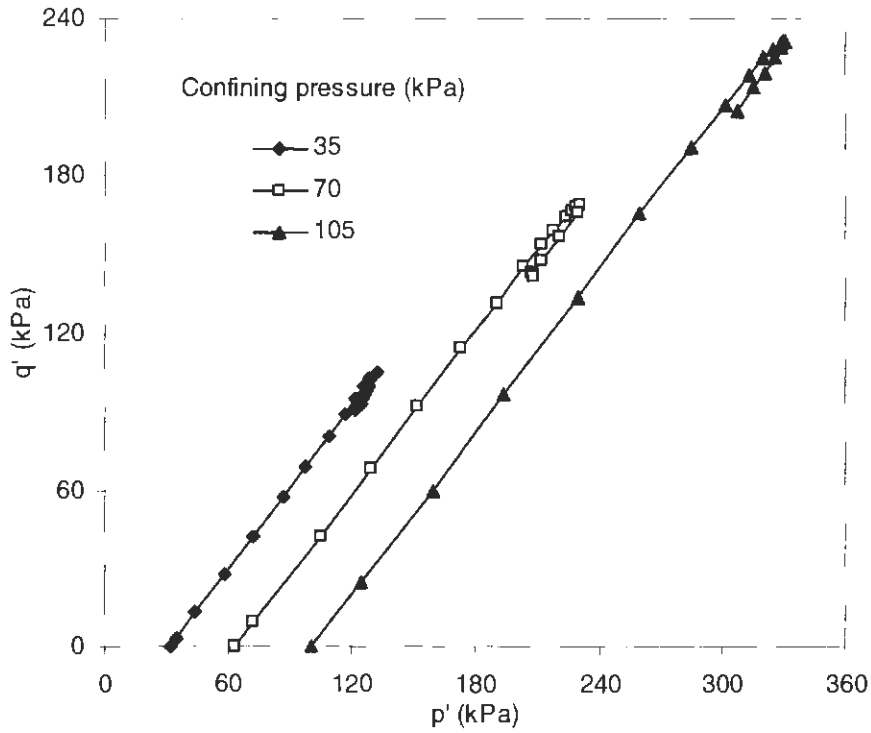

Figure D23. p' – q' plots for WF triaxial specimens at compaction energy of 2693 kJ/m^3 and average initial moisture content of 13.3%

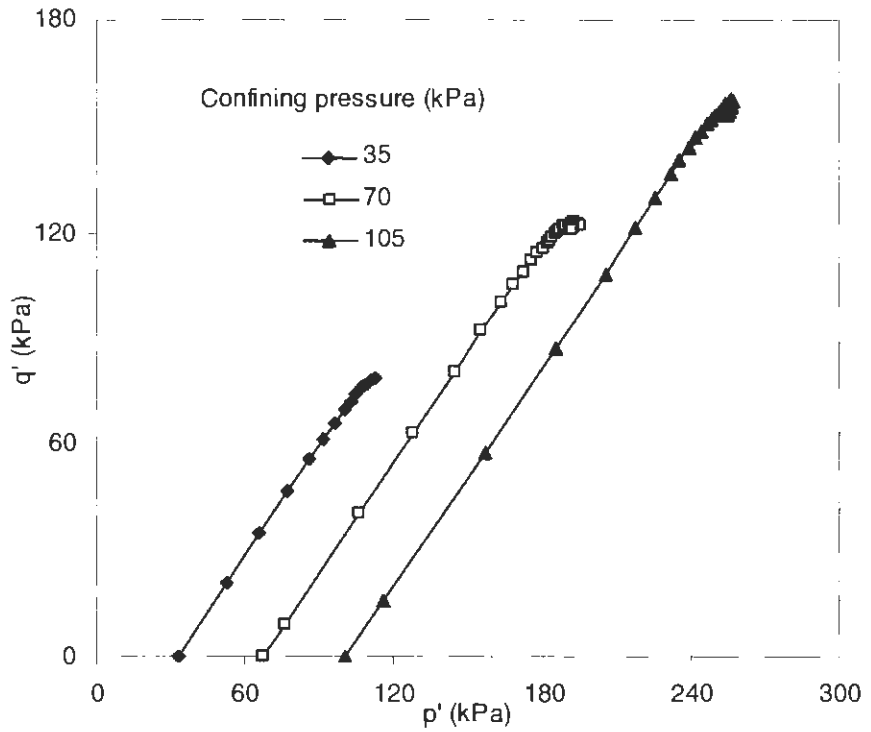

Figure D24. p' – q' plots for WF triaxial specimens at compaction energy of 355 kJ/m^3 and average initial moisture content of 19.5%

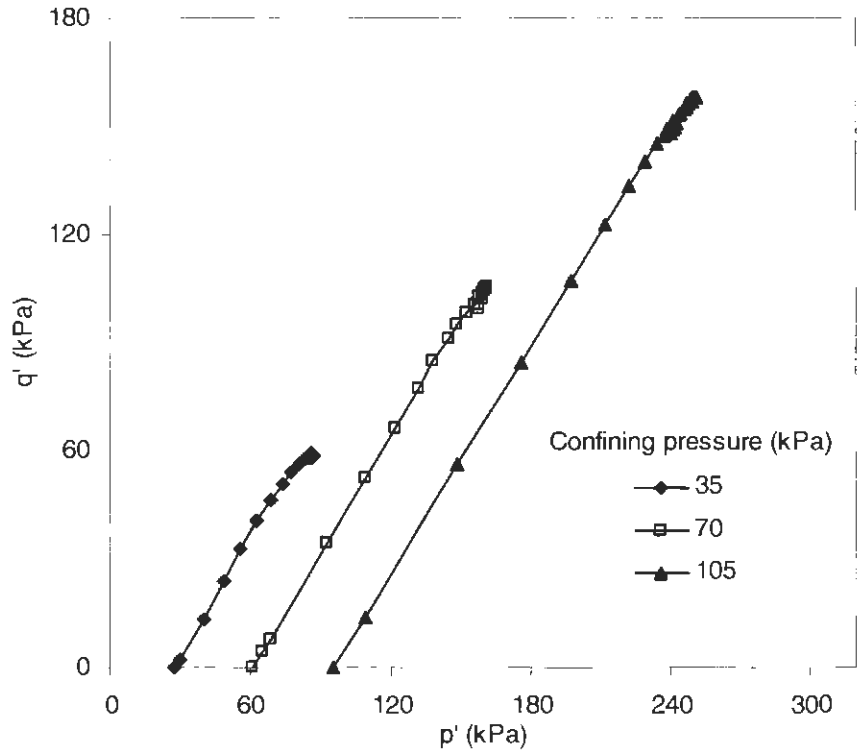

Figure D25. p' – q' plots for WF triaxial specimens at compaction energy of 592 kJ/m^3 and average initial moisture content of 18.2%

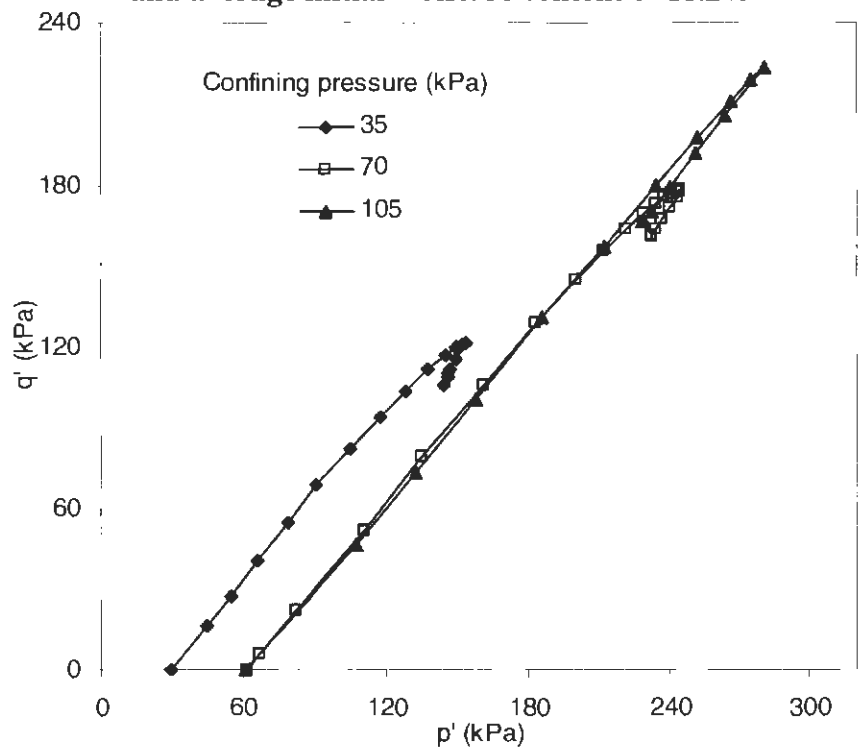

Figure D26. p' – q' plots for WF triaxial specimens at compaction energy of 2693 kJ/m^3 and average initial moisture content of 20.1%

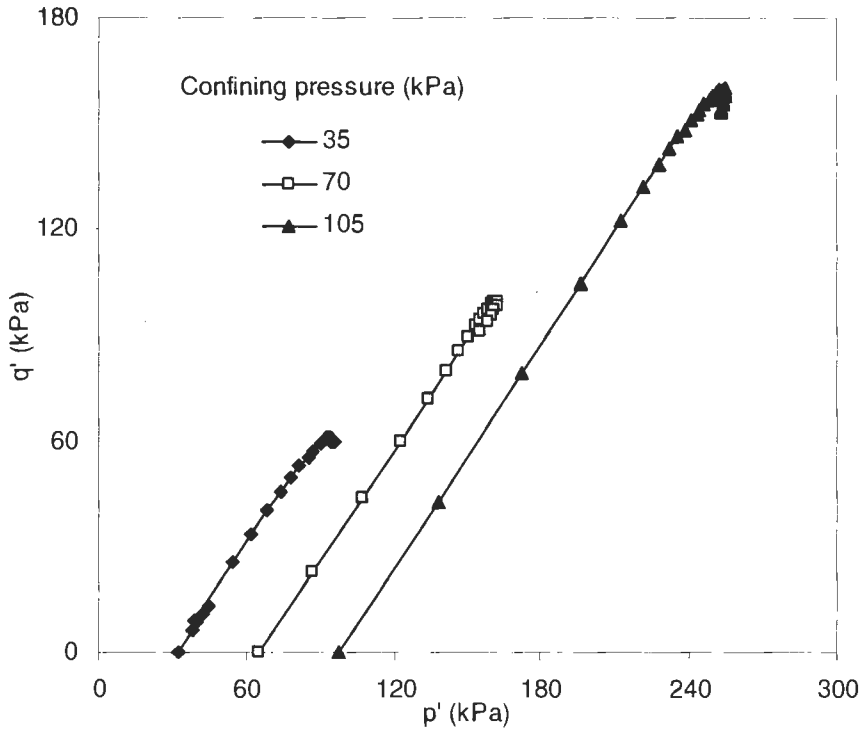

Figure D27. p' – q' plots for WF triaxial specimens at compaction energy of 355 kJ/m^3 and average initial moisture content of 21.3%

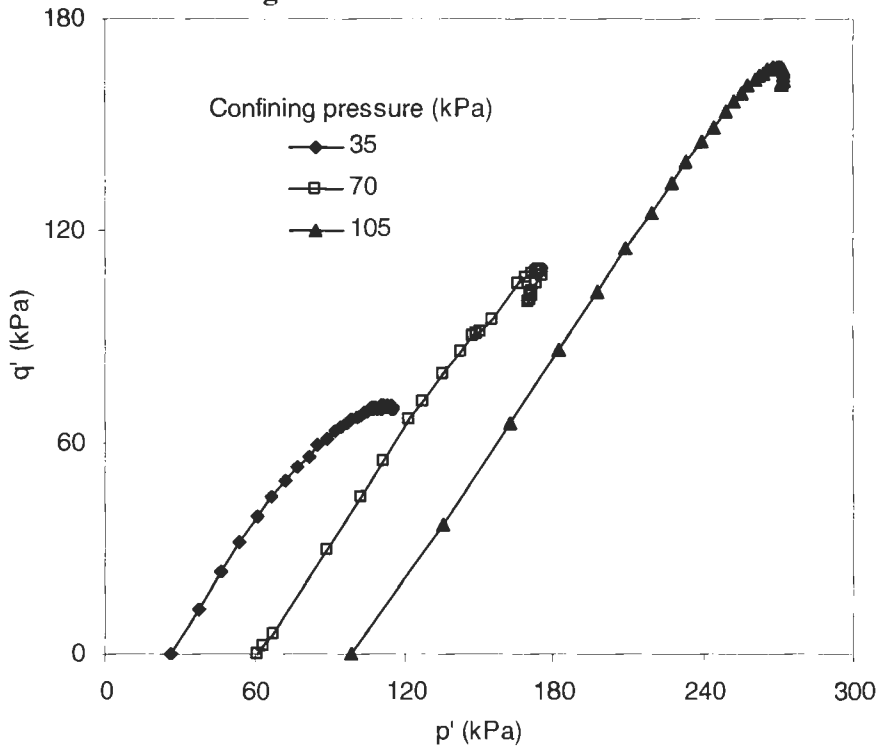

Figure D28. p' – q' plots for WF triaxial specimens at compaction energy of 592 kJ/m^3 and average initial moisture content of 22.3%

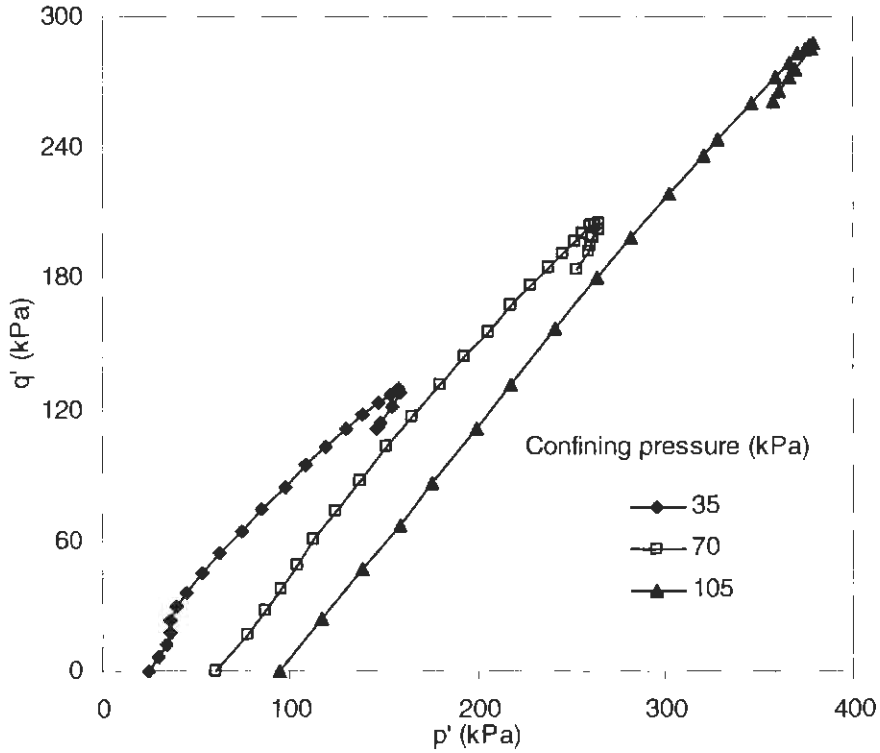

Figure D29. p' – q' plots for WF triaxial specimens at compaction energy of 2693 kJ/m^3 and average initial moisture content of 21.7%

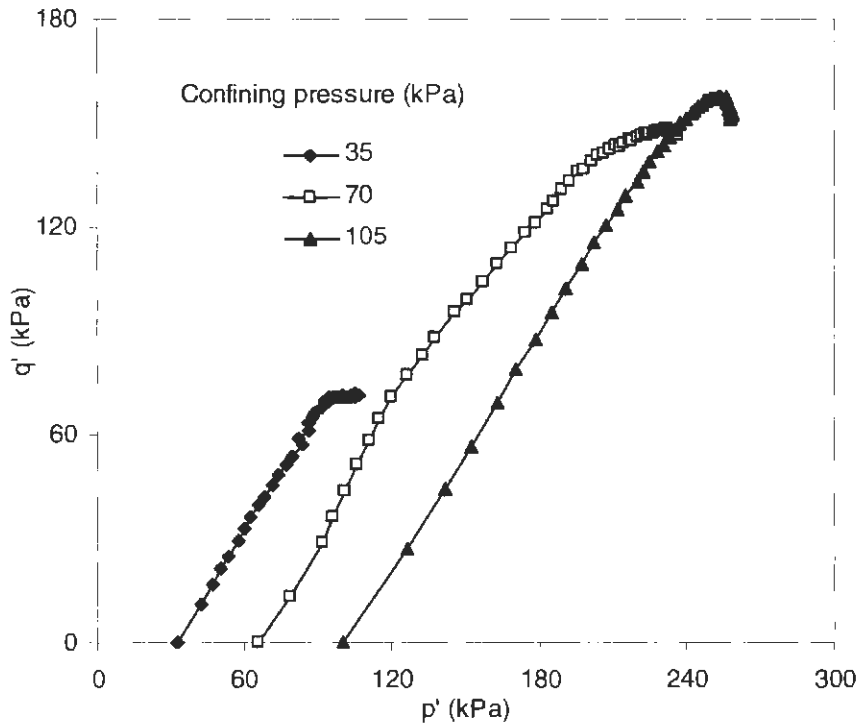

Figure D30. p' – q' plots for WF triaxial specimens at compaction energy of 355 kJ/m^3 and average initial moisture content of 25.7%

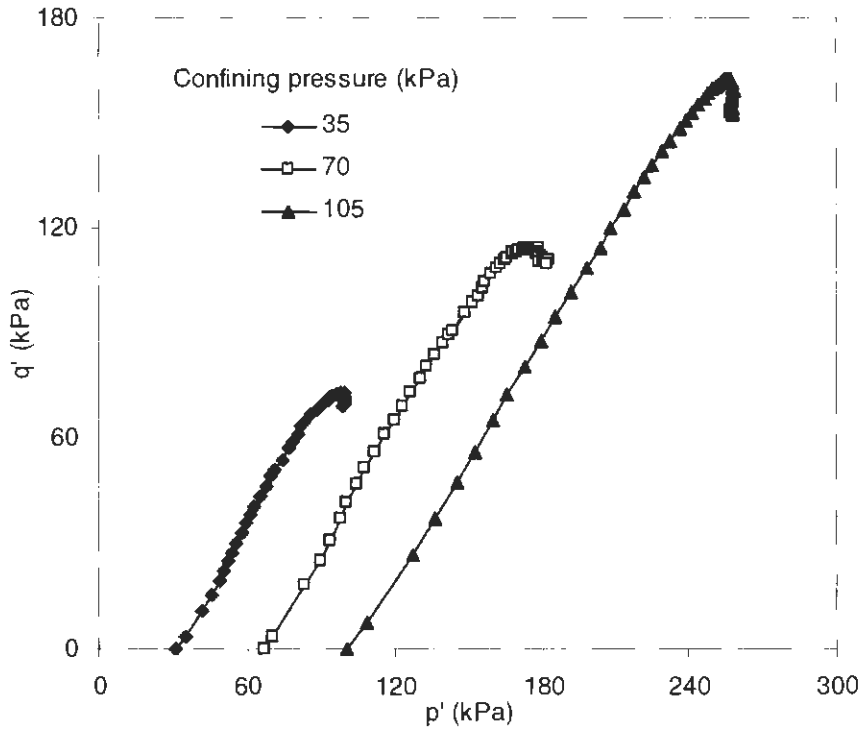

Figure D31. p' – q' plots for WF triaxial specimens at compaction energy of 592 kJ/m^3 and average initial moisture content of 25.9%

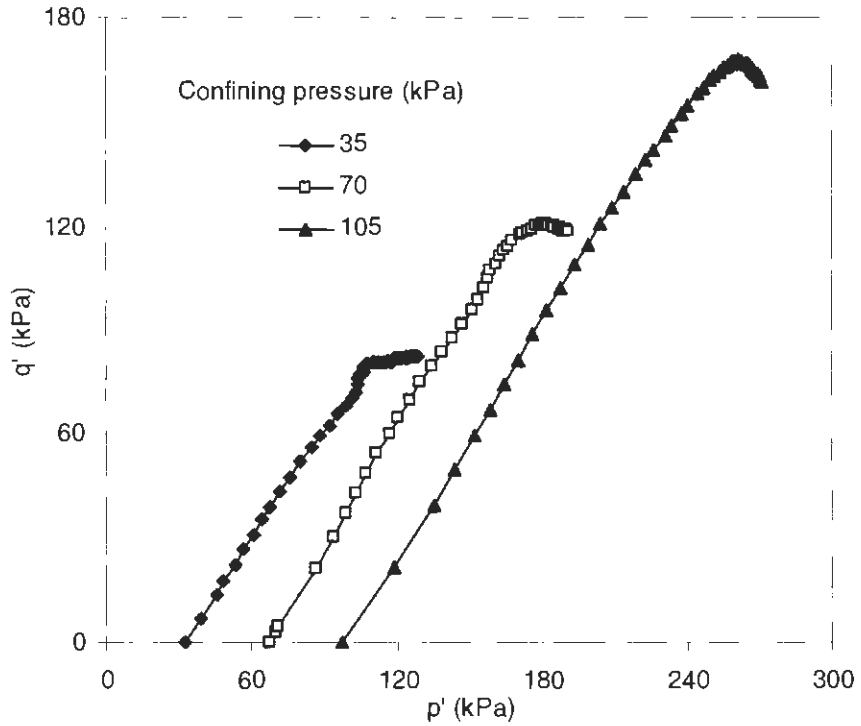

Figure D32. p' – q' plots for WF triaxial specimens at compaction energy of 987 kJ/m^3 and average initial moisture content of 25.6%

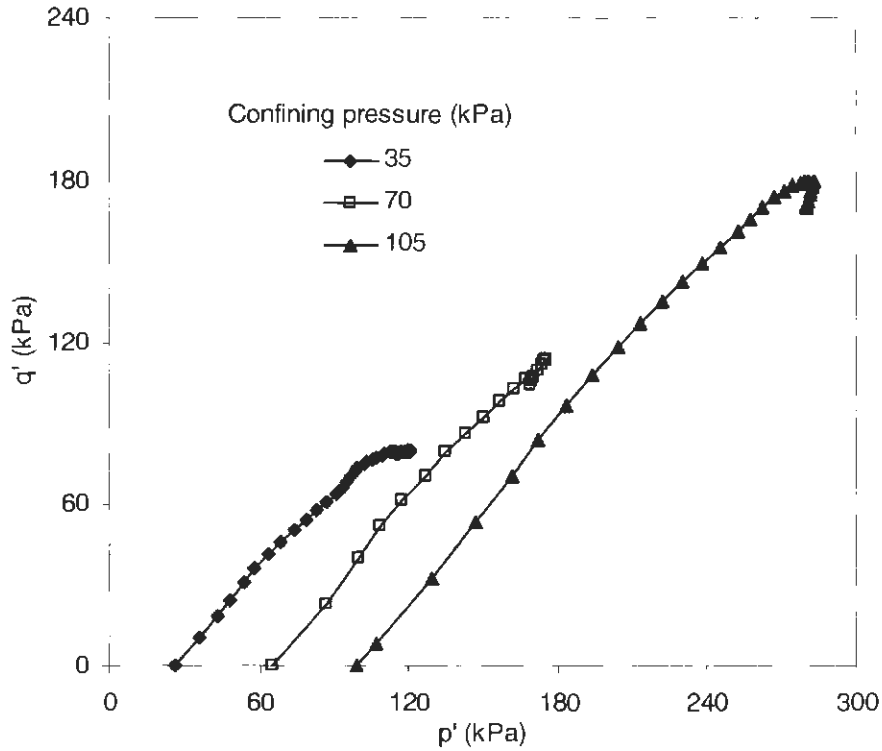

Figure D33. p' – q' plots for WF triaxial specimens at compaction energy of 1643 kJ/m^3 and average initial moisture content of 25.5%

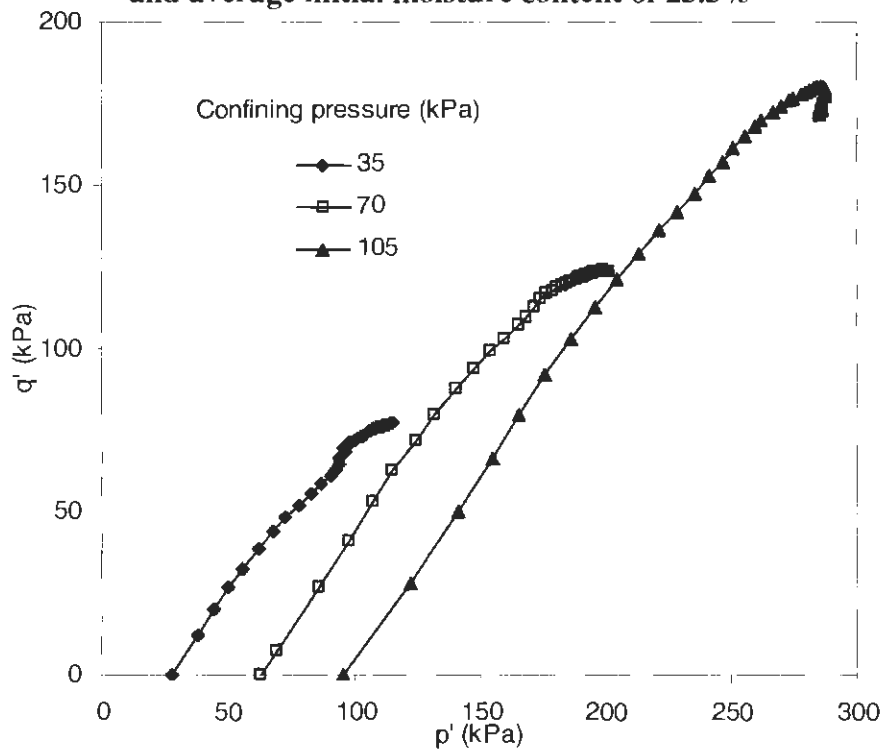

Figure D34. p' – q' plots for WF triaxial specimens at compaction energy of 2693 kJ/m^3 and average initial moisture content of 25.7%

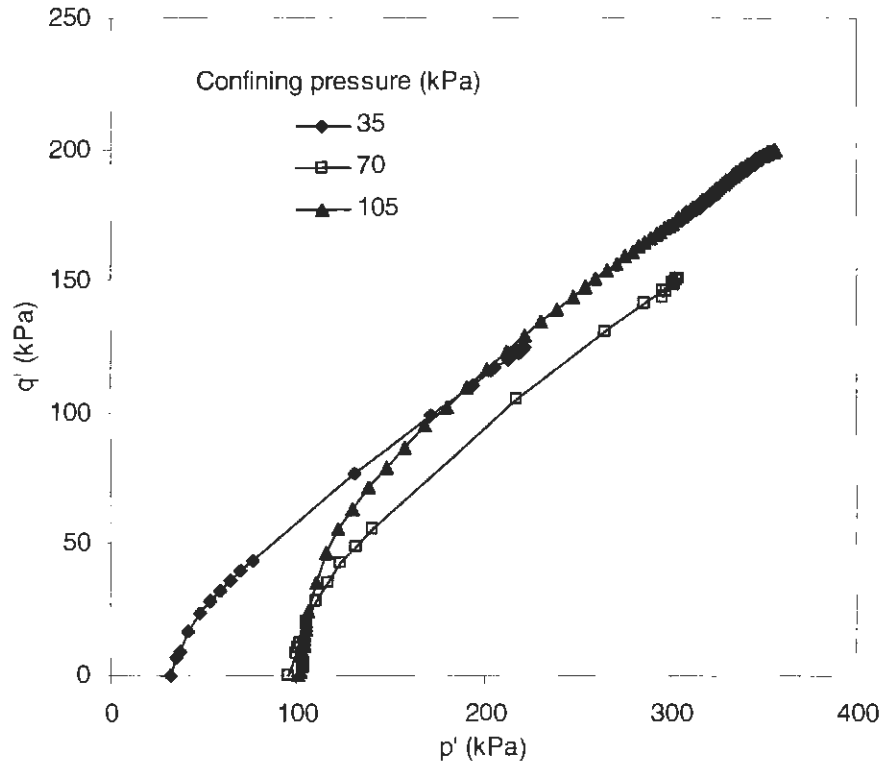

Figure D35. p' – q' plots for ELE triaxial specimens at compaction energy of 592 kJ/m^3 and average initial moisture content of 18.9%

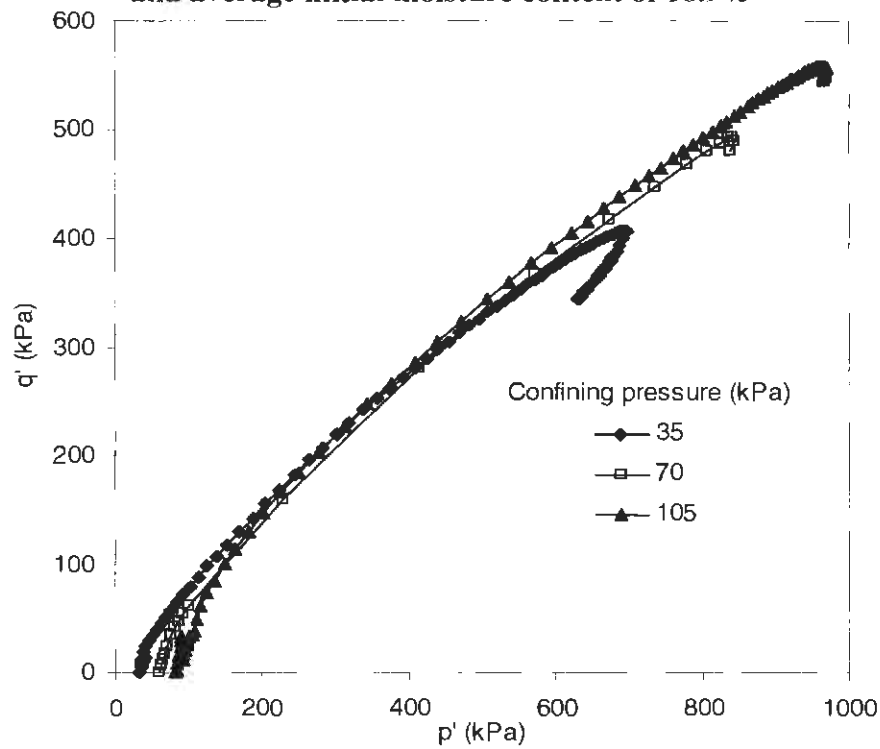

Figure D36. p' – q' plots for ELE triaxial specimens at compaction energy of 2693 kJ/m^3 and average initial moisture content of 18.1%

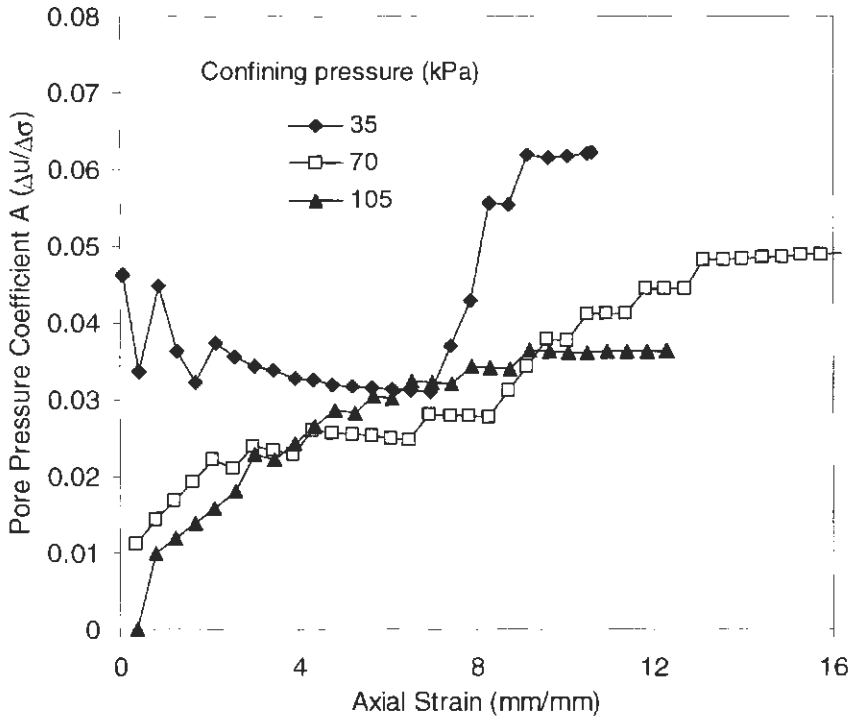

Figure D37. Pore pressure coefficient A as a function of axial strain for WF triaxial specimens at compaction energy of 355 kJ/m^3 and moisture content of 13.5%

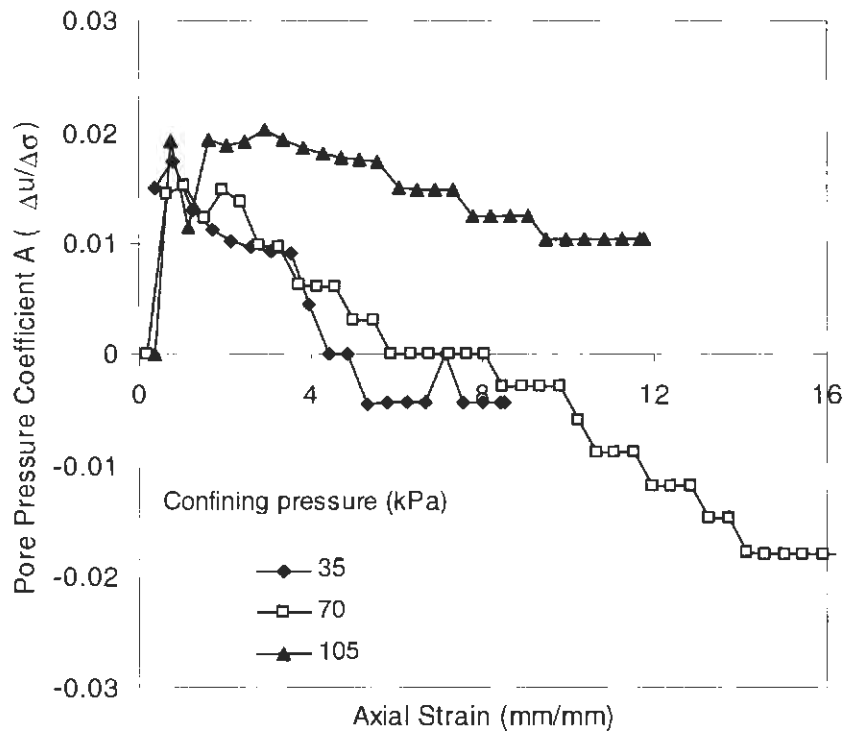

Figure D38. Pore pressure coefficient A as a function of axial strain for WF triaxial specimens at compaction energy of 592 kJ/m^3 and moisture content of 13.4%

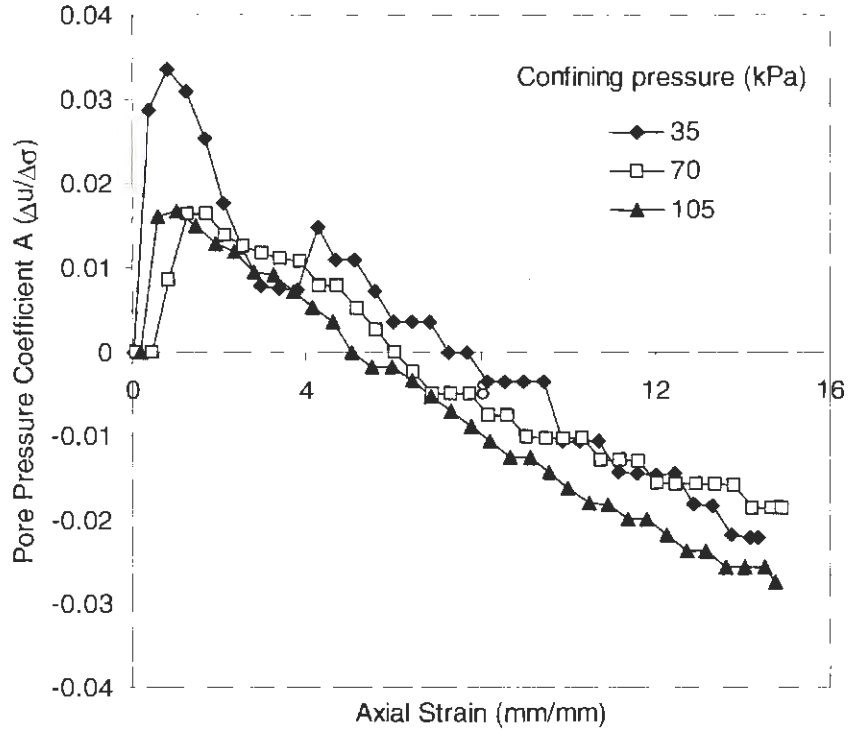

Figure D39. Pore pressure coefficient A as a function of axial strain for WF triaxial specimens at compaction energy of 987 kJ/m^3 and moisture content of 13.9%

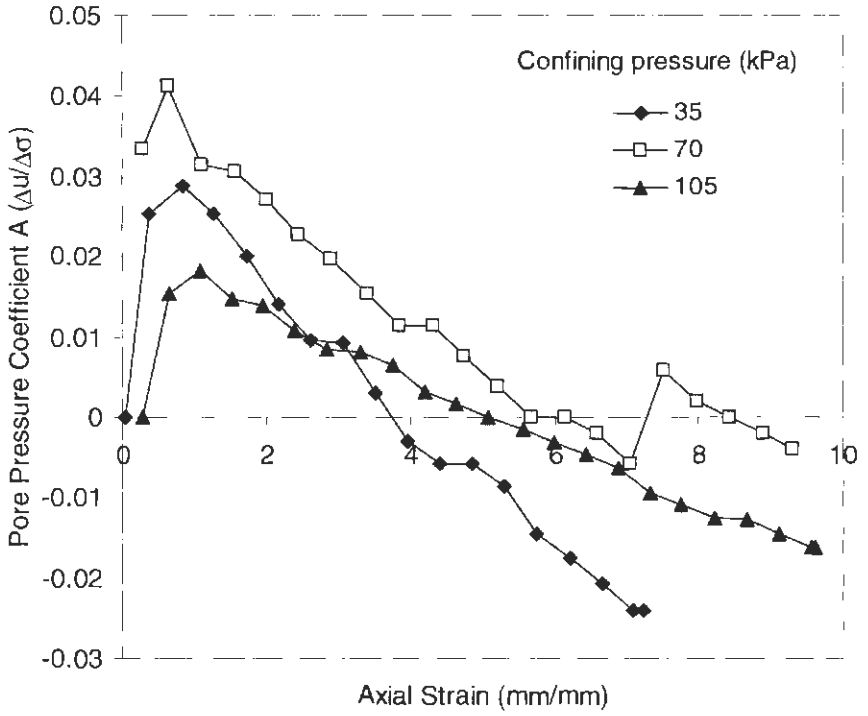

Figure D40. Pore pressure coefficient A as a function of axial strain for WF triaxial specimens at compaction energy of 1643 kJ/m^3 and moisture content of 13.7%

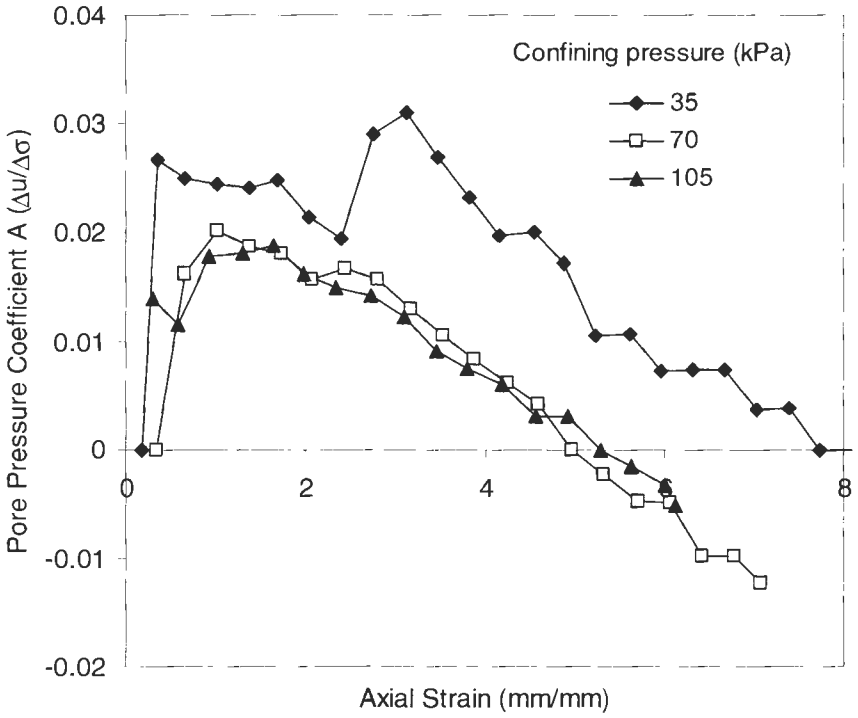

Figure D41. Pore pressure coefficient A as a function of axial strain for WF triaxial specimens at compaction energy of 2693 kJ/m^3 and moisture content of 13.3%

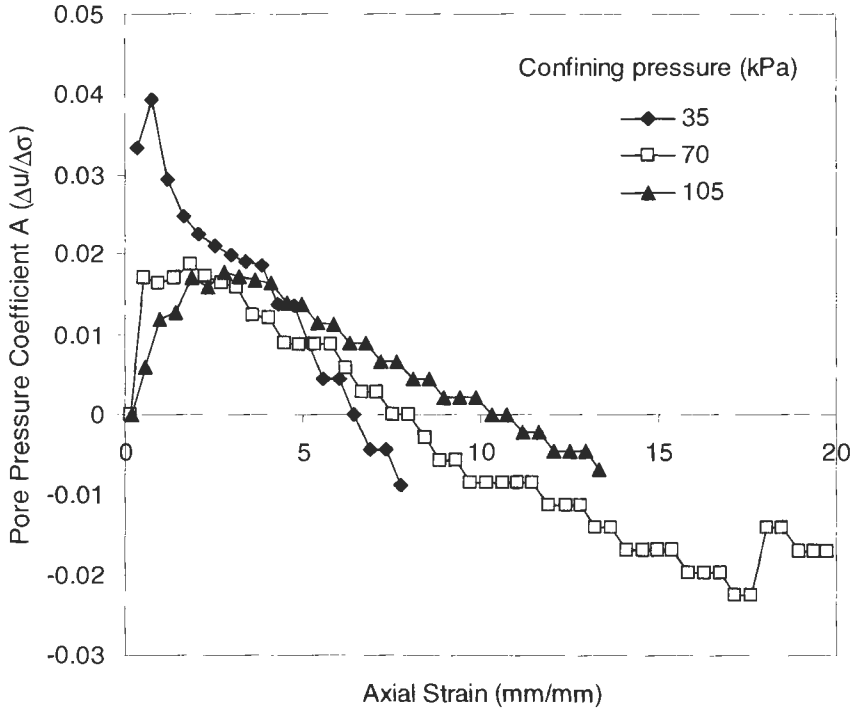

Figure D42. Pore pressure coefficient A as a function of axial strain for WF triaxial specimens at compaction energy of 355 kJ/m^3 and moisture content of 19.5%

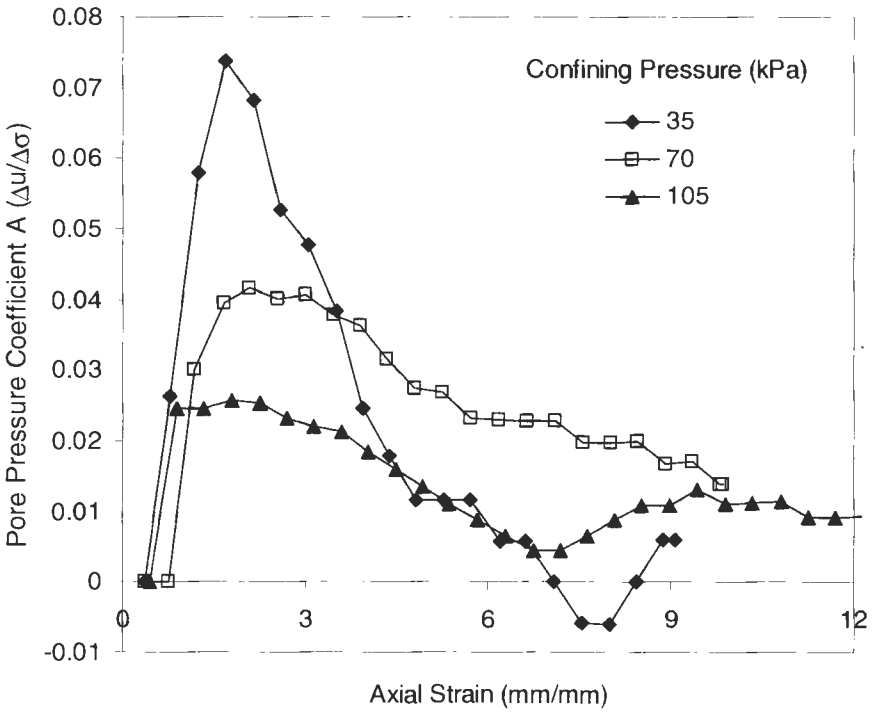

Figure D43. Pore pressure coefficient A as a function of axial strain for WF triaxial specimens at compaction energy of 592 kJ/m^3 and moisture content of 18.2%

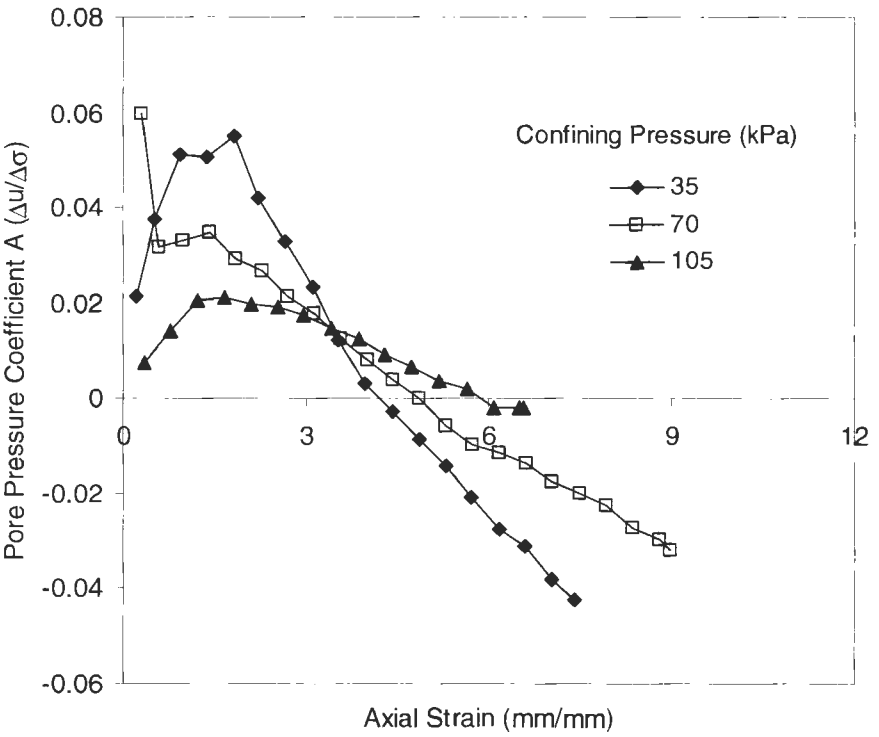

Figure D44. Pore pressure coefficient A as a function of axial strain for WF triaxial specimens at compaction energy of 2693 kJ/m^3 and moisture content of 20.1%

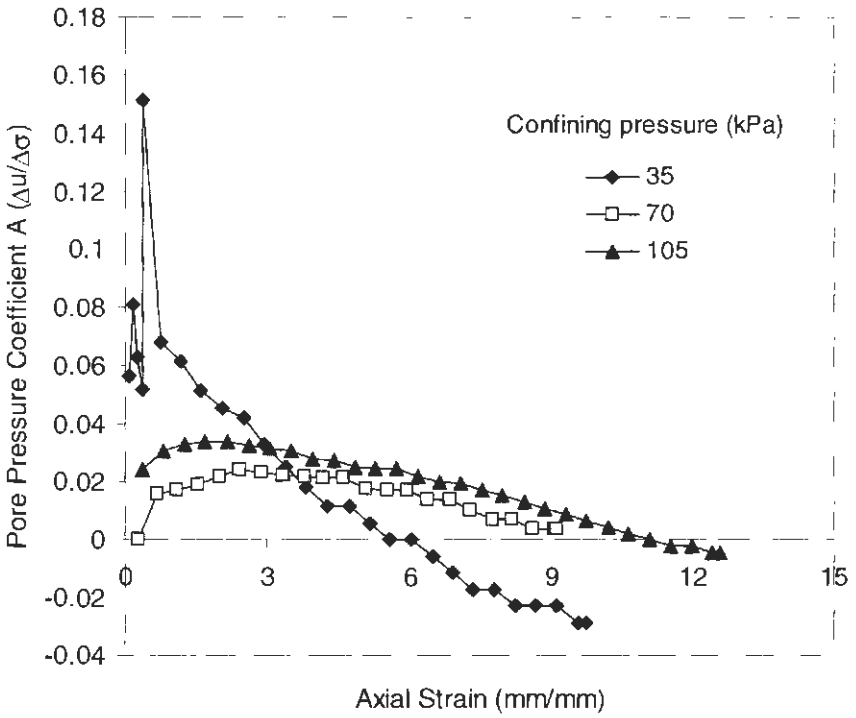

Figure D45. Pore pressure coefficient A as a function of axial strain for WF triaxial specimens at compaction energy of 355 kJ/m^3 and moisture content of 21.3%

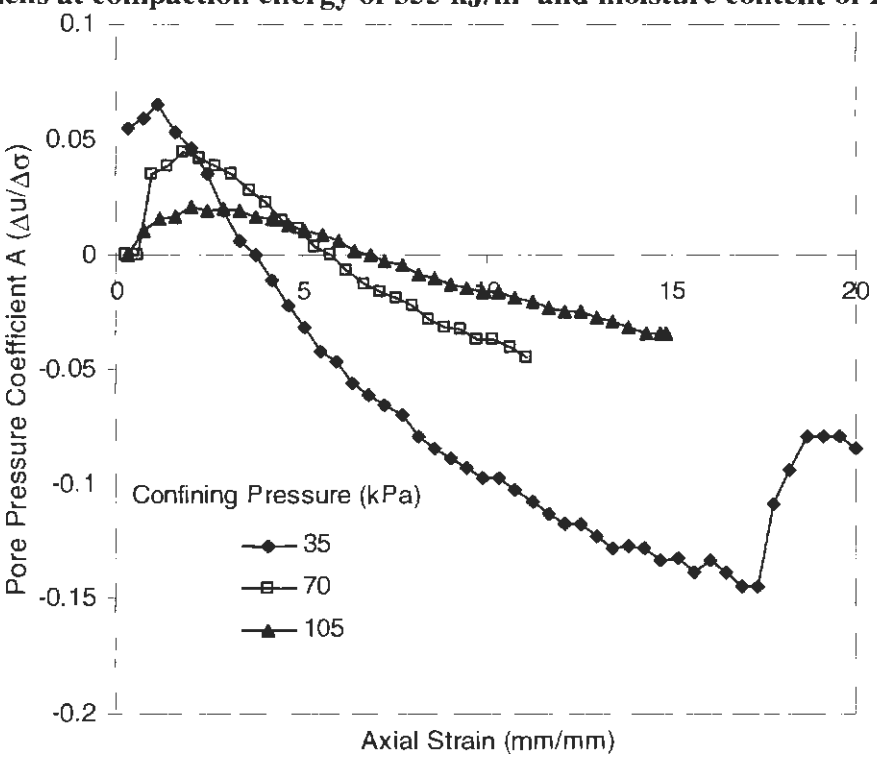

Figure D46. Pore pressure coefficient A as a function of axial strain for WF triaxial specimens at compaction energy of 592 kJ/m^3 and moisture content of 22.3%

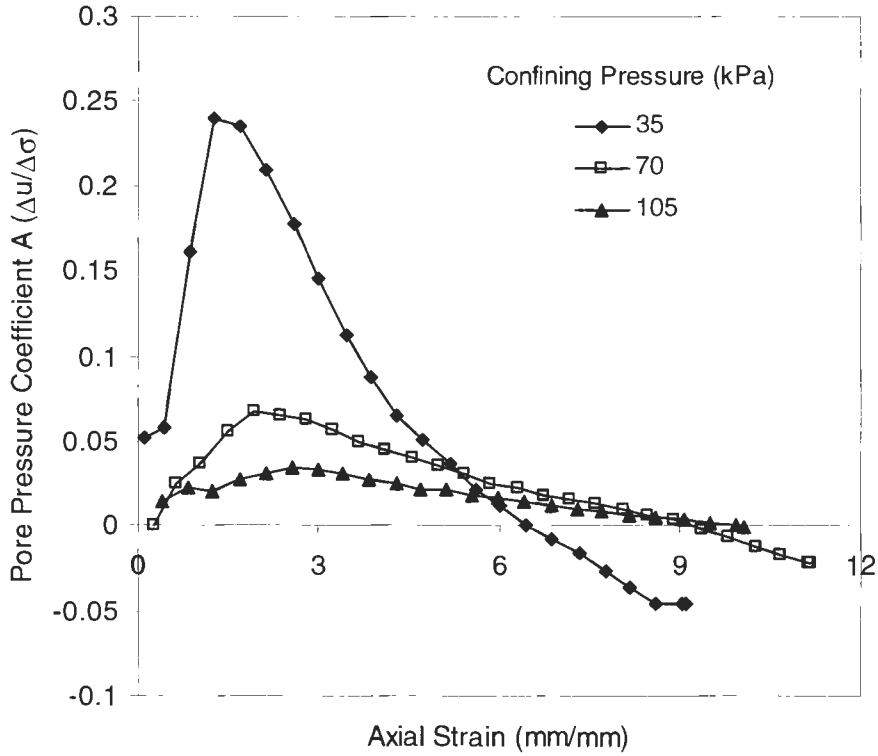

Figure D47. Pore pressure coefficient A as a function of axial strain for WF triaxial specimens at compaction energy of 2693 kJ/m^3 and moisture content of 21.7%

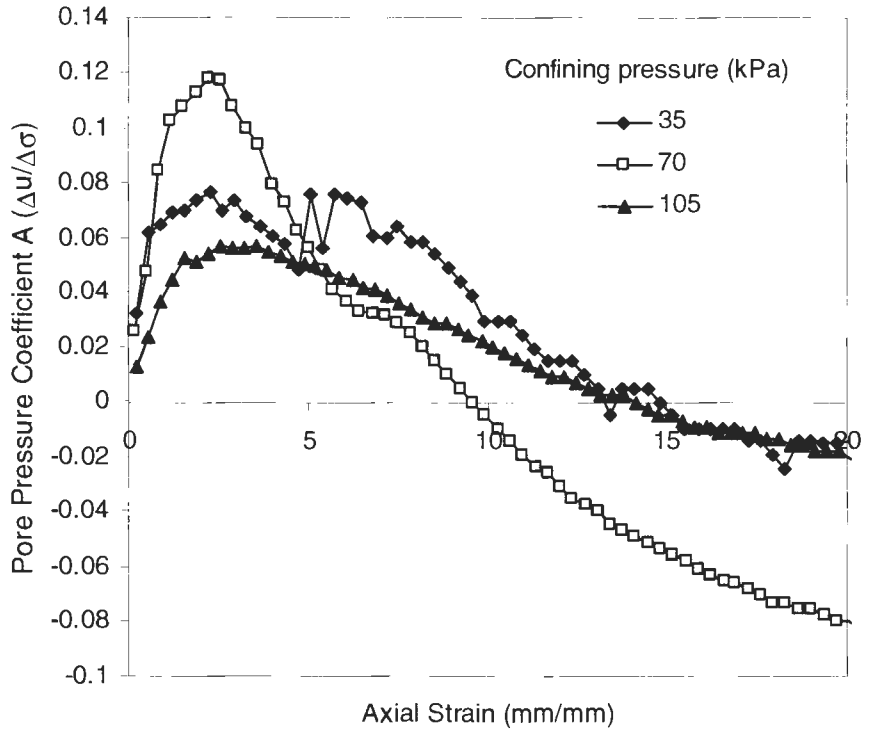

Figure D48. Pore pressure coefficient A as a function of axial strain for WF triaxial specimens at compaction energy of 355 kJ/m^3 and moisture content of 25.7%

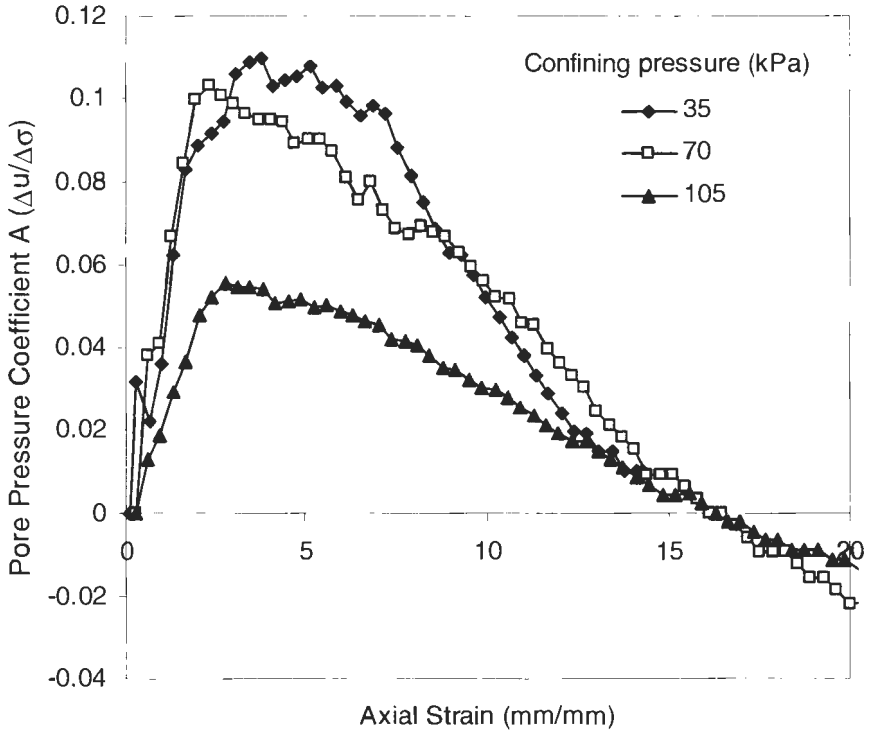

Figure D49. Pore pressure coefficient A as a function of axial strain for WF triaxial specimens at compaction energy of 592 kJ/m^3 and moisture content of 25.9%

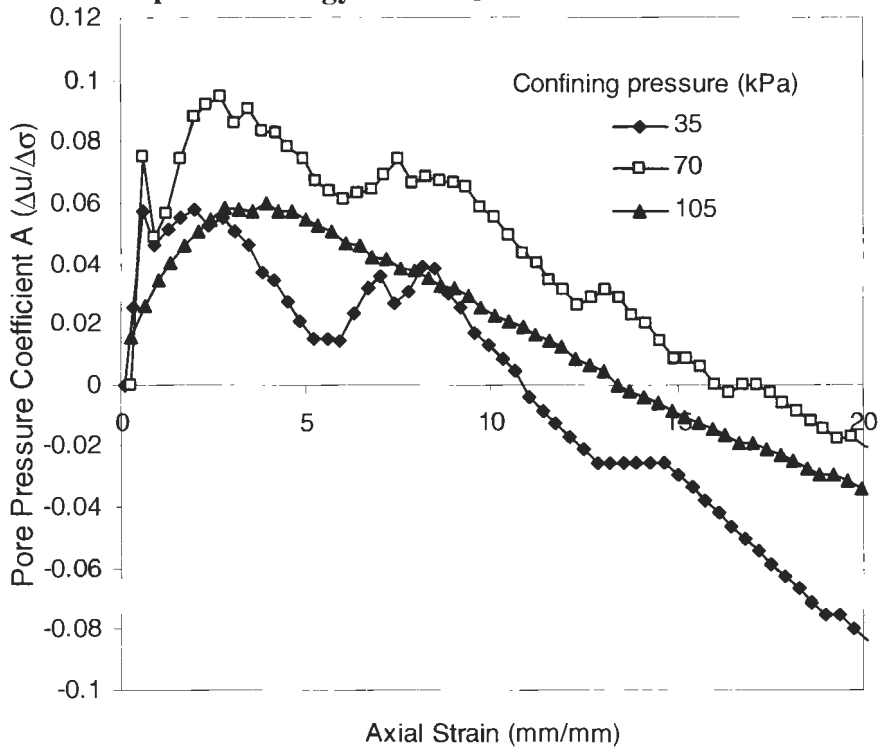

Figure D50. Pore pressure coefficient A as a function of axial strain for WF triaxial specimens at compaction energy of 987 kJ/m^3 and moisture content of 25.6%

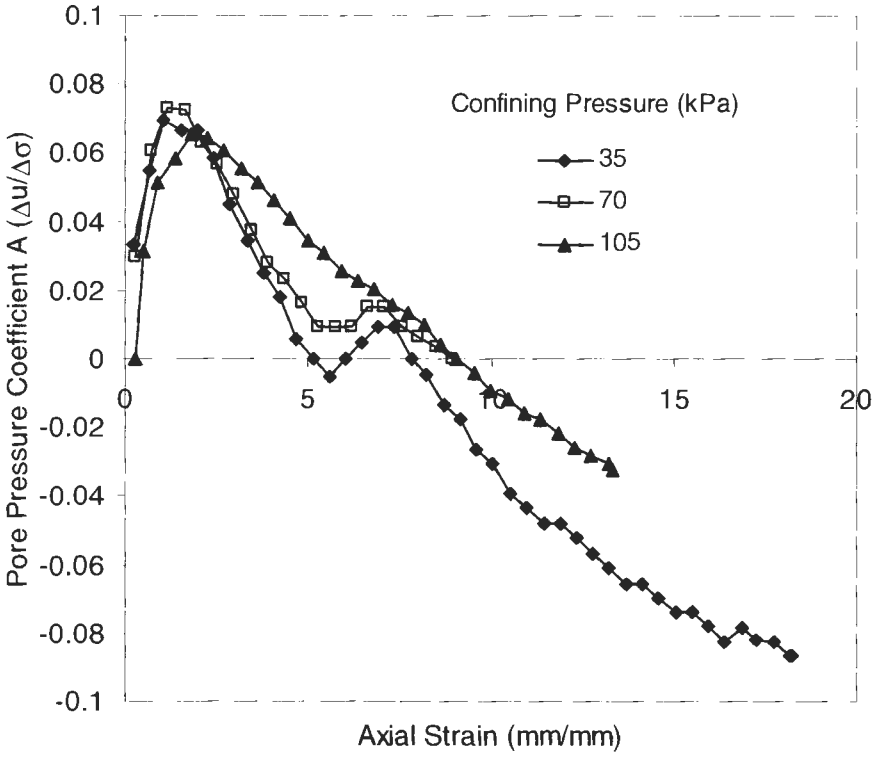

Figure D51. Pore pressure coefficient A as a function of axial strain for WF triaxial specimens at compaction energy of 1643 kJ/m^3 and moisture content of 25.5%

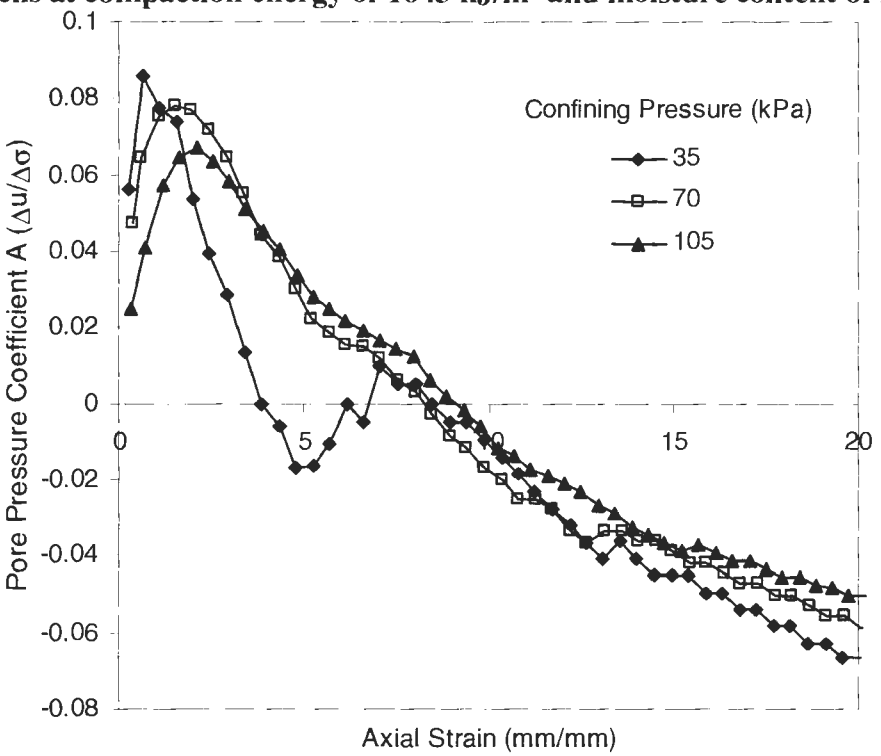

Figure D52. Pore pressure coefficient A as a function of axial strain for WF triaxial specimens at compaction energy of 2693 kJ/m^3 and moisture content of 25.7%

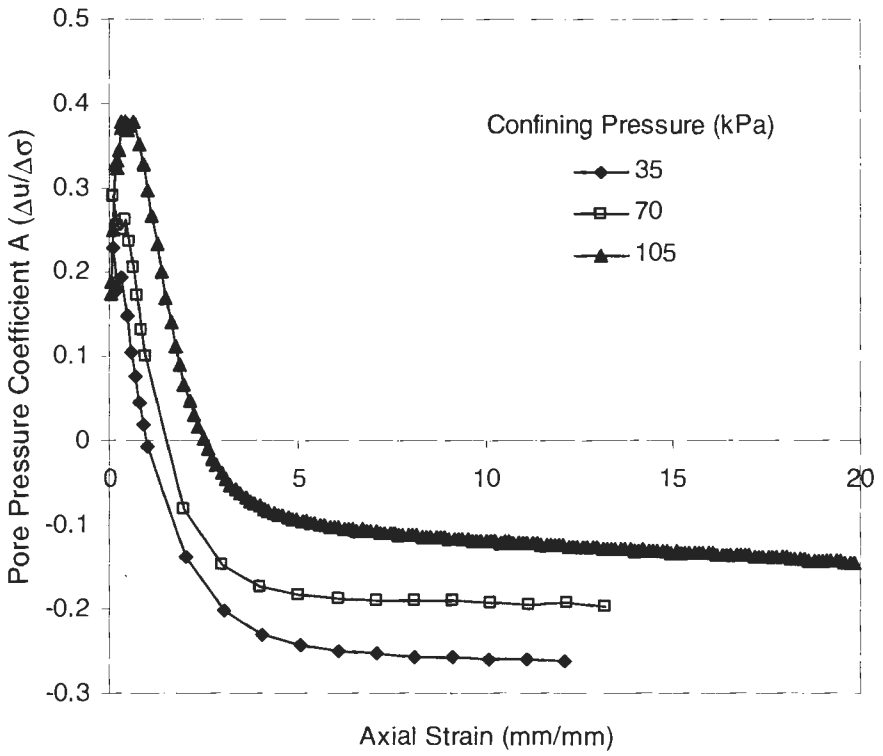

Figure D53. Pore pressure coefficient A as a function of axial strain for ELE triaxial specimens at compaction energy of 592 kJ/m^3 and moisture content of 18.9%

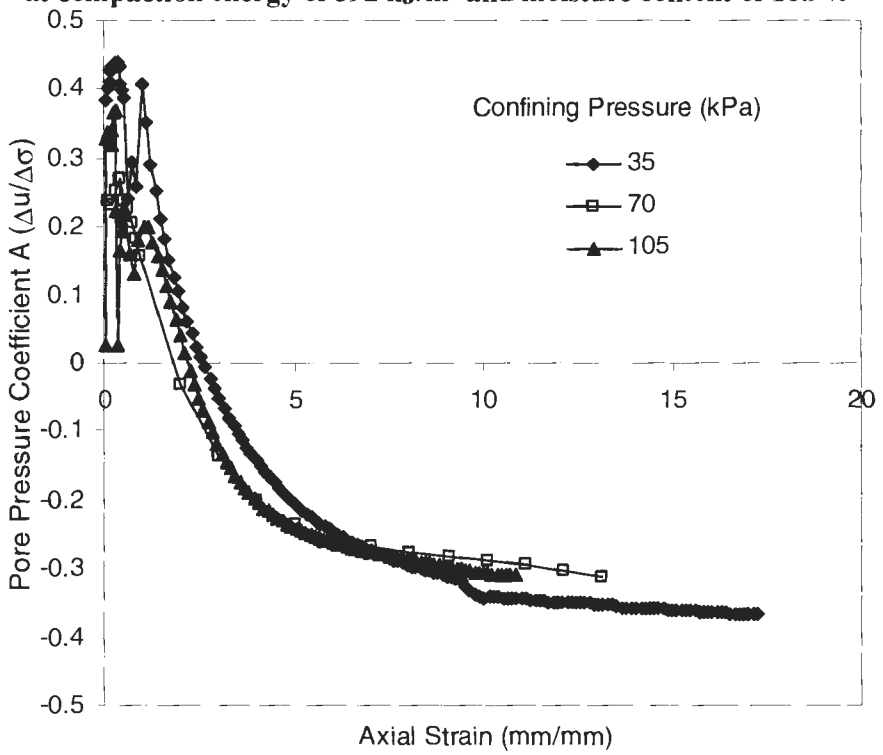

Figure D54. Pore pressure coefficient A as a function of axial strain for ELE triaxial specimens at compaction energy of 2693 kJ/m^3 and moisture content of 18.1%

APPENDIX E. TRIAX REGRESSION FIGURES

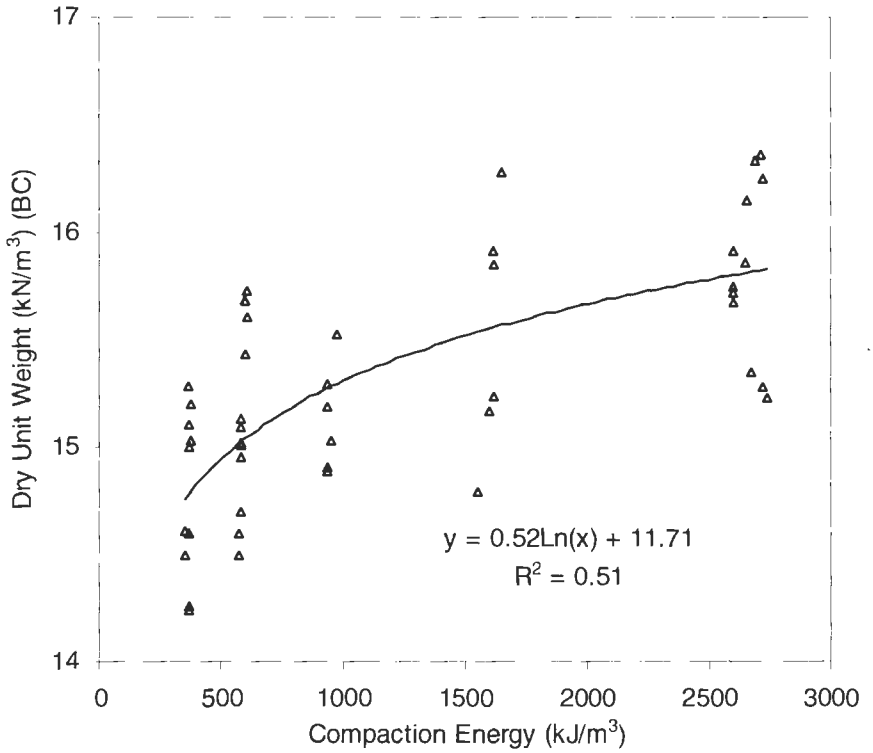

Figure E1. Regression of initial dry unit weight with compaction energy for WF triax

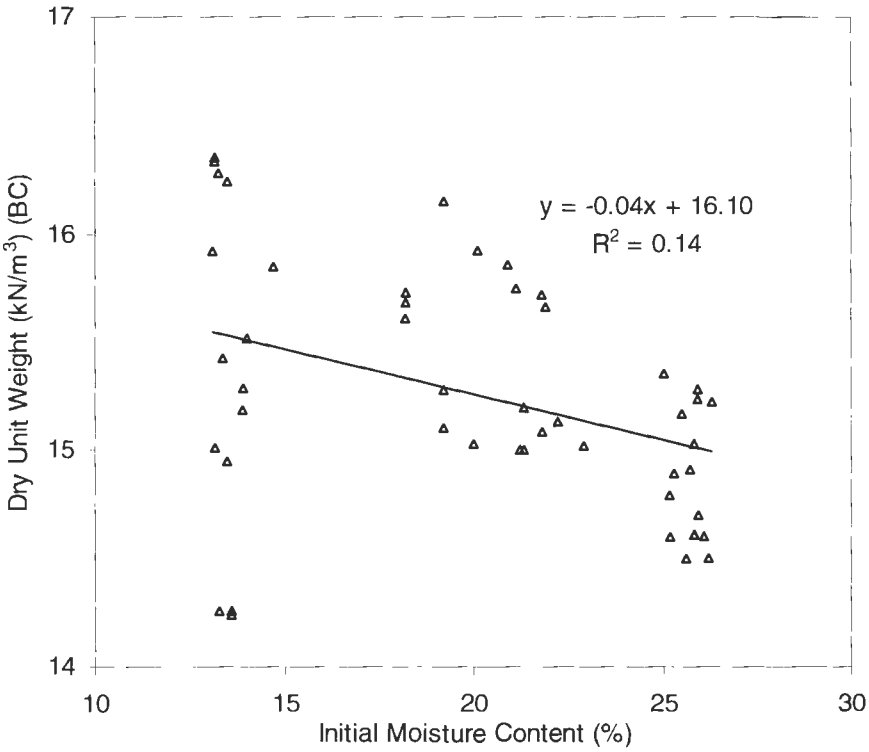

Figure E2. Regression of initial dry unit weight with initial moisture content for WF triax

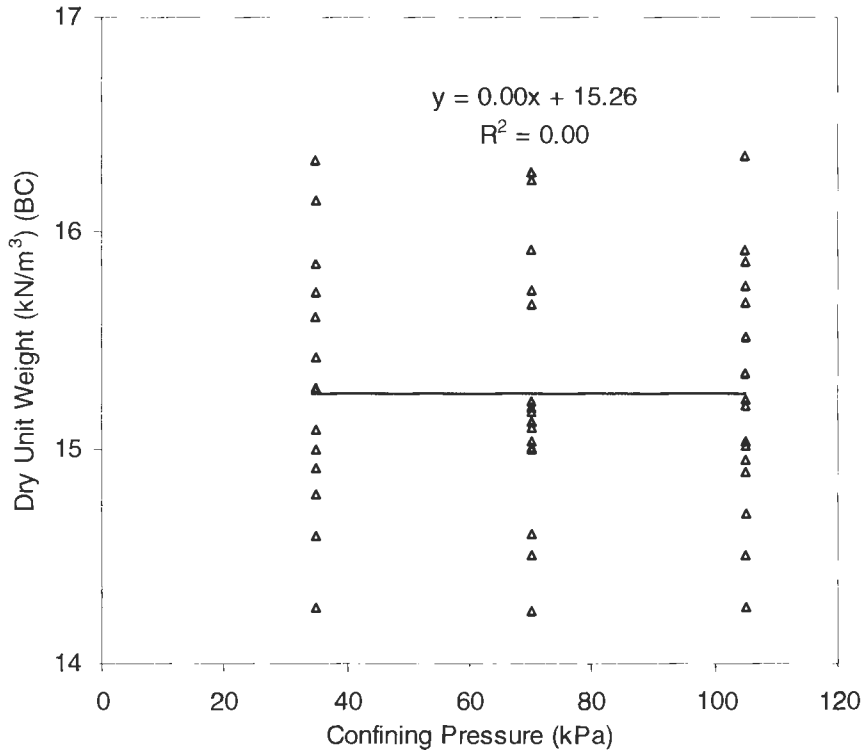

Figure E3. Regression of initial dry unit weight with confining pressure for WF triax

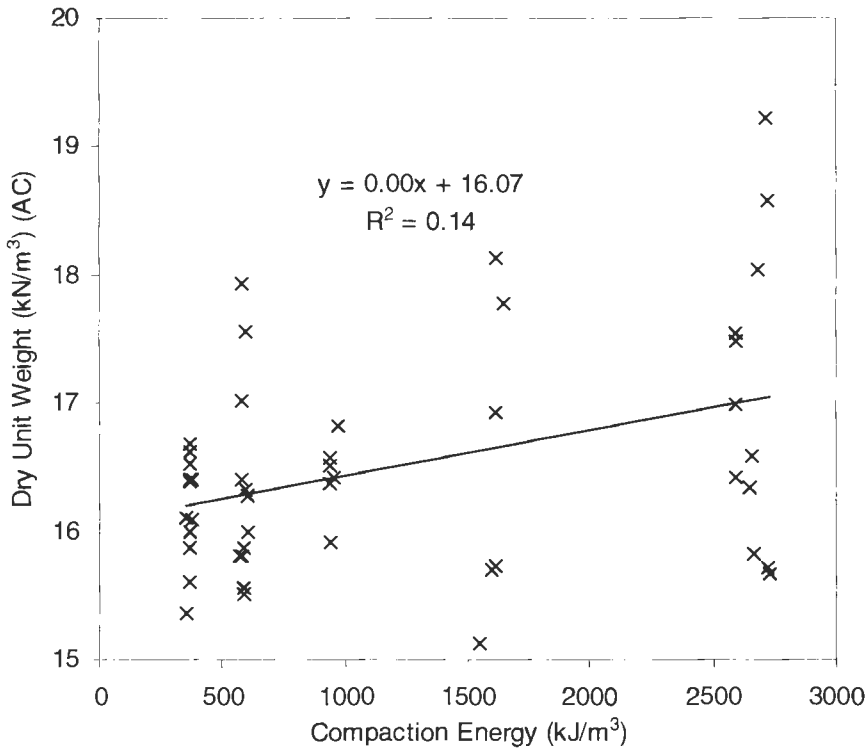

Figure E4. Regression of final dry unit weight with compaction energy for WF triax

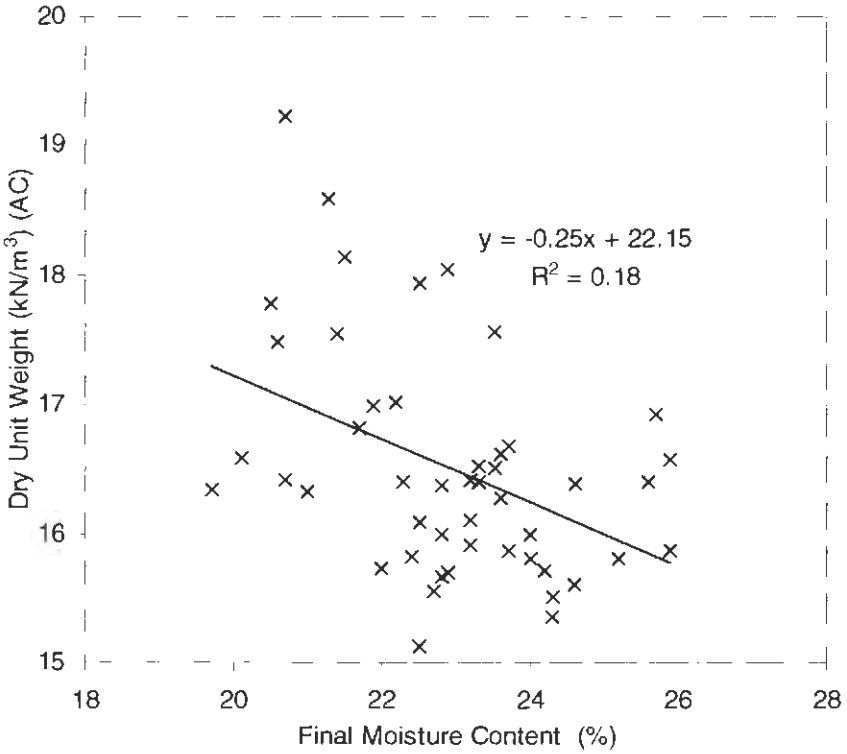

Figure E5. Regression of final dry unit weight with final moisture content for WF triax

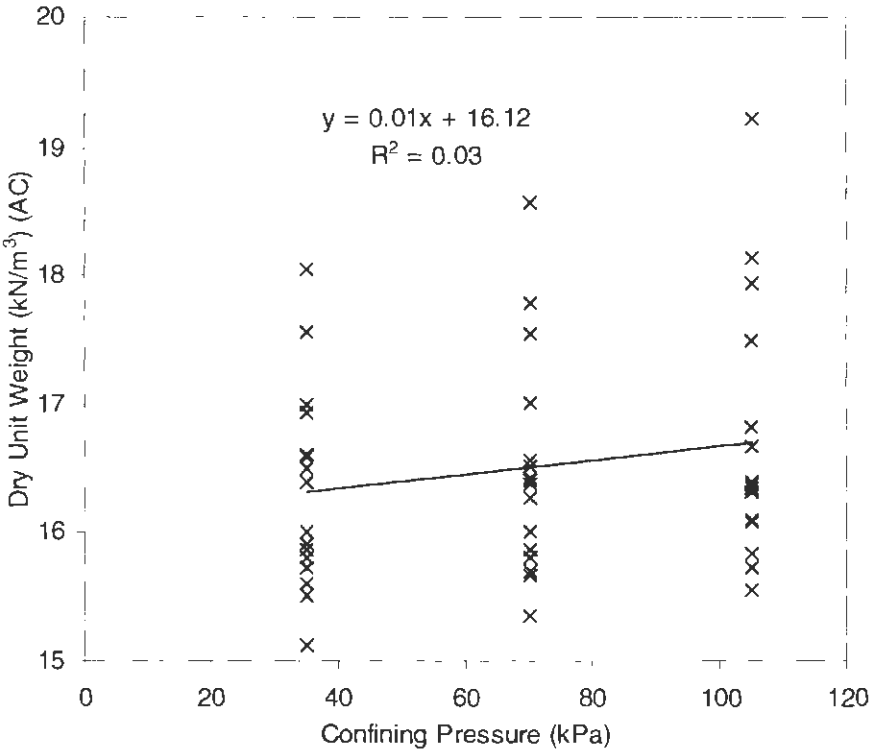

Figure E6. Regression of final dry unit weight with confining pressure for WF triax

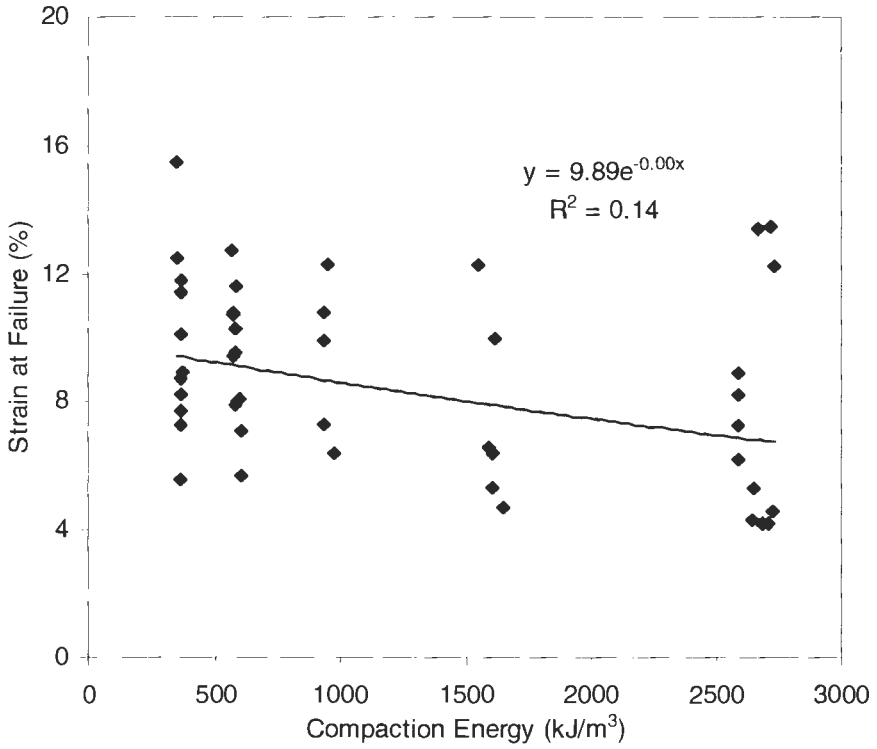

Figure E7. Regression of strain at failure with compaction energy for WF triax

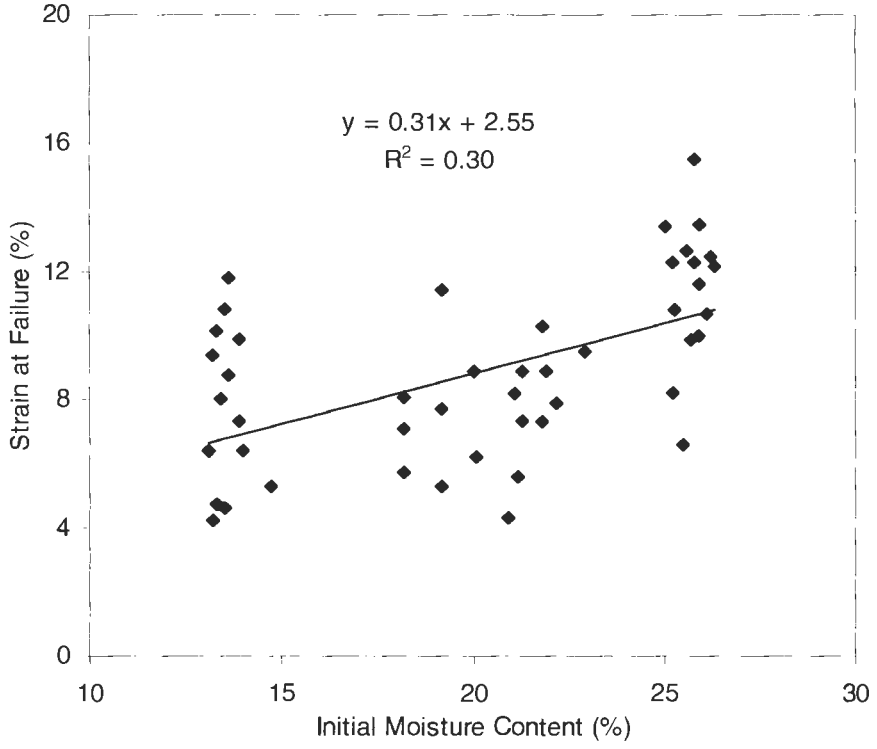

Figure E8. Regression of strain at failure with initial moisture content for WF triax

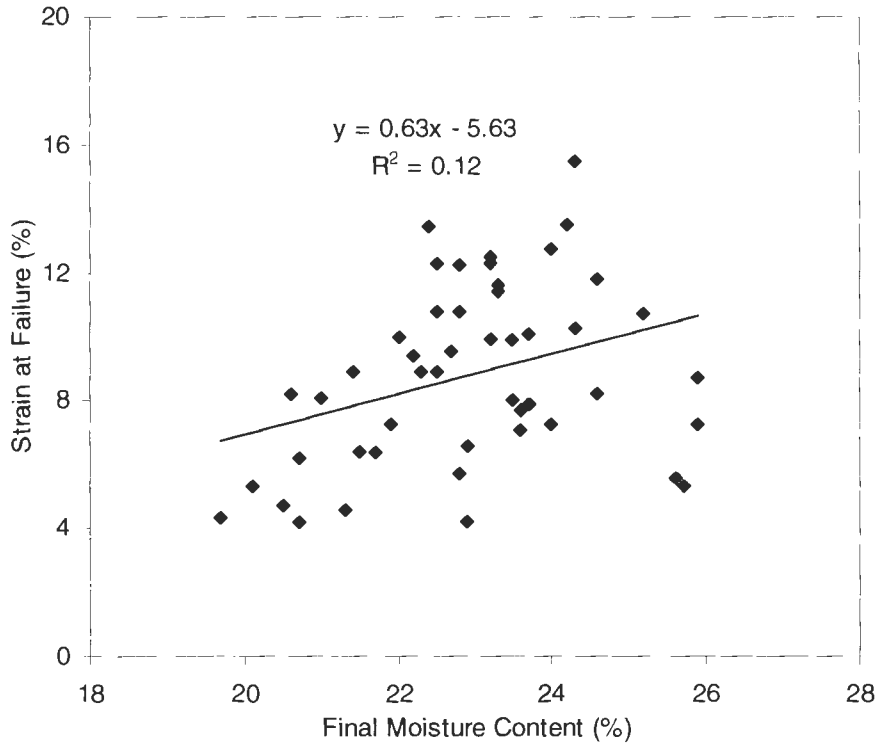

Figure E9. Regression of strain at failure with final moisture content for WF triax

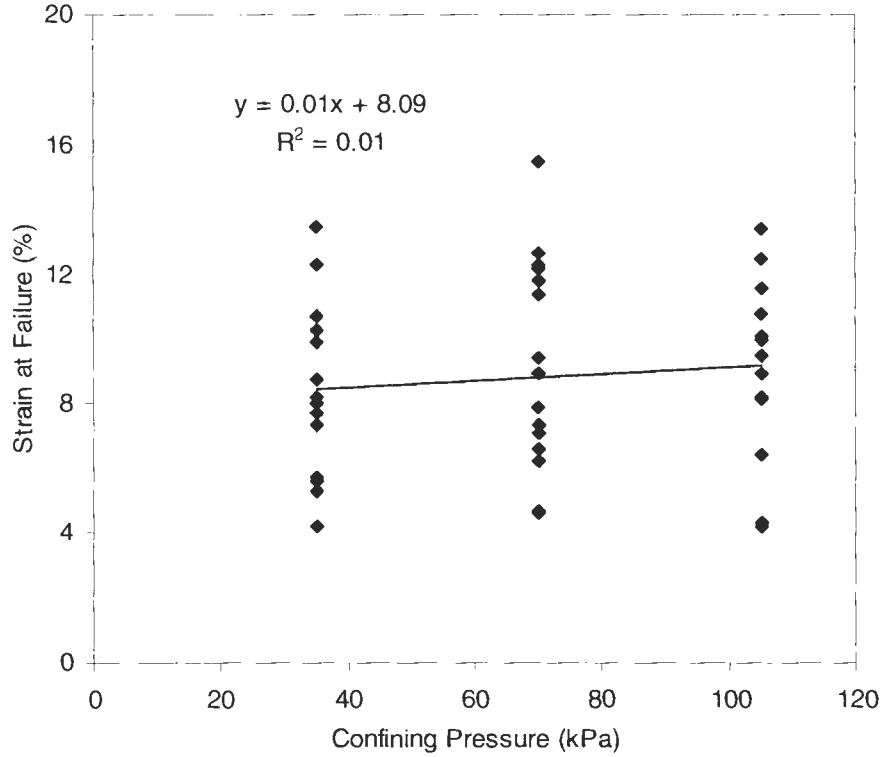

Figure E10. Regression of strain at failure with confining pressure for WF triax

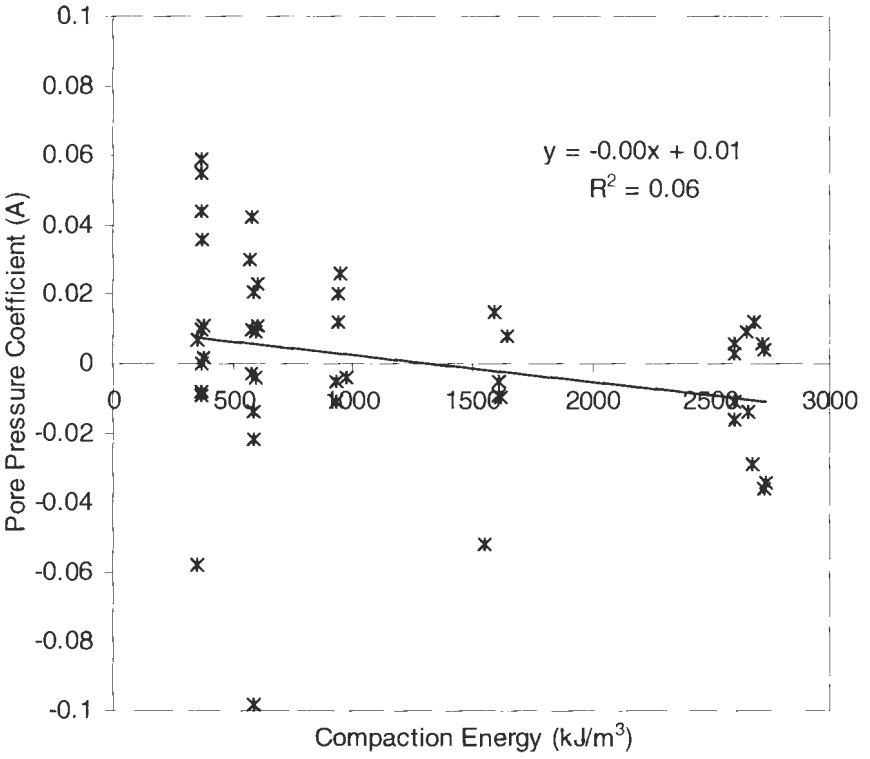

Figure E11. Regression of pore pressure coefficient A with compaction energy for WF triax

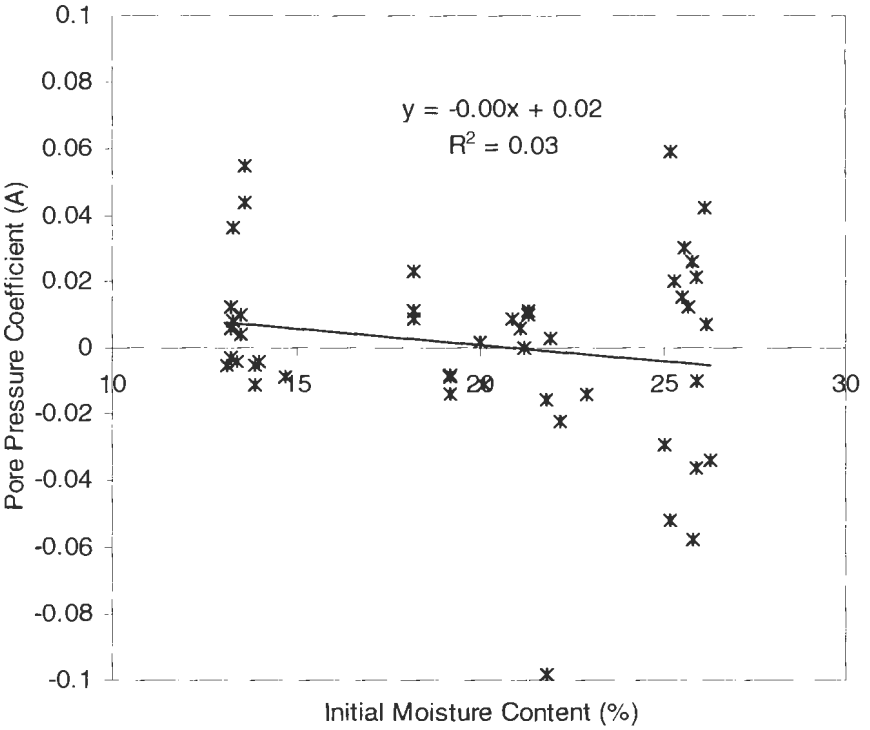

Figure E12. Regression of pore pressure coefficient A with initial moisture content for WF triax

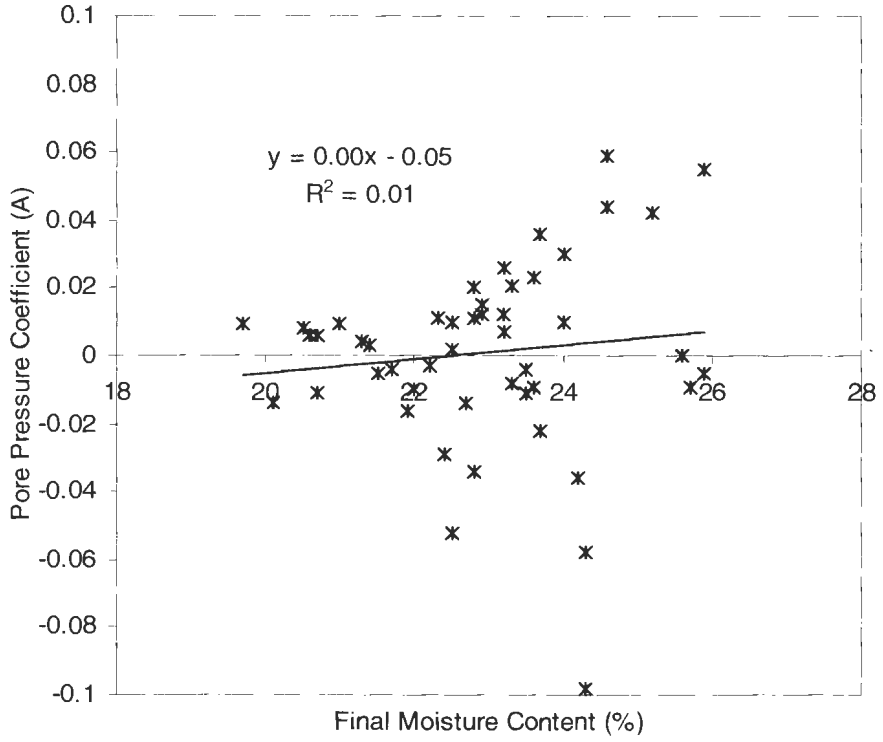

Figure E13. Regression of pore pressure coefficient A with final moisture content for WF triax

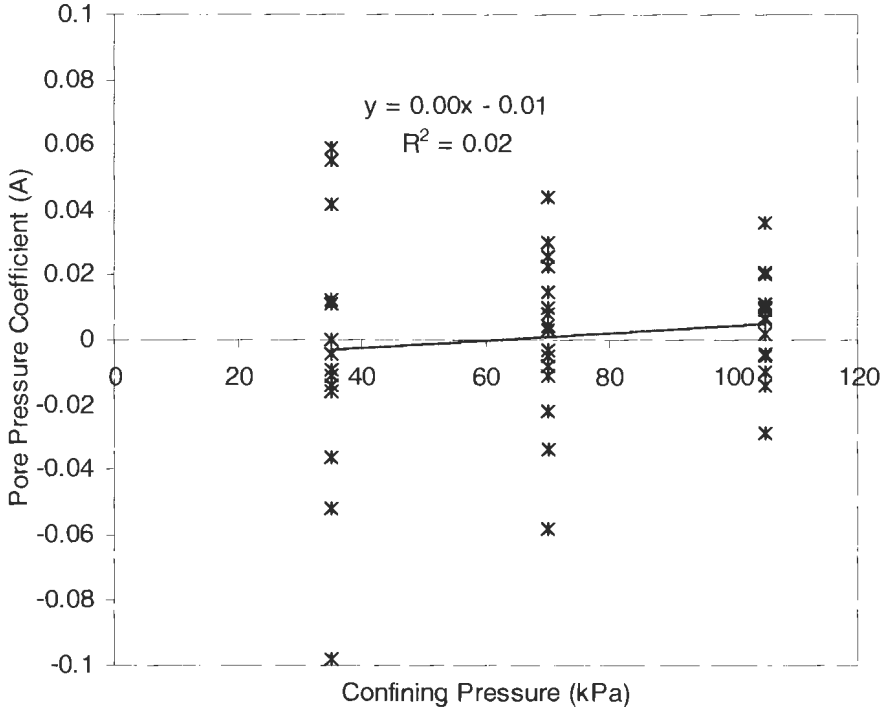

Figure E14. Regression of pore pressure coefficient A with confining pressure for WF triax

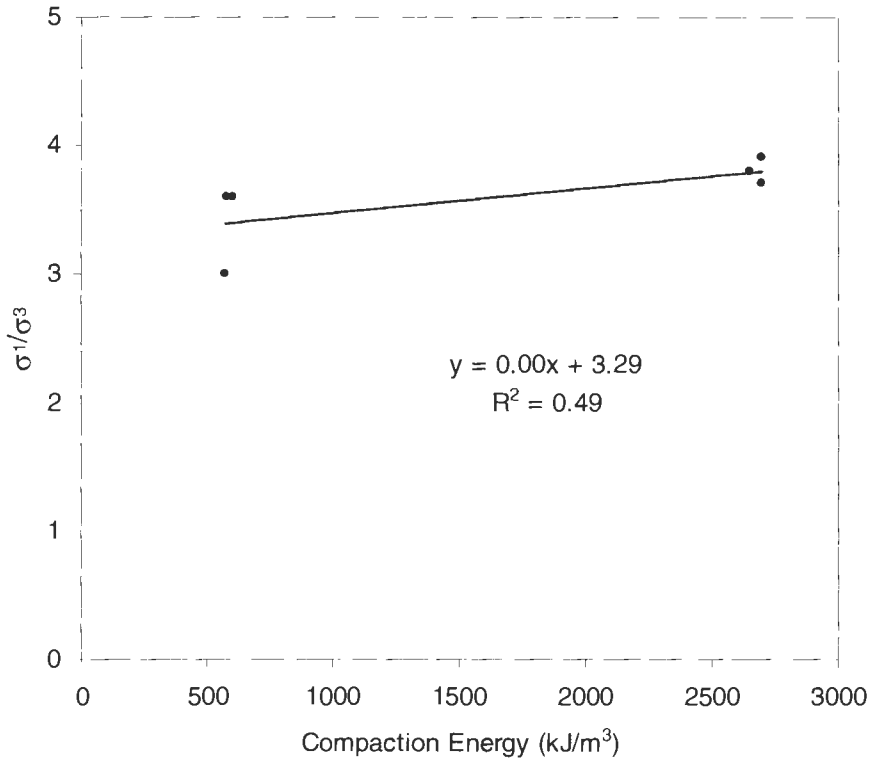

Figure E15. Regression of principal stress ratio with compaction energy for ELE triax

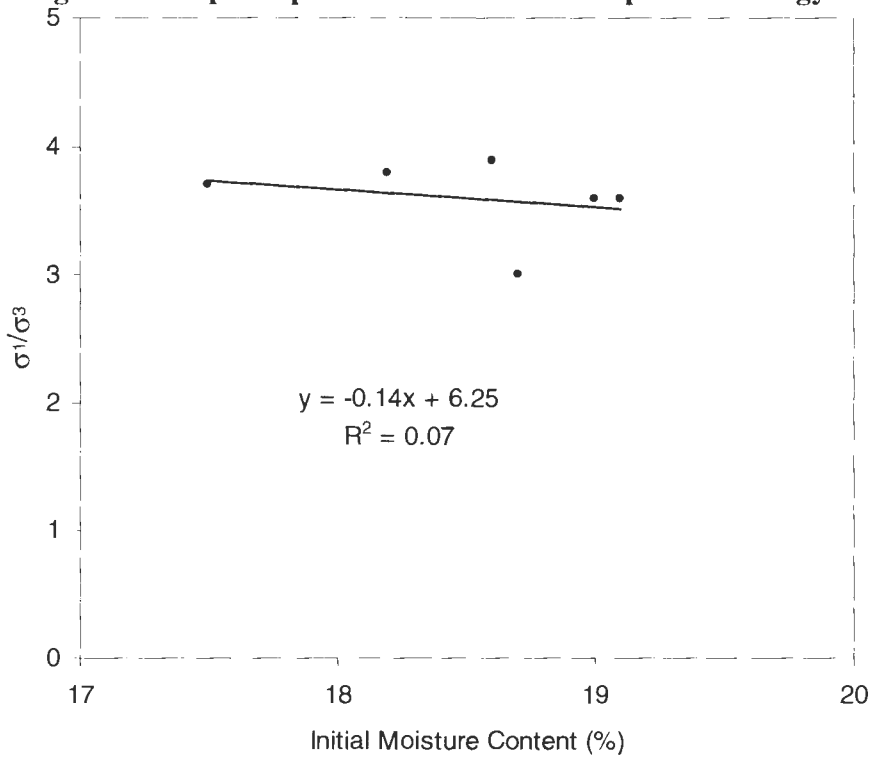

Figure E16. Regression of principal stress ratio with initial moisture content for ELE triax

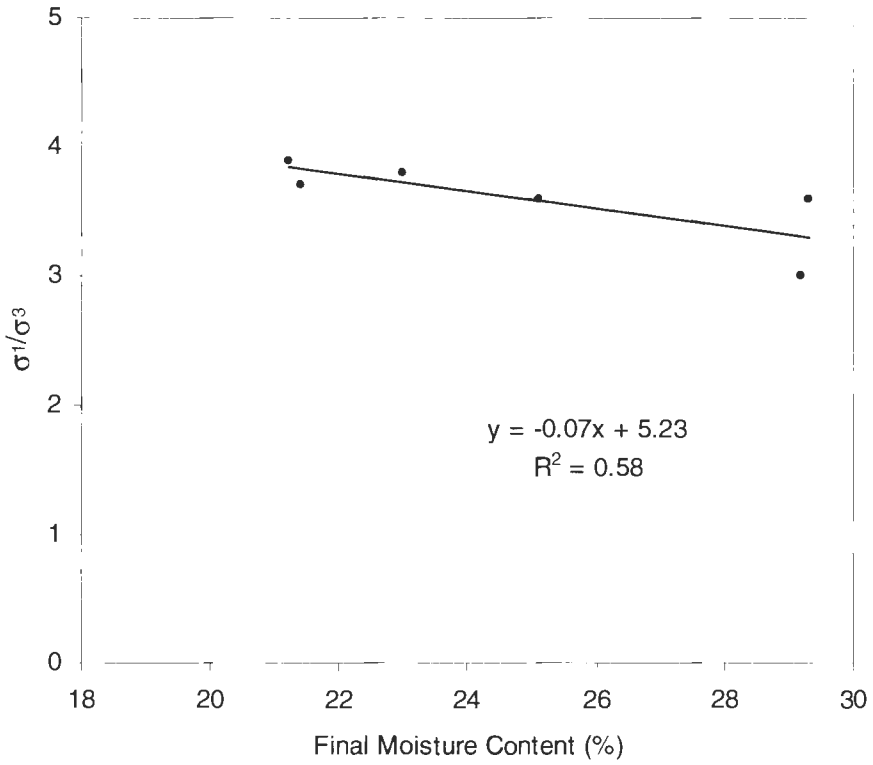

Figure E17. Regression of principal stress ratio with final moisture content for ELE triax

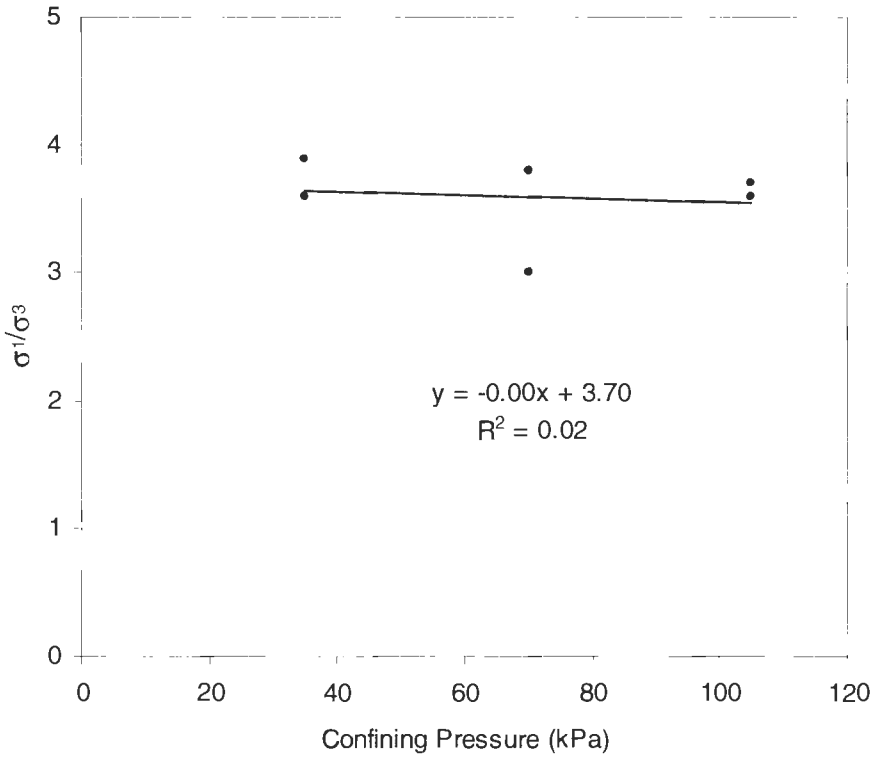

Figure E18. Regression of principal stress ratio with confining pressure for ELE triax

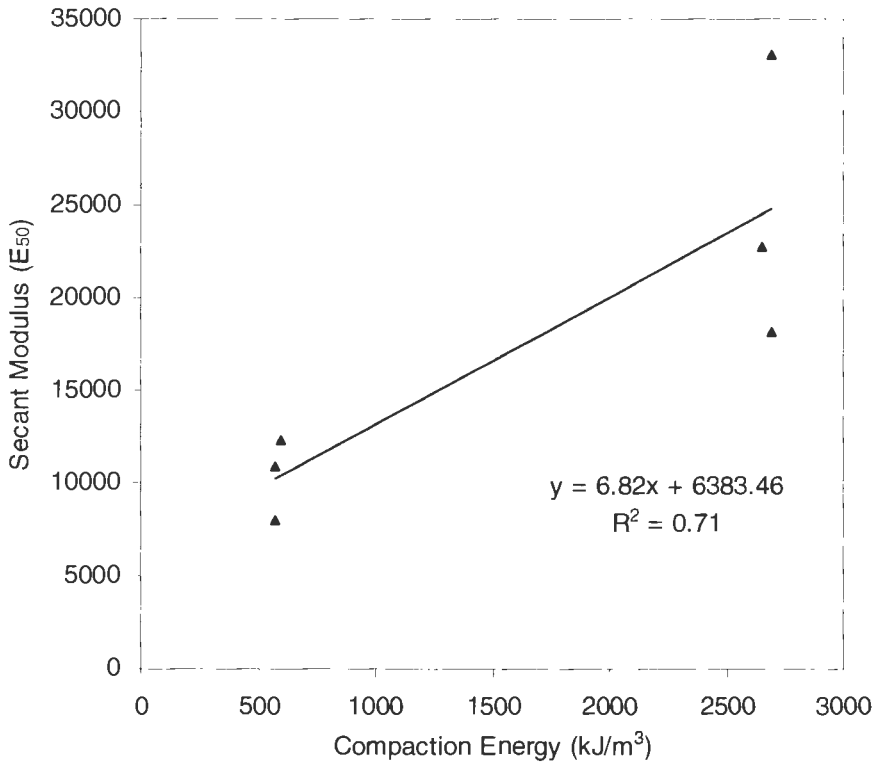

Figure E19. Regression of secant modulus with compaction energy for ELE triax

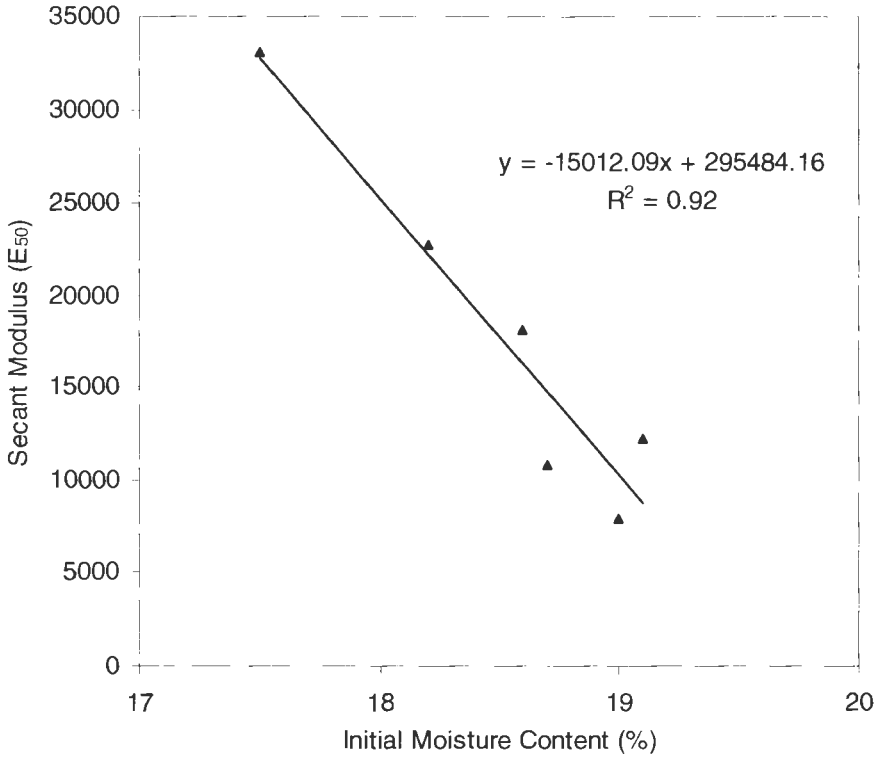

Figure E20. Regression of secant modulus with initial moisture content for ELE triax

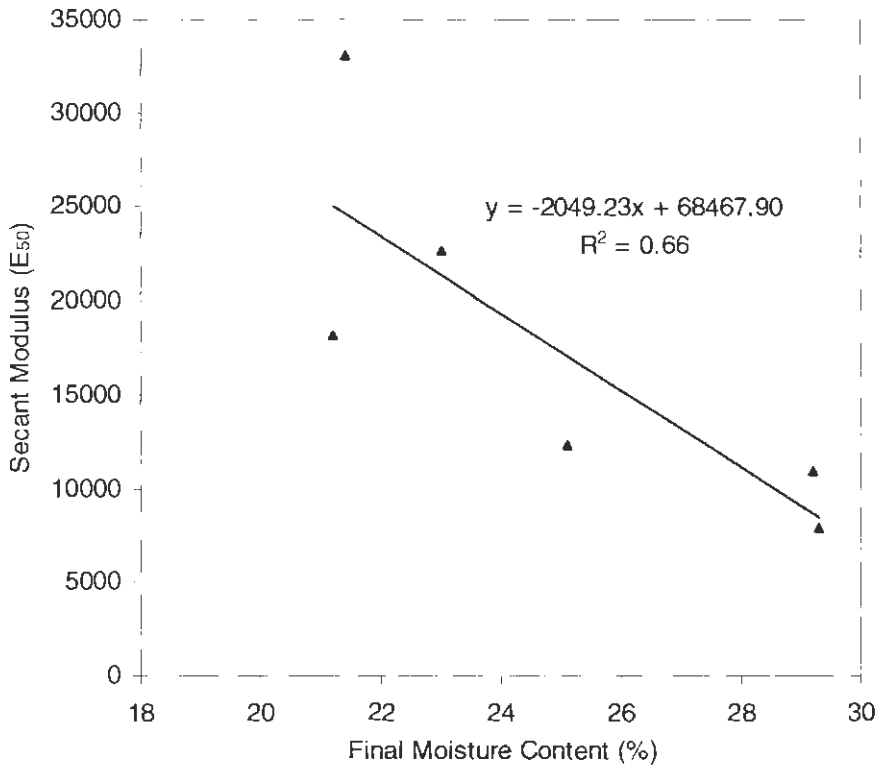

Figure E21. Regression of secant modulus with final moisture content for ELE triax

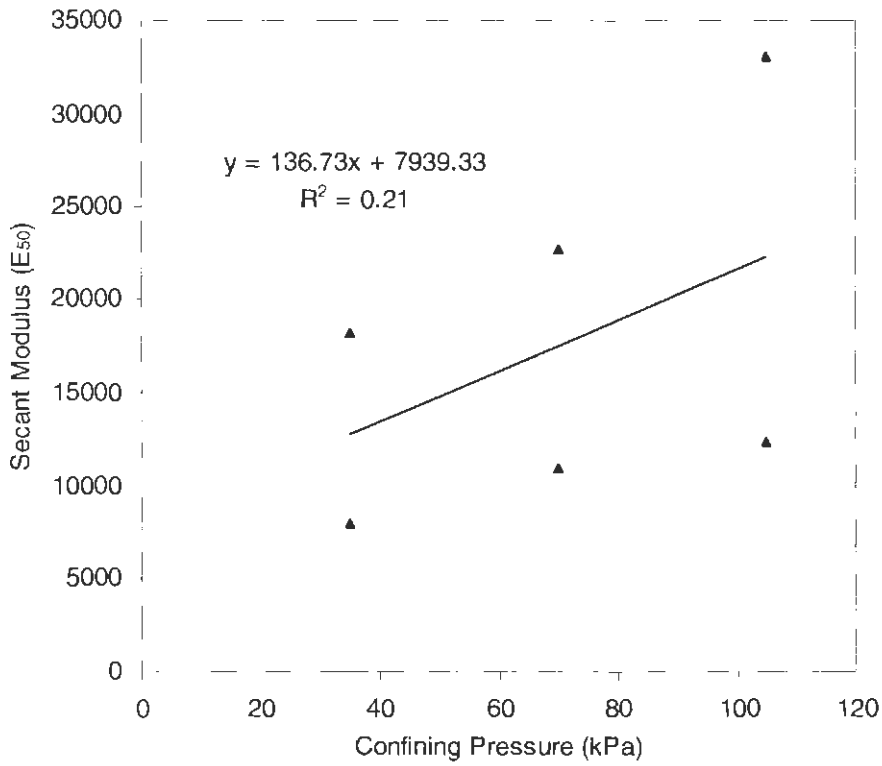

Figure E22. Regression of secant modulus with confining pressure for ELE triax

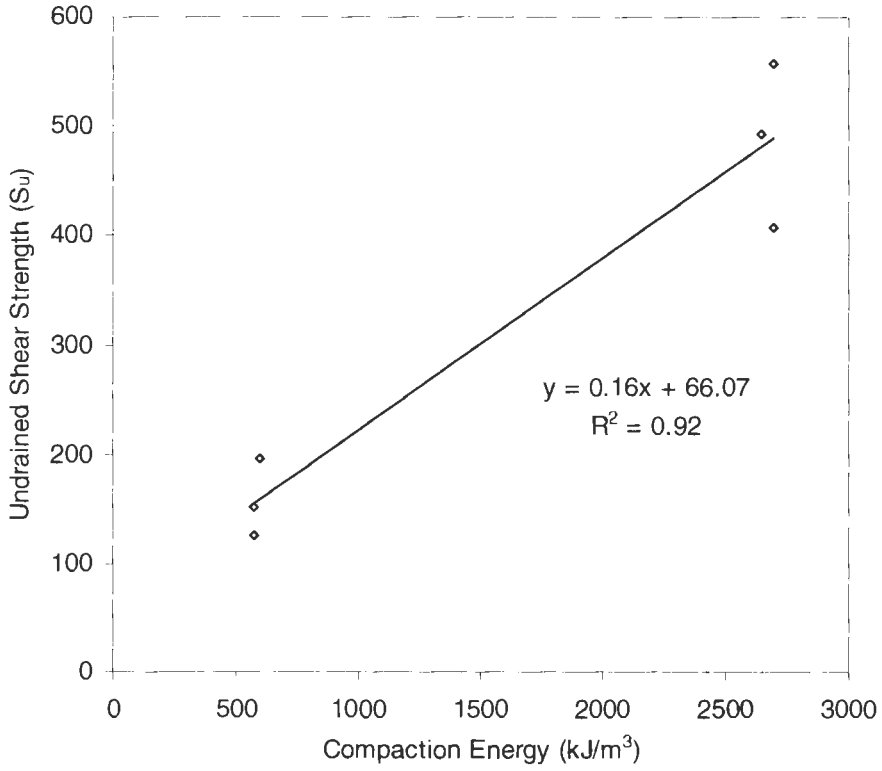

Figure E23. Regression of undrained shear strength with compaction energy for ELE triax

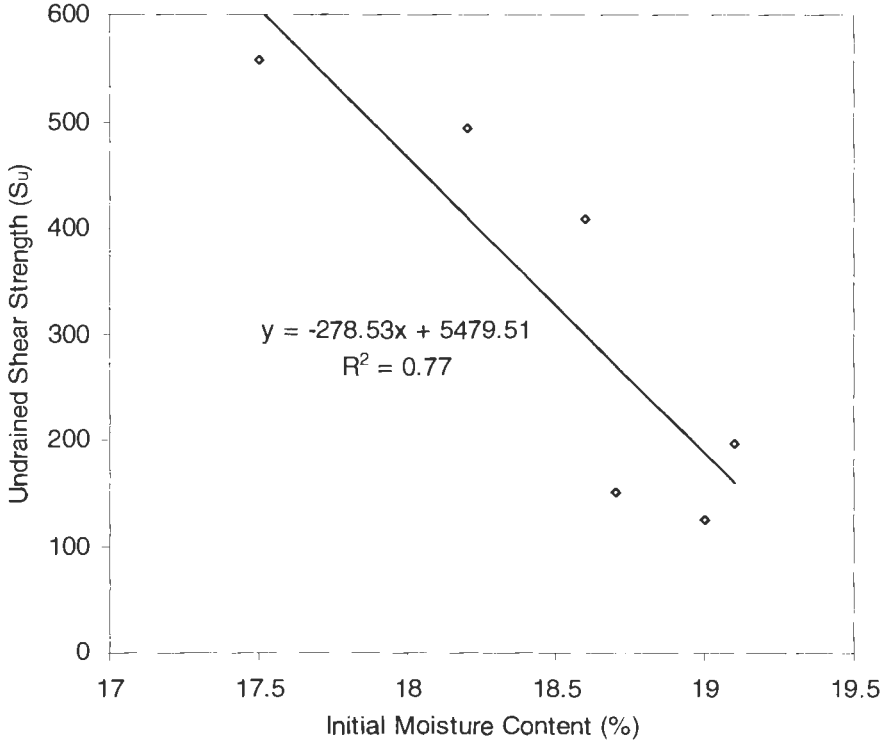

Figure E24. Regression of undrained shear strength with initial moisture content for ELE triax

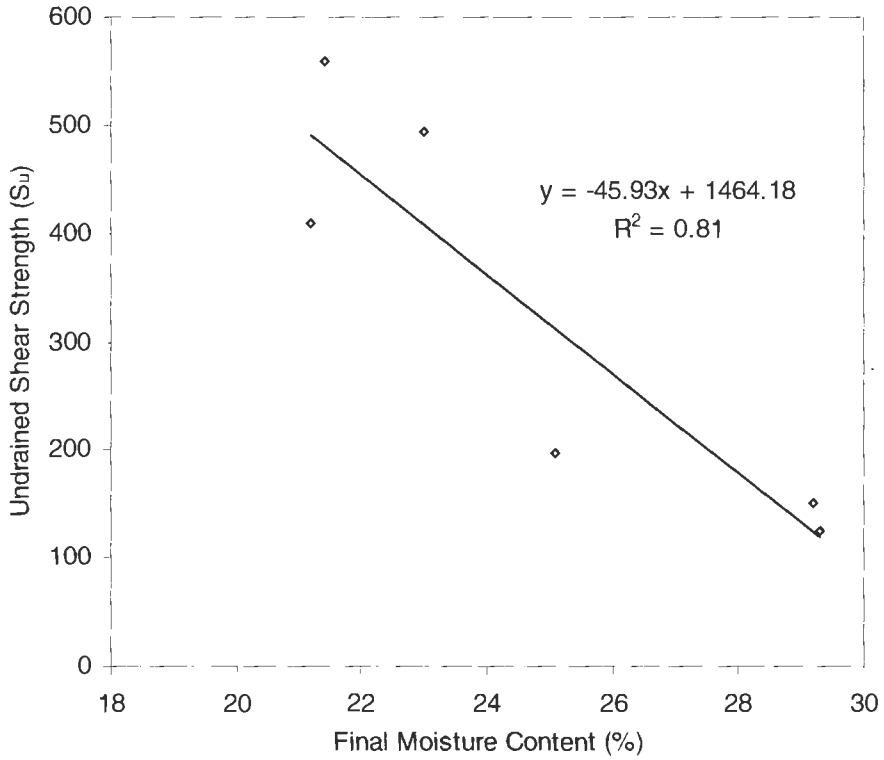

Figure E25. Regression of undrained shear strength with final moisture content for ELE triax

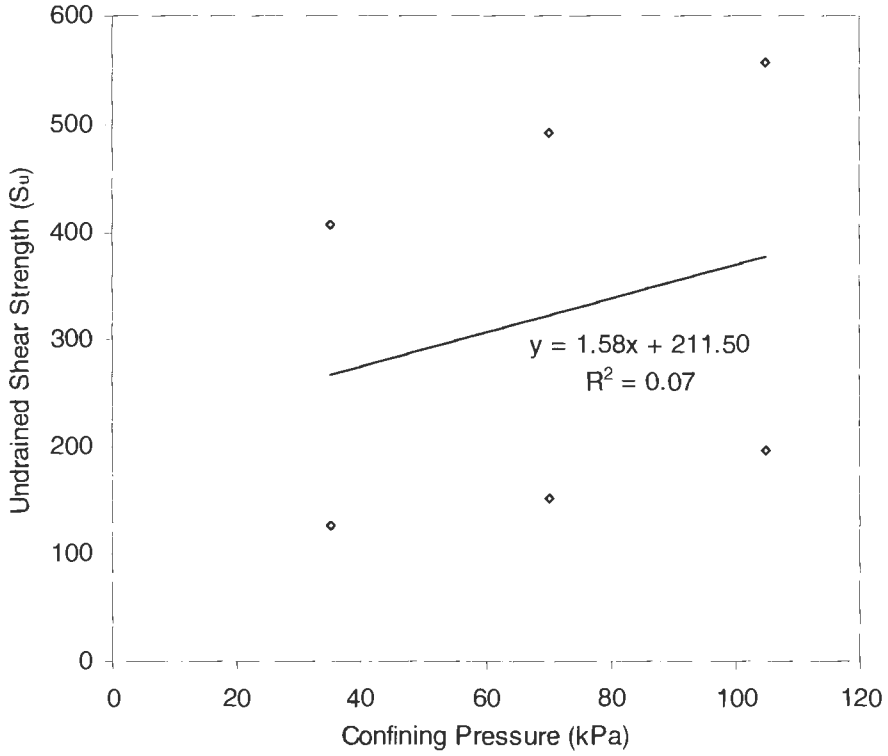

Figure E26. Regression of undrained shear strength with confining pressure for ELE triax

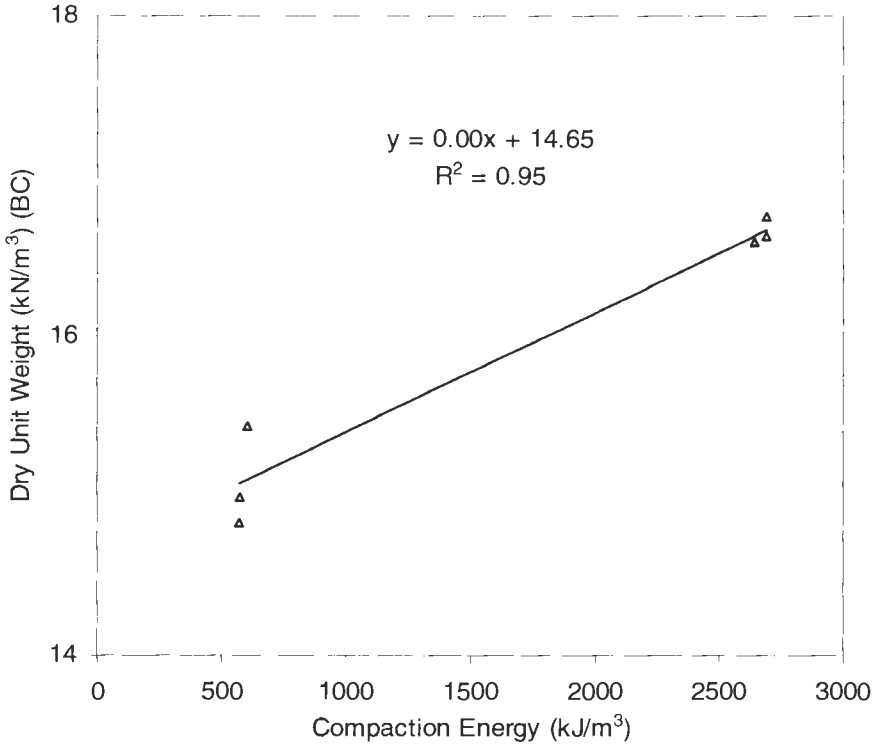

Figure E27. Regression of initial dry unit weight with compaction energy for ELE triax

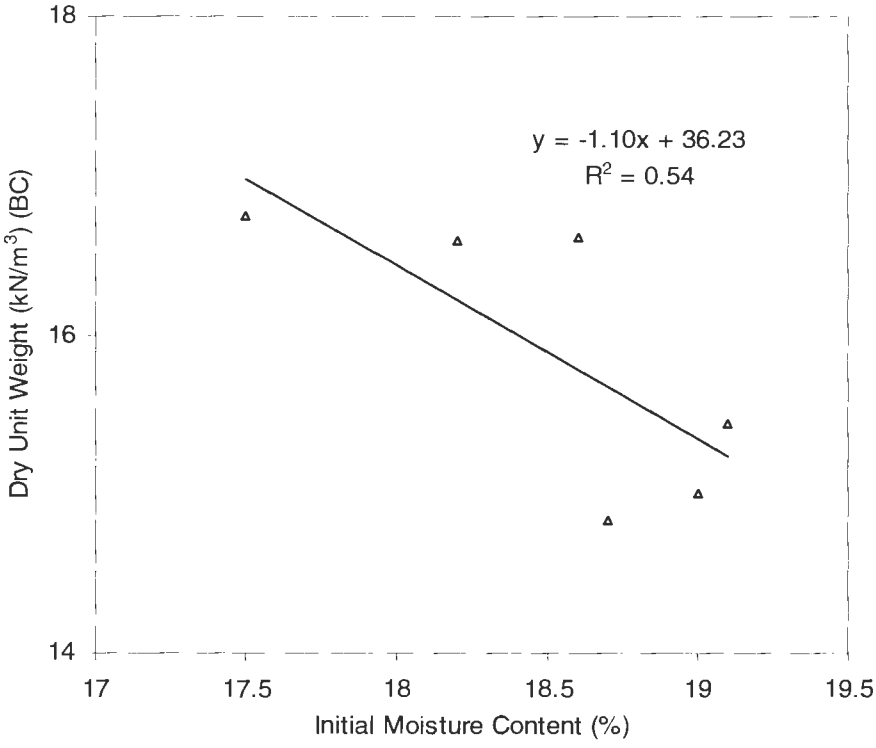

Figure E28. Regression of initial dry unit weight with initial moisture content for ELE triax

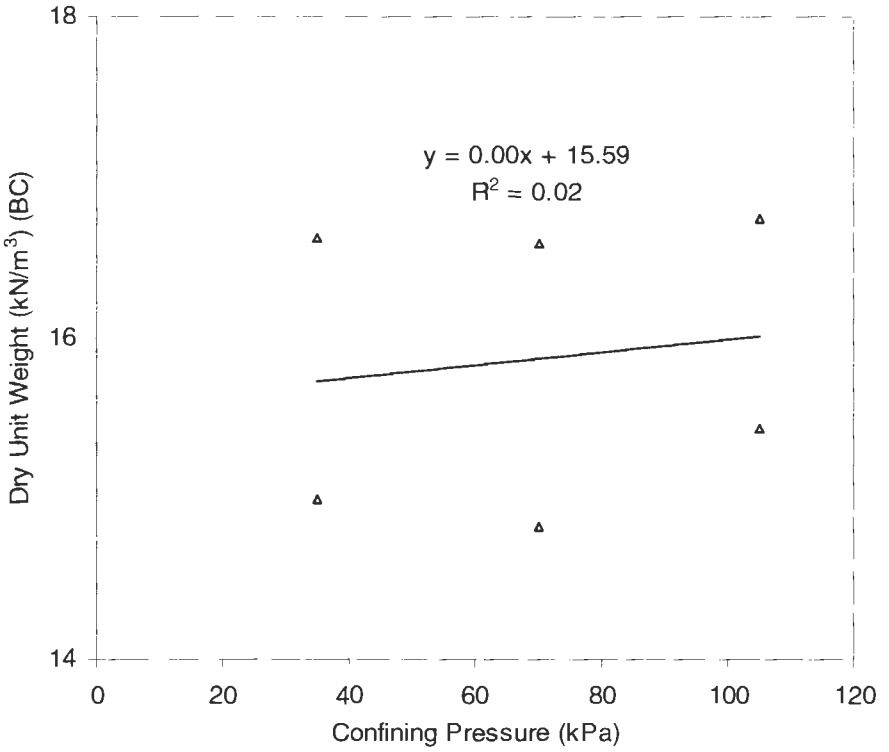

Figure E29. Regression of initial dry unit weight with confining pressure for ELE triax

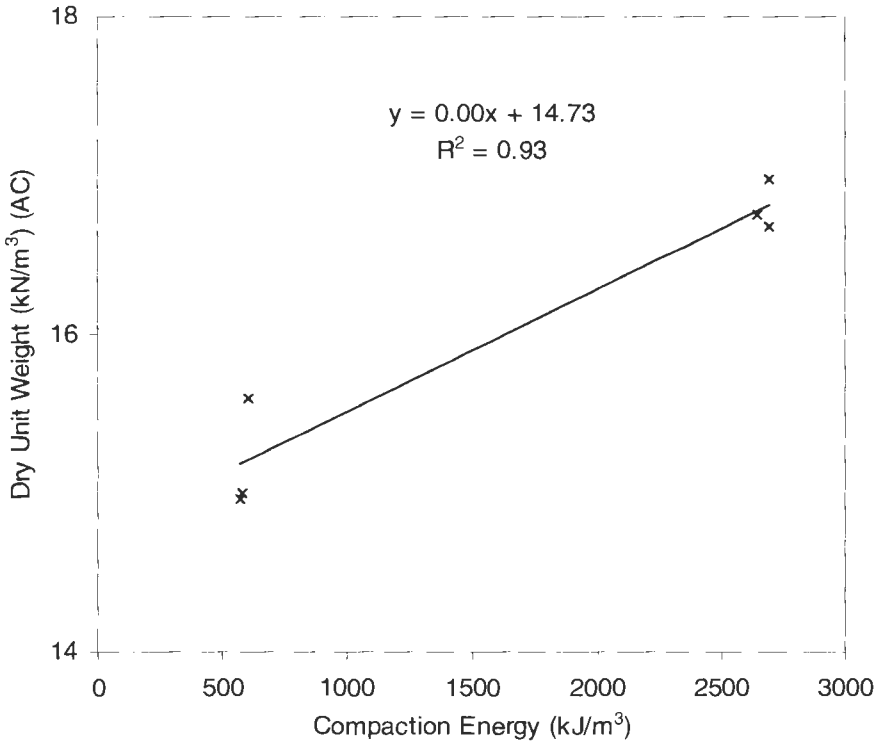

Figure E30. Regression of final dry unit weight with compaction energy for ELE triax

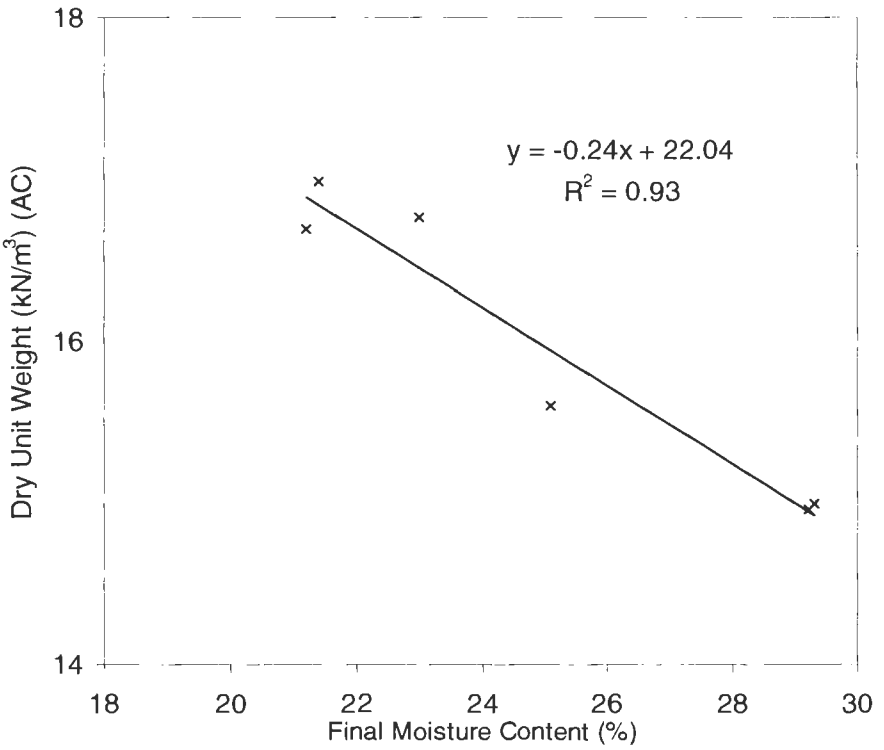

Figure E31. Regression of final dry unit weight with final moisture content for ELE triax

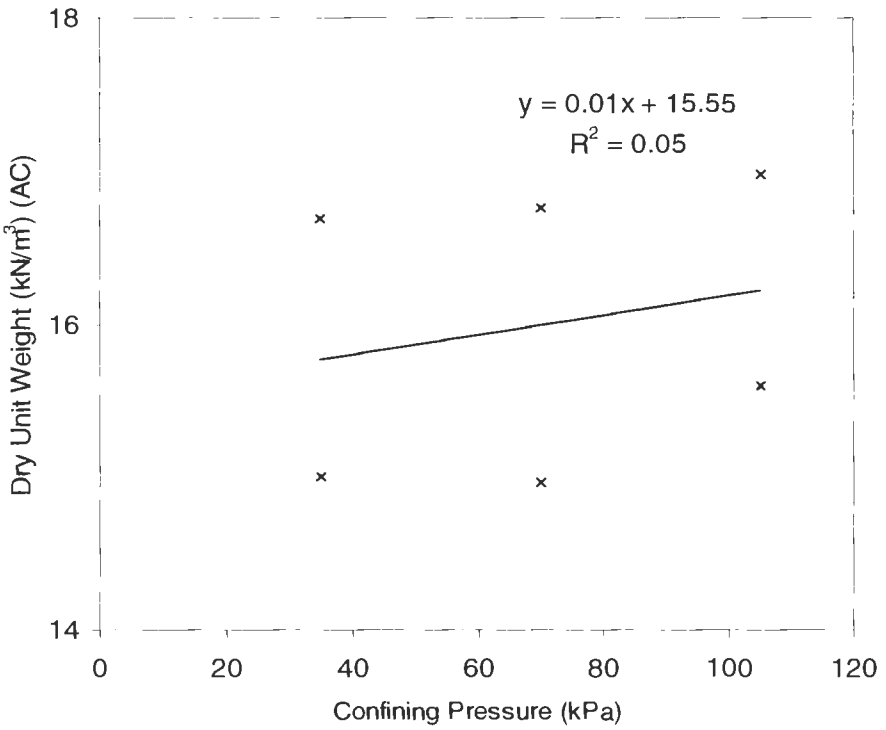

Figure E32. Regression of final dry unit weight with confining pressure for ELE triax

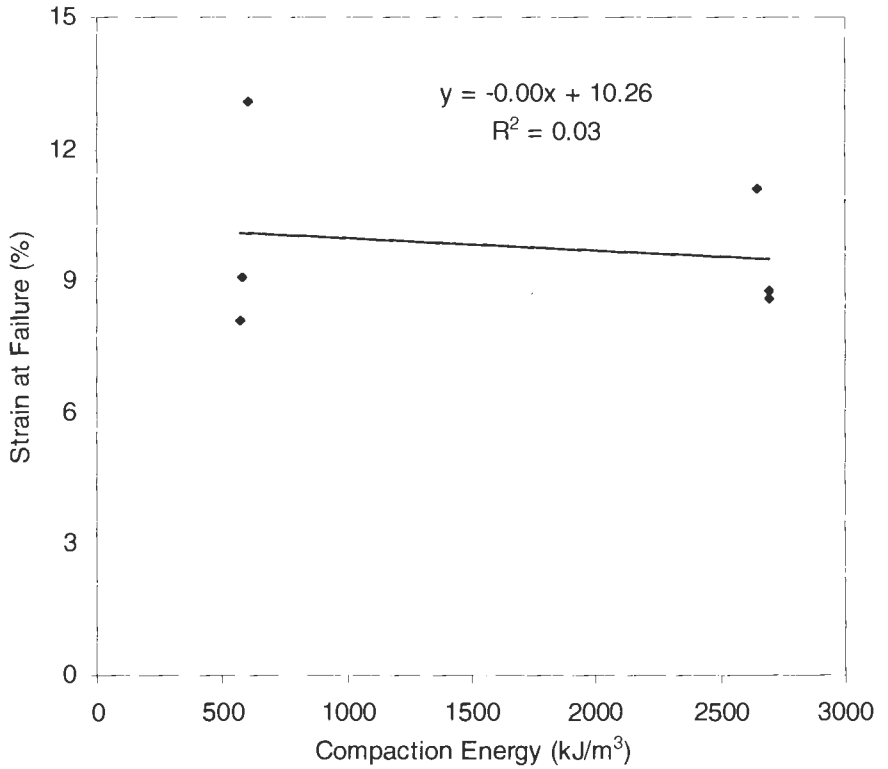

Figure E33. Regression of strain at failure with compaction energy for ELE triax

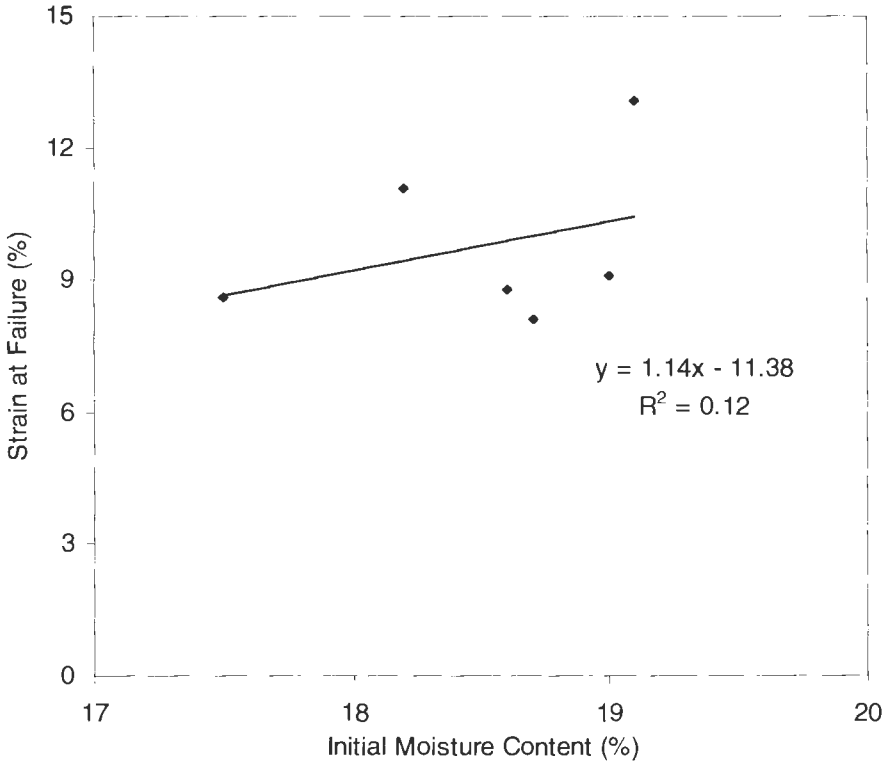

Figure E34. Regression of strain at failure with initial moisture content for ELE triax

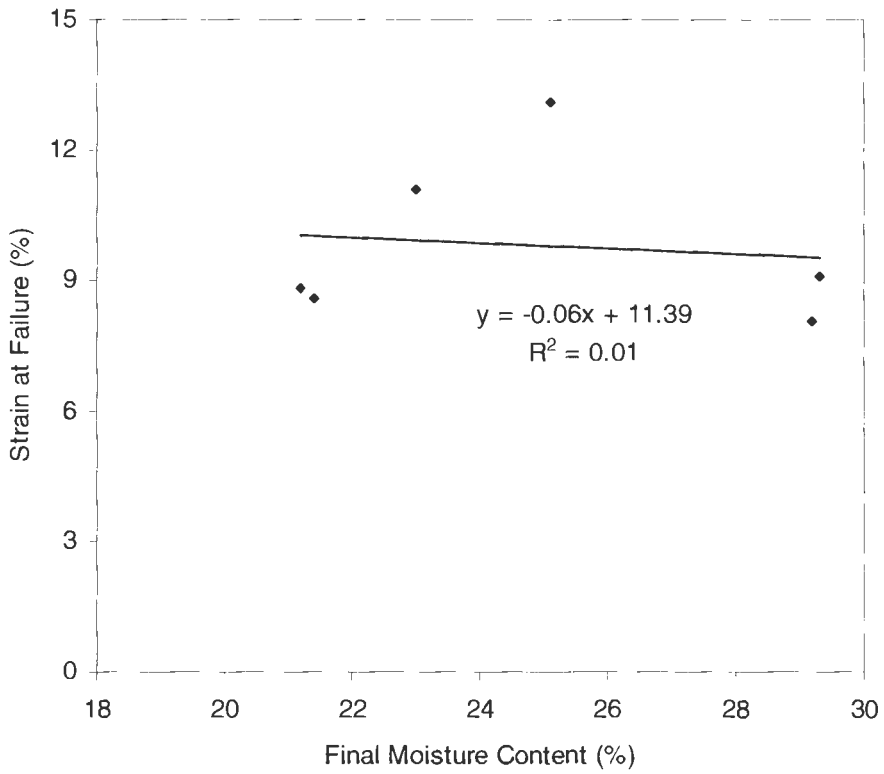

Figure E35. Regression of strain at failure with final moisture content for ELE triax

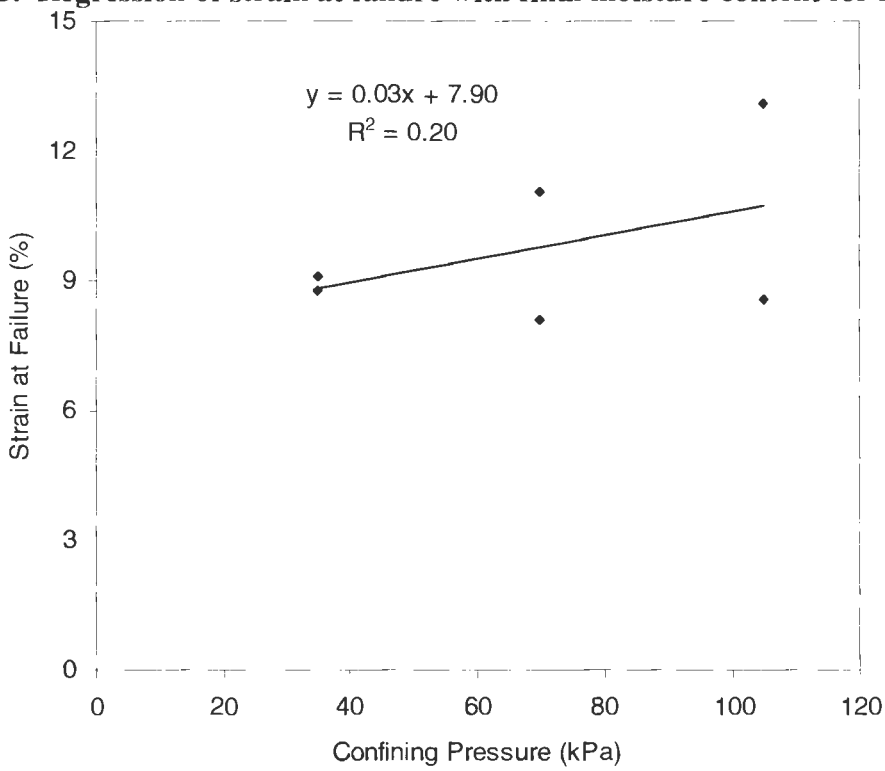

Figure E36. Regression of strain at failure with confining pressure for ELE triax

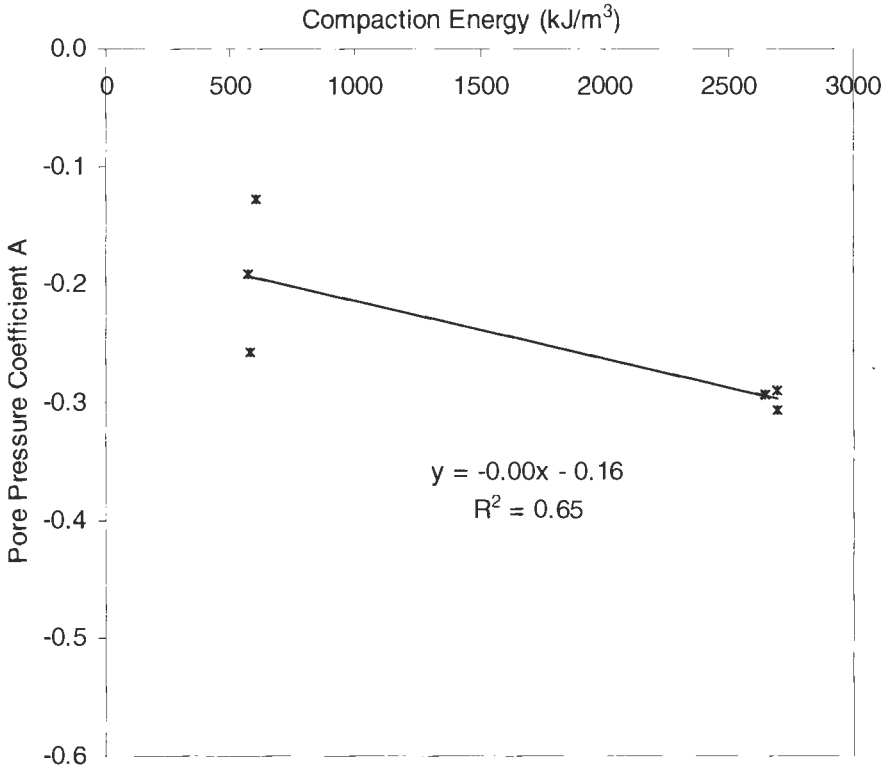

Figure E37. Regression of pore pressure coefficient A with compaction energy for ELE triax

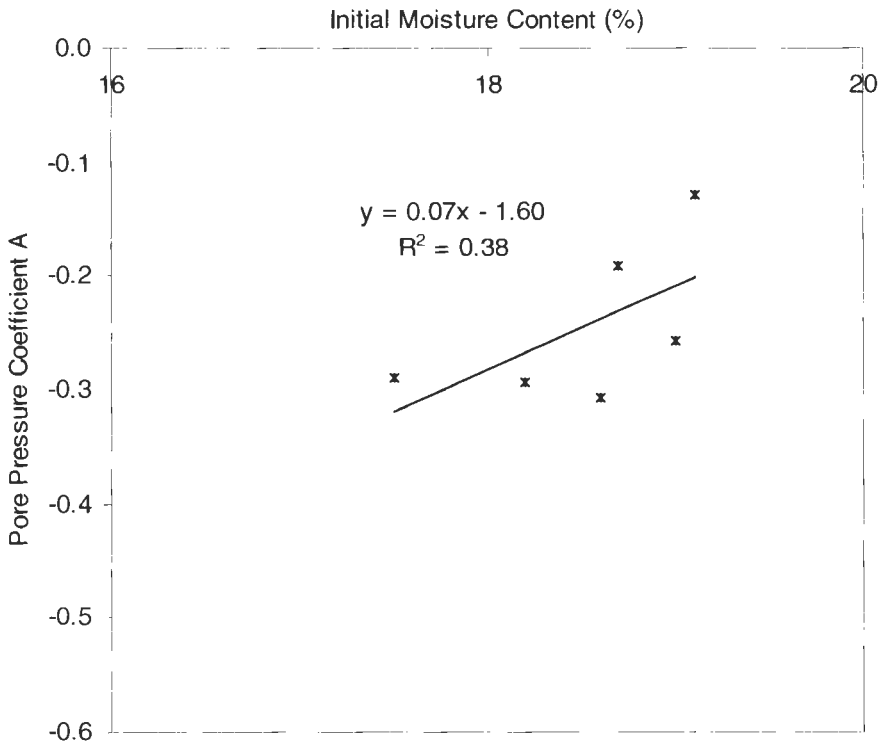

Figure E38. Regression of pore pressure coefficient A with initial moisture content for ELE triax

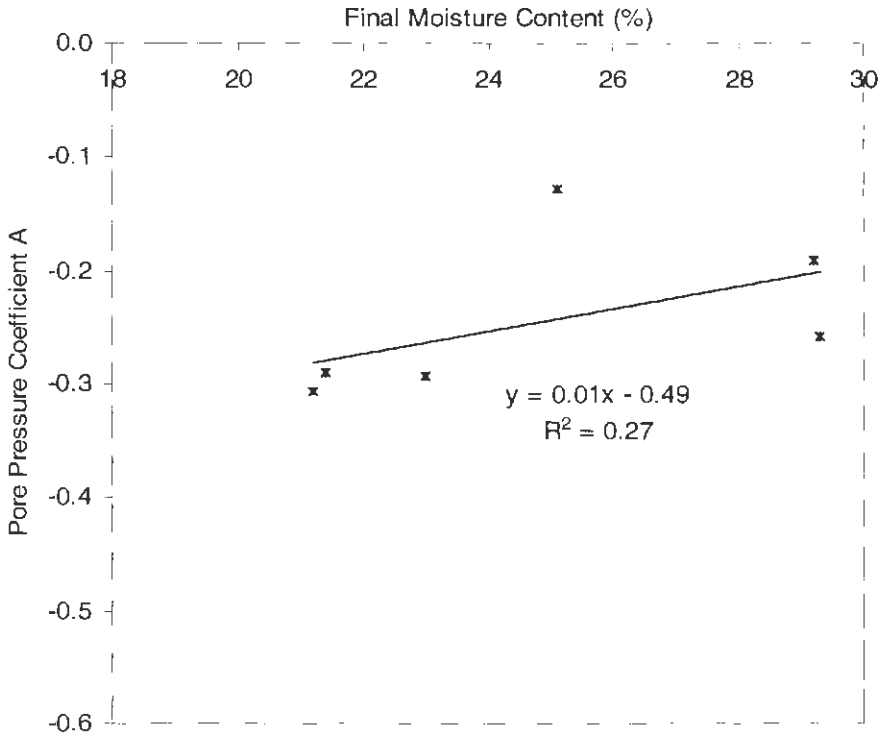

Figure E39. Regression of pore pressure coefficient A with final moisture content for ELE triax

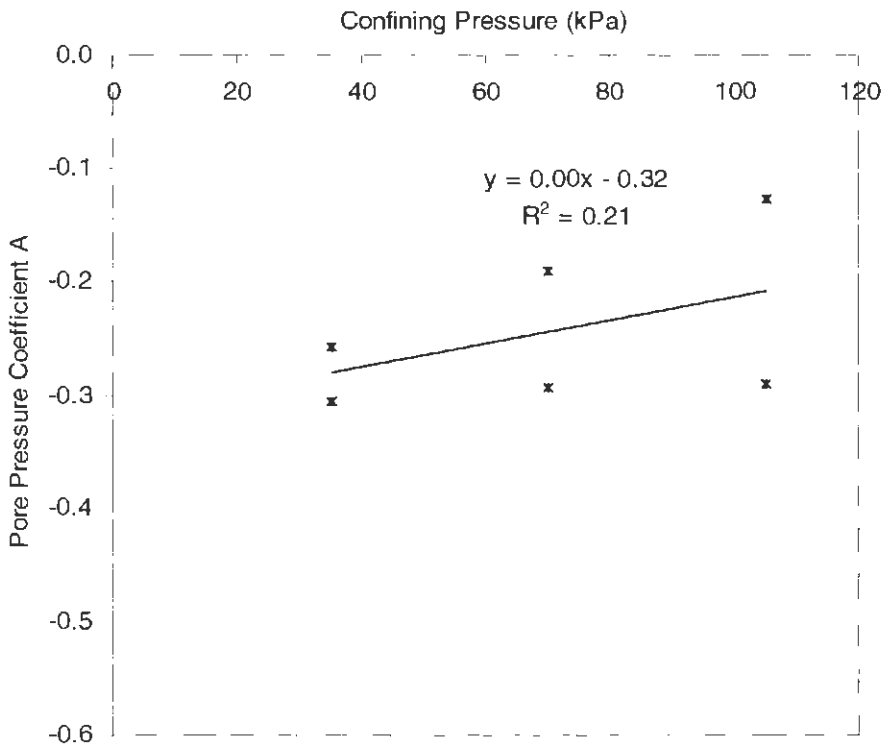

Figure E40. Regression of pore pressure coefficient A with confining pressure for ELE triax

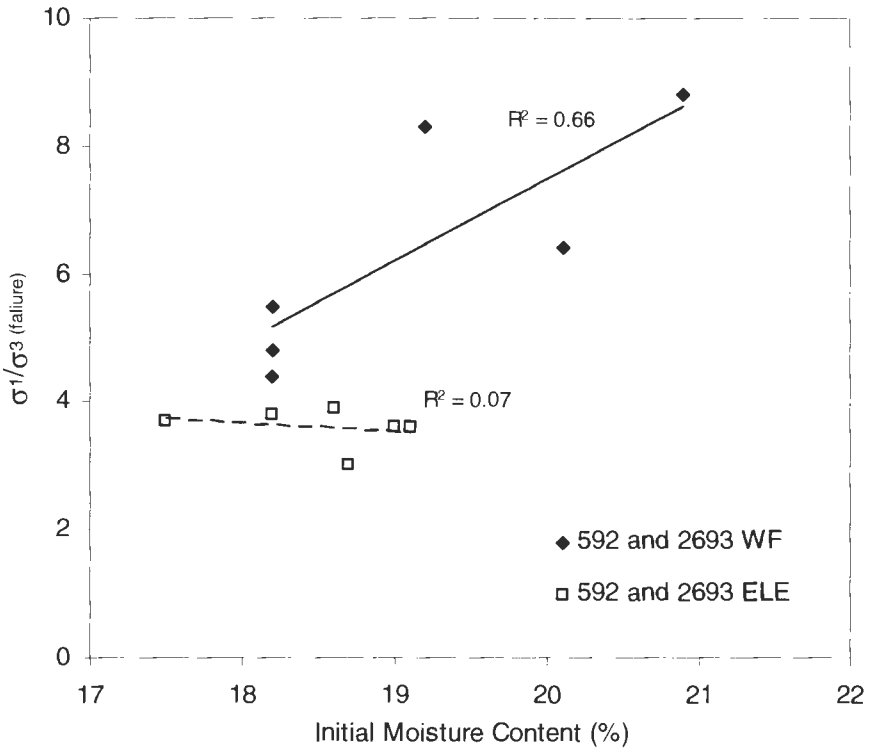

Figure E41. Comparison of principle stress ratios with initial moisture content between WF and ELE

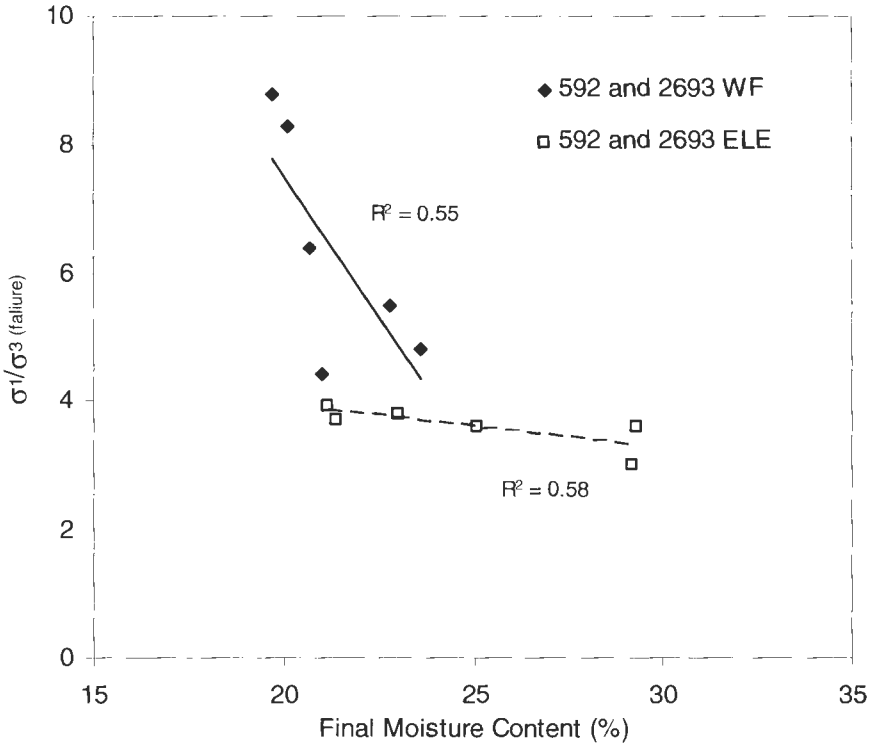

Figure E42. Comparison of principle stress ratios with final moisture content between WF and ELE

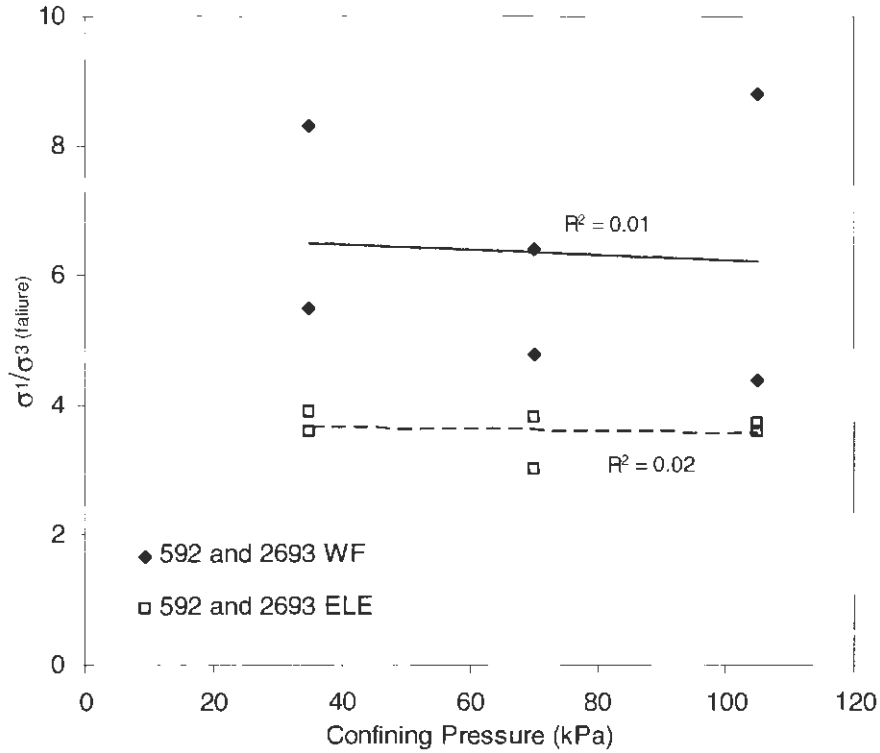

Figure E43. Comparison of principle stress ratios with confining pressure between WF and ELE

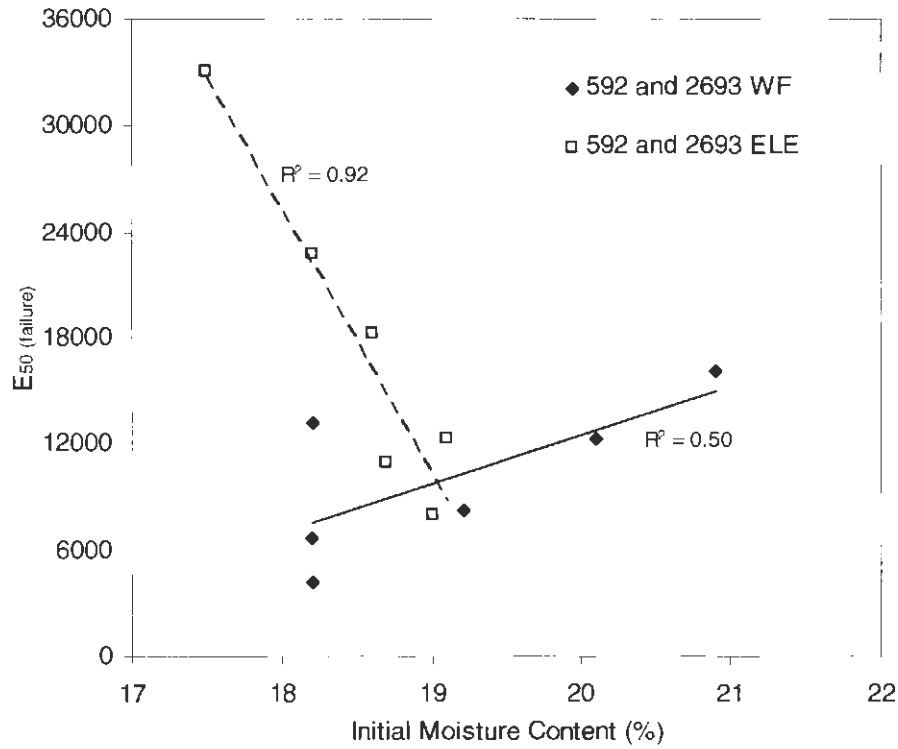

Figure E44. Comparison of secant modulus with initial moisture content between WF and ELE

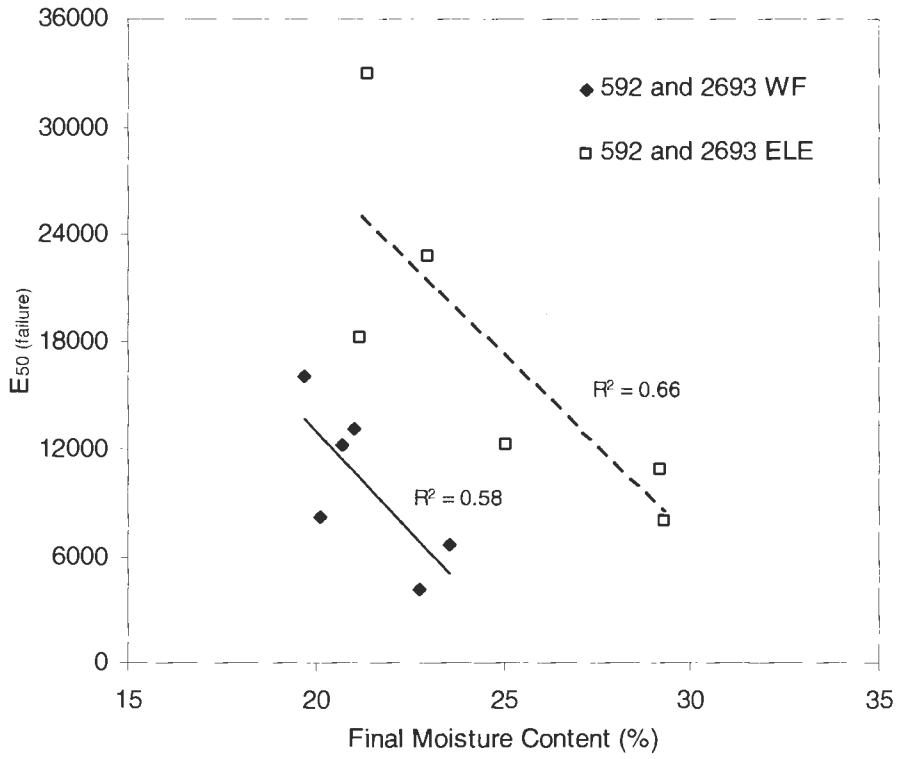

Figure E45. Comparison of secant modulus with final moisture content between WF and ELE

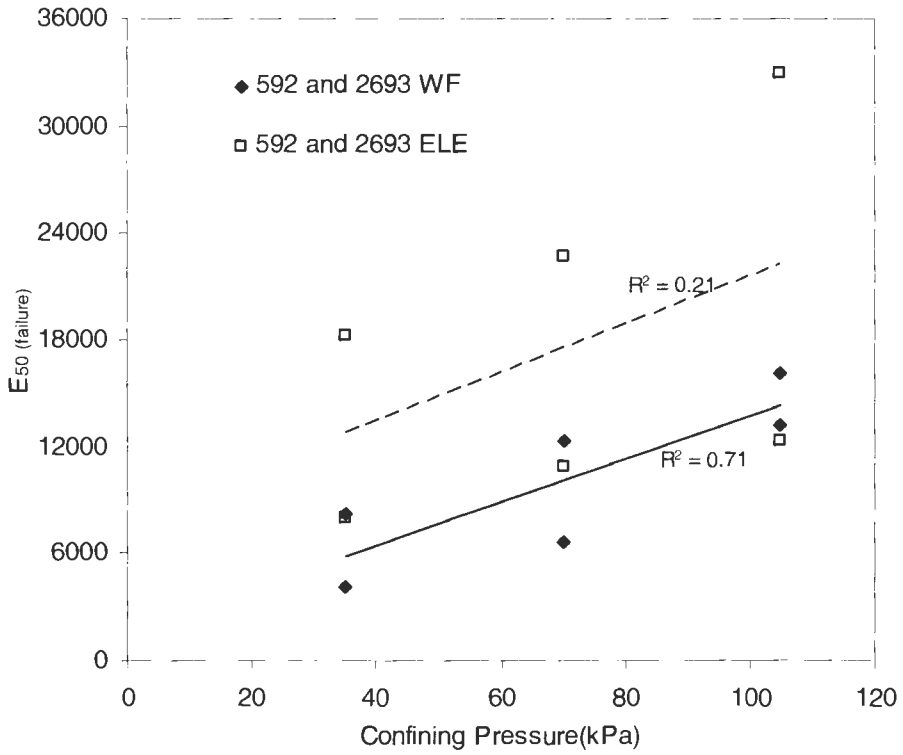

Figure E46. Comparison of secant modulus with confining pressure between WF and ELE

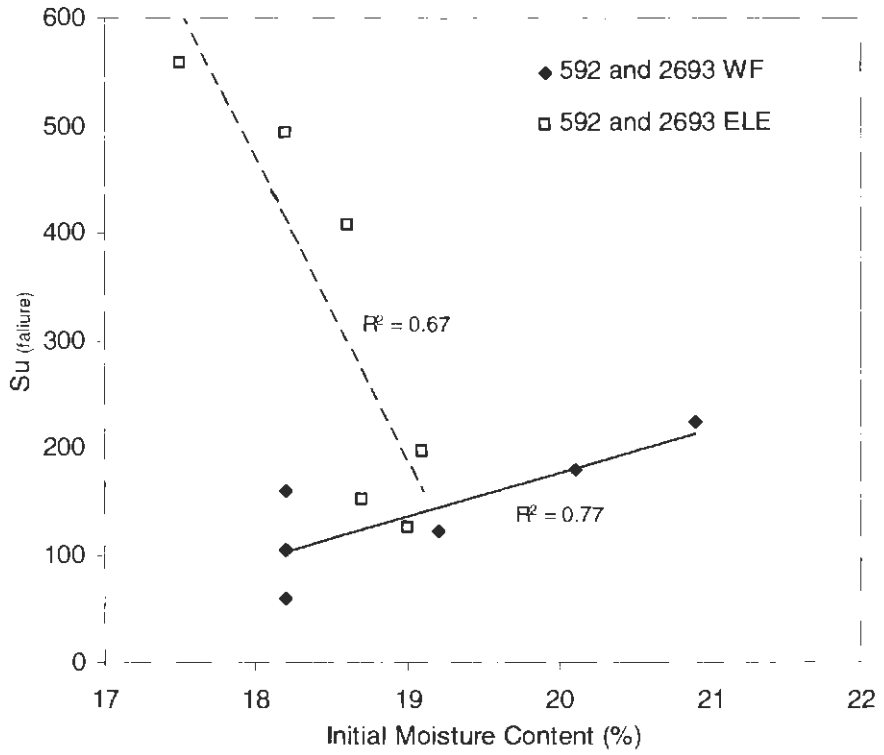

Figure E47. Comparison of undrained shear strength with initial moisture content between WF and ELE

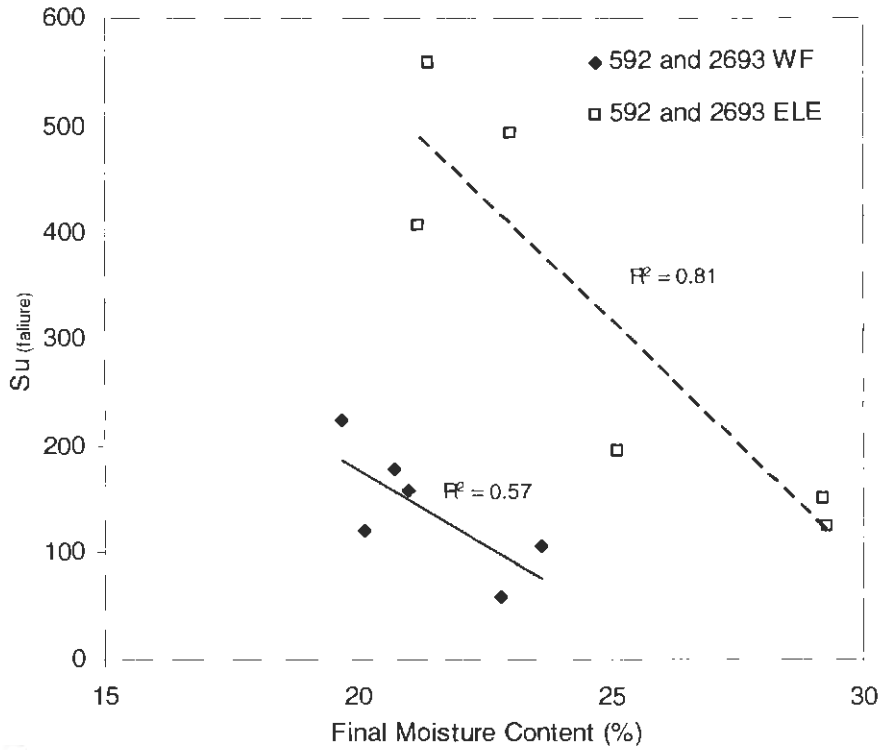

Figure E48. Comparison of undrained shear strength with final moisture content between WF and ELE

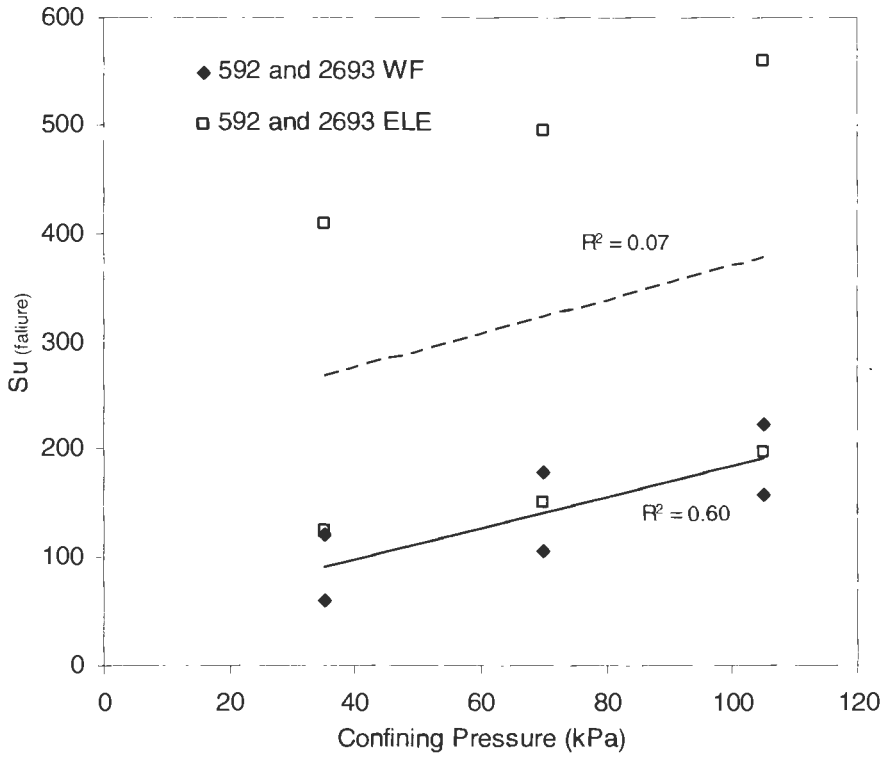

Figure E49. Comparison of undrained shear strength with confining pressure between WF and ELE

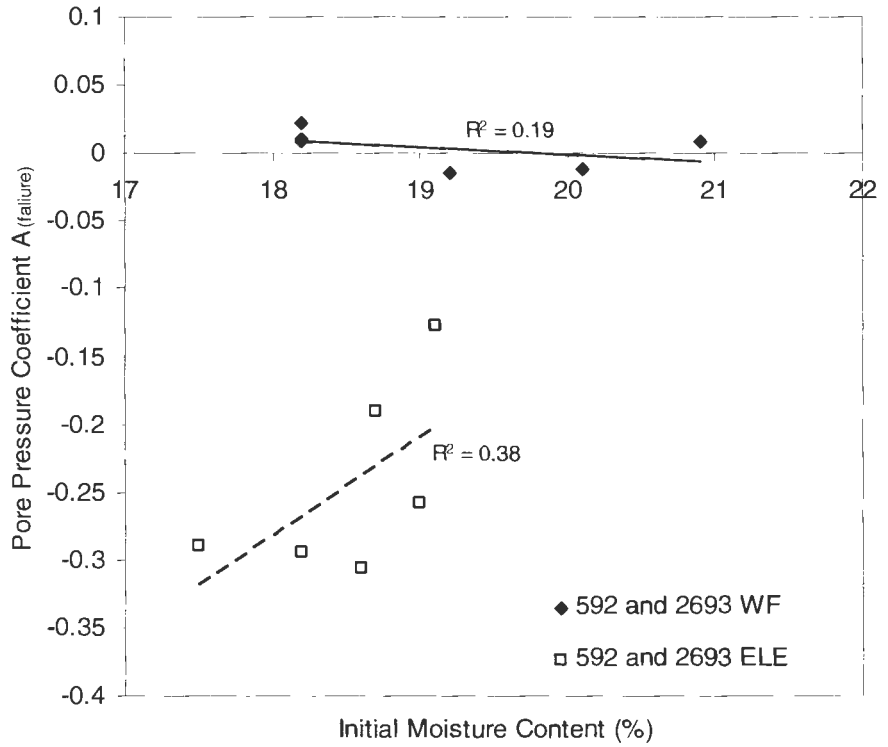

Figure E50. Comparison of pore pressure coefficient A with initial moisture content between WF and ELE

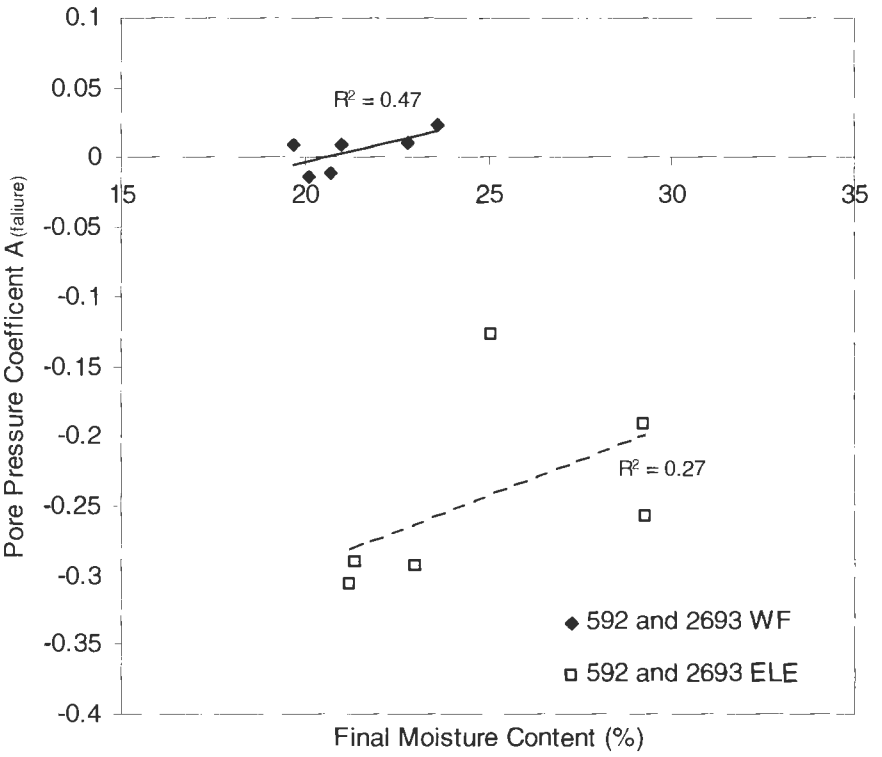

Figure E51. Comparison of pore pressure coefficient A with final moisture content between WF and ELE

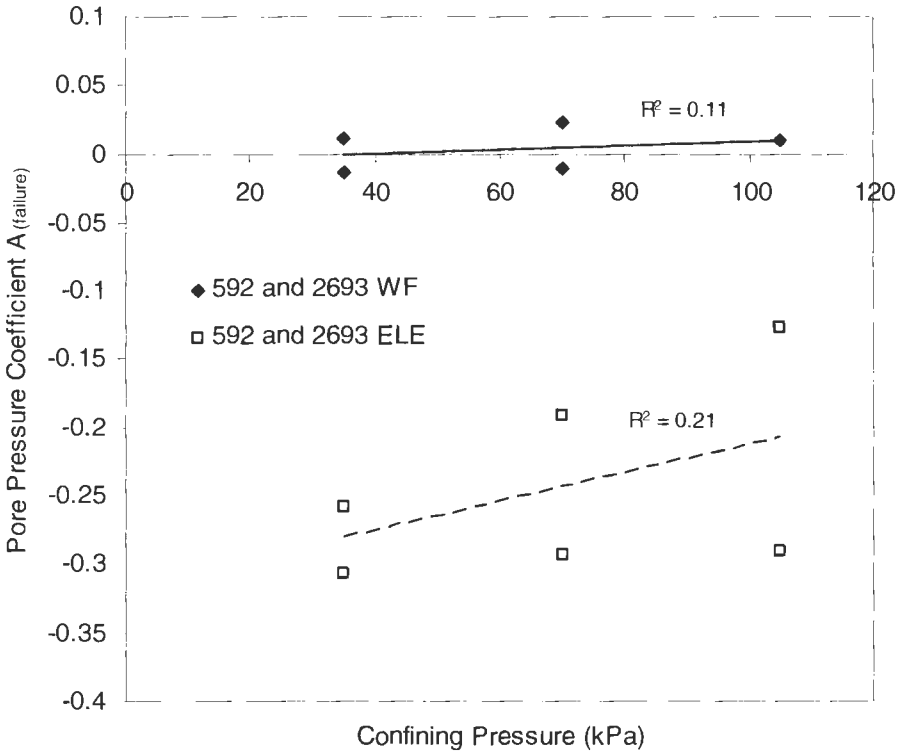

Figure E52. Comparison of pore pressure coefficient A with confining pressure between WF and ELE

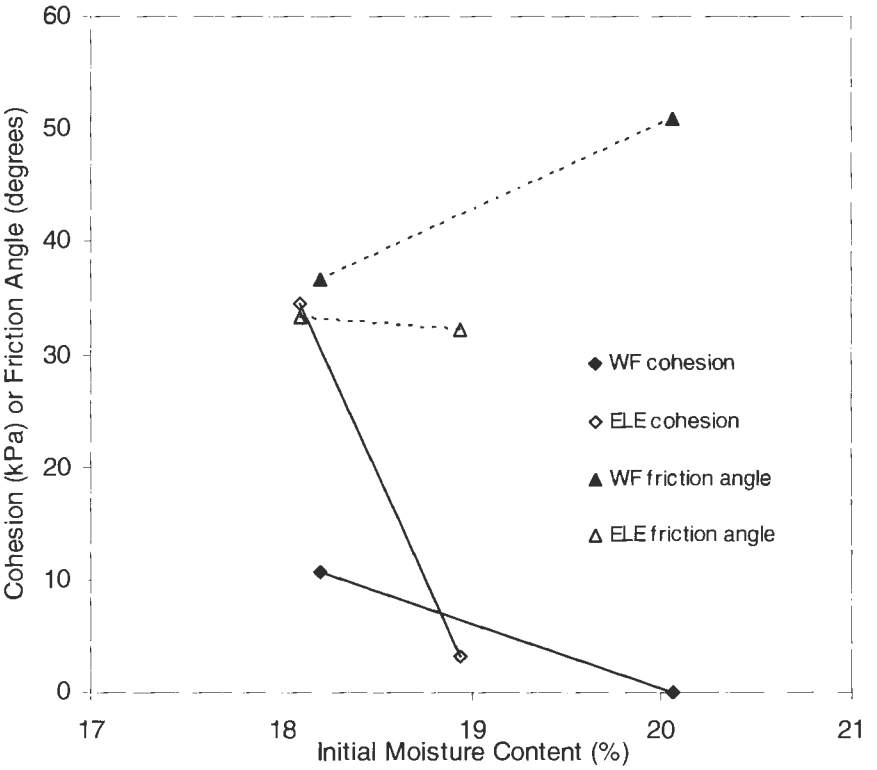

Figure E53. Comparison of limit state parameters with initial moisture content between WF and ELE

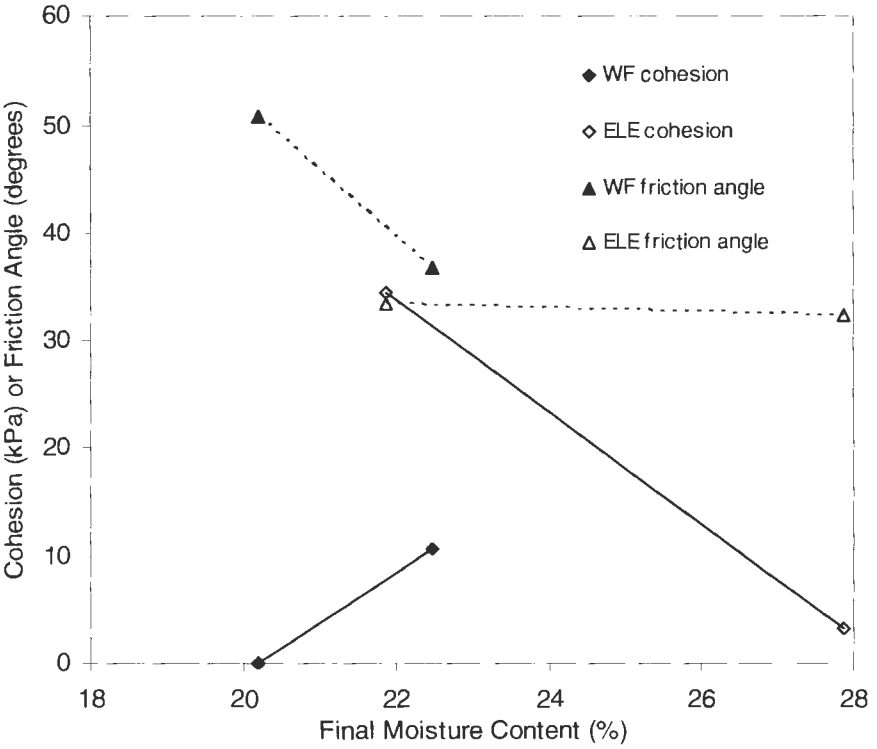

Figure E54. Comparison of limit state parameters with final moisture content between WF and ELE

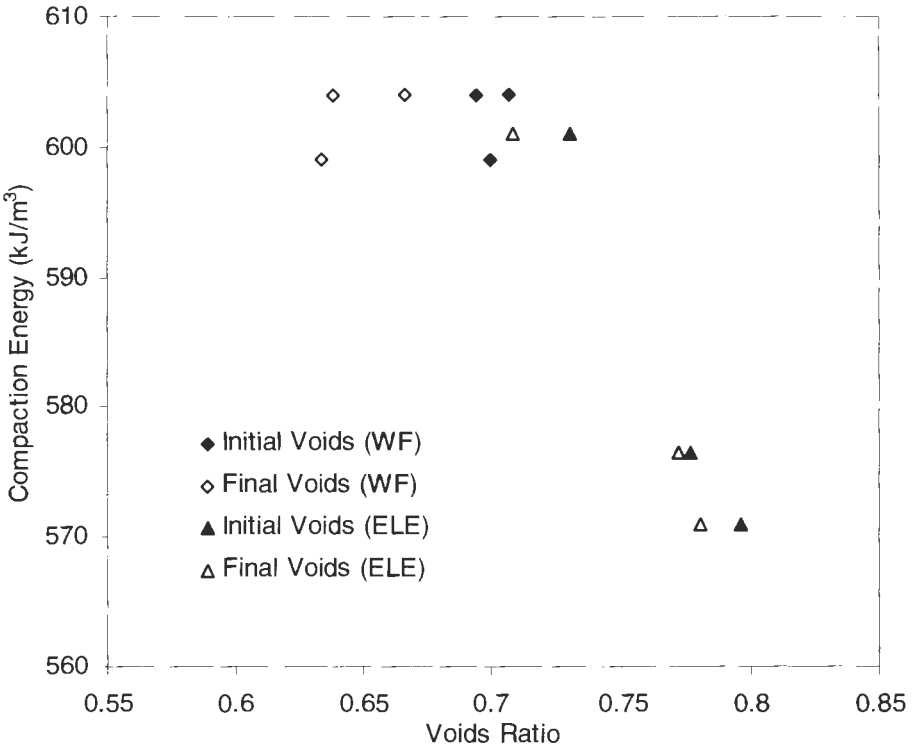

Figure E55. Comparison of void ratios with compaction energy between WF and ELE

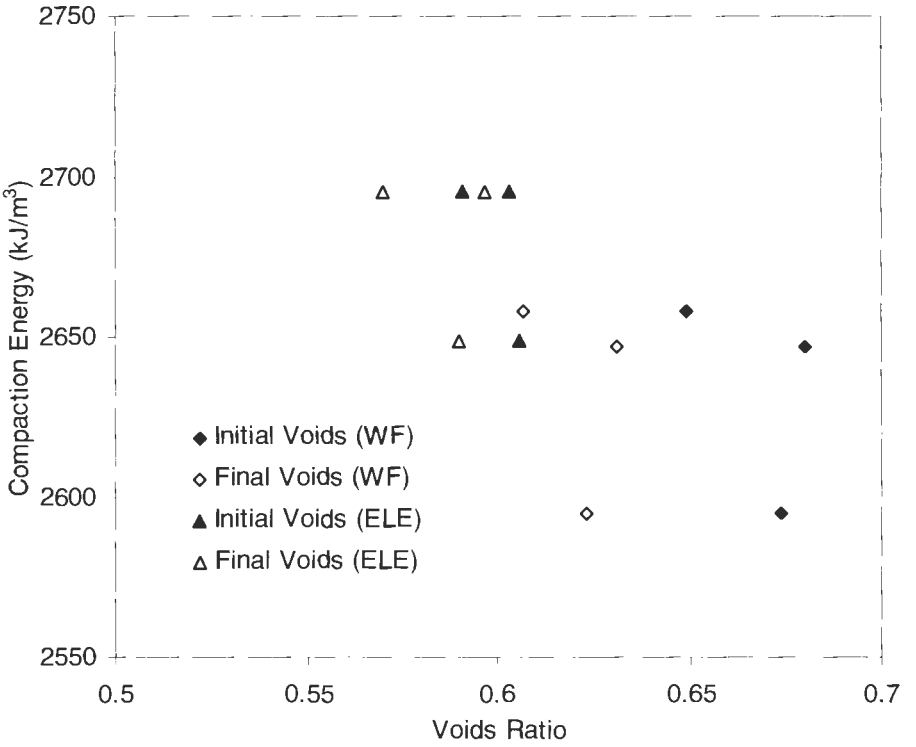

Figure E55. Comparison of void ratios with compaction energy between WF and ELE

APPENDIX F. FIELD DATA

Table F1. In-situ measurements from test strip 1A (PPG till) after 1 roller pass and an initial loose lift thickness of 30 cm.

	Nuclear					GeoGauge	
Test Point	Moisture Content (%)*	Dry Unit Weight (kN/m^3)*	Percent Standard Compaction (%)	Clegg Impact Value	DCP Index (mm/blow)	Stiffness (MN/m)	Modulus (MPa)
1	10.0	18.03	86	16.0	11	12.00	104.07
2	8.9	16.19	77	7.1	21	7.85	68.14
3	9.7	15.54	74	3.8	35	5.58	48.43
4	8.1	14.88	71	4.9	38	7.48	64.85
5	8.6	15.86	76	5.6	31	8.04	69.75
6	7.3	16.74	80	6.1	26	7.56	65.59
7	8.5	15.84	75	6.2	55	5.86	50.85
8	8.9	16.00	76	4.3	24	7.13	61.88
9	8.8	16.20	77	7.8	---	6.44	55.85
10	9.7	15.83	75	5.9	---	10.52	91.22

* - Denotes average of two measurements

Table F2. In-situ measurements from test strip 1B (PPG till) after 1 roller pass and an initial loose lift thickness of 30 cm.

	Nuclear					GeoGauge	
Test Point	Moisture Content (%)*	Dry Unit Weight (kN/m^3)*	Percent Standard Compaction (%)	Clegg Impact Value	DCP Index (mm/blow)	Stiffness (MN/m)	Modulus (MPa)
11	8.1	16.09	77	7.7	---	10.03	87.01
12	8.8	16.78	80	6.4	---	7.12	61.76
13	9.4	16.21	77	5.7	---	6.69	58.00
14	9.5	15.72	75	5.4	29	5.17	44.88
15	7.0	16.68	79	5.2	29	5.47	47.43
16	8.4	16.38	78	6.4	33	8.56	74.28
17	7.6	16.33	78	3.9	25	7.35	63.77
18	7.6	15.46	74	8.0	45	7.95	68.99
19	8.0	16.68	79	5.5	17	8.05	69.81
20	8.8	17.80	85	10.8	---	11.67	101.20

* - Denotes average of two measurements

Table F3. In-situ measurements from test strip 2A (PPG till) after 2 roller passes and an initial loose lift thickness of 30 cm.

	Nuclear					GeoGauge	
Test Point	Moisture Content (%)*	Dry Unit Weight (kN/m^3)*	Percent Standard Compaction (%)	Clegg Impact Value	DCP Index (mm/blow)	Stiffness (MN/m)	Modulus (MPa)
21	7.7	17.48	83	10.3	---	11.69	101.41
22	10.8	16.93	81	5.6	31	7.53	65.32
23	9.9	17.04	81	6.7	28	8.12	70.48
24	8.4	16.63	79	5.2	39	5.99	51.92
25	9.1	17.48	83	5.9	47	8.24	71.47
26	9.9	16.74	80	5.1	26	6.8	59.02
27	8.6	16.23	77	4.8	19	6.00	52.08
28	8.3	16.63	79	6.3	24	7.41	64.28
29	10.2	15.65	75	5.0	---	6.14	53.30
30	9.3	16.04	76	4.8	---	5.75	49.91

* - Denotes average of two measurements

Table F4. In-situ measurements from test strip 2B (PPG till) after 2 roller passes and an initial loose lift thickness of 30 cm.

	Nuclear					GeoGauge	
Test Point	Moisture Content (%)*	Dry Unit Weight (kN/m^3)*	Percent Standard Compaction (%)	Clegg Impact Value	DCP Index (mm/blow)	Stiffness (MN/m)	Modulus (MPa)
31	8.7	16.81	80	4.4	---	5.35	46.41
32	10.0	16.30	78	8.3	---	5.92	51.35
33	7.5	17.35	83	7.3	45	4.90	42.47
34	8.4	17.33	83	4.9	23	5.56	48.28
35	8.6	17.26	82	5.1	31	5.23	45.35
36	7.7	18.13	86	4.2	27	7.15	62.05
37	8.0	18.21	87	8.5	23	9.14	79.28
38	7.6	17.24	82	8.2	17	7.15	62.07
39	7.9	17.17	82	7.3	28	7.45	64.60
40	8.7	16.88	80	6.2	---	6.76	58.67

* - Denotes average of two measurements

Table F5. In-situ measurements from test strip 3A (PPG till) after 3 roller passes and an initial loose lift thickness of 30 cm.

	Nuclear					GeoGauge	
Test Point	Moisture Content (%)*	Dry Unit Weight (kN/m^3)*	Percent Standard Compaction (%)	Clegg Impact Value	DCP Index (mm/blow)	Stiffness (MN/m)	Modulus (MPa)
41	8.0	17.54	84	9.9	---	7.95	68.95
42	8.0	17.22	82	5.0	38	7.25	62.92
43	8.4	17.51	83	7.2	21	7.41	64.36
44	8.3	18.79	89	6.4	17	8.05	69.87
45	8.6	18.41	88	8.1	18	10.85	94.09
46	9.9	17.29	82	5.9	31	9.42	81.68
47	10.8	16.46	78	4.8	26	9.52	82.57
48	11.2	17.19	82	5.4	31	7.81	67.74
49	11.3	16.94	81	6.0	---	7.79	67.57
50	11.4	18.00	86	6.1	---	6.41	55.59

* - Denotes average of two measurements

Table F6. In-situ measurements from test strip 3B (PPG till) after 3 roller passes and an initial loose lift thickness of 30 cm.

	Nuclear					GeoGauge	
Test Point	Moisture Content (%)*	Dry Unit Weight (kN/m^3)*	Percent Standard Compaction (%)	Clegg Impact Value	DCP Index (mm/blow)	Stiffness (MN/m)	Modulus (MPa)
51	9.5	18.55	88	6.3	---	9.64	83.60
52	9.0	17.63	84	6.8	---	9.65	83.70
53	9.0	17.49	83	4.6	14	10.32	89.51
54	9.8	17.76	85	5.8	13	9.24	80.12
55	8.0	19.23	92	8.1	17	11.78	102.22
56	9.4	19.00	90	5.9	20	7.66	66.44
57	7.9	19.63	93	10.7	5	9.21	79.90
58	10.3	19.99	95	6.9	4	9.63	83.52
59	9.5	17.25	82	7.7	13	8.30	71.97
60	8.8	18.43	88	6.8	---	6.87	59.57

* - Denotes average of two measurements

Table F7. In-situ measurements from test strip A (Edwards till) after 6 roller passes and an initial loose lift thickness of 30 cm.

	Nuclear		Actual				
Test Point	Moisture Content (%)*	Dry Unit Weight (kN/m^3)*	Moisture Content (%)	Dry Unit Weight (kN/m^3)	Clegg Impact Value	DCP Index (mm/blow)	Percent Standard Compaction (%)
1A	9.0	16.55	8.3	18.17	17.2	14	88
2A	8.0	16.74	8.5	---	16.7	17	89
3A	12.9	15.66	8.2	---	10.5	41	84
4A	10.8	15.51	9.3	17.76	15.4	20	83
5A	9.7	16.67	8.5	---	14.9	15	89
6A	9.4	16.07	9.1	---	13.7	26	86
7A	9.5	15.70	8.6	---	11.8	27	84
8A	10.0	15.97	9.3	16.99	10.6	29	85
9A	7.2	16.96	7.8	---	11.7	18	91
10A	8.9	16.01	8.5	---	7.5	29	85

* - Denotes average of two measurements

Table F8. In-situ measurements from test strip B (Edwards till) after 6 roller passes and an initial loose lift thickness of 40 cm.

	Nuclear		Actual				
Test Point	Moisture Content (%)*	Dry Unit Weight (kN/m^3)*	Moisture Content (%)	Dry Unit Weight (kN/m^3)	Clegg Impact Value	DCP Index (mm/blow)	Percent Standard Compaction (%)
1B	14.3	16.23	12.9	---	10.5	46	87
2B	13.8	16.01	13.2	17.61	7.1	55	85
3B	13.4	15.75	12.7	---	6.8	53	84
4B	14.5	16.00	12.4	17.76	7.5	52	85
5B	13.6	15.91	12.5	---	11.5	45	85
6B	13.5	16.15	12.7	---	9.1	51	86
7B	15.3	16.35	12.8	---	8.1	50	87
8B	12.6	15.89	12.1	---	11.2	46	85
9B	13.5	15.67	12.2	15.98	8.3	52	84
10B	11.4	15.99	11.4	---	9.7	42	85

* - Denotes average of two measurements

Table F9. In-situ measurements from test strip C (Edwards till) after 6 roller passes and an initial loose lift thickness of 40 cm.

	Nuclear		Actual				
Test Point	Moisture Content (%)*	Dry Unit Weight (kN/m^3)*	Moisture Content (%)	Dry Unit Weight (kN/m^3)	Clegg Impact Value	DCP Index (mm/blow)	Percent Standard Compaction (%)
1C	13.8	17.37	14.0	---	8.3	54	93
2C	17.2	16.26	15.7	17.66	3.7	116	87
3C	19.2	15.96	15.5	---	3.5	116	85
4C	14.6	16.43	14.1	---	7.0	67	88
5C	16.1	16.20	14.7	---	5.3	92	86
6C	16.7	17.18	14.0	---	5.3	91	92
7C	15.3	17.30	14.1	18.17	6.8	66	92
8C	14.3	16.46	14.3	---	5.7	91	88
9C	14.9	16.35	14.4	17.01	4.4	64	87
10C	12.3	16.26	12.9	---	7.3	58	87

* - Denotes average of two measurements

Table F10. In-situ measurements from test strip D (Edwards till) after 6 roller passes and an initial loose lift thickness of 40 cm.

	Nuclear		Actual				
Test Point	Moisture Content (%)*	Dry Unit Weight (kN/m^3)*	Moisture Content (%)	Dry Unit Weight (kN/m^3)	Clegg Impact Value	DCP Index (mm/blow)	Percent Standard Compaction (%)
1D	13.2	17.22	14.1	---	6.5	37	92
2D	15.6	17.21	14.8	---	6.4	51	92
3D	16.1	16.25	15.0	17.09	3.5	103	87
4D	15.4	15.42	13.8	---	4.3	79	82
5D	17.4	15.76	14.7	---	4.6	93	84
6D	14.7	16.35	13.8	16.76	6.4	83	87
7D	15.9	16.33	14.7	---	5.3	72	87
8D	16.6	17.61	15.3	---	4.8	83	94
9D	15.9	15.88	14.8	17.98	4.7	122	85
10D	16.1	15.82	14.1	---	4.7	76	84

* - Denotes average of two measurements

Table F11. In-situ measurements from test strip E (Edwards till) after 10 roller passes and an initial loose lift thickness of 25 cm.

	Nuclear		Actual				
Test Point	Moisture Content (%)*	Dry Unit Weight (kN/m^3)*	Moisture Content (%)	Dry Unit Weight (kN/m^3)	Clegg Impact Value	DCP Index (mm/blow)	Percent Standard Compaction (%)
1E	10.3	16.49	8.5	---	19.8	12	88
2E	7.6	16.74	8.2	17.05	19.0	18	89
3E	8.4	16.63	8.3	---	22.7	10	89
4E	9.3	15.70	8.4	---	13.4	20	84
5E	8.9	16.97	8.3	17.82	21.7	12	90
6E	8.5	16.63	8.3	---	14.5	18	89
7E	8.7	16.71	8.2	---	24.7	24	89
8E	8.5	16.49	9.1	18.11	16.6	17	88
9E	9.6	16.73	8.2	---	19.1	17	89
10E	9.2	17.00	8.2	---	31.3	9	91

* - Denotes average of two measurements

Table F12. In-situ measurements from test strip F (Edwards till) after 10 roller passes and an initial loose lift thickness of 70 cm.

	Nuclear		Actual				
Test Point	Moisture Content (%)*	Dry Unit Weight (kN/m^3)*	Moisture Content (%)	Dry Unit Weight (kN/m^3)	Clegg Impact Value	DCP Index (mm/blow)	Percent Standard Compaction (%)
1F	18.4	15.83	13.7	18.12	6.1	60	84
2F	18.0	16.34	13.6	---	6.9	65	87
3F	15.8	17.01	14.1	---	7.5	73	91
4F	14.4	16.64	12.3	---	8.0	54	89
5F	13.3	17.53	12.1	19.12	7.1	65	93
6F	17.2	16.88	15.1	---	4.6	99	90
7F	15.5	17.58	14.5	18.40	5.7	60	94
8F	13.1	17.35	13.5	---	7.5	47	92
9F	15.5	16.21	12.5	---	8.7	58	86
10F	14.7	16.59	12.6	---	14.1	54	88

* - Denotes average of two measurements

Table F13. In-situ measurements from test strip G (Edwards till) after 10 roller passes and an initial loose lift thickness of 65 cm.

	Nuclear		Actual				
Test Point	Moisture Content (%)*	Dry Unit Weight (kN/m^3)*	Moisture Content (%)	Dry Unit Weight (kN/m^3)	Clegg Impact Value	DCP Index (mm/blow)	Percent Standard Compaction (%)
1G	12.8	17.74	12.1	19.40	10.4	52	95
2G	12.7	17.15	12.2	19.34	12.4	46	91
3G	12.7	16.11	12.0	18.15	9.2	41	86
4G	12.9	17.42	12.0	---	12.9	42	93
5G	13.0	17.57	11.6	---	13.1	42	94

* - Denotes average of two measurements

Table F14. In-situ measurements from test strip H (Edwards till) after 10 roller passes and an initial loose lift thickness of 30 cm.

	Nuclear		Actual				
Test Point	Moisture Content (%)*	Dry Unit Weight (kN/m^3)*	Moisture Content (%)	Dry Unit Weight (kN/m^3)	Clegg Impact Value	DCP Index (mm/blow)	Percent Standard Compaction (%)
1H	12.7	19.14	12.6	19.32	11.3	19.	102
2H	13.0	17.79	11.9	---	11.5	26	95
3H	13.6	16.58	12.6	---	10.5	19	88
4H	12.9	17.71	12.2	19.12	11.7	25	94
5H	13.8	17.81	12.1	---	11.7	27	95
6H	13.3	17.69	11.8	---	13.2	24	94
7H	10.6	17.81	11.1	---	16.4	16	95
8H	13.1	18.07	12.4	---	11.8	28	96
9H	13.0	17.29	11.7	---	14.9	17	92
10H	12.8	17.26	11.0	18.75	17.3	18	92

* - Denotes average of two measurements

Table F15. In-situ measurements from test strip A (WDSM clay 1) after 1 roller pass and an initial loose lift thickness of 40 cm.

	Nuclear				
Test Point	Moisture Content (%)*	Dry Unit Weight (kN/m^3)*	Percent Standard Compaction (%)	Clegg Impact Value	DCP Index (mm/blow)
A1	28.0	13.42	85	3.4	213
A2	29.9	11.46	71	1.9	123
A3	29.3	12.01	74	2.9	132
A4	28.2	10.97	68	3.0	109
A5	23.6	13.71	84	3.2	75

* - Denotes average of two measurements

Table F16. In-situ measurements from test strip A (WDSM clay 1) after 2 roller passes and an initial loose lift thickness of 40 cm.

	Nuclear				
Test Point	Moisture Content (%)*	Dry Unit Weight (kN/m^3)*	Percent Standard Compaction (%)	Clegg Impact Value	DCP Index (mm/blow)
A1	32.0	12.88	79	3.8	90
A2	29.3	13.19	81	3.4	232
A3	26.2	13.87	85	3.1	131
A4	24.5	12.58	77	4.1	101
A5	22.3	13.64	84	4.2	107

* - Denotes average of two measurements

Table F17. In-situ measurements from test strip A (WDSM clay 1) after 3 roller passes and an initial loose lift thickness of 40 cm.

	Nuclear				
Test Point	Moisture Content (%)*	Dry Unit Weight (kN/m^3)*	Percent Standard Compaction (%)	Clegg Impact Value	DCP Index (mm/blow)
A1	28.0	13.20	81	1.0	89
A2	29.9	13.16	81	2.5	106
A3	29.3	13.59	84	2.5	126
A4	28.2	11.65	72	3.7	120
A5	23.6	12.44	77	3.7	68

* - Denotes average of two measurements

Table F18. In-situ measurements from test strip A (WDSM clay 1) after 4 roller passes and an initial loose lift thickness of 40 cm.

	Nuclear				
Test Point	Moisture Content (%)*	Dry Unit Weight (kN/m^3)*	Percent Standard Compaction (%)	Clegg Impact Value	DCP Index (mm/blow)
A1	28.0	13.49	83	2.0	134
A2	29.9	12.29	76	3.1	90
A3	29.3	14.45	89	3.2	115
A4	28.2	13.38	82	4.5	102
A5	23.6	13.83	85	4.1	66

* - Denotes average of two measurements

Table F19. In-situ measurements from test strip B (WDSM clay 1) after 1 roller pass and an initial loose lift thickness of 45 cm.

	Nuclear				
Test Point	Moisture Content (%)*	Dry Unit Weight (kN/m^3)*	Percent Standard Compaction (%)	Clegg Impact Value	DCP Index (mm/blow)
B1	23.2	13.85	85	1.9	175
B2	24.2	13.07	81	3.6	113
B3	25.5	13.11	81	3.1	144
B4	27.1	12.54	77	2.9	98
B5	27.3	13.32	82	2.5	266

* - Denotes average of two measurements

Table F20. In-situ measurements from test strip B (WDSM clay 1) after 2 roller passes and an initial loose lift thickness of 45 cm.

	Nuclear				
Test Point	Moisture Content (%)*	Dry Unit Weight (kN/m^3)*	Percent Standard Compaction (%)	Clegg Impact Value	DCP Index (mm/blow)
B1	24.2	13.93	86	3.7	116
B2	21.0	12.95	80	3.1	140
B3	24.0	13.09	81	3.4	220
B4	21.8	13.53	83	2.5	155
B5	20.9	13.78	85	2.7	142

* - Denotes average of two measurements

Table F21. In-situ measurements from test strip B (WDSM clay 1) after 3 roller passes and an initial loose lift thickness of 45 cm.

	Nuclear				
Test Point	Moisture Content (%)*	Dry Unit Weight (kN/m^3)*	Percent Standard Compaction (%)	Clegg Impact Value	DCP Index (mm/blow)
B1	20.5	14.19	87	4.1	97
B2	24.1	12.91	80	3.8	98
B3	22.9	13.42	83	2.8	138
B4	22.2	12.47	77	2.7	120
B5	20.2	14.41	89	4.7	162

* - Denotes average of two measurements

Table F22. In-situ measurements from test strip B (WDSM clay 1) after 4 roller passes and an initial loose lift thickness of 45 cm.

	Nuclear				
Test Point	Moisture Content (%)*	Dry Unit Weight (kN/m^3)*	Percent Standard Compaction (%)	Clegg Impact Value	DCP Index (mm/blow)
B1	18.8	14.57	90	5.7	92
B2	22.3	13.89	86	2.4	149
B3	23.7	14.11	87	4.1	143
B4	20.4	14.05	87	2.8	102
B5	21.2	14.53	90	3.8	127

* - Denotes average of two measurements

Table F23. In-situ measurements from test strip B (WDSM clay 1) after 6 roller passes and an initial loose lift thickness of 45 cm.

	Nuclear				
Test Point	Moisture Content (%)*	Dry Unit Weight (kN/m^3)*	Percent Standard Compaction (%)	Clegg Impact Value	DCP Index (mm/blow)
B1	23.1	14.71	91	3.7	106
B2	22.3	14.67	90	2.4	162
B3	22.4	14.15	87	4.7	97
B4	20.1	14.39	89	5.1	222
B5	21.5	14.41	89	2.9	109

* - Denotes average of two measurements

Table F24. In-situ measurements from test strip C (WDSM clay 2) after 2 roller passes and an initial loose lift thickness of 40 cm.

	Nuclear				
Test Point	Moisture Content (%)*	Dry Unit Weight (kN/m^3)*	Percent Standard Compaction (%)	Clegg Impact Value	DCP Index (mm/blow)
C1	29.4	11.54	73	4.9	54
C2	25.9	12.54	79	4.7	73
C3	23.9	13.25	84	4.7	74

* - Denotes average of two measurements

Table F25. In-situ measurements from test strip C (WDSM clay 2) after 4 roller passes and an initial loose lift thickness of 40 cm.

	Nuclear				
Test Point	Moisture Content (%)*	Dry Unit Weight (kN/m^3)*	Percent Standard Compaction (%)	Clegg Impact Value	DCP Index (mm/blow)
C1	26.2	12.81	81	5.6	42
C2	25.9	12.79	81	6.6	98
C3	25.3	13.86	88	6.9	56

* - Denotes average of two measurements

Table F26. In-situ measurements from test strip C (WDSM clay 2) after 6 roller passes and an initial loose lift thickness of 40 cm.

	Nuclear				
Test Point	Moisture Content (%)*	Dry Unit Weight (kN/m^3)*	Percent Standard Compaction (%)	Clegg Impact Value	DCP Index (mm/blow)
C1	25.0	13.05	82	6.4	53
C2	25.5	13.03	82	7.2	79
C3	26.8	13.13	83	6.0	49

* - Denotes average of two measurements

Table F27. In-situ measurements from test strip CV (WDSM clay 2) after 2 roller passes and an initial loose lift thickness of 40 cm.

	Nuclear				
Test Point	Moisture Content (%)*	Dry Unit Weight (kN/m^3)*	Percent Standard Compaction (%)	Clegg Impact Value	DCP Index (mm/blow)
CV1	29.8	11.84	75	6.1	68
CV2	28.0	12.74	80	---	55
CV3	33.5	12.54	79	6.7	42
CV4	24.2	13.99	88	---	60
CV5	28.6	11.99	76	5.4	75

* - Denotes average of two measurements

Table F28. In-situ measurements from test strip CV (WDSM clay 2) after 4 roller passes and an initial loose lift thickness of 40 cm.

	Nuclear				
Test Point	Moisture Content (%)*	Dry Unit Weight (kN/m^3)*	Percent Standard Compaction (%)	Clegg Impact Value	DCP Index (mm/blow)
CV1	30.1	12.80	81	7.0	59
CV2	28.1	13.05	82	---	48
CV3	27.8	13.90	88	7.9	48
CV4	28.6	13.60	86	---	57
CV5	25.3	13.45	85	5.9	59

* - Denotes average of two measurements

Table F29. In-situ measurements from test strip CV (WDSM clay 2) after 6 roller passes and an initial loose lift thickness of 40 cm.

	Nuclear				
Test Point	Moisture Content (%)*	Dry Unit Weight (kN/m^3)*	Percent Standard Compaction (%)	Clegg Impact Value	DCP Index (mm/blow)
CV1	25.8	13.00	82	5.2	51
CV2	21.0	13.86	88	---	45
CV3	24.6	13.54	86	7.5	48
CV4	26.8	13.76	87	---	61
CV5	25.4	13.24	84	7.9	49

* - Denotes average of two measurements

APPENDIX G. FIELD REGRESSION FIGURES

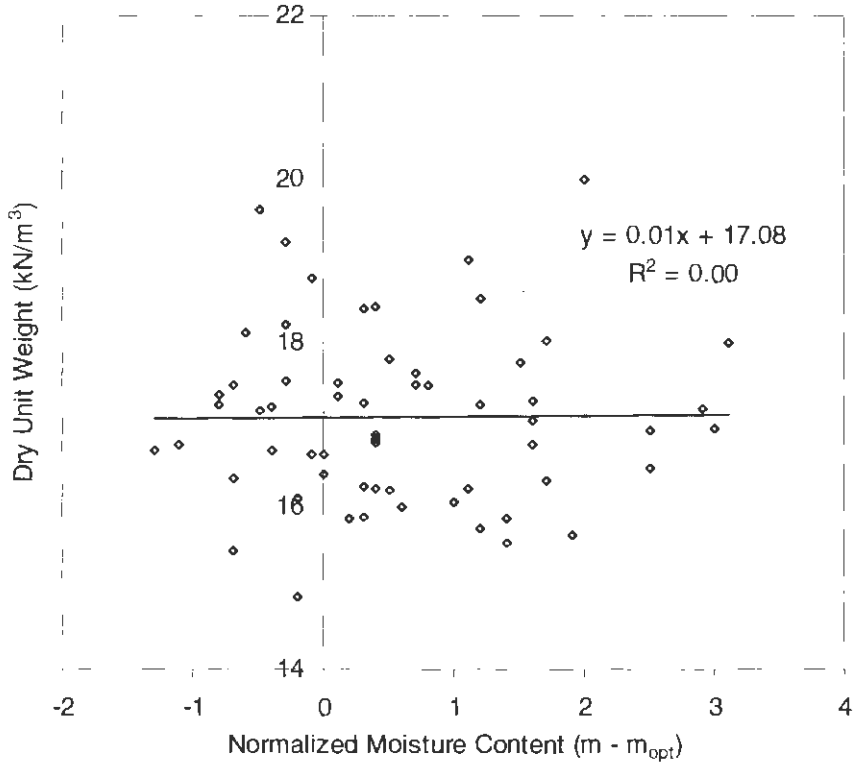

Figure G1. Regression for dry unit weight with normalized moisture content (PPG)

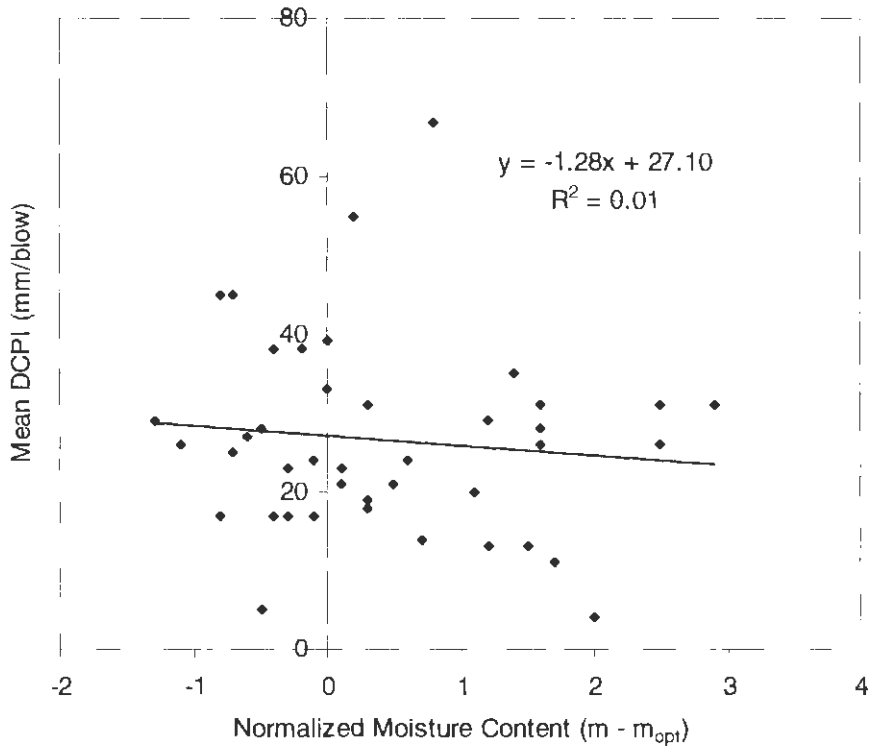

Figure G2. Regression for mean DCPI with normalized moisture content (PPG)

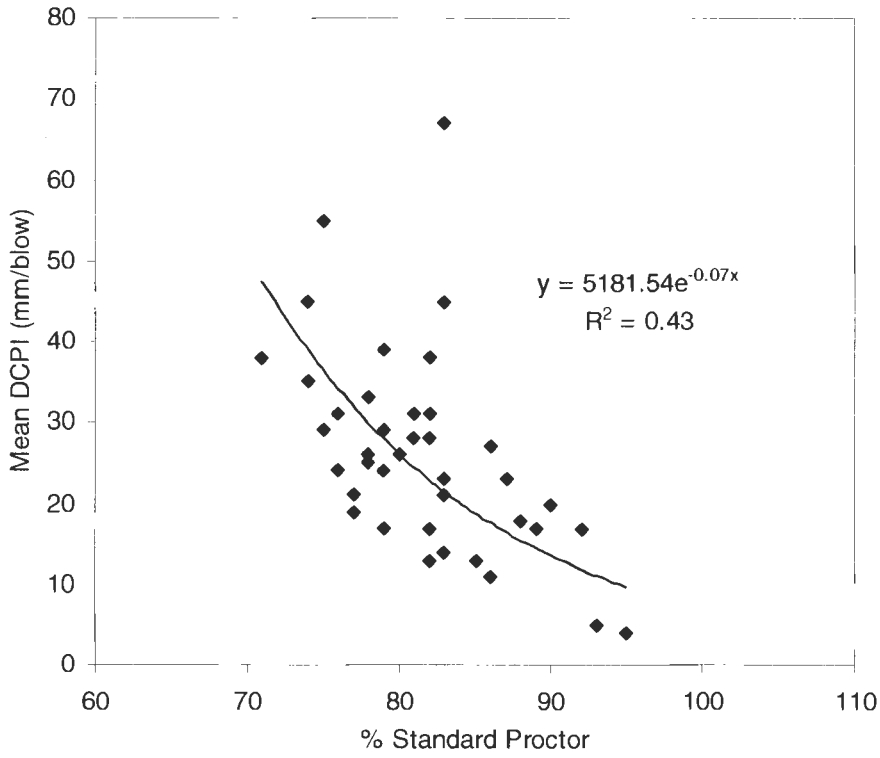

Figure G3. Regression for mean DCPI with relative compaction (PPG)

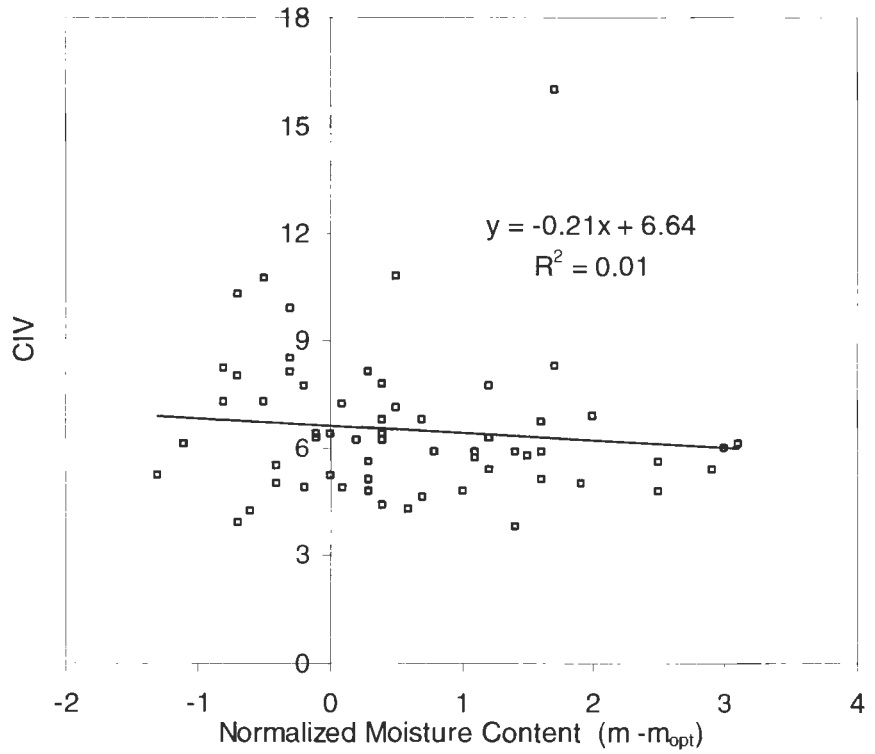

Figure G4. Regression for CIV with normalized moisture content (PPG)

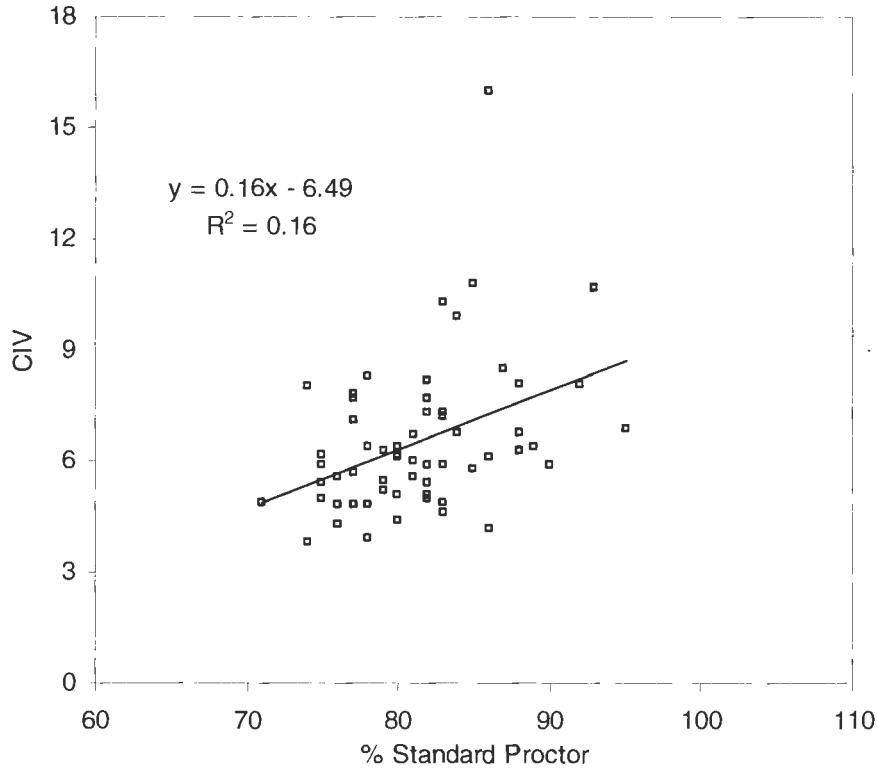

Figure G5. Regression for CIV with relative compaction (PPG)

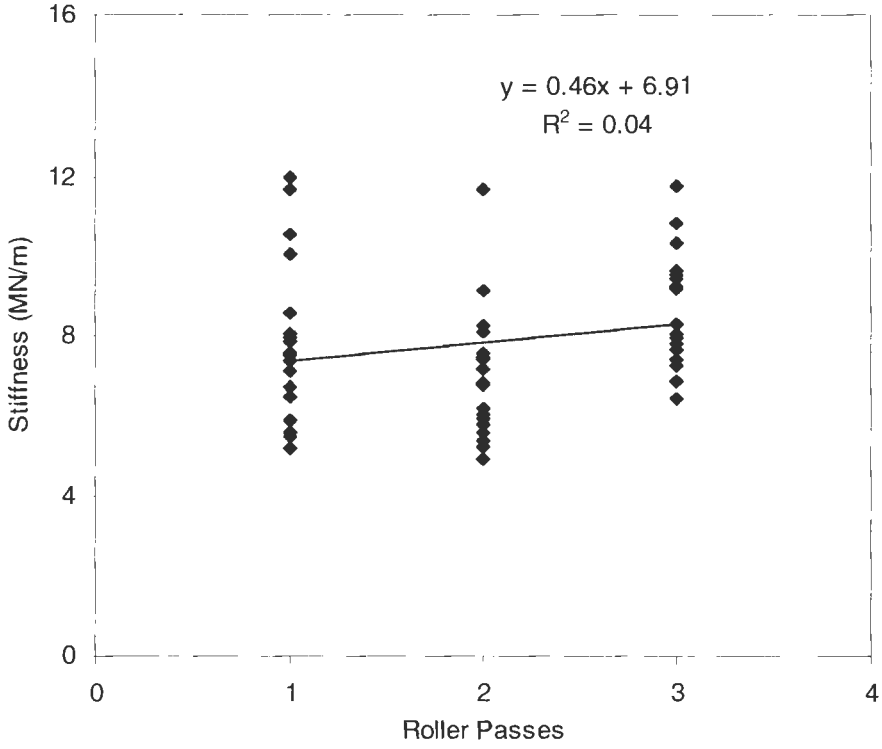

Figure G6. Regression for stiffness with roller passes (PPG)

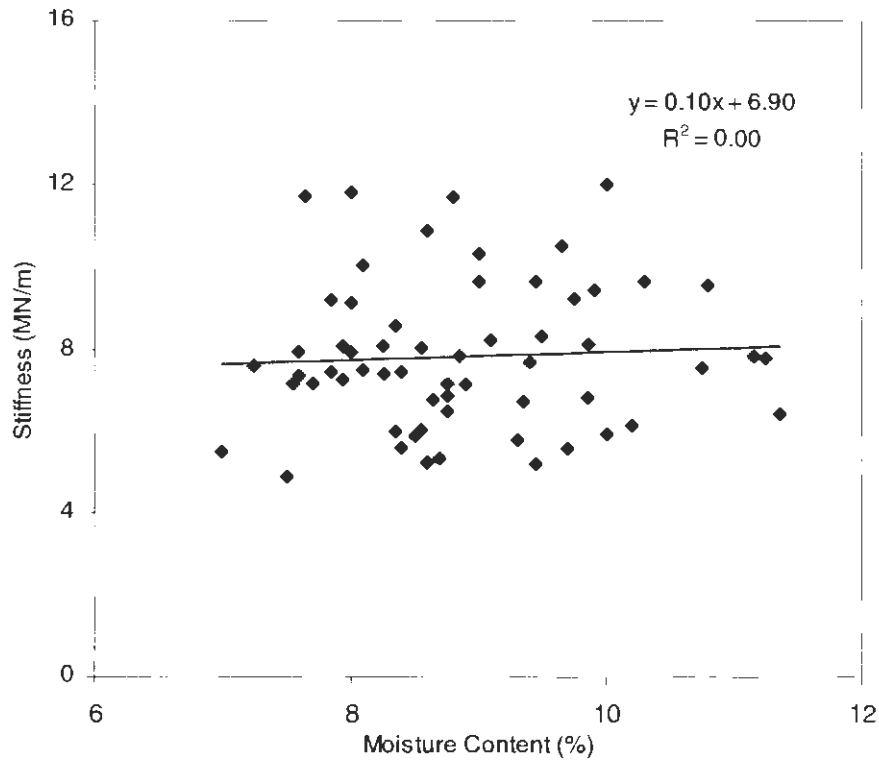

Figure G7. Regression for stiffness with moisture content (PPG)

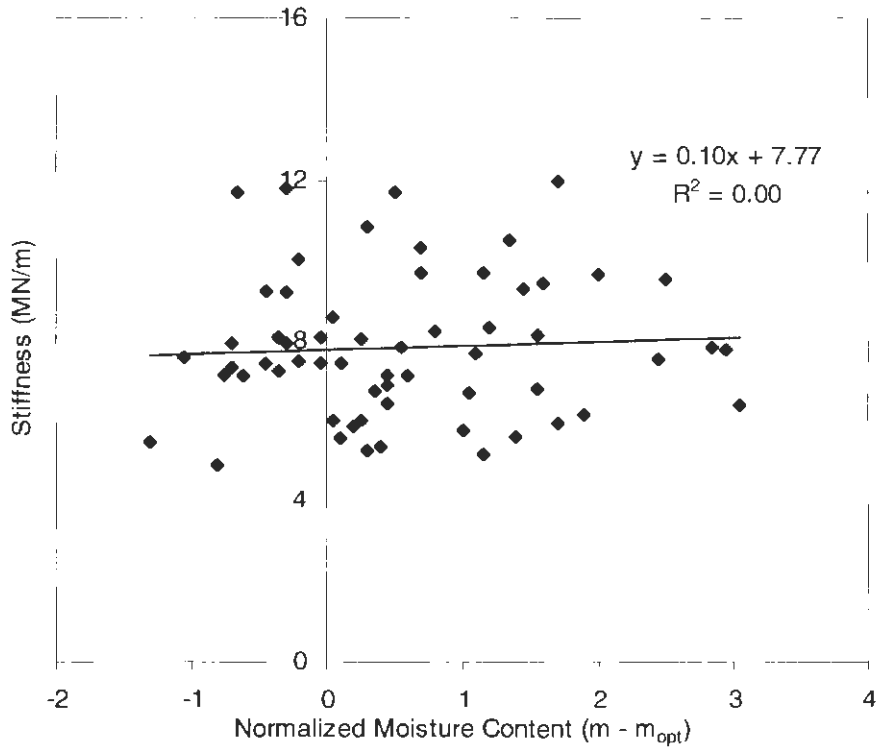

Figure G8. Regression for stiffness with normalized moisture content (PPG)

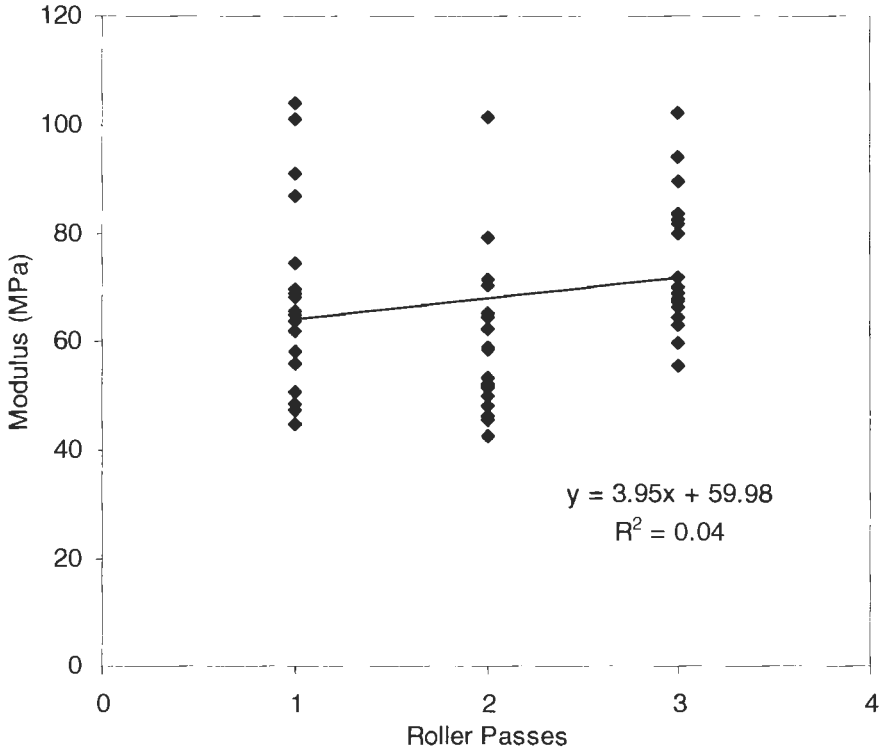

Figure G9. Regression for modulus with roller passes (PPG)

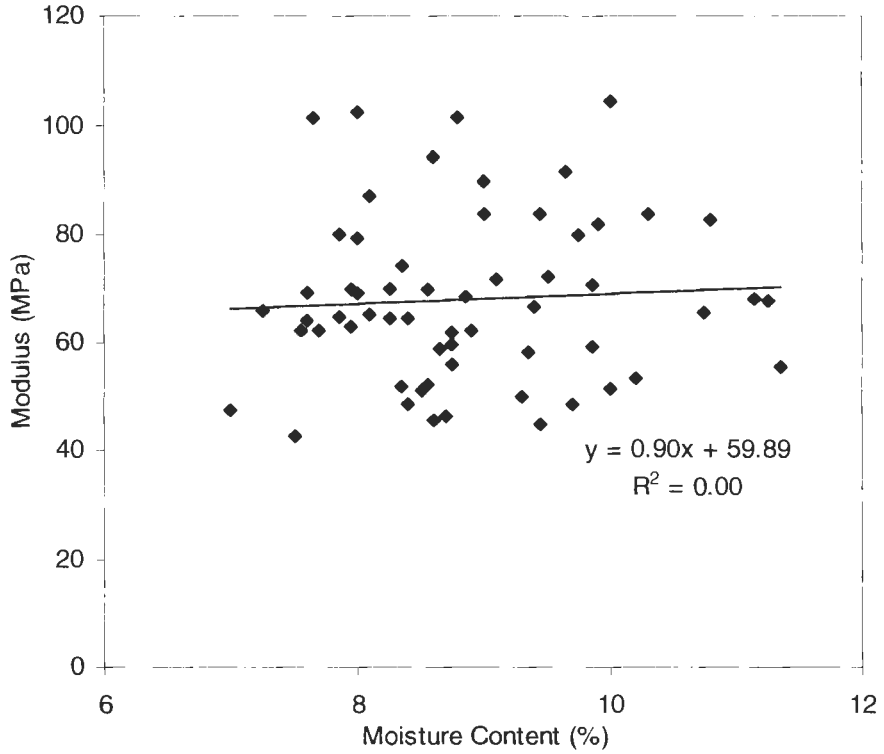

Figure G10. Regression for modulus with moisture content (PPG)

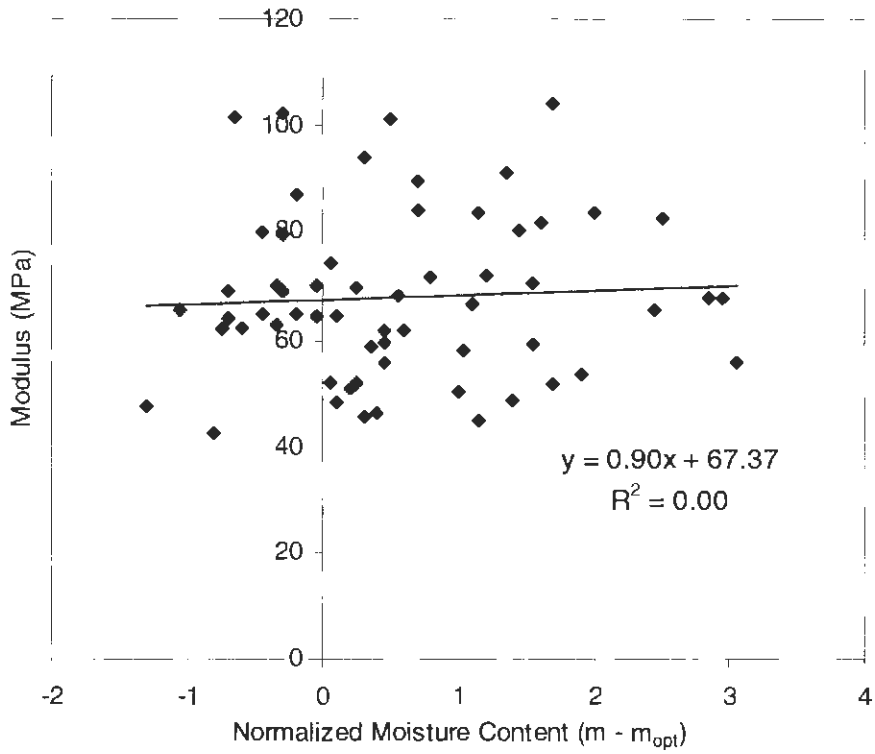

Figure G11. Regression for modulus with normalized moisture content (PPG)

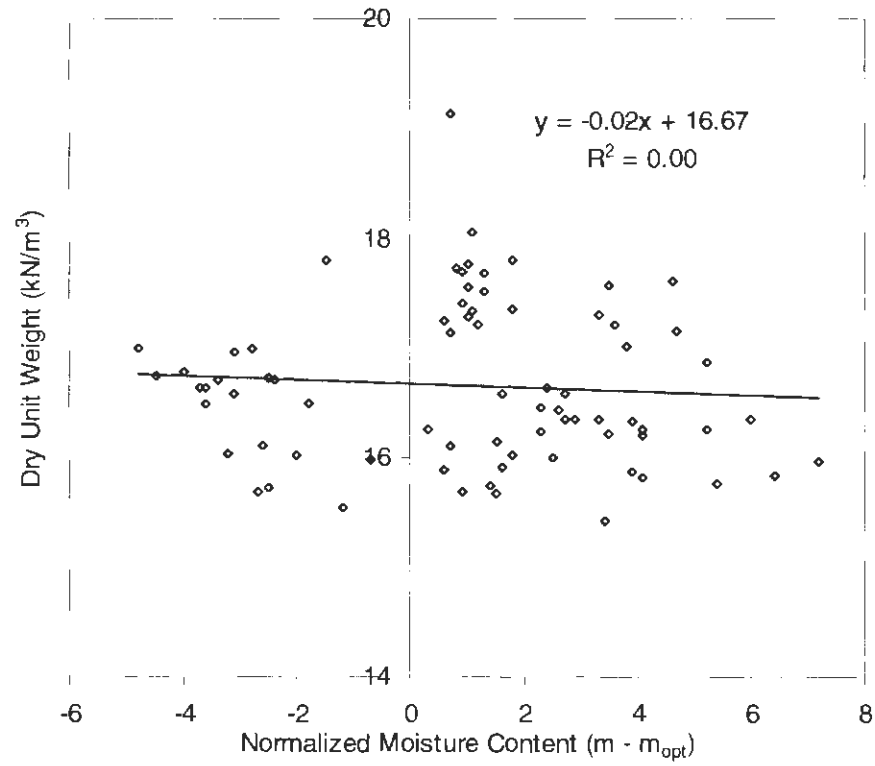

Figure G12. Regression for dry unit weight with normalized moisture content (Edwards)

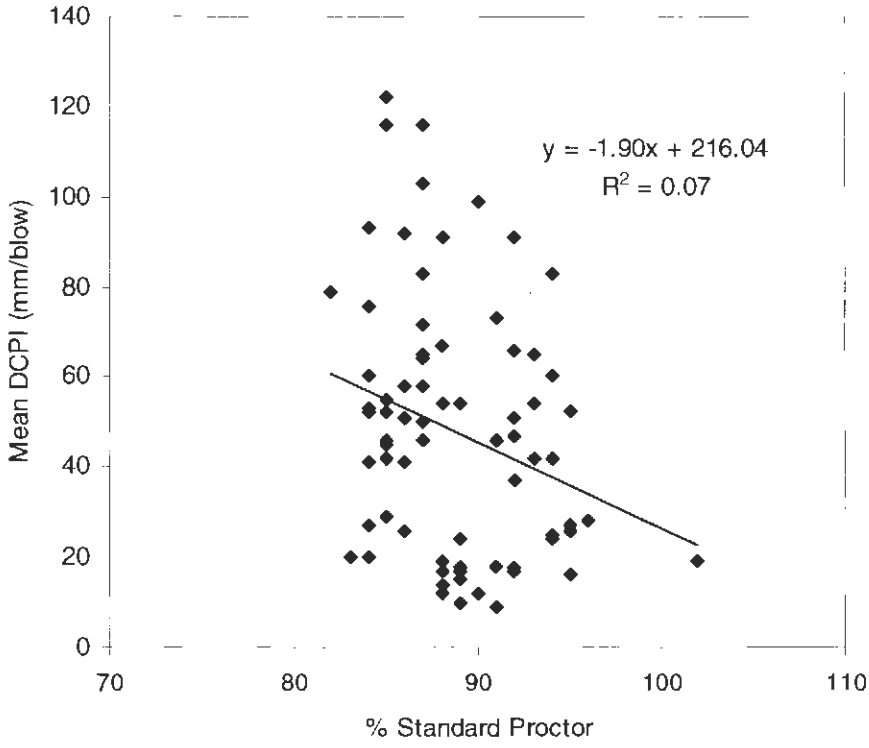

Figure G13. Regression for mean DCPI with relative compaction (Edwards)

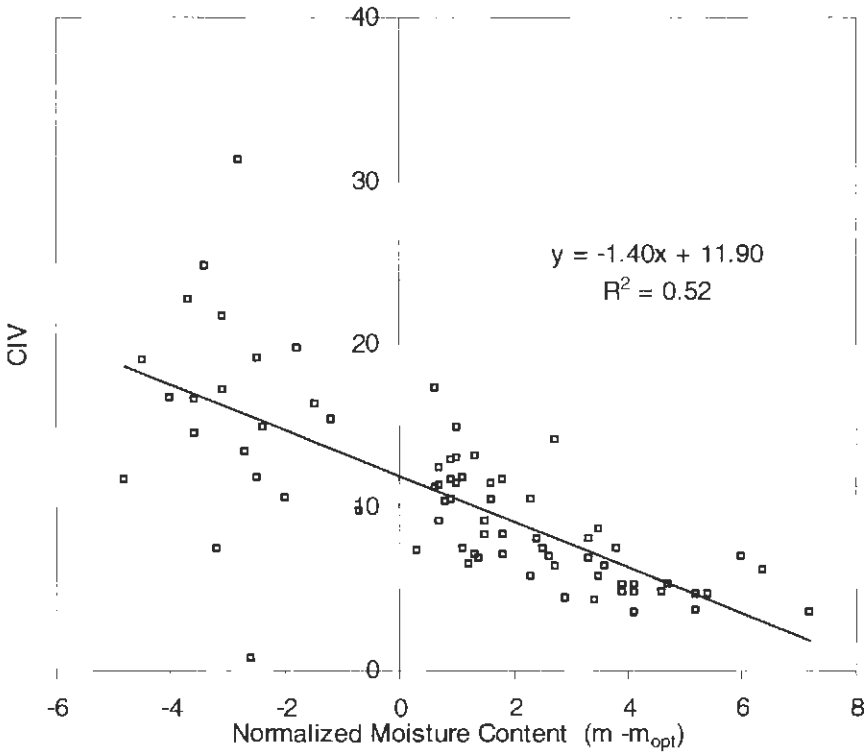

Figure G14. Regression for CIV with normalized moisture content (Edwards)

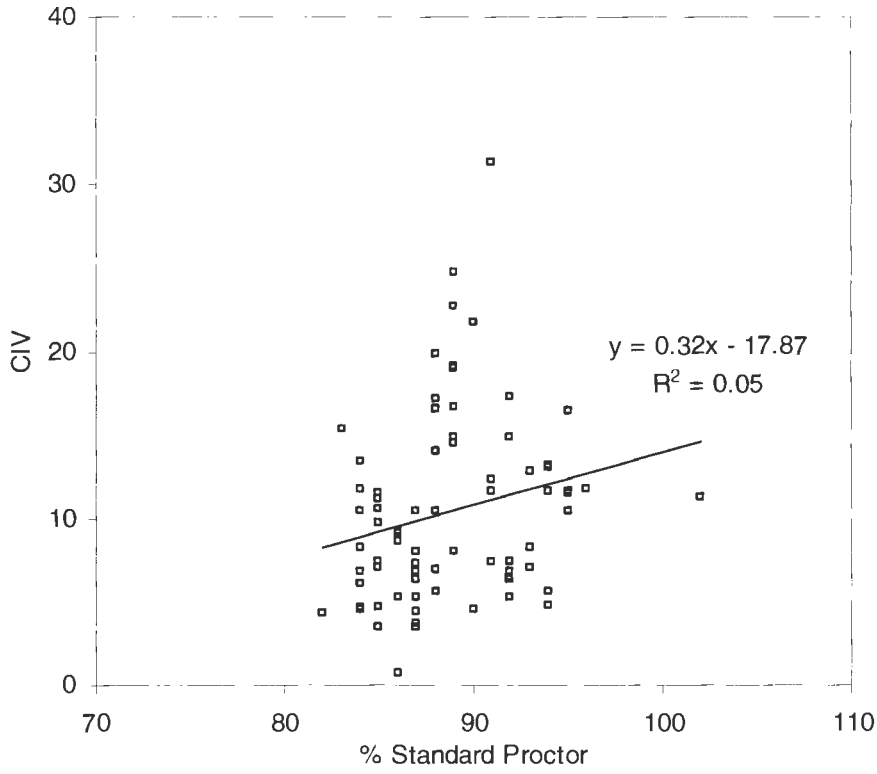

Figure G15. Regression for CIV with relative compaction (Edwards)

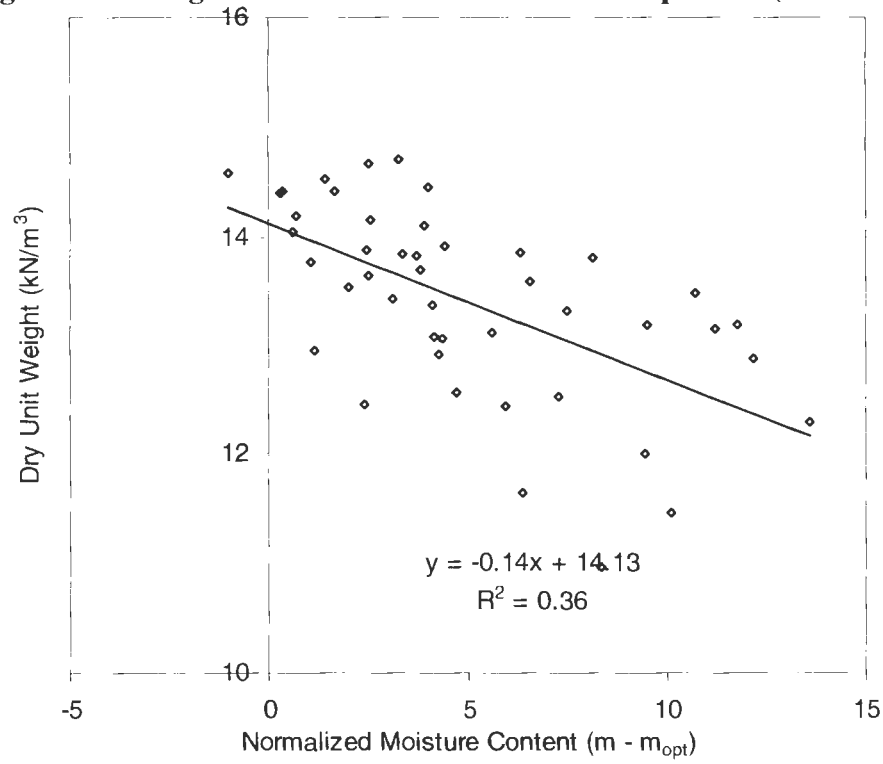

Figure G16. Regression for dry unit weight with normalized moisture content (WDSM existing clay)

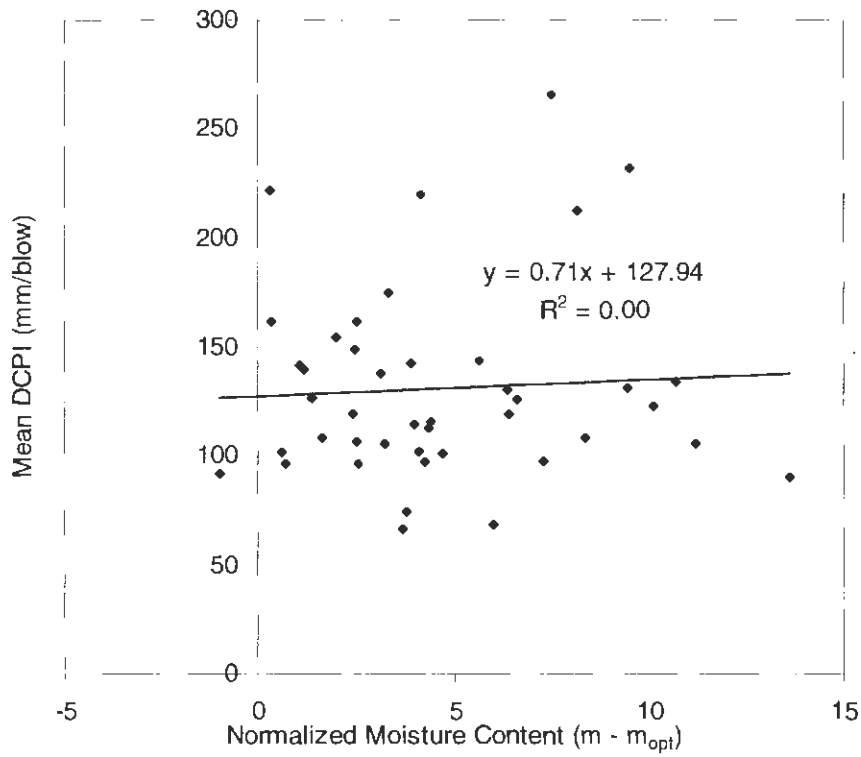

Figure G17. Regression for mean DCPI with normalized moisture content (WDSM existing clay)

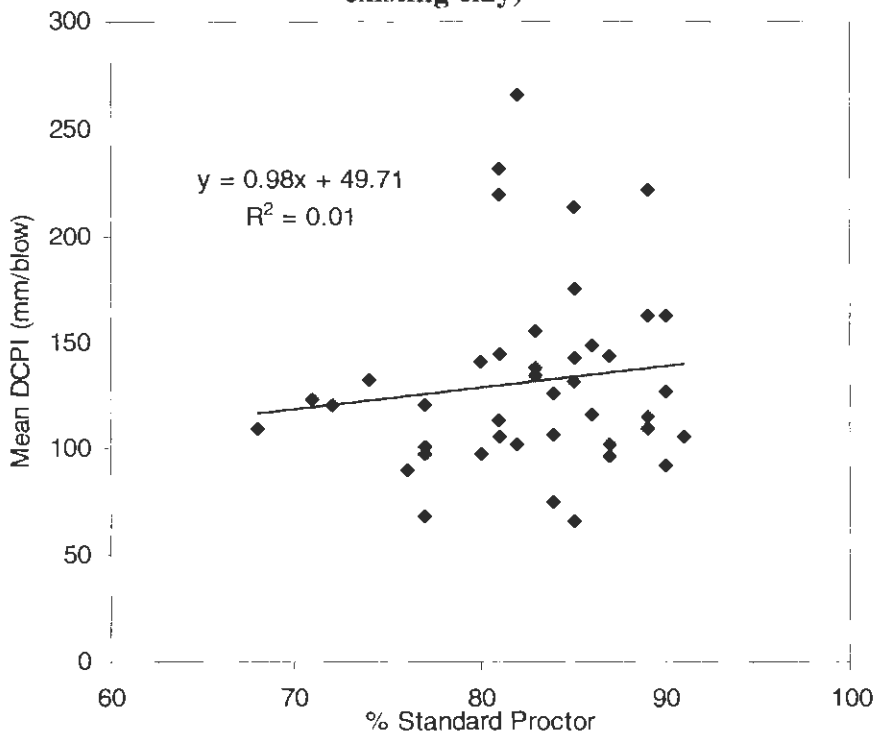

Figure G18. Regression for mean DCPI with relative compaction (WDSM existing clay)

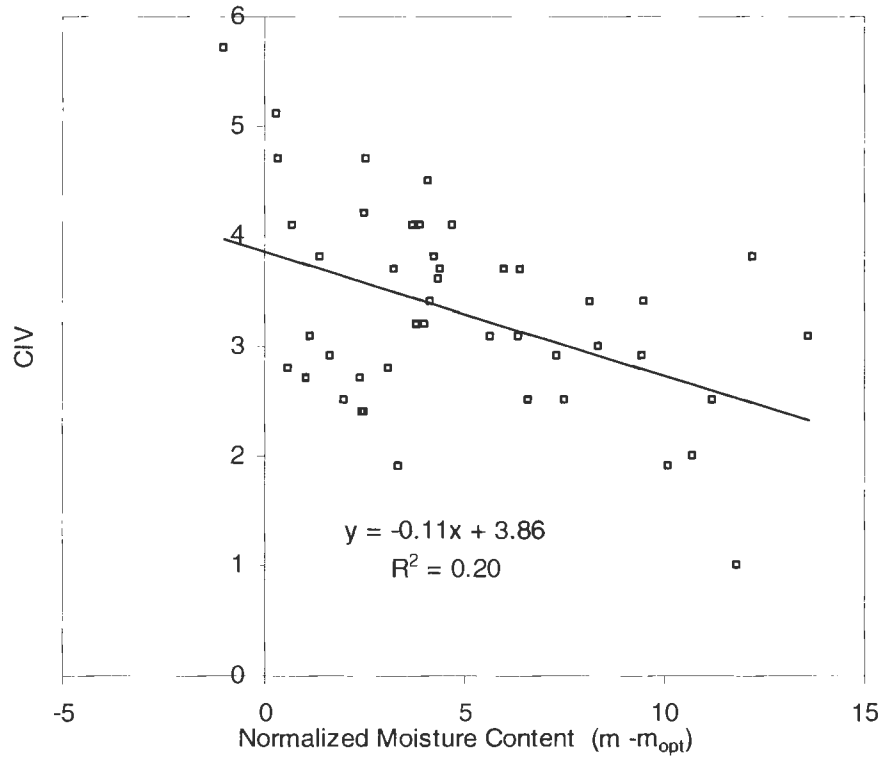

Figure G19. Regression for CIV with normalized moisture content (WDSM existing clay)

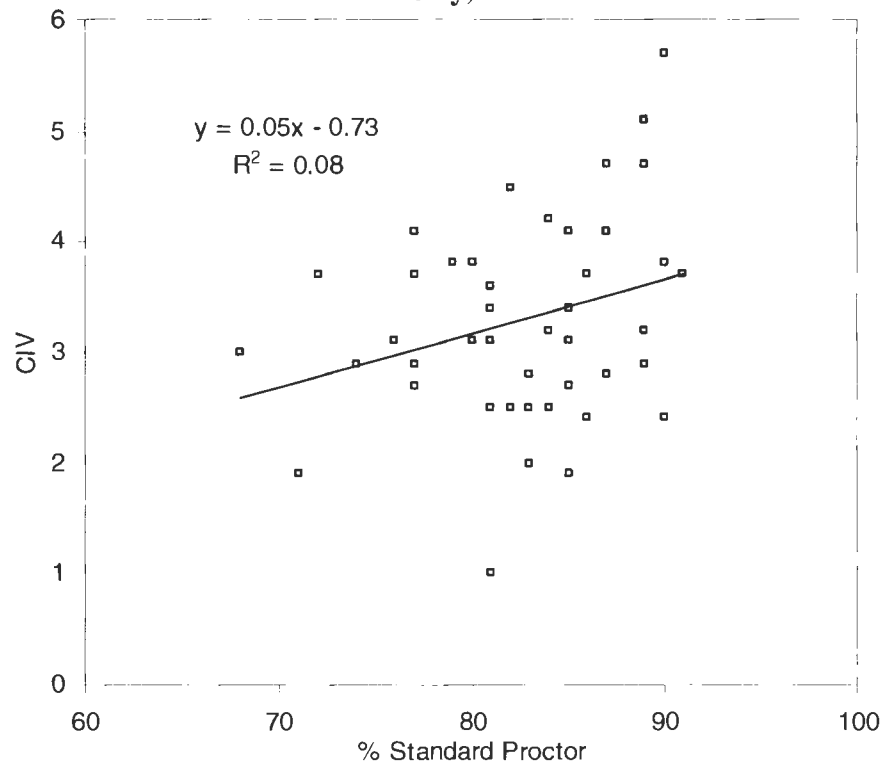

Figure G20. Regression for CIV with relative compaction (WDSM existing clay)

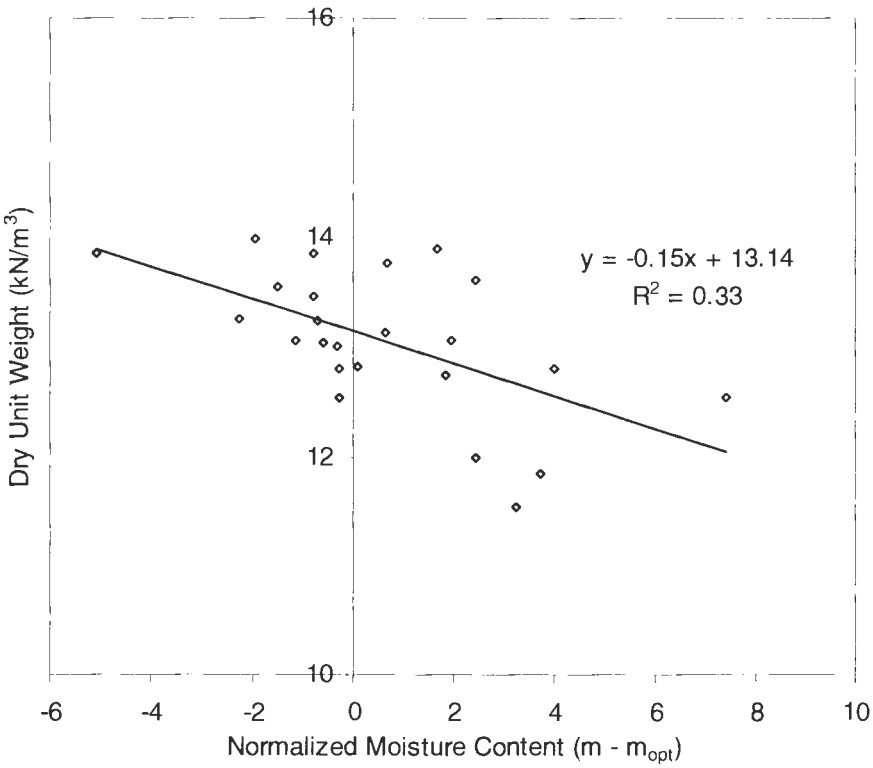

Figure G21. Regression for dry unit weight with normalized moisture content (WDSM fill clay)

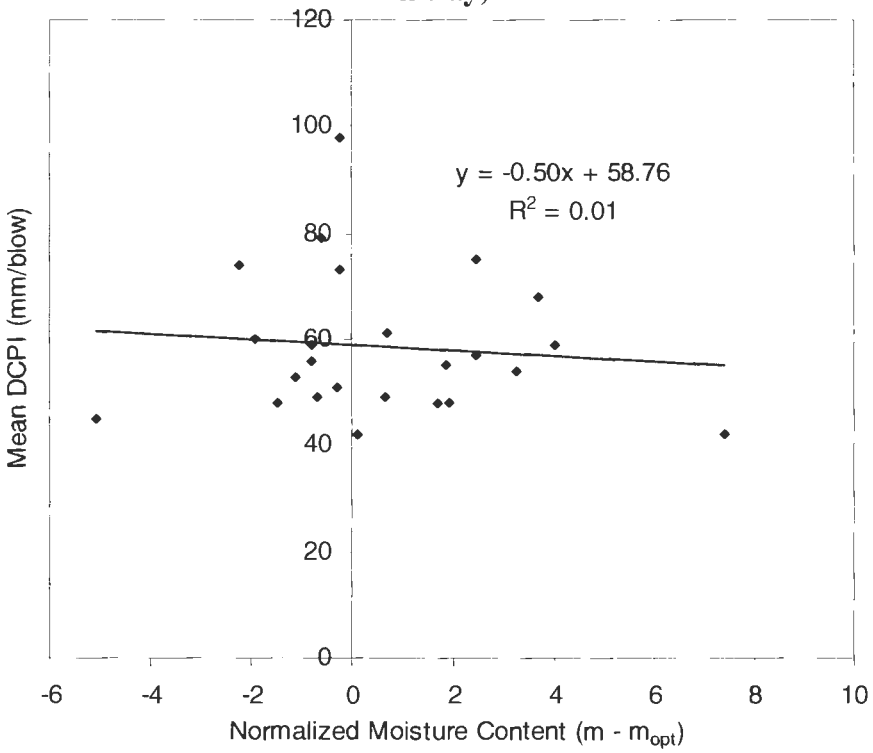

Figure G22. Regression for mean DCPI with normalized moisture content (WDSM fill clay)

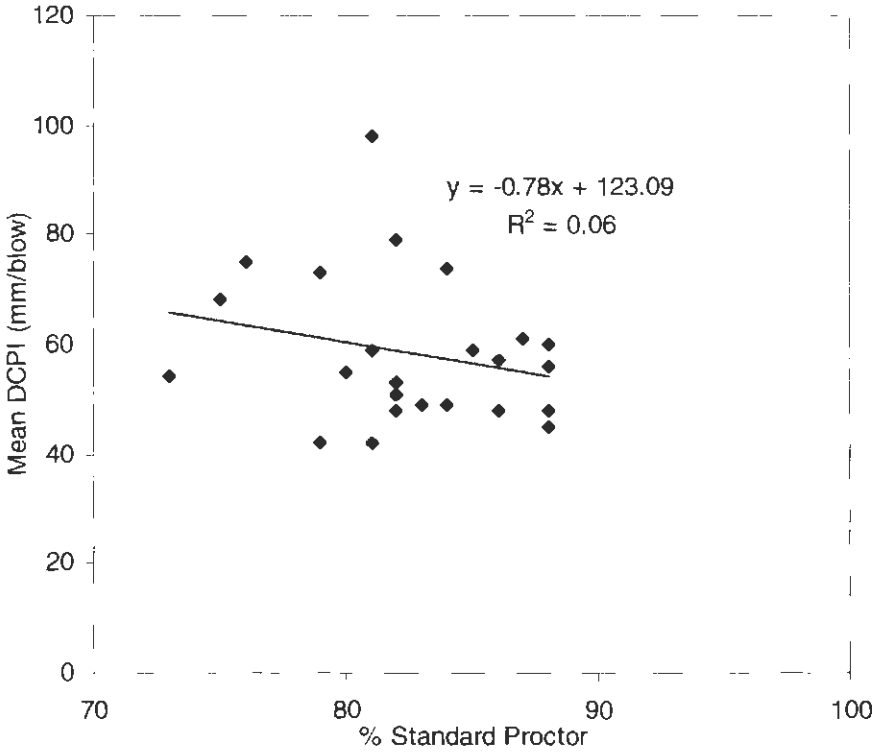

Figure G23. Regression for mean DCPI with relative compaction (WDSM fill clay)

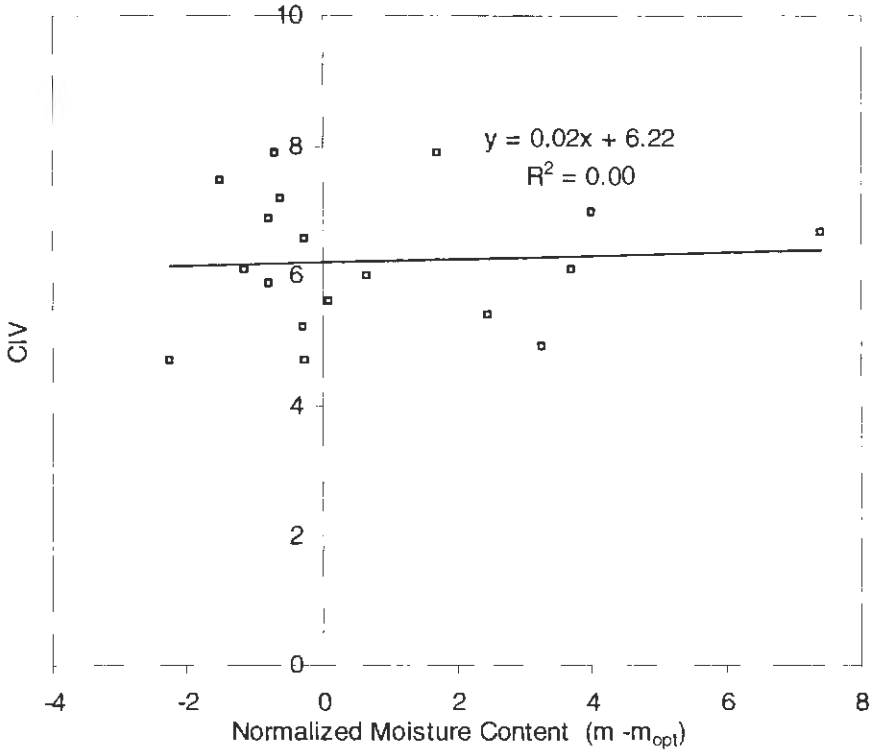

Figure G24. Regression for CIV with normalized moisture content (WDSM fill clay)

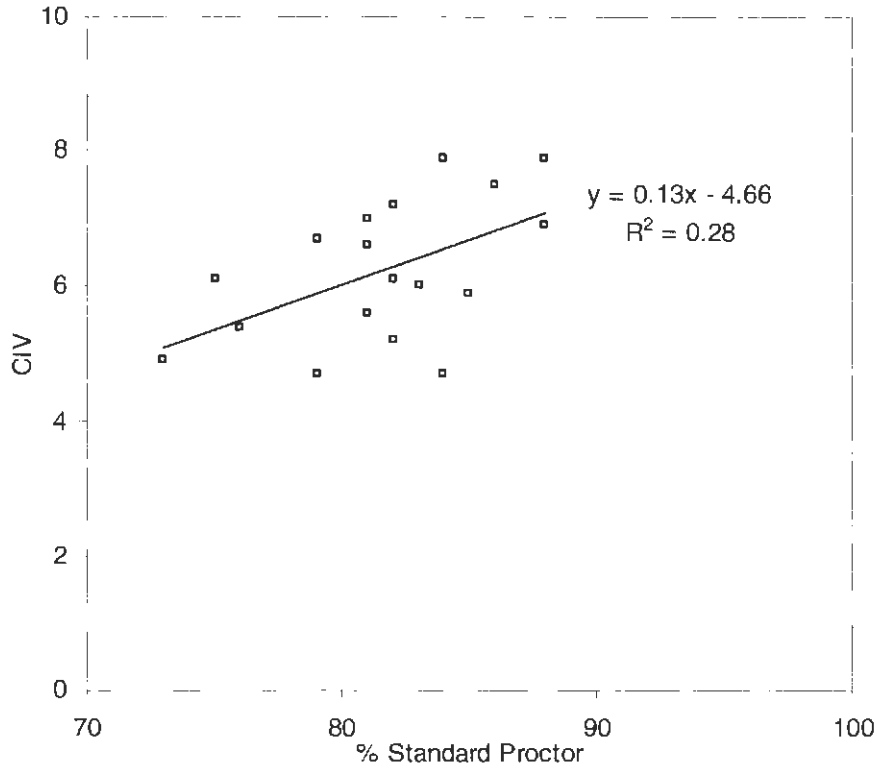

Figure G25. Regression for CIV with relative compaction (WDSM fill clay)

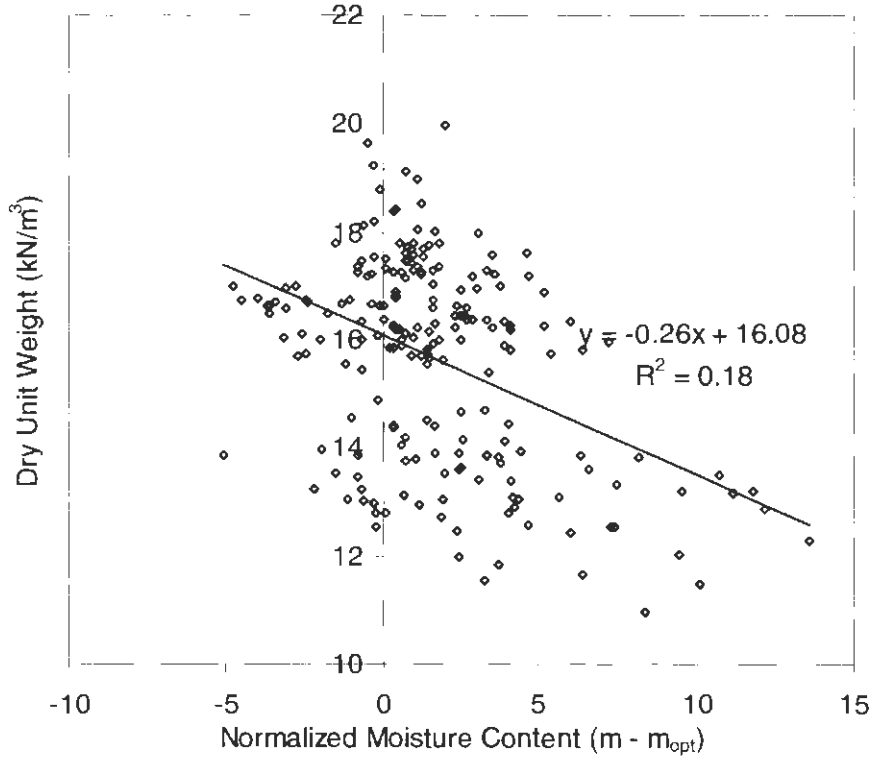

Figure G26. Regression for dry unit weight with normalized moisture content (all field soils)

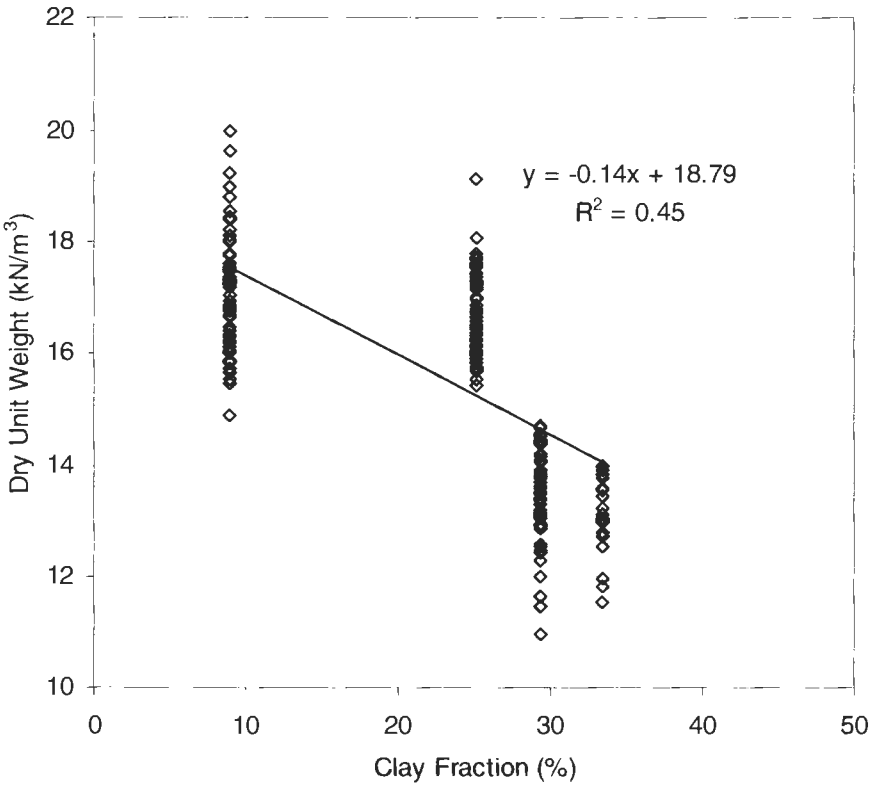

Figure G27. Regression for dry unit weight with clay fraction (all field soils)

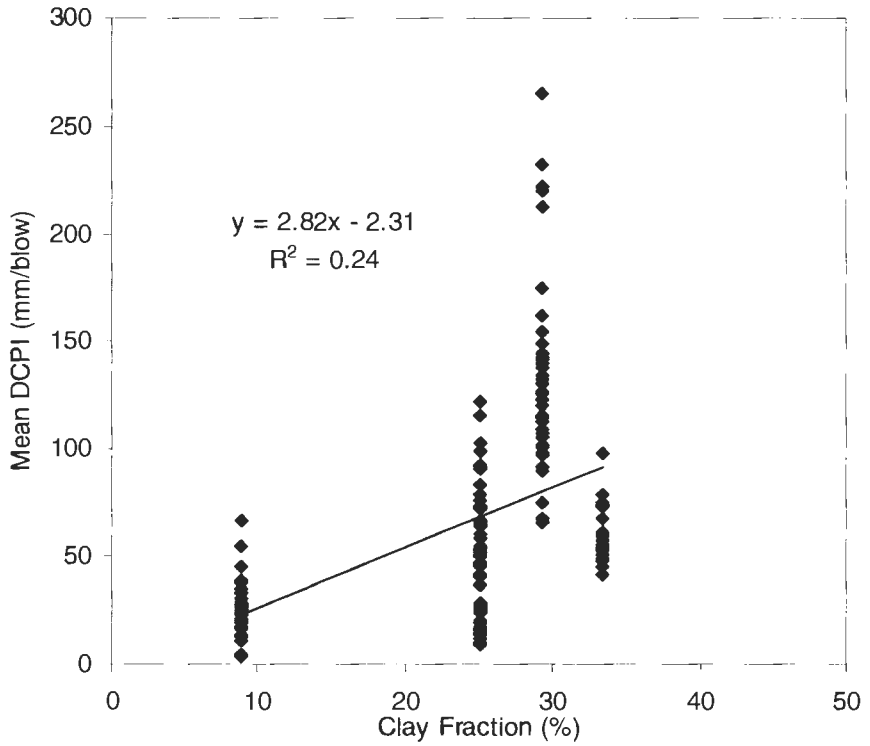

Figure G28. Regression for mean DCPI with clay fraction (all field soils)

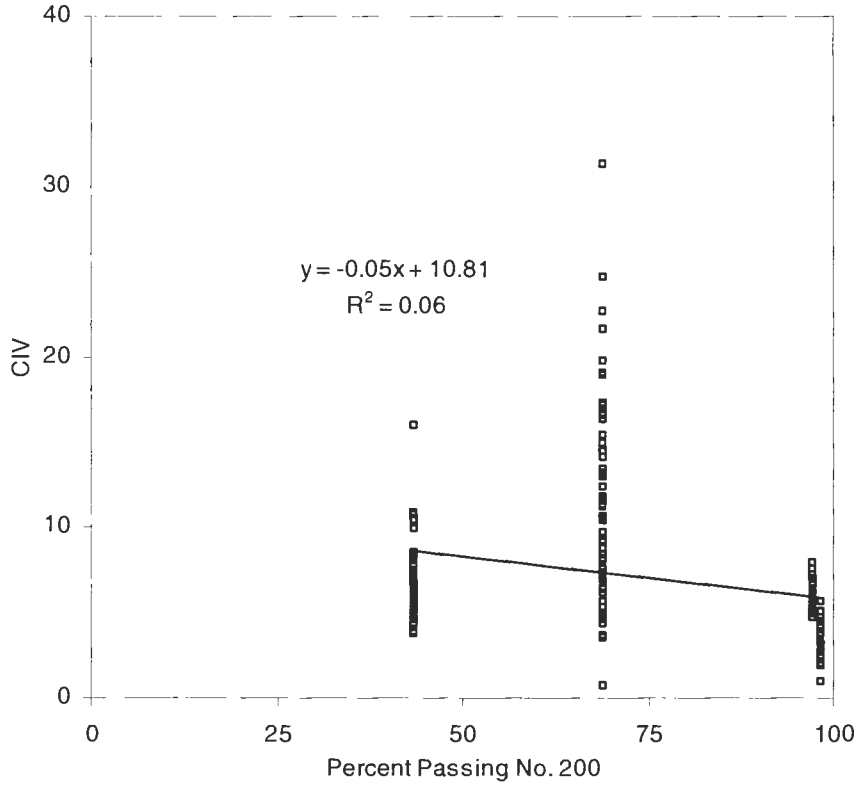

Figure G29. Regression for CIV with percent passing No. 200 sieve (all field soils)

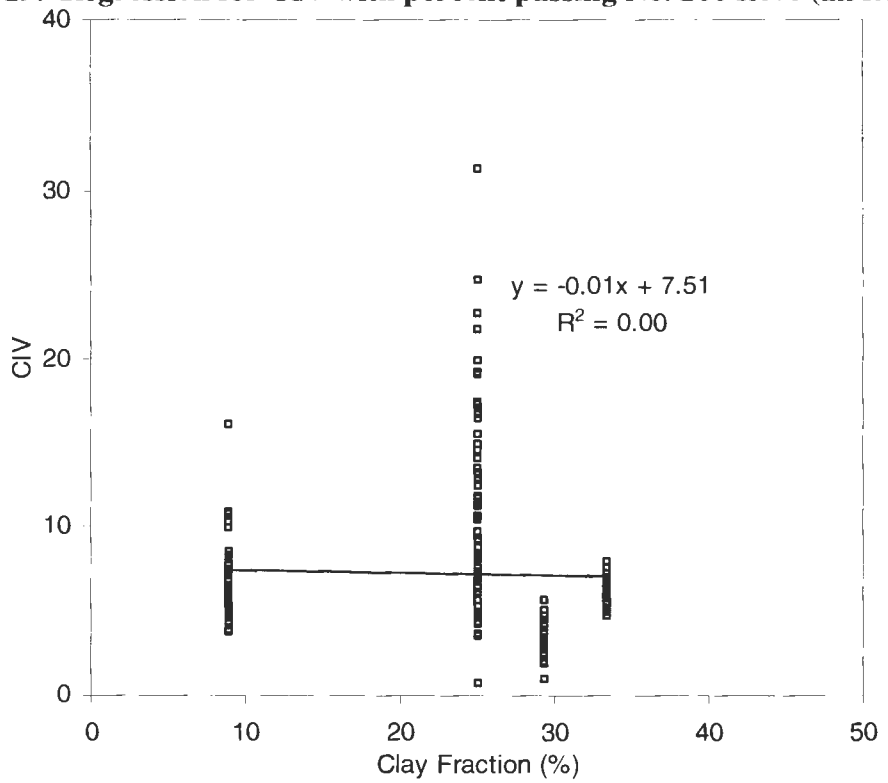

Figure G30. Regression for CIV with clay fraction (all field soils)

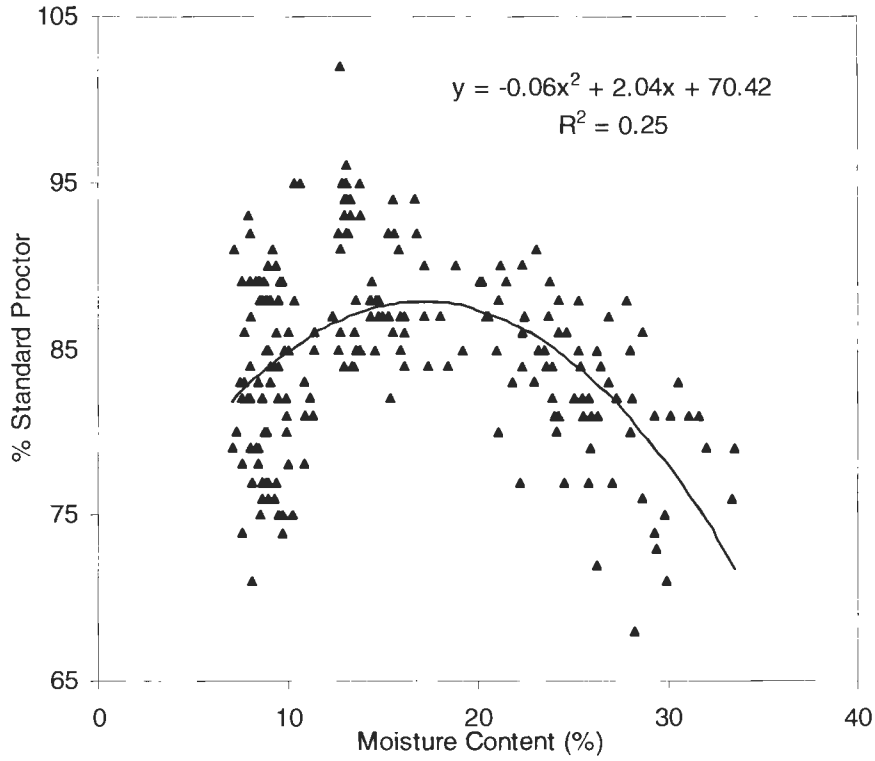

Figure G30. Regression for relative compaction with moisture content (all field soils)

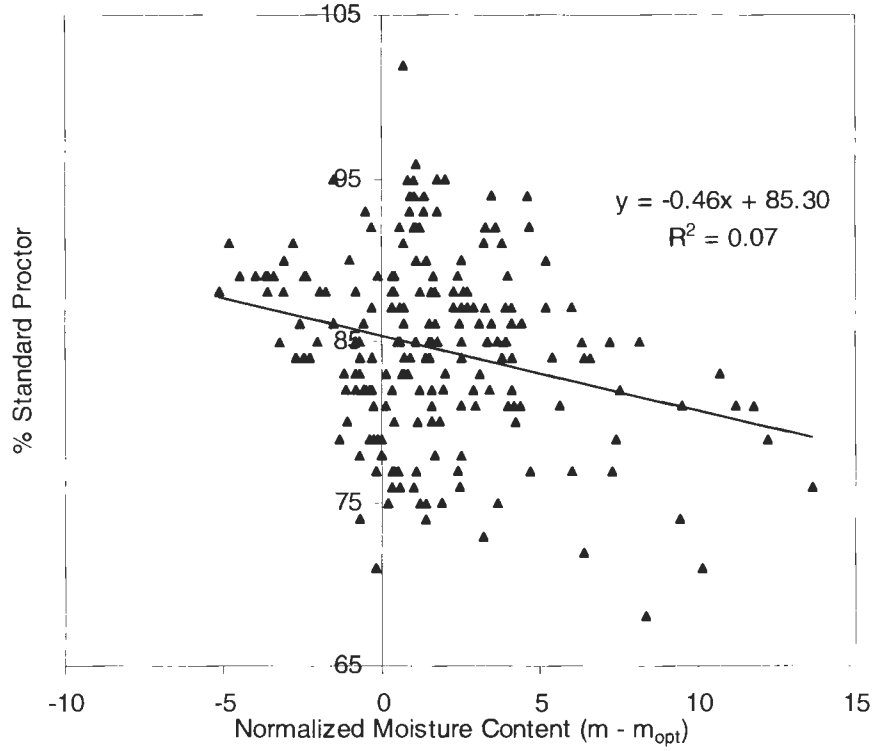

Figure G31. Regression for relative compaction with normalized moisture content (all field soils)

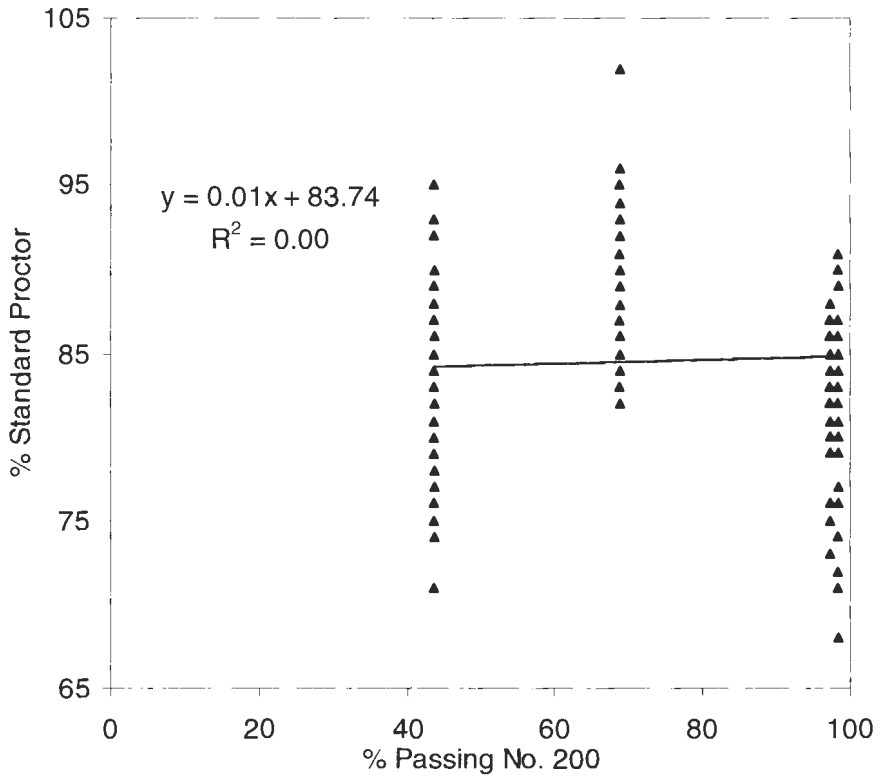

Figure G32. Regression for relative compaction with percent passing No. 200 sieve (all field soils)

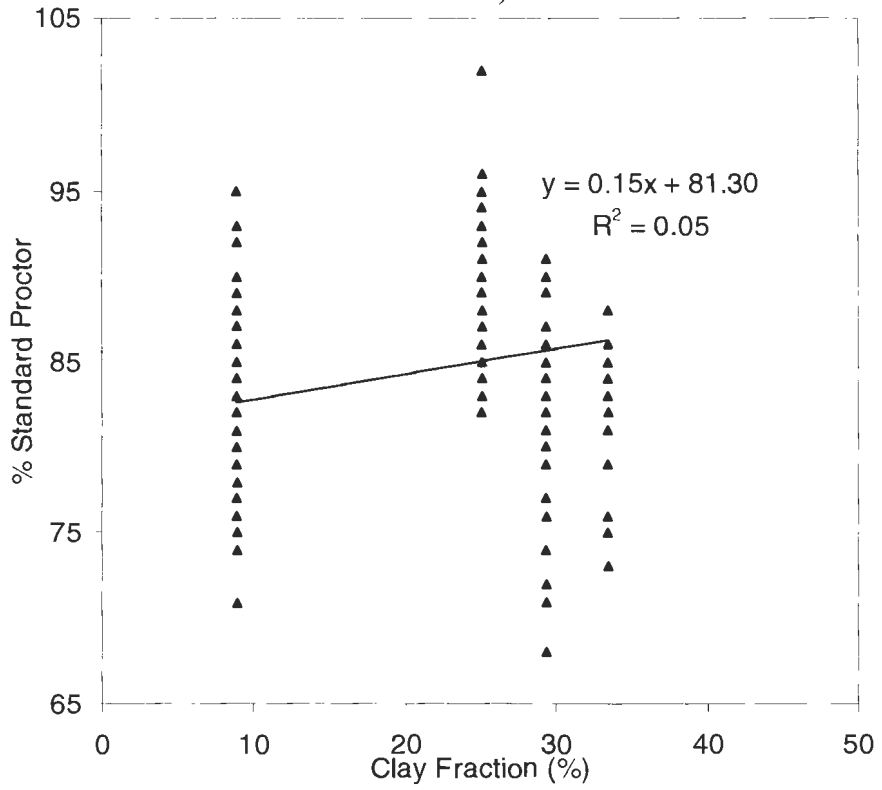

Figure G33. Regression for relative compaction with clay fraction (all field soils)

REFERENCES CITED

Attom, M.F. (1997). "The Effect of Compactive Energy Level on Some Soil Properties." *Applied Clay Science*, 12, 61-72.

Attom, M.F., Abu-Zreig, M.M., and Obaidat M.T. (2001). "Changes in Clay Swelling and Shear Strength Properties with Different Sample Preparation Techniques." *Geotechnical Testing Journal*, 24, 157-63.

Bell, J.R. (1977). "Compaction Energy Relationships of Cohesive Soils." *Transportation Research Record*, 641, 29-34.

Boltz, L., Benson, C., and Boutwell, G. (1998). "Estimating Optimum Water Content and Maximum Dry Unit Weight for Compacted Clays." *J. of Geo. and Geoenv. Eng.*, 124(9), 907-912.

Charles, J.A., Skinner, H.D., and Watts, K.S. (1998). "The Specification of Fill to Support Buildings on Shallow Foundations: The 95% Fixation." *Ground Engineering*, 29-33.

Davidson, D.T. and Gardiner, W.P. (1949). "Calculation of Standard Proctor Density and Optimum Moisture Content from Mechanical Analysis, Shrinkage Factors, and Plasticity Index." *Proc., of the 29th Annual Meeting, Highway Research Board*, 29, 477-481.

Fernandez. F. and Corcoran, P.T. (2001). "A Concept for Assessing Soil Compaction Efficiency." *Foundations and Ground Improvement.* 325-339.

Handy, R.L. (2002). "First-Order Rate Equations in Geotechnical Engineering." *J. of Geo. and Geoenv. Eng.*, 128(5), 416-425.

Humboldt Scientific, Inc. (1999). "H-4140 Geogauge. Soil Compaction Control via In-place Stiffness and Modulus." 14 pp.

Jumikis, A.R. (1958) "Geology and Soils of the Newark (N.J.) Metropolitan Area." *Proc., of the ASCE, J. of Soil Mech. and Found. Div.*, 84(1646), 1-41.

Kouassi, P., Breysse, D., Girard, H., and Poulain, D. (2000). "A New Technique of Kneading Compaction in the Laboratory." *Geotechnical Testing Journal*, 23, 72-82.

Lambe, T.W. (1958). "The Engineering Behavior of Compacted Clays." *J. of the Soil Mech. and Found. Div.*, 84(1655), 1-35.

Lawton E.C., Fragazy R.J., and Hardcastle J.H. (1989). "Collapse of Compacted Clayey Sand." *J. of Geo. Eng.*, 115(9), 1252-1267.

Malama, J.C. (2005). *Evaluation of the Dynamic Cone Penetrometer (DCP) and Geotechnical Remote Acquisition of Data System (G-RAD) for Earthwork Quality Control Testing for Cohesive Soils.* Master's Thesis. Iowa State Univ., Ames, Iowa, 144 pp.

McRae, J.L. and Rutledge, P.C. (1952). "Laboratory Kneading of Soil to Stimulate Field Compaction." *Highway Research Board*, 593-600.

Pagen, C.A. and Jagannath, B.N. (1968). *Effect of Gyratory Compaction on the Rheological Characteristics of Clay.* Report No. EES 248-3. Engineering Experiment Station, Ohio State Univ., Columbus, Ohio, 59 pp.

Ping, W.V., Yang, Z., Leonard, M., and Putcha, S. (2002). "Laboratory Simulation of Field Compaction Characteristics on Sandy Soils." *Transportation Research Record*, 84-95.

Proctor, R. R. (1933a). "Fundamental Principles of Soil Compaction." *Engineering News-Record*, 111, 245-248.

Proctor, R. R. (1933b). "Description of Field and Laboratory Methods." *Engineering News-Record*, 111, 289-289.

Proctor, R. R. (1933d). "Field and Laboratory Verification of Soil Suitability." *Engineering News-Record*, 111, 372-376.

Proctor, R.R. (1948b). "Laboratory Soil Compaction Methods, Penetration Resistance Measurements and the Indicated Saturated Penetration Resistance." *Proc., of the 2nd Int. Conf. on Soil Mech. and Found. Eng.*, 5, 242-247.

Ramiah, B., Viswanath, V., and Krishnamurthy, H. (1970). "Interrelationships of Compaction and Index Properties." *Proc., of the 2nd Southeast Asian Conf. on Soil Eng.*, Rotterdam, The Netherlands, 577-587.

Ring, G.W., Sallberg, J.R., and Collins, W.H. (1962). "Correlation of Compaction and Classification Test Data of Soils." *Public Roads*, 32(4), 77-87.

Rowan, W.H., and Graham, W.W. (1948). "Proper Compaction Eliminates Curing Period in Constructing Fills." *Civil Engineering*, 118(7), 450-451.

Trenter, N.A. and Charles, J.A. (1996). "A Model Specification for Engineered Fills for Building Purposes." *Proc., of Institution of Civil Engineers, Geo. Eng.*, 119(4), 219-230.

Turnbull, J.M. (1948). "Computation of Optimum Moisture Content in the Moisture-Density Relationship of Soils." *Proc., of the 2nd Int. Conf. on Soil Mech. and Found. Eng.*, Rotterdam, 4, 256-262.

Walsh, K.D., Houston, W.N., and Houston, S.L. (1997) "Field Implications of Current Compaction Specification Design Practices." *J. of Const. Eng. and Management*, 123(4), 363-370.

White, D.J., Bergeson, K.L., and Jahren, C.T. (1999). *Embankment Quality: Phase II.* Center for Transportation and Research Education, Iowa State Univ., Ames, Iowa.

White, D.J., Bergeson, K.L., and Jahren, C.T. (2002). *Embankment Quality: Phase III.* Iowa DOT Project TR-401, CTRE Project 97-08. Center for Transportation and Research Education, Iowa State Univ., Ames, Iowa, 171 pp.

Woods, K.B. and Litehiser, R.R. (1938). "Soil Mechanics Applied to Highway Engineering in Ohio." *Ohio State University Studies*, 7(2)

Yemington, E.G. (1958). "Correlation of Compaction Test Results with Plasticity Characteristics of Soils." *Public Roads*.

ACKNOWLEDGEMENTS

I am deeply indebted to many people who helped me in different ways to accomplish this labor of love the reader has read. First, I must thank Dr. David White for the direction, motivation, and encouragement he has given me throughout my time at Iowa State University. I am officially now a geotechnical disciple from the school of Dr. White…or as he would say, "Just call me Dave." So thanks Dave! Next, I want to thank all sponsors of this research including: IDOT, IAAGC, Iowa Paving Assoc., and CAT, Inc. Most importantly, thank you taxpayers of Iowa for giving me a livable income to support myself and a wife for the last two years! Thank-you Dr. Ed Jaselskis and Dr. Max Morris for your time and effort in helping me at your respective offices, out in the field, or during POS committee meetings. I am deeply grateful to all the graduate and undergraduate students who helped me in the lab and/or field. These students include: Dianna, Martinique, Clinton, Mark, Matt V., Lifeng Li, Don Chen, and the "Malama man", Joels C. Malama, master of the DCP; who probably answered more of my questions on soil engineering than anyone else (including Dr. White). A special thank you to my lovely bride, who has endured much more than I have throughout the writing of this paper, and at times has become a "thesis widow". I love you babe! Thank you to any other friends and family that have lovingly encouraged and supported me during this time. Finally, thank you Father for giving me an opportunity to use the gifts and talents that you gave to me. You created man from the soil of the earth and to soil they all return. You are my foundation, my Rock, and my Redeemer.